

TESIS DOCTORAL

MARCO DE TRABAJO TERMODINÁMICO INTEGRADO  
PARA LA ABSORCIÓN DE REFRIGERANTES  
FLUORADOS EN LÍQUIDOS IÓNICOS

PhD THESIS

AN INTEGRATED THERMODYNAMIC FRAMEWORK  
FOR THE ABSORPTION OF FLUORINATED  
REFRIGERANTS IN IONIC LIQUIDS

AUTOR

SALVADOR ASENSIO DELGADO

DIRECTORES

PROF.<sup>a</sup> DR.<sup>a</sup> ANE URTIAGA MENDÍA

DR. GABRIEL ZARCA LAGO

UNIVERSIDAD DE CANTABRIA

Escuela de **Doctorado** de la Universidad de Cantabria

Santander 2023

**UNIVERSIDAD DE CANTABRIA**

DOCTORADO EN INGENIERÍA QUÍMICA, DE LA ENERGÍA Y DE PROCESOS



PhD THESIS

**An integrated thermodynamic framework for the absorption of  
fluorinated refrigerants in ionic liquids**

TESIS DOCTORAL

**Marco de trabajo termodinámico integrado para la absorción  
de refrigerantes fluorados en líquidos iónicos**

Realizada por:

**Salvador Asensio Delgado**

Dirigida por:

Prof.<sup>a</sup> Dr.<sup>a</sup> Ane Urutiaga Mendía

Dr. Gabriel Zarca Lago

Escuela de Doctorado de Universidad de Cantabria

**Santander 2023**



El presente documento recoge la tesis doctoral titulada “AN INTEGRATED THERMODYNAMIC FRAMEWORK FOR THE ABSORPTION OF FLUORINATED REFRIGERANTS IN IONIC LIQUIDS” presentada por Salvador Asensio Delgado para optar al título de Doctor por la Universidad de Cantabria dentro del Programa de Doctorado en Ingeniería Química, de la Energía y de Procesos (BOE núm. 16, de 19 de enero de 2015, RUCT: 5601000).

La tesis ha sido desarrollada en el grupo de investigación de Tecnologías Ambientales y Bioprocesos del Departamento de Ingenierías Química y Biomolecular de la Universidad de Cantabria, bajo la supervisión de la Profesora Ana María Urriaga Mendía y el Doctor Gabriel Zarca Lago.

La tesis se presenta en forma de compendio de artículos. El documento aúna y resume trabajos previamente publicados en revistas científicas incluidas en el *Journal of Citation Reports – Science Citation Index (JCR)*, cumpliendo con la normativa vigente en la Universidad de Cantabria y en el Programa de Doctorado en Ingeniería Química, de la Energía y de Procesos referente a la elaboración de tesis doctorales por compendio de artículos previamente publicados.

En concreto, esta tesis se compone de ocho artículos científicos. De ellos, dos han sido publicados en revistas de primer decil de su categoría, tres en revistas de primer cuartil de su categoría y tres en revistas de segundo cuartil de su categoría.

A continuación, se listan las contribuciones científicas que componen la tesis, así como las contribuciones a congresos realizadas durante la tesis. El orden de presentación de los artículos no es el estrictamente cronológico de su publicación, sino el que se utilizará en el documento de tesis doctoral, una vez adaptado a los objetivos globales y específicos de la tesis:

- Artículos en revistas científicas, indicando la lista de autores por orden de firma, título del artículo, título de la revista, volumen de la revista, año de publicación, números de página, factor de impacto, denominación del área temática de la revista, cuartil en el área temática, y posición relativa en el área temática.

1. Salvador Asensio-Delgado, Fernando Pardo, Gabriel Zarca, Ane Urriaga. Absorption separation of fluorinated refrigerant gases with ionic liquids: Equilibrium, mass transport, and process design. *Separation and Purification Technology*, 276 (2021), 119363. Factor de impacto JCR: 9.136. Chemical engineering: primer cuartil, primer decil, 14/142.
2. Salvador Asensio-Delgado, Daniel Jovell, Gabriel Zarca, Ane Urriaga, Fèlix Llovell. Thermodynamic and process modeling of the recovery of R410A compounds

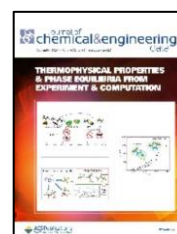




with ionic liquids. *International Journal of Refrigeration*, 118 (2020), 365-375. Factor de impacto JCR: 3.629. Mechanical engineering: segundo cuartil, 34/133. Thermodynamics: segundo cuartil, 17/60.



3. Salvador Asensio-Delgado, Fernando Pardo, Gabriel Zarca, Ane Urtiaga. Vapor-liquid equilibria and diffusion coefficients of difluoromethane, 1,1,1,2-tetrafluoroethane, and 2,3,3,3-tetrafluoropropene in low-viscosity ionic liquids. *Journal of Chemical & Engineering Data*, 65 (2020), 4242-4251. Factor de impacto JCR: 2.694. Thermodynamics: segundo cuartil, 27/63.

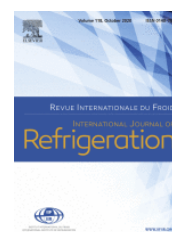


Chemical engineering: tercer cuartil, 77/143. Multidisciplinary chemistry: tercer cuartil, 98/179.

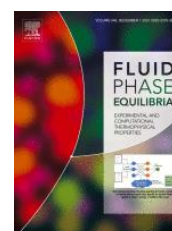
4. Salvador Asensio-Delgado, Fernando Pardo, Gabriel Zarca, Ane Urtiaga. Enhanced absorption separation of hydrofluorocarbon/hydrofluoroolefin refrigerant blends using ionic liquids. *Separation and Purification Technology*, 249 (2020), 117136. Factor de impacto JCR: 7.312. Chemical engineering: primer cuartil, 16/143.



5. José M. Asensio-Delgado, Salvador Asensio-Delgado, Gabriel Zarca, Ane Urtiaga. Analysis of hybrid compression absorption refrigeration using low-GWP HFC or HFO/ionic liquid working pairs. *International Journal of Refrigeration*, 134 (2022), 232-241. Factor de impacto JCR (año 2021): 4.140. Mechanical engineering: primer cuartil, 34/137. Thermodynamics: segundo cuartil, 17/63.



6. Salvador Asensio-Delgado, Miguel Viar, Fernando Pardo, Gabriel Zarca, Ane Urtiaga. Gas solubility and diffusivity of hydrofluorocarbons and hydrofluoroolefins in cyanide-based ionic liquids for the separation of refrigerant mixtures. *Fluid Phase Equilibria*, 549 (2021), 113210. Factor de impacto JCR: 2.745. Thermodynamics: segundo cuartil, 29/63. Chemical engineering: tercer cuartil, 81/142. Physical chemistry: tercer cuartil, 110/163.

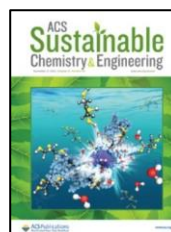


7. Salvador Asensio-Delgado, Fernando Pardo, Gabriel Zarca, Ane Urtiaga. Machine learning for predicting the solubility of high-GWP fluorinated refrigerants in ionic liquids. *Journal of Molecular Liquids*, 367 (2022), 120472.

Factor de impacto JCR (año 2021): 6.633. Atomic, molecular & chemical physics: primer cuartil, 6/36. Physical chemistry: segundo cuartil, 48/163.



8. Salvador Asensio-Delgado, Miguel Viar, Agílio A.H. Pádua, Gabriel Zarca, Ane Urriaga. Understanding the molecular features controlling the solubility differences of R-134a, R-1234ze(E) and R-1234yf in 1-alkyl-3-methylimidazolium tricyanomethanide ionic liquids. *ACS Sustainable Chemistry & Engineering*, 10 (2022), 15124-15134. Factor de impacto JCR (año 2021): 9.224. Chemical engineering: primer cuartil, primer decil, 13/143. Multidisciplinary chemistry: primer cuartil, 29/179. Green & sustainable science & technology: primer cuartil, 10/47.



- Contribuciones a congresos.

1. Salvador Asensio-Delgado, Fernando Pardo, Gabriel Zarca, Ane Urriaga. Novel ionic liquid-based separation processes for the recycling of fluorinated refrigerant gases. Comunicación oral. 13<sup>th</sup> European Congress of Chemical Engineering and 6<sup>th</sup> European Congress of Applied Biotechnology. Celebrado de modo virtual. 20-23 de septiembre de 2021.



2. Salvador Asensio-Delgado, Fernando Pardo, Gabriel Zarca, Ane Urriaga. Ionic liquids as entrainers of fluorinated refrigerant gases: from vapor-liquid equilibrium to separation process design. Presentación flash y póster. 31<sup>st</sup> European Symposium on Applied Thermodynamics. Celebrado de modo virtual. 5-7 de julio de 2021.



3. Salvador Asensio-Delgado, Fernando Pardo, Gabriel Zarca, Ane Urriaga. Using the Regular Solution Theory to select ionic liquids for the separation of fluorinated refrigerants. Comunicación oral. 6<sup>th</sup> Iberoamerican Meeting on Ionic Liquids. Celebrado de modo virtual. 24-26 de mayo 2021.



4. Salvador Asensio-Delgado, Fernando Pardo, Gabriel Zarca, Ane Urriaga. Solubility differences of refrigerant gases in ionic liquids. Comunicación oral. 14<sup>th</sup> Mediterranean Congress of Chemical Engineering. Celebrado de modo virtual. 16-20 de noviembre de 2020. ISBN: 978-84-09-25244-2.

El autor de la tesis, Salvador Asensio Delgado, ha contado con una Ayuda del Programa de Formación de Profesorado Universitario (FPU) del Ministerio de Ciencia, Innovación y Universidades con referencia FPU18/03939 (MCIN/AEI/10.1039/501100011033).

Además, la investigación de esta tesis ha sido parcialmente financiada por el Fondo Europeo de Desarrollo Regional en el marco del programa Interreg-Sudoe a través del proyecto KET4F-Gas-SOE2/P1/P0823 “KET4F-GAS: Reducción del impacto ambiental de los gases fluorados en el espacio SUDOE mediante tecnologías facilitadoras esenciales” y por el Ministerio de Ciencia e Innovación a través de la Agencia Estatal de Investigación (MCIN/AEI/10.1039/501100011033) en el marco del proyecto PID2019-105827RB-I00 “Funcionalización de membranas como elemento clave en el desarrollo de procesos avanzados de separación”, correspondiente a la convocatoria de 2019 «Proyectos de I+D+i», en el marco del Programa Estatal de Generación de Conocimiento y Fortalecimiento Científico y Tecnológico del Sistema de I+D+i Orientada a los Retos de la Sociedad, del Pla Estatal de Investigación Científica y Técnica y de Innovación 2017-2020.

Asimismo, durante la elaboración de la tesis doctoral, Salvador Asensio Delgado ha disfrutado de una “Ayuda complementaria para beneficiarios de ayudas (FPU): Estancias Breves y Traslados Temporales. 2021” con la referencia EST21/00100 para la realización de una estancia de investigación predoctoral de tres meses de duración (septiembre-diciembre de 2021) en el Ionic Liquids Group del Laboratoire de Chimie de la École Normale Supérieure de Lyon (Lyon, Francia) bajo la supervisión del Profesor Agílio A.H. Pádua.

Por ende, tanto el autor como los directores expresan su más sincero agradecimiento hacia la financiación y apoyo aportado por dichas instituciones y entidades.

## Agradecimientos

Me gustaría expresar mi agradecimiento a todas las personas que me han apoyado y contribuido durante la tesis.

A mis directores de tesis, la profesora Ane Urtiaga y el doctor Gabriel Zarca, por darme la oportunidad de desarrollar mi labor de investigación en el Departamento de Ingenierías Química y Biomolecular y por su guía y consejos indispensables para la realización de esta tesis doctoral.

I am also very grateful to Professor Agílio Pádua for giving me the opportunity to learn about molecular dynamics at the Ionic Liquids group of the Laboratoire de Chimie of the ENS de Lyon, and work with all the wonderful people that work with him in the computational part and with Margarida Costa Gomes in the experimental matters.

A todos los compañeros del Departamento de Ingenierías Química y Biomolecular. A Fernando Pardo por su contribución a esta tesis y por acuñar términos que enriquecen el idioma, como caFer y Ferpecto. A Marta Romay, por su ayuda en el diseño de presentaciones y graphical abstracts varios, y a Andrea Arguillarena por sus consideraciones filosóficas, como sus valiosos argumentos sobre por qué deberíamos usar la palabra zincado en el lenguaje cotidiano. A Carmen Barquín y Sophie Schröder, por dejarme ir a ver qué hacen en sus tesis y porqué les gusta tanto usar el HPLC. A Sergio San Martín, porque para investigar hay que tener ideas. Y a todos los demás que harían la lista demasiado larga, gracias por las charlas, cafés, conversaciones, consejos y ratos compartidos.

Y a mi familia. Porque sí y punto.



# **Índice**

---



<b>RESUMEN .....</b>	<b>1</b>
<b>ABSTRACT .....</b>	<b>3</b>
<b>1. INTRODUCTION.....</b>	<b>9</b>
1.1. GENERAL CONTEXT .....	9
1.2. ENVIRONMENTAL IMPACTS.....	9
1.3. FLUORINATED REFRIGERANTS.....	12
1.4. ADVANCED SEPARATION PROCESSES .....	15
1.5. IMPROVEMENT OF THE REFRIGERATION ENERGY EFFICIENCY .....	17
1.6. THE NEED FOR A FRAMEWORK FOR THE STUDY OF F-GAS ABSORPTION IN ILS .....	18
1.7. OBJECTIVES AND STRUCTURE .....	19
1.8. REFERENCES TO CHAPTER 1 .....	22
<b>2. METHODOLOGY .....</b>	<b>33</b>
2.1. EXPERIMENTAL METHODS .....	33
2.1.1. <i>Experimental apparatus and procedure</i> .....	33
2.1.2. <i>Solubility measurements</i> .....	34
2.1.3. <i>Diffusivity calculation</i> .....	39
2.2. MODELING METHODS .....	43
2.2.1. <i>Nonrandom two-liquid model</i> .....	43
2.2.2. <i>Soft Statistical Associating Fluid Theory</i> .....	46
2.2.3. <i>Artificial neural networks</i> .....	49
2.2.4. <i>Molecular dynamics simulations</i> .....	51
2.3. PROCESS DESIGN .....	53
2.4. REFERENCES TO CHAPTER 2 .....	56
<b>3. SCIENTIFIC PUBLICATIONS.....</b>	<b>63</b>
3.1. SCIENTIFIC PUBLICATION 1. "ABSORPTION SEPARATION OF FLUORINATED REFRIGERANT GASES WITH IONIC LIQUIDS: EQUILIBRIUM, MASS TRANSPORT, AND PROCESS DESIGN", SALVADOR ASENSIO-DELGADO, FERNANDO PARDO, GABRIEL ZARCA, ANE URTIAGA, <i>SEPARATION AND PURIFICATION TECHNOLOGY</i> , 276 (2021) 119363 .....	63
3.2. SCIENTIFIC PUBLICATION 2. "THERMODYNAMIC AND PROCESS MODELING OF THE RECOVERY OF R410A COMPOUNDS WITH IONIC LIQUIDS", SALVADOR ASENSIO-DELGADO, DANIEL JOVELL, GABRIEL ZARCA, ANE URTIAGA, FÈLIX LLOVELL, <i>INTERNATIONAL JOURNAL OF REFRIGERATION</i> , 118 (2020) 365-375 .....	93
3.3. SCIENTIFIC PUBLICATION 3. "VAPOR-LIQUID EQUILIBRIA AND DIFFUSION COEFFICIENTS OF DIFLUOROMETHANE, 1,1,1,2-TETRAFLUOROETHANE, AND 2,3,3,3-TETRAFLUOROPROPENE IN LOW-VISCOSITY IONIC LIQUIDS", SALVADOR ASENSIO-DELGADO, FERNANDO PARDO, GABRIEL ZARCA, ANE URTIAGA, <i>JOURNAL OF CHEMICAL &amp; ENGINEERING DATA</i> , 65 (2020) 4242-4251 .....	113



3.4. SCIENTIFIC PUBLICATION 4. “ENHANCED ABSORPTION SEPARATION OF HYDROFLUOROCARBON/HYDROFLUOROOLEFIN REFRIGERANT BLENDS USING IONIC LIQUIDS”, SALVADOR ASENSIO-DELGADO, FERNANDO PARDO, GABRIEL ZARCA, ANE URTIAGA, <i>SEPARATION AND PURIFICATION TECHNOLOGY</i> , 249 (2020) 117136.....	127
3.5. SCIENTIFIC PUBLICATION 5. “ANALYSIS OF HYBRID COMPRESSION ABSORPTION REFRIGERATION USING LOW-GWP HFC OR HFO/IONIC LIQUID WORKING PAIRS”, JOSÉ M. ASENSIO-DELGADO, SALVADOR ASENSIO-DELGADO, GABRIEL ZARCA, ANE URTIAGA, <i>INTERNATIONAL JOURNAL OF REFRIGERATION</i> , 134 (2022) 232-241 .....	143
3.6. SCIENTIFIC PUBLICATION 6. “GAS SOLUBILITY AND DIFFUSIVITY OF HYDROFLUOROCARBONS AND HYDROFLUOROOLEFINS IN CYANIDE-BASED IONIC LIQUIDS FOR THE SEPARATION OF REFRIGERANT MIXTURES”, SALVADOR ASENSIO-DELGADO, MIGUEL VIAR, FERNANDO PARDO, GABRIEL ZARCA, ANE URTIAGA, <i>FLUID PHASE EQUILIBRIA</i> , 549 (2021) 113210 .....	171
3.7. SCIENTIFIC PUBLICATION 7. “MACHINE LEARNING FOR PREDICTING THE SOLUBILITY OF HIGH-GWP FLUORINATED REFRIGERANTS IN IONIC LIQUIDS”, SALVADOR ASENSIO-DELGADO, FERNANDO PARDO, GABRIEL ZARCA, ANE URTIAGA, <i>JOURNAL OF MOLECULAR LIQUIDS</i> , 367 (2022) 120472 .....	193
3.8. SCIENTIFIC PUBLICATION 8. “UNDERSTANDING THE MOLECULAR FEATURES CONTROLLING THE SOLUBILITY DIFFERENCES OF R-134A, R-1234ZE(E) AND R-1234YF IN 1-ALKYL-3-METHYLIMIDAZOLIUM TRICYANOMETHANIDE IONIC LIQUIDS”, SALVADOR ASENSIO-DELGADO, MIGUEL VIAR, AGÍLIO A.H. PÁDUA, GABRIEL ZARCA, ANE URTIAGA, <i>ACS SUSTAINABLE CHEMISTRY &amp; ENGINEERING</i> , 10 (2022), 15124-15134. ....	209
<b>4. RESULTS SUMMARY .....</b>	<b>253</b>
4.1. EXPERIMENTAL RESULTS .....	253
4.2. COMPUTATIONAL RESULTS .....	255
4.2.1. <i>Data regression</i> .....	255
4.2.2. <i>Data prediction</i> .....	256
4.2.3. <i>Interaction analysis</i> .....	256
4.3. PROCESS DESIGN .....	257
4.4. ASSEMBLING THE FRAMEWORK .....	258
<b>4. RESUMEN DE RESULTADOS .....</b>	<b>260</b>
4.1. RESULTADOS EXPERIMENTALES.....	260
4.2. RESULTADOS COMPUTACIONALES .....	262
4.2.1. <i>Regresión de datos</i> .....	262
4.2.2. <i>Predicción de datos</i> .....	263
4.2.3. <i>Análisis de interacciones</i> .....	264
4.3. DISEÑO DE PROCESOS.....	264
4.4. CREACIÓN DEL MARCO DE TRABAJO.....	265
<b>5. CONCLUSIONS AND FUTURE PERSPECTIVES .....</b>	<b>271</b>
<b>5. CONCLUSIONES Y PERSPECTIVAS FUTURAS.....</b>	<b>275</b>
<b>ANEXO. DIFUSIÓN DE RESULTADOS .....</b>	<b>280</b>

1. ARTÍCULOS EN REVISTAS CIENTÍFICAS .....	280
2. CONTRIBUCIONES A CONGRESOS .....	281
3. CONTRIBUCIONES A CONGRESOS COMO COAUTOR .....	282
4. CONTRIBUCIONES A CONGRESOS ANTERIORES AL DOCTORADO .....	282
5. OTRAS ACTIVIDADES.....	283

### Listado de Figuras/List of figures

<b>FIGURE 1. VARIATION IN THE EMISSIONS OF GREENHOUSE GASES BETWEEN 1990 AND 2020 [16]. THE EMISSIONS OF SOME GASES STARTED TO DECREASE GREATLY THANKS TO THE NEW ENACTED POLICIES. ....</b>	<b>11</b>
<b>FIGURE 2. ASHRAE REFRIGERANT CODE SYSTEM. ....</b>	<b>12</b>
<b>FIGURE 3. EXAMPLES OF VAPOR-LIQUID EQUILIBRIUM BEHAVIORS OF HFC REFRIGERANT MIXTURES. R32 (1) + R134A (2) AT 303 K (▼), R143A (1) + R134A (2) AT 293 K (◆), R32 (1) + R143A (2) AT 293 K (▲), R32 (1) + R125 (2) AT 275 K (■), AND R125 (1) + R143A (2) AT 273 K (●).....</b>	<b>16</b>
<b>FIGURE 4. BASIC FLOWSHEET OF THE EXTRACTIVE DISTILLATION PROCESS FOR THE SEPARATION OF F-GASES USING ILS .....</b>	<b>17</b>
<b>FIGURE 5. BASIC FLOWSHEET OF THE ABSORPTION REFRIGERATION CYCLE. ....</b>	<b>18</b>
<b>FIGURE 6. SUMMARY OF THE CONTRIBUTIONS OF THIS THESIS.....</b>	<b>21</b>
<b>FIGURE 7. EXPERIMENTAL SETUP FOR OBTAINING GAS-IL VLE SOLUBILITY DATA. ....</b>	<b>34</b>
<b>FIGURE 8. ASSESSMENT OF THE EFFECT OF VOLUME EXPANSION IN THE DETERMINATION OF SOLUBILITY OF GASES IN ILS: (TOP) CO<sub>2</sub> IN [C<sub>4</sub>MIM][BF<sub>4</sub>] COMPARED TO [6], (MIDDLE) R1234YF IN [C<sub>4</sub>MIM][BF<sub>4</sub>] COMPARED TO [7], AND (BOTTOM) R134A IN [C<sub>4</sub>MIM][OTF].....</b>	<b>36</b>
<b>FIGURE 9. DETERMINATION OF THE DIFFUSION COEFFICIENT AT INFINITE DILUTION FOR THE SYSTEM OF R32 IN [C<sub>2</sub>MIM][TCM] AT 283.15 K: (TOP) DATA REGISTERED DURING THE EXPERIMENT, (MIDDLE) REGRESSION OF EQ. (5), AND (BOTTOM) REGRESSION OF EQ. (8).....</b>	<b>43</b>
<b>FIGURE 10. REPRESENTATION OF THE MOLECULAR PARAMETERS OF THE SOFT-SOFT EOS.....</b>	<b>48</b>
<b>FIGURE 11. STRUCTURE OF A TWO-HIDDEN-LAYER NEURAL NETWORK.....</b>	<b>49</b>
<b>FIGURE 12. EXAMPLE OF INITIAL PERIODIC BOX FOR THE MOLECULAR DYNAMICS SIMULATIONS. ....</b>	<b>52</b>
<b>FIGURE 13. SCHEME OF THE FEP CALCULATION. ....</b>	<b>53</b>
<b>FIGURE 14. SCHEMATICS OF (A) A SINGLE-EFFECT ABSORPTION REFRIGERATION SYSTEM, AND (B) A COMPRESSION-ASSISTED ABSORPTION REFRIGERATION SYSTEM. ....</b>	<b>54</b>

FIGURE 15. GRAPHICAL ABSTRACT OF THE ARTICLE “ABSORPTION SEPARATION OF FLUORINATED REFRIGERANT GASES WITH IONIC LIQUIDS: EQUILIBRIUM, MASS TRANSPORT, AND PROCESS DESIGN” . .....	63
FIGURE 16. GRAPHICAL ABSTRACT OF THE ARTICLE “THERMODYNAMIC AND PROCESS MODELING OF THE RECOVERY OF R410A COMPOUNDS WITH IONIC LIQUIDS” .	93
FIGURE 17. GRAPHICAL ABSTRACT OF THE ARTICLE “VAPOR-LIQUID EQUILIBRIA AND DIFFUSION COEFFICIENTS OF DIFLUOROMETHANE, 1,1,1,2-TETRAFLUOROETHANE, AND 2,3,3,3-TETRAFLUOROPROPENE IN LOW-VISCOSITY IONIC LIQUIDS”	113
FIGURE 18. GRAPHICAL ABSTRACT OF THE ARTICLE “ENHANCED ABSORPTION SEPARATION OF HYDROFLUOROCARBON/HYDROFLUOROOLEFIN REFRIGERANT BLENDS USING IONIC LIQUIDS”	127
FIGURE 19. GRAPHICAL ABSTRACT OF THE ARTICLE “EXPERIMENTAL AND MOLECULAR DYNAMICS STUDY ON THE ABSORPTION OF R134A, R1234ZE(E), AND R1234YF IN 1-ALKYL-3-METHYLIMIDAZOLIUM TRICYANOMETHANIDE IONIC LIQUIDS”	209

Listado de Tablas/List of tables

TABLE 1. ASHRAE DESIGNATIONS FOR ISOMER DIFFERENTIATION.	13
TABLE 2. SELECTION OF SOME COMMON COMMERCIAL REFRIGERANT BLENDS.	14
TABLE 3. PROPERTIES OF COMMON HFCS AND HFOS CONTAINED IN NEW REFRIGERANT BLENDS.	15
TABLE 4. F-GAS/IL SYSTEMS EXPERIMENTALLY STUDIED DURING THE THESIS.	38
TABLE 5. NRTL PARAMETERS OF THE SYSTEMS STUDIED IN THIS THESIS. $\alpha$ VALUE WAS SET TO 0.2 FOR EVERY SYSTEM.	45
TABLE 6. SYSTEMS STUDIED IN THE SCIENTIFIC PUBLICATION 3.	114
TABLE 7. SUMMARY OF F-GAS/IL SYSTEMS STUDIED DURING THE THESIS. (P): PUBLISHED SYSTEM, (V): SYSTEM USED FOR VALIDATION OF THE EXPERIMENTAL SETUP AND PUBLISHED, AND (F): SYSTEM TO BE PUBLISHED IN THE FUTURE.	255
TABLA 8. RESUMEN DE SISTEMAS DE GASES FLUORADOS REFRIGERANTES Y LÍQUIDOS IÓNICOS ESTUDIADOS DURANTE LA TESIS. (P): SISTEMA PUBLICADO, (V): SISTEMA UTILIZADO PARA VALIDAR EL EQUIPO EXPERIMENTAL Y PUBLICADO, Y (F): SISTEMA A PUBLICAR EN EL FUTURO.	262

**Resumen**

**Abstract**



## Resumen

La refrigeración es uno de los logros ingenieriles más importantes del siglo XX y aumentó el bienestar de las personas de forma significativa. Desde su invención, el sector de la refrigeración y aire acondicionado (RAC) ha experimentado transformaciones continuamente para aumentar su eficiencia y reducir el impacto medioambiental relacionado con su actividad. A lo largo del tiempo, son varios los factores que han impulsado los cambios en el sector, como la demanda de equipos más pequeños, o por la necesidad de sustituir los clorofluorocarbonos, sustancias que estaban consumiendo la capa de ozono al liberarlos a la atmósfera, por otras sustancias que no afectaban al ozono atmosférico, los hidrofluorocarbonos (HFCs). En la actualidad, la fuerza motora de la evolución del sector son los Objetivos de Desarrollo Sostenible impulsados por la Organización de Naciones Unidas, que buscan la acción por el clima, comunidades sostenibles y producción y consumos responsables. El sector RAC está inmerso en una revolución que busca reducir el impacto ambiental de su actividad. Este impacto se debe, por una parte, a que los equipos de refrigeración son grandes consumidores de electricidad porque, dentro del ciclo de refrigeración, el fluido refrigerante debe pasar por una etapa de presurización a la salida del evaporador del circuito. Normalmente, esto se consigue con compresores, que son equipos de alto consumo de energía eléctrica. Por otro lado, los fluidos refrigerantes basados en HFCs y contenidos en equipos RAC en su fin de vida no se recuperan, sino que se recogen e incineran o, desafortunadamente, se emiten ilegalmente a la atmósfera. La emisión difusa o intencionada de gases HFCs es un asunto de preocupación global por sus altos potenciales de calentamiento atmosférico, y su emisión es un problema que debe resolverse. La contribución del sector RAC al calentamiento global se ve agravada por el crecimiento de la población mundial y de su desarrollo económico, que aumenta la cantidad de equipos RAC instalados y, por tanto, sus cargas ambientales asociadas.

Esta tesis forma parte los esfuerzos de investigación encaminados a mejorar la sostenibilidad del sector RAC a través del desarrollo de un marco de trabajo integrado para el estudio e implementación de procesos basados en la absorción de gases refrigerantes fluorados (F-gases) en líquidos iónicos (LIs), una familia de compuestos que han llamado la atención por sus propiedades únicas. Para abordar la problemática de la eficiencia de los equipos, el compresor del ciclo de refrigeración se podría sustituir por un conjunto de absorbedor-bomba-desorbedor con un LI en su interior para absorber el refrigerante, presurizarlo y desorberlo a alta presión. La eficiencia aumentaría porque el consumo eléctrico de las bombas es más bajo que el de los compresores, y el proceso da la oportunidad de valorizar otras fuentes de energía térmica de

bajo grado para aumentar la circularidad de recursos. Con respecto al problema de las emisiones, los LIs podrían utilizarse como disolventes en procesos de destilación extractiva para recuperar gases fluorados de interés para la formulación de las nuevas mezclas refrigerantes que se están sintetizando en la actualidad, caracterizadas por su bajo potencial de calentamiento atmosférico, mientras que los gases fluorados de alto impacto ambiental seguirían un tratamiento de gestión como residuo peligroso. Además, este paradigma abre la oportunidad de reducir la producción primaria de refrigerantes, promoviendo un modelo de economía circular en el sector RAC.

El marco de trabajo de esta tesis se ha establecido en base a estudios experimentales y computacionales, incluyendo una extensa y rigurosa revisión de la bibliografía disponible sobre la absorción de F-gases en LIs, la creación de una extensa base de datos, la determinación experimental de la solubilidad de HFCs e hidrofluoroolefinas (HFOs) en LIs de sistemas potencialmente de mayor interés que los estudiados hasta el momento, su regresión paramétrica con el extendido modelo NRTL y la ecuación de estado avanzada soft-SAFT, la simulación de procesos de destilación extractiva y de refrigeración por absorción, la predicción de la solubilidad utilizando aprendizaje automático y el estudio de las interacciones soluto-disolvente por medio de simulaciones de dinámica molecular. En base a toda esta investigación, el flujo de trabajo propuesto para el diseño futuro de procesos consiste en revisar la información publicada tras la revisión de esta tesis, realizar un estudio computacional de la solvatación para entender las interacciones moleculares, predecir el equilibrio utilizando la herramienta de aprendizaje automático de esta tesis para preseleccionar LIs de interés, confirmar la solubilidad de forma experimental para esos LIs, realizar la regresión de los datos y diseñar el proceso *per se*.

Los resultados de esta tesis son más que la definición del flujo de trabajo. Gracias a la revisión crítica, se infirieron tendencias en la solubilidad y selectividad y se seleccionaron LIs en base a ellas. Las tendencias mostraron que los LIs con volúmenes molares bajos y poco fluorados solubilizaban cantidades menores de F-gases, pero presentaban selectividades de absorción más altas frente a las mezclas de F-gases utilizadas como fluidos refrigerantes. Así, se probaron LIs con aniones basados en el cianuro, estudiando experimentalmente el equilibrio de absorción de gases puros, con lo que se obtuvo la selectividad ideal más alta hasta la fecha para la separación del gas R32 de sus mezclas con R125 y R1234yf, con el LI  $[C_2mim][SCN]$ , y de R134a de R1234yf con  $[C_2mim][dca]$ , lo que permitiría su separación y recuperación futuras de forma eficiente. Por otra parte, LIs con aniones muy fluorados y gran volumen molar como el  $[C_2mim][Tf_2N]$  solubilizarían mayores cantidades de gas, y serían los candidatos elegidos para aumentar la

eficiencia de los ciclos de refrigeración basados en absorción-desorción. La dinámica molecular y el aprendizaje automático son metodologías de modelado potentes que se encuentran en crecimiento hoy en día. El uso de la dinámica molecular permite el estudio teórico de los sistemas a nivel microscópico y de interacciones. En este estudio mostró que los F-gases interactúan principalmente con el anión y con la cadena alquílica del catión en LIs de base imidazolio, sin casi interacción con el ciclo aromático catiónico, lo que indica que LIs que busquen alcanzar altos valores de selectividad deberían sintetizarse buscando aniones o cadenas alquílicas que interaccionen con diferente intensidad con los gases a separar. La red neuronal artificial entrenada durante esta tesis permite realizar predicciones de los equilibrios líquido-vapor binarios a partir de propiedades de los compuestos puros como las propiedades críticas, factor acéntrico y presión de vapor de los refrigerantes y las masas molecular, átomos de flúor y volumen molar de los refrigerantes y LIs, con una desviación relativa absoluta media del 10%, incluso para F-gases que no existían en la base de datos utilizada para el entrenamiento de la red.

## **Abstract**

Refrigeration is one of the greatest engineering achievements of the 20<sup>th</sup> century that increased human wellbeing significantly. Since its invention, the sector of refrigeration and air conditioning (RAC) has undergone continuous transformations to increase its efficiency and reduce its environmental impacts. Over time, different factors have driven the evolution of the sector, as the demand for smaller equipment or the need to substitute chlorofluorocarbons, substances which were depleting the atmospheric ozone layer when emitted, by other substances not depleting the atmospheric ozone, the hydrofluorocarbons (HFCs). Currently, the driving force stimulating the evolution of the sector are the Sustainable Development Goals promoted by the United Nations Organization, that look for climate action, sustainable communities and responsible consumption and production. The RAC sector is immersed in a revolution aimed at reducing the environmental impact of its activity. On the one hand, this impact is due to the electricity consumption of refrigeration equipment since, inside the refrigeration cycle, the refrigerant fluid must be pressurized when it exits the evaporator of the circuit. Normally, this pressurization is made by means of compressors, which are devices of high electrical energy consumption. On the other hand, refrigerant fluids based on HFCs from RAC equipment in its end of life are not recovered, but incinerated or, unfortunately, illegally emitted. The sporadic or intentional emission of HFC gases is a matter of concern due to their high global warming potentials, and their emission is a problem that must be addressed. The two aforementioned



problems are aggravated by the increase of world's population and its economic development, which increases the amount of installed RAC equipment and, consequently, their associated burdens.

This thesis forms part of the research efforts toward the improvement of the sustainability of the RAC sector through the development of an integrated framework for the study and implementation of processes based on the absorption of fluorinated refrigerant gases (F-gases) in ionic liquids (ILs), a family of compounds that have attracted attention because of their unique properties. To address the problem of equipment efficiency, the refrigeration cycle compressor could be substituted by an absorber-pump-desorber ensemble with an IL inside, which would absorb the refrigerant, get the liquid mixture pressurized, and release the refrigerant at high pressure. The efficiency would increase because the electrical consumption of pumps is lower than that of compressors, and the process gives the opportunity of valorizing other sources of low-grade thermal energy to increase resource circularity. With respect to the problem of the emissions, ILs could be used as entrainers in extractive distillation processes to recover the refrigerant gases of interest due to their lower environmental impact to reuse them in the formulation of new refrigerant mixtures that are currently being synthesized and characterized by their low global warming potential, while the fluorinated gases of higher environmental impact would be treated as harmful waste. Interestingly, this paradigm opens the opportunity to reduce the primary production of fresh refrigerant gases, promoting a circular economy model in the RAC sector.

The framework developed in this thesis was established based on experimental and computational studies, including an extensive and rigorous revision of the available literature on the absorption of F-gases in ILs, the creation of an extensive database, the experimental determination of solubility of HFCs and hydrofluoroolefins (HFOs) in ILs for systems of potential higher interest than those studied to date, their parametrical regression with the extended NRTL model and with the advanced soft-SAFT equation of state, the simulation of extractive distillation and absorption refrigeration processes, the prediction of solubility using machine learning, and the study of solvent-solute interactions by means of molecular dynamics simulations. Based on all this research, the workflow proposed for the future design of process would consist of reviewing the information published after the revision of this thesis, a computational study of the solvation to understand the molecular interactions happening in the systems, predicting vapor-liquid equilibria using the machine learning tool developed in this thesis to preselect ILs of interest, confirming experimentally the data for the ILs of interest, regression of data, and designing the process of interest itself.

The results of this thesis have been more than the workflow definition. Thanks to the critical revision work, trends on solubility and selectivity were inferred and potentially good ILs were selected. The trends showed that the ILs with low molar volumes and low fluorination solubilized lesser amounts of F-gases but increased the absorption selectivity against F-gas mixtures used as refrigerant fluids substantially. Thus, ILs with cyanide-based anions were tested in experimental absorption studies of pure gases, resulting on the higher ideal selectivity to date for the separation of the gas R32 from its mixtures with R125 and R1234yf using the IL [C<sub>2</sub>mim][SCN], and [C<sub>2</sub>mim][dca] for separating R134a from R1234yf, allowing their future efficient separation and recovery. On the other hand, ILs with highly-fluorinated anions and high molar volume such as [C<sub>2</sub>mim][Tf<sub>2</sub>N] would solubilize greater amounts of gas, and would be the candidates chosen to increase the absorption refrigeration cycle efficiencies. Molecular dynamics and machine learning are powerful modeling methodologies that are still growing nowadays. The use of molecular dynamics allows the theoretical study of the system at the microscopic and interaction level. This study showed that F-gases interact mainly with the anion and the cation alkyl chain of imidazolium ILs, with almost no interaction with the cation head groups, which indicates the ILs aiming at reaching high selectivity values should be synthesized looking for anions or alkyl chains that interact with different intensity with the gases to be separated. The artificial neural network trained during the thesis can predict binary vapor-liquid equilibria from pure component data such as the critical properties, acentric factor and vapor pressure of the refrigerants and the molar masses, fluorine atoms and molar volume of refrigerants and ILs, with an average absolute relative deviation of 10%, even for F-gases not existent in the dataset used to train it.

The work developed during this thesis helps to move the RAC sector towards a more sustainable and circular economy model.



# **Introduction**



# 1. Introduction

## 1.1. General context

Refrigeration is considered one of the 20 greatest engineering achievements of the 20th century [1]. Thanks to refrigeration equipment, we can preserve food and medicaments during their supply chain, use air conditioning in buildings and transport, and develop industrial processes working at low temperatures [2]. Since the development of cooling and chilling equipment, the market of refrigeration, air conditioning, and heat pumps (RACHP) has evolved and developed itself to match the customers' needs [3]. However, this growth carries some associated problems. According to two European Union's reports published in 2020, the heating and cooling sector grew to account for 51% of the total energy consumption and 27% of the total greenhouse gas (GHG) emissions in Europe –mostly due to the fossil fuel origin of the consumed electricity, and not just to direct and fugitive GHG emissions–, and it will continue to grow worldwide as developing countries gain access to electricity and cover their infrastructural needs [4], [5]. In addition, the progressive raise of the Earth's average temperature sets global warming as a factor that will increase the global refrigeration requirements.

The United Nations Development Programme 2030 Agenda sets 17 Sustainable Development Goals [6], among which “Affordable and clean energy” and “Climate action” affect directly the RACHP sector, as well as other goals such as “Sustainable cities and communities” and “Responsible consumption and production” do, aimed at improving the sustainability through the reduction of waste and the promotion of resilient economic models. The scientific community and RACHP industry are engaged in the development and adaptation of the sector to a more sustainable model through various ways, e.g., the synthesis and implementation of new refrigerants, the increase of the equipment efficiency, the minimization of waste, and the shift towards a circular economy [7]–[10].

This thesis forms part of these efforts towards improving the sustainability of the RACHP sector through the development of an integrated framework for the study and implementation of processes based on the absorption of fluorinated refrigerant gases (F-gases) in ionic liquids (ILs), whose use as solvents allows the design of more energy-efficient refrigeration equipment and the recycling of mild-GWP F-gases through extractive distillation processes as discussed below.

## 1.2. Environmental impacts

The main problems related to the increase in the installed cooling capacity are clear. On the one hand, more equipment in service requires more electricity to work and, considering that in the

current grid mix more than half of the energy comes from fossil fuels, this leads to an increase in the indirect CO<sub>2</sub> emissions of refrigeration [8], [11]. The other problem is related to the release of the refrigerant fluids from RACHP equipment once they reach their end of life [9], which implies direct emissions of fluorinated GHGs.

A refrigerant is a fluid that evaporates to extract the heat required from a source, after which it is compressed, condensed, and expanded to be used again as a heat extractor in what is known as a refrigeration cycle. The refrigerants used in RACHP equipment have been evolving, starting with the natural refrigerants NH<sub>3</sub>, SO<sub>2</sub> and CO<sub>2</sub> used in the early days of refrigeration. They were substituted by the synthetic chlorofluorocarbons (CFCs) and hydrochlorofluorocarbons (HCFCs) as a solution to avoid using flammable and toxic compounds. However, the synthetic CFC and HCFC refrigerants were discovered to be harmful to the stratospheric ozone layer, and they had to be phased out to comply with the Montreal Protocol [12]. Research efforts of the leading refrigerant companies resulted at that time in a novel family of refrigerants, the non-chlorinated hydrofluorocarbons (HFCs), which started to replace CFCs and HCFCs since 1990 [3], [13].

HFCs have been used for the last thirty years and are prevalent in RACHP equipment nowadays thanks to their zero ozone depletion potential (ODP), but they still have high global warming potentials (GWP), sometimes thousands of times higher than that of the reference CO<sub>2</sub>, which poses them as substances of environmental concern [13], [14]. The contribution of HFCs to global GHG emissions was estimated as being 0.46, 0.73, and 1.1 Gt CO<sub>2</sub>-eq in 2005, 2010, and 2015, respectively [15]. In fact, while the average emissions of all other GHGs decreased in the European Union between 1990 and 2019, fluorinated gases were the only group whose emissions increased, up to 79%, as shown in Figure 1 [16]. Furthermore, different scenarios predict a further rise of HFCs global emissions up to more than 8 Gt CO<sub>2</sub>-eq·yr<sup>-1</sup> by 2050, if mitigation or abatement policies are not enacted [17]. The Kigali Amendment to the Montreal Protocol (2016) defined a schedule for phasing down the production and consumption of HFCs by 85% of the 2011-2013 average by the late 2040s. In line with this, several international regulations have defined stages of progressive restrictions that are adapted to the different HFC applications and GWP, as is the case of the European F-Gas Regulation (EU 517/2014) transposed to Spanish regulation in the Royal Decree RD 115/2017 [18]–[21]. The effect of these new policies is starting to make effect. Using data released by the European Environment Agency, Figure 1 shows that the 79% increase in emissions of HFCs in 2018 has reduced to 57% in 2020, and this trend will continue as more restrictive stages of the legislation enter into force [16].

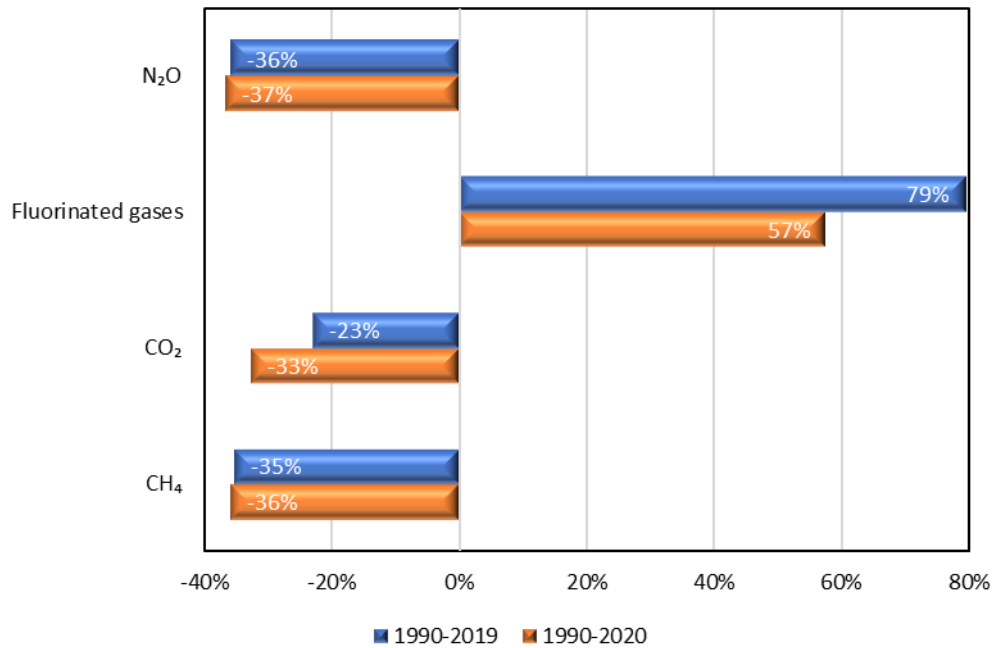


Figure 1. Variation in the emissions of greenhouse gases between 1990 and 2020 [16]. The emissions of some gases started to decrease greatly thanks to the new enacted policies.

Different compounds have been tested to replace HFCs, such as hydrofluoroolefins (HFOs) or hydrochlorofluoroolefins (HCFOs), which are analogous to HFCs and HCFCs, but contain unsaturated double bonds that make molecules more reactive and degradable in the atmosphere and, therefore, less pollutant [3], [10], [22]. However, the main conclusion of the studies to date is that there is not any quintessential refrigerant that will be able to fully replace the HFCs in the form of a pure compound. Instead, HFOs and HCFOs will have to be mixed with HFCs and other compounds as hydrocarbons or CO<sub>2</sub> to form low-GWP refrigerant blends adequate for each type of application [23].

In this context, recovering the HFC blends from end-of-life equipment and separating these into their pure components allows the reuse of those with lower environmental impacts in new, more eco-friendly blends. Furthermore, some of these HFC/HFO blends that have been introduced recently into the RAC market will be short-lived because of the staggered reduction in the GWP limits established by some regulations. Therefore, the recovery, reclamation and reuse of refrigerants is a promising approach to increase their lifetime while minimizing the amount of new HFCs introduced into the market and their subsequent release to the atmosphere, shifting the RACHP market towards a more circular economy model [9].



### 1.3. Fluorinated refrigerants

Nowadays, most refrigeration systems employ F-gas mixtures. F-gases and their mixtures are normally referred to following the American Society of Heating, Refrigerating and Air-Conditioning Engineering (ASHRAE) [10], [24]. Figure 2 describes the ASHRAE code used to name refrigerants, in which four figures describe the molecular structure, followed by letters that distinguish between isomers. The first digit is the number of unsaturated bonds in the molecule, the second is the number of carbon atoms minus one, the third is the number of hydrogen atoms plus one, and the last digit accounts for the number of fluorine atoms. Chlorine atoms, if any, are calculated from the available carbon bonds after subtracting the number of fluorine and hydrogen atoms present in the molecule. For instance, R22 is a one-carbon molecule with two fluorine atoms, one hydrogen atom, and one chlorine atom, i.e., R22 stands for chlorodifluoromethane.

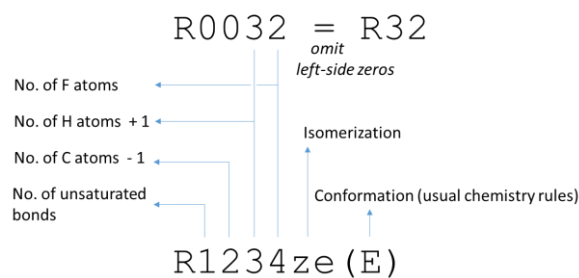


Figure 2. ASHRAE refrigerant code system. The code used is exemplified in the molecules of difluoromethane (R32) and trans-1,3,3,3-tetrafluoropropene (R1234ze(E)). Figure from publication 1 [9] of this thesis article compendium.

Isomer designations depend on the molecule chain length. In the case of ethane-based molecules, no letter at the end of the name refers to the most symmetrical molecule in terms of the distribution of mass around each carbon atom. For instance, 1,1,2,2-tetrafluoroethane is R134, while R134a designates 1,1,1,2-tetrafluoroethane. The isomer coding becomes more complicated for longer chain molecules, with different letters depending on the carbon segment substitution as shown in Table 1 [10].

Other considerations include the safety classification of refrigerants. F-gases are nontoxic, so they receive the letter A. Moreover, the flame propagation behavior of refrigerants means they are nonflammable, low flammable, and mildly flammable compounds (designated as A1, A2L, and A2, respectively). As a reference point, the HFO R1234ze(E), classified as A2L, requires

approximately 250 000 times more energy to ignite than its equivalent hydrocarbon propene [10].

Table 1. ASHRAE designations for isomer differentiation. Table from publication 1 [9] of this thesis article compendium.

Segment	Letter	Segment	Letter
CCl <sub>2</sub>	a	CHCl <sub>2</sub>	n
CClF	b	CH <sub>2</sub> Cl	o
CF <sub>2</sub>	c	CHF <sub>2</sub>	p
CHCl	d	CH <sub>2</sub> F	q
CHF	e	CHClF	r
CH <sub>2</sub>	f	CH <sub>3</sub>	s
CCl <sub>3</sub>	j	C	t
CCl <sub>2</sub> F	k	CCl	x
CClF <sub>2</sub>	l	CF	y
CF <sub>3</sub>	m	CH	z

With respect to mixtures, ASHRAE classifies refrigerant blends as zeotropic mixtures, codified as the 400 series, and azeotropic mixtures, with code numbers in the 500 series. For all mixtures, the numeric code is followed by an uppercase letter denoting the different mixture compositions of the same refrigerant compounds [24]. However, for separation purposes, it should be noted that a mixture of compounds belonging to the 400 series may also present azeotropic behavior with a different composition. One example is R410A, an equimass mixture of R32 and R125 with an azeotropic point at 92 mol % of R32.

Table 2 is a list of some of the most important third- and fourth-generation mixtures of fluorinated refrigerants together with their ASHRAE safety classification and composition. As can be seen, binary, ternary, quaternary, and even more complicated mixtures exist currently. New mixture formulations that are being introduced into the market include HFOs (namely, R1234yf and R1234ze(E)), driven by the need to reduce the GWP of refrigerants and achieve higher refrigeration efficiencies, whereas the proportion of high-GWP HFCs, such as R125, is dropping [25]. Further insights can be extracted from Table 2, where it can be seen that when blending HFOs with the HFCs R134a and R125, the resulting mixtures have no flame propagation (A1 safety classification) but at the expense of achieving only moderate reductions of the GWP. On the other hand, blending HFOs with R32 provides mixtures with a significantly lower GWP than the phased-out HFC mixtures, yet with low flammability (A2L) [3]. In addition, the presence of HFCs such as R32, R134a, and R125 in new blends highlights the importance of recovering compounds from end-of-life equipment as a way of reducing the environmental impact of this

sector and advancing towards a sustainable production and consumption model in harmony with current environmental protection and GWP mitigation policies.

Table 2. Selection of some common commercial refrigerant blends. Table from publication 1 [9] of this thesis article compendium.

Alternative blends	Phase-out subject mixtures	ASHRAE safety classification	GWP	Application	Composition (wt%)					
					R32	R143a	R134a	R125	R1234yf	R1234ze(E)
R404A	R404A	A1	3922	medium and low temperature commercial refrigeration		52.0	4.0	44.0		
R407C	R407C	A1	1774	air-conditioning units heat-pumps, chillers, industrial and commercial medium temperature refrigeration	23.0		52.0	25.0		
R410A	R410A	A1	2088	air-conditioning units heat pumps; cold storage; industrial and commercial and low temperature refrigeration	50.0			50.0		
R507A	R507A	A1	3985	medium and low temperature commercial refrigeration		50.0		50.0		
R447A	R447A	A2L	583	replacement for R410A in stationary air-conditioners		68.0		3.5		28.5
R448A	R448A	A1	1387	non-flammable replacement for R404A in low and medium temperature commercial and transport refrigeration	26.0		21.0	26.0	20.0	7.0
R449A	R449A	A1	1397	non-flammable replacement for R404A in low and medium temperature commercial and transport refrigeration	24.3		25.7	24.7	25.3	
R452B	R452B	A2L	698	replacement for R410A in chillers		67.0		7.0	26.0	
R454A	R454A	A2L	239	replacement for R404A in low and medium temperature commercial refrigeration		35.0			65.0	
R454B	R454B	A2L	466	replacement for R410A		68.9			31.1	
R454C	R454C	A2L	148	replacement for R404A in low and medium temperature commercial refrigeration (hermetic units)		21.5			78.5	
R513A	R513A	A1	631	non-flammable replacement for R134a in medium temperature commercial refrigeration and chillers			44.0		56.0	

## 1.4. Advanced separation processes

The scientific community is working to address the two problems associated with the RACHP sector, which are the indirect emissions due to the energy consumption of the refrigeration cycles and the refrigerant emissions at the end of life of the equipment. The solution to the high energy consumption lies in an improvement of the equipment efficiency or its adaptation to work with renewable energy sources [8], [26]–[28]. The recovery of single refrigerants is hindered because their mixtures have close bubble and dew points and often exhibit azeotropic behavior because they are designed to mimic the behavior of a single fluid [29]. Table 3 presents relevant properties of the main HFCs and HFOs that are being used in new HFC/HFO blends [22], [30], [31].

Table 3. Properties of common HFCs and HFOs contained in new refrigerant blends. Table from publication 4 [29] of this thesis article compendium.

Properties	HFCs			HFOs	
	R32	R125	R134a	R1234yf	R1234ze(E)
Molecular formula	CH <sub>2</sub> F <sub>2</sub>	C <sub>2</sub> HF <sub>5</sub>	C <sub>2</sub> H <sub>2</sub> F <sub>4</sub>	C <sub>3</sub> H <sub>2</sub> F <sub>4</sub>	C <sub>3</sub> H <sub>2</sub> F <sub>4</sub>
GWP	675	3500	1430	4	6
Molar mass (g mol <sup>-1</sup> )	52.02	120.02	102.03	114.04	114.04
Critical temperature (K)	351.26	339.17	374.21	367.85	382.52
Critical pressure (bar)	57.82	36.18	40.59	33.82	36.35
Critical volume (cm <sup>3</sup> mol <sup>-1</sup> )	122.70	209.25	199.32	239.81	233.10
Acentric factor	0.2769	0.3052	0.3268	0.2760	0.3131
Normal boiling point (°C)	-51.65	-48.09	-26.07	-29.45	-18.95
ASHRAE-34 flammability	A2L	A1	A1	A2L	A2L

Some examples of the separation challenges are presented in Figure 3 [32]–[36], where the mixture of R32 + R134a is an example of an easy-to-separate mixture, and the rest are progressively more difficult to separate: close boiling points (R143a + R134a), pinch effect at high compositions (R32 + R143a), an azeotrope at a single composition (R32 + R125) and azeotrope over the whole range of composition (R125 + R143a). Thus, conventional technologies like distillation will not be able to separate refrigerant blends and only advanced separation processes present a real alternative for recovering them.

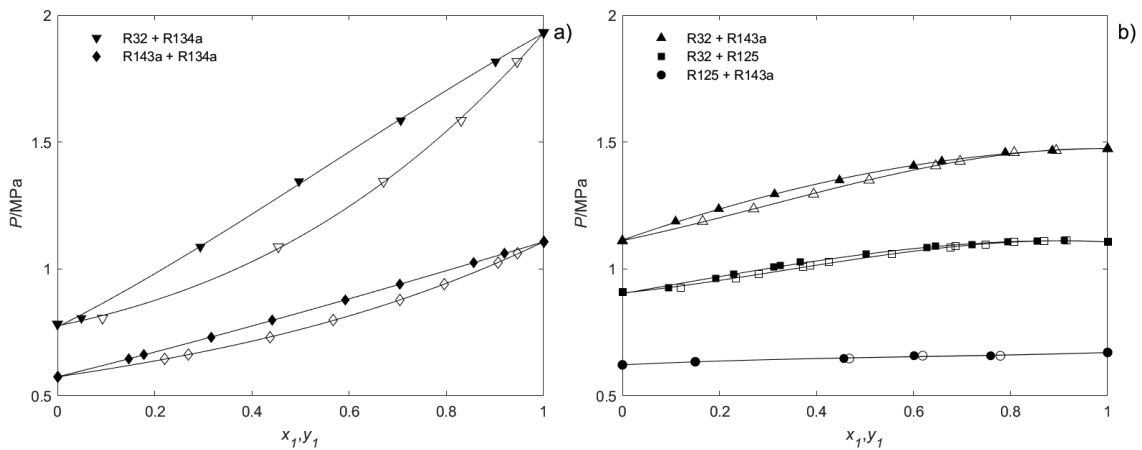


Figure 3. Examples of vapor-liquid equilibrium behaviors of HFC refrigerant mixtures. R32 (1) + R134a (2) at 303 K ( $\blacktriangledown$ ), R143a (1) + R134a (2) at 293 K ( $\blacklozenge$ ), R32 (1) + R143a (2) at 293 K ( $\blacktriangle$ ), R32 (1) + R125 (2) at 275 K ( $\blacksquare$ ), and R125 (1) + R143a (2) at 273 K ( $\bullet$ ). Filled and empty symbols are the molar liquid and vapor phase composition, respectively [32]–[36]. Figure from publication 1 [9] of this thesis article compendium.

Some of the alternatives proposed use adsorbent materials both for the reduction of energy consumption in adsorption refrigeration processes [37], [38] and for the separation of refrigerants in adsorption-based processes [39], [40]. Likewise, membranes have shown to reduce the energy consumption of RACHP equipment [41], [42] and to successfully separate refrigerant gases from their mixtures [43]–[46]. Lately, the absorption of F-gases in ILs is the option that has been attracting the most attention in the form of absorption refrigeration processes [27] and absorption-based separations such as extractive distillations [9], [47]. ILs are ionic compounds comprising highly asymmetric cations and anions that make them be liquids at room temperature despite their internal attractive forces due to its low cohesive energy [48]. They have attracted attention in different fields such as separation [49]–[52], synthesis and catalysis [53], [54], energy [55], analytical applications [56], and as building blocks for advanced materials [57]. Their unique properties explain their spread among so many disciplines, including the separation and recovery of refrigerant compounds from mixtures: they present good chemical and thermal stability, they are non-flammable and have a wide liquid range, the ability to solubilize both polar and nonpolar compounds through various mechanisms, and negligible vapor pressure [58], [59]. In the design of extractive distillation processes like that presented in Figure 4, ILs are advantageous because they can separate the components of a mixture without leaving traces in the distillate stream and without requiring a rectification section in the column above the solvent feed to avoid the distillate solvent losses [50], [60]. Furthermore, the bottoms stream can be easily regenerated without needing a second distillation column [52].

Additionally, the selectivity of the separation is potentially high if the cation-anion combination is carefully selected to suit the mixture of interest [51].

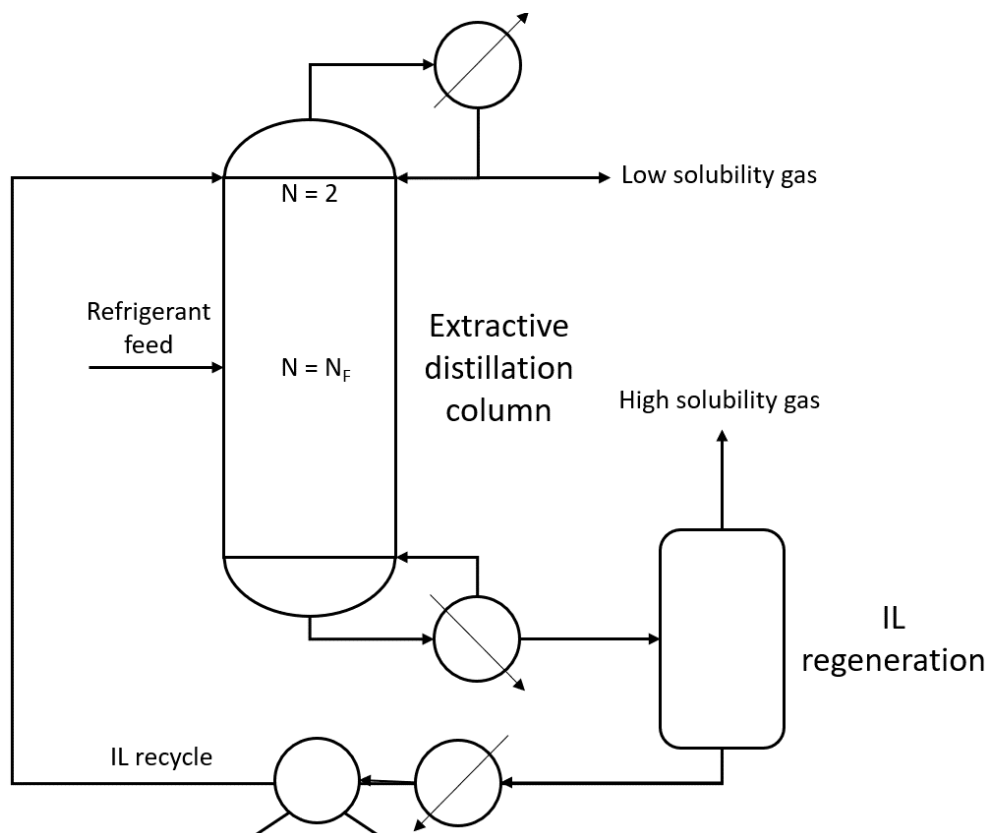


Figure 4. Basic flowsheet of the extractive distillation process for the separation of F-gases using ILs.

### 1.5. Improvement of the refrigeration energy efficiency

Figure 5 shows an absorption refrigeration system, which involves replacing the compressor of a typical compression refrigeration system by an absorption-desorption cycle where the refrigerant is solubilized in a solvent, compressed in liquid state, and desorbed at high pressure and temperature. The advantage of this system comes from the lower electric energy consumption related to the pressure increase in the liquid state, as a pump consumes less energy than a compressor, and to the opportunity for using low-grade thermal energy in the desorber, valorizing heat sources that normally would be wasted [8], [26], [27]. These sources include either renewable energy, e.g., solar or geothermal energy, and waste heat generated in industrial facilities, such as the heat lost in an oven or generated in an exothermic reaction [28]. Current commercial absorption refrigeration systems mostly rely on the use of two absorption pairs,  $\text{H}_2\text{O-LiBr}$  or  $\text{NH}_3\text{-H}_2\text{O}$ . However, refrigerant-IL pairs can surpass the performance of both because ILs are liquid in a wide range of temperature, so they do not risk crystallization as  $\text{H}_2\text{O-}$

LiBr do, they are not corrosive, and the refrigerant and IL can be easily separated in the desorber without the need for a rectification unit as it is the case for  $\text{NH}_3\text{-H}_2\text{O}$  [61].

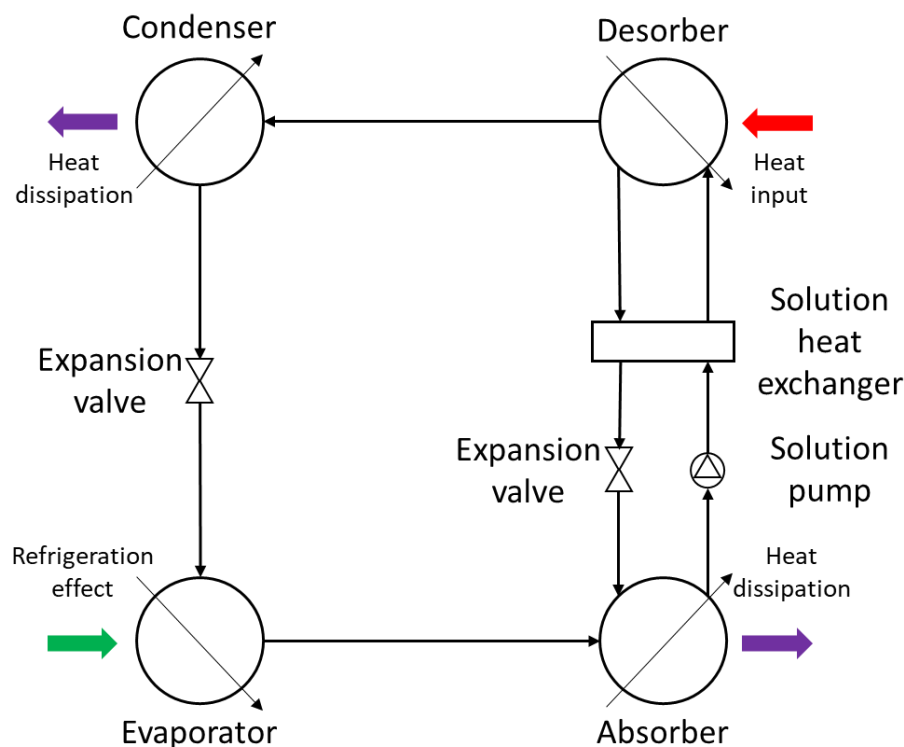


Figure 5. Basic flowsheet of the absorption refrigeration cycle.

### 1.6. The need for a framework for the study of F-gas absorption in ILs

Given the level of interest raised for the use of ILs in the two processes previously described, this thesis aimed at developing a framework for the study, characterization, and assessment of the absorption of F-gases in ILs to reduce the overall environmental footprint of the RACHP sector. At the beginning of this thesis, the heterogeneity of the publications in the topic incurred in difficulties to make educated guesses aimed at setting the path to follow during the initial experiments of the thesis. While some publications covered the solubility of several F-gases in one IL, or alternatively the solubility of an F-gas in several ILs and analyzed the results looking for physical explanations of the results, other publications were limited to the determination of the vapor-liquid equilibrium without any kind of analysis or even a reason behind the choice of the studied IL. Modelling studies suffered of the same issues: while some of the articles applied advanced equations of state (EoS) or even developed new activity-coefficient methods and compared their accuracy to other available models, other publications were limited to the regression of the phase equilibrium of some F-gas/IL systems without any comparison with other models or considerations on the physical meaning of the parameters, neither on the applicability

---

and transferability of their modeling approach. Furthermore, while classical approaches like EoS and activity-coefficient models had been studied profusely, novel computational approaches such as molecular dynamics or artificial intelligence had received little attention. Especially, these alternatives should be studied as complementary tools to increase the knowledge of the absorption mechanisms and trends depending on the solute and solvent physical properties and interactions, rather than limiting them to the regression of experimental data. Therefore, apart from reaching meaningful results and conclusions in the fields of separation and absorption refrigeration of F-gases with ILs, this thesis sets an integrated framework covering the basic steps for the design of processes based on the absorption of F-gases in ILs. The recommendations reached in this thesis are not definitive. They are taken considering the current existent models, their availability in commercial process simulators and the maturity of the advanced computational techniques. Future improvements may result in a change of the specific models recommended for each step, but the basic skeleton of the framework should remain the same and be of great help to tackle complex process design.

In this manner, this thesis is aligned with the Spanish Strategy of Science, Technology and Innovation 2021-2027 (Estrategia Española de Ciencia, Tecnología e Innovación 2021-2027) that establishes the challenge of “Climate, energy and mobility” aiming at reducing climate change and increase the productive processes sustainability [62]. Likewise, the thesis is also aligned with the objective of “Climate, energy and mobility” of the Horizon Europe 2030 [63] and the goals of “Affordable and clean energy”, “Climate action”, “Sustainable cities and communities”, and “Responsible consumption and production” of Sustainable Development Goals of the United Nations Development Programme [6].

## **1.7. Objectives and structure**

In the context of the thesis motivation, the objective of this thesis is to develop an integrated framework for decision making in the design of new processes based on the absorption of HFCs and HFOs in ILs. This can be used both for the design of advanced separation systems for the selective recovery of HFCs and HFOs through extractive distillation processes, promoting the development of technologies for climate change mitigation, and for the design of absorption refrigeration systems using F-gas/IL working pairs, promoting the reduction of the energy consumption of refrigeration equipment.

To achieve the global objective, the following specific objectives are tackled:



- Review of the state of the art for the absorption of F-gases using ILs, analysis of trends in the available information, and selection of potential systems for their study (Publication 1 [9]).
- Preparation of a database compiling all the available data on the absorption of F-gases using ILs (Publication 1 [9]).
- Experimental assessment of the absorption of F-gases in ILs of interest to increase the selectivity for the separation of refrigerant compounds present in current commercial blends and for the solubilization of F-gases in ILs and its application in absorption refrigeration systems (Publications 3 to 6 and 8 [29], [61], [64], [65], [68]).
- Model assessment for the description of the vapor-liquid equilibria of F-gas/IL mixtures and its implementation in the design of separation and absorption refrigeration processes through activity coefficient models such as NRTL (Publications 3 to 6 [29], [61], [64], [65]) and advanced equations of state such as soft-SAFT (Publication 2 [66]).
- Development of a tool based on machine learning techniques for the prediction of the solubility of F-gases in ILs to allow the prescreening of solvents before the costly and time-consuming experimental phase (Publication 7 [67]).
- Study of the solute-solvent interactions between F-gases and ILs in the microscale using advanced theoretical methods based on molecular dynamics simulations (Publication 8 [68]).

The scientific articles compiled in this study address the different objectives of the thesis according to Figure 6, which could be subdivided in three main steps. The first step is the critical step, as it leads to the selection of the optimal solvent for each of the processes of interest, and consists of the intertwined use of literature data, molecular dynamics studies, machine learning regression and experimental confirmation of the taken decisions. The classical approach consists of testing different solvents and select the best one. This thesis proposes a screening based on three complementary axes, two of them of mathematical nature and one of them of bibliographical analysis. Molecular dynamics give meaningful information on the interactions between chemical species that point towards families of compounds that present suitable properties to result in certain behaviors to improve the overall process. Artificial intelligence can manage enormous amounts of data and learn complex relationships between properties, providing with fast and accurate screening possibilities that increase the research efficiency. Reviewing all the available information from other authors has long been known as a useful and powerful procedure to learn and know the state of the art before wasting time in researching already-known topics. Critically analyzing this information is even more important, as having the

whole picture can shed light on trends that could not be seen with the limited information contained in each of the individual references. Figure 6 shows that these three axes are related to experimental data. This thesis validates and trains the two mathematical approaches considered and compiled all the bibliographical information until August 2021 on the absorption of F-gases using ILs with a critical analysis of the compiled information. The second and third steps are more easily understandable: the second one involves the regression of the vapor-liquid equilibrium (VLE) of the F-gases and ILs of interest with adequate models and the third one is the process design itself. Thanks to this thesis, future work in the topic will need lower effort because the framework is already developed, so that the process design would consist of the following steps: complementary solvent screening based on the aforementioned three axes, experimental validation of the selected solvent, data regression with thermodynamic models, and definitive process design.

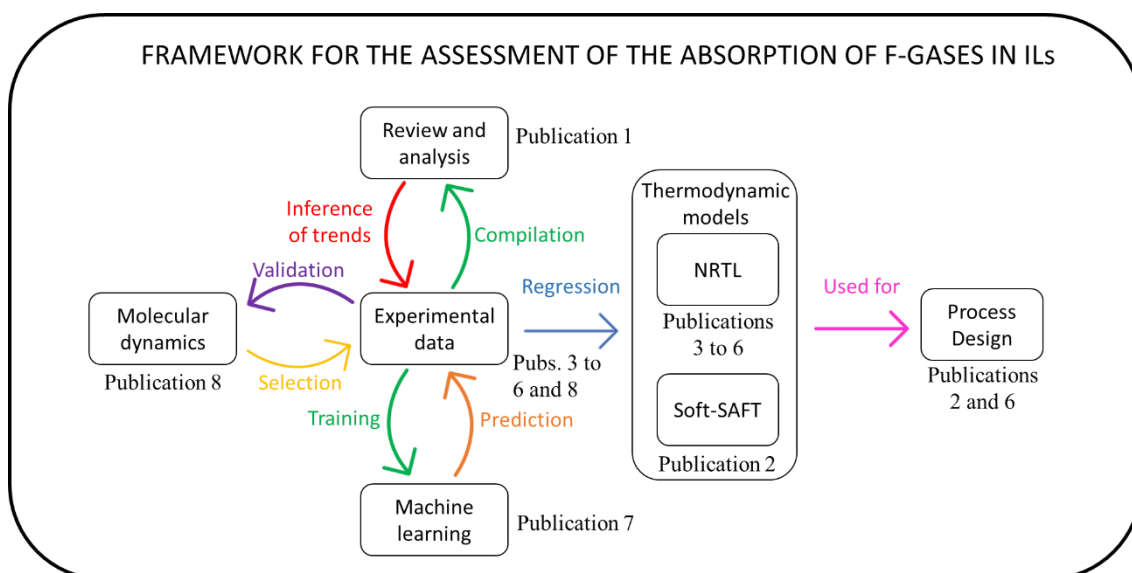


Figure 6. Summary of the contributions of this thesis.

Fulfilling these objectives and considering the regulations of the University of Cantabria [69] and the Doctorate Program of Chemical Engineering, Energy, and Process [70] for the presentation of doctoral thesis as previously published article compendia, the present thesis follows the structure:

- Chapter 1. Introduction. The thesis research line is presented, including its general context and objectives.
- Chapter 2. Methodology. The procedure and methods used for the different tasks that form this thesis are described, both for the experimental and modeling parts.

- Chapter 3. Scientific articles. It includes the articles forming the core of this thesis. These articles develop the general objective of the thesis through both experimental and modeling studies. The eight articles have been published in relevant journals of the field, including two publications in the first decile of the chemical engineering category. Each of the articles is preceded by a short explanation of its contents and its relationship with the rest of the articles in the context of the thesis. For that reason, the articles are not presented in the same order they were published, but an order coherent with the thesis topic and objectives is applied. For example, the critical review is presented in first place, although it was published the fourth. Although the work it includes was carried out since the beginning of the thesis through the creation of the extensive database, the analysis of trends and results required a wiser and more measured work that made possible an advancement in knowledge beyond a simple bibliographical data compilation.
- Chapter 4. Results summary. As its name indicates, it summarizes the main results obtained during the thesis.
- Chapter 5. Conclusions. This section compiles the conclusions achieved during this work and presents the possible future work that could continue this thesis.

To comply with the rules of the University of Cantabria for the presentation and defense of thesis with international mention [69], the thesis is written in English, and the abstract, results summary and conclusions are also presented in Spanish.

### 1.8. References to chapter 1

- [1] G. Constable and B. Somerville, *A century of innovation: Twenty engineering achievements that transformed our lives*. Joseph Henry Press, 2003.
- [2] M. O. McLinden, C. J. Seeton, and A. Pearson, "New refrigerants and system configurations for vapor-compression refrigeration," *Science*, vol. 370, no. 6518, pp. 791–796, 2020, doi: 10.1126/science.abe3692.
- [3] M. O. McLinden and M. L. Huber, "(R)Evolution of Refrigerants," *J. Chem. Eng. Data*, vol. 65, no. 9, pp. 4176–4193, 2020, doi: 10.1021/acs.jced.0c00338.
- [4] European Environment Agency, "Annual European Union greenhouse gas inventory 1990-2018 and inventory report 2020," Brussels, 2020. [Online]. Available: <https://www.eea.europa.eu/publications/european-union-greenhouse-gas-inventory-2020>.
- [5] European Commission Directorate-General for Energy, "Executive summary. Mapping

- and analyses of the current and future (2020 - 2030) heating/cooling fuel deployment (fossil/renewables),” 2020.
- [6] United Nations Department of Economic and Social Affairs, “Do you know all 17 SDGs?” <https://sdgs.un.org/goals> (accessed Jan. 09, 2022).
- [7] P. Giménez-Prades, J. Navarro-Esbrí, C. Arpagaus, A. Fernández-Moreno, and A. Mota-Babiloni, “Novel molecules as working fluids for refrigeration, heat pump and organic Rankine cycle systems,” *Renew. Sustain. Energy Rev.*, vol. 167, no. November 2021, p. 112549, 2022, doi: 10.1016/j.rser.2022.112549.
- [8] M. Seiler, A. Kühn, F. Ziegler, and X. Wang, “Sustainable cooling strategies using new chemical system solutions,” *Ind. Eng. Chem. Res.*, vol. 52, no. 47, pp. 16519–16546, 2013, doi: 10.1021/ie401297u.
- [9] S. Asensio-Delgado, F. Pardo, G. Zarca, and A. Urtiaga, “Absorption separation of fluorinated refrigerant gases with ionic liquids: Equilibrium, mass transport, and process design,” *Sep. Purif. Technol.*, vol. 276, p. 119363, 2021, doi: 10.1016/j.seppur.2021.119363.
- [10] A. J. Sicard and R. T. Baker, “Fluorocarbon Refrigerants and their Syntheses: Past to Present,” *Chem. Rev.*, vol. 120, pp. 9164–9303, 2020, doi: 10.1021/acs.chemrev.9b00719.
- [11] E. J. Garcia, D. Bahamon, and L. F. Vega, “Systematic Search of Suitable Metal-Organic Frameworks for Thermal Energy-Storage Applications with Low Global Warming Potential Refrigerants,” *ACS Sustain. Chem. Eng.*, vol. 9, pp. 3157–3171, 2021, doi: 10.1021/acssuschemeng.0c07797.
- [12] United Nations, *Montreal Protocol on Substances that Deplete the Ozone Layer*. USA, 1987.
- [13] J. M. Calm, “The next generation of refrigerants - Historical review, considerations, and outlook,” *Int. J. Refrig.*, vol. 31, no. 7, pp. 1123–1133, 2008, doi: 10.1016/j.ijrefrig.2008.01.013.
- [14] C. Booten, S. Nicholson, M. Mann, and O. Abdelaziz, “Refrigerants: Market Trends and Supply Chain Assessment,” Golden, Colorado, 2020. [Online]. Available: <https://www.nrel.gov/docs/fy20osti/70207.pdf>.
- [15] P. Purohit *et al.*, “Electricity savings and greenhouse gas emission reductions from global

- phase-down of hydrofluorocarbons,” *Atmos. Chem. Phys.*, vol. 20, no. 19, pp. 11305–11327, 2020, doi: 10.5194/acp-20-11305-2020.
- [16] European Environment Agency, “EEA greenhouse gas-data viewer.” <https://www.eea.europa.eu/data-and-maps/data/data-viewers/greenhouse-gases-viewer> (accessed Sep. 25, 2020).
- [17] G. J. M. Velders, D. W. Fahey, J. S. Daniel, M. McFarland, and S. O. Andersen, “The large contribution of projected HFC emissions to future climate forcing,” *Proc. Natl. Acad. Sci. U. S. A.*, vol. 106, no. 27, pp. 10949–10954, 2009, doi: 10.1073/pnas.0902817106.
- [18] United Nations, “Amendment to the Montreal protocol on substances that deplete the ozone layer,” *United Nations Treaty Collection*, Chapter XXVII, 2.f. 2016. [https://treaties.un.org/Pages/ViewDetails.aspx?src=IND&mtdsg\\_no=XXVII-2-f&chapter=27&clang=\\_en](https://treaties.un.org/Pages/ViewDetails.aspx?src=IND&mtdsg_no=XXVII-2-f&chapter=27&clang=_en) (accessed February 5, 2023).
- [19] E. A. Heath, “Amendment to the Montreal Protocol on Substances that Deplete the Ozone Layer (Kigali Amendment),” *Int. Leg. Mater.*, vol. 56, no. 1, pp. 193–205, 2017, doi: 10.1017/ilm.2016.2.
- [20] European Parliament and Council, “EU 517/2014”, *Official Journal of the European Union*, vol. 150, pp. 195–230, 2014.
- [21] Gobierno de España, “Real Decreto 115/2017”, *Boletín Oficial del Estado*, vol. 42, pp. 11096-11150, 2017.
- [22] A. Mota-Babiloni, J. Navarro-Esbrí, Á. Barragán-Cervera, F. Molés, and B. Peris, “Analysis based on EU Regulation No 517/2014 of new HFC/HFO mixtures as alternatives of high GWP refrigerants in refrigeration and HVAC systems,” *Int. J. Refrig.*, vol. 52, pp. 21–31, 2015, doi: 10.1016/j.ijrefrig.2014.12.021.
- [23] M. O. McLinden, J. S. Brown, R. Brignoli, A. F. Kazakov, and P. A. Domanski, “Limited options for low-global-warming-potential refrigerants,” *Nat. Commun.*, vol. 8, no. 1, pp. 1–9, 2017, doi: 10.1038/ncomms14476.
- [24] R. and A.-C. E. American Society of Heating, “ASHRAE Refrigerant Designations.” <https://www.ashrae.org/technical-resources/standards-and-guidelines/ashrae-refrigerant-designations> (accessed Sep. 25, 2020).
- [25] European Fluorocarbons Technical Committee, “Refrigerants Subject To The F-Gas Regulation 517/2014.” <https://www.fluorocarbons.org/library/> (accessed Sep. 25, 2020).

- 
- [26] A. Altamirano, N. Le Pierrès, and B. Stutz, "Review of small-capacity single-stage continuous absorption systems operating on binary working fluids for cooling: Theoretical, experimental and commercial cycles," *Int. J. Refrig.*, vol. 106, pp. 350–373, 2019, doi: 10.1016/j.ijrefrig.2019.06.033.
- [27] D. Zheng, L. Dong, W. Huang, X. Wu, and N. Nie, "A review of imidazolium ionic liquids research and development towards working pair of absorption cycle," *Renew. Sustain. Energy Rev.*, vol. 37, pp. 47–68, 2014, doi: 10.1016/j.rser.2014.04.046.
- [28] W. Jiang *et al.*, "A comprehensive review on the pre-research of nanofluids in absorption refrigeration systems," *Energy Reports*, vol. 8, pp. 3437–3464, 2022, doi: 10.1016/j.egyr.2022.02.087.
- [29] S. Asensio-Delgado, F. Pardo, G. Zarca, and A. Urtiaga, "Enhanced absorption separation of hydrofluorocarbon/hydrofluoroolefin refrigerant blends using ionic liquids," *Sep. Purif. Technol.*, vol. 249, no. January, p. 117136, 2020, doi: 10.1016/j.seppur.2020.117136.
- [30] A. Mota-Babiloni, P. Makhnatch, and R. Khodabandeh, "Recent investigations in HFCs substitution with lower GWP synthetic alternatives: Focus on energetic performance and environmental impact," *Int. J. Refrig.*, vol. 82, pp. 288–301, 2017, doi: 10.1016/j.ijrefrig.2017.06.026.
- [31] I. H. Bell, J. Wronski, S. Quoilin, and V. Lemort, "Pure and Pseudo-pure Fluid Thermophysical Property Evaluation and the Open-Source Thermophysical Property Library CoolProp," *Ind. Eng. Chem. Res.*, vol. 53, no. 6, pp. 2498–2508, 2014, doi: 10.1021/ie4033999.
- [32] B. G. Lee, J. Y. Park, J. S. Lim, S. Y. Cho, and K. Y. Park, "Phase Equilibria of Chlorofluorocarbon Alternative Refrigerant Mixtures," *J. Chem. Eng. Data*, vol. 44, pp. 190–192, 1999, doi: 10.1021/je980180g.
- [33] M. Nagel and K. Bier, "Vapour-liquid equilibrium of ternary mixtures of the refrigerants R32, R125 and R134a," *Int. J. Refrig.*, vol. 18, no. 8, pp. 534–543, 1995, doi: 10.1016/0140-7007(96)81780-4.
- [34] J. S. Lim, J. Y. Park, B. G. Lee, and Y. W. Lee, "Phase equilibria of 1,1,1-trifluoroethane (HFC-143a) + 1,1,1,2-tetrafluoroethane (HFC-134a), and + 1,1-difluoroethane (HFC-152a) at 273.15, 293.15, 303.15, and 313.15 K," *Fluid Phase Equilib.*, vol. 193, no. 1–2, pp. 29–39, 2002, doi: 10.1016/S0378-3812(01)00632-X.

- [35] C. N. Kim and Y. M. Park, "Vapor-liquid equilibria for the difluoromethane (HFC-32)+1,1,1-trifluoroethane (HFC-143a) system," *J. Chem. Eng. Data*, vol. 45, no. 1, pp. 34–37, 2000, doi: 10.1021/je9901379.
- [36] Y. Higashi, "Vapor-Liquid Equilibrium, Coexistence Curve, and Critical Locus for Pentafluoroethane +1,1,1-Trifluoroethane (R125/R143a)," *J. Chem. Eng. Data*, vol. 44, pp. 333–337, 1999, doi: 10.1021/je980266+.
- [37] P. Goyal, P. Baredar, A. Mittal, and A. R. Siddiqui, "Adsorption refrigeration technology - An overview of theory and its solar energy applications," *Renew. Sustain. Energy Rev.*, vol. 53, pp. 1389–1410, 2016, doi: 10.1016/j.rser.2015.09.027.
- [38] P. R. Chauhan, S. C. Kaushik, and S. K. Tyagi, "Current status and technological advancements in adsorption refrigeration systems: A review," *Renew. Sustain. Energy Rev.*, vol. 154, no. September 2021, p. 111808, 2022, doi: 10.1016/j.rser.2021.111808.
- [39] A. D. Yancey, S. J. Terian, B. J. Shaw, T. M. Bish, D. R. Corbin, and M. B. Shiflett, "A review of fluorocarbon sorption on porous materials," *Microporous Mesoporous Mater.*, vol. 331, no. August 2021, p. 111654, 2022, doi: 10.1016/j.micromeso.2021.111654.
- [40] D. K. J. A. Wanigarathna, J. Gao, and B. Liu, "Metal organic frameworks for adsorption-based separation of fluorocompounds: a review," *Mater. Adv.*, vol. 1, pp. 310–320, 2020, doi: 10.1039/d0ma00083c.
- [41] J. Woods, "Membrane processes for heating, ventilation, and air conditioning," *Renew. Sustain. Energy Rev.*, vol. 33, pp. 290–304, 2014, doi: 10.1016/j.rser.2014.01.092.
- [42] F. Asfand and M. Bourouis, "A review of membrane contactors applied in absorption refrigeration systems," *Renew. Sustain. Energy Rev.*, vol. 45, pp. 173–191, 2015, doi: 10.1016/j.rser.2015.01.054.
- [43] F. Pardo, G. Zarca, and A. Urriaga, "Effect of feed pressure and long-term separation performance of Pebax-ionic liquid membranes for the recovery of difluoromethane (R32) from refrigerant mixture R410A," *J. Memb. Sci.*, vol. 618, p. 118744, 2021, doi: 10.1016/j.memsci.2020.118744.
- [44] F. Pardo, G. Zarca, and A. Urriaga, "Separation of Refrigerant Gas Mixtures Containing R32, R134a, and R1234yf through Poly(ether- block -amide) Membranes," *ACS Sustain. Chem. Eng.*, vol. 8, pp. 2548–2556, 2020, doi: 10.1021/acssuschemeng.9b07195.
- [45] F. Pardo *et al.*, "Integration of Stable Ionic Liquid-Based Nanofluids into Polymer

- Membranes. Part II: Gas Separation Properties toward Fluorinated Greenhouse Gases,” *Nanomaterials*, vol. 11, no. 3, pp. 1–19, 2021, doi: 10.3390/nano11030607.
- [46] F. Pardo, S. Gutiérrez-Hernández, G. Zarca, and A. Urtiaga, “Toward the recycling of low-GWP hydrofluorocarbon/hydrofluoroolefin refrigerant mixtures using composite ionic liquid-polymer membranes,” *ACS Sustain. Chem. Eng.*, vol. 9, pp. 7012–7021, 2021, doi: 10.1021/acssuschemeng.1c00668.
- [47] B. R. Mellein, A. M. Scurto, and M. B. Shiflett, “Gas Solubility in Ionic Liquids,” *Curr. Opin. Green Sustain. Chem.*, vol. 28, no. 6, p. 100425, 2020, doi: 10.1016/j.cogsc.2020.100425.
- [48] G. Zarca, A. Urtiaga, I. Ortiz, P. Cañizares, and M. A. Rodrigo, “Carbon monoxide reactive separation with basic 1-hexyl-3-methylimidazolium chlorocuprate (I) ionic liquid: Electrochemical determination of mass transport properties,” *Sep. Purif. Technol.*, vol. 141, pp. 31–37, 2015, doi: 10.1016/j.seppur.2014.11.027.
- [49] D. Han and K. H. Row, “Recent Applications of Ionic Liquids in Separation Technology,” *Molecules*, vol. 15, pp. 2405–2426, 2010, doi: 10.3390/molecules15042405.
- [50] J. D. Seader, E. J. Henley, and D. K. Roper, *Separation process principles*, 3rd ed. New Jersey, USA: John Wiley & Sons, Ltd, 2010.
- [51] Z. Lei, C. Dai, J. Zhu, and B. Chen, “Extractive Distillation with Ionic Liquids: A Review,” *AIChE J.*, vol. 60, pp. 3312–3329, 2014, doi: 10.1002/aic.14537.
- [52] A. B. Pereiro, J. M. M. Araújo, J. M. S. S. Esperança, I. M. Marrucho, and L. P. N. Rebelo, “Ionic liquids in separations of azeotropic systems - A review,” *Journal of Chemical Thermodynamics*, vol. 46, pp. 2–28, 2012, doi: 10.1016/j.jct.2011.05.026.
- [53] T. Welton, “Room-Temperature Ionic Liquids. Solvents for Synthesis and Catalysis,” *Chem. Rev.*, vol. 99, no. 8, pp. 2071–2083, 1999, doi: 10.1021/cr980032t.
- [54] V. I. Pârvulescu and C. Hardacre, “Catalysis in Ionic Liquids,” *Chem. Rev.*, vol. 107, pp. 2615–2665, 2007, doi: 10.1021/cr050948h.
- [55] D. R. MacFarlane *et al.*, “Energy Applications of Ionic Liquids,” *Energy Environ. Sci.*, vol. 7, no. 1, pp. 232–250, 2014, doi: 10.1039/C3EE42099J.
- [56] T. D. Ho, C. Zhang, L. W. Hantao, and J. L. Anderson, “Ionic liquids in analytical chemistry: Fundamentals, advances, and perspectives,” *Anal. Chem.*, vol. 86, no. 1, pp. 262–285, 2014, doi: 10.1021/ac4035554.



- [57] S. Zhang, Q. Zhang, Y. Zhang, Z. Chen, M. Watanabe, and Y. Deng, "Beyond solvents and electrolytes: Ionic liquids-based advanced functional materials," *Prog. Mater. Sci.*, vol. 77, pp. 80–124, 2016, doi: 10.1016/j.pmatsci.2015.10.001.
- [58] G. Zarca, I. Ortiz, and A. Urriaga, "Novel solvents based on thiocyanate ionic liquids doped with copper(I) with enhanced equilibrium selectivity for carbon monoxide separation from light gases," *Sep. Purif. Technol.*, vol. 196, pp. 47–56, 2018, doi: 10.1016/j.seppur.2017.06.069.
- [59] Z. Lei, C. Dai, and B. Chen, "Gas Solubility in Ionic Liquids," *Chem. Rev.*, vol. 114, no. 2, pp. 1289–1326, 2014, doi: 10.1021/cr300497a.
- [60] V. Gerbaud, I. Rodriguez-Donis, L. Hegely, P. Lang, F. Denes, and X. Q. You, "Review of extractive distillation. Process design, operation, optimization and control," *Chem. Eng. Res. Des.*, vol. 141, pp. 229–271, 2019, doi: 10.1016/j.cherd.2018.09.020.
- [61] J. M. Asensio-Delgado, S. Asensio-Delgado, G. Zarca, and A. Urriaga, "Analysis of hybrid compression absorption refrigeration using low-GWP HFC or HFO/ionic liquid working pairs," *Int. J. Refrig.*, vol. 134, pp. 232–241, 2022, doi: 10.1016/j.ijrefrig.2021.11.013.
- [62] Gobierno de España and Ministerio de Ciencia e Innovación, "Estrategia Española de Ciencia, Tecnología e Innovación 2021-2027." 2021.
- [63] European Commission, "Horizon Europe - Investing to shape our future" [https://health.ec.europa.eu/system/files/2021-11/ev\\_20211021\\_co07\\_en\\_0.pdf](https://health.ec.europa.eu/system/files/2021-11/ev_20211021_co07_en_0.pdf) (accessed February 5, 2023).
- [64] S. Asensio-Delgado, F. Pardo, G. Zarca, and A. Urriaga, "Vapor–Liquid Equilibria and Diffusion Coefficients of Difluoromethane, 1,1,1,2-Tetrafluoroethane, and 2,3,3,3-Tetrafluoropropene in Low-Viscosity Ionic Liquids," *J. Chem. Eng. Data*, vol. 65, no. 9, pp. 4242–4251, 2020, doi: 10.1021/acs.jced.0c00224.
- [65] S. Asensio-Delgado, M. Viar, F. Pardo, G. Zarca, and A. Urriaga, "Gas solubility and diffusivity of hydrofluorocarbons and hydrofluoroolefins in cyanide-based ionic liquids for the separation of refrigerant mixtures," *Fluid Phase Equilib.*, vol. 549, p. 113210, 2021, doi: 10.1016/j.fluid.2021.113210.
- [66] S. Asensio-Delgado, D. Jovell, G. Zarca, A. Urriaga, and F. Llovel, "Thermodynamic and process modeling of the recovery of R410A compounds with ionic liquids," *Int. J. Refrig.*, vol. 118, pp. 365–375, 2020, doi: 10.1016/j.ijrefrig.2020.04.013.

- 
- [67] S. Asensio-delgado, F. Pardo, G. Zarca, and A. Urriaga, "Machine learning for predicting the solubility of high-GWP fluorinated refrigerants in ionic liquids," *J. Mol. Liq.*, vol. 367, p. 120472, 2022, doi: 10.1016/j.molliq.2022.120472.
- [68] S. Asensio-Delgado, M. Viar, A. A. H. Pádua, G. Zarca, and A. Urriaga, "Understanding the Molecular Features Controlling the Solubility Differences of R-134a, R-1234ze(E), and R-1234yf in 1-Alkyl-3-methylimidazolium Tricyanomethanide Ionic Liquids," *ACS Sustain. Chem. Eng.*, vol. 10, no. 46, pp. 15124–15134, 2022, doi: 10.1021/acssuschemeng.2c04561.
- [69] U. de Cantabria, "Normativa de gestión académica de los estudios de doctorado regulados por el Real Decreto 99/2011." 2020, [Online]. Available: <https://web.unican.es/estudios/Documents/TESIS/RCT-D9-IQUIMICA.pdf>.
- [70] Programa de Doctorado en Ingeniería Química de la Energía y de Procesos, "Normativa Para La Elaboración De Tesis Doctorales Como Compendio De Artículos En El Programa De Doctorado En 'Ingeniería Química, De La Energía Y De Procesos' De La Universidad De Cantabria," 2017, [Online]. Available: <https://web.unican.es/estudios/Documents/TESIS/RCT-D9-IQUIMICA.pdf>.



# **Methodology**

---



---

## 2. Methodology

This thesis has tackled the development of a framework to study the absorption of F-gases using ILs. To that end, the solubility and diffusivity of F-gases in ILs has been determined experimentally and different modeling approaches have been used with the objectives of regressing and predicting vapor-liquid equilibrium (VLE) and understanding the solute-solvent interactions. This section summarizes the methods used during the thesis. The extended explanations are available in the articles forming the core of this thesis.

### 2.1. Experimental methods

The isochoric saturation method was used to measure the solubility of F-gases in ILs [1]. Using this method, the diffusion coefficients at infinite dilution can be determined using data collected at the beginning of each experiment following the semi-infinite volume model [2], [3]. Then, the experiments for determining solubility and diffusivity of F-gases in ILs were made in the same equipment.

#### 2.1.1. Experimental apparatus and procedure

The experimental system consists of a gas absorption chamber and a gas storage cylinder connected by a valve as shown in Figure 7. The absorption chamber is a jacketed stirred tank reactor (Buchi, model Picoclave, 170 mL), equipped with a pressure transducer (Aplisens, model PCE-28,  $\pm 0.001$  bar) and a Pt 100 temperature sensor. The thermal fluid flows through the jacket connected to a cryothermostatic bath (Julabo, model F25-ME,  $\pm 0.01$  K). The storage cylinder (140 mL) was initially equipped with an absolute digital manometer (Keller, model Leo 2,  $\pm 0.001$  bar). However, the tank pressure transducer and the manometer of the storage cylinder were substituted by two pressure transducers that allowed their connection to a computer for automatic data recording (Keller, series PAA-33X, 0.01% accuracy). To ensure a low IL humidity, the ILs were dried for two days at 60 °C and vacuum and their water content was measured to be lower than 50 ppm by Karl-Fischer titration. The absorption chamber was loaded with  $\sim 35$  g ( $\pm 0.0001$  g) of the vacuum-dried IL. The difference between the total available volume and loaded IL volume is large enough to ensure that the measurements are independent of IL volumetric expansion. Before each experiment, the IL was degassed at 333 K under vacuum for a minimum of 6 h. As mentioned, this experimental system allows for the determination of both solubility and diffusivity in a single experiment. First, the temperature and pressure of the gas-filled storage cylinder were recorded. Then, the valve connecting both sections was opened, and the absorption process was allowed to proceed spontaneously for the first 20 min for diffusivity

measurements without stirring. After that, the stirrer was set at 500 rpm and gas absorption proceeded until the system reached equilibrium conditions, this is, when pressure remained constant for more than 20 min.

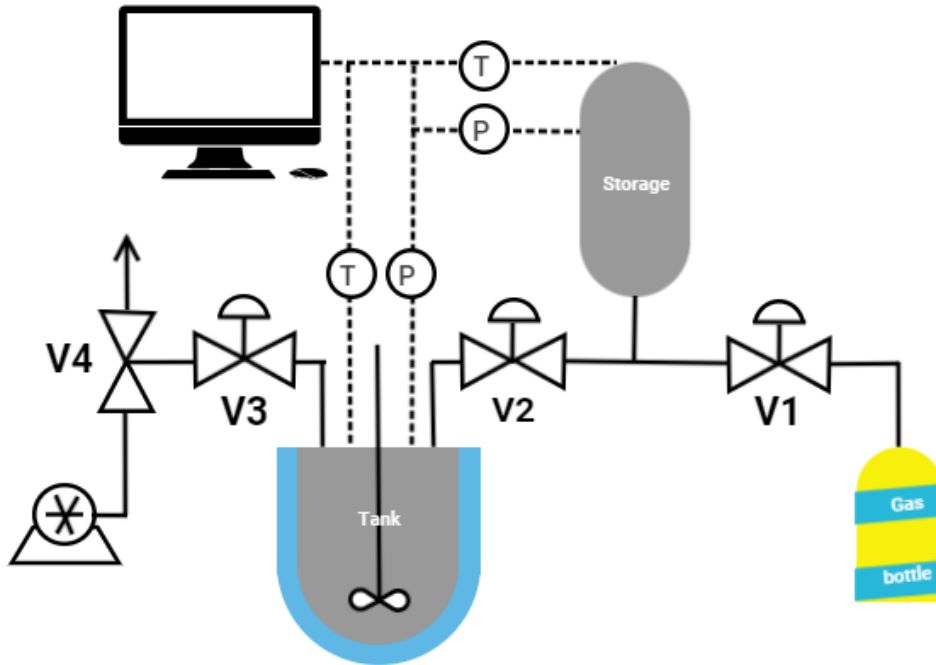


Figure 7. Experimental setup for obtaining gas-IL VLE solubility data.

### 2.1.2. Solubility measurements

The isochoric saturation method is one of the synthetic methods available for the determination of the vapor-liquid equilibria (VLE) and solubility of pure gases in ILs. It is considered synthetic rather than analytic because the compositions are not directly measured, but they are derived from the recording of the gas pressure and temperature at the initial and final states of the experiment [4]. Using pressure and temperature, the molar density is calculated using the Peng-Robinson equation of state (EoS). Knowing the volume of the equipment, the moles of gas can be calculated, and the difference between the final and initial moles is the amount that has been absorbed:

$$n_{step} = \rho_{(i,s)} \cdot V_S + \rho_{(i-1,c)} \cdot (V_c - V_l) - \rho_{(i,eq)} \cdot (V_S + V_c - V_l) \quad (1)$$

where  $V_S$ ,  $V_c$ , and  $V_l$  are the storage cylinder, sorption chamber, and loaded IL volumes (L), and  $\rho_s$ ,  $\rho_c$ , and  $\rho_{eq}$  are the gas molar densities ( $\text{mol} \cdot \text{L}^{-1}$ ) in the storage cylinder, in the sorption chamber, and in the whole system at equilibrium conditions, respectively. For consecutive stages, the dissolved moles are calculated as the moles absorbed in one step ( $n_{step}$ ) plus the moles dissolved in the previous steps ( $n_k$ ):

$$n_{abs} = n_{step} + \sum_{k=1}^{i-1} n_k \quad (2)$$

And then, the molar fraction is calculated using the moles of IL charged in the system ( $n_l$ ):

$$x = \frac{n_{abs}}{n_l + n_{abs}} \quad (3)$$

As mentioned in section 2.1.1., the experimental system has been designed to ensure that the measurements are independent of the IL volumetric expansion. The previous equations show that the amount of gas dissolved is indirectly calculated from the difference between the moles in the gas phase and at the beginning of each step and the remaining at equilibrium conditions, so that this method relies on gas phase measurements. Maximizing the gas to liquid volume ratio can minimize the effect of volume expansion in the measurements, so the experimental setup in this thesis was designed with gas to liquid ratio around 25:1 with a total volume of 310 mL of which only ~12 mL are occupied by liquid. Here, the effect of volume expansion on the measurements performed in the experimental setup is assessed more thoroughly. In Figure 13 of the work by Aki et al. [5], it is observed that volume expansion follows an approximately linear increase with the mole fraction of absorbed gas. For the case of CO<sub>2</sub> absorption in [C<sub>4</sub>mim][BF<sub>4</sub>], a CO<sub>2</sub> mole fraction of 0.4 yields a volume expansion of approximately 15%. Denoting  $\alpha$  as the volumetric expansion factor, Eq. (1) can be modified to Eq. (1.b) as follows:

$$n_{step} = \rho_{(i,s)} \cdot V_S + \rho_{(i-1,c)} \cdot (V_c - V_l) - \rho_{(i,eq)} \cdot (V_S + V_c - V_l) \quad (1)$$

$$n_{step} = \rho_{(i,s)} \cdot V_S + \rho_{(i-1,c)} \cdot (V_c - V_l \cdot (1 + \alpha \cdot x_{i-1})) - \rho_{(i,eq)} \cdot (V_S + V_c - V_l \cdot (1 + \alpha \cdot x_i)) \quad (1.b)$$

When volume expansion is considered, Eq. (1.b) and (3) need to be solved iteratively. This procedure is applied to some example systems in this section to show that volume effect has not a meaningful impact in the results and every other value in this thesis is calculated using Eq. (1). Figure 8 shows the examples. First, the solubility of CO<sub>2</sub> in [C<sub>4</sub>mim][BF<sub>4</sub>] measured by Shiflett and Yokozeki in a microgravimetric balance [6] is compared with the results using the isochoric saturation method in the system of this thesis considering and neglecting volume expansion. The parameter  $\alpha$  is calculated equal to  $\frac{0.15}{4} = 0.0375$  from Aki et al. [5]. The isotherm is well replicated and the difference in each value for the molar composition is between 0.2 and 1.2% when the volume expansion is considered, which is lower than the experimental uncertainty.



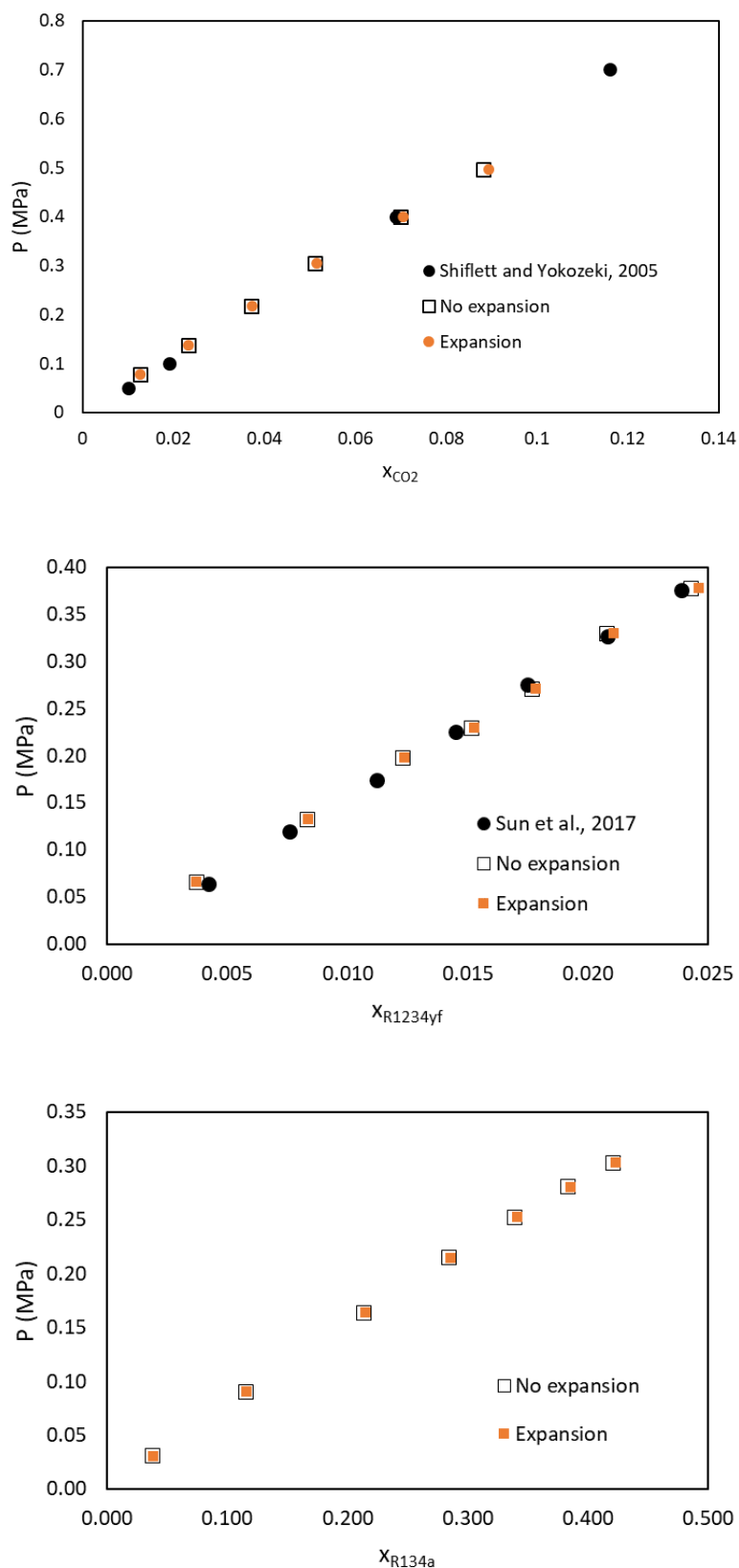


Figure 8. Assessment of the effect of volume expansion in the determination of solubility of gases in ILs: (top)  $CO_2$  in  $[C_4mim][BF_4]$  compared to [6], (middle) R1234yf in  $[C_4mim][BF_4]$  compared to [7], and (bottom) R134a in  $[C_4mim][OTf]$ .

To continue with the demonstration, the solubility of R1234yf in the same IL, [C<sub>4</sub>mim][BF<sub>4</sub>], was determined and compared to data published by Sun et al. [7]. As F-gases are not available in the work by Aki, we assumed a volumetric expansion higher and more unfavorable than any value presented in the work, a 25% expansion for a molar fraction of 0.4. The isotherm is well replicated and the difference between the values considering and neglecting volume expansion is still lower than the experimental uncertainty. However, the solubility of R1234yf is low, so the independence of results of volumetric expansion is further shown with a system studied in this thesis characterized by a high gas absorption capacity, the one formed by R134a and [C<sub>4</sub>mim][OTf], assuming again a 25% volume expansion for a refrigerant molar fraction equal to 0.4. As it can be easily observed, the results are independent of the volume expansion.

This thesis has studied the solubility of five refrigerant gases in ten ILs. The F-gases considered have been difluoromethane, 1,1,1,2-tetrafluoroethane, pentafluoroethane, 2,3,3,3-tetrafluoropropene, and trans-1,3,3,3-tetrafluoropropene (R32, R134a, R125, R1234yf, and R1234ze(E), respectively) because of their current importance in the refrigeration market. The ILs have been selected progressively as results were obtained as it will be explained in the results section. They consisted of the 1-alkyl-3-methylimidazolium cation ([C<sub>n</sub>mim]<sup>+</sup>) with the ethyl, butyl, hexyl or octyl as alkyl chain (n = 2, 4, 6, or 8) and tetrafluoroborate, trifluoromethane, bis(trifluoromethylsulfonyl)imide, thiocyanate, dicyanamide, and tricyanomethanide as anions ([BF<sub>4</sub>]<sup>-</sup>, [OTf]<sup>-</sup>, [Tf<sub>2</sub>N]<sup>-</sup>, [SCN]<sup>-</sup>, [dca]<sup>-</sup>, and [tcm]<sup>-</sup>, respectively). Table 4 summarizes the F-gas/IL systems studied in this thesis together with the number of data points obtained and the range of experimental conditions observed during the experiments (temperature, pressure, and molar fraction). This table present the imidazolium ILs with the shorter alkyl chains first. For those IL having the same cation, the order is alphabetical with respect to the short name chosen for their anions. When the solubility of several refrigerant gases is studied in the same IL, the gas solutes appear according to their increasing number of carbon atoms. Within each of these groups, refrigerants with the lowest molar masses come first. Isomers appear alphabetically. A total of 36 F-gas/IL binary systems have been determined experimentally in this thesis, 34 of them are completely new absorption pairs and the remaining 2 were studied for validation of the experimental system. Apart from the systems contained in this thesis, 8 additional systems consisting of the absorption of R32 and R125 in [C<sub>n</sub>mim][tcm] with n = 2, 4, 6, and 8 were also studied. They do not form part of the thesis because they are not published yet, but they will be published in the near future.

Table 4. F-gas/IL systems experimentally studied during the thesis.

<b>Ionic liquid</b>	<b>Gas</b>	<b>T/K</b>	<b>P/MPa</b>	<b>x/mol·mol<sup>-1</sup></b>	<b>No.</b>
[C <sub>2</sub> mim][BF <sub>4</sub> ]	R32	283.15-323.15	0.0369-0.8753	0.0132-0.5245	32
	R134a	283.15-323.15	0.0374-0.4946	0.0104-0.4266	36
	R1234yf	303.15	0.0607-0.4223	0.0038-0.0277	5
[C <sub>2</sub> mim][dca]	R32	283.15-323.15	0.0384-0.9329	0.0141-0.3505	25
	R134a	283.15-323.15	0.0447-0.4061	0.0094-0.1724	26
	R125	283.15-323.15	0.0679-0.8940	0.0024-0.1248	25
	R1234yf	283.15-323.15	0.0658-0.4277	0.0022-0.0419	25
	R1234ze(E)	283.15-323.15	0.0523-0.3438	0.0068-0.1137	25
[C <sub>2</sub> mim][OTf]	R32	298.15	0.0492-0.4404	0.0296-0.2469	6
	R134a	283.15-323.15	0.0308-0.4216	0.0185-0.4208	31
	R1234yf	283.15-323.15	0.0511-0.4825	0.0051-0.1577	25
	R1234ze(E)	283.15-323.15	0.0367-0.3292	0.0177-0.2651	26
[C <sub>2</sub> mim][SCN]	R32	283.15-313.15	0.0578-0.7396	0.0130-0.2411	22
	R134a	283.15-313.15	0.0648-0.4342	0.0071-0.1276	20
	R125	283.15-323.15	0.0638-0.7337	0.0008-0.0628	27
	R1234yf	283.15-313.15	0.0635-0.4593	0.0007-0.0366	20
	R1234ze(E)	283.15-323.15	0.0554-0.3505	0.0042-0.0783	25
[C <sub>2</sub> mim][tcm]	R134a	283.15-323.15	0.0406-0.4151	0.0133-0.2254	25
	R1234yf	283.15-323.15	0.0632-0.4449	0.0037-0.0739	25
	R1234ze(E)	283.15-323.15	0.0435-0.3837	0.0108-0.1748	25
[C <sub>2</sub> mim][Tf <sub>2</sub> N]	R1234yf	283.15-323.15	0.0499-0.4796	0.0134-0.3602	25
	R1234ze(E)	283.15-323.15	0.0321-0.3218	0.0252-0.3474	26
[C <sub>4</sub> mim][dca]	R32	283.15-323.15	0.0435-0.9008	0.0158-0.4242	25
	R134a	283.15-323.15	0.0514-0.4095	0.0122-0.2337	25
	R125	283.15-323.15	0.0670-0.7460	0.0038-0.1681	25
	R1234yf	283.15-323.15	0.0615-0.4397	0.0026-0.0717	24
	R1234ze(E)	283.15-323.15	0.0470-0.3679	0.0095-0.1922	25
[C <sub>4</sub> mim][tcm]	R134a	283.15-323.15	0.0432-0.4077	0.0159-0.2613	25
	R1234yf	283.15-323.15	0.0598-0.4365	0.0047-0.0983	24
	R1234ze(E)	283.15-323.15	0.0447-0.3633	0.0117-0.2158	25
[C <sub>6</sub> mim][tcm]	R134a	283.15-323.15	0.0401-0.4085	0.0180-0.2809	25
	R1234yf	283.15-323.15	0.0594-0.4427	0.0070-0.1260	25
	R1234ze(E)	283.15-323.15	0.0404-0.3572	0.0164-0.2394	25
[C <sub>8</sub> mim][tcm]	R134a	283.15-323.15	0.0417-0.4079	0.0167-0.3152	25
	R1234yf	283.15-323.15	0.0580-0.4402	0.0088-0.1625	25
	R1234ze(E)	283.15-323.15	0.0408-0.3546	0.0190-0.2793	25
<b>Total</b>					<b>875</b>

In all cases, the uncertainty in molar fraction was calculated from the instrumental uncertainty of the directly measured data (temperature, pressure and IL charged mass as discussed in 2.1.1.) using the quadratic expansion of errors. In this sense, the uncertainty of a variable  $y = f(x_i)$  is calculated as:

$$u(y) = \sqrt{\sum_i \left(\frac{\partial y}{\partial x_i}\right)^2 \cdot u(x_i)^2} \quad (4)$$

With the experimental system used in this thesis, accurate results with low experimental errors were measured. For systems of high solubility, the relative error derived from instrument uncertainty could be lower than 1% in some cases. For systems of low solubility, the error was higher, sometimes around 5%. For some specific systems of very low solubility, such as the absorption of R125 and R1234yf in [C<sub>2</sub>mim][SCN], the solubility at high temperatures was so low that only 4 points could be reliably determined in their isotherms instead of the minimum of 5 that were determined for all the rest of the systems.

### 2.1.3. Diffusivity calculation

The diffusion coefficients of F-gases in ILs at infinite dilution ( $D$ ) are calculated using the semi-infinite volume model [2], [3]. For experimental systems as the one used in this thesis, some assumptions are made [3]:

1. Concentration does not vary radially.
2. The volume is considered infinite in the direction orthogonal to the liquid surface, where the  $z = 0$  corresponds to the IL surface.
3. Joule-Thomson effects are negligible for the time interval used in determining the diffusion coefficient.
4. The surface concentration is at equilibrium with the gas at time higher than 2 min.

Further considerations of these assumptions were considered in [3]. In this case, the gas surface concentration  $C_{z=0}$  can be modeled using:

$$C_{z=0} = C_{z=t=0} + m \sqrt{t} \quad (5)$$

where  $C_{z=t=0}$  is the concentration of the surface at time 0 and  $m$  is a mass transfer coefficient. The surface concentration is calculated as [8]:

$$C_{z=0} = \frac{\rho_{IL}}{M_{IL} \cdot \left(\frac{k_H}{f} - 1\right)} \quad (6)$$

where  $\rho_{IL}$  and  $M_{IL}$  are the density and molar mass of the IL, respectively and  $k_H$  is the Henry's law constant (MPa) obtained from the solubility data [9], [10]:

$$k_H(T) = \lim_{x \rightarrow 0} \frac{\bar{f}(P, T)}{x} \quad (5)$$

where  $\bar{f}$  is the refrigerant fugacity (MPa) calculated using the Peng–Robinson EoS and  $x$  is the molar fraction from the solubility experiments. The surface concentration is used to calculate the initial concentration in the surface ( $C_{z=t=0}$ ) and the mass transfer coefficient ( $m$ ) from a linear fitting of the absorption data to Eq. (5). Then, these two parameters ( $C_{z=t=0}$  and  $m$ ) are used to calculate the accumulated dissolved moles per unit area ( $M_t$ ) by integrating the Fickian diffusion expression (Eq. (8)), and the diffusion coefficient is calculated from the slope of the linear fitting:

$$M_t = \int_0^t \left( D \left( \frac{\partial C}{\partial z} \right)_{z=0} \right) dt = \sqrt{D} \left( 2C_{z=t=0} \sqrt{\frac{t}{\pi}} - \frac{1}{2} mt \sqrt{\pi} \right) = \sqrt{D} \varepsilon \quad (8)$$

For properties that are obtained as the regression coefficients of a regression, the error was calculated following the rigorous least squares adjustment as explained by Wentworth [11]. If the function to be adjusted is expressed as  $F = 0$ , where  $F = w - a - bv - cv^2$ , the regression is made iteratively in a matrix form:

$$\mathbf{B} \cdot \mathbf{\Delta} = \mathbf{C} \quad (6)$$

where

$$\mathbf{B} = \begin{bmatrix} \sum \frac{F_{ai} \cdot F_{ai}}{L_i} & \sum \frac{F_{ai} \cdot F_{bi}}{L_i} & \sum \frac{F_{ai} \cdot F_{ci}}{L_i} \\ \sum \frac{F_{bi} \cdot F_{ai}}{L_i} & \sum \frac{F_{bi} \cdot F_{bi}}{L_i} & \sum \frac{F_{bi} \cdot F_{ci}}{L_i} \\ \sum \frac{F_{ci} \cdot F_{ai}}{L_i} & \sum \frac{F_{ci} \cdot F_{bi}}{L_i} & \sum \frac{F_{ci} \cdot F_{ci}}{L_i} \end{bmatrix} \quad (7)$$

$$\mathbf{C} = \begin{bmatrix} \sum \frac{F_{ai} \cdot F_i^0}{L_i} \\ \sum \frac{F_{bi} \cdot F_i^0}{L_i} \\ \sum \frac{F_{ci} \cdot F_i^0}{L_i} \end{bmatrix} \quad (8)$$

Here,  $F_i^0$  is the value of the function with the initial guessed parameters ( $a_0, b_0, c_0$ ) in each experimental point  $i$ , formed by two values  $v_i$  and  $w_i$ .  $F_{ai}$  is the derivative of the function with

respect to parameter  $a$  evaluated at point  $i$ ,  $F_{bi}$  is the derivative of the function with respect to parameter  $b$  evaluated at point  $i$ , and  $F_{ci}$  is the derivative of the function with respect to parameter  $c$  evaluated at point  $i$ .  $L_i$  is a variable of variance inherent to each experimental point that includes the uncertainty weighting:

$$L_i = (u(v_i))^2 \cdot F_{vi}^2 + (u(w_i))^2 \cdot F_{wi}^2 \quad (9)$$

Here, the derivative is made with respect to the variables instead of the parameters, so that  $F_{vi}$  and  $F_{wi}$  are the derivatives of the function with respect to  $v$  and  $w$ , respectively, in each experimental point.

The matrix  $\Delta$  is a column vector of the form:

$$\Delta = \begin{bmatrix} \Delta a \\ \Delta b \\ \Delta c \end{bmatrix} \quad (10)$$

where  $\Delta a$ ,  $\Delta b$ , and  $\Delta c$  are the difference between the initial value of the parameters and the value estimated using least squares regression. Once converged, the uncertainty of the parameters is the square root of the main diagonal of the inverse matrix of the coefficient matrix  $B$ .

Figure 9 shows the procedure to obtain the diffusion coefficient from experimental data. First, data must be registered. Using Eq. (6), the surface concentration is calculated. Then, the parameters  $C_{z=t=0}$  and  $m$  are regressed according to Eq. (5). These two parameters are used to calculate  $\varepsilon$ , and then activity coefficient is obtained from the square of the slope of the regression of data to Eq. (8).

The system presented in Figure 9 is a favorable one because the IL  $[\text{C}_2\text{mim}][\text{tcm}]$  has an acceptable absorption capacity of the F-gas R32. For systems where the solubility of the gas is lower, the results have a high uncertainty due to two main reasons. First, the uncertainty of the Henry's law constant is higher due to the quadratic propagation of errors. Second, the low gas solubility results in a much slower absorption and, therefore, less decrease in pressure during the first 20 minutes of experiments. The smaller decrease in pressure results in less data to regress and more horizontal regression lines, which have higher associated uncertainties. For that reason, throughout the thesis it can be observed that the uncertainty of the diffusion coefficient is higher in conditions of low solubility. Due to the stated reasons, the diffusivity of R125 in  $[\text{C}_2\text{mim}][\text{SCN}]$  could not be determined because pressure did not fall within the sensors sensitivity during the experiment, even when the exposure time was increased to 40 minutes. This low solubility of R125 was very positive for process design because it would not be absorbed

in the IL in an extractive distillation column, but measuring the diffusivity would require of a different method.

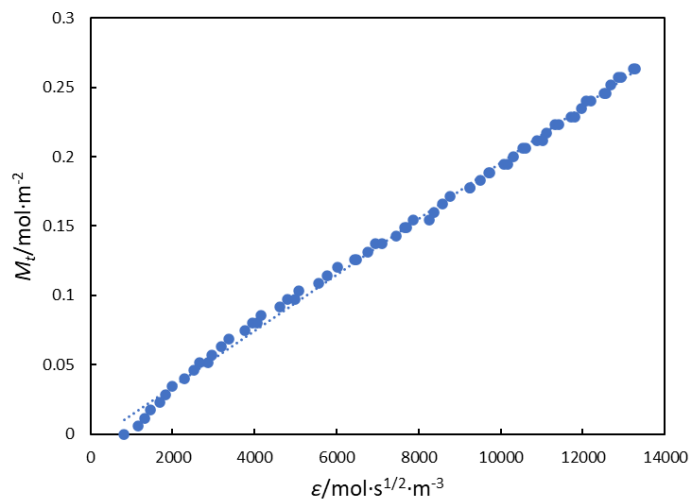
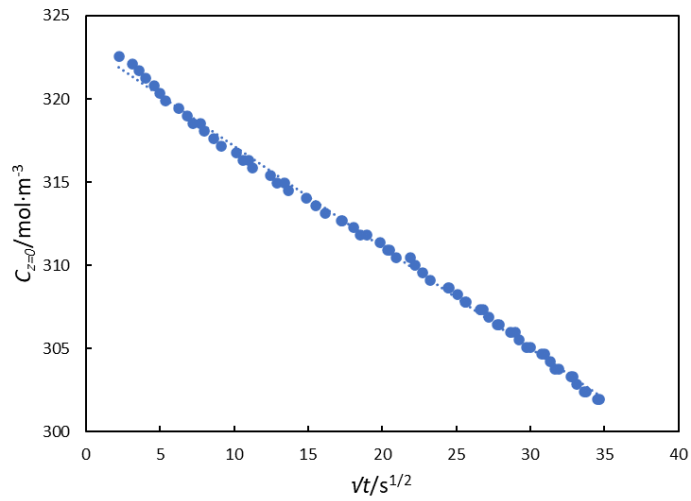
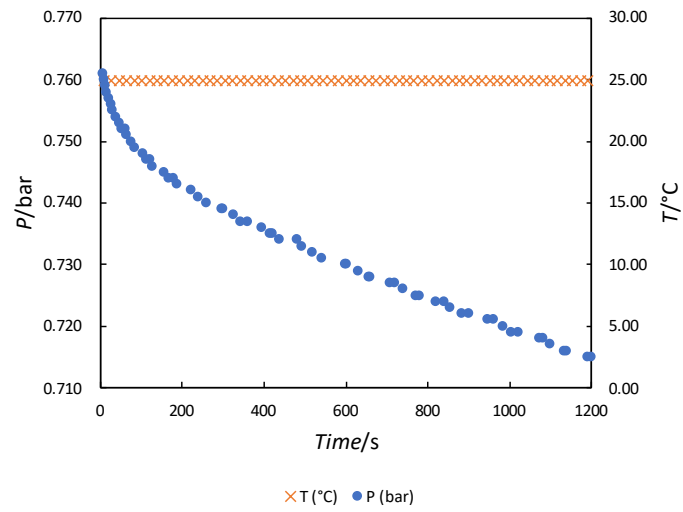


Figure 9. Determination of the diffusion coefficient at infinite dilution for the system of R32 in [C<sub>2</sub>mim][tcm] at 283.15 K: (top) data registered during the experiment, (middle) regression of Eq. (5), and (bottom) regression of Eq. (8).

## 2.2. Modeling methods

Different modeling methods have been used during the thesis. These different methods were chosen to progress from traditional approaches like EoS and activity coefficient models towards advanced computational techniques such as molecular dynamics and artificial intelligence methods that are generating high interest. Assessing how they can complement each other and increasing the knowledge of each of them to identify potential synergies to be used in future studies were also part of the objectives. The three main goals of the modeling part have been (1) the VLE data regression by means of the NRTL activity coefficient model and the soft-SAFT EoS for their use in process simulation, (2) the VLE data prediction by means of artificial neural networks (ANNs) for the fast screening of ILs and selection of those with high selectivity for the separation of interest, and (3) the understanding of the interactions between solutes and solvents by means of molecular dynamics simulations for deepening the knowledge of the absorption of F-gases in ILs and pointing towards the design of novel ILs with high selectivity based on molecular features.

### 2.2.1. Nonrandom two-liquid model

The experimental solubility data are modeled using the nonrandom two-liquid activity-coefficient model (NRTL), which has been widely used in literature and process simulation to model the VLE of fluorinated refrigerant gases in ILs. The experimental VLE can be described by:

$$y_i p \Phi_i = x_i \gamma_i p_i^S \quad (i \in \mathbb{Z} [1, N]) \quad (11)$$

where  $y_i$  and  $x_i$  are the molar fractions of the  $i$  species in the vapor and liquid phases, respectively, and  $\gamma_i$  and  $p_i^S$  are the activity coefficient and the vapor pressure, respectively.

The correction factor  $\Phi$  is calculated as

$$\Phi_i = \exp \left[ \frac{(B_i - V_i^L)(p - p_i^S)}{RT} \right] \quad (12)$$

where  $R$  is the ideal gas constant,  $B_i$  is the second virial coefficient and  $V_i^L$  is the saturated liquid molar volume.  $p_i^S$ ,  $B_i$  and  $V_i^L$  were calculated using the advanced EoS based on Helmholtz energy formulations that are implemented in CoolProp 6.4.0 [12]–[17]. Substitution of Eq. (12) in Eq. (11) leads to the following expression of the activity coefficients:



$$\gamma_1 = \frac{p}{x_1 p_1^S} \exp \left[ \frac{(B_1 - V_1^L)(p - p_1^S)}{RT} \right] \quad (13)$$

For a binary mixture, the NRTL activity coefficients are expressed according to Eq. (14):

$$\ln \gamma_1 = x_2^2 \left[ \tau_{21} \left( \frac{G_{21}}{x_1 + x_2 G_{21}} \right)^2 + \frac{\tau_{12} G_{12}}{(x_2 + x_1 G_{12})^2} \right] \quad (14)$$

where

$$G_{12} = \exp(-\alpha \tau_{12}), \quad G_{21} = \exp(-\alpha \tau_{21}) \quad (15)$$

$$\tau_{12} = \tau_{12}^0 + \frac{\tau_{12}^1}{T}, \quad \tau_{21} = \tau_{21}^0 + \frac{\tau_{21}^1}{T} \quad (16)$$

The parameter  $\alpha$  can be treated as an adjustable parameter, but it is usually assumed constant and equal to 0.2 for fluorocarbons, a convention that we followed for consistency with previous works [6]. Thus, only the temperature-dependent binary interaction parameters  $\tau_{12}$  and  $\tau_{21}$  are optimized in this work. In Eq. (13),  $\tau_{12}^1$  and  $\tau_{21}^1$  represent the excess free energy of Gibbs divided by the ideal gas constant, while  $\tau_{12}^0$  and  $\tau_{21}^0$  are used in this work to model systems with large deviations from the ideal behavior. The NRTL activity coefficients are modeled to fit the experimental activity coefficients using the average absolute relative deviation (AARD), and we also provide the deviation in pressure (AARD<sub>p</sub>).

$$AARD = \frac{100}{N} \sum_{i=1}^N \left| \frac{\gamma_{exp} - \gamma_{calc}}{\gamma_{exp}} \right| \quad (17)$$

$$AARD_p = \frac{100}{N} \sum_{i=1}^N \left| \frac{P_{exp} - P_{calc}}{P_{exp}} \right| \quad (18)$$

Table 5 summarizes the systems modeled in this thesis with their NRTL parameters and deviations. The parameters  $\tau_{12}^0$  and  $\tau_{21}^0$  are only used when the deviations using only two parameters are higher than 10%. This case happens mostly for systems where the solubility of the F-gas in the IL is very low, and the activity coefficients are far from ideal. Especially remarkable are the parameters for the two systems with the lowest F-gas solubility, R125 and R1234yf in [C<sub>2</sub>mim][SCN], for which all the NRTL parameters have very high absolute values due to their high deviations from ideal behavior.

Table 5. NRTL parameters of the systems studied in this thesis.  $\alpha$  value was set to 0.2 for every system.

<b>Ionic liquid</b>	<b>Gas</b>	$\tau_{12}^0$	$\tau_{12}^1/K$	$\tau_{21}^0$	$\tau_{21}^1/K$	<b>AARD/%</b>	<b>AARD<sub>p</sub>/%</b>
[C <sub>2</sub> mim][BF <sub>4</sub> ]	R32	0	6148.1	0	51.99	3.64	4.06
	R134a	0	4794.7	0	278.90	2.56	2.27
[C <sub>2</sub> mim][dca]	R32	0	4524.4	0	-27.31	3.10	3.27
	R134a	0	3322.5	0	198.32	1.98	2.08
	R125	2.02	2739.8	3.88	-731.37	6.56	6.96
	R1234yf	4.89	399.13	4.40	-843.39	6.32	6.70
	R1234ze(E)	0	2848.5	0	286.69	4.66	4.86
[C <sub>2</sub> mim][OTf]	R134a	0	5076.4	0	99.29	2.20	2.31
	R1234yf	6.23	414.60	4.34	-1126.1	5.97	6.35
	R1234ze(E)	0	3782.8	0	97.71	2.41	2.52
[C <sub>2</sub> mim][SCN]	R32	0	1025.6	0	-210.04	2.45	2.54
	R134a	0	2682.6	0	254.58	3.63	3.82
	R125	187.11	-51435	23.86	-6466.3	7.32	7.82
	R1234yf	179.52	-47781	21.89	-5506.8	10.92	11.59
	R1234ze(E)	4.06	372.70	2.46	-428.68	4.03	4.25
[C <sub>2</sub> mim][tcm]	R134a	0	1360.3	0	-111.37	2.17	2.29
	R1234yf	6.25	121.84	2.67	-477.81	6.57	6.95
	R1234ze(E)	0	2579.7	0	117.56	2.15	2.27
[C <sub>2</sub> mim][Tf <sub>2</sub> N]	R1234yf	0	3844.6	0	135.20	1.68	1.79
	R1234ze(E)	0	3083.8	0	-175.03	5.00	5.14
[C <sub>4</sub> mim][dca]	R32	0	5061.3	0	-29.55	1.94	2.05
	R134a	0	3760.7	0	155.39	1.75	1.84
	R125	-0.58	4144.8	3.84	-812.88	5.64	6.00
	R1234yf	10.13	-906.24	3.420	-671.41	9.77	10.21
	R1234ze(E)	0	3136.7	0	206.22	4.08	4.32
[C <sub>4</sub> mim][tcm]	R134a	0	3569.7	0	45.06	2.52	2.61
	R1234yf	8.00	-341.56	2.21	-428.00	6.43	6.75
	R1234ze(E)	0	3540.7	0	203.68	4.34	4.52
[C <sub>6</sub> mim][tcm]	R134a	0	1222.9	0	-202.90	1.34	1.40
	R1234yf	0	2521.7	0	199.54	4.52	4.78
	R1234ze(E)	0	1954.3	0	-86.48	1.48	1.56
[C <sub>8</sub> mim][tcm]	R134a	0	4618.6	0	107.52	3.75	3.91
	R1234yf	0	2535.2	0	119.92	4.50	4.75
	R1234ze(E)	0	1604.04	0	-153.53	0.86	0.90

### 2.2.2. Soft Statistical Associating Fluid Theory

Molecular-based models such as those based on the Statistical Associating Fluid Theory (SAFT) have shown their capability to describe phase equilibria of systems composed by several gases plus ILs. In this regard, the soft-SAFT EoS [18] has been employed successfully to describe the absorption of gases like CO<sub>2</sub>, CO, CH<sub>4</sub>, or SO<sub>2</sub> by physical [19] or reactive [20] methods. Hence, soft-SAFT EoS was used as it should be able to describe the behavior of the systems formed by fluorinated gases plus ILs with a good balance between accuracy and simplicity.

SAFT is a molecular-based EoS that models fluids theoretically as chains of homonuclear spheres and follows Wertheim's first-order perturbation theory, which accounts explicitly for the effects of intermolecular association and chain length (molecular shape), in addition to the usual effects of short range repulsion and dispersion forces included in traditional EoS [18]. This means that the effects of interactions and molecular shapes have specific terms that can be separated and quantified on its own. SAFT equations are written in terms of the Helmholtz energy of the system as a sum of different molecular contributions, and the derivation of this expression allows the calculation of thermodynamic properties. Soft-SAFT differs from original SAFT in that it uses a Lennard-Jones intermolecular potential to account for the interactions in the reference term of the equation instead of a model composed by hard spheres. So, the general expression for soft-SAFT is given in terms of the residual Helmholtz energy,  $A^{res}$ , defined as the total energy of the system,  $A^{total}$ , relative to that of an ideal gas,  $A^{ideal}$ , at the same temperature and density. This is expressed as a sum of contributions: a reference term,  $A^{ref}$ , a chain contribution,  $A^{chain}$  (accounts for the connectivity between segments), and an intermolecular association contribution,  $A^{assoc}$ ,

$$\frac{A^{res}}{Nk_B T} = \frac{A^{total}}{Nk_B T} - \frac{A^{ideal}}{Nk_B T} = \frac{A^{ref}}{Nk_B T} + \frac{A^{chain}}{Nk_B T} + \frac{A^{assoc}}{Nk_B T} \quad (19)$$

where  $N$  is the number of molecules,  $k_B$  is the Boltzmann constant and  $T$  is the temperature [21].

The Lennard-Jones reference term accounts in a single term for the repulsive and attractive interaction of the monomers forming the chain, allowing associating sites to be located inside the repulsion region of the potential if desired, mimicking hydrogen-bonding situations where distances between molecule centres are shorter than the diameter of the segments forming the model [18]. The monomers are characterized by two molecular parameters: the segment diameter  $\sigma$  and the dispersive energy between segments  $\varepsilon$ . The reference term is extended to mixtures using van der Waals one-fluid theory, where the residual Helmholtz free energy of the mixture is approximated by the residual Helmholtz free energy of a pure hypothetical fluid with generalized Lorentz-Berthelot mixing rules:

$$\sigma_{ij} = \eta_{ij} \left( \frac{\sigma_{ii} + \sigma_{jj}}{2} \right) \quad (20)$$

$$\varepsilon_{ij} = \xi_{ij} (\varepsilon_{ii} \varepsilon_{jj})^{\frac{1}{2}} \quad (21)$$

where  $\eta_{ij}$  and  $\xi_{ij}$  are respectively the size and energy binary adjustable parameters for the species  $i$  and  $j$ . They account for differences in size and energy of the monomers of two compounds in the mixture and are usually fitted to binary mixture data, being equal to one for ideal mixtures.

The chain term is obtained as a function of the chain length  $m_i$  and  $g_{LJ}$ , which is the radial distribution function of a fluid of Lennard-Jones spheres at density  $\rho = m_i \rho_m$ :

$$\frac{A^{chain}}{Nk_B T} = \sum_i x_i (1 - m_i) \ln g_{LJ} \quad (22)$$

The association term for  $n$  associating sites on the molecule  $i$  is

$$\frac{A^{assoc}}{Nk_B T} = \sum_i x_i \sum_a \left( \ln X_{a,i} - \frac{X_{a,i}}{2} \right) + \frac{M_i}{2} \quad (23)$$

where  $X_{a,i}$  is the fraction of component  $i$  not bonded at sites of type  $a$  and  $M_i$  is the number of association sites of type  $a$  on component  $i$ . The value of  $X_{a,i}$  comes from the solution of the following mass action equation:

$$X_{a,i} = \frac{1}{1 + \rho \sum_{j=1}^n x_j \sum_{b=1}^s X_{b,j} \Delta_{ab,ij}} \quad (24)$$

where the specific site-site function  $\Delta_{ab,ij}$  is approximated by

$$\Delta_{ab,ij} = \kappa_{ab,ij}^{HB} f_{ab,ij} \mathcal{G}_{ij}^{LJ} \quad (25)$$

which includes two additional molecular parameters related to association: the site-site bonding-volume of association  $\kappa_{ab,ij}^{HB}$ , and the site-site association energy  $\varepsilon_{ab,ij}^{HB}$ , included in the Mayer f-function  $f_{ab,ij}$ .

$$f_{ab,ij} = \exp \left( \frac{\varepsilon_{ab,ij}^{HB}}{\kappa_{ab,ij}^{HB}} \right) \quad (26)$$

For binary mixtures, cross-associating interactions are possible, and the cross-interaction values for the volume and energy of association are described by Lorentz-Berthelot combining rules using the mean arithmetic and geometric average of the pure component values, respectively [22].

$$\kappa_{ab,ij}^{HB} = \left( \frac{\kappa_{ab,ii}^{HB (1/3)} + \kappa_{ab,jj}^{HB (1/3)}}{2} \right)^3 \quad (27)$$

$$\varepsilon_{ab,ij}^{HB} = (\varepsilon_{ab,ii}^{HB} \varepsilon_{ab,jj}^{HB})^{\frac{1}{2}} \quad (28)$$

Figure 10 shows a representation of how soft-SAFT models the different compounds with an explanation of the meaning of each of the molecular parameters. In this sense, refrigerant gases are modeled as homonuclear chain-like molecules with two associating sites, A and B, of different nature to account for the dipole moment of the molecules, where only A-B interactions are allowed between refrigerant molecules as in a positive negative interaction of two dipoles [23], [24]. Following previous works using ILs, the imidazolium-based IL with  $[\text{PF}_6]^-$  as anion was modeled with only one associating site (C) to represent cation-cation interactions [25] and those with  $[\text{Tf}_2\text{N}]^-$  as anion contain three sites to model the delocalization of the anion electric charge, where one site (D) represents the anion nitrogen atom interactions with the cation and two sites of the same type represent the anion oxygen interactions (type E) [26]. The C—C interaction is allowed because this site has a dual nature, but only D—E interactions are allowed. In mixtures of refrigerants with ILs, interactions are allowed between sites of opposite or dual nature charge, i.e., only A—C, B—C, A—D, and B—E interactions are considered [23].

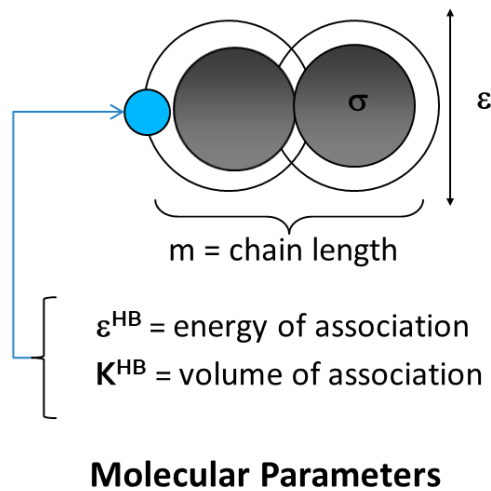


Figure 10. Representation of the molecular parameters of the soft-SAFT EoS.

During the work related to this thesis, the objective function to fit the experimental data using the soft-SAFT EoS has been the average absolute deviation (AAD) in the molar fraction as advised by the equation developers:

$$AAD = \frac{100}{N} \sum_{i=1}^N |x_{exp} - x_{calc}| \quad (29)$$

### 2.2.3. Artificial neural networks

An ANN is formed by processing units called neurons that are organized in layers. Figure 11 shows a schematic representation of a two-hidden-layer neural network. The first layer of the network is the input layer, through which the input data is fed to the ANN. The input data provides useful and relevant information, the so-called features, to the network. These features are then fed to the hidden layers, where they suffer a series of transformations. Next, the information is sent from the last hidden layer to the output layer, which provides the results [27], [28].

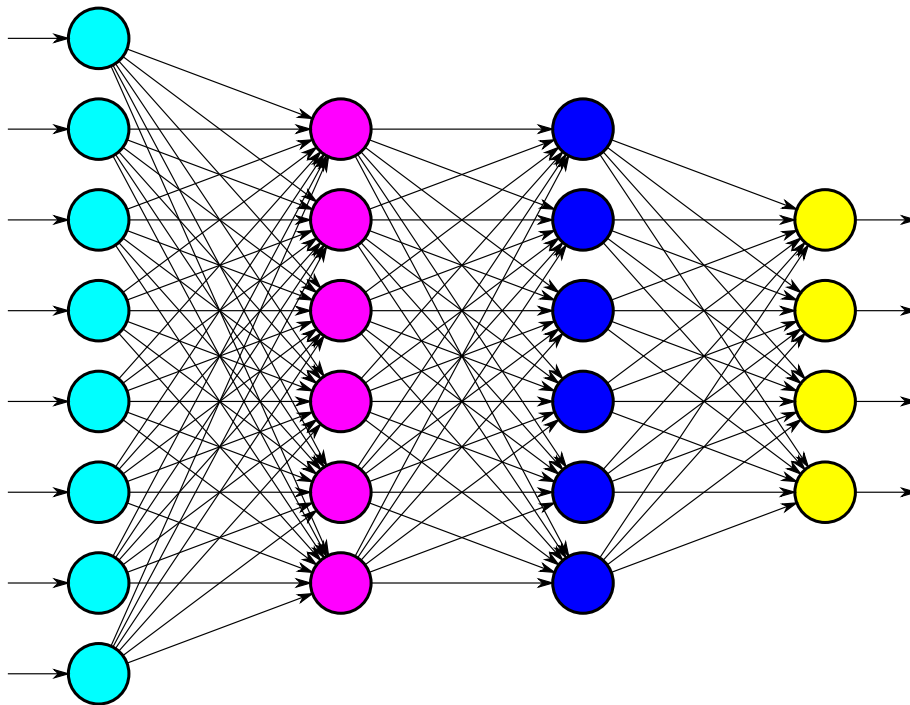


Figure 11. Structure of a two-hidden-layer neural network.

Each of the hidden layers communicates with their adjacent layers, this is, the ones that are immediately before and after. To that end, each neuron  $j$  in layer  $i$  receives  $k$  inputs ( $u_{i-1,k}$ ) from the previous layer ( $k$  is the number of neurons in the previous layer), multiplies them by their corresponding weights ( $w_{ijk}$ ) and adds the bias ( $b_{ij}$ ):

$$y_{ij} = b_{ij} + \sum_k w_{ijk} u_{i-1,k} \quad (30)$$

---

The calculated value of each neuron ( $y_{ij}$ ), normalized with a transfer function, represents the input to the neurons of the next layer. In this work, we have used the hyperbolic tangent sigmoid function (*tansig*) to normalize the neuron output [29]:

$$u_{ij} = \frac{2}{1 + \exp(-2y_{ij})} - 1 \quad (31)$$

where  $u_{ij}$  is the normalized neuron output which will be used as an input for the following layer.

After the last hidden layer, the normalized outputs are multiplied by the output layer weights and summed using the *purelin* function [29]. An extended explanation of the ANN calculation can be found in the Supplementary Material of Publication 7.

To develop the ANN, all the weights,  $w_{ijk}$ , and biases,  $b_{ij}$ , are parametrized for every neuron in every layer. Unfortunately, there is not an explicit rule that determines the number of hidden layers or the number of neurons in each layer, so they must be selected by trial and error [30]. In this work, we focused in three-hidden-layers structures containing between 1 and 10 neurons in each layer. This decision was made after checking that the structures containing only one or two hidden layers resulted in much worse performances. For each possible combination, 50 different networks were trained and only the best one was kept. The training was made using the Neural Network Toolbox of MATLAB R2021a software using the BFGS Quasi-Newton training function (*trainbfg*). The maximum number of epochs was set to 10000, but the maximum number of fails was kept at 50 to avoid overfitting, so that the final network was only trained for 1544 epochs.

For the ANN developed in this thesis, the VLE database compiled in Publication 1 was used to train the model. This database, containing data for 24 F-gases and 52 ILs, was randomly divided in training, validation, and test sets in the proportion 70/15/15. For an easier use of the tool, it was developed using as input variables easily accessible and well-known properties of the pure solvents and solutes, namely, molar mass of the refrigerant and the IL cation and anion, IL and refrigerant molar volumes, number of fluorine atoms in the IL and refrigerant, and the refrigerant critical properties, acentric factor, and vapor pressure. This way, feeding to the ANN common properties, the user can have a fast calculation of the refrigerant solubility in ILs without needing time-consuming experiments.

The average absolute relative deviation (*AARD*) was used as the performance function because minimizing the *AARD* allowed the accurate prediction of the solubility of low-sorbing gases, while it also provided low absolute errors for the prediction of highly soluble gases. However,

the root mean square error (*RMSE*) and mean absolute error (*MAE*) were also evaluated as performance indicators of the ANN.

$$\begin{aligned}
 AARD &= \frac{100}{N} \sum_i \left| \frac{x_{calc,i} - x_{exp,i}}{x_{exp,i}} \right| \\
 RMSE &= \sqrt{\frac{1}{N} \sum_i (x_{calc,i} - x_{exp,i})^2} \\
 MAE &= \frac{1}{N} \sum_i |x_{calc,i} - x_{exp,i}|
 \end{aligned} \tag{32}$$

#### 2.2.4. Molecular dynamics simulations

Molecular dynamics simulations were performed in LAMMPS software using the CL&Pol polarizable force field for the ILs [31]–[33]. The F-gases were described using available sets of parameters [34]–[36] compatible with the CL&Pol force field. In the CL&Pol force field, the explicit polarization effects are represented by Drude induced dipoles where each atomic site is represented by a positively charged Drude core and a negatively charged Drude particle with mass equal to 0.4 atomic units attached by a spring of constant  $k_D$  equal to 4184 kJ/mol to the core. The polarization procedure presented in Goloviznina et al. [31] for ILs was followed for the fixed-charge force fields of the gases, of which a short summary follows, using the polarizer and scaleLJ tools available in Pádua's group repositories [37]. The partial charges of the Drude particles were evaluated from atomic polarizabilities according to  $\alpha = q_D^2/k_D$  using the atomic polarizabilities from the work of Heid et al. [38] Heavy atoms are considered as polarizable, while the polarizability of the H atoms was merged into those of the atoms they are attached to. The Thole function [39] was used to damp short-range interactions between induced dipoles to avoid instabilities with the  $\alpha$  parameter set to 2.6. The temperature of the Drude particles was kept at 1 K to approximate the dynamics to the self-constant regime [31]. The Lennard-Jones potential from the non-polarizable CL&P force field was scaled to avoid counting twice the induction effect [31]. The cut-off radius was set to 12 Å applying the tail correction to energy and pressure and the electrostatic interactions were calculated up to long-range using the particle-particle-particle-mesh method with a relative accuracy of 10<sup>-5</sup>. The bond lengths involving H atoms were constrained using the SHAKE algorithm to allow simulations with a time step of 1 fs.

Periodic cubic boxes containing 300 IL ion pairs with 12 molecules of F-gas were prepared using Packmol [40] and fftool [41], giving initial box configurations as shown in Figure 12. Then, they



were equilibrated for 5 ns at 343 K and 1 bar using a Nosé-Hoover thermostat and barostat followed by 10 ns production runs to perform the local structure analysis. The RDF data were directly calculated in LAMMPS, while the SDF contours were calculated from the LAMMPS trajectories using TRAVIS and represented using the VMD software. Twelve systems were simulated, studying the interaction of R134a, R1234ze(E), and R1234yf with the IIs [C<sub>n</sub>mim][tcm], with n = 2, 4, 6, and 8.

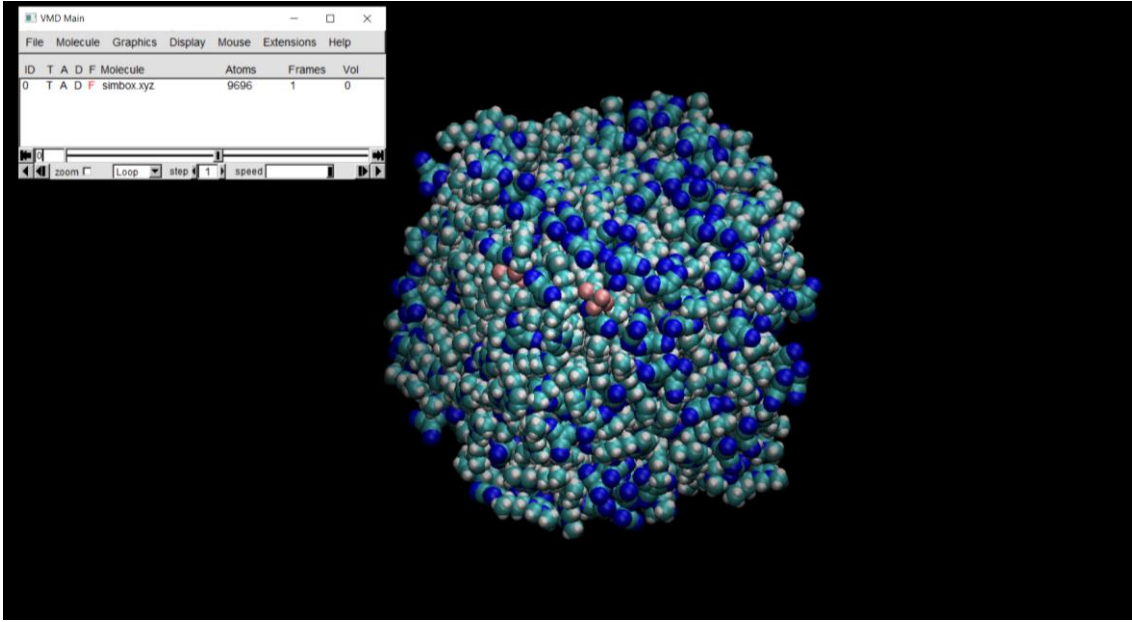


Figure 12. Example of initial periodic box for the molecular dynamics simulations.

For validation of the applied procedure, 1 molecule of F-gas placed in boxes of 100 IL ion pairs were used to obtain residual chemical potential ( $\mu^{res}$ ) following the FEP method. This calculation was done only for the mixtures with the IL [C<sub>2</sub>mim][tcm]. First, the Lennard-Jones interaction was progressively activated followed by van der Waals interactions and the electrostatic interactions resulting from the induced dipoles, thus passing from a molecule of gas present in the box but not interacting with the solvent to a state with the molecule fully interacting with the solvent. To do this progressive increase of the interaction, a coupling parameter  $\lambda$  was increased from 0 to 1 in steps of 0.05 for the Lennard-Jones interaction and 0.1 for the other two, and then decreased from 1 to 0 to confirm that the hysteresis is negligible. The chemical potential is then the difference between the initial and final states calculated as:

$$\Delta\mu = -kT \sum_{i=0}^{i-1} \ln \frac{\langle V \exp\left(-\frac{U_{\lambda_{i+1}} - U_{\lambda_i}}{kT}\right) \rangle_{\lambda_i}}{\langle V \rangle_{\lambda_i}} \quad (33)$$

The  $\mu^{res}$  is calculated subtracting the  $\Delta\mu$  for the F-gas in vacuum to the  $\Delta\mu$  for the F-gas in the IL to avoid counting the intramolecular interactions as shown in Figure 13. Then, the Henry's law constants were evaluated according to:

$$k_H = \rho_{solvent} RT \ln \left( \frac{\mu^{res}}{RT} \right) \quad (34)$$

where  $\rho_{solvent}$  is the density of the IL. For the FEP calculations, the Langevin thermostat was used to improve the stability of the simulations.

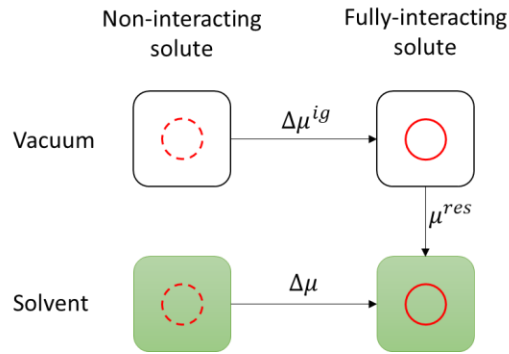


Figure 13. Scheme of the FEP calculation.

### 2.3. Process design

The two different processes studied in this thesis have been flash separators and absorption refrigeration cycles, both using NRTL as the thermodynamic method.

The binary regressed parameters were used to perform flash calculations of ternary mixtures (two F-gases and one IL) to assess the separation factor of different ILs at 5 bar and 303 K. The compositions of each constituent of the multicomponent systems are calculated using the NRTL expression for multicomponent mixtures [42]:

$$\ln \gamma_i = \frac{\sum_j \tau_{ji} G_{ji} x_j}{\sum_k G_{ki} x_k} + \sum_j \left[ \frac{x_j G_{ij}}{\sum_k G_{kj} x_k} \left( \tau_{ij} - \frac{\sum_k x_k \tau_{kj} G_{kj}}{\sum_k G_{kj} x_k} \right) \right] \quad (35)$$

Once predicted the phase equilibria of the ternary mixtures, the mass balance for an isothermal flash was solved using the Rachford-Rice equation:

$$\sum_i \frac{z_i (K_i - 1)}{1 + \beta (K_i - 1)} = 0 \quad (36)$$

$$x_i = \frac{z_i}{1 + \beta (K_i - 1)}$$

where  $z_i$  is the molar fraction of each component in the feed,  $\beta$  is the fraction of feed that is vaporized, and  $K_i$  is the equilibrium constant equal to the ratio of the vapor and liquid phase compositions,  $y_i$  and  $x_i$ . To solve the flash separator, the IL to gas mixture ratio was set to 2:3 in moles and the molar composition of the gas mixtures was set to 70:30 for R32/R125, 50:50 for R134a/R1234yf, and 80:20 for R32:R1234yf, which are the compositions of interest for each of the mixtures as explained in Publication 6.

The design of the absorption refrigeration systems (Figure 14) was based on the mass and energy balances of the condenser, evaporator, absorber, desorber, solution heat exchanger, and compressor forming the system. Some assumptions were considered:

1. The system operates at steady state.
2. The absorber and generator outlet solutions are in equilibrium
3. Heat losses, flow resistance, and pressure drops are not considered.
4. The expansion valves produce isenthalpic pressure decrements.
5. The liquid and vapor phases are in the saturated state.
6. The efficiency of the solution heat exchanger is set at 0.8.
7. Following ASHRAE considerations [43], the temperature of the refrigerant leaving the generator is the same as that of the solution inlet.
8. The compressor isentropic efficiency and compression ratio are set to 0.7 and 1.5, respectively [44].

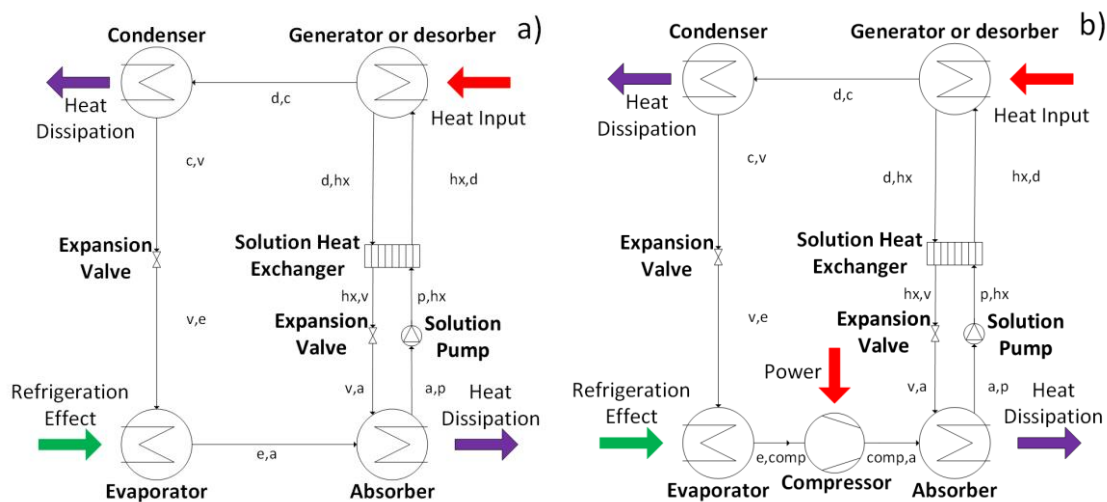


Figure 14. Schematics of (a) a Single-Effect Absorption Refrigeration System, and (b) a Compression-Assisted Absorption Refrigeration System. Figure from Publication 5 [45] of this article compendium.

The mass and energy balances (Eqs. (37) to (45)) must be solved simultaneously for each element in the system to determine the thermodynamic performance, so they were solved writing a Matlab program. The enthalpy subscripts indicate the equipment a stream comes from and goes to, e.g.,  $h_{d,c}$  represents the specific enthalpy of the stream that comes from the desorber and goes to the condenser. In addition,  $h_{(comp,a),s}$  is the ideal enthalpy of the stream leaving the compressor.

$$Q_g + m_r f h_{hx,d} = m_r h_{d,c} + m_r (f - 1) h_{d,hx} \quad (37)$$

$$Q_a + m_r f h_{a,p} = m_r h_{comp,a} + m_r (f - 1) h_{v,a} \quad (38)$$

$$Q_c - m_r h_{c,v} = m_r h_{d,c} \quad (39)$$

$$Q_e - m_r h_{v,e} = m_r h_{e,ecomp} \quad (40)$$

$$m_r f h_{p,hx} = m_r f h_{a,p} + W_p \Rightarrow h_{b,hx} = h_{a,b} \quad (41)$$

$$W_{comp} = m_r (h_{comp,a} - h_{e,a}) = \frac{m_r (h_{(comp,a),s} - h_{e,a})}{\eta_i} \quad (42)$$

$$p_a = p_e CR \quad (43)$$

$$Q_{hx} = m_r (f - 1) (h_{d,hx} - h_{hx,v}) = m_r (f - 1) (h_{hx,d} - h_{b,hx}) \quad (44)$$

$$\eta_{hx} = \frac{T_{hx,d} - T_{b,hx}}{T_{d,hx} - T_{b,hx}} \quad (45)$$

The thermodynamic properties of the refrigerants were obtained using CoolProp 6.4.0 software [12]. The specific enthalpy of the solution can be calculated from:

$$h = x_1 h_1 + x_2 h_2 + h_{ex} \quad (46)$$

where  $x_1$  and  $x_2$  are the refrigerant and absorbent molar fractions, and  $h_{ex}$  is the excess enthalpy of the mixture calculated from the NRTL parameters:

$$h_{ex} = -RT^2 \left[ x_1 \left( \frac{\partial \ln \gamma_1}{\partial T} \right)_{p,x} + x_2 \left( \frac{\partial \ln \gamma_2}{\partial T} \right)_{p,x} \right] \quad (47)$$

The enthalpies of the ILs were obtained from their heat capacities, which were fitted to a quadratic expression from experimental data as shown in the Supplementary Information of Publication 5.

---

## 2.4. References to chapter 2

- [1] M. F. Costa Gomes, "Low-pressure solubility and thermodynamics of solvation of carbon dioxide, ethane, and hydrogen in 1-hexyl-3-methylimidazolium bis(trifluoromethylsulfonyl) amide between temperatures of 283 K and 343 K," *J. Chem. Eng. Data*, vol. 52, no. 2, pp. 472–475, 2007, doi: 10.1021/je0604129.
- [2] J. Crank, *The Mathematics of Diffusion*, 2nd ed. Oxford, UK: Clarendon Press, 1975.
- [3] D. Camper, C. Becker, C. Koval, and R. D. Noble, "Diffusion and solubility measurements in room temperature ionic liquids," *Ind. Eng. Chem. Res.*, vol. 45, no. 1, pp. 445–450, 2006, doi: 10.1021/ie0506668.
- [4] S. Peper, J. M. S. Fonseca, and R. Dohrn, "High-pressure fluid-phase equilibria: Trends, recent developments, and systems investigated (2009–2012)," *Fluid Phase Equilib.*, vol. 484, pp. 126–224, 2019, doi: 10.1016/j.fluid.2018.10.007.
- [5] S. N. V. K. Aki, B. R. Mellein, E. M. Saurer, and J. F. Brennecke, "High-pressure phase behavior of carbon dioxide with imidazolium-based ionic liquids," *J. Phys. Chem. B*, vol. 108, pp. 20355–20365, 2004, doi: 10.1021/je8000443.
- [6] M. B. Shiflett and A. Yokozeki, "Solubilities and Diffusivities of Carbon Dioxide in Ionic Liquids: [bmim][PF6] and [bmim][BF4]," *Ind. Eng. Chem. Res.*, vol. 44, pp. 4453–4464, 2005, doi: 10.1021/ie058003d.
- [7] Y. Sun, Y. Zhang, X. Wang, J. M. Prausnitz, and L. Jin, "Gaseous absorption of 2,3,3,3-tetrafluoroprop-1-ene in three imidazolium-based ionic liquids," *Fluid Phase Equilib.*, vol. 450, pp. 65–74, 2017, doi: 10.1016/j.fluid.2017.07.013.
- [8] M. He, S. Peng, X. Liu, P. Pan, and Y. He, "Diffusion coefficients and Henry's constants of hydrofluorocarbons in [HMIM][Tf2N], [HMIM][TfO], and [HMIM][BF4]," *J. Chem. Thermodyn.*, vol. 112, pp. 43–51, 2017, doi: 10.1016/j.jct.2017.04.009.
- [9] M. B. Shiflett and A. Yokozeki, "Solubility and Diffusivity of Hydrofluorocarbons in Room-Temperature Ionic Liquids," *AIChE J.*, vol. 52, no. 3, pp. 1205–1219, 2006, doi: 10.1002/aic.10685.
- [10] L. F. Lepre, D. Andre, S. Denis-Quanquin, A. Gautier, A. A. H. Pádua, and M. F. Costa Gomes, "Ionic liquids can enable the recycling of fluorinated greenhouse gases," *ACS Sustain. Chem. Eng.*, vol. 7, pp. 16900–16906, 2019, doi: 10.1021/acssuschemeng.9b04214.

- 
- [11] W. E. Wentworth, "Rigorous Least Squares Adjustment: Application to some non-linear equations, I," *J. Chem. Educ.*, vol. 42, no. 2, pp. 96–103, 1965, doi: 10.1021/ed042p96.
- [12] I. H. Bell, J. Wronski, S. Quoilin, and V. Lemort, "Pure and Pseudo-pure Fluid Thermophysical Property Evaluation and the Open-Source Thermophysical Property Library CoolProp," *Ind. Eng. Chem. Res.*, vol. 53, no. 6, pp. 2498–2508, 2014, doi: 10.1021/ie4033999.
- [13] R. Tillner-Roth and A. Yokozeki, "An international standard equation of state for difluoromethane (R-32) for temperatures from the triple point at 136.34 K to 435 K and pressures up to 70 MPa," *J. Phys. Chem. Ref. Data*, vol. 26, no. 6, pp. 1273–1328, 1997, doi: 10.1063/1.556002.
- [14] R. Tillner-Roth and H. D. Baehr, "An International Standard Formulation for the Thermodynamic Properties of 1,1,1,2-Tetrafluoroethane (HFC-134a) for Temperatures from 170 K to 455 K and Pressures up to 70 MPa," *J. Phys. Chem. Ref. Data*, vol. 23, no. 5, pp. 657–729, 1994, doi: 10.1063/1.555958.
- [15] M. Richter, M. O. McLinden, and E. W. Lemmon, "Thermodynamic properties of 2,3,3,3-tetrafluoroprop-1-ene (R1234yf): Vapor pressure and  $p - \phi - T$  Measurements and an Equation of State," *J. Chem. Eng. Data*, vol. 56, no. 7, pp. 3254–3264, 2011, doi: 10.1021/je200369m.
- [16] E. W. Lemmon and R. T. Jacobsen, "A new functional form and new fitting techniques for equations of state with application to pentafluoroethane (HFC-125)," *J. Phys. Chem. Ref. Data*, vol. 34, no. 1, pp. 69–108, 2005, doi: 10.1063/1.1797813.
- [17] M. Thol and E. W. Lemmon, "Equation of State for the Thermodynamic Properties of trans-1,3,3,3-Tetrafluoropropene [R-1234ze(E)]," *Int. J. Thermophys.*, vol. 37, no. 3, pp. 1–16, 2016, doi: 10.1007/s10765-016-2040-6.
- [18] F. J. Blas and L. F. Vega, "Thermodynamic behaviour of homonuclear and heteronuclear Lennard-Jones chains with association sites from simulation and theory," *Mol. Phys.*, vol. 92, no. 1, pp. 135–150, 1997.
- [19] F. Llovel, M. B. Oliveira, J. A. P. Coutinho, and L. F. Vega, "Solubility of greenhouse and acid gases on the [C4mim][MeSO4] ionic liquid for gas separation and CO2 conversion," *Catal. Today*, vol. 255, pp. 87–96, 2015, doi: 10.1016/j.cattod.2014.12.049.

- 
- [20] G. Zarca, I. Ortiz, A. Urtiaga, and F. Llovell, "Accurate Thermodynamic Modeling of Ionic Liquids/Metal Salt Mixtures: Application to Carbon Monoxide Reactive Absorption," *AIChE J.*, vol. 63, no. 8, pp. 3532–3543, 2017, doi: 10.1002/aic.
- [21] I. I. I. Alkhatib, C. G. Albà, A. S. Darwish, F. Llovell, and L. F. Vega, "Searching for Sustainable Refrigerants by Bridging Molecular Modeling with Machine Learning," *Ind. Eng. Chem. Res.*, vol. 61, no. 21, pp. 7414–7429, 2022, doi: 10.1021/acs.iecr.2c00719.
- [22] C. G. Albà, L. F. Vega, and F. Llovell, "A consistent thermodynamic molecular model of n-hydrofluoroolefins and blends for refrigeration applications," *Int. J. Refrig.*, vol. 113, pp. 145–155, 2020, doi: 10.1016/j.ijrefrig.2020.01.008.
- [23] C. G. Albà, L. F. Vega, and F. Llovell, "Assessment on Separating Hydrofluoroolefins from Hydrofluorocarbons at the Azeotropic Mixture R513A by Using Fluorinated Ionic Liquids: A Soft-SAFT Study," *Ind. Eng. Chem. Res.*, vol. 59, no. 29, pp. 13315–13324, 2020, doi: 10.1021/acs.iecr.0c02331.
- [24] O. Vilaseca, F. Llovell, J. Yustos, R. M. Marcos, and L. F. Vega, "Phase equilibria, surface tensions and heat capacities of hydrofluorocarbons and their mixtures including the critical region," *J. Supercrit. Fluids*, vol. 55, pp. 755–768, 2010, doi: 10.1016/j.supflu.2010.10.015.
- [25] F. Llovell, O. Vilaseca, and L. F. Vega, "Thermodynamic Modeling of Imidazolium-Based Ionic Liquids with the [PF6]<sup>-</sup> Anion for Separation Purposes," *Sep. Sci. Technol.*, vol. 47, no. 2, pp. 399–410, 2012, doi: 10.1080/01496395.2011.635625.
- [26] F. Llovell, E. Valente, O. Vilaseca, and L. F. Vega, "Modeling Complex Associating Mixtures with [Cn-mim][Tf2N] Ionic Liquids: Predictions from the Soft-SAFT Equation," *J. Phys. Chem. B*, vol. 115, pp. 4387–4398, 2011.
- [27] J. Li, L. Pan, M. Suvarna, and X. Wang, "Machine learning aided supercritical water gasification for H<sub>2</sub>-rich syngas production with process optimization and catalyst screening," *Chem. Eng. J.*, vol. 426, no. March, p. 131285, 2021, doi: 10.1016/j.cej.2021.131285.
- [28] D. Serrano and D. Castelló, "Tar prediction in bubbling fluidized bed gasification through artificial neural networks," *Chem. Eng. J.*, vol. 402, no. April, 2020, doi: 10.1016/j.cej.2020.126229.

- 
- [29] A. Tarafdar, N. C. Shahi, A. Singh, and R. Sirohi, "Artificial Neural Network Modeling of Water Activity: a Low Energy Approach to Freeze Drying," *Food Bioprocess Technol.*, vol. 11, no. 1, pp. 164–171, 2018, doi: 10.1007/s11947-017-2002-4.
- [30] C. A. Faúndez, R. A. Campusano, and J. O. Valderrama, "Misleading results on the use of artificial neural networks for correlating and predicting properties of fluids. A case on the solubility of refrigerant R-32 in ionic liquids," *J. Mol. Liq.*, vol. 298, p. 112009, 2020, doi: 10.1016/j.molliq.2019.112009.
- [31] K. Goloviznina, J. N. Canongia Lopes, M. F. Costa Gomes, and A. A. H. Pádua, "Transferable, Polarizable Force Field for Ionic Liquids," *J. Chem. Theory Comput.*, vol. 15, no. 11, pp. 5858–5871, 2019, doi: 10.1021/acs.jctc.9b00689.
- [32] K. Goloviznina, Z. Gong, M. F. Costa Gomes, and A. A. H. Pádua, "Extension of the CL&Pol Polarizable Force Field to Electrolytes, Protic Ionic Liquids, and Deep Eutectic Solvents," *J. Chem. Theory Comput.*, vol. 17, no. 3, 2021, doi: 10.1021/acs.jctc.0c01002.
- [33] K. Goloviznina, Z. Gong, and A. A. H. Pádua, "The CL&Pol polarizable force field for the simulation of ionic liquids and eutectic solvents," *Wiley Interdiscip. Rev. Comput. Mol. Sci.*, no. July 2021, pp. 1–16, 2021, doi: 10.1002/wcms.1572.
- [34] R. P. S. Peguin, G. Kamath, J. J. Potoff, and S. R. P. da Rocha, "All-atom force field for the prediction of vapor - liquid equilibria and interfacial properties of HFA134a," *J. Phys. Chem. B*, vol. 113, no. 1, pp. 178–187, 2009, doi: 10.1021/jp806213w.
- [35] G. Raabe and E. J. Maginn, "A force field for 3,3,3-fluoro-1-propenes, including HFO-1234yf," *J. Phys. Chem. B*, vol. 114, no. 31, pp. 10133–10142, 2010, doi: 10.1021/jp102534z.
- [36] G. Raabe, "Molecular modeling of fluoropropene refrigerants," *J. Phys. Chem. B*, vol. 116, no. 19, pp. 5744–5751, 2012, doi: 10.1021/jp300991t.
- [37] K. Goloviznina and A. A. H. Pádua, "clandpol." <https://github.com/paduagroup/clandpol> (accessed Sep. 25, 2022).
- [38] E. Heid, A. Szabadi, and C. Schröder, "Quantum mechanical determination of atomic polarizabilities of ionic liquids," *Phys. Chem. Chem. Phys.*, vol. 20, pp. 10992–10996, 2018, doi: 10.1039/C8CP01677A.



- [39] A. Dequidt, J. Devémy, and A. A. H. Pádua, "Thermalized Drude Oscillators with the LAMMPS Molecular Dynamics Simulator," *J. Chem. Inf. Model.*, vol. 56, no. 1, pp. 260–268, 2016, doi: 10.1021/acs.jcim.5b00612.
- [40] L. Martínez, R. Andrade, E. G. Birgin, and J. M. Martínez, "PACKMOL: A Package for Building Initial Configurations for Molecular Dynamics Simulation," *J. Comput. Chem.*, vol. 30, pp. 2157–2164, 2009, doi: 10.1002/jcc.21224
- [41] A. A. H. Pádua, "fftool." <https://github.com/paduagroup/fftool> (accessed Sep. 25, 2022).
- [42] J. D. Seader, E. J. Henley, and D. K. Roper, *Separation process principles*, 3rd ed. New Jersey, USA: John Wiley & Sons, Ltd, 2010.
- [43] T. Circle, 2013 ASHRAE Handbook—Fundamentals. *American Society of Heating*, 2013.
- [44] W. Wu, T. You, H. Zhang, and X. Li, "Comparisons of different ionic liquids combined with trans-1,3,3,3-tetrafluoropropene (R1234ze(E)) as absorption working fluids," *Int. J. Refrig.*, vol. 88, pp. 45–57, 2018, doi: 10.1016/j.ijrefrig.2017.12.011.
- [45] J. M. Asensio-Delgado, S. Asensio-Delgado, G. Zarca, and A. Urtiaga, "Analysis of hybrid compression absorption refrigeration using low-GWP HFC or HFO/ionic liquid working pairs," *Int. J. Refrig.*, vol. 134, pp. 232–241, 2022, doi: 10.1016/j.ijrefrig.2021.11.013.

**Scientific**

---

**publications**

---



### 3. Scientific publications

This section collects the scientific publications that form this doctoral thesis.

**3.1. Scientific publication 1. “Absorption separation of fluorinated refrigerant gases with ionic liquids: Equilibrium, mass transport, and process design”, Salvador Asensio-Delgado, Fernando Pardo, Gabriel Zarca, Ane Urriaga, *Separation and Purification Technology*, 276 (2021) 119363**

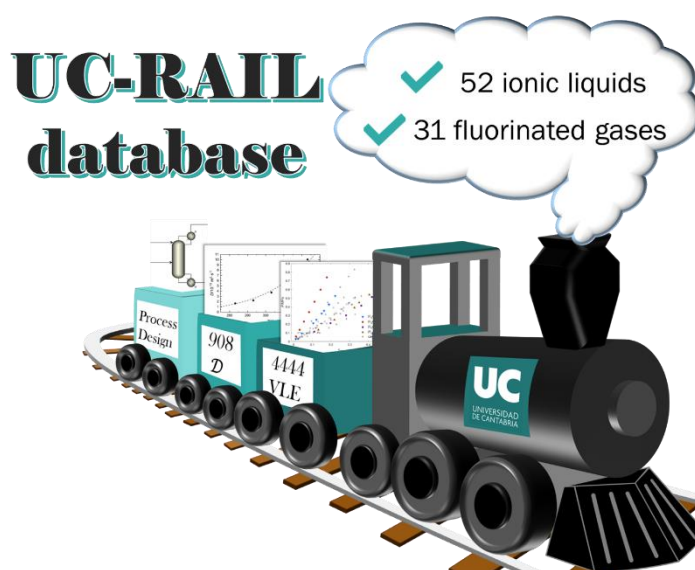


Figure 15. Graphical abstract of the article “Absorption separation of fluorinated refrigerant gases with ionic liquids: Equilibrium, mass transport, and process design”.

The objective of this article is to compile and analyze the information available in the literature relating to the absorption of F-gases in ILs. The first part addresses general information about F-gases, namely, their definition, classification used by the refrigeration sector, their GWP values in CO<sub>2</sub>-eq., and new F-gas normative. Afterwards, the article performs an extensive review of thermodynamic and mass transport properties and the process design of refrigerant separations using ILs. The data include the VLE of ILs with HFCs, HFOs, HCFOs, CFCs, HCFCs, perfluorocarbons (PFCs), and bromodifluoromethane (R22B1), as well as the VLLE of ILs with HFCs, HCFCs, and CFCs, critical fluid-liquid equilibria (CLE) of HFCs in ILs, viscosity of mixtures of ILs with HFCs and HFOs, and the diffusion coefficients of HFCs, HFOs, HCFOs, HCFCs, and R22B1 in ILs. Its general objective is to serve as a reference document for guidance in future studies on the absorption of F-gases in ILs. To that end, an extensive database called UC-RAIL (University of Cantabria Refrigerant Absorption in Ionic Liquids) has been compiled and prepared as Supplementary

Material of the review article containing all the aforementioned data. Additionally, several trends were identified such as the one seen by using the Regular Solution Theory, which showed that ILs with low molar volume provide higher selectivity for the separation of F-gas mixtures. Figure 15 shows the graphical abstract available in the online version of the article and the electronic version of the article contains the UC-RAIL database provided as Supplementary Material.



# Absorption separation of fluorinated refrigerant gases with ionic liquids: Equilibrium, mass transport, and process design

Salvador Asensio-Delgado, Fernando Pardo, Gabriel Zarca, Ane Urtiaga\*

Department of Chemical and Biomolecular Engineering, Universidad de Cantabria, Av. Los Castros 46, Santander 39005, Spain

## ARTICLE INFO

### Keywords:

Hydrofluorocarbons  
Hydrofluoroolefins  
Ionic liquids  
Solubility  
Diffusivity  
Membrane separation

## ABSTRACT

Interest in recovering and reclaiming refrigerant gases is growing as a consequence of increasing concern about the high global warming potential of some hydrofluorocarbons (HFCs). However, advanced separation processes, like extractive distillation, are required to selectively separate azeotropic and close-boiling refrigerant mixtures. In this regard, ionic liquids (ILs) arise as promising entrainers because of their favorable properties, including nonvolatility and good HFC solubility selectivity. The aim of this review is to become a reference text for the research and design of novel separation processes for mixtures of fluorinated gases based on the use of ILs. We include an extensive compilation of publications on equilibrium, mass transport, and absorption and membrane separation related to the use of ILs to selectively separate, not only the most relevant refrigerants employed nowadays, namely, HFCs, hydrofluoroolefins, and hydrochlorofluoroolefins, but also other relevant refrigerant families, such as chlorofluorocarbons, hydrochlorofluorocarbons, and perfluorocarbons. The UC-RAIL database provided as [Supplementary Information](#) compiles more than 5000 data points that are comprehensively analyzed in the review focusing on process design. Finally, we provide a set of directions that lead to the recovery of fluorinated refrigerant gases, to shift the refrigeration and air conditioning sector towards a more circular economy.

## 1. Introduction

Hydrofluorocarbons (HFCs) are synthetic compounds used primarily as refrigerant gases, but also as foam blowing agents, aerosols, and fire extinguishers [1,2]. The HFC family of refrigerants rapidly universalized after ratification of the Montreal Protocol (1987), an international agreement aimed at avoiding the depletion of stratospheric ozone by phasing out the use of chlorofluorocarbons (CFCs) and hydrochlorofluorocarbons (HCFCs) [3–5].

The implementation of HFCs in various sectors of the refrigeration and air conditioning (RAC) market led to a consequent increase in their emissions to the atmosphere. Fig. 1 presents a summary of the data collected from inventory reports published recently by the US and European Union environmental agencies, considering the main sources of HFC emissions, among which refrigeration and air conditioning applications clearly predominate [6,7].

Despite their zero ozone depletion potential (ODP), HFCs are still greenhouse gases (GHGs) of very high concern, with global warming potential (GWP) values of up to 12,400 CO<sub>2</sub> equivalents. The

contribution of HFCs to global GHG emissions was estimated as being 0.46, 0.73, and 1.1 Gt CO<sub>2</sub>-eq in 2005, 2010, and 2015, respectively [8]. In fact, while the average emissions of all other GHGs decreased in the European Union between 1990 and 2018, fluorinated gases were the only group whose emission increased, up to 77.6% [9]. Furthermore, different scenarios predict a further rise of HFCs global emissions up to more than 8 Gt CO<sub>2</sub>-eq·yr<sup>-1</sup> by 2050, if mitigation or abatement policies are not enacted [10].

The international consensus on the negative contribution of HFCs to climate change led to the promulgation of the Kigali Amendment to the Montreal Protocol (2016), a global agreement aimed at reducing emissions of fluorinated gases. The Kigali Amendment defined a schedule for phasing down the production and consumption of HFCs by 85% of the 2011–2013 average by the late 2040s [11,12]. In line with this, some regions and nations have already implemented regulations for meeting the objectives of this agreement. For example, the European F-Gas Regulation (EU 517/2014) aims to achieve a 79% reduction in the 2009–2012 HFC sales by 2030 [13], and the USA has implemented incentive credits for the use of low-GWP refrigerants according to the US

\* Corresponding author.

E-mail address: [urtiaga@unican.es](mailto:urtiaga@unican.es) (A. Urtiaga).

<https://doi.org/10.1016/j.seppur.2021.119363>

Received 26 May 2021; Received in revised form 23 July 2021; Accepted 23 July 2021

Available online 26 July 2021

1383-5866/© 2021 The Author(s).

Published by Elsevier B.V. This is an open access article under the CC BY-NC-ND license

(<http://creativecommons.org/licenses/by-nc-nd/4.0/>).

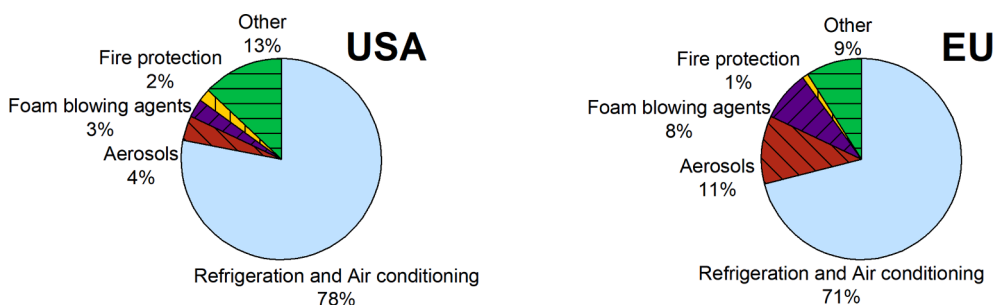


Fig. 1. Main sources of F-gases emissions in the USA and the European Union in 2018. This figure has been produced using data collected from references [6] and [7].

Environmental Protection Agency’s Significant New Alternatives Policy (SNAP). Other countries, including Australia, Norway, Switzerland, and Turkey, have also put into effect new policies that will enable full compliance with the requirements of the Kigali Amendment [8]. Most of these rules define stages of progressive restrictions that are adapted to HFC applications and GWP. Fig. 2 summarizes the prohibitions for introducing HFCs into the European market [13,14]. As can be seen, from 2020 on, movable air-conditioning equipment and foams must contain refrigerants with a maximum GWP of 150, and stationary and commercial use equipment cannot contain with a GWP of more than 2500.

These limitations on the use of HFCs have drastically affected refrigeration, air conditioning, and heat pump (RACHP) equipment, as well as foam and aerosol production, and, in the short term, new low-GWP refrigerants are being adopted to substitute the high-GWP HFC blends [15]. It is clear, therefore, that low GWP is a new environmental constraint that must be considered in the formulation of refrigerants in addition to ODP, flammability, stability, energy efficiency, and system complexity [4,16,17]. In response to this need, hydrofluoroolefins (HFOs) have emerged as a new family of refrigerants with zero ODP and

very low GWP. HFO molecules have a carbon-carbon double bond that increases their reactivity, reducing their atmospheric lifetimes and, thus, their GWP. Unfortunately, the greater reactivity also translates into slightly increased flammability [3,4]. Hydrochlorofluoroolefins (HCFOs) are also considered for the same reasons as HFOs, with the caveat of their small ODP, as the molecule contains chlorine. At present, there is no pure compound that satisfies all these constraints simultaneously, for which reason new refrigerants are actually formed by mixing HFCs with moderate GWP and HFOs, sometimes even including small proportions of hydrocarbons and CO<sub>2</sub> [18].

In addition, the new regulations establish a new paradigm in the RACHP sector by including the term “reclamation” of fluorinated refrigerants, referring to the reprocessing of a fluorinated greenhouse gas recovered during maintenance or prior to disposal, to match the equivalent performance of a virgin substance [13]. Therefore, recovering the HFC blends from end-of-life equipment and separating these into their pure components allows the reuse of those with lower environmental impacts in new, more eco-friendly blends. Furthermore, some of these HFC/HFO blends that have recently been introduced into the RAC market will be short-lived because of the staggered reduction in the

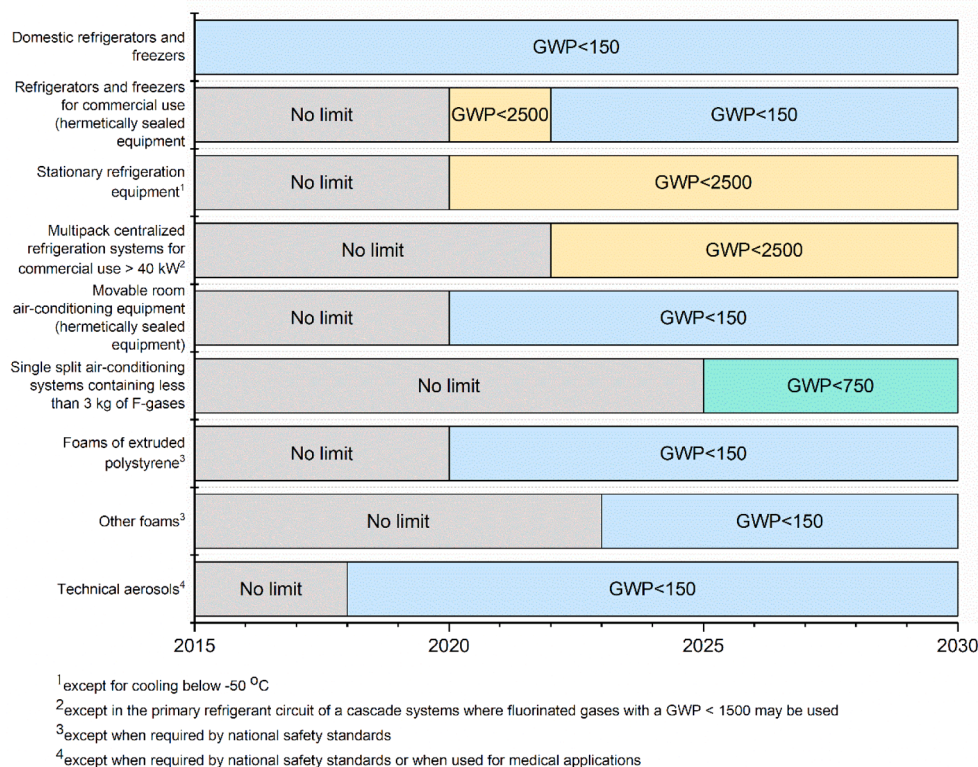


Fig. 2. Prohibitions on HFCs market in the European Union. This figure has been prepared with data collected from reference [13].

GWP limits established by some regulations. The recovery, reclamation and reuse of refrigerants is a promising approach that increases their lifetime while minimizing the amount of new HFCs introduced into the market and their subsequent release to the atmosphere, shifting the RACHP market towards a more circular economy.

However, separating most refrigerant blends using conventional gas separation processes like distillation is not straightforward, as these are close-boiling mixtures that often exhibit azeotropic behavior, as shown in Section 3 [19]. For these systems, only advanced separation processes present a real alternative for recovering refrigerant blends. In this context, absorption in liquid entrainers, adsorption on particulate materials, and membrane separation technologies emerge as candidates for separating fluorocarbon mixtures. A recent review analyzed the use of metal organic frameworks (MOFs) as adsorbent materials [20], and there is some pioneering work on the use of polymer membranes [21,22]. However, it is absorption in ionic liquids (ILs) that has attracted the most research attention. ILs are compounds comprising highly asymmetric cations and anions, and these have attracted attention in many different fields, including separation [23,24], synthesis and catalysis [25,26], energy [27], analytical applications [28], and as building blocks for advanced materials [29]. Their unique properties explain their spread among so many disciplines, including the separation and recovery of refrigerant compounds from mixtures: they present good chemical and thermal stability, they are non-flammable, have a wide liquid range, the ability to solubilize both polar and nonpolar compounds through various mechanisms, and they have negligible vapor pressure [30,31]. In the design of absorption or extractive distillation processes, the use of ILs is advantageous as there are no trace amounts of these in the distillate, the bottoms stream can be easily regenerated, and the selectivity of the separation is potentially high if the cation–anion combination is carefully selected to suit the mixture of interest [32].

Given the level of interest in developing novel separation processes for refrigerant mixtures, this review comprehensively analyzes the research carried out over the last two decades in terms of the absorption of different fluorocarbon gases (F-gases) into ILs. Knowing the vapor–liquid equilibrium (VLE) of the systems of interest is crucially important for the design of refrigerant separations using advanced absorption and extractive distillation processes. Moreover, other properties like mixture viscosity and gas diffusivity have important effects on process operation, as these can determine whether equilibrium is reached, therefore impacting the equipment sizing and the operating costs of a real separation facility. For that reason, this review includes a number of studies that consider these mass transport properties. In summary, we provide a complete compilation and analysis of equilibrium and transport data for a wide number of F-gas–IL systems containing 4444 vapor–liquid equilibrium points (193 absorption pairs formed by 52 ILs and 26 F-gases), 86 vapor–liquid–liquid equilibrium (VLLE) points (25 absorption pairs formed by 3 ILs and 16 gases), 908 diffusion coefficients (81 absorption pairs formed by 31 ILs and 14 F-gases), and 249 mixture viscosity points (4 systems). All these data are collected in the extensive UC-RAIL (Refrigerant Absorption in Ionic Liquids) database provided as [Supplementary Information](#).

The review is organized as follows: firstly, we explain the refrigerant coding system with considerations regarding gas mixture characteristics followed by a general classification of the phase behavior of refrigerant systems and their separation challenges. After that, we present and analyze F-gas–IL equilibrium and mass transport experimental data. Finally, the solubility selectivity of ILs is assessed using the Regular Solution Theory to determine the ideal characteristics an IL should have to yield efficient separations, and we review examples of recovery systems that could be used to introduce a circular economy model to the refrigerant market, including the use of ILs with polymer materials in membrane technology.

## 2. Fluorinated refrigerants

### 2.1. Pure compounds

Refrigerant fluids are designated according to the American Society of Heating, Refrigerating and Air-Conditioning Engineers (ASHRAE) [3,33]. Fig. 3 describes the ASHRAE code used to name refrigerants, in which four figures describe the molecular structure, followed by letters that distinguish between isomers. The first digit is the number of unsaturated bonds in the molecule, the second is the number of carbon atoms minus one, the third is the number of hydrogen atoms plus one, and the last digit accounts for the number of fluorine atoms. Chlorine atoms, if any, are calculated from the available carbon bonds after subtracting the number of fluorine and hydrogen atoms present in the molecule. For instance, R22 is a one-carbon molecule with two fluorine atoms, one hydrogen atom, and one chlorine atom, i.e., R22 stands for chlorodifluoromethane. In the event that the molecule has atoms of other elements, the refrigerant code indicates the element and the number of atoms at the end [34]. For example, this review includes information on bromodifluoromethane, whose refrigerant name is R22B1 (notice that the letter is just “B” instead of “Br” for its chemical symbol).

Isomer designations depend on the molecule chain length. In the case of ethane-based molecules, no letter at the end of the name refers to the most symmetrical molecule in terms of the distribution of mass around each carbon atom. For instance, 1,1,1,2-tetrafluoroethane is R134, while R134a designates 1,1,1,2-tetrafluoroethane. The isomer coding becomes more complicated for longer chain molecules, with different letters depending on the carbon segment substitution as shown in Table 1 [3]. Table S1 in the [Supplementary information](#) gives the list of gases in this review including their name, code, and chemical formula.

Other considerations include the safety classification of refrigerants. F-gases are nontoxic, so they receive the letter A. Moreover, the flame propagation behavior of refrigerants means they are nonflammable, low flammable, and mildly flammable compounds (designated as A1, A2L, and A2, respectively). As a reference point, HFO R1234ze(E), classified as A2L, requires approximately 250 000 times more energy to ignite than its equivalent hydrocarbon [3].

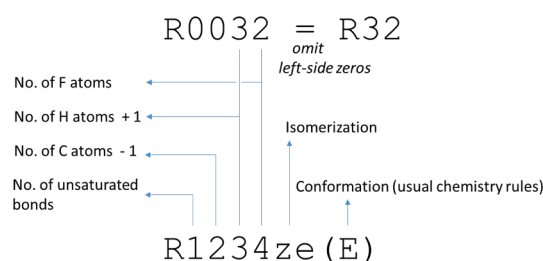


Fig. 3. ASHRAE refrigerant code system.

Table 1  
ASHRAE designations for isomer differentiation.

Segment	Letter	Segment	Letter
CCl <sub>2</sub>	a	CHCl <sub>2</sub>	n
CClF	b	CH <sub>2</sub> Cl	o
CF <sub>2</sub>	c	CHF <sub>2</sub>	p
CHCl	d	CH <sub>2</sub> F	q
CHF	e	CHClF	r
CH <sub>2</sub>	f	CH <sub>3</sub>	s
CCl <sub>3</sub>	j	C	t
CCl <sub>2</sub> F	k	CCl	x
CClF <sub>2</sub>	l	CF	y
CF <sub>3</sub>	m	CH	z



**Table 2**  
Selection of some common commercial refrigerant blends.

ASHRAE mixtures	ASHRAE safety classification	GWP	Application	Composition (wt%)						
				R32	R143a	R134a	R125	R1234yf	R1234ze(E)	
Phase-out subject mixtures	R404A	3922	medium and low temperature commercial refrigeration							
	R407C	1774	air-conditioning units heat-pumps, chillers, industrial and commercial medium temperature refrigeration	23.0	52.0	4.0	44.0			
Alternative blends	R410A	2088	air-conditioning units heat pumps; cold storage, industrial and commercial and low temperature refrigeration	50.0			50.0			
	R507A	3985	medium and low temperature commercial refrigeration		50.0		50.0			
	R447A	583	replacement for R410A in stationary air-conditioners	68.0			3.5		28.5	
	R448A	1387	non-flammable replacement for R404A in low and medium temperature commercial and transport refrigeration	26.0		21.0	26.0	20.0	7.0	
	R449A	1397	non-flammable replacement for R404A in low and medium temperature commercial and transport refrigeration	24.3		25.7	24.7	25.3		
	R452B	698	replacement for R410A in chillers	67.0			7.0	26.0		
	R454A	239	replacement for R404A in low and medium temperature commercial refrigeration	35.0				65.0		
ASHRAE mixtures	R454B	466	replacement for R410A	68.9				31.1		
	R454C	148	replacement for R404A in low and medium temperature commercial refrigeration (hermetic units)	21.5				78.5		
	R513A	631	non-flammable replacement for R134a in medium temperature commercial refrigeration and chillers			44.0				56.0

## 2.2. Refrigerant mixtures

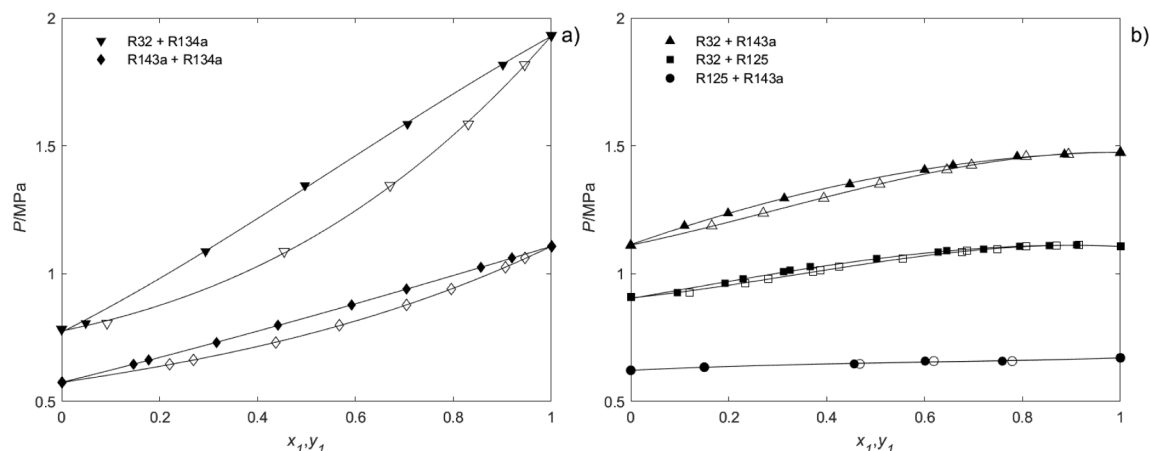
Nowadays, most refrigeration systems employ F-gas mixtures. ASHRAE classifies refrigerant blends as zeotropic mixtures, codified as the 400 series, and azeotropic mixtures, with code numbers in the 500 series. For all mixtures, the numeric code is followed by an uppercase letter denoting the different mixture compositions of the same refrigerant compounds [33]. However, for separation purposes, it should be noted that a mixture of compounds belonging to the series 400 may also present azeotropic behavior with a different composition. One example of this is R410A, an equimass mixture of R32 and R125 with an azeotropic point at 92 mol % of R32.

Table 2 is a list of some of the most important third- and fourth-generation mixtures of fluorinated refrigerants together with their ASHRAE safety classification and composition. As can be seen, binary, ternary, quaternary, and even more complicated mixtures exist currently. New mixture formulations that are being introduced into the market include HFOs (namely, R1234yf and R1234ze(E)), driven by the need to reduce the GWP of refrigerants and achieve higher refrigeration efficiencies, whereas the proportion of high-GWP HFCs, such as R125, is dropping [35]. Further insights can be extracted from Table 2, where it can be seen that when blending HFOs with the HFCs R134a and R125, the resulting mixtures have no flame propagation (A1 safety classification) but at the expense of achieving only a moderately reduced GWP. On the other hand, blending HFOs and R32 provides mixtures with a significantly lower GWP than the phased-out HFC mixtures, yet with low flammability (A2L) [4]. In addition, the presence of HFCs such as R32, R134a, and R125 in new blends highlights the importance of recovering compounds from end-of-life equipment as a way of reducing the environmental impact of this sector and advancing towards a sustainable production and consumption model in harmony with current environmental protection and GWP mitigation policies.

## 3. Mixture separation challenges

Refrigerant mixtures show different behaviors in their VLE. Usually, the RACHP sector leans towards the design of azeotropic (R500 series) and near-azeotropic blends because in refrigeration systems these mixtures behave as if they were pure fluids [19]. Although R400 series blends are near-azeotropic mixtures, they exhibit a very low temperature glide, that is, the difference in the dew and bubble points of the mixture is very narrow at a constant pressure. In addition to their pure-fluid behavior, another advantage of using azeotropic or near-azeotropic blends is that their heat transfer coefficients are higher than those of zeotropic mixtures [36]. Furthermore, in the event of leaks during the operation of a refrigeration system, zeotropic mixtures undergo compositional changes that can decrease the efficiency of the cycle [37–39]. In general, refrigeration systems with azeotropic mixtures use less energy, and have higher refrigeration capacity and a better coefficient of performance [40].

Overall, using the best refrigerants for RACHP equipment is disadvantageous for the recycling and recovery of individual gases from the mixture because their behavior is very close to that of a single fluid. In this article, we classify the phase behavior of binary refrigerant mixtures into five different types posing separation challenges of increasing difficulty. This classification does not intend to describe the global phase behavior [41], as its purpose is to provide a simplified view of the separation requirements of the refrigerant mixtures. For a clear explanation, Fig. 4 shows the pressure-molar fraction diagram of five representative binary mixtures of the third-generation HFC commercial blends that are to be phased out. Other examples that appear with the launch of HFOs in the market are also disclosed. Two lines represent each mixture, describing the pressure dependence of the liquid- and vapor-phase composition at a fixed temperature. The different behaviors are described below:



**Fig. 4.** Examples of vapor–liquid equilibrium behaviors of third-generation refrigerant mixtures. Type 1: R32 (1) + R134a (2) at 303 K (▼), Type 2: R143a (1) + R134a (2) at 293 K (◆), Type 3: R32 (1) + R143a (2) at 293 K (▲), Type 4: R32 (1) + R125 (2) at 275 K (■), and Type 5: R125 (1) + R143a (2) at 273 K (●). Filled and empty symbols are the molar liquid and vapor phase composition, respectively [42,44,45,50,55].

1. Zeotropic mixtures with a high temperature glide. These mixtures are easy to separate using conventional vapor–liquid equilibrium technologies, as the phase change significantly increases the proportion in which one of the components is found with respect to the other. Fig. 4a shows the VLE of the system R32 + R134a, and other examples of interest are the systems R32 + R1234ze(E) and R134a + R125 [42–44].
2. Zeotropic mixtures with a very low temperature glide. These close-boiling mixtures can be separated using distillation, but at the cost of an excessive number of equilibrium stages. Fig. 4a shows the VLE of R134a + R143a [45]. Other examples are the mixtures of R1234ze (E) and R1234yf with R161, which seem attractive for formulating new blends thanks to their low GWP and extremely low temperature glide [46,47].
3. Zeotropic mixtures showing the “pinch effect” or “bird’s beak”, in other words, the bubble and dew lines tend to overlap when approaching pure compound composition [48,49]. Fig. 4b presents the case of R32 + R143a, which is encountered in mixtures such as R427A [50]. Another example is the system R32 + R1234yf (e.g., the R454C mixture) [51].
4. Azeotropic mixtures at a certain composition. This is the case of the system of R32 + R125, which presents an azeotrope at around 92 mol % of R32 [52–54], and the vapor and liquid compositions are very close throughout the entire range of composition (Fig. 4b) [44].
5. Azeotropic mixtures over the entire range of composition. This behavior usually occurs in mixtures of compounds with very similar vapor pressures. Fig. 4b shows the R125 + R143a system [55]. The mixture of R134a + R1234yf is another example of an azeotrope among the fourth-generation blends. The commercialization of mixtures based on R134a and R1234yf is currently gaining importance, so it is expected that these azeotropic mixtures will be collected as residual gas from end-of-life RACHP equipment in the near future [18,51,56].

Accordingly, the recovery, reclamation and reuse of refrigerants from end-of-life RACHP equipment requires in most cases the use of advanced separation technologies to break the azeotropic behavior or enhance the separation of near-azeotropic mixtures. For this purpose, ILs are interesting solvents that present promising properties enabling the successful separations of F-gases and allowing the design of new reclamation technologies and processes.

#### 4. Experimental methods

This section summarizes the main experimental techniques

employed to determine the VLE and VLLE as well as to characterize mixture viscosity and gas diffusivity. The methods are divided into analytical and synthetic methods. Analytical methods analyze the phases by taking samples or using gravimetric methods at different pressures and temperatures. Conversely, in synthetic methods the exact total composition is known, and the change in pressure, temperature and volume are used to calculate the composition of each of the phases [57].

##### 4.1. Phase equilibrium

Two methods are predominant in the studies of F-gas solubility in ILs: the gravimetric microbalance (GM) method and the isochoric saturation (IS) method. These two methods measure the VLE and allow the calculation of the diffusion coefficients in the same measurement.

The GM method is an analytical technique based on monitoring the mass of the sample in the balance, which increases as gas dissolves into the liquid [57,58]. Initially, the IL sample is loaded into a balance with a counterweight inside a pressure vessel. Two different modes of operation can be applied. In one mode, with temperature and pressure control, gas is admitted and the exhaust valves open and close to adjust the pressure to the set point for a sufficiently long time (3 to 8 h) to ensure proper equilibrium [59]. Another option consists of a temperature controlled stepwise supply of gas where the pressure falls during the absorption process and both the mass and pressure variations are recorded in equilibrium [60]. The IL swells when absorbing gas, making buoyancy corrections necessary to determine the actual mass of gas absorbed [59].

The IS method is a synthetic pressure-decay technique based on putting known amounts of gas in contact with a mass of IL in a constant volume vessel. The system is formed of two parts: a reservoir where the gas is stored, and the equilibrium cell where the IL and the gas are in contact under continuous stirring. The temperature and pressure of both chambers are recorded at initial and equilibrium conditions to determine the amount of gas in each condition, and the difference between the two quantities is the amount of gas absorbed. Volume expansion effects should also be considered with this technique. However, the effect of IL expansion may be negligible in systems employing sufficiently large gas volumes relative to the IL sample volume.

In the synthetic isochoric method (SI), the gas reservoir is replaced by a syringe pump that allows the amount of gas absorbed to be determined from the difference between the volume injected by the pump and the final volume in the system calculated from the temperature and pressure readings [61].

There is a further synthetic method, known as the synthetic isobaric method (SIP) that allows direct readings of the volume change during

the absorption process. The pressure of the system remains constant thanks to the control of a linear actuator that adjusts the position of a piston, and its displacement represents the volume of gas dissolved [62].

Lastly, one study used an analytical method referred to as the weight method (WM). The gas enters the solvent-loaded equilibrium cell from a syringe pump and pressure decays to its equilibrium value. The solute and solvent mole fractions are determined from the mass increase of the liquid. Unlike the GM method, the WM does not use buoyancy corrections [63].

Vapor-liquid-liquid equilibrium (VLLE) methods are visual. One of the methods uses the same equipment as the synthetic isochoric method, i.e., uses a syringe pump for determining the VLLE. In this case, to determine the VLLE, the gas is added to the IL until a droplet of a very thin film of condensed refrigerant (with a negligible mass) is seen through a view cell in the apparatus at the vapor pressure of the F-gas [61].

The other technique is a visual volumetric method based only on mass and volume measurements. In the case of a non-volatile IL, two sample containers with different quantities of F-gas and IL are prepared. The VLLE is reached in each container when three separated phases form and their heights remain constant, a process that normally takes several days. The height of each phase can then be related to the phase compositions in the two containers using linear algebra [64].

#### 4.2. Viscosity of gas-ionic liquid mixtures

Determining the viscosity of gas-IL mixtures requires the sample to be in equilibrium conditions. Two methods have been used to study the viscosity of ILs as a function of the concentration of gas absorbed. One consists of letting the refrigerant and the IL reach equilibrium conditions in a vessel and then introducing the mixture into the viscometer with a constant flow pump under saturated pressure [65]. In the other method, the liquid phase continuously circulates from the equilibrium cell to the viscometer, which accelerates the mixing with the F-gas; once the pressure stops decaying the mixture is isolated in the viscometer to measure its viscosity [66].

#### 4.3. Diffusion coefficients

As previously mentioned, both the GM and IS methods allow the diffusion coefficients to be determined at the same time the VLE data are obtained. With the IS method, the semi-infinite volume model can be

applied to obtain the diffusion coefficients at infinite dilution [67,68], while the GM allows the measurement of concentration-dependent diffusion coefficients [69].

### 5. Refrigerant absorption in ionic liquids

The refrigerant gases in this review are synthetic fluorocarbons, namely, HFCs and HFOs, but we also report the data available for HCFOs, CFCs, HCFCs, and perfluorocarbons (PFCs). Most articles focus on describing the VLE of binary mixtures where one IL dissolves one refrigerant gas. In addition, a few articles study the three-phase VLLE that is achieved when the IL reaches its maximum absorption capacity, and the refrigerant gas starts to condense in a separate phase. Most articles examine the absorption of gases in imidazolium-based ILs, as this cation is the most commonly known and readily available. Other cations considered in a lesser extent are pyridinium, phosphonium, and ammonium. Table 3 lists the name of the cations and anions of the ILs found in this review, and Table S2 in the UC-RAIL database in the Supporting Information also discloses their structure. The colored matrix in Fig. 5 provides a complete overview of the studied pairs and indicates whether the information comprises many different temperatures and pressures or just a limited set of conditions. In this matrix, fluorinated gases are grouped according to their family, showing that the available information on HFCs is more extensive both in number of gases considered and total absorption pairs studied.

#### 5.1. Hydrofluorocarbons

Table 4 summarizes the experimental absorption pairs formed by an HFC and an IL found in the literature together with the experimental method, the number of data points and the range of experimental conditions ( $T$ - $P$ - $x$ ). In addition, the complete UC-RAIL database containing all the data series has been constructed and this is provided in Table S3 as Supporting Information. These tables present ILs with imidazolium cations first, followed by pyridinium and phosphonium cations, and finally ammonium cations. Within each cation group, ILs with fewer and shorter alkyl chains in the cation appear first. The order for ILs with the same cation is alphabetical with respect to the short name of their anions. When there is information on the absorption of several refrigerant gases in one IL, the gas solutes appear according to their increasing number of carbon atoms. Within each of these groups, refrigerants with the lowest molar masses come first. If several authors have studied the

**Table 3**  
List of IL cations and anions.

Cation	Cation name	Anion	Anion name
[C <sub>2</sub> mim] <sup>+</sup>	1-ethyl-3-methylimidazolium	[Ac] <sup>-</sup>	acetate
[C <sub>4</sub> mim] <sup>+</sup>	1-butyl-3-methylimidazolium	[BEI] <sup>-</sup>	bis(pentafluoroethylsulfonyl)imide
[C <sub>6</sub> mim] <sup>+</sup>	1-hexyl-3-methylimidazolium	[BF <sub>4</sub> ] <sup>-</sup>	tetrafluoroborate
[C <sub>7</sub> mim] <sup>+</sup>	1-heptyl-3-methylimidazolium	[Cl] <sup>-</sup>	chloride
[C <sub>8</sub> mim] <sup>+</sup>	3-octyl-1-methylimidazolium	[Et <sub>2</sub> PO <sub>4</sub> ] <sup>-</sup>	diethylphosphate
[(C <sub>8</sub> ) <sub>2</sub> im] <sup>+</sup>	1,3-dioctylimidazolium	[FEP] <sup>-</sup>	tris(pentafluoroethyl)trifluorophosphate
[C <sub>8</sub> H <sub>4</sub> F <sub>13</sub> mim] <sup>+</sup>	1-(3,3,4,4,5,5,6,6,7,7,8,8,8-tridecafluorooctyl)-3-methylimidazolium	[FS] <sup>-</sup>	2-(1,2,2,2-tetrafluoroethoxy)-1,1,2,2-tetrafluoroethanesulfonate
[C <sub>12</sub> mim] <sup>+</sup>	1-dodecyl-3-methylimidazolium	[HFPS] <sup>-</sup>	1,1,2,3,3,3-hexafluoropropanesulfonate
[(C <sub>1</sub> ) <sub>2</sub> C <sub>3</sub> im] <sup>+</sup>	1,2-dimethyl-3-propylimidazolium	[I] <sup>-</sup>	iodide
[C <sub>2</sub> mpy] <sup>+</sup>	1-ethyl-3-methylpyridinium	[MeSO <sub>4</sub> ] <sup>-</sup>	methylsulfate
[C <sub>3</sub> mpy] <sup>+</sup>	3-methyl-1-propylpyridinium	[OTf] <sup>-</sup>	trifluoromethanesulfonate
[C <sub>4</sub> mpy] <sup>+</sup>	1-butyl-3-methylpyridinium	[Pe] <sup>-</sup>	pentanoate
[P <sub>4441</sub> ] <sup>+</sup>	tributyl(methyl)phosphonium	[PF <sub>6</sub> ] <sup>-</sup>	hexafluorophosphate
[P <sub>4442</sub> ] <sup>+</sup>	tributyl(ethyl)phosphonium	[Pr] <sup>-</sup>	propionate
[P <sub>44414</sub> ] <sup>+</sup>	tributyl(tetradecyl)phosphonium	[PFBS] <sup>-</sup>	perfluorobutanesulfonate
[P <sub>66614</sub> ] <sup>+</sup>	triethyl(tetradecyl)phosphonium	[PPF] <sup>-</sup>	perfluoropentanoate
[m-2-HEA] <sup>+</sup>	N-methyl-2-hydroxyethylammonium	[SCN] <sup>-</sup>	thiocyanate
		[TF <sub>2</sub> N] <sup>-</sup>	bis(trifluoromethylsulfonyl)imide
		[TFES] <sup>-</sup>	1,1,2,2-tetrafluoroethanesulfonate
		[TMeM] <sup>-</sup>	tris(trifluoromethylsulfonyl)methide
		[TMPP] <sup>-</sup>	bis(2,4,4-trimethylpentyl)phosphinate
		[TPES] <sup>-</sup>	1,1,2-trifluoro-2-(perfluoroethoxy)ethanesulfonate
		[TTES] <sup>-</sup>	1,1,2-trifluoro-2-(trifluoromethoxy)ethanesulfonate

		Fluorinated refrigerant gases																									
		HFCs										HFOs/HCFO				CFCs/HCFCs				PFCs							
		R41	R32	R23	R161	R152a	R143a	R134	R134a	R125	R245fa	R236fa	R227ea	R1234yf	R1234ze(E)	R1336mzz(E)	R1336mzz(Z)	R1233zd(E)	R22	R114	R114a	R124	R124a	R14	R116	R218	R22B1
Ionic liquids	[C <sub>2</sub> mim][Ac]																										
	[C <sub>2</sub> mim][BEI]																										
	[C <sub>2</sub> mim][BF <sub>4</sub> ]																										
	[C <sub>2</sub> mim][OTf]																										
	[C <sub>2</sub> mim][PF <sub>6</sub> ]																										
	[C <sub>2</sub> mim][PFBS]																										
	[C <sub>2</sub> mim][PPP]																										
	[C <sub>2</sub> mim][SCN]																										
	[C <sub>2</sub> mim][Tf <sub>2</sub> N]																										
	[C <sub>2</sub> mim][TFES]																										
	[C <sub>2</sub> mpy][PFBS]																										
	[C <sub>3</sub> mpy][Tf <sub>2</sub> N]																										
	[C <sub>4</sub> mim][Ac]																										
	[C <sub>4</sub> mim][BF <sub>4</sub> ]																										
	[C <sub>4</sub> mim][FS]																										
	[C <sub>4</sub> mim][HFPS]																										
	[C <sub>4</sub> mim][MeSO <sub>4</sub> ]																										
	[C <sub>4</sub> mim][OTf]																										
	[C <sub>4</sub> mim][PF <sub>6</sub> ]																										
	[C <sub>4</sub> mim][SCN]																										
	[C <sub>4</sub> mim][TFES]																										
	[C <sub>4</sub> mim][TPES]																										
	[C <sub>4</sub> mim][TTES]																										
	[C <sub>4</sub> mpy][Tf <sub>2</sub> N]																										
	[C <sub>6</sub> mim][BF <sub>4</sub> ]																										
	[C <sub>6</sub> mim][Cl]																										
	[C <sub>6</sub> mim][FEP]																										
	[C <sub>6</sub> mim][OTf]																										
	[C <sub>6</sub> mim][PF <sub>6</sub> ]																										
	[C <sub>6</sub> mim][Tf <sub>2</sub> N]																										
	[C <sub>7</sub> mim][TFES]																										
	[C <sub>8</sub> mim][BEI]																										
	[C <sub>8</sub> mim][BF <sub>4</sub> ]																										
	[C <sub>8</sub> mim][I]																										
	[C <sub>8</sub> mim][PF <sub>6</sub> ]																										
[C <sub>8</sub> mim][Tf <sub>2</sub> N]																											
[C <sub>8</sub> mim][TFES]																											
[(C <sub>8</sub> ) <sub>2</sub> im][I]																											
[C <sub>8</sub> H <sub>4</sub> F <sub>13</sub> mim][BEI]																											
[C <sub>8</sub> H <sub>4</sub> F <sub>13</sub> mim][Tf <sub>2</sub> N]																											
[C <sub>12</sub> mim][TFES]																											
[(C <sub>1</sub> ) <sub>2</sub> C <sub>9</sub> im][Tf <sub>2</sub> N]																											
[(C <sub>1</sub> ) <sub>2</sub> C <sub>9</sub> im][TMeM]																											
[P <sub>4441</sub> ][MeSO <sub>4</sub> ]																											
[P <sub>4442</sub> ][Et <sub>3</sub> PO <sub>4</sub> ]																											
[P <sub>44412</sub> ][HFPS]																											
[P <sub>66614</sub> ][Cl]																											
[P <sub>66614</sub> ][Tf <sub>2</sub> N]																											
[P <sub>66614</sub> ][TMPP]																											
[P <sub>66614</sub> ][TPES]																											
[m-2-HEA][Pr]																											
[m-2-HEA][Pe]																											

Fig. 5. F-gas—IL VLE pairs studied. Green color stands for systems studied in a wide set of pressure and temperature conditions, purple color marks absorption pairs studied at a single temperature, and yellow color indicates systems studied at a single pressure. (For interpretation of the references to color in this figure legend, the reader is referred to the web version of this article.)

same absorption pair, they appear in chronological order of publication.

The data on HFCs—IL VLE range from 273.13 to 353.15 K and 0.0094 to 2.16 MPa. The most common temperature range is from 295 to 305 K, which accounts for 37% of the total volume of solubility data. The next temperature range, in order of available experimental solubility data (19%), is from 315 to 325 K, while the other temperatures ranges

distribute more or less equally. In terms of pressure, 78% of the data was obtained at less than 0.5 MPa, and 44% at less than 0.2 MPa, the main reason being that some of the refrigerant gases are highly condensable, so they liquefy at moderate pressures. Currently, there are data available for the absorption of 12 HFCs in 50 different ILs. Almost 50% of the data provides information on the solubility of R32 or R134a. The outstanding

**Table 4**  
Summary of solubility data of HFCs in ILs. Table S3 of the UC-RAIL database collects all the data.

Ionic liquid	Gas	Method*	T/K	P/MPa	$x/\text{mol}\cdot\text{mol}^{-1}$	No.	Ref.
[C <sub>2</sub> mim][Ac]	R32	GM	303.15	0.0294–0.5246	0.0117–0.2229	9	[60]
	R134a	GM	303.15	0.0259–0.5007	0.0111–0.2851	11	[60]
	R125	GM	303.15	0.0486–0.4940	0.0168–0.3067	10	[60]
[C <sub>2</sub> mim][BEI]	R32	GM	283.15–348.15	0.0096–1.0005	0.001–0.802	31	[70]
	R134	GM	283.12–348.16	0.010–0.350	0.010–0.980	31	[71]
	R134a	GM	283.10–348.10	0.0103–0.3505	0.006–0.795	32	[72]
[C <sub>2</sub> mim][BF <sub>4</sub> ]	R32	IS	283.15–323.15	0.0369–0.8753	0.0132–0.5245	32	[73]
	R134a	IS	283.15–323.15	0.0374–0.4946	0.0104–0.4266	36	[73]
	R125	WM	313.15–353.15	0.072–0.835	0.0076–0.0773	25	[74]
[C <sub>2</sub> mim][OTf]	R32	IS	273.14–348.16	0.097–0.857	0.029–0.630	27	[75]
	R32	GM	303.15	0.0402–0.5093	0.0229–0.2689	8	[60]
	R32	IS	298.15	0.0492–0.4404	0.0296–0.2469	6	[73]
	R152a	IS	273.16–348.17	0.040–0.848	0.048–0.473	24	[75]
	R134a	GM	303.15	0.0460–0.4994	0.0369–0.3518	10	[60]
	R134a	IS	283.15–323.15	0.0308–0.4216	0.0185–0.4208	31	[73]
	R125	GM	303.15	0.0245–0.6173	0.0068–0.1904	8	[60]
	R23	GM	332.90–348.00	0.0097–1.9999	0.001–0.151	17	[76]
	R32	GM	303.15	0.0283–0.5025	0.0244–0.3276	11	[60]
[C <sub>2</sub> mim][PF <sub>6</sub> ]	R23	GM	332.90–348.00	0.0097–1.9999	0.001–0.151	17	[76]
[C <sub>2</sub> mim][PFBS]	R32	GM	303.15	0.0283–0.5025	0.0244–0.3276	11	[60]
	R134a	GM	303.15	0.0155–0.4928	0.0271–0.4791	12	[60]
	R125	GM	303.15	0.0266–0.6084	0.0284–0.3835	10	[60]
[C <sub>2</sub> mim][PPFP]	R32	GM	303.15	0.0402–0.5093	0.0315–0.3299	8	[60]
	R134a	GM	303.15	0.0460–0.4994	0.0674–0.5277	10	[60]
	R125	GM	303.15	0.0245–0.6173	0.0266–0.4548	8	[60]
[C <sub>2</sub> mim][SCN]	R32	IS	283.15–313.15	0.0578–0.7396	0.0130–0.2411	22	[77]
	R134a	IS	283.15–313.15	0.0648–0.4342	0.0071–0.1276	20	[77]
[C <sub>2</sub> mim][Tf <sub>2</sub> N]	R41	SIP	288.15–308.19	0.10128–0.10763	0.03988–0.05714	5	[78]
	R32	GM	283.15–348.05	0.0096–1.0005	0.002–0.786	31	[70]
	R32	SIP	288.11–308.19	0.10203–0.10447	0.07150–0.1135	5	[78]
	R32	GM	303.15	0.0283–0.5025	0.0228–0.3225	11	[60]
	R32	IS	303.15	0.024–0.208	0.0129–0.145	9	[79]
	R23	GM	298.0–323.2	0.0265–1.9993	0.007–0.481	35	[80]
	R23	SIP	288.13–308.17	0.09897–0.10659	0.02542–0.03627	5	[78]
	R23	IS	303.15	0.100–0.302	0.0451–0.127	6	[79]
	R152a	GM	298.1–298.2	0.025–0.550	0.041–0.823	35	[81]
	R134	GM	282.9–348.1	0.0099–0.3505	0.006–0.964	31	[82]
	R134a	GM	282.7–348.1	0.0100–0.3503	0.000–0.755	32	[82]
	R134a	SI	298–348	0.028–2.160	0.0087–0.8183	47	[83]
	R134a	GM	303	0.0249–0.3499	0.0308–0.3708	6	[84]
	R134a	GM	303.15	0.0155–0.4928	0.0257–0.4420	12	[60]
	R134a	IS	303.15	0.018–0.155	0.0147–0.156	7	[79]
R125	GM	283.10–348.20	0.0100–1.0001	0.004–0.681	36	[85]	
R125	GM	303.15	0.0266–0.6084	0.0201–0.2787	10	[60]	
[C <sub>2</sub> mim][TFES]	R32	GM	298.05–298.15	0.0099–1.0016	0.006–0.477	8	[70]
[C <sub>4</sub> mim][Ac]	R32	GM	289.05–298.25	0.0099–1.0004	0.010–0.518	8	[70]
	R32	GM	298.15	0.05–1.0	0.054–0.510	7	[86]
	R125	GM	298.15	0.05–1.0	0.060–0.692	7	[86]
[C <sub>4</sub> mim][BF <sub>4</sub> ]	R32	GM	283.0–348.2	0.0097–0.9999	0.002–0.759	31	[69]
	R32	GM	298.15	0.05–1.0	0.024–0.545	7	[86]
	R125	GM	298.15	0.05–1.0	0.008–0.378	7	[86]
[C <sub>4</sub> mim][FS]	R32	GM	298.15	0.0100–1.0005	0.009–0.638	8	[70]
[C <sub>4</sub> mim][HFPS]	R32	GM	298.15	0.0095–1.0004	0.010–0.670	8	[70]
	R134a	GM	283.10–348.10	0.0099–0.3506	0.003–0.677	32	[72]
[C <sub>4</sub> mim][MeSO <sub>4</sub> ]	R32	GM	298.15	0.0099–1.0006	0.012–0.489	8	[70]
[C <sub>4</sub> mim][OTf]	R32	IS	273.13–348.24	0.098–0.902	0.033–0.683	26	[75]
	R152a	IS	273.22–348.18	0.056–0.879	0.060–0.536	24	[75]
	R41	GM	283.09–348.18	0.0097–1.9995	0.002–0.637	34	[87]
[C <sub>4</sub> mim][PF <sub>6</sub> ]	R32	GM	283.20–348.20	0.0097–0.9999	0.003–0.815	31	[69]
	R32	GM	298.15	0.05–1.0	0.039–0.574	7	[86]
	R23	GM	282.6–348.1	0.0096–2.0002	0.000–0.535	34	[69]
	R161	GM	283.06–348.16	0.0099–0.7005	0.003–0.575	30	[87]
	R152a	GM	283.1–348.2	0.0097–0.4505	0.005–0.799	28	[69]
	R143a	GM	284.9–348.2	0.0095–1.0004	0.000–0.241	36	[69]
	R134	GM	283.11–348.16	0.0101–0.3505	0.006–0.789	30	[87]
	R134a	GM	283.0–348.2	0.0097–0.3500	0.000–0.724	32	[69]
	R125	GM	283.1–348.3	0.0098–0.9998	0.000–0.660	36	[69]
	R125	GM	298.15	0.05–1.0	0.012–0.323	7	[86]
	R32	GM	298.15	0.0095–0.9992	0.004–0.379	8	[70]
	R32	GM	298.15	0.05–1.0	0.004–0.349	7	[86]
	R125	GM	298.15	0.05–1.0	0.001–0.105	7	[86]
	R32	GM	298.15	0.0097–0.9989	0.007–0.556	8	[70]
	[C <sub>4</sub> mim][TPES]	R32	GM	298.15	0.0095–0.9994	0.010–0.674	8
[C <sub>4</sub> mim][TTES]	R134a	GM	283.05–348.10	0.0102–0.3505	0.006–0.798	32	[72]
	R32	GM	298.15	0.0095–0.9992	0.010–0.650	8	[70]
R134a	GM	282.10–348.15	0.0102–0.3505	0.005–0.748	32	[72]	

(continued on next page)



Table 4 (continued)

Ionic liquid	Gas	Method*	T/K	P/MPa	x/mol·mol <sup>-1</sup>	No.	Ref.	
[C <sub>6</sub> mim][BF <sub>4</sub> ]	R32	IS	303.2–343.2	0.0406–0.0603	0.01795–0.02800	5	[88]	
	R161	IS	303.2–343.2	0.0457–0.0640	0.01662–0.02787	5	[88]	
	R152a	IS	303.2–343.2	0.0326–0.0529	0.02011–0.03196	5	[88]	
	R143a	IS	303.2–343.2	0.1076–0.1569	0.01501–0.02196	5	[88]	
	R134a	SI	298–348	0.081–1.970	0.0000–0.7071	17	[89]	
	R125	IS	303.2–343.2	0.0954–0.1294	0.01592–0.02953	5	[88]	
	R245fa	IS	303.15–343.15	0.011–0.125	0.0213–0.1358	25	[90]	
	R236fa	IS	303.15–343.15	0.039–0.263	0.0285–0.1462	25	[90]	
	R227ea	IS	303.15–343.15	0.073–0.332	0.0201–0.1150	25	[90]	
[C <sub>6</sub> mim][Cl]	R32	GM	298.15	0.05–1.0	0.021–0.410	7	[86]	
	R125	GM	298.15	0.05–1.0	0.040–0.654	7	[86]	
[C <sub>6</sub> mim][FEP]	R32	IS	293.1–343.2	0.051–0.493	0.0467–0.3493	36	[91]	
	R32	GM	298.15	0.05–1.0	0.067–0.720	7	[86]	
	R161	IS	293.0–343.2	0.036–0.548	0.0615–0.4895	36	[91]	
	R152a	IS	293.0–343.2	0.031–0.525	0.0691–0.5225	36	[91]	
	R134	GM	283.07–348.14	0.010–0.350	0.009–0.959	31	[71]	
	R125	GM	298.15	0.05–1.0	0.038–0.578	7	[86]	
[C <sub>6</sub> mim][OTf]	R32	IS	303.2–343.2	0.0522–0.0683	0.02015–0.03263	5	[88]	
	R161	IS	303.2–343.2	0.0405–0.0587	0.02466–0.03932	5	[88]	
	R152a	IS	303.2–343.2	0.0329–0.0563	0.02843–0.04113	5	[88]	
	R143a	IS	303.2–343.2	0.0646–0.0837	0.01426–0.02307	5	[88]	
	R125	IS	303.2–343.2	0.0609–0.0804	0.01393–0.02486	5	[88]	
	R134a	SI	298–348	0.081–2.057	0.0295–0.7677	21	[89]	
[C <sub>6</sub> mim][PF <sub>6</sub> ]	R32	IS	302.5–344.1	0.1144–1.2208	0.0923–0.4972	35	[92]	
[C <sub>6</sub> mim][Tf <sub>2</sub> N]	R161	IS	302.2–344.3	0.0300–0.6730	0.0305–0.3878	49	[93]	
	R152a	IS	302.3–343.4	0.0376–0.3074	0.0573–0.2528	30	[92]	
	R143a	IS	302.7–343.0	0.130–1.545	0.0434–0.3561	42	[93]	
	R134a	SI	298–348	0.042–2.075	0.0247–0.8572	29	[89]	
	R134a	SI	343.15	0.084–2.075	0.0397–0.9440	11	[66]	
	R125	IS	302.6–343.2	0.1091–1.0592	0.0530–0.3282	30	[92]	
	R245fa	IS	303.15–343.15	0.016–0.144	0.049–0.196	30	[94]	
	R236fa	IS	303.15–343.15	0.030–0.315	0.046–0.279	30	[94]	
	R227ea	IS	303.15–343.15	0.058–0.485	0.042–0.284	30	[94]	
	[C <sub>7</sub> mim][TFES]	R32	GM	298.15	0.0099–0.9980	0.008–0.592	8	[70]
	[C <sub>8</sub> mim][BEI]	R134a	GM	303–343	0.0248–0.3495	0.0191–0.4523	18	[84]
	[C <sub>8</sub> mim][I]	R32	GM	298.0–298.2	0.01007–1.00022	0.004–0.416	8	[76]
	[C <sub>8</sub> mim][Tf <sub>2</sub> N]	R134a	GM	303–343	0.0248–0.3496	0.0161–0.3976	18	[84]
	[C <sub>8</sub> mim][TFES]	R23	GM	298.1–323.2	0.0501–2.0007	0.007–0.462	37	[95]
	[(C <sub>8</sub> ) <sub>2</sub> mim][I]	R32	GM	297.9–298.0	0.01002–1.00024	0.007–0.468	8	[76]
[C <sub>8</sub> H <sub>4</sub> F <sub>13</sub> mim][BEI]	R134a	GM	303–343	0.0248–0.3499	0.0208–0.4761	18	[84]	
[C <sub>8</sub> H <sub>4</sub> F <sub>13</sub> mim][Tf <sub>2</sub> N]	R134a	GM	303–343	0.0248–0.3493	0.0210–0.4586	18	[84]	
[C <sub>12</sub> mim][TFES]	R32	GM	298.15	0.0096–1.0010	0.006–0.569	8	[70]	
[(C <sub>1</sub> ) <sub>2</sub> C <sub>3</sub> mim][Tf <sub>2</sub> N]	R32	GM	298.05–298.15	0.0099–1.0011	0.008–0.651	8	[70]	
[(C <sub>1</sub> ) <sub>2</sub> C <sub>3</sub> mim][TMeM]	R32	GM	283.15–348.15	0.0094–1.0005	0.000–0.805	31	[70]	
	R134	GM	283.03–348.14	0.010–0.350	0.006–0.963	31	[71]	
[C <sub>2</sub> mppy][PFBS]	R32	GM	303.15	0.0294–0.5246	0.0248–0.3634	9	[60]	
	R134a	GM	303.15	0.0259–0.5007	0.0330–0.4989	11	[60]	
	R125	GM	303.15	0.0486–0.4940	0.0361–0.3587	10	[60]	
[C <sub>3</sub> mppy][Tf <sub>2</sub> N]	R32	GM	283.15–348.05	0.0095–1.0004	0.003–0.782	31	[70]	
	R134	GM	283.00–348.14	0.010–0.350	0.005–0.925	31	[71]	
[C <sub>4</sub> mppy][Tf <sub>2</sub> N]	R32	GM	298.15	0.0096–1.0000	0.010–0.654	8	[70]	
[P <sub>4441</sub> ][MeSO <sub>4</sub> ]	R41	SIP	288.15–308.33	0.09953–0.10633	0.03176–0.04397	5	[96]	
	R32	SIP	288.15–308.39	0.10054–0.10356	0.08052–0.11740	5	[96]	
	R23	SIP	288.15–308.45	0.09981–0.10401	0.05197–0.09487	5	[96]	
[P <sub>4442</sub> ][Et <sub>2</sub> PO <sub>4</sub> ]	R41	SIP	288.15–308.15	0.10086–0.10228	0.03891–0.05634	5	[96]	
	R32	SIP	288.15–308.21	0.09993–0.10344	0.1306–0.1950	5	[96]	
	R23	SIP	288.15–308.27	0.09908–0.10363	0.1942–0.2512	5	[96]	
[P <sub>4441</sub> 4][HFPS]	R134a	GM	283.05–348.10	0.0099–0.3504	0.009–0.763	32	[72]	
[P <sub>6661</sub> 4][Cl]	R41	SIP	288.15–308.55	0.10081–0.10600	0.04901–0.06752	5	[96]	
	R32	SIP	288.15–308.15	0.09997–0.10589	0.1210–0.1705	5	[96]	
	R23	SIP	288.17–308.17	0.09976–0.10759	0.1704–0.2299	5	[96]	
[P <sub>6661</sub> 4][Tf <sub>2</sub> N]	R41	SIP	288.15–308.15	0.09911–0.10313	0.06653–0.09092	5	[78]	
	R32	SIP	288.15–308.23	0.10249–0.10686	0.1004–0.1330	5	[78]	
	R23	SIP	288.15–308.39	0.09704–0.10168	0.04360–0.05886	5	[78]	
[P <sub>6661</sub> 4][TMPP]	R32	IS	302.4–343.6	0.1347–1.0693	0.1030–0.4629	30	[97]	
	R161	IS	302.2–343.3	0.097–0.595	0.139–0.479	30	[98]	
	R152a	IS	302.2–343.2	0.055–0.561	0.067–0.413	30	[98]	
	R143a	IS	302.3–343.8	0.169–1.136	0.087–0.385	30	[98]	
	R134a	IS	302.9–343.6	0.164–0.801	0.199–0.488	30	[98]	
	R125	IS	302.4–343.6	0.114–0.847	0.180–0.536	25	[98]	
	R245fa	IS	292.5–333.4	0.0216–0.1750	0.0803–0.2583	30	[97]	
	R236fa	IS	292.9–333.4	0.0109–0.2945	0.0338–0.3807	30	[97]	
	R227ea	IS	292.5–333.2	0.0134–0.3211	0.1017–0.4570	25	[97]	
[P <sub>6661</sub> 4][TPES]	R134a	GM	282.80–348.10	0.0098–0.3505	0.003–0.799	32	[72]	
[m-2-HEA][Pr]	R41	SIP	288.15–308.23	0.09993–0.10449	0.01095–0.01542	5	[78]	
	R32	SIP	288.15–308.23	0.10005–0.10571	0.02435–0.03624	5	[78]	

(continued on next page)

Table 4 (continued)

Ionic liquid	Gas	Method*	T/K	P/MPa	$x/\text{mol}\cdot\text{mol}^{-1}$	No.	Ref.
[m-2-HEA][Pe]	R23	SIP	288.15–308.23	0.10005–0.10571	0.01035–0.01444	5	[78]
	R41	SIP	288.15–308.17	0.10023–0.10414	0.01678–0.02153	5	[78]
	R32	SIP	283.15–308.21	0.10268–0.10650	0.03055–0.04684	5	[78]
	R23	SIP	288.15–308.36	0.10043–0.10556	0.01549–0.02040	5	[78]

\* GM: gravimetric microbalance. IS: isochoric saturation. SI: synthetic isochoric. SIP: synthetic isobaric. WM: weight method.

research effort of Shiflett's group makes  $[\text{C}_2\text{mim}][\text{TF}_2\text{N}]$  and  $[\text{C}_4\text{mim}][\text{PF}_6]$  the most well-studied ILs, followed by  $[\text{C}_6\text{mim}][\text{TF}_2\text{N}]$  and  $[\text{P}_{66614}][\text{TMPP}]$ , studied by He's group.

The UC-RAIL database compiled in this review permits a deeper analysis of the solubility of fluorinated gases in ILs. The solubility assessment is made in terms of mole fraction,  $x$  ( $\text{mol}\cdot\text{mol}^{-1}$ ), which is the most widely used composition expression in articles evaluating the VLE. However, we also compare the solubility according to molality,  $m$  ( $\text{mol}\cdot\text{kg}^{-1}$ ), for two different reasons. Firstly, because the dependence on the molar mass of the ILs is eliminated; the wide range of IL molar masses (149–781  $\text{g}\cdot\text{mol}^{-1}$ ) can lead to misleading conclusions when comparing the F-gas solubility between ILs with a large difference. As will be shown, in some extreme cases an IL with a high molar fraction absorption capacity results in one of the lowest molality capacities. Furthermore, expressing the solubility in molality helps process design as it is a useful engineering unit to compare the mass of solvent required for a given separation.

Knowing what determines the solubility of F-gases in ILs is helpful for selecting the optimal IL for the intended application. However, many

different factors affect the solubility of F-gases, so there is no single driving mechanism that can describe the solubility of all gases in every IL. Both enthalpic and entropic effects are present in the solvation process, and it seems that the predominance of either one mechanism or the other depends on the type of absorbed gas. For example, Lepre et al. [84] showed that the absorption capacity for the polar R134a increases when the  $[\text{C}_8\text{mim}]^+$  cation is replaced by its fluorinated analogue  $[\text{C}_8\text{H}_4\text{F}_{13}\text{mim}]^+$  due to the more favorable entropy of solvation. On the other hand, for the case of apolar PFCs, they found that the higher solubility in the IL with fluorinated cation can be attributed to a more favorable enthalpy of solvation [99], the difference being related to the polarity of the solutes and the existence of polar and apolar regions in the nanosegregated domains of the ILs. These facts were further confirmed by means of molecular dynamics simulations, which showed that the polar R134a dissolves in the polar domain of  $[\text{C}_8\text{mim}][\text{TF}_2\text{N}]$ , but in the apolar domain of  $[\text{C}_8\text{H}_4\text{F}_{13}\text{mim}][\text{TF}_2\text{N}]$  due to a shielding effect observed on R134a fluorine atoms that occurs upon fluorination of the cation alkyl side chain; while apolar PFCs dissolve in the apolar domain of both ILs [84,99].

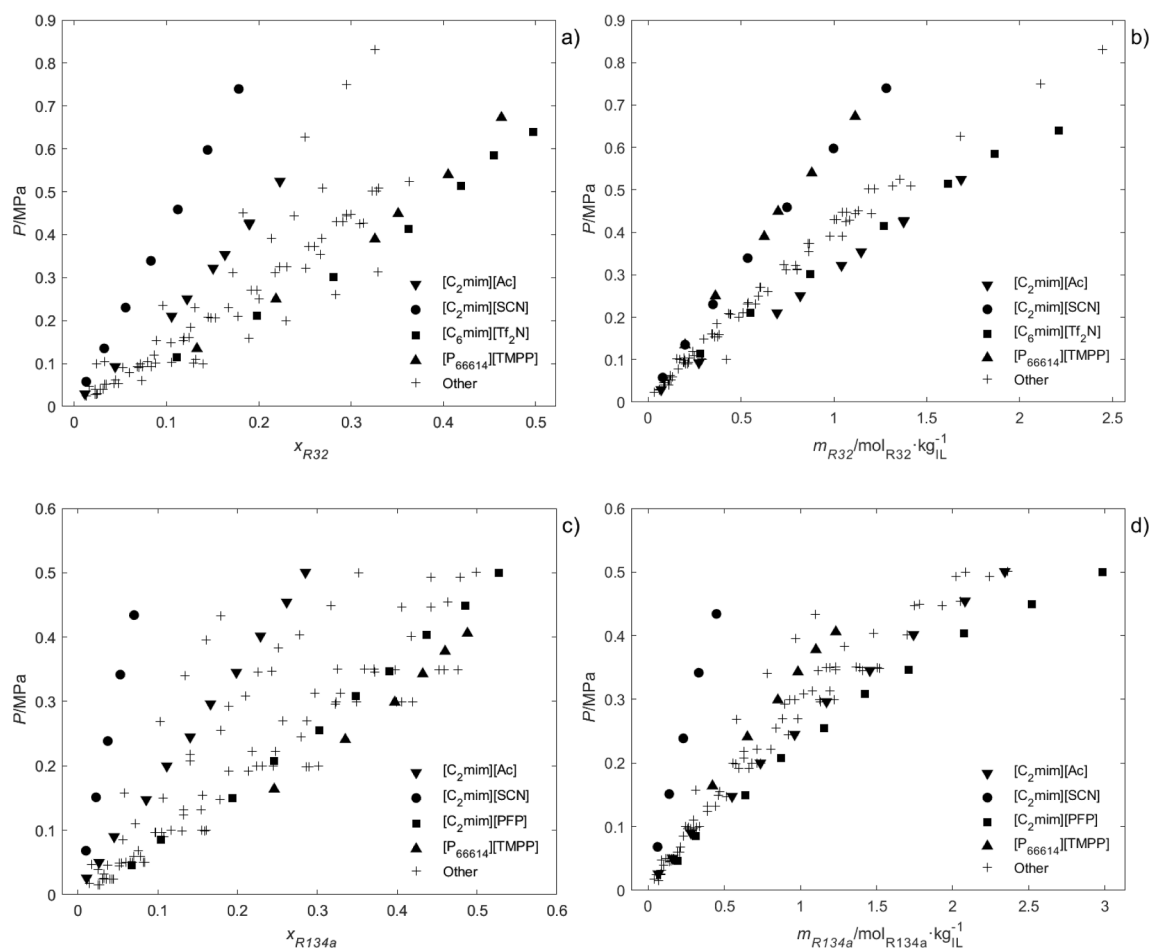


Fig. 6. Solubility of HFCs in different ILs at 303 K: R32 in (a) mole fraction,  $x/\text{mol}\cdot\text{mol}^{-1}$ , and (b) molality,  $m/\text{mol}\cdot\text{kg}^{-1}$ ; and R134a in (c) mole fraction,  $x/\text{mol}\cdot\text{mol}^{-1}$ , and (d) molality,  $m/\text{mol}\cdot\text{kg}^{-1}$ . Data from references [60,73,77–79,84,88,91,92,96–98].

Enthalpic effects relate to different gas–liquid interactions, such as ion–dipole interactions or the H-bonding capability of the compounds. The dipole moment of the solute was proposed as a possible driver for F-gas solubility in ILs, but there is not clear correlation between the electric dipole moment of a series of F-gases and their solubility in a given IL because other interactions also affect solubility [69,97]. Moreover, HFCs form clusters that increase their effective dipole moment, further hindering the analysis of the dipole effect in solubility [100–102]. On the other hand, the H-bonding interaction makes the solubility of F-gases in fluorinated anions higher than in non-fluorinated anions [60,70,72,90–92]. In that sense, Fig. 6 shows the absorption isotherms at 303 K for R32 and R134a, two HFC gases of interest in current refrigeration mixtures for which abundant datasets are available (see Table 4 and Fig. 5). For R32 the lowest solubility occurs with a non-fluorinated anion, [SCN]<sup>−</sup>, while the highest is seen with the most common fluorinated anion, [Tf<sub>2</sub>N]<sup>−</sup>. In the case of R134a, [SCN]<sup>−</sup> again presents the lowest capacity, while the highest solubility of this gas occurs with [PFPP]<sup>−</sup>, a heavily fluorinated perfluoroanion. In addition, it is worth noticing the solubility of gases in [C<sub>2</sub>mim][Ac]. Contrary to what is expected, the absorption capacity of this low-molecular-weight IL is comparably high when expressed in molality (Fig. 6b and 6d), even analogous to that of [C<sub>6</sub>mim][Tf<sub>2</sub>N]. A possibility for the high absorption capacity of [C<sub>2</sub>mim][Ac] is that the two resonant oxygen atoms of acetate act as electron donors in forming H-bonds (as happens in its mixtures with water [103]), making the anion highly polar, but this hypothesis needs to be confirmed.

Entropic effects relate to the degree of order achieved in the solvation process and the free volume available in the IL. In general, the solvation entropy determines the absorption capacity in such a way that the gas solubility is higher for less negative values of the solvation entropy [60,73,77,84]. The available free volume therefore plays a key role in determining the solubility of F-gases in ILs [104,105]. For this reason, solubility (in the mole fraction basis) increases with increasing IL molar volume [106]. Additionally, fluorinated ILs have higher free volumes because of the greater rigidity of the fluorinated chains [84]. The effect of IL size and degree of fluorination becomes clear in Fig. 6a and 6c. [C<sub>2</sub>mim][SCN], a small IL with no fluorine atoms, presents the lowest R32 and R134a solubility values, while the large [P<sub>66614</sub>][TMPP] and the very fluorinated [C<sub>6</sub>mim][Tf<sub>2</sub>N] display high solubility values for these two gases.

However, the solubility range of ILs narrows when expressed in molality basis, as previously noted by Carvalho et al. [107] for the case of CO<sub>2</sub> solubility in ILs, and leads to a fairer comparison between solvents. For example, some studies support the idea that phosphonium-ILs have a higher absorption capability than imidazolium-ILs. Nevertheless, although [P<sub>66614</sub>][TMPP] seems to have a high R32 absorption capacity in mole fraction (Fig. 6a), it actually exhibits the lowest capacity per unit mass of solvent, similar to that of [C<sub>2</sub>mim][SCN] (Fig. 6b). A similar, yet

less-pronounced decrease in the [P<sub>66614</sub>][TMPP] capacity is observed for the absorption of R134a when expressed in mass units (Fig. 6c and d).

For a fixed cation, the solubility of polar F-gases is reported to scale with increasing anion size and charge density, as larger anions can have a more dispersed negative charge [89]. This effect is depicted in Fig. 7a, which shows that the solubility of R32 at 303 K increases in the order [C<sub>2</sub>mim][BF<sub>4</sub>] < [C<sub>2</sub>mim][OTf] < [C<sub>2</sub>mim][Tf<sub>2</sub>N]. However, Fig. 7b shows that, when represented in molality, the three ILs have a very similar absorption capacity. In this manner, while Fig. 6 shows that IL fluorination has an important effect on the F-gas solubility, Fig. 7 suggests that the size of similarly fluorinated anions has little effect on the solubility of a given F-gas.

An interesting analysis of the solubility of HFCs in ILs comes from the assessment of the Henry's law constants. These constants relate the fugacity of gases with the absorbed molar fraction at low concentrations:

$$k_H(T) = \lim_{x \rightarrow 0} \frac{f(p, T)}{x} \quad (1)$$

where  $f$  is the refrigerant fugacity and  $x$  is the absorbed gas molar fraction. To unify the criteria, we have recalculated Henry's law constants from the experimental data compiled from the literature in the UC-RAIL database. To this end, refrigerant fugacity is calculated using the Peng-Robinson equation of state (EoS) and Eq. (1) is simplified to obtain the Henry's law constants as the first derivative of a second-order polynomial fit evaluated at zero composition [69,73,77,84]:

$$k_H \approx \left( \frac{df}{dx} \right)_{x=0} \quad (2)$$

Considering that the critical temperature of pure compounds is a property closely related to the intermolecular potential well depth, and that the Henry's law constants are directly related to the excess chemical potential of a solute at infinite dilution, Shiflett and Yokozeki [87] postulated that, for a given solvent, the Henry's law constants must be related to the solute critical temperature. They demonstrated that  $\ln k_H$  is linearly correlated to the critical temperature of pure HFCs, which exhibit different slopes for the methane and ethane series of HFCs. In other words, the solubility increases as the well depth (or the attractive interaction) becomes greater [87]. In 2006, the authors speculated whether the relationship holds for other compounds in a given IL [87], a hypothesis that can now be tested given the amount of new experimental data. In this review, we extend this analysis to other ILs, to propene fluorinated derivatives, as well as the methane series of HCFCs and halons (R22 and R22B1). Fig. 8 shows the results for two different ILs, [C<sub>4</sub>mim][PF<sub>6</sub>] and [C<sub>6</sub>mim][Tf<sub>2</sub>N], demonstrating that the relationship holds when extending the mentioned systems, and that varying slopes are obtained for different families of compounds.

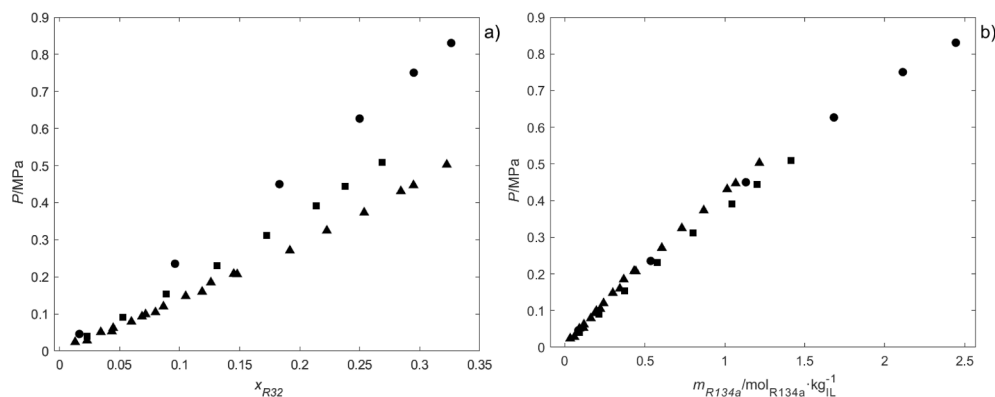
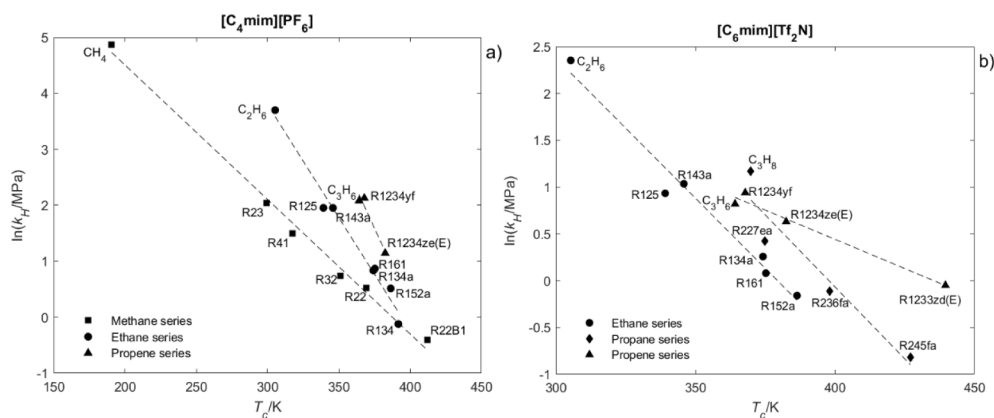


Fig. 7. Solubility of R32 at 303 K in [C<sub>2</sub>mim][BF<sub>4</sub>] (●), [C<sub>2</sub>mim][OTf] (■), and [C<sub>2</sub>mim][Tf<sub>2</sub>N] (▲) in (a) mole fraction,  $x/\text{mol}\cdot\text{mol}^{-1}$ , and (b) molality,  $m/\text{mol}\cdot\text{kg}^{-1}$ . Data from references [60,73].





**Fig. 8.** Correlation between solute critical temperature and their Henry's law constants for absorption of fluorinated refrigerants at 323 K in (a)  $[C_4mim][PF_6]$  and (b)  $[C_6mim][Tf_2N]$ . The Henry's law constants for F-gases are calculated fitting data from references [69,81,87,89,92–94,108–112] to Eq. (2), and the Henry's law constants for hydrocarbons come from various references [113–116].

**Table 5**

Summary of solubility data of HFOs and HCFOs in ILs. Table S4 of the UC-RAIL database collects all the data.

Ionic liquid	Gas	Method*	T/K	P/MPa	x/mol·mol <sup>-1</sup>	No.	Ref.
$[C_2mim][Ac]$	R1234yf	IS	283.15–343.15	0.073–0.568	0.003–0.060	49	[121]
$[C_2mim][BF_4]$	R1234yf	IS	283.15–343.15	0.0592–0.4399	0.0019–0.0398	49	[118]
	R1234yf	IS	303.15	0.0607–0.4223	0.0038–0.0277	5	[73]
	R1234ze(E)	IS	283.15–343.15	0.050–0.438	0.0063–0.1814	49	[119]
$[C_2mim][OTf]$	R1234yf	IS	283.15–323.15	0.0511–0.4825	0.0051–0.1577	25	[73]
$[C_2mim][SCN]$	R1234yf	IS	283.15–313.15	0.0635–0.4593	0.0007–0.0366	20	[77]
$[C_2mim][Tf_2N]$	R1234yf	IS	283.15–323.15	0.0499–0.4796	0.0134–0.3602	25	[73]
	R1336mzz(E)	N.A.	293.1–353.8	0.194–0.800	0.093–0.173	11	[123]
	R1336mzz(Z)	N.A.	293.1–353.8	0.05–0.41	0.280–0.589	12	[123]
$[C_4mim][Ac]$	R1234yf	IS	283.15–343.15	0.078–0.811	0.007–0.133	66	[121]
$[C_4mim][PF_6]$	R1234yf	IS	283.15–343.15	0.0460–0.4339	0.0063–0.0954	49	[110]
	R1234ze(E)	IS	283.15–343.15	0.0854–0.4347	0.0289–0.2969	42	[108]
$[C_6mim][BF_4]$	R1234yf	IS	303.2–343.2	0.1109–0.1587	0.01530–0.02515	5	[88]
	R1234yf	IS	283.15–343.15	0.0548–0.4384	0.0063–0.1388	49	[118]
	R1234yf	IS	303.20–353.23	0.109–0.660	0.012–0.149	30	[122]
	R1234ze(E)	IS	283.15–343.15	0.044–0.434	0.0160–0.3241	49	[119]
	R1233zd(E)	IS	303.07–343.19	0.007–0.142	0.004–0.081	30	[111]
$[C_6mim][OTf]$	R1234yf	IS	303.2–343.2	0.0619–0.0824	0.01629–0.02866	5	[88]
	R1234yf	IS	303.02–353.7	0.127–0.752	0.019–0.151	30	[122]
	R1233zd(E)	IS	303.15–343.17	0.009–0.139	0.006–0.103	30	[111]
$[C_6mim][PF_6]$	R1234yf	IS	283.15–343.15	0.0506–0.4303	0.0100–0.1366	49	[110]
	R1234yf	IS	303.05–353.27	0.138–0.747	0.012–0.138	30	[122]
	R1234ze(E)	IS	283.15–343.15	0.0847–0.4342	0.0344–0.3472	42	[108]
$[C_6mim][Tf_2N]$	R1234yf	IS	292.29–353.21	0.0993–0.9251	0.0376–0.3536	35	[112]
	R1234ze(E)	IS	292.98–353.23	0.0497–0.6937	0.0228–0.3312	35	[112]
	R1233zd(E)	IS	303.12–343.17	0.009–0.130	0.010–0.113	30	[111]
$[C_8mim][BF_4]$	R1234yf	IS	283.15–343.15	0.0548–0.4379	0.0108–0.1847	49	[118]
	R1234ze(E)	IS	283.15–343.15	0.045–0.433	0.0200–0.3614	49	[119]
$[C_8mim][PF_6]$	R1234yf	IS	283.15–343.15	0.0538–0.4377	0.0125–0.1894	49	[110]
	R1234ze(E)	IS	283.15–343.15	0.0850–0.4340	0.0403–0.3877	42	[108]
$[P_{66614}][Cl]$	R1234yf	IS	283.15–343.15	0.064–0.825	0.061–0.641	66	[121]

\* GM: gravimetric microbalance. IS: isochoric saturation. SI: synthetic isochoric. SIP: synthetic isobaric. WM: weight method.

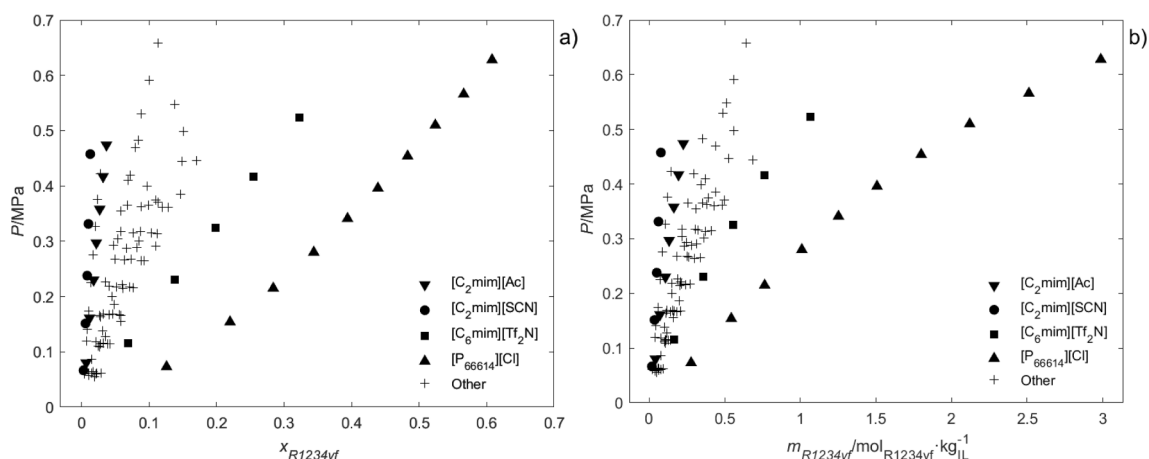
## 5.2. Hydrofluoroolefins and hydrochlorofluoroolefins

Table 5 lists the experimental absorption pairs formed by HFO or HCFO and an IL found in the literature, with information on the method, number of data points and experimental conditions. Table S4 in the UC-RAIL database in the Supporting Information contains all the composition data. The organization of the information contained in the two tables is the same as for HFCs.

The study of HFOs and HCFO-1233zd(E) solubility in ILs started later than work on HFCs. Some information appeared in the early 2010s, but the quantity of data in the literature increases most significantly from 2017 on. The VLE data are reported for temperature and pressure ranges from 283.15 to 353.27 K and 0.0070 to 0.9251 MPa. The solubility data are distributed uniformly within that temperature range, while most

data are reported at low pressures (90% of the data at 0.5 MPa or less). R1234yf is the most widely studied refrigerant in this group, and accounts for 62% of the data. In general, the solubility of R1234yf is lower than the solubility of R32 or R134a, but higher than other HFCs like R143a. On the other hand, R1234ze(E) is more soluble than its isomer R1234yf, at least with the studied ILs. The solubility of R1233zd(E) in the same ILs is higher [111] than that of the two R1234 isomers, as shown in Fig. 8, behavior that is attributed to the increased attractive interaction when the terminal fluorine is substituted by the more polar chlorine atom. Additionally, temperature affects the solubility of HFOs more than that of HFCs with higher absolute values of solvation enthalpy [112], and the solvation entropy determines the absorption capacity as it does for HFCs [73,77].

Fig. 9 compiles the absorption isotherms of R1234yf at 303 K.



**Fig. 9.** Solubility of R1234yf in different ILs at 303 K in (a) mole fraction,  $x/\text{mol}\cdot\text{mol}^{-1}$ , and (b) molality,  $m/\text{mol}\cdot\text{kg}^{-1}$ . Data from references [73,77,88,110,112,118,121,122].

Similarly to the results shown for R32 and R134a in Fig. 6, the solubility of R1234yf in most of the absorption pairs falls between the non-fluorinated [SCN]<sup>-</sup> and the fluorinated [Tf<sub>2</sub>N]<sup>-</sup>. The only exception is the solubility in [P<sub>66614</sub>][Cl], which presents a very high absorption capacity (both in molar and mass basis), which can be attributed to the electronegative anion and the high free volume of the IL [117].

The influence of the cation alkyl chain length has scarcely been studied in the literature. Fig. 10 shows that the solubility of R1234yf is enhanced with increasing alkyl chain length [77,118,119], which has been attributed to stronger van der Waals interactions between the IL and R1234yf [118,120].

A comparison between the solubility of HFCs and HFOs permits preliminary screening for a suitable G-L absorption system to selectively separate HFOs from their mixtures with HFCs. Fig. 9b shows that the solubility of R1234yf in [C<sub>2</sub>mim][Ac] is very low, unlike the absorption of R32 and R134a in this same IL (Fig. 6b and 6d). This initial assessment therefore suggests that [C<sub>2</sub>mim][Ac] is a good possibility for separating mixtures of R1234yf and R32 or R134a such as, for example, the azeotropic R513A (R134a + R1234yf).

### 5.3. Other refrigerant gases

Table 6 lists the experimental absorption pairs formed by CFCs, HCFCs, PFCs, or R22B1 and an IL found in the literature. Table S5 in the Supporting Information is a database containing all the composition data as a function of temperature and pressure.

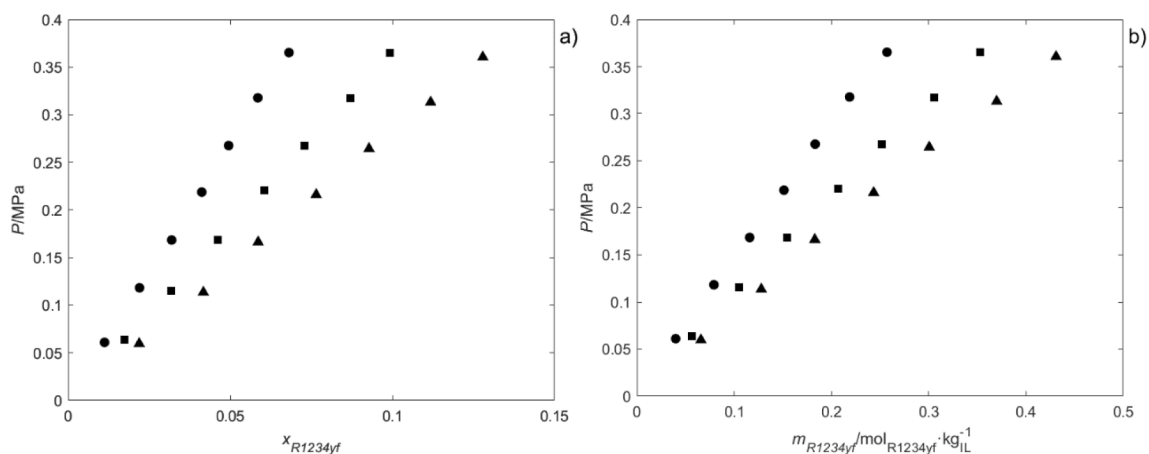


**Fig. 10.** Solubility of R1234yf in [C<sub>4</sub>mim][PF<sub>6</sub>] (●), [C<sub>6</sub>mim][PF<sub>6</sub>] (■), and [C<sub>8</sub>mim][PF<sub>6</sub>] (▲) in (a) mole fraction,  $x/\text{mol}\cdot\text{mol}^{-1}$ , and (b) molality,  $m/\text{mol}\cdot\text{kg}^{-1}$ . Data from reference [110].

CFCs and HCFCs are compounds of interest in the current context of F-gas emissions control, as they still appear in waste mixtures of refrigerant gases, from old RACHP equipment that is reaching its end of life. However, the phase down of ozone-depleting substances retired CFCs and HCFCs from the market, and the availability of absorption data in ILs for these substances is very scarce. Research efforts should also focus on these as they appear in residual gases from equipment that is nearing its end of life, and they are often intermediates in the synthesis routes to HFOs or HCFOs [3].

Shiflett and Yokozeki [82] related the solubility and miscibility differences when mixing CFCs and HFCs with [C<sub>2</sub>mim][Tf<sub>2</sub>N] to the dipole moments of the refrigerants as chlorine atoms are substituted by hydrogen atoms. They found that the solubility of CF<sub>3</sub>-CFCl<sub>2</sub> in [C<sub>2</sub>mim][Tf<sub>2</sub>N] is lower than the solubility of CF<sub>3</sub>-CHFCl and much lower than the solubility of CF<sub>3</sub>-CH<sub>2</sub>F. Furthermore, refrigerant gases with increasingly electronegative and polar groups, like chloride, show higher solubility in [C<sub>2</sub>mim][Tf<sub>2</sub>N]. Thus, the order of solubility is CHF<sub>2</sub>-Cl > CHF<sub>2</sub>-F > CHF<sub>2</sub>-CH<sub>3</sub> > CHF<sub>2</sub>-CF<sub>3</sub> when represented against normalized pressure to remove any bias due to the different saturation pressures of the gases [81].

The solubility of bromodifluoromethane (R22B1), which also appears in F-gases collected from end-of-life equipment, has been reported in some ILs. The authors state that fluorocarbon molecules with polar, electronegative groups like bromide are more soluble in ILs than those with an alkyl functionality [109].

PFCs are used in ultra-low temperature applications (below -50 °C)

**Table 6**

Summary of solubility data of CFCs, HCFCs, PFCs, and R22B1. Table S5 of the UC-RAIL database collects all the data.

Ionic liquid	Gas	Method*	T/K	P/MPa	$x/\text{mol}\cdot\text{mol}^{-1}$	No.	Ref.	
[C <sub>2</sub> mim][Tf <sub>2</sub> N]	R22	GM	283.1–348.2	0.0500–0.9000	0.024–0.835	46	[81]	
	R14	IS	303.15	0.044–0.474	0.0034–0.0583	6	[79]	
	R22B1	GM	283.2–348.2	0.0249–0.4000	0.025–0.788	45	[109]	
	R114	GM	283.0–348.1	0.0103–0.1504	0.000–0.126	22	[82]	
	R114a	GM	283.1–348.1	0.0102–0.1504	0.001–0.142	22	[82]	
	R124	GM	283.0–348.1	0.0101–0.3004	0.001–0.757	26	[82]	
[C <sub>2</sub> mim][TFES]	R22	GM	283.1–348.2	0.0498–0.8999	0.016–0.810	46	[81]	
	[C <sub>4</sub> mim][BF <sub>4</sub> ]	R22	GM	283.1–348.2	0.0500–0.9000	0.017–0.827	46	[81]
[C <sub>4</sub> mim][PF <sub>6</sub> ]	R22	GM	283.2–348.2	0.0500–0.9001	0.017–0.814	46	[81]	
	R22B1	GM	283.1–348.2	0.0249–0.4000	0.017–0.759	45	[109]	
[C <sub>6</sub> mim][Tf <sub>2</sub> N]	R14	IS	293.3–413.3	1.127–9.582	0.0122–0.0889	27	[126]	
	R14	IS	303.42–343.44	0.11465–0.12991	0.00106–0.00150	5	[125]	
[C <sub>8</sub> mim][BEI]	R14	IS	303.16–343.20	0.07073–0.08203	0.00228–0.00328	10	[99]	
	R116	IS	303.15–343.18	0.06335–0.07466	0.00310–0.00589	14	[99]	
	R218	IS	303.17–343.12	0.06632–0.08028	0.00681–0.01198	10	[99]	
	R14	IS	303.18–342.76	0.06945–0.08352	0.00117–0.00165	12	[99]	
[C <sub>8</sub> mim][Tf <sub>2</sub> N]	R116	IS	303.17–343.19	0.06675–0.07594	0.00219–0.00318	10	[99]	
	[C <sub>8</sub> H <sub>4</sub> F <sub>13</sub> mim][BEI]	R14	IS	318.15–343.07	0.07261–0.07827	0.00419–0.00526	7	[99]
	R116	IS	318.16–343.24	0.06339–0.07963	0.00662–0.01097	11	[99]	
[C <sub>8</sub> H <sub>4</sub> F <sub>13</sub> mim][Tf <sub>2</sub> N]	R218	IS	318.18–343.17	0.06927–0.07872	0.01403–0.02508	7	[99]	
	R14	IS	303.16–343.16	0.06824–0.07794	0.00319–0.00455	9	[99]	
	R116	IS	303.15–343.19	0.06280–0.07412	0.00528–0.01048	16	[99]	
[P <sub>66614</sub> ][Tf <sub>2</sub> N]	R218	IS	303.16–343.21	0.06181–0.07168	0.01132–0.02538	9	[99]	
	R14	IS	303.41–343.49	0.10459–0.12410	0.00163–0.00297	13	[125]	
	R116	IS	303.19–343.23	0.10554–0.13135	0.00296–0.00545	8	[125]	
	R218	IS	303.43–343.70	0.04120–0.11984	0.00690–0.0116	10	[125]	

\* GM: gravimetric microbalance. IS: isochoric saturation. SI: synthetic isochoric. SIP: synthetic isobaric. WM: weight method.

either alone or in mixtures with R23 (mixtures R508A and R508B) and in the manufacture of electronic semiconductors. The use of PFCs is not restricted by the F-gas regulations due to the limited number of units in operation [124], but their high-GWP makes them GHGs of concern that may well be regulated in the future. The little data available in the literature show that the solubility of PFCs in ILs is very low, the order of solubility being perfluoromethane < perfluoroethane < perfluoropropane. For these gases, Pison et al. [125] found that the solubility in [P<sub>66614</sub>][Tf<sub>2</sub>N] increases with the molecular size due to a more favorable entropy of solvation given that the enthalpy of solvation was similar for all gases. However, for ILs with different cations, the solubility becomes larger as the apolar domains in the IL increase, for example, the solubility of perfluoromethane is higher in [P<sub>66614</sub>][Tf<sub>2</sub>N] than in [C<sub>6</sub>mim][Tf<sub>2</sub>N] due to a more favorable enthalpic contribution.

#### 5.4. Global phase behavior

Most of the information on the equilibrium of F-gases with ILs that is available in the literature has already been covered in the previous sections in relation to VLE. The global phase behavior (VLE, cloud points, critical fluid-liquid equilibrium) is much less well studied, but it can still provide meaningful insights of the phase equilibrium of F-gases and ILs mixtures. To illustrate the type of equilibrium, Fig. 11 presents the global phase behavior of the mixture of R134a and [C<sub>4</sub>mim][PF<sub>6</sub>]. Compared to previous figures, this covers the entire range of composition up to the pure refrigerant and shows that when the saturation pressure of the refrigerant is reached, it condenses in a separate phase if the IL does not have enough absorption capacity (which may only occur at sufficiently high temperatures). The global phase behavior is organized according to the van Konynenburg and Scott classification, which labels the binary phase behavior as types I through VI. For the case of HFC–IL mixtures, the behavior is usually a type V, that is, there is a VLE region at low pressures, followed by the VLE region with a lower critical solution temperature (LCST) point where only one liquid phase exists, such as that illustrated in Fig. 11. In some cases, the behavior falls into a type III, where there is no LCST and the VLE region exists at low

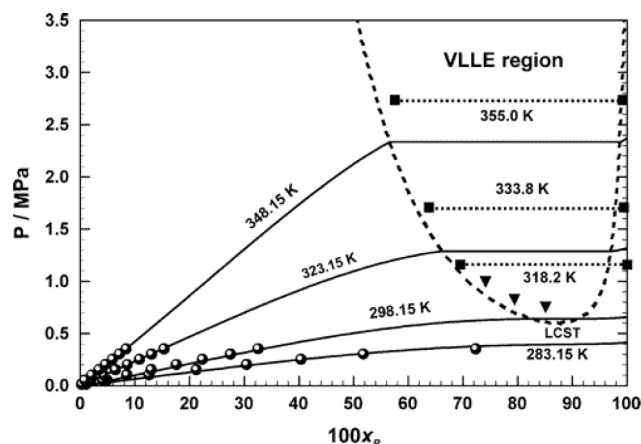


Fig. 11. Pressure-composition phase diagram for R134a + [C<sub>4</sub>mim][PF<sub>6</sub>]. Solid and dashed lines represent the modeling of a modified-RK equation of state, and symbols are experimental data: VLE (●), VLE (■), and cloud-points (▼). Reprinted with permission from reference [129]. Copyright 2006 American Chemical Society.

temperatures until the IL freezing point is reached [64,127–129].

The studies that consider VLE cover different families of gases such as HFCs (R41, R23, R161, R152a, R143a, R134a, and R125), HCFCs (R124, R124a, R123, and R123a), and CFCs (R11, R114, R114a, R113 and R113a) in the ILs [C<sub>2</sub>mim][Tf<sub>2</sub>N] and [C<sub>4</sub>mim][PF<sub>6</sub>] [64,82,85,128–130]. The VLE of binary mixtures of R134a with [C<sub>6</sub>mim][BF<sub>4</sub>], [C<sub>6</sub>mim][PF<sub>6</sub>] and [C<sub>6</sub>mim][Tf<sub>2</sub>N] has also been reported [66,89]. Table S6 in the Supporting Information presents these data. The studies show that the miscibility of HFCs with ILs is higher and much higher than the miscibility of HCFCs and CFCs with ILs, respectively, as evidenced by a much wider VLE region in the phase diagram of the latter compounds.

Cloud points have been reported in studies dedicated to VLE for mixtures of [C<sub>2</sub>mim][Tf<sub>2</sub>N] with R123, R123a, R124, R124a, R134,

R134a, and R125 [82,85], and mixtures of [C<sub>6</sub>mim][PF<sub>6</sub>] with the refrigerants R23, R123, R152a, R134a, and R125 [64,128–130]. Moreover, some articles consider the phase behavior of supercritical R23 with ILs to gain insights into the use of this gas as an extractant of solutes from the IL; these are compiled in Table S7 of the Supporting Information [131,132].

## 6. Mass transport properties

Mass transfer influences the operation of equilibrium-based separation processes [133], therefore affecting both the chemical and economic design [134]. If the diffusion of the gaseous species is slow, column stages will likely operate in non-equilibrium conditions. For example, the CO<sub>2</sub> absorption completion in [C<sub>2</sub>mim][Tf<sub>2</sub>N] in flow conditions has been determined to be around 70% of the equilibrium concentration [135]. Diffusion is slower in more viscous solvents, thus decreasing mass transfer rates [133]. Also, if the viscosity is too high, pumping costs go up and the separation target may not be achievable [136]. Mass transport properties that influence the kinetics of the separation process therefore require further assessment.

### 6.1. Viscosity of gas-ionic liquid mixtures

Mixture viscosity is one of the key properties to consider when applying ILs to gas separations [120]. Some screening and design studies constrain the maximum IL viscosity to 100 mPa·s at 298.15 K in order to consider it a feasible solvent [137,138]. Then, an IL like [C<sub>2</sub>mim][Ac], which we noted in previous sections as a promising candidate for separating the constituents of the R513A mixture would simply not be considered due to its high viscosity (143.6 mPa·s at 298.15 K [139]). However, the viscosity of the IL-gas mixture may be considerably lower than that of the pure IL, and this mixed viscosity property could make the operation viable.

In line with this thinking, the viscosity of [C<sub>6</sub>mim][Tf<sub>2</sub>N] mixed with various HFCs and HFOs has recently been published, as summarized in Table 7. A compilation of all the data from the literature is included in Table S8 of the UC-RAIL database in the Supplementary Information. [C<sub>6</sub>mim][Tf<sub>2</sub>N] is an IL with a relatively low viscosity, between 153 mPa·s at 283.15 K and 14.6 mPa·s at 343.15 K for the pure IL [140], so the effects discussed in this section may be more pronounced for more viscous ILs.

The data in the literature show that the viscosity of the IL [C<sub>6</sub>mim][Tf<sub>2</sub>N] decreases sharply as the gas pressure increases, in other words, at increased F-gas content absorbed in the IL. This effect is particularly remarkable at low temperatures that promote gas absorption, so process design stages should consider this carefully. For example, the viscosity of the mixture of R152a with [C<sub>6</sub>mim][Tf<sub>2</sub>N] at 283.15 K and 1 bar is 66 mPa·s, one third of the viscosity of the pure IL. Fig. 12 shows the viscosity data of mixtures of refrigerants with [C<sub>6</sub>mim][Tf<sub>2</sub>N] as a function of molar fraction of gas dissolved at 323.15 K [65,66,141]. The viscosity of pure refrigerants is calculated using CoolProp 6.4.0 [142]. The viscosity of refrigerants in their liquid phase is in the range 0.10–0.15 mPa·s, two orders of magnitude lower than [C<sub>6</sub>mim][Tf<sub>2</sub>N], explaining why the viscosity of the mixture is so low in comparison with the pure IL. Fig. 12 also includes the mixture viscosity predicted with the Arrhenius (Eq. (3)) and the Kendall and Monroe's (Eq. (4)) models considering

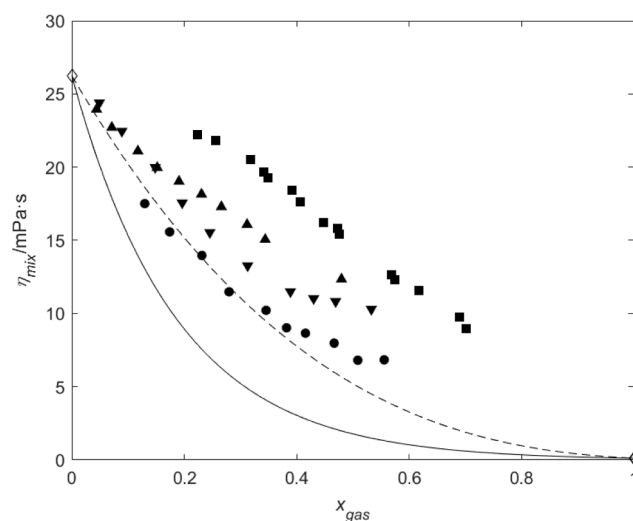


Fig. 12. Viscosity of mixtures of [C<sub>6</sub>mim][Tf<sub>2</sub>N] with refrigerant gases at 323.15 K. Experimental points for different F-gases: R152a [65] (●), R134a [65,66] (■), R1234yf [141] (▲), and R1234ze(E) [141] (▼). Pure [C<sub>6</sub>mim][Tf<sub>2</sub>N] viscosity [140] and pure refrigerant viscosity [142] presented as diamonds (◇). The lines represent the Arrhenius (solid line, —) and Kendall-Monroe (dashed line, - -) ideal behaviors of mixture viscosity.

ideal mixture behavior [143]:

$$\ln \eta_{mix} = x_1 \ln \eta_1 + x_2 \ln \eta_2 \quad (3)$$

$$\eta_{mix} = \left( x_1 \cdot \eta_1^{1/3} + x_2 \cdot \eta_2^{1/3} \right)^3 \quad (4)$$

It can be observed that, although the Kendall-Monroe model performs better than the Arrhenius model, the mixture viscosity of all systems present positive deviations for the ideal behavior that are particularly significant for R134a and almost negligible for R152a. To account for these deviations, the variation of the viscosity with the mixture composition has been described using both empirical correlations, like the Setschenow equation [65], and more accurate semi-theoretical models based on Eyring's viscosity theory, like the Eyring-NRTL and Eyring-modified two-suffix Margules (Eyring-MTSM) models [141,144], that include a nonideal term based on the excess Gibbs free energy ( $G^E$ ) of the mixture.

$$\ln(\eta_{mix}) = x_1 \ln(\eta_1) + x_2 \ln(\eta_2) + \frac{G^E}{RT} \quad (5)$$

### 6.2. Diffusion coefficients

Gas separations with ILs are driven by differences in solubility, rather than diffusivity differences [145]. However, diffusion coefficients are one of the most important transport properties, necessary for calculating mass transfer rates [146,147]. In the case of fluorinated refrigerant gases, the research has mainly focused on assessing the diffusion coefficients of R32, as shown in the summary presented in Fig. 13, followed by those of R134a, R125, and R1234yf. Diffusion coefficients have been determined either using a GM method or through the IS

Table 7

Summary of the viscosity ( $\eta$ ) of mixtures of HFCs and HFOs with [C<sub>6</sub>mim][Tf<sub>2</sub>N]. Table S8 of the UC-RAIL database collects all the data.

Gas	T/K	P/MPa	x/mol·mol <sup>-1</sup>	$\eta$ /mPa·s	No.	Ref.
R152a	283.15–343.15	0.053–0.786	0.1143–0.6978	118.24–4.92	70	[65]
R134a	298.15–343.15	0.29–2.03	0.148–0.813	55.8–3.24	15	[66]
R134a	298.15–343.15	0.158–1.930	0.127–0.768	66.435–4.301	24	[65]
R1234yf	283.15–343.15	0.086–1.301	0.0286–0.4796	145.28–10.31	70	[141]
R1234ze(E)	283.15–343.15	0.096–1.420	0.0302–0.5510	119.21–9.34	70	[141]

		Fluorinated refrigerant gases													
		HFCs								Other					
		R32	R23	R161	R152a	R143a	R134a	R125	R245fa	R236fa	R227ea	R1234yf	R1234ze(E)	R22	R22B1
Ionic liquids	[C <sub>2</sub> mim][BEI]														
	[C <sub>2</sub> mim][BF <sub>4</sub> ]														
	[C <sub>2</sub> mim][OTf]														
	[C <sub>2</sub> mim][PF <sub>6</sub> ]														
	[C <sub>2</sub> mim][SCN]														
	[C <sub>2</sub> mim][Tf <sub>2</sub> N]														
	[C <sub>2</sub> mim][TFES]														
	[C <sub>3</sub> mpy][Tf <sub>2</sub> N]														
	[C <sub>4</sub> mim][Ac]														
	[C <sub>4</sub> mim][BF <sub>4</sub> ]														
	[C <sub>4</sub> mim][FS]														
	[C <sub>4</sub> mim][HFPS]														
	[C <sub>4</sub> mim][MeSO <sub>4</sub> ]														
	[C <sub>4</sub> mim][PF <sub>6</sub> ]														
	[C <sub>4</sub> mim][SCN]														
	[C <sub>4</sub> mim][TFES]														
	[C <sub>4</sub> mim][TPES]														
	[C <sub>4</sub> mim][TTES]														
	[C <sub>4</sub> mpy][Tf <sub>2</sub> N]														
	[C <sub>6</sub> mim][BF <sub>4</sub> ]														
	[C <sub>6</sub> mim][Cl]														
	[C <sub>6</sub> mim][FEP]														
	[C <sub>6</sub> mim][OTf]														
	[C <sub>6</sub> mim][Tf <sub>2</sub> N]														
	[C <sub>7</sub> mim][TFES]														
	[C <sub>8</sub> mim][I]														
	[(C <sub>8</sub> ) <sub>2</sub> mim][I]														
	[C <sub>12</sub> mim][TFES]														
[(C <sub>1</sub> ) <sub>2</sub> C <sub>3</sub> mim][Tf <sub>2</sub> N]															
[(C <sub>1</sub> ) <sub>2</sub> C <sub>3</sub> mim][TMeM]															
[P <sub>44414</sub> ][HFPS]															
[P <sub>66614</sub> ][TPES]															

**Fig. 13.** F-gas—IL diffusion coefficient pairs studied. Green color stands for pressure-dependent data at several temperatures, purple color marks pressure-dependent diffusion studied at a single temperature and yellow color indicates systems studied at a single pressure with the same method, while light orange are systems studied using the semi-infinite dilution model. (For interpretation of the references to color in this figure legend, the reader is referred to the web version of this article.)

method with a semi-infinite volume model. The former provides data at different concentrations (Table 8), while the latter only determines the diffusion coefficients at infinite dilution (Table 9). A compilation of all the data from the literature is included in Table S9 of the UC-RAIL database in the Supplementary Information.

The number of systems for which the diffusion coefficients have been studied is much lower than for the characterization of the VLE, so it is difficult to find trends and correlations in the data. A comparison of the different diffusion coefficients at infinite dilution shows that the relationship of diffusivity with viscosity is not clear. In fact, strong deviations occur with [OTf]<sup>-</sup> and [Tf<sub>2</sub>N]<sup>-</sup> anions, something that was also observed for CO<sub>2</sub> and which led to the formulation of different correlations for those anions [148]. In general, the published data on diffusivity of fluorinated gases are not yet sufficient to infer any family behavior. Future studies should focus on assessing the impact of alkyl chain length in 1-alkyl-3-methylimidazolium ILs for different anion families, to achieve a deeper understanding of diffusion coefficients behavior.

Self-diffusion of refrigerant gases and IL mixtures has been studied in two recent articles. One of these experimentally assessed the self-diffusion of R134a + [C<sub>6</sub>mim][Tf<sub>2</sub>N] [66], while the other used molecular dynamics simulations to calculate the self-diffusion of R1234yf + [C<sub>4</sub>mim][Tf<sub>2</sub>N] [149]. When compared with data for the pure compound, the refrigerant self-diffusion coefficient is lower, while the cation and anion of the IL diffuse faster. This is attributed to the fact that the solution reduces the free volume of the refrigerant and increases the IL free volume.

## 7. Fluorinated gas separation analysis

The wide range of ILs makes it complicated to select the optimal entrainer, due to the heterogeneity of the cations and anions available. For that reason, this section first applies the Regular Solution Theory (RST) as a screening tool for elucidating trends in IL solubility selectivity and setting meaningful guidelines for selecting optimal entrainers. After that, we analyze the available information on modeling and process design for the separation of F-gases using ILs and, finally, we present the process intensification strategy through the synthesis of mixed matrix membranes formed by an IL and a polymer, with the aim of improving the selectivity and reducing the equipment size.

### 7.1. Prediction of ionic liquid selectivity using the Regular solution Theory

The RST is a simple model used to describe the solubility of gases in ILs [150]. A simplified version of the RST relates the Henry's law constant to the squared difference between the solubility parameters of the solvent ( $\delta_{IL}$ ) and solute ( $\delta_{F-gas}$ ). These solubility parameters can be estimated from the lattice energy density of the IL using the Kapustinskii equation [116], which can be solved to relate the Henry's law constants to the molar volume of the IL ( $V_m^{IL}$ ), as shown in Eq. (6) [145,151]:

$$\ln(k_H(\text{bar})) = \alpha + \frac{\beta}{(V_m^{IL}(\text{cm}^3 \cdot \text{mol}^{-1}))^{4/3}} \quad (6)$$

The parameters  $\alpha$  and  $\beta$  in Eq. (6) are constants that depend only on the gas being absorbed and the temperature. In Fig. 14a we have adjusted the Henry's law constants of R32, R134a, R1234yf and R1234ze(E) at 303 K to  $V_m^{IL-4/3}$  to determine the  $\alpha$  and  $\beta$  parameters. The good fit of the data to Eq. (6) shows that the RST provides a reasonable description of the absorption of fluorinated gases in ILs, and ILs with increasing molar volume present lower Henry's law constants, i.e., higher solubility. Table 10 presents the values of  $\alpha$  and  $\beta$  calculated from the y-intersect and the slope of the linear fitting in Fig. 14a. The Henry's law constants have been calculated from absorption data included in the UC-RAIL database, as explained in Section 5.1. We focus on two HFCs (R32 and R134a) and two HFOs (R1234yf and R1234ze(E)) as these are widely applied in current RACHP equipment, and there is interest in developing separation processes to selectively recover these refrigerant gases.

The absorption capacity of ILs at 1 bar can be predicted as a function of the IL molar volume by rearranging of Eq. (6) [145] as

$$\text{Absorption capacity} \left( \frac{\text{mol gas}}{\text{L IL}} \right) = \frac{1}{\left[ \exp \left( \alpha + \frac{\beta}{(v_m^{IL})^{4/3}} \right) - 1 \right] v_m^{IL}} \quad (7)$$

Fig. 14b shows the gas absorption capacity of ILs as predicted by Eq. (7) for a wide range of IL molar volumes. As can be seen, the absorption capacity increases with the IL molar volume until it reaches a maximum, after which the absorption capacity tends to descend or stabilize. The prediction of the CO<sub>2</sub> absorption capacity of ILs is also presented as a reference [145].

The definition of the RST used in this work considers only the IL molar volume as the solubility driving factor [145], although enthalpic effects can also exert an important influence, as previously explained in



**Table 8**

Summary of diffusion coefficients of refrigerants in ILs data from a gravimetric microbalance. Table S9 in the UC-RAIL database collects all the data.

Ionic liquid	Gas	T/K	P/MPa	$x/\text{mol}\cdot\text{mol}^{-1}$	$D/10^{-11} \text{ m}^2\cdot\text{s}^{-1}$	No.	Ref.	
[C <sub>2</sub> mim][BEI]	R32	283.15–348.15	0.0096–0.8505	0.010–0.802	3.8–35	25	[70]	
	R134a	283.10–348.10	0.0103–0.3005	0.006–0.673	1.9–17	27	[72]	
[C <sub>2</sub> mim][PF <sub>6</sub> ]	R23	332.9–348.0	0.00965–1.99990	0.001–0.151	10.2–72.2	15	[76]	
[C <sub>2</sub> mim][Tf <sub>2</sub> N]	R22B1	283.2–348.2	0.0499–0.4000	0.051–0.760	13.1–73.7	22	[109]	
	R22	283.1–348.2	0.0500–0.9000	0.024–0.835	4.5–86	15	[81]	
[C <sub>2</sub> mim][TFES]	R32	283.15–348.05	0.0096–0.8504	0.005–0.672	4.1–48	24	[70]	
	R22	283.2–348.2	0.0498–0.8999	0.016–0.810	1.7–47	15	[81]	
	R32	298.05	0.2484–1.0016	0.133–0.477	2.9–12	6	[70]	
[C <sub>3</sub> mpy][Tf <sub>2</sub> N]	R32	283.15–348.05	0.0095–1.0002	0.003–0.782	5.7–55	25	[70]	
[C <sub>4</sub> mim][Ac]	R32	298.05–298.25	0.0099–1.0004	0.010–0.518	2.2–21	8	[70]	
	R32	298.15	0.05	0.054	0.5	1	[86]	
	R125	298.15	0.05	0.060	0.4	1	[86]	
[C <sub>4</sub> mim][BF <sub>4</sub> ]	R22B1	283.1–348.2	0.0500–0.4000	0.039–0.763	6.14–119	22	[109]	
	R22	283.1–348.2	0.0500–0.9000	0.017–0.827	3.1–160	15	[81]	
	R32	283.0–348.2	0.0097–0.9999	0.002–0.759	1.7–19	31	[69]	
	R32	298.15	0.05	0.024	7.8	1	[86]	
	R125	298.15	0.05	0.008	2.4	1	[86]	
[C <sub>4</sub> mim][FS]	R32	298.15	0.0100–1.0005	0.009–0.638	4.3–28	7	[70]	
[C <sub>4</sub> mim][HFPS]	R32	298.15	0.0095–1.0004	0.010–0.670	3.3–17	8	[70]	
	R134a	283.10–348.10	0.0099–0.3506	0.003–0.677	0.9–8.1	25	[72]	
[C <sub>4</sub> mim][MeSO <sub>4</sub> ]	R32	298.15	0.0099–1.0006	0.012–0.489	2.1–12	8	[70]	
[C <sub>4</sub> mim][PF <sub>6</sub> ]	R22B1	283.1–348.2	0.0500–0.4000	0.037–0.732	4.18–119	22	[109]	
	R22	283.2–348.2	0.0500–0.9001	0.017–0.814	1.5–76	15	[81]	
	R32	283.2–348.2	0.0099–0.9999	0.003–0.815	1.7–12	28	[69]	
	R32	298.15	0.05	0.039	8.5	1	[86]	
	R23	282.6–348.1	0.0098–2.0000	0.000–0.419	1.5–23	28	[69]	
	R152a	283.1–348.2	0.0099–0.4505	0.005–0.577	1.1–15	22	[69]	
	R143a	285.1–348.2	0.1000–1.0003	0.009–0.241	0.8–14	26	[69]	
	R134a	283.0–348.2	0.0097–0.3500	0.000–0.724	0.4–8.4	29	[69]	
	R125	283.1–348.3	0.0996–0.9998	0.007–0.660	0.6–11	31	[69]	
	R125	298.15	0.05	0.012	1.7	1	[86]	
	R32	298.15	0.0095–0.9992	0.004–0.379	8.1–21	7	[70]	
	[C <sub>4</sub> mim][TFES]	R32	298.15	0.0999–0.9989	0.072–0.556	1.5–14	7	[70]
	[C <sub>4</sub> mim][TPES]	R32	298.15	0.0095–0.9994	0.010–0.674	4.5–21	8	[70]
R134a		283.05–348.10	0.0102–0.3505	0.006–0.673	0.9–15	29	[72]	
[C <sub>4</sub> mim][TTES]	R32	298.15	0.0095–0.9992	0.010–0.650	4.3–25	8	[70]	
	R134a	282.10–348.15	0.0102–0.3502	0.005–0.630	1.0–14	30	[72]	
[C <sub>4</sub> mpy][Tf <sub>2</sub> N]	R32	298.15	0.0096–1.0000	0.010–0.654	6.8–23	6	[70]	
[C <sub>6</sub> mim][Cl]	R32	298.15	0.05	0.021	1.5	1	[86]	
	R125	298.15	0.05	0.040	0.4	1	[86]	
	R32	298.15	0.05	0.067	19.6	1	[86]	
[C <sub>6</sub> mim][FEP]	R125	298.15	0.05	0.038	5.5	1	[86]	
	R32	298.15	0.0099–0.9980	0.008–0.592	3.9–16	8	[70]	
[C <sub>7</sub> mim][TFES]	R32	298.15	0.0099–0.9980	0.008–0.592	3.9–16	8	[70]	
[C <sub>8</sub> mim][I]	R32	298.0–298.2	0.01007–1.00022	0.004–0.416	1.75–6.37	8	[76]	
[(C <sub>8</sub> ) <sub>2</sub> im][I]	R32	297.9–298.0	0.01002–1.00024	0.007–0.468	1.78–5.77	8	[76]	
[C <sub>12</sub> mim][TFES]	R32	298.15	0.0995–1.0010	0.074–0.569	4.7–13	7	[70]	
[(C <sub>1</sub> ) <sub>2</sub> C <sub>3</sub> im][Tf <sub>2</sub> N]	R32	298.05–298.15	0.0099–1.0011	0.008–0.651	6.3–23	8	[70]	
[(C <sub>1</sub> ) <sub>2</sub> C <sub>3</sub> im][TMeM]	R32	283.15–348.05	0.0099–1.0005	0.004–0.805	1.4–21	25	[70]	
[P <sub>44414</sub> ][HFPS]	R134a	283.05–348.10	0.0100–0.3504	0.009–0.763	1.3–20.2	30	[72]	
[P <sub>66614</sub> ][TPES]	R134a	282.85–348.10	0.0098–0.3505	0.003–0.718	1.7–23	30	[72]	

**Section 5.1 and 5.2.** Despite the good fit of the data to the RST, Fig. 14a contains some points that deviate significantly from the model. The R32 and R134a absorption data in three ILs with molar volumes of around  $150 \text{ cm}^3\cdot\text{mol}^{-1}$ , [C<sub>2</sub>mim][Ac], [C<sub>2</sub>mim][BF<sub>4</sub>], and [C<sub>2</sub>mim][SCN], may shed some light on the solubility of fluorinated gases, so the differences between the experimental and predicted values are presented in Fig. 15. The RST accurately describes the capacity of [C<sub>2</sub>mim][BF<sub>4</sub>], but fails for the other two ILs. In the case of [SCN]<sup>-</sup>, the lower absorption capacity may be related to a lower electron donor capacity. Conversely, [Ac]<sup>-</sup> may have a higher capacity to form hydrogen bonds as discussed previously, favoring the absorption capacity. In fact, the highest R134a capacity is observed for the [PF<sub>6</sub>]<sup>-</sup> anion, reinforcing the idea that carboxylate-based ILs provide increased F-gas solubility, higher than expected. Interestingly, the solubility of R1234yf in the three ILs with a molar volume of around  $150 \text{ cm}^3\cdot\text{mol}^{-1}$  is very low, so that all three are expected to enhance the solubility selectivity when separating this HFO from its mixtures with HFCs.

Some of these deviations from the RST may be a result of chemical interactions and should be explored further. For example, the [Ac]<sup>-</sup> and

[Cl]<sup>-</sup> anions present such a high R125 absorption capacity [60,86] that their behavior strongly deviates from the RST predictions. Table 10 presents the  $\alpha$  and  $\beta$  parameters for R125. Fig. 15 shows the differences between the RST prediction and the experimental Henry's law constant for R125 in [C<sub>4</sub>mim][Ac] and [C<sub>6</sub>mim][Cl] at 298 K and [C<sub>2</sub>mim][Ac] at 303 K, where deviations become clear: the ILs with [Ac]<sup>-</sup> and [Cl]<sup>-</sup> anions have very low Henry's law constant values and therefore a higher absorption capacity (at low pressure) than expected from the physical solubility description of the RST.

Using the RST, it is possible to infer the expected trend in solubility selectivity of gas–liquid absorption separation, which is calculated as the ratio of absorption capacities [145]. In this work, we have calculated the selectivity for some interesting mixtures that present the azeotropic or pinch behaviors discussed in Section 3. Fig. 16a shows the absorption selectivity of R32 over R1234yf and R134a over R1234yf and R1234ze (E); Fig. 16b shows the absorption selectivity of R32 over R125. The lines were obtained from the model (Eq. (7)) and the  $\alpha$  and  $\beta$  parameters in Table 10, and the points are calculated from the experimental data reported in the UC-RAIL database.

Table 9

Summary of diffusion coefficients of refrigerants in ILs data calculated with a semi-infinite volume model. Table S9 in the UC-RAIL database collects all the data.

Ionic liquid	Gas	T/K	$D/10^{-10} \text{ m}^2 \cdot \text{s}^{-1}$	No.	Ref.	
[C <sub>2</sub> mim][BF <sub>4</sub> ]	R32	283.15–323.15	1.67–10.04	5	[73]	
	R134a	283.15–323.15	1.27–9.57	5	[73]	
[C <sub>2</sub> mim][OTf]	R134a	283.15–323.15	1.06–5.42	5	[73]	
	R1234yf	283.15–323.15	0.97–8.01	5	[77]	
[C <sub>2</sub> mim][SCN]	R32	283.15–313.15	5.1–13.3	4	[77]	
	R134a	283.15–313.15	1.5–13.2	4	[77]	
	R1234yf	283.15–313.15	0.5–9.8	4	[77]	
[C <sub>2</sub> mim][Tf <sub>2</sub> N]	R1234yf	283.15–323.15	0.36–5.14	5	[73]	
[C <sub>6</sub> mim][BF <sub>4</sub> ]	R32	303.2–343.2	1.29–4.76	5	[88]	
	R161	303.2–343.2	1.23–4.20	5	[88]	
	R152a	303.2–343.2	0.74–2.56	5	[88]	
	R143a	303.2–343.2	0.77–3.39	5	[88]	
	R125	303.2–343.2	0.63–3.66	5	[88]	
	R245fa	303.15–343.15	0.53–4.87	5	[90]	
	R236fa	303.15–343.15	0.56–6.24	5	[90]	
	R227ea	303.15–343.15	1.26–7.79	5	[90]	
	R1234yf	303.2–343.2	0.69–3.59	5	[88]	
	R1233zd(E)	303.2–343.2	3.3–16.8	5	[111]	
	[C <sub>6</sub> mim][FEP]	R32	293.5–343.2	1.75–11.42	6	[91]
		R161	293.2–343.2	0.56–8.78	6	[91]
		R152a	293.2–343.2	0.41–6.36	6	[91]
	[C <sub>6</sub> mim][OTf]	R32	303.2–343.2	3.01–8.35	5	[88]
R161		303.2–343.2	2.08–5.91	5	[88]	
R152a		303.2–343.2	1.48–4.73	5	[88]	
R143a		303.2–343.2	1.96–6.13	5	[88]	
R125		303.2–343.2	2.38–6.19	5	[88]	
R1234yf		303.2–343.2	1.46–4.97	5	[88]	
R1233zd(E)		303.2–343.2	5.2–26.2	5	[111]	
R32		303.0–343.2	1.55–4.78	5	[88]	
R161		303.2–343.2	1.28–4.13	5	[88]	
R152a		302.8–343.0	0.99–3.16	5	[88]	
[C <sub>6</sub> mim][Tf <sub>2</sub> N]	R143a	303.4–342.8	1.84–5.10	5	[88]	
	R125	303.1–342.9	1.02–4.21	5	[88]	
	R245fa	303.15–343.15	0.84–3.47	5	[94]	
	R236fa	303.15–343.15	1.55–8.42	5	[94]	
	R227ea	303.15–343.15	2.72–12.6	5	[94]	
	R1234yf	303.1–343.2	1.39–5.96	5	[88]	
	R1233zd(E)	303.2–343.2	2.9–8.3	5	[111]	

In general, Fig. 16 shows that ILs with a small molar volume offer greater solubility selectivity for separating of HFC/HFO mixtures, so research efforts in the design of separation processes should be directed towards characterizing ILs with a molar volume near to  $150 \text{ cm}^3 \cdot \text{mol}^{-1}$ . [C<sub>2</sub>mim][Ac] would provide the greatest selectivity because it dissolves small amounts of R1234yf while presenting a high solubility for R32 and R134a, as shown in Fig. 6. In contrast, the selectivity of [C<sub>2</sub>mim][Ac] for separating mixtures of R32 and R125 is very low, behavior attributed to its strong interaction with R125 (Fig. 16b). In the same manner, [C<sub>4</sub>mim][Ac] and [C<sub>6</sub>mim][Cl] display a selectivity value lower than one for separating the gas pair R32 and R125, meaning that both ILs absorb more R125 than R32. Recovering R32 from R410A (the commercial equimass mixture of R32 and R125) would therefore need an IL that interacts with R125 strongly enough to give a high selectivity of R125 over R32. Finally, Fig. 16a shows that separating R134a and R1234ze(E) using G-L absorption may be cumbersome because the predicted selectivity is close to one for a wide range of IL molar volumes, so in this case, the efforts should be focused on systems that deviate from the RST.

The assessment would also require further information relating to the description of the solubility mechanism, in order to explain the solubility selectivity deviations from the RST, as observed for the IL with the [SCN]<sup>-</sup> and [Ac]<sup>-</sup> anions, where the former presents a low absorption capacity and the latter provides high solubility as discussed in Section 5.1. Another interesting deviation from the RST is the case of [C<sub>6</sub>mim][FEP], which offers much greater selectivity than predicted for the separation of R32 and R125 mixtures; this may be related to repulsive interactions between the large number of fluorine atoms in R125 and the IL anion [FEP]<sup>-</sup>.

## 7.2. Thermodynamic models

A barrier identified for the implementation of ILs in industrial applications is the lack of fundamental understanding of their performance in relation with their compositional structure [152]. Accurate models for the description of thermodynamic properties and phase behavior are tools whose use is fundamental to advance in the design of novel separation processes. In the field of F-gases mixtures with ILs there is a good number of publications interested in describing the thermodynamic behavior of these complex mixtures, a challenge that has been addressed through the different approaches reviewed in this section, namely, activity coefficient models, cubic EoS, statistical mechanics EoS, quantum chemistry calculations and artificial intelligence models.

In the previous section, we modeled the absorption of refrigerant gases in ILs using RST and showed that it does not capture the real behavior of these binary mixtures because the molecular interactions between the IL and the F-gases are neglected. Furthermore, the RST analysis is based on Henry's law constants, which are defined at infinite dilution. To consider the Henry's law constant dependence on pressure, some authors have applied empirical correlations based on the Krichevsky-Kasarnovsky and Krichevsky-Ilinskaya equations [92,93,97,98,108,112,118,153].

Most frequently, the VLE is described using activity coefficient approaches based on excess Gibbs free energy models [23], among which the nonrandom two-liquid (NRTL) model is the most widely applied. Despite being developed for nonelectrolyte solutions, a total of 91 F-gas–IL systems have been modeled using NRTL with good accuracy [69–73,75,77,81,82,85,87,90,91,108–111,118,119,122,130,154,155]. Other activity coefficient models have also been evaluated providing

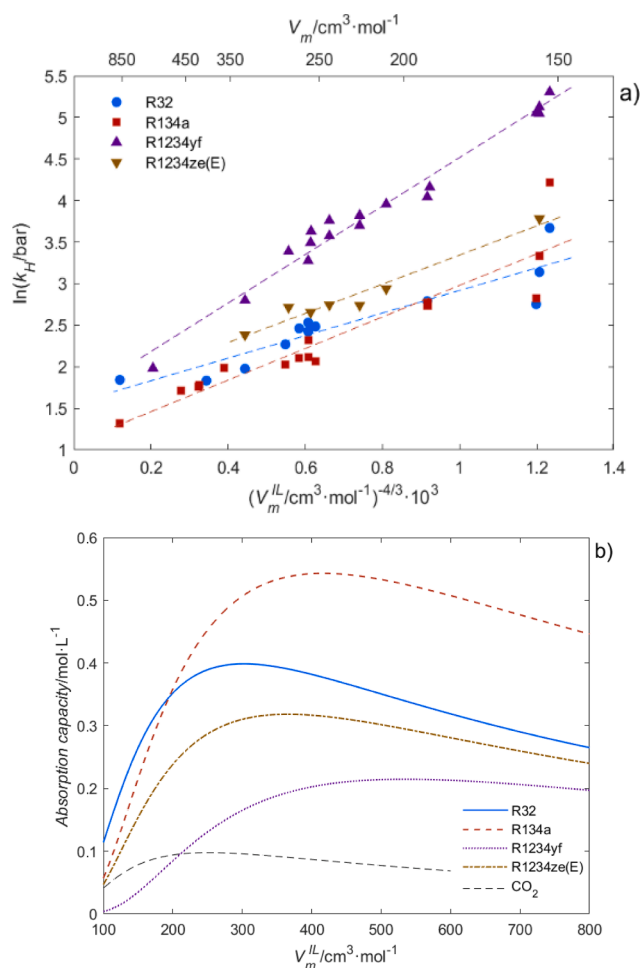


**Fig. 14.** RST applied to HFC/HFO absorption in ILs: (a) regression plot to Eq. (4), (b) predicted absorption capacity of ILs (Eq. (5)). Symbols represent each of the gases: R32 (blue ●), R134a (red ■), R1234yf (purple ▲), R1234ze(E) (brown ▼), and CO<sub>2</sub> (dashed line). (For interpretation of the references to color in this figure legend, the reader is referred to the web version of this article.)

**Table 10**

Values of  $\alpha$  and  $\beta$  for different refrigerant gases at 303 K.

T/K	Parameter	R32	R134a	R125	R1234yf	R1234ze(E)
303	$\alpha$	1.56	1.08	0.98	1.60	1.59
	$\beta$	1358	1900	2771	2918	1755
298	$\alpha$	1.87		1.49		
	$\beta$	893		2746		

similar accuracy to the NRTL model. Mainly, the UNIFAC group contribution method, for which Dong et al. [156] fitted 16 new group interaction parameters to describe the interaction between fluorinated segments and ILs from VLE data of 18 HFC—IL mixtures, and to a lesser degree, a new version of the e-NRTL equation developed to consider the size difference of the molecules and ions in the solution [157].

Cubic EoS, which treat the IL as a whole molecule with a certain volume and cohesive energy [152], have also been extensively used to model the VLE and to predict the VLLE of fluorinated refrigerants and ILs. However, ILs have no measurable critical properties, so their pseudocritical properties have to be predicted applying different methods. Nevertheless, Morais et al. [86] demonstrated that the van der Waals EoS was not sensitive to the IL critical parameters above a certain critical pressure, a hypothesis that should be tested for other cubic EoS. The Redlich-Kwong EoS and the van der Waals EoS modified by

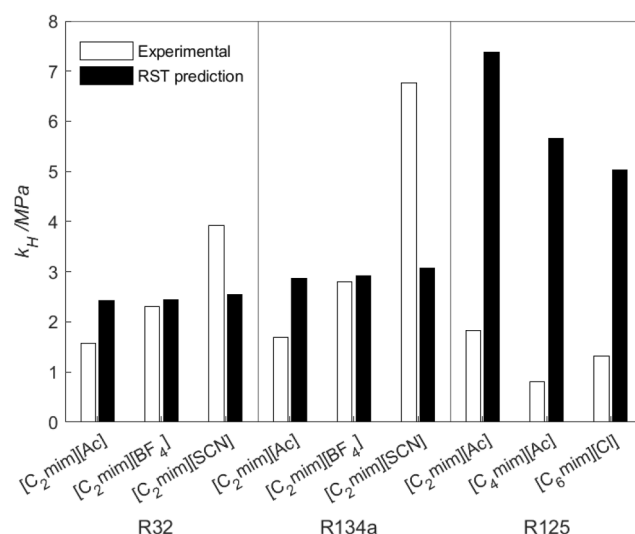


**Fig. 15.** Deviations from RST in the absorption of R32, R134a, and R125 with a selection of ILs.

Yokozeki [158] were originally applied to model the solubility of refrigerants in lubricant oils, and then used to model 33 F-gas—IL systems [64,76,80,82,85,95,126,128,129,159,160] and 13 F-gas—IL systems [86,161], respectively. The Soave-Redlich-Kwong and the Peng-Robinson EoS with typical van der Waals-two parameter mixing rules are other cubic EoS used for modeling systems of HFCs and ILs (5 F-gas—IL systems were modeled using that approach [89,162]). In addition, the Peng-Robinson EoS has also been applied combined with either the Wong-Sandler (17 F-gas—IL systems [163]) or the Adachi and Sugie (R23 + [C<sub>2</sub>mim][PF<sub>6</sub>] [131]) mixing rules. Additionally, the cubic EoS of Peng-Robinson and Valderrama-Patel-Teja modified by Kwak and Mansoori have been used to model the VLE equilibrium of 19 and 13 F-gas—IL mixtures, respectively [153,164,165]. All these cubic EoS and the associated mixing rules are collected in Tables 11 and 12, respectively.

Statistical mechanics EoS are molecular-based approaches that describe the physics of the system, which enhances the model predictive ability and extends its range of application [152]. Both lattice models and chain fluid theories have been used for the description of the equilibrium of refrigerants and ILs. Regarding lattice models, Hekayati et al. used the Sanchez-Lacombe and the  $\epsilon^*$ -modified Sanchez-Lacombe EoS to model 14 refrigerant—IL mixtures [166]. The  $\epsilon^*$ -modified EoS treat the interaction energy as a temperature-dependent parameter, an approach that reported great improvements in the calculation of liquid densities of polar fluids and ILs, especially at high pressures [167]. Shojaeian and Fatoorehchi [168] developed a relatively simple cubic plus association EoS named Peng-Robinson-two state EoS and modeled 20 refrigerant—IL mixtures. The rest of the statistical mechanics EoS used for modeling the equilibrium of refrigerant—IL mixtures belongs to the family of the Statistical Associating Fluid Theory (SAFT), of which the soft-SAFT version has been the most widely applied. The soft-SAFT EoS, which is written in terms of the residual Helmholtz free energy of the system using a Lennard-Jones intermolecular potential as the reference fluid, has shown accurate descriptions of the mixture phase behavior and VLLE predictions [56,79,169]. Other SAFT type equations are the perturbed chain PC-SAFT, which has been implemented to calculate absorption refrigeration cycles [170], the truncated PC-SAFT (tPC-SAFT), only used to model the system R23—[C<sub>4</sub>mim][PF<sub>6</sub>] [171], and the critical-point-based modified PC-SAFT (CP-PC-SAFT), used to purely predict the solubility of R134a and R1234ze(E) in [C<sub>6</sub>mim][Tf<sub>2</sub>N] based on the pure-compound critical properties [172].

The conductor-like screening model for real solvents (COSMO-RS) has been used to predict the VLE of refrigerant—IL mixtures. COSMO-RS



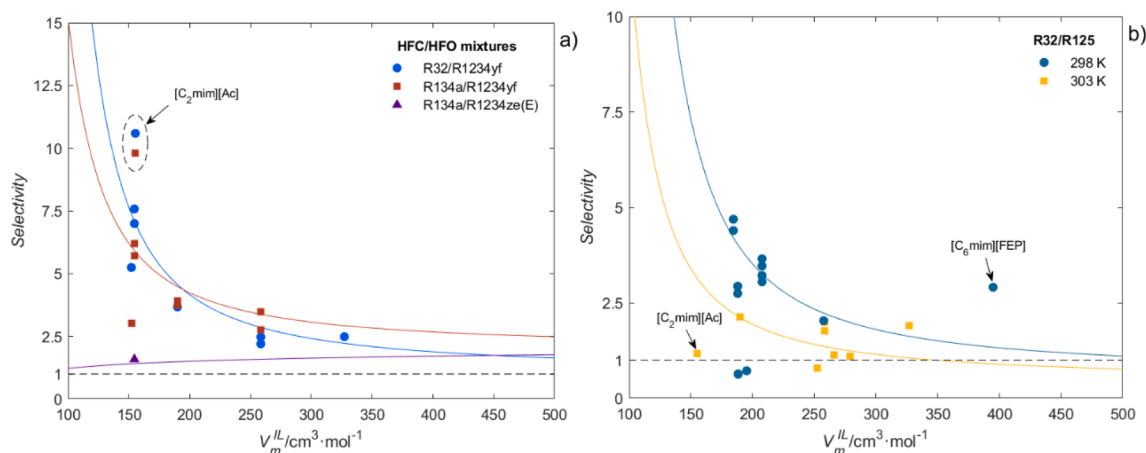


**Fig. 16.** Absorption selectivity for mixtures of (a) R32 and R1234yf (blue ●), R134a and R1234yf (red ■), R134a and R1234ze(E) at 303 K (purple ▲), and (b) R32 and R125 at 298 K (blue ●) and 303 K (yellow ■). The points present the ideal selectivity calculated from experimental data. Continuous lines present the selectivity calculated using the RST model. (For interpretation of the references to color in this figure legend, the reader is referred to the web version of this article.)

calculates the equilibrium using molecular surface polarity distributions obtained from quantum chemical calculations of the pure compounds of the mixture [152]. For the case of refrigerant absorption in ILs, COSMO-RS was used to screen the Henry's law constants of three fluorocarbons

(R134a, R125, and R1234ze(E)) in 900 ILs [173]. The estimated solubility of R134a and R125 in ILs was pretty accurate considering that this is a fully predictive approach, but the absorption of R1234ze(E) was very much overestimated. Furthermore, COSMO-RS has been used to

**Table 11**

Cubic equations of state used to model F-gas—IL mixtures.

Equation	Expression	Parameters	References
Modified van der Waals	$P = \frac{RT}{V_m - b} - \frac{a}{V_m^2}$	$a = \frac{0.421875R^2T_c^2}{P_c} \alpha(T)$ $b = \frac{0.125RT_c}{P_c}$ $\alpha = \sum_{k=0}^{\leq 3} \beta_k \left(\frac{1}{T_r} - T_r\right)^k \quad T_r \leq 1$ $\alpha = \beta_0 + \beta_1 \exp(2(1 - T_r) - 1) T_r \quad T_r > 1$	[86,161]
Modified Redlich-Kwong	$P = \frac{RT}{V_m - b} - \frac{a}{V_m^2 + bV_m}$	$a = \frac{0.42748R^2T_c^2}{P_c} \alpha(T)$ $b = \frac{0.08664RT_c}{P_c}$ $a \text{ equal to that of the modified van der Waals EoS}$	[64,76,80,82,85,95,126,128,129,159,160]
Soave-Redlich-Kwong	$P = \frac{RT}{V_m - b} - \frac{a}{V_m^2 + bV_m}$	$a = \frac{0.42748R^2T_c^2}{P_c} (1 + \kappa(1 - \sqrt{T_r}))^2$ $b = \frac{0.08664RT_c}{P_c}$ $\kappa = 0.480 + 1.574\omega - 0.176\omega^2$	[162]
Peng-Robinson	$P = \frac{RT}{V_m - b} - \frac{a}{V_m^2 + 2bV_m - b^2}$	$a = \frac{0.45724R^2T_c^2}{P_c} (1 + \kappa(1 - \sqrt{T_r}))^2$ $b = \frac{0.07780RT_c}{P_c}$ $\kappa = 0.37464 + 1.54226\omega - 0.26992\omega^2$	[89,131,162,163]
Peng-Robinson/ Kwak-Mansoori	$P = \frac{RT}{V_m - b} - \frac{a + RTd - 2\sqrt{RTad}}{V_m^2 + 2bV_m - b^2}$	$a = a_c(1 + \kappa)^2$ $b = \frac{0.07780RT_c}{P_c}$ $d = \frac{a_c\kappa^2}{RT_c}$ $a_c = \frac{0.45724R^2T_c^2}{P_c}$ $\kappa = 0.37464 + 1.54226\omega - 0.26992\omega^2$	[164]

(continued on next page)

**Table 12**  
Mixing rules used with the cubic equations of state.

Mixing rule	Parameters	Ref.
van der Waals 2-parameter	$a = \sum_{i,j} \sqrt{a_i a_j} (1 - k_{ij}) x_i x_j$ $b = \frac{1}{2} \sum_{i,j} (b_i + b_j) (1 - l_{ij}) x_i x_j$ $k_{ij} = k_{ji} \quad l_{ij} = l_{ji} \quad k_{ii} = l_{ii} = 0$	[89,162]
Yokozeki	$a = \sum_{i,j} \sqrt{a_i a_j} f_{ij} (1 - k_{ij}) x_i x_j$ $b = \frac{1}{2} \sum_{i,j} (b_i + b_j) (1 - k_{ij}) (1 - m_{ij}) x_i x_j$ $f_{ij} = 1 + \frac{\tau_{ij}}{T}$ $k_{ij} = \frac{l_{ij} l_{ji} (x_i + x_j)}{l_{ij} x_i + l_{ji} x_j}$ $l_{ij} = l_{ji} \quad m_{ij} = m_{ji} \quad \tau_{ij} = \tau_{ji} \quad l_{ii} = m_{ii} = \tau_{ii} = 0$	[64,76,80,82,85,86,95,126,128,129,159–161]
Kwak-Mansoori	$a = \sum_{i,j} \sqrt{a_i a_j} f_{ij} (1 - k_{ij}) x_i x_j$ $M = \sum_{i,j} \left( \frac{M_i^{1/3} + M_j^{1/3}}{2} \right)^3 (1 - \mu_{ij}) x_i x_j$ $M \equiv b, c, d \quad \mu \equiv l, m, n \quad k_{ij} = k_{ji} \quad l_{ij} = l_{ji}$ $m_{ij} = m_{ji} \quad k_{ii} = l_{ii} = m_{ii} = 0$	[153,164,165]
Wong-Sandler	$b - \frac{a}{RT} = \sum_{i,j} \left( b - \frac{a}{RT} \right)_{ij} (1 - k_{ij}) x_i x_j$ $b = \frac{\sum_{i,j} \left( b - \frac{a}{RT} \right)_{ij} x_i x_j}{1 - \frac{G^{ex}}{CRT} - \sum_i x_i \frac{a_i}{b_i RT}}$ $a = b \left( \frac{G^{ex}}{C} + \sum_i x_i \frac{a_i}{b_i} \right)$ $\left( b - \frac{a}{RT} \right)_{ij} = \frac{1}{2} \left( \left( b_i - \frac{a_i}{RT} \right) + \left( b_j - \frac{a_j}{RT} \right) \right)$ $k_{ij} = k_{ji} \quad k_{ii} = 0$ <p>For Peng-Robinson, <math>C = -0.62322</math>. <math>G^{ex}</math> can be calculated with NRTL:</p> $\frac{G^{ex}}{RT} = x_1 x_2 \left( \frac{\tau_{21} G_{21}}{x_1 + x_2 G_{21}} + \frac{\tau_{12} G_{12}}{x_2 + x_1 G_{12}} \right)$	[163]
Adachi and Sugie	$a = \sum_{i,j} \sqrt{a_i a_j} (1 - k_{ij} - \lambda_{ij} (x_i - x_j)) x_i x_j$ $b = \frac{1}{2} \sum_{i,j} (b_i + b_j) (1 - l_{ij}) x_i x_j$ $k_{ij} = k_{ji} \quad l_{ij} = l_{ji} \quad \lambda_{ij} = \lambda_{ji} \quad k_{ii} = l_{ii} = \lambda_{ii} = 0$	[131]

predict the R32 and R134a solubility in ILs in order to address the initial stages of the conceptual design of separation processes [174].

Artificial neural networks have also been applied to calculate the solubility of R32 in 17 ILs [175], a work recently extended to cover the solubility of 10 F-gases in 8 ILs for a total of 22 systems [176]. Considering the good results achieved, these networks could be used as a pre-screening tool for the selection of adequate IL solvents.

### 7.3. Process design for separating fluorinated refrigerants using ionic liquids

In addition to systematically describing the phase equilibria of refrigerant gases and ILs and modeling this equilibrium following different approaches, some studies have evaluated the potential use of ILs as entrainers in extractive distillation processes, showing they are promising solvents for separating complex mixtures [32,177].

Two works simulated extractive distillation columns for separating R410A into R32 and R125 using equilibrium models [169,178]. Both

articles used the NRTL model to describe the phase equilibrium and simulated 28 column stages at 1 MPa with two flashes connected in series as shown in Fig. 17. Comparing the results of the two articles reveals that similar purities can be achieved using [C<sub>4</sub>mim][PF<sub>6</sub>] and [C<sub>2</sub>mim][Tf<sub>2</sub>N], while [C<sub>4</sub>mim][PF<sub>6</sub>] resulted in a lower IL flow rate and a reduced reboiler heat duty thanks to its greater solubility selectivity. Further aspects related to the scale-up and the influence of feed composition were evaluated in a patent by Shiflett and Yokozeki [179].

One recent article simulated the capture of either R134a or R32 from streams with 98% argon in an absorption column using equilibrium and rate-based models [174]. In that work, the phase equilibrium was calculated using the COSMO-SAC property model of Aspen Plus v10 treating the ILs as independent ions. Also, the viscosity of the IL was fitted from experimental data using an Arrhenius-like expression. The simulated absorption column (with no reboiler) was operated at 1 bar and the IL was regenerated in another column with a reboiler operating at 423.15 K. For low viscosity ILs, the separation performance predicted by rate-based models was 40% lower than that of equilibrium-based

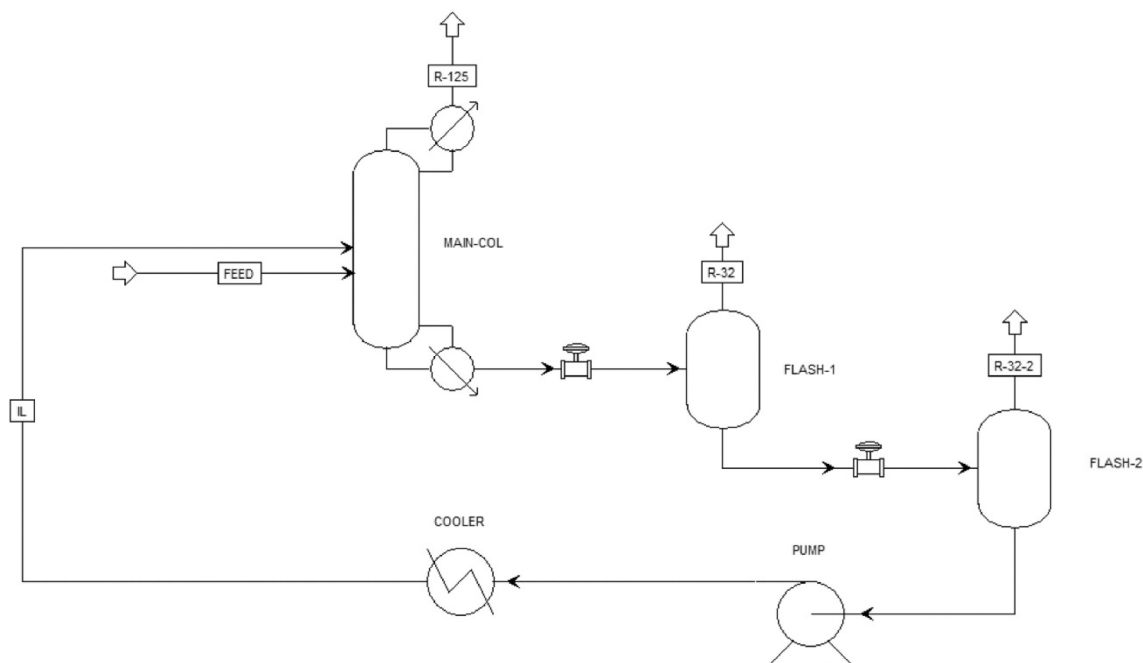


Fig. 17. Process flowsheet of a R410A separation unit using ILs as entrainer. Reprinted with permission from reference [169]. Copyright 2020 Elsevier.

simulations at low temperatures, the difference being attributed to mass transfer limitations. For highly viscous ILs, the rate-based models indicated that the operation would be extremely hindered by the mass transfer limitations at any temperature. Additionally, our review on the viscosity of refrigerant–IL mixtures presented in Section 6.1 suggests that the mixture viscosity does not follow ideal behavior, and therefore, the rate-based models should also consider the non-ideal mixture behavior to obtain more accurate simulation results.

Performing simulations using rate-based models is a step further towards accounting for the reduced separation efficiency caused by the high viscosity of ILs [134,180]. In fact, kinetics and mass transfer have been demonstrated to play a key role in absorption and extractive distillation processes where rate-based models produce accurate descriptions of pilot plant studies [134,136,180,181]. However, these models may require additional data such as mixture viscosities and surface tensions, which are often not available, in order to increase their accuracy. In the absence of mass transfer data, equilibrium model simulations are the best alternative for assessing the performance of extractive distillation columns considering that high viscosity ILs may have low applicability. However, setting a maximum viscosity value above which the IL is not even considered may be too drastic, especially if the sharp decrease expected in the viscosity of the mixture is taken into account.

Another IL property that must be considered in process design is the thermal stability of ILs, particularly regarding the regeneration stages. Typically, short-term ramped temperature analyses are performed to determine the point of thermal degradation, that is, the onset temperature ( $T_{onset}$ ). However, this information should be complemented with long-term isothermal measurements which have proved that significant IL weight losses may occur at temperatures lower than  $T_{onset}$  [182–184]. In general, pyrrolidinium cation cores are more temperature resistant than their imidazolium, pyridinium and tetraalkyl ammonium counterparts; whereas the influence of the anion type has been well correlated to the anion hydrophobicity [182]. For instance, acetate- and halide-based anions significantly reduce the thermal stability while the [Tf<sub>2</sub>N] anion can withstand much higher temperatures [185–187].

So far, the selection of an appropriate IL entrainer with high absorption capacity and selectivity has been the principal approach

followed for the design of F-gases separation processes using ILs. Further steps should evaluate the optimal column design and the IL regeneration stage to minimize the energy requirements and the amount of IL solvent used, while maximizing the final product purity and recovery of the value-added refrigerant gases, as well as perform the cost analysis. In addition, theoretical studies should be validated by experimental work and case studies. In this sense, the phase equilibria of ternary mixtures should be researched experimentally to check whether the equilibrium models provide an accurate description. Also, the first steps should be given to evaluate the separation process at bench scale, as this would provide relevant information about whether the performance of conventional pressure drop and mass transfer correlations for column internals can be extrapolated to IL solvents, especially those with higher viscosity [32,188].

#### 7.4. Refrigerant separations with IL-based membranes

Research into ILs combined with polymer materials has become increasingly important for gas separation using membrane technology. Such hybrid materials can be prepared in different ways: in the form of supported ionic liquid membranes (SILMs); physically blended into composite ionic liquid and polymer membranes (CILPMs); or as polymerizable ionic liquids (PILs) that may contain non-polymerizable ILs (PIL-IL membranes) [189,190]. To date, numerous studies have reported noticeable improvements in the separation of CO<sub>2</sub>/N<sub>2</sub>, CO<sub>2</sub>/CH<sub>4</sub> and CO<sub>2</sub>/H<sub>2</sub> gas pairs, commonly exceeding the so-called Robeson's upper bounds given by conventional polymers [191–193]. These types of IL-based hybrid membranes take advantage of the superior CO<sub>2</sub> solubility in the IL, with respect to that of H<sub>2</sub>/N<sub>2</sub>/CH<sub>4</sub>, to yield membranes that in most cases exhibit improved solubility selectivity values and higher permeability than the base polymer membranes.

The separation of refrigerant mixtures using IL-based membranes has recently been addressed by Pardo et al. [21,22,194–196]. In these works, CILPMs are fabricated by immobilizing the ILs [C<sub>2</sub>mim][SCN], [C<sub>2</sub>mim][BF<sub>4</sub>], [C<sub>2</sub>mim][OTf], and [C<sub>2</sub>mim][Tf<sub>2</sub>N] within the thermoplastic elastomer Pebax®1657, a block copolymer comprising interlinked polyethylene oxide and polyamide-6 segments. In these works, the constituents of the mixtures R410A (50 wt% R32 and R125) and two

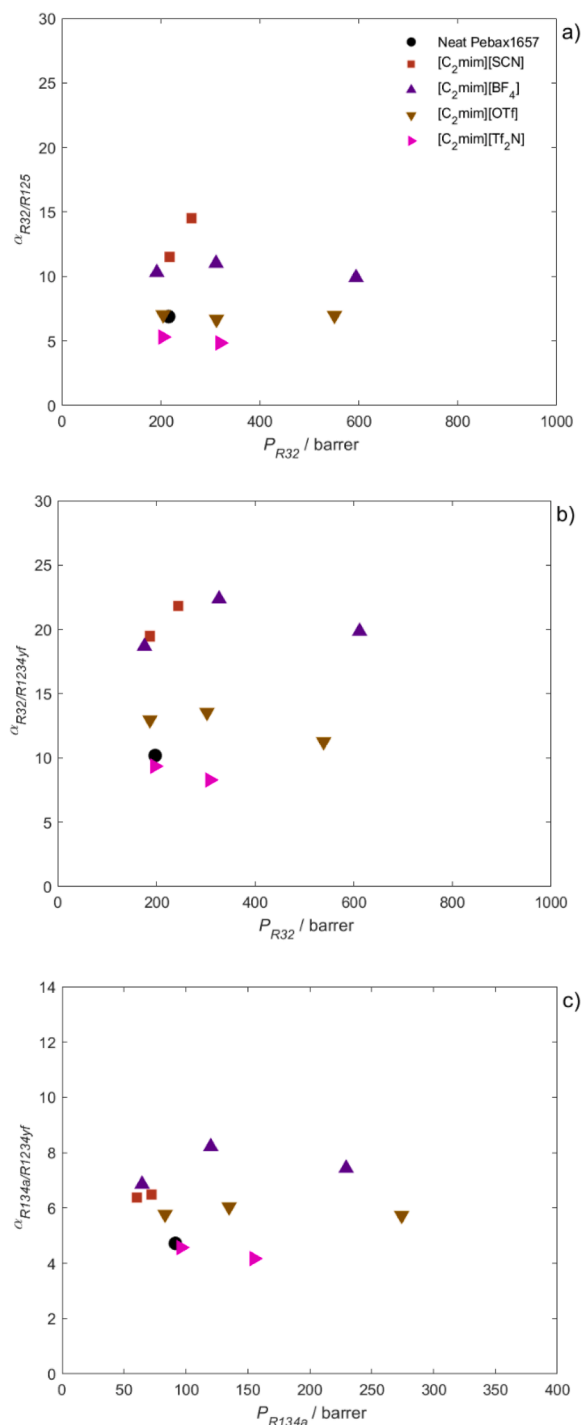


**Fig. 18.** Non-competitive selectivity vs single gas permeability of the fastest gas in neat Pebax® 1657 and CILPMs with [C<sub>2</sub>mim][SCN], [C<sub>2</sub>mim][BF<sub>4</sub>], [C<sub>2</sub>mim][OTf] and [C<sub>2</sub>mim][Tf<sub>2</sub>N] for the gas pairs: a) R32/R125 (T = 303 K, P = 1.86 bar), b) R32/R1234yf (T = 303 K, P = 1.3 bar) and c) R134a/R1234yf (T = 303 K, P = 1.3 bar). Data are taken with permissions from references [22] and [161].

different HFC/HFO mixtures, namely R454B (68.9 wt% R32 and 31.1 wt% R1234yf) and R513A (44 wt% R134a and 56 wt% R1234yf), are separated. The results are shown in Fig. 18, where the ideal (non-competitive) permeability selectivity is plotted against the permeability of the most permeable compound for each separation. In all cases, the CILPMs prepared with the small molar volume ILs [C<sub>2</sub>mim][SCN] and [C<sub>2</sub>mim][BF<sub>4</sub>] significantly improved the ideal selectivity for the gas pairs R32/R125, R32/R1234yf and R134a/R1234yf over the neat polymer membrane.

On the other hand, the ILs [C<sub>2</sub>mim][OTf] and [C<sub>2</sub>mim][Tf<sub>2</sub>N] did not

remarkably improve the permeability selectivity. These results agree well with the observed sorption behavior (Fig. 16), indicating that small molar volume ILs generally favor the solubility difference between pairs of gases. In addition, for both HFC/HFO separations, it was observed that a differential advantage provided by CILPMs containing [C<sub>2</sub>mim][SCN] and [C<sub>2</sub>mim][BF<sub>4</sub>] is that the permeability of R1234yf is blocked due to a sharp solubility decrease in the composite matrix that improves the separation performance towards the recovery of either R32 or R134a. This behavior agrees very well with the predicted R1234yf solubility in small molar volume ILs using the RST (Fig. 14b).

In regard to the IL content of CILPMs, although the increased IL content in this type of hybrid materials significantly increases gas permeability, the mechanical stability of the membrane is compromised. For example, the authors reported that CILPMs with 60 wt% [C<sub>2</sub>mim][BF<sub>4</sub>] did not withstand continuous operation at pressures higher than 4 bar, whereas CILPMs containing 40 wt% [C<sub>2</sub>mim][SCN] were tested for almost one month at pressures up to 12 bar [22].

In conclusion, given that the combined application of IL and polymer membranes currently represent a relatively unexplored field for F-gas separations, it is expected that future studies will focus on the search for novel materials using new polymers and ILs. Those studies should also test the mechanical and functional properties of the composite membranes over long operational periods and at process conditions close to those of the intended applications. Furthermore, the possibility of manufacturing IL-based composite membranes with industrial scale configurations, such as hollow fiber or spiral wound membrane modules, should be explored to determine the real separation potential of these novel materials [197–199].

## 8. Conclusions and prospective view

The international consensus on the negative contribution of HFCs to climate change led to the formulation of several agreements and regulations aimed at reducing the emissions of fluorinated gases. Among others, the global Kigali Amendment to the Montreal Protocol, the SNAP program in the US, and European Regulation 517/2014 schedule 85% reductions in the emission of HFCs by the late 2040s and propose the reclamation of fluorinated gases. This reclamation consists of reprocessing the refrigerant gas recovered during maintenance or prior to disposal to match the equivalent performance of a virgin substance. This context favors the recovery of HFC blends from end-of-life equipment, to then separate the mixtures into their pure components, which would allow those with lower environmental impact to be reused in new, more eco-friendly blends. However, most refrigerant blends behave as azeotropic or close-boiling mixtures that mimic pure compound behavior in terms of vapor–liquid equilibria, complicating the separation and recovery.

ILs are promising as entrainers in the separation process, so this review exhaustively compiles and analyzes the absorption of synthetic fluorinated refrigerants in ILs to act as a reference document for the future design of extractive distillation processes. The wide scope of this review covers the analysis of experimental results of thermodynamic and mass transport properties and the design of refrigerant separations based on the use of ILs in extractive distillation and membrane processes. We have proposed various milestones and guidelines to help authors make decisions with regard to future studies on the absorption of fluorinated gases in ILs:

- The UC-RAIL database provided as [Supplementary Information](#) in this review compiles all the experimental data published up to February 2021 on the absorption of fluorinated refrigerants in ILs. This includes 4444 vapor–liquid equilibrium points for 193 absorption pairs comprising 52 ILs and 26 F-gases, 86 vapor–liquid–liquid equilibrium points of 25 absorption pairs comprising 3 ILs and 16 gases, 249 F-gas–IL mixture viscosity points for 4 systems and 908 diffusion coefficients for 81 absorption pairs comprising 31 ILs and 14 F-gases.
- Our analysis using Henry's law constants establishes that ILs with low molar volumes are the most promising for achieving high selectivity values. Also, one option worth exploring involves those ILs that have strong interactions with fluorinated gases, as is the case of carboxylate anions that deviate from the Regular Solution Theory.
- The mass transport properties have also been compiled, but there is much less information on this, and it should be assessed again in the future. Particularly, the viscosity decay of ILs when they contain absorbed F-gas should be assessed, as the dissolution of refrigerant

gases sharply decreases IL viscosity. This means that ILs which are *a priori* too viscous for operation may still be interesting for the design of extractive distillation processes. This information should also be implemented in process simulators, enabling the process design using robust results that consider the important positive values in excess mixture viscosity.

- There are some examples of process simulations for separating and purifying HFCs from blends in gas–liquid absorption configurations. However, further work is needed to define process integration and optimal design. Furthermore, given the high viscosity of many ILs, the use of rate-based models is recommended.
- Incipient results are available showing the potential of using ILs in membrane processes. Further assessment is needed to determine the optimal operating conditions for separating the refrigerant systems of interest. In addition, although the results are promising, IL-based membranes are still at an early stage of development and more efforts are required to build robust and compact membrane modules with large surface areas and to synthesize IL-based membranes with thin-film selective layers.

Overall, the knowledge of the thermodynamic properties of mixtures of F-gases and ILs is sufficient to allow educated guesses in terms of selecting ILs with potentially high selectivity that could be used to separate many different refrigerant mixtures. Future efforts should focus on evaluating mass transport properties and process design to pave the way to pilot plants and the upscaling of separation process based on the use of ILs, and to shift the refrigeration sector towards a more circular economy model.

## Declaration of Competing Interest

The authors declare that they have no known competing financial interests or personal relationships that could have appeared to influence the work reported in this paper.

## Acknowledgements

The authors fully acknowledge the financial support received from Project KET4F-Gas-SOE2/P1/P0823, which is co-financed by the European Regional Development Fund within the framework of Interreg Sudoe Programme, and project PID2019-105827RB-I00 – Agencia Estatal de Investigación, Spain. S. A.-D. and F. P. acknowledge the FPU grant (18/03939) and the post-doctoral fellowship (FJCI-2017-32884 Juan de la Cierva Formación), respectively, awarded by the Spanish Ministry of Science and Innovation. Marta Romay's graphical abstract is gratefully acknowledged.

## Appendix A. Supplementary material

Supplementary data to this article can be found online at <https://doi.org/10.1016/j.seppur.2021.119363>.

## References

- [1] C. Booten, S. Nicholson, M. Mann, O. Abdelaziz, *Refrigerants: Market Trends and Supply Chain Assessment*, Golden, Colorado, 2020.
- [2] J.M. Calm, The next generation of refrigerants - Historical review, considerations, and outlook, *Int. J. Refrig.* 31 (7) (2008) 1123–1133, <https://doi.org/10.1016/j.ijrefrig.2008.01.013>.
- [3] A.J. Sicard, R.T. Baker, Fluorocarbon Refrigerants and their Syntheses: Past to Present, *Chem. Rev.* 120 (17) (2020) 9164–9303, <https://doi.org/10.1021/acs.chemrev.9b00719>.
- [4] M.O. McLinden, M.L. Huber, (R)Evolution of Refrigerants, *J. Chem. Eng. Data.* 65 (9) (2020) 4176–4193, <https://doi.org/10.1021/acs.jced.0c00338>.
- [5] United Nations, Montreal Protocol on Substances that Deplete the Ozone Layer, USA, 1987. [https://treaties.un.org/Pages/ViewDetails.aspx?src=TREATY&mtdsg\\_no=XXVII-2-a&Chapter=27&lang=en](https://treaties.un.org/Pages/ViewDetails.aspx?src=TREATY&mtdsg_no=XXVII-2-a&Chapter=27&lang=en).



- [6] European Environment Agency, Annual European Union greenhouse gas inventory 1990-2018 and inventory report 2020, Brussels, 2020. <https://www.eea.europa.eu/publications/european-union-greenhouse-gas-inventory-2020>.
- [7] United States Environmental Protection Agency, Inventory of U.S. greenhouse gas emissions and sinks: 1990-2018, 2020. <https://www.epa.gov/gghemissions/inventory-us-greenhouse-gas-emissions-and-sinks-1990-2018>.
- [8] P. Purohit, L. Höglund-Isaksson, J. Dulac, N. Shah, M. Wei, P. Rafaj, W. Schöpp, Electricity savings and greenhouse gas emission reductions from global phase-down of hydrofluorocarbons, *Atmos. Chem. Phys.* 20 (19) (2020) 11305–11327, <https://doi.org/10.5194/acp-20-11305-2020>.
- [9] European Environment Agency, EEA greenhouse gas- data viewer, (n.d.). <https://www.eea.europa.eu/data-and-maps/data/data-viewers/greenhouse-gases-viewer> (accessed September 25, 2020).
- [10] G.J.M. Velders, D.W. Fahey, J.S. Daniel, M. McFarland, S.O. Andersen, The large contribution of projected HFC emissions to future climate forcing, *Proc. Natl. Acad. Sci. U. S. A.* 106 (27) (2009) 10949–10954, <https://doi.org/10.1073/pnas.0902817106>.
- [11] United Nations, Amendment to the Montreal protocol on substances that deplete the ozone layer, (2016).
- [12] E.A. Heath, Amendment to the Montreal Protocol on Substances that Deplete the Ozone Layer (Kigali Amendment), *Int. Leg. Mater.* 56 (1) (2017) 193–205, <https://doi.org/10.1017/ilm.2016.2>.
- [13] European Parliament and Council, EU 517/2014, (2014) 195–230.
- [14] A. Mota-Babiloni, J. Navarro-Esbrí, A. Barragán-Cervera, F. Molés, B. Peris, Analysis based on EU Regulation No 517/2014 of new HFC/HFO mixtures as alternatives of high GWP refrigerants in refrigeration and HVAC systems, *Int. J. Refrig.* 52 (2015) 21–31, <https://doi.org/10.1016/j.ijrefrig.2014.12.021>.
- [15] A. Mota-Babiloni, J. Navarro-Esbrí, F. Molés, A.B. Cervera, B. Peris, G. Verdú, A review of refrigerant R1234ze(E) recent investigations, *Appl. Therm. Eng.* 95 (2016) 211–222, <https://doi.org/10.1016/j.applthermaleng.2015.09.055>.
- [16] M.O. McLinden, J.S. Brown, R. Brignoli, A.F. Kazakov, P.A. Domanski, Limited options for low-global-warming-potential refrigerants, *Nat. Commun.* 8 (2017) 1–9, <https://doi.org/10.1038/ncomms14476>.
- [17] M.O. McLinden, C.J. Seaton, A. Pearson, New refrigerants and system configurations for vapor-compression refrigeration, *Science* (80-) 370 (2020) 791–796, <https://doi.org/10.1126/science.abe3692>.
- [18] A. Mota-Babiloni, P. Makhnatch, R. Khodabandeh, Recent investigations in HFCs substitution with lower GWP synthetic alternatives: Focus on energetic performance and environmental impact, *Int. J. Refrig.* 82 (2017) 288–301, <https://doi.org/10.1016/j.ijrefrig.2017.06.026>.
- [19] G. Morrison, M.O. McLinden, Azeotropy in refrigerant mixtures, *Int. J. Refrig.* 16 (1993) 129–138, [https://doi.org/10.1016/0140-7007\(93\)90069-K](https://doi.org/10.1016/0140-7007(93)90069-K).
- [20] D.K.J.A. Wanigarathna, J. Gao, B. Liu, Metal organic frameworks for adsorption-based separation of fluorocompounds: a review, *Mater. Adv.* 1 (3) (2020) 310–320, <https://doi.org/10.1039/D0MA00083C>.
- [21] F. Pardo, G. Zarca, A. Urtiaga, Separation of Refrigerant Gas Mixtures Containing R32, R134a, and R1234yf through Poly(ether-block-amide) Membranes, *ACS Sustain. Chem. Eng.* 8 (6) (2020) 2548–2556, <https://doi.org/10.1021/acssuschemeng.9b0719510.1021/acssuschemeng.9b07195.s001>.
- [22] F. Pardo, G. Zarca, A. Urtiaga, Effect of feed pressure and long-term separation performance of Pebax-ionic liquid membranes for the recovery of difluoromethane (R32) from refrigerant mixture R410A, *J. Memb. Sci.* 618 (2021) 118744, <https://doi.org/10.1016/j.memsci.2020.118744>.
- [23] J.D. Seader, E.J. Henley, D.K. Roper, *Separation process principles*, 3rd ed, John Wiley & Sons Ltd, New Jersey, USA, 2010.
- [24] D. Han, K.H. Row, Recent Applications of Ionic Liquids in Separation Technology, *Molecules* 15 (2010) 2405–2426, <https://doi.org/10.3390/molecules15042405>.
- [25] T. Welton, Room-Temperature Ionic Liquids. Solvents for Synthesis and Catalysis, *Chem. Rev.* 99 (8) (1999) 2071–2084, <https://doi.org/10.1021/cr980032t>.
- [26] V.I. Părvulescu, C. Hardacre, Catalysis in Ionic Liquids, *Chem. Rev.* 107 (6) (2007) 2615–2665, <https://doi.org/10.1021/cr050948h>.
- [27] D.R. MacFarlane, N. Tachikawa, M. Forsyth, J.M. Pringle, P.C. Howlett, G. D. Elliott, J.H. Davis, M. Watanabe, P. Simon, C.A. Angell, Energy Applications of Ionic Liquids, *Energy Environ. Sci.* 7 (1) (2014) 232–250, <https://doi.org/10.1039/C3EE42099J>.
- [28] T.D. Ho, C. Zhang, L.W. Haantao, J.L. Anderson, Ionic liquids in analytical chemistry: Fundamentals, advances, and perspectives, *Anal. Chem.* 86 (1) (2014) 262–285, <https://doi.org/10.1021/ac4035554>.
- [29] S. Zhang, Q. Zhang, Y. Zhang, Z. Chen, M. Watanabe, Y. Deng, Beyond solvents and electrolytes: Ionic liquids-based advanced functional materials, *Prog. Mater. Sci.* 77 (2016) 80–124, <https://doi.org/10.1016/j.pmatsci.2015.10.001>.
- [30] G. Zarca, I. Ortiz, A. Urtiaga, Novel solvents based on thiocyanate ionic liquids doped with copper(I) with enhanced equilibrium selectivity for carbon monoxide separation from light gases, *Sep. Purif. Technol.* 196 (2018) 47–56, <https://doi.org/10.1016/j.seppur.2017.06.069>.
- [31] Z. Lei, C. Dai, B. Chen, Gas Solubility in Ionic Liquids, *Chem. Rev.* 114 (2) (2014) 1289–1326, <https://doi.org/10.1021/cr300497a>.
- [32] Z. Lei, C. Dai, J. Zhu, B. Chen, Extractive Distillation with Ionic Liquids: A Review, *AIChE J.* 60 (9) (2014) 3312–3329, <https://doi.org/10.1002/aic.v60.910.1002/aic.14537>.
- [33] R. and A.-C.E. American Society of Heating, ASHRAE Refrigerant Designations, (n.d.). <https://www.ashrae.org/technical-resources/standards-and-guidelines/ashrae-refrigerant-designations> (accessed September 25, 2020).
- [34] U.K. Deiters, Some remarks on the nomenclature of refrigerants, *Fluid Phase Equilib.* 132 (1–2) (1997) 265–270, [https://doi.org/10.1016/S0378-3812\(96\)03232-3](https://doi.org/10.1016/S0378-3812(96)03232-3).
- [35] European Fluorocarbons Technical Committee, Refrigerants Subject To The F-Gas Regulation 517/2014, (n.d.). <https://www.fluorocarbons.org/library/> (accessed September 25, 2020).
- [36] C. Kondou, D. BaBa, F. Mishima, S. Koyama, Flow boiling of non-azeotropic mixture R32/R1234ze(E) in horizontal microfin tubes, *Int. J. Refrig.* 36 (8) (2013) 2366–2378, <https://doi.org/10.1016/j.ijrefrig.2013.07.009>.
- [37] Y. Maalem, A. Zarfa, Y. Tamene, S. Fedali, H. Madani, Prediction of thermodynamic properties of the ternary azeotropic mixtures, *Fluid Phase Equilib.* 517 (2020) 112613, <https://doi.org/10.1016/j.fluid.2020.112613>.
- [38] Y. Zhao, Z. Li, X. Zhang, X. Wang, X. Dong, B. Gao, M. Gong, J. Shen, Azeotropic refrigerants and its application in vapor compression refrigeration cycle, *Int. J. Refrig.* 108 (2019) 1–13, <https://doi.org/10.1016/j.ijrefrig.2019.08.024>.
- [39] B.O. Bolaji, Performance investigation of ozone-friendly R404A and R507 refrigerants as alternatives to R22 in a window air-conditioner, *Energy Build.* 43 (11) (2011) 3139–3143, <https://doi.org/10.1016/j.enbuild.2011.08.011>.
- [40] Y. Zhao, M. Gong, X. Dong, H. Zhang, H. Guo, J. Wu, Prediction of ternary azeotropic refrigerants with a simple method, *Fluid Phase Equilib.* 425 (2016) 72–83, <https://doi.org/10.1016/j.fluid.2016.05.010>.
- [41] R. Privat, J.-N. Jaubert, Classification of global fluid-phase equilibrium behaviors in binary systems, *Chem. Eng. Res. Des.* 91 (10) (2013) 1807–1839, <https://doi.org/10.1016/j.cherd.2013.06.026>.
- [42] B.G. Lee, J.Y. Park, J.S. Lim, S.Y. Cho, K.Y. Park, Phase Equilibria of Chlorofluorocarbon Alternative Refrigerant Mixtures, *J. Chem. Eng. Data.* 44 (2) (1999) 190–192, <https://doi.org/10.1021/je980180g>.
- [43] L. Kou, Z. Yang, X. Tang, W. Zhang, J. Lu, Experimental measurements and correlation of isothermal vapor-liquid equilibria for HFC-32 + HFO-1234ze(E) and HFC-134a + HFO-1234ze(E) binary systems, *J. Chem. Thermodyn.* 139 (2019), 105798, <https://doi.org/10.1016/j.jct.2019.04.020>.
- [44] M. Nagel, K. Bier, Vapour-liquid equilibrium of ternary mixtures of the refrigerants R32, R125 and R134a, *Int. J. Refrig.* 18 (8) (1995) 534–543, [https://doi.org/10.1016/0140-7007\(96\)81780-4](https://doi.org/10.1016/0140-7007(96)81780-4).
- [45] J.S. Lim, J.Y. Park, B.G. Lee, Y.W. Lee, Phase equilibria of 1,1,1-trifluoroethane (HFC-143a) + 1,1,1,2-tetrafluoroethane (HFC-134a), and + 1,1-difluoroethane (HFC-152a) at 273.15, 293.15, 303.15, and 313.15 K, *Fluid Phase Equilib.* 193 (2002) 29–39, [https://doi.org/10.1016/S0378-3812\(01\)00632-X](https://doi.org/10.1016/S0378-3812(01)00632-X).
- [46] L.-X. Chen, P. Hu, W.-B. Zhu, L. Jia, Z.-S. Chen, Vapor-liquid equilibria of fluoroethane (HFC-161) + 2,3,3,3-tetrafluoroprop-1-ene (HFO-1234yf), *Fluid Phase Equilib.* 392 (2015) 19–23, <https://doi.org/10.1016/j.fluid.2015.02.014>.
- [47] X. Meng, X. Hu, T. Yang, J. Wu, Vapor liquid equilibria for binary mixtures of difluoromethane (R32) + fluoroethane (R161) and fluoroethane (R161) + trans-1,3,3,3-tetrafluoropropene (R1234ze(E)), *J. Chem. Thermodyn.* 118 (2018) 43–50, <https://doi.org/10.1016/j.jct.2017.10.015>.
- [48] R. Stryjek, P.S. Chappellear, R. Kobayashi, Low-Temperature Vapor-Liquid Equilibria of Nitrogen-Methane System, *J. Chem. Eng. Data.* 19 (1974) 334–339, <https://doi.org/10.1021/je60063a023>.
- [49] S.G. Levy, M.F. Doherty, A simple exact method for calculating tangent pinch points in multicomponent nonideal mixtures by bifurcation theory, *Chem. Eng. Sci.* 41 (12) (1986) 3155–3160, [https://doi.org/10.1016/0009-2509\(86\)85052-7](https://doi.org/10.1016/0009-2509(86)85052-7).
- [50] C.N. Kim, Y.M. Park, Vapor-liquid equilibria for the difluoromethane (HFC-32)+ 1,1,1-trifluoroethane (HFC-143a) system, *J. Chem. Eng. Data.* 45 (1) (2000) 34–37, <https://doi.org/10.1021/je9901379>.
- [51] T. Kamiaka, C. Dang, E. Hihara, Vapor-liquid equilibrium measurements for binary mixtures of R1234yf with R32, R125, and R134a, *Int. J. Refrig.* 36 (3) (2013) 965–971, <https://doi.org/10.1016/j.ijrefrig.2012.08.016>.
- [52] M.H. Barley, J.D. Morrison, A. O'Donnell, I.B. Parker, S. Petherbridge, R. W. Wheelhouse, Vapour-liquid equilibrium data for binary mixtures of some new refrigerants, *Fluid Phase Equilib.* 140 (1–2) (1997) 183–206, [https://doi.org/10.1016/S0378-3812\(97\)00146-5](https://doi.org/10.1016/S0378-3812(97)00146-5).
- [53] S. Horstmann, M. Wilken, K. Fischer, J. Gmehling, Isothermal vapor-liquid equilibrium and excess enthalpy data for the binary systems propylene oxide + 2-methylpentane and difluoromethane (R32) + pentafluoroethane (R125), *J. Chem. Eng. Data.* 49 (6) (2004) 1504–1507, <https://doi.org/10.1021/je034253u>.
- [54] M.B. Shiflett, S.I. Sandler, Modeling fluorocarbon vapor-liquid equilibria using the Wong-Sandler model, *Fluid Phase Equilib.* 147 (1–2) (1998) 145–162, [https://doi.org/10.1016/S0378-3812\(98\)00253-2](https://doi.org/10.1016/S0378-3812(98)00253-2).
- [55] Y. Higashi, Vapor-Liquid Equilibrium, Coexistence Curve, and Critical Locus for Pentafluoroethane + 1,1,1-Trifluoroethane (R125/R143a), *J. Chem. Eng. Data.* 44 (1999) 333–337, <https://doi.org/10.1021/je980266+>.
- [56] C.G. Alba, L.F. Vega, F. Llovel, Assessment on Separating Hydrofluoroolefins from Hydrofluorocarbons at the Azeotropic Mixture R513A by Using Fluorinated Ionic Liquids: A Soft-SAFT Study, *Ind. Eng. Chem. Res.* 59 (29) (2020) 13315–13324, <https://doi.org/10.1021/acs.iecr.0c02331>.
- [57] S. Peper, J.M.S. Fonseca, R. Dohrn, High-pressure fluid-phase equilibria: Trends, recent developments, and systems investigated (2009–2012), *Fluid Phase Equilib.* 484 (2019) 126–224, <https://doi.org/10.1016/j.fluid.2018.10.007>.
- [58] B.R. Mellein, A.M. Scurto, M.B. Shiflett, Gas Solubility in Ionic Liquids, *Curr. Opin. Green Sustain. Chem.* 28 (2021) 100425, <https://doi.org/10.1016/j.cogsc.2020.100425>.
- [59] M.B. Shiflett, A. Yokozeki, Solubilities and Diffusivities of Carbon Dioxide in Ionic Liquids: [bmim][PF6] and [bmim][BF4], *Ind. Eng. Chem. Res.* 44 (2005) 4453–4464, <https://doi.org/10.1021/ie058003d>.
- [60] J.E. Sosa, R.P.P.L. Ribeiro, P.J. Castro, J.P.B. Mota, J.M.M. Araújo, A.B. Pereira, Absorption of Fluorinated Greenhouse Gases Using Fluorinated Ionic Liquids, *Ind.*

- Eng. Chem. Res. 58 (45) (2019) 20769–20778, <https://doi.org/10.1021/acs.iecr.9b04648>10.1021/acs.iecr.9b04648.s001.
- [61] W. Ren, A.M. Scurto, High-pressure phase equilibria with compressed gases, *Rev. Sci. Instrum.* 78 (12) (2007) 125104, <https://doi.org/10.1063/1.2814025>.
- [62] I.M.A. Fonseca, J.P.B. Almeida, H.C. Fachada, Automated apparatus for gas solubility measurements, *J. Chem. Thermodyn.* 39 (10) (2007) 1407–1411, <https://doi.org/10.1016/j.jct.2007.05.013>.
- [63] Z. Lei, J. Yuan, J. Zhu, Solubility of CO<sub>2</sub> in Propanone, 1-Ethyl-3-methylimidazolium Tetrafluoroborate, and Their Mixtures, *J. Chem. Eng. Data.* 55 (10) (2010) 4190–4194, <https://doi.org/10.1021/jc100343v>.
- [64] M.B. Shiflett, A. Yokozeki, Vapor-Liquid-Liquid Equilibria of Pentafluoroethane and Ionic Liquid [bmim][PF<sub>6</sub>] Mixtures Studied with the Volumetric Method, *J. Phys. Chem. B.* 110 (29) (2006) 14436–14443, <https://doi.org/10.1021/jp062437k>.
- [65] Y. Zhang, X. Wang, J. Yin, Viscosity of saturated mixtures of 1-hexyl-3-methylimidazolium bis(trifluoromethylsulfonyl)amide with R600a and R152a, *J. Chem. Thermodyn.* 141 (2020) 105970, <https://doi.org/10.1016/j.jct.2019.105970>.
- [66] A. Aghosseini, W. Ren, L.R. Weatherley, A.M. Scurto, Viscosity and self-diffusivity of ionic liquids with compressed hydrofluorocarbons: 1-Hexyl-3-methylimidazolium bis(trifluoromethylsulfonyl)amide and 1,1,1,2-tetrafluoroethane, *Fluid Phase Equilib.* 437 (2017) 34–42, <https://doi.org/10.1016/j.fluid.2016.11.022>.
- [67] D. Camper, C. Becker, C. Koval, R. Noble, Diffusion and solubility measurements in room temperature ionic liquids, *Ind. Eng. Chem. Res.* 45 (1) (2006) 445–450, <https://doi.org/10.1021/ie0506668>.
- [68] J. Crank, in: *The Mathematics of Diffusion*, 2nd ed, Clarendon Press, Oxford, UK, 1975, [https://doi.org/10.1016/0306-4549\(77\)90072-X](https://doi.org/10.1016/0306-4549(77)90072-X).
- [69] M.B. Shiflett, A. Yokozeki, Solubility and Diffusivity of Hydrofluorocarbons in Room-Temperature Ionic Liquids, *AIChE J.* 52 (3) (2006) 1205–1219, <https://doi.org/10.1002/aic.v52:310.1002/aic.10685>.
- [70] M.B. Shiflett, M.A. Harmer, C.P. Junk, A. Yokozeki, Solubility and Diffusivity of Difluoromethane in Room-Temperature Ionic Liquids, *J. Chem. Eng. Data.* 51 (2) (2006) 483–495, <https://doi.org/10.1021/jc050386z>.
- [71] M.B. Shiflett, A. Yokozeki, J.P. Knapp, Process for the separation of fluorocarbons using ionic liquids, US Patent 7,964,760 B2, 2011.
- [72] M.B. Shiflett, M.A. Harmer, C.P. Junk, A. Yokozeki, Solubility and diffusivity of 1,1,1,2-tetrafluoroethane in room-temperature ionic liquids, *Fluid Phase Equilib.* 242 (2) (2006) 220–232, <https://doi.org/10.1016/j.fluid.2006.01.026>.
- [73] S. Asensio-Delgado, F. Pardo, G. Zarca, A. Urriaga, Vapor–Liquid Equilibria and Diffusion Coefficients of Difluoromethane, 1,1,1,2-Tetrafluoroethane, and 2,3,3,3-Tetrafluoropropene in Low-Viscosity Ionic Liquids, *J. Chem. Eng. Data.* 65 (9) (2020) 4242–4251, <https://doi.org/10.1021/acs.jced.0c00224>.
- [74] G. Yu, Y. Jiang, Z. Lei, Pentafluoroethane Dehydration with Ionic Liquids, *Ind. Eng. Chem. Res.* 57 (36) (2018) 12225–12234, <https://doi.org/10.1021/acs.iecr.8b02790>.
- [75] L.i. Dong, D. Zheng, G. Sun, X. Wu, Vapor–Liquid Equilibrium Measurements of Difluoromethane + [Emim]OTf, Difluoromethane + [Bmim]OTf, Difluoroethane + [Emim]OTf, and Difluoroethane + [Bmim]OTf Systems, *J. Chem. Eng. Data.* 56 (9) (2011) 3663–3668, <https://doi.org/10.1021/jc2005566>.
- [76] M.B. Shiflett, A. Yokozeki, Absorption cycle utilizing ionic liquid as working fluid, US Patent 8715521 B2 (2014).
- [77] S. Asensio-Delgado, F. Pardo, G. Zarca, A. Urriaga, Enhanced absorption separation of hydrofluorocarbon/hydrofluoroolefin refrigerant blends using ionic liquids, *Sep. Purif. Technol.* 249 (2020) 117136, <https://doi.org/10.1016/j.seppur.2020.117136>.
- [78] J.M.M.V. Sousa, J.F.O. Granjo, A.J. Queimada, A.G.M. Ferreira, N.M.C. Oliveira, I.M.A. Fonseca, Solubilities of hydrofluorocarbons in ionic liquids: Experimental and modelling study, *J. Chem. Thermodyn.* 73 (2014) 36–43, <https://doi.org/10.1016/j.jct.2013.07.013>.
- [79] D. Jovell, S. B. Gómez, M.E. Zakrzewska, A.V.M. Nunes, J.M.M. Araújo, A. B. Pereira, F. Llovent, Insight on the Solubility of R134a in Fluorinated Ionic Liquids and Deep Eutectic Solvents, *J. Chem. Eng. Data.* 65 (10) (2020) 4956–4969, <https://doi.org/10.1021/acs.jced.0c00588>10.1021/acs.jced.0c00588.s001.
- [80] M.B. Shiflett, D.R. Corbin, B.A. Elliott, A. Yokozeki, Sorption of trifluoromethane in zeolites and ionic liquid, *J. Chem. Thermodyn.* 64 (2013) 40–49, <https://doi.org/10.1016/j.jct.2013.04.018>.
- [81] D.L. Minnick, M.B. Shiflett, Solubility and Diffusivity of Chlorodifluoromethane in Imidazolium Ionic Liquids: [emim][TF<sub>2</sub>N], [bmim][BF<sub>4</sub>], [bmim][PF<sub>6</sub>], and [emim][TFES], *Ind. Eng. Chem. Res.* 58 (25) (2019) 11072–11081, <https://doi.org/10.1021/acs.iecr.9b02419>.
- [82] M.B. Shiflett, A. Yokozeki, Solubility Differences of Halocarbon Isomers in Ionic Liquid [emim][TF<sub>2</sub>N], *J. Chem. Eng. Data.* 52 (5) (2007) 2007–2015, <https://doi.org/10.1021/jc700295e>.
- [83] W. Ren, A.M. Scurto, M.B. Shiflett, A. Yokozeki, Phase behavior and equilibria of ionic liquids and refrigerants: 1-ethyl-3-methylimidazolium bis(trifluoromethylsulfonyl)imide ([EMIm][TF<sub>2</sub>N]) and R-134a, in: *Gas-Expanded Liq. Near-Critical Media*, 2009, pp. 112–128. <https://doi.org/10.1021/bk-2009-1006.ch006>.
- [84] L.F. Lepre, D. Andre, S. Denis-Quanquin, A. Gautier, A.A.H. Pádua, M. Costa Gomes, Ionic liquids can enable the recycling of fluorinated greenhouse gases, *ACS Sustain. Chem. Eng.* 7 (19) (2019) 16900–16906, <https://doi.org/10.1021/acssuschemeng.9b04214>.
- [85] M.B. Shiflett, A. Yokozeki, Binary Vapor-Liquid and Vapor–Liquid–Liquid Equilibria of Hydrofluorocarbons (HFC-125 and HFC-143a) and Hydrofluoroethers (HFE-125 and HFE-143a) with Ionic Liquid [emim][TF<sub>2</sub>N], *J. Chem. Eng. Data.* 53 (2) (2008) 492–497, <https://doi.org/10.1021/jc700588d>.
- [86] A.R.C. Morais, A.N. Harders, K.R. Baca, G.M. Olsen, B.J. Befort, A.W. Dowling, E. J. Maginn, M.B. Shiflett, Phase Equilibria, Diffusivities, and Equation of State Modeling of HFC-32 and HFC-125 in Imidazolium-based Ionic Liquids for the Separation of R-410A, *Ind. Eng. Chem. Res.* 59 (40) (2020) 18222–18235, <https://doi.org/10.1021/acs.iecr.0c02820>10.1021/acs.iecr.0c02820.s001.
- [87] M.B. Shiflett, A. Yokozeki, Gaseous Absorption of Fluoromethane, Fluoroethane, and 1,1,2,2-Tetrafluoroethane in 1-Butyl-3-Methylimidazolium Hexafluorophosphate, *Ind. Eng. Chem. Res.* 45 (18) (2006) 6375–6382, <https://doi.org/10.1021/ie060192s>.
- [88] M. He, S. Peng, X. Liu, P. Pan, Y. He, Diffusion coefficients and Henry's constants of hydrofluorocarbons in [HMIM][TF<sub>2</sub>N], [HMIM][TfO], and [HMIM][BF<sub>4</sub>], *J. Chem. Thermodyn.* 112 (2017) 43–51, <https://doi.org/10.1016/j.jct.2017.04.009>.
- [89] W. Ren, A.M. Scurto, Phase equilibria of imidazolium ionic liquids and the refrigerant gas, 1,1,1,2-tetrafluoroethane (R-134a), *Fluid Phase Equilib.* 286 (1) (2009) 1–7, <https://doi.org/10.1016/j.fluid.2009.07.007>.
- [90] X. Liu, M.Q. Nguyen, S. Xue, C. Song, M. He, Vapor-Liquid Equilibria and Inter-Diffusion Coefficients for Working Pairs for Absorption Refrigeration Systems Composed of [HMIM][BF<sub>4</sub>] and Fluorinated Propanes, *Int. J. Refrig.* 104 (2019) 34–41, <https://doi.org/10.1016/j.ijrefrig.2019.04.023>.
- [91] X. Liu, P. Pan, M. He, Vapor-liquid equilibrium and diffusion coefficients of R32 + [HMIM][FEP], R152a + [HMIM][FEP] and R161 + [HMIM][FEP], *J. Mol. Liq.* 253 (2018) 28–35, <https://doi.org/10.1016/j.molliq.2018.01.032>.
- [92] X. Liu, M. He, N. Lv, X. Qi, C. Su, Vapor–Liquid Equilibrium of Three Hydrofluorocarbons with [HMIM][TF<sub>2</sub>N], *J. Chem. Eng. Data.* 60 (5) (2015) 1354–1361, <https://doi.org/10.1021/je501069b>.
- [93] X. Liu, M. He, N. Lv, X. Qi, C. Su, Solubilities of R-161 and R-143a in 1-Hexyl-3-methylimidazolium bis(trifluoromethylsulfonyl)imide, *Fluid Phase Equilib.* 388 (2015) 37–42, <https://doi.org/10.1016/j.fluid.2014.12.026>.
- [94] X. Liu, P. Pan, F. Yang, M. He, Solubilities and diffusivities of R227ea, R236fa and R245fa in 1-hexyl-3-methylimidazolium bis(trifluoromethylsulfonyl)imide, *J. Chem. Thermodyn.* 123 (2018) 158–164, <https://doi.org/10.1016/j.jct.2018.04.004>.
- [95] M.B. Shiflett, D.R. Corbin, A. Yokozeki, Comparison of the sorption of trifluoromethane (R-23) on zeolites and in an ionic liquid, *Adsorpt. Sci. Technol.* 31 (1) (2013) 59–83, <https://doi.org/10.1260/0263-6174.31.1.59>.
- [96] J.M.M.V. Sousa, J.F.O. Granjo, A.J. Queimada, A.G.M. Ferreira, N.M.C. Oliveira, I.M.A. Fonseca, Solubility of hydrofluorocarbons in phosphonium-based ionic liquids: Experimental and modelling study, *J. Chem. Thermodyn.* 79 (2014) 184–191, <https://doi.org/10.1016/j.jct.2014.08.001>.
- [97] X. Liu, N. Lv, C. Su, M. He, Solubilities of R32, R245fa, R227ea and R236fa in a phosphonium-based ionic liquid, *J. Mol. Liq.* 218 (2016) 525–530, <https://doi.org/10.1016/j.molliq.2016.02.041>.
- [98] X. Liu, X. Qi, N. Lv, M. He, Gaseous absorption of fluorinated ethanes by ionic liquids, *Fluid Phase Equilib.* 405 (2015) 1–6, <https://doi.org/10.1016/j.fluid.2015.07.001>.
- [99] L.F. Lepre, L. Pison, I. Otero, A. Gautier, J. Dévemy, P. Husson, A.A.H. Pádua, M. Costa Gomes, Using hydrogenated and perfluorinated gases to probe the interactions and structure of fluorinated ionic liquids, *Phys. Chem. Chem. Phys.* 21 (17) (2019) 8865–8873, <https://doi.org/10.1039/C9CP00593E>.
- [100] B.J. Costa Cabral, R.C. Guedes, R.S. Pai-Pandikar, C.A. Nieto de Castro, Hydrogen bonding and the dipole moment of hydrofluorocarbons by density functional theory, *Phys. Chem. Chem. Phys.* 3 (2001) 4200–4207, <https://doi.org/10.1039/b102879k>.
- [101] E. Kryachko, S. Scheiner, CH...F hydrogen bonds. Dimers of fluoromethanes, *J. Phys. Chem. A.* 108 (2004) 2527–2535, <https://doi.org/10.1021/jp0365108>.
- [102] M. Karamodini, F. Varaminian, Solubility of R22, R23, R32, R134a, R152a, R125 and R744 refrigerants in water by using equations of state, *Int. J. Refrig.* 36 (6) (2013) 1681–1688, <https://doi.org/10.1016/j.ijrefrig.2013.04.013>.
- [103] Q.R. Sheridan, W.F. Schneider, E.J. Maginn, Role of Molecular Modeling in the Development of CO<sub>2</sub>-Reactive Ionic Liquids, *Chem. Rev.* 118 (2018) 5242–5260, <https://doi.org/10.1021/acs.chemrev.8b00017>.
- [104] T. Endo, Y. Nishisaka, Y. Kin, Y. Kimura, Systematic estimation and interpretation of fractional free volume in 1-alkyl-3-methylimidazolium-based ionic liquids, *Fluid Phase Equilib.* 498 (2019) 144–150, <https://doi.org/10.1016/j.fluid.2019.06.027>.
- [105] X. Liu, K.E. O'Harra, J.E. Bara, C.H. Turner, Molecular Insight into the Anion Effect and Free Volume Effect of CO<sub>2</sub> Solubility in Multivalent Ionic Liquids, *Phys. Chem. Chem. Phys.* 22 (36) (2020) 20618–20633, <https://doi.org/10.1039/D0CP03424J>.
- [106] M.S. Shannon, J.M. Tedstone, S.P.O. Danielsen, M.S. Hindman, A.C. Irvin, J. E. Bara, Free volume as the basis of gas solubility and selectivity in imidazolium-based ionic liquids, *Ind. Eng. Chem. Res.* 51 (15) (2012) 5565–5576, <https://doi.org/10.1021/ie202916e>.
- [107] P.J. Carvalho, K.A. Kurnia, J.A.P. Coutinho, Dispelling some myths about the CO<sub>2</sub> solubility in ionic liquids, *Phys. Chem. Chem. Phys.* 18 (22) (2016) 14757–14771, <https://doi.org/10.1039/C6CP01896C>.
- [108] Y. Sun, Y. Zhang, G. Di, X. Wang, J.M. Prausnitz, L. Jin, Vapor-Liquid Equilibria for R1234ze(E) and Three Imidazolium-Based Ionic Liquids as Working Pairs in Absorption-Refrigeration Cycle, *J. Chem. Eng. Data.* 63 (8) (2018) 3053–3060, <https://doi.org/10.1021/acs.jced.8b00314>10.1021/acs.jced.8b00314.s001.
- [109] D.L. Minnick, M.B. Shiflett, Solubility and Diffusivity of Bromodifluoromethane (Halon-1201) in Imidazolium Ionic Liquids: [C2C1im][TF<sub>2</sub>N], [C4C1im][BF<sub>4</sub>], and [C4C1im][PF<sub>6</sub>], *J. Chem. Eng. Data.* 65 (7) (2020) 3277–3286, <https://doi.org/10.1021/acs.jced.0c00022>.

- [110] Y. Zhang, J. Yin, X. Wang, Vapor-liquid equilibrium of 2,3,3,3-tetrafluoroprop-1-ene with 1-butyl-3-methylimidazolium hexafluorophosphate, 1-hexyl-3-methylimidazolium hexafluorophosphate, and 1-octyl-3-methylimidazolium hexafluorophosphate, *J. Mol. Liq.* 260 (2018) 203–208, <https://doi.org/10.1016/j.molliq.2018.03.112>.
- [111] M. He, P. Pan, F. Yang, T. Wang, X. Liu, Gaseous Absorption of trans-1-Chloro-3,3,3-trifluoropropene in Three Imidazolium-Based Ionic Liquids, *J. Chem. Eng. Data.* 63 (5) (2018) 1780–1788, <https://doi.org/10.1021/acs.jced.8b00110>.
- [112] X. Liu, L. Bai, S. Liu, M. He, Vapor–Liquid Equilibrium of R1234yf/[HMIM][TF2N] and R1234ze (E)/[HMIM][TF2N] Working Pairs for the Absorption Refrigeration Cycle, *J. Chem. Eng. Data.* 61 (11) (2016) 3952–3957, <https://doi.org/10.1021/acs.jced.6b00731>.
- [113] J.L. Anthony, E.J. Maginn, J.F. Brennecke, Solubilities and thermodynamic properties of gases in the ionic liquid 1-n-butyl-3-methylimidazolium hexafluorophosphate, *J. Phys. Chem. B.* 106 (29) (2002) 7315–7320, <https://doi.org/10.1021/jp020631a>.
- [114] M.F. Costa Gomes, Low-pressure solubility and thermodynamics of solvation of carbon dioxide, ethane, and hydrogen in 1-hexyl-3-methylimidazolium bis(trifluoromethylsulfonyl) amide between temperatures of 283 K and 343 K, *J. Chem. Eng. Data.* 52 (2) (2007) 472–475, <https://doi.org/10.1021/je0604129>.
- [115] C.M. Sanchez, T. Song, J.F. Brennecke, B.D. Freeman, Hydrogen Stable Supported Ionic Liquid Membranes with Silver Carriers: Propylene and Propane Permeability and Solubility, *Ind. Eng. Chem. Res.* 59 (12) (2020) 5362–5370, <https://doi.org/10.1021/acs.iecr.9b04886>.
- [116] D. Camper, C. Becker, C. Koval, R. Noble, Low pressure hydrocarbon solubility in room temperature ionic liquids containing imidazolium rings interpreted using regular solution theory, *Ind. Eng. Chem. Res.* 44 (6) (2005) 1928–1933, <https://doi.org/10.1021/ie049312r>.
- [117] F.A.M.M. Gonçalves, C.S.M.F. Costa, C.E. Ferreira, J.C.S. Bernardo, I. Johnson, I. M.A. Fonseca, A.G.M. Ferreira, Pressure-volume-temperature measurements of phosphonium-based ionic liquids and analysis with simple equations of state, *J. Chem. Thermodyn.* 43 (6) (2011) 914–929, <https://doi.org/10.1016/j.jct.2011.01.009>.
- [118] Y. Sun, Y. Zhang, X. Wang, J.M. Prausnitz, L. Jin, Gaseous absorption of 2,3,3,3-tetrafluoroprop-1-ene in three imidazolium-based ionic liquids, *Fluid Phase Equilib.* 450 (2017) 65–74, <https://doi.org/10.1016/j.fluid.2017.07.013>.
- [119] X. Wang, Y. Zhang, D. Wang, Y. Sun, Phase Equilibria of trans-1,3,3,3-Tetrafluoropropene with Three Imidazolium Ionic Liquids, *J. Chem. Eng. Data.* 62 (6) (2017) 1825–1831, <https://doi.org/10.1021/acs.jced.7b00047>.
- [120] Y.F. Hu, Z.C. Liu, C.M. Xu, X.M. Zhang, The molecular characteristics dominating the solubility of gases in ionic liquids, *Chem. Soc. Rev.* 40 (2011) 3802–3823, <https://doi.org/10.1039/c0cs00006j>.
- [121] Y. Sun, G. Di, J. Wang, Y. Hu, X. Wang, M. He, Gaseous solubility and thermodynamic performance of absorption system using R1234yf / IL working pairs, *Appl. Therm. Eng.* 172 (2020) 115161, <https://doi.org/10.1016/j.applthermaleng.2020.115161>.
- [122] X. Liu, Z. Ye, L. Bai, M. He, Performance comparison of two absorption-compression hybrid refrigeration systems using R1234yf/ionic liquid as working pair, *Energy Convers. Manag.* 181 (2019) 319–330, <https://doi.org/10.1016/j.enconman.2018.12.030>.
- [123] K. Kontomaris, N.C. Moull, M.B. Shiflett, Compositions comprising ionic liquids and fluoroolefins and use thereof in absorption cycle systems, US Patent Application 2011/0088418 A1, 2011.
- [124] A. Mota-Babiloni, M. Mastani Joybari, J. Navarro-Esbrí, C. Mateu-Royo, Á. Barragán-Cervera, M. Amat-Albuixech, F. Molés, Ultralow-temperature refrigeration systems: Configurations and refrigerants to reduce the environmental impact, *Int. J. Refrig.* 111 (2020) 147–158, <https://doi.org/10.1016/j.ijrefrig.2019.11.016>.
- [125] L. Pison, J.N. Canongia Lopes, L.P.N. Rebelo, A.A.H. Padua, M.F. Costa Gomes, Interactions of fluorinated gases with ionic liquids: Solubility of CF<sub>4</sub>, C<sub>2</sub>F<sub>6</sub>, and C<sub>3</sub>F<sub>8</sub> in trihexyltetradecylphosphonium bis(trifluoromethylsulfonyl)amide, *J. Phys. Chem. B.* 112 (39) (2008) 12394–12400, <https://doi.org/10.1021/jp8051714>.
- [126] J. Kumelan, Á. Pérez-Salado Kamps, D. Tuma, A. Yokozeki, M.B. Shiflett, G. Maurer, Solubility of tetrafluoromethane in the ionic liquid [hmim][TF2N], *J. Phys. Chem. B.* 112 (10) (2008) 3040–3047, <https://doi.org/10.1021/jp076737t>.
- [127] W. Ren, A.M. Scurto, Global phase behavior of imidazolium ionic liquids and compressed 1,1,1,2-tetrafluoroethane (R-134a), *AIChE J.* 55 (2) (2009) 486–493, <https://doi.org/10.1002/aic.v55:210.1002/aic.11657>.
- [128] A. Yokozeki, M.B. Shiflett, Global phase behaviors of trifluoromethane in ionic liquid [bmim][PF6], *AIChE J.* 52 (11) (2006) 3952–3957, [https://doi.org/10.1002/\(ISSN\)1547-5905.10.1002/aic.v52:1110.1002/aic.11007](https://doi.org/10.1002/(ISSN)1547-5905.10.1002/aic.v52:1110.1002/aic.11007).
- [129] M.B. Shiflett, A. Yokozeki, Vapor-Liquid-Liquid Equilibria of Hydrofluorocarbons + 1-Butyl-3-methylimidazolium Hexafluorophosphate, *J. Chem. Eng. Data.* 51 (5) (2006) 1931–1939, <https://doi.org/10.1021/je060275f10.1021/je060275f.s001>.
- [130] M.B. Shiflett, A. Yokozeki, Hydrogen substitution effect on the solubility of perhalogenated compounds in ionic liquid [bmim][PF6], *Fluid Phase Equilib.* 259 (2) (2007) 210–217, <https://doi.org/10.1016/j.fluid.2007.07.035>.
- [131] A. Shariati, C.J. Peters, High-pressure phase behavior of systems with ionic liquids: measurements and modeling of the binary system fluoroform + 1-ethyl-3-methylimidazolium hexafluorophosphate, *J. Supercrit. Fluids.* 25 (2) (2003) 109–117, [https://doi.org/10.1016/S0896-8446\(02\)00160-2](https://doi.org/10.1016/S0896-8446(02)00160-2).
- [132] A. Shariati, K. Gutkowski, C.J. Peters, Comparison of the Phase Behavior of Some Selected Binary Systems with Ionic Liquids, *AIChE J.* 51 (5) (2005) 1532–1540, <https://doi.org/10.1002/aic.v51:510.1002/aic.10384>.
- [133] K. Dong, X. Liu, H. Dong, X. Zhang, S. Zhang, Multiscale Studies on Ionic Liquids, *Chem. Rev.* 117 (10) (2017) 6636–6695, <https://doi.org/10.1021/acs.chemrev.6b00776>.
- [134] M.T. Mota-Martinez, P. Brandl, J.P. Hallett, N. Mac Dowell, Challenges and opportunities for the utilisation of ionic liquids as solvents for CO<sub>2</sub> capture, *Mol. Syst. Des. Eng.* 3 (3) (2018) 560–571, <https://doi.org/10.1039/C8ME00009C>.
- [135] K. Li, W. Wu, J. Wu, H. Liang, H. Zhang, Experiments on vapour-liquid equilibrium of CO<sub>2</sub>-ionic liquid under flow conditions and influence on its refrigeration cycle, *Appl. Therm. Eng.* 180 (2020) 115865, <https://doi.org/10.1016/j.applthermaleng.2020.115865>.
- [136] J. Palomar, M. Larriba, J. Lemus, D. Moreno, R. Santiago, C. Moya, J. de Riva, G. Pedrosa, Demonstrating the key role of kinetics over thermodynamics in the selection of ionic liquids for CO<sub>2</sub> physical absorption, *Sep. Purif. Technol.* 213 (2019) 578–586, <https://doi.org/10.1016/j.seppur.2018.12.059>.
- [137] J. Wang, Z. Song, H. Cheng, L. Chen, L. Deng, Z. Qi, Multilevel screening of ionic liquid absorbents for simultaneous removal of CO<sub>2</sub> and H<sub>2</sub>S from natural gas, *Sep. Purif. Technol.* 248 (2020) 117053, <https://doi.org/10.1016/j.seppur.2020.117053>.
- [138] J. Wang, Z. Song, H. Cheng, L. Chen, L. Deng, Z. Qi, Computer-Aided Design of Ionic Liquids as Absorbent for Gas Separation Exemplified by CO<sub>2</sub> Capture Cases, *ACS Sustain. Chem. Eng.* 6 (9) (2018) 12025–12035, <https://doi.org/10.1021/acsuschemeng.8b0232110.1021/acsuschemeng.8b02321.s001>.
- [139] M.G. Freire, A.R.R. Teles, M.A.A. Rocha, B. Schröder, C.M.S.S. Neves, P. J. Carvalho, D.V. Evtuguin, L.M.N.B.F. Santos, J.A.P. Coutinho, Thermophysical Characterization of Ionic Liquids Able To Dissolve Biomass, *J. Chem. Eng. Data.* 56 (12) (2011) 4813–4822, <https://doi.org/10.1021/je200790q>.
- [140] J.A. Widegren, J.W. Magee, Density, viscosity, speed of sound, and electrolytic conductivity for the ionic liquid 1-hexyl-3-methylimidazolium bis(trifluoromethylsulfonyl)imide and its mixtures with water, *J. Chem. Eng. Data.* 52 (6) (2007) 2331–2338, <https://doi.org/10.1021/je700329a>.
- [141] Y. Zhang, X. Jia, X. Wang, Experimental investigation on the viscosity of [Hmim][TF2N] saturated with R1234ze(E) or R1234yf, *Int. J. Refrig.* 117 (2020) 338–345, <https://doi.org/10.1016/j.ijrefrig.2020.04.018>.
- [142] I.H. Bell, J. Wronski, S. Quoilin, V. Lemort, Pure and Pseudo-pure Fluid Thermophysical Property Evaluation and the Open-Source Thermophysical Property Library CoolProp, *Ind. Eng. Chem. Res.* 53 (6) (2014) 2498–2508, <https://doi.org/10.1021/ie4033999>.
- [143] J. Kendall, K.P. Monroe, The viscosity of liquids. II. The viscosity-composition curve for ideal liquid mixtures, *J. Am. Chem. Soc.* 39 (1917) 1787–1802, <https://doi.org/10.1021/cen-v023n003.p224>.
- [144] S. Atashrouz, M. Zarghampour, S. Abdollahi, G. Pazuki, B. Nasernejad, Estimation of the viscosity of ionic liquids containing binary mixtures based on the Eyring's theory and a modified Gibbs energy model, *J. Chem. Eng. Data.* 59 (11) (2014) 3691–3704, <https://doi.org/10.1021/je500572t>.
- [145] D. Camper, J. Bara, C. Koval, R. Noble, Bulk-fluid solubility and membrane feasibility of Rmim-based room-temperature ionic liquids, *Ind. Eng. Chem. Res.* 45 (18) (2006) 6279–6283, <https://doi.org/10.1021/ie060177n>.
- [146] S. Zeng, X. Zhang, L.u. Bai, X. Zhang, H. Wang, J. Wang, D.i. Bao, M. Li, X. Liu, S. Zhang, Ionic-Liquid-Based CO<sub>2</sub> Capture Systems: Structure, Interaction and Process, *Chem. Rev.* 117 (14) (2017) 9625–9673, <https://doi.org/10.1021/acs.chemrev.7b00072>.
- [147] G. Zarca, I. Ortiz, A. Urriaga, Recovery of carbon monoxide from flue gases by reactive absorption in ionic liquid imidazolium chlorocuprate(I): Mass transfer coefficients, *Chinese J. Chem. Eng.* 23 (5) (2015) 769–774, <https://doi.org/10.1016/j.cjche.2014.06.040>.
- [148] S.S. Moganty, R.E. Baltus, Diffusivity of carbon dioxide in room-temperature ionic liquids, *Ind. Eng. Chem. Res.* 49 (19) (2010) 9370–9376, <https://doi.org/10.1021/ie101260j>.
- [149] T. Wang, X. Liu, J. Chu, Y. Shi, J. Li, M. He, Molecular dynamics simulation of diffusion and interaction of [bmim][TF2N] + HFO-1234yf mixture, *J. Mol. Liq.* 312 (2020), 113390, <https://doi.org/10.1016/j.molliq.2020.113390>.
- [150] J.E. Bara, T.K. Carlisle, C.J. Gabriel, D. Camper, A. Finotello, D.L. Gin, R.D. Noble, Guide to CO<sub>2</sub> separations in imidazolium-based room-temperature ionic liquids, *Ind. Eng. Chem. Res.* 48 (6) (2009) 2739–2751, <https://doi.org/10.1021/ie8016237>.
- [151] S.S. Moganty, R.E. Baltus, Regular solution theory for low pressure carbon dioxide solubility in room temperature ionic liquids: Ionic liquid solubility parameter from activation energy of viscosity, *Ind. Eng. Chem. Res.* 49 (12) (2010) 5846–5853, <https://doi.org/10.1021/ie901837k>.
- [152] L.F. Vega, O. Vilaseca, F. Llovel, J.S. Andreu, Modeling ionic liquids and the solubility of gases in them: Recent advances and perspectives, *Fluid Phase Equilib.* 294 (1–2) (2010) 15–30, <https://doi.org/10.1016/j.fluid.2010.02.006>.
- [153] C.A. Faúndez, J.O. Valderrama, R.A. Campusano, Henry's law constant as a function of temperature and pressure to calculate the solubility of difluoromethane (R-32) in ionic liquids, *Int. J. Refrig.* 119 (2020) 401–409, <https://doi.org/10.1016/j.ijrefrig.2020.05.024>.
- [154] W. Wu, T. You, H. Zhang, X. Li, Comparisons of different ionic liquids combined with trans-1,3,3,3-tetrafluoropropene (R1234ze(E)) as absorption working fluids, *Int. J. Refrig.* 88 (2018) 45–57, <https://doi.org/10.1016/j.ijrefrig.2017.12.011>.
- [155] Y.J. Kim, S. Kim, Y.K. Joshi, A.G. Fedorov, P.A. Kohl, Thermodynamic analysis of an absorption refrigeration system with ionic-liquid/refrigerant mixture as a working fluid, *Energy.* 44 (1) (2012) 1005–1016, <https://doi.org/10.1016/j.energy.2012.04.048>.
- [156] L.i. Dong, D. Zheng, X. Wu, Working pair selection of compression and absorption hybrid cycles through predicting the activity coefficients of hydrofluorocarbon +



- ionic liquid systems by the UNIFAC model, *Ind. Eng. Chem. Res.* 51 (12) (2012) 4741–4747, <https://doi.org/10.1021/ie202029d>.
- [157] L. Bai, M. He, X. Liu, Z. Ye, A new activity coefficient model for the solution of molecular solute + ionic liquid, *Fluid Phase Equilib.* 493 (2019) 144–152, <https://doi.org/10.1016/j.fluid.2019.04.016>.
- [158] A. Yokozeki, Solubility of refrigerants in various lubricants, *Int. J. Thermophys.* 22 (2001) 1057–1071, <https://doi.org/10.1023/A:1010695705260>.
- [159] S. Kim, P.A. Kohl, Analysis of [hmim][PF<sub>6</sub>] and [hmim][TF<sub>2</sub>N] ionic liquids as absorbents for an absorption refrigeration system, *Int. J. Refrig.* 48 (2014) 105–113, <https://doi.org/10.1016/j.ijrefrig.2014.09.003>.
- [160] S. Kim, N. Patel, P.A. Kohl, Performance simulation of ionic liquid and hydrofluorocarbon working fluids for an absorption refrigeration system, *Ind. Eng. Chem. Res.* 52 (19) (2013) 6329–6335, <https://doi.org/10.1021/ie400261g>.
- [161] A. Yokozeki, M.B. Shiflett, Gas solubilities in ionic liquids using a generic van der Waals equation of state, *J. Supercrit. Fluids.* 55 (2) (2010) 846–851, <https://doi.org/10.1016/j.supflu.2010.09.015>.
- [162] A.C.D. Freitas, L.P. Cunico, M. Aznar, R. Guirardello, Modeling vapor liquid equilibrium of ionic liquids + gas binary systems at high pressure with cubic equations of state, *Brazilian J. Chem. Eng.* 30 (1) (2013) 63–73, <https://doi.org/10.1590/S0104-66322013000100008>.
- [163] K. Parvaneh, A. Rasoolzadeh, A. Shariati, Modeling the phase behavior of refrigerants with ionic liquids using the QC-PC-SAFT equation of state, *J. Mol. Liq.* 274 (2019) 497–504, <https://doi.org/10.1016/j.molliq.2018.10.116>.
- [164] C.A. Faúndez, L.A. Barrientos, J.O. Valderrama, Modeling and thermodynamic consistency of solubility data of refrigerants in ionic liquids, *Int. J. Refrig.* 36 (8) (2013) 2242–2250, <https://doi.org/10.1016/j.ijrefrig.2013.06.006>.
- [165] J.O. Valderrama, C.A. Faúndez, R. Campusano, An overview of a thermodynamic consistency test of phase equilibrium data. Application of the versatile VPT equation of state to check data of mixtures containing a gas solute and an ionic liquid solvent, *J. Chem. Thermodyn.* 131 (2019) 122–132, <https://doi.org/10.1016/j.jct.2018.09.019>.
- [166] J. Hekayati, A. Roosta, J. Javanmardi, Thermodynamic modeling of refrigerants solubility in ionic liquids using original and e<sup>\*</sup>-Modified Sanchez-Lacombe equations of state, *Fluid Phase Equilib.* 403 (2015) 14–22, <https://doi.org/10.1016/j.fluid.2015.05.046>.
- [167] H. Machida, Y. Sato, R.L. Smith, Simple modification of the temperature dependence of the Sanchez-Lacombe equation of state, *Fluid Phase Equilib.* 297 (2) (2010) 205–209, <https://doi.org/10.1016/j.fluid.2010.03.024>.
- [168] A. Shojaeian, H. Fatoorehchi, Modeling solubility of refrigerants in ionic liquids using Peng Robinson-Two State equation of state, *Fluid Phase Equilib.* 486 (2019) 80–90, <https://doi.org/10.1016/j.fluid.2019.01.003>.
- [169] S. Asensio-Delgado, D. Jovell, G. Zarca, A. Urriaga, F. Llovel, Thermodynamic and process modeling of the recovery of R410A compounds with ionic liquids, *Int. J. Refrig.* 118 (2020) 365–375, <https://doi.org/10.1016/j.ijrefrig.2020.04.013>.
- [170] I. Sujatha, G. Venkatarathnam, Comparison of performance of a vapor absorption refrigeration system operating with some hydrofluorocarbons and hydrofluoroolefins as refrigerants along with ionic liquid [hmim][TF<sub>2</sub>N] as the absorbent, *Int. J. Refrig.* 88 (2018) 370–382, <https://doi.org/10.1016/j.ijrefrig.2018.03.004>.
- [171] E.K. Karakatsani, I.G. Economou, M.C. Kroon, C.J. Peters, G.J. Witkamp, tPC-SAFT modeling of gas solubility in imidazolium-based ionic liquids, *J. Phys. Chem. C* 111 (2007) 15487–15492, <https://doi.org/10.1021/jp070556+>.
- [172] I. Polishuk, Implementation of CP-PC-SAFT for Predicting Thermodynamic Properties and Gas Solubility in 1-Alkyl-3-methylimidazolium Bis (trifluoromethylsulfonyl)imide Ionic Liquids without Fitting Binary Parameters, *Ind. Eng. Chem. Res.* 56 (27) (2017) 7845–7857, <https://doi.org/10.1021/acs.iecr.7b01846>.
- [173] D. Moreno, V.R. Ferro, J. de Riva, R. Santiago, C. Moya, M. Larriba, J. Palomar, Absorption refrigeration cycles based on ionic liquids: Refrigerant/absorbent selection by thermodynamic and process analysis, *Appl. Energy* 213 (2018) 179–194, <https://doi.org/10.1016/j.apenergy.2018.01.034>.
- [174] J.E. Sosa, R. Santiago, D. Hospital-Benito, M.F. Costa Gomes, J.M.M. Araújo, A. B. Pereiro, J. Palomar, Process Evaluation of Fluorinated Ionic Liquids as F-Gases Absorbents, *Environ. Sci. Technol.* (2020), <https://doi.org/10.1021/acs.est.0c05305>.
- [175] C.A. Faúndez, R.A. Campusano, J.O. Valderrama, Misleading results on the use of artificial neural networks for correlating and predicting properties of fluids. A case on the solubility of refrigerant R-32 in ionic liquids, *J. Mol. Liq.* 298 (2020) 112009, <https://doi.org/10.1016/j.molliq.2019.112009>.
- [176] E.N. Fierro, C.A. Faúndez, A.S. Muñoz, Influence of thermodynamically inconsistent data on modeling the solubilities of refrigerants in ionic liquids using an artificial neural network, *J. Mol. Liq.* 337 (2021) 116417, <https://doi.org/10.1016/j.molliq.2021.116417>.
- [177] A.B. Pereiro, J.M.M. Araújo, J.M.S.S. Esperança, I.M. Marrucho, L.P.N. Rebelo, Ionic liquids in separations of azeotropic systems - A review, *J. Chem. Thermodyn.* 46 (2012) 2–28, <https://doi.org/10.1016/j.jct.2011.05.026>.
- [178] M.B. Shiflett, A. Yokozeki, Separation of difluoromethane and pentafluoroethane by extractive distillation using ionic liquid, *Chem. Today* 24 (2006) 28–30.
- [179] M.B. Shiflett, A. Yokozeki, Utilizing ionic liquids for hydrofluorocarbon separation, US Patent 8,628,644 B2, 2014.
- [180] E. Quijada-Maldonado, T.A.M. Aelmans, G.W. Meindersma, A.B. de Haan, Pilot plant validation of a rate-based extractive distillation model for water-ethanol separation with the ionic liquid [emim][DCA] as solvent, *Chem. Eng. J.* 223 (2013) 287–297, <https://doi.org/10.1016/j.cej.2013.02.111>.
- [181] E. Quijada-Maldonado, G.W. Meindersma, A.B. De Haan, Pilot plant study on the extractive distillation of toluene-methylcyclohexane mixtures using NMP and the ionic liquid [hmim][TfCB] as solvents, *Sep. Purif. Technol.* 166 (2016) 196–204, <https://doi.org/10.1016/j.seppur.2016.04.041>.
- [182] C. Maton, N. De Vos, C.V. Stevens, Ionic liquid thermal stabilities: Decomposition mechanisms and analysis tools, *Chem. Soc. Rev.* 42 (2013) 5963–5977, <https://doi.org/10.1039/c3cs60071h>.
- [183] Y. Huang, Z. Chen, J.M. Crosthwaite, S. N.V.K. Aki, J.F. Brennecke, Thermal Stability of Ionic Liquids in Nitrogen and Air Environments, *J. Chem. Thermodyn.* 161 (2021) 106560, <https://doi.org/10.1016/j.jct.2021.106560>.
- [184] N. Meine, F. Benedetto, R. Rinaldi, Thermal stability of ionic liquids assessed by potentiometric titration, *Green Chem.* 12 (2010) 1711–1714, <https://doi.org/10.1039/c0gc00091d>.
- [185] E. Fabre, S.M.S. Murshed, A review of thermophysical properties and potential of ionic liquids for thermal applications, *J. Mater. Chem. A* (2021), <https://doi.org/10.1039/d1ta03656d>.
- [186] Y. Cao, T. Mu, Comprehensive investigation on the thermal stability of 66 ionic liquids by thermogravimetric analysis, *Ind. Eng. Chem. Res.* 53 (20) (2014) 8651–8664, <https://doi.org/10.1021/ie5009597>.
- [187] M. Villanueva, A. Coronas, J. García, J. Salgado, Thermal stability of ionic liquids for their application as new absorbents, *Ind. Eng. Chem. Res.* 52 (45) (2013) 15718–15727, <https://doi.org/10.1021/ie401656e>.
- [188] V. Gerbaud, I. Rodríguez-Donis, L. Hegely, P. Lang, F. Denes, X.Q. You, Review of extractive distillation. Process design, operation, optimization and control, *Chem. Eng. Res. Des.* 141 (2019) 229–271, <https://doi.org/10.1016/j.cherd.2018.09.020>.
- [189] K. Friess, P. Izák, M. Kárászová, M. Pasichnyk, M. Lanč, D. Nikolaeva, P. Luis, J. C. Jansen, A review on ionic liquid gas separation membranes, *Membranes* (Basel). 11 (2021) 1–58, <https://doi.org/10.3390/membranes11020097>.
- [190] G. Zarca, W.J. Horne, I. Ortiz, A. Urriaga, J.E. Bara, Synthesis and gas separation properties of poly(ionic liquid)-ionic liquid composite membranes containing a copper salt, *J. Memb. Sci.* 515 (2016) 109–114, <https://doi.org/10.1016/j.memsci.2016.05.045>.
- [191] P. Bernardo, J.C. Jansen, F. Bazzarelli, F. Tasselli, A. Fuoco, K. Friess, P. Izák, V. Jarmarova, M. Kacirkova, G. Clarizia, Gas transport properties of Pebax®/room temperature ionic liquid gel membranes, *Sep. Purif. Technol.* 97 (2012) 73–82, <https://doi.org/10.1016/j.seppur.2012.02.041>.
- [192] J.E. Bara, E.S. Hatakeyama, D.L. Gin, R.D. Noble, Improving CO<sub>2</sub> permeability in polymerized room-temperature ionic liquid gas separation membranes through the formation of a solid composite with a room-temperature ionic liquid, *Polym. Adv. Technol.* (2008) 229–236, <https://doi.org/10.1002/pat.1209>.
- [193] P. Scovazzo, D. Hvard, M. McShea, S. Mixon, D. Morgan, Long-term, continuous mixed-gas dry fed CO<sub>2</sub>/CH<sub>4</sub> and CO<sub>2</sub>/N<sub>2</sub> separation performance and selectivities for room temperature ionic liquid membranes, *J. Memb. Sci.* 327 (1-2) (2009) 41–48, <https://doi.org/10.1016/j.memsci.2008.10.056>.
- [194] F. Pardo, S.V. Gutiérrez-Hernández, G. Zarca, A. Urriaga, Toward the recycling of low-GWP hydrofluorocarbon/hydrofluoroolefin refrigerant mixtures using composite ionic liquid-polymer membranes, *ACS Sustain. Chem. Eng.* 9 (20) (2021) 7012–7021, <https://doi.org/10.1021/acssuschemeng.1c00668>.
- [195] C. Hermida-Merino, F. Pardo, G. Zarca, J.M.M. Araújo, A. Urriaga, M.M. Piñeiro, A.B. Pereiro, Integration of stable ionic liquid-based nanofluids into polymer membranes, Part I: Membrane synthesis and characterization, *Nanomaterials* 11 (2021) 607–623, <https://doi.org/10.3390/nano11030607>.
- [196] F. Pardo, S. Gutiérrez-Hernández, C. Hermida-Merino, J.M.M. Araújo, M. M. Piñeiro, A.B. Pereiro, G. Zarca, A. Urriaga, Integration of Stable Ionic Liquid-Based Nanofluids into Polymer Membranes. Part II: Gas Separation Properties toward Fluorinated Greenhouse Gases, *Nanomaterials* 11 (2021) 1–19, <https://doi.org/10.3390/nano11030607>.
- [197] W. Fam, J. Mansouri, H. Li, V. Chen, Improving CO<sub>2</sub> separation performance of thin film composite hollow fiber with Pebax®1657/ionic liquid gel membranes, *J. Memb. Sci.* 537 (2017) 54–68, <https://doi.org/10.1016/j.memsci.2017.05.011>.
- [198] Z. Dai, L.u. Bai, K.N. Hval, X. Zhang, S. Zhang, L. Deng, Pebax®/TSIL blend thin film composite membranes for CO<sub>2</sub> separation, *Sci. China Chem.* 59 (5) (2016) 538–546, <https://doi.org/10.1007/s11426-016-5574-3>.
- [199] G. Zarca, A. Urriaga, L.T. Biegler, I. Ortiz, An optimization model for assessment of membrane-based post-combustion gas upcycling into hydrogen or syngas, *J. Memb. Sci.* 563 (2018) 83–92, <https://doi.org/10.1016/j.memsci.2018.05.038>.

**3.2. Scientific publication 2. “Thermodynamic and process modeling of the recovery of R410A compounds with ionic liquids”, Salvador Asensio-Delgado, Daniel Jovell, Gabriel Zarca, Ane Urtiaga, Fèlix Llovell, *International Journal of Refrigeration*, 118 (2020) 365-375**

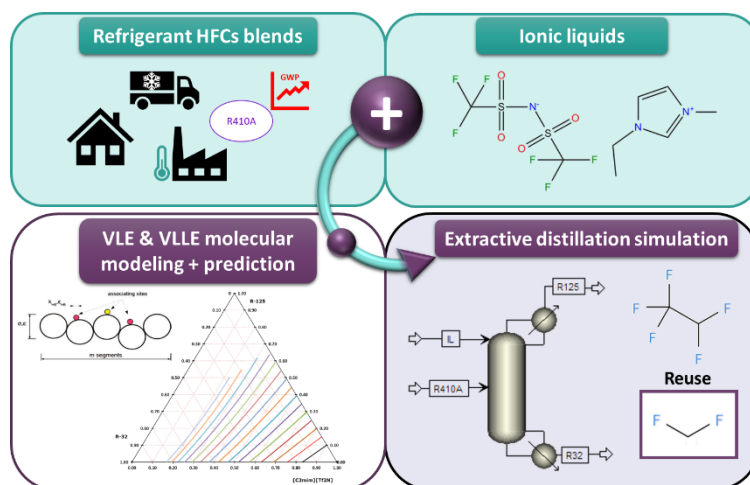
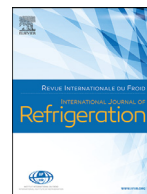


Figure 16. Graphical abstract of the article “Thermodynamic and process modeling of the recovery of R410A compounds with ionic liquids”.

This article is the result of a collaboration with Dr. Fèlix Llovell and the research group in the Institut Químic de Sarrià (IQS), Universitat Ramon Llull. Here, we explore the use of the advanced soft-SAFT EoS for the modeling of mixtures of F-gases and ILs, demonstrating that the soft-SAFT EoS is an adequate model for the description of the thermodynamic behavior of mixtures formed by these compounds. To that end, the VLE for the absorption of R32 and R125 in the ILs  $[C_4\text{mim}][PF_6]$ ,  $[C_2\text{mim}][Tf_2N]$ , and  $[C_6\text{mim}][Tf_2N]$  are fitted, achieving good predictions of the vapor-liquid-liquid equilibria (VLLE) of the binary mixtures. These three liquids were chosen because the experimental data for the absorption of R32 and R125 were available. Later in the thesis, better ILs for the separation were identified, while these ILs remain interesting for application where high absorption capacities are required. Then, a ternary mixture with the most interesting IL was predicted at 300 K and pressures between 0.2 and 1.6 MPa, predicting a liquid-liquid immiscibility at higher pressures due to the refrigerant condensation. This prediction was used to calculate the process one-stage selectivity in a flash evaporator using the Rachford-Rice equation. Finally, the article concludes with a process design of an extractive distillation column performed in collaboration with the coauthors affiliated to the IQS for the separation of the commercial mixture R410A, an equimass mixture of R32 and R125. Figure 16 shows the graphical abstract available in the online version of the article.



## Thermodynamic and process modeling of the recovery of R410A compounds with ionic liquids



S. Asensio-Delgado<sup>a</sup>, D. Jovell<sup>b</sup>, G. Zarca<sup>a</sup>, A. Urriaga<sup>a</sup>, F. Llovell<sup>b,\*</sup>

<sup>a</sup> Department of Chemical and Biomolecular Engineering, Universidad de Cantabria, Av. Los Castros s/n, Santander 39005, Spain

<sup>b</sup> Department of Chemical Engineering and Materials Science, IQS School of Engineering, Universitat Ramon Llull, Via Augusta 390, Barcelona 08017, Spain

### ARTICLE INFO

#### Article history:

Received 20 December 2019

Revised 2 March 2020

Accepted 13 April 2020

Available online 12 May 2020

#### Keywords:

Ionic liquid  
R410A  
Soft-SAFT  
Solubility  
Selectivity  
Process simulation

### ABSTRACT

European regulations are limiting the use of hydrofluorocarbons (HFCs) as refrigerants because of their elevated global warming potentials (GWPs). Apart from their substitution by other compounds with lower environmental impact, one of the plausible approaches to meet the legal requirements is the formulation of new refrigerant blends containing a low GWP compound (e.g., hydrofluoroolefins) mixed with one HFC that provides the necessary thermodynamic characteristics to act as an effective refrigerant. Thus, the recovery and reuse of HFCs seems a promising approach to increase their lifespan and reduce their production. However, current regeneration technologies that are based on distillation are highly energy-intensive. Therefore, the development of novel separation processes to selectively separate HFCs is needed for the practical implementation of circular economy principles in the use of refrigerants. This work is a step forward on using ionic liquids (ILs) to selectively separate F-gases. The advanced molecular-based soft-SAFT equation of state (EoS) is used as a tool to assess the potential of ILs as a solvent platform for the selective separation of the compounds forming the R410A refrigerant blend: R32 and R125. Soft-SAFT is employed to model the absorption of these HFCs into different ILs with different fluorinated anions. Ternary diagrams are then predicted for the absorption of R32/R125 mixtures into selected ILs to evaluate the competitive selectivity between both compounds. Based on this study, a potential ionic liquid candidate is chosen and a process simulation is performed to estimate the approximate energy cost of the separation and recovery process.

© 2020 Elsevier Ltd and IIR. All rights reserved.

## Modélisation thermodynamique et du processus de récupération des composés du R410A avec des liquides ioniques

Mots-clés: Liquide ionique; R410A; Équation soft-SAFT; Solubilité; Sélectivité; Simulation de processus

### 1. Introduction

Since the phase-out of ozone-depleting substances under the Montreal Protocol, the use of hydrofluorocarbons (HFCs) as alternative refrigerants with a negligible impact on the atmospheric ozone layer grew rapidly. Today, the concentration of HFCs in the atmosphere is still increasing due to fugitive emissions, the lack of end-life recovery protocols and the non-recyclability of refrigerants (Mota-Babiloni et al., 2017). However, the release of HFCs

to the atmosphere is also a matter of concern because they are powerful greenhouse gases that, in some cases, exhibit very high Global Warming Potentials (GWPs). Therefore, international initiatives aiming at the reduction of HFCs emissions have been recently adopted. In this respect, EU Regulation No. 517/2014 (Schulz and Kourkoulas, 2014) established restrictions on the placing on the market of several products and equipment based on the intended application and the GWP of the HFC to be used. Moreover, the Kigali Amendment to Montreal Protocol, which schedules an ambitious program to reduce the production and consumption of HFCs (Heath, 2017), was ratified by numerous parties and entered into force on January 2019 intending to avoid up to 0.5 °C of warm-

\* Corresponding author: Phone: ±34 93 2670000.

E-mail addresses: [felix.llovell@iqs.edu](mailto:felix.llovell@iqs.edu), [felixllovell@gmail.com](mailto:felixllovell@gmail.com) (F. Llovell).

## Nomenclature

AAD	Absolute Average Deviation
EOS(s)	Equation(s) of State
EU	European Union
GWP	Global Warming Potential
HFC	Hydrofluorocarbons
IG	Ideal Gas
IL(s)	Ionic Liquid(s)
LJ	Lennard-Jones
LLE	Liquid-Liquid Equilibria
LLV	Liquid-Liquid-Vapor
NIST	National Institute of Standards and Technology
NRTL	Non-Random Two-Liquid
SAFT	Statistical Association Fluid Theory
VLE	Vapor-Liquid Equilibria
VLLE	Vapor-Liquid-Liquid Equilibria
WEEE	Waste Electrical and Electronic Equipment

### Latin symbols

$A$	Helmholtz free energy
$f$	Fugacity
$g$	Radial distribution function
$k_B$	Boltzmann constant
$k_H$	Henry's coefficients
$K^{HB}$	Volume of association
$m$	Chain length
$M$	Total number of association sites
$P$	Pressure
$R$	Ideal gas constant
$S$	Gaseous absorption selectivity
$T$	Temperature
$V$	Volume
$x$	Liquid mole fraction
$X$	Fraction of molecules not bonded to the site
$y$	Vapor mole fraction
$z$	Feed mole fraction

### Greek symbols

$\alpha$	Ideal selectivity
$\varepsilon$	Lennard-Jones energy parameter
$\varepsilon^{HB}$	Square-well energy parameter of an association site
$\eta$	Lorentz-Berthelot size binary parameter
$\xi$	Lorentz-Berthelot energy binary parameter
$\sigma$	Lennard-Jones size parameter (diameter of the sphere)
$\rho$	Density
$\omega$	Acentric factor

### Superscripts

Assoc	Association
HB	Hydrogen bonding
Id	Ideal
Res	Residual
V	Vapor

### Subscripts

$\alpha, \beta$	Association sites
$i, j$	Compound

One of the plausible approaches to meet both the legal and technical requirements is the formulation of new refrigerant mixtures, based on a low GWP compound (e.g., hydrofluorolefins) combined with small amounts of at least one the following HFCs: difluoromethane (R32), pentafluoroethane (R125), 1,1,1,2-tetrafluoroethane (R134a) and 1,1-difluoroethane (R152a) (Mota-Babiloni et al., 2015). Moreover, EU Directive 2012/19 on waste electrical and electronic equipment (WEEE) (European Parliament and Council, 2012) compels the Member States to remove refrigerant fluids from separately collected WEEEs and ensure a proper treatment. Thus, this regulatory framework provides an excellent opportunity to shift towards a more circular economy as the waste refrigeration equipment that will be generated within the next decades will represent an important source of HFCs that could be reused (Pardo et al., 2020). Consequently, in order to boost the recyclability of refrigerants, the selective recovery of HFCs from end-of-life equipment and reuse in new refrigerant mixtures must be sought. However, currently used HFC blends are characterized for behaving almost like pure fluids (near-azeotropic mixtures), with virtually no variation of composition between the vapor and liquid phases and almost constant evaporation/condensation temperature at a given pressure. Under these premises, the separation of the different HFCs by means of cryogenic distillation processes becomes challenging (Ren and Scurto, 2009). Thus, it is necessary to develop new cost-effective processes to selectively separate refrigerant mixtures into their primary constituents.

In this regard, ionic liquids (ILs) have been proposed as a novel solvent platform in new gas separation processes because of their unique features, e.g., extremely low vapor pressure, high thermal and chemical stability, liquid state in a wide temperature range, and enhanced solvation properties, among others (Lei et al., 2014; Zarca et al., 2018; Zhao et al., 2017). Up to date, several studies have been conducted on the solubility of fluorinated refrigerants into ILs (Liu et al., 2015a, 2015b, 2015c, 2018; Shiflett and Yokozeki, 2006a, 2006b, 2006c, 2007, 2008; Yokozeki and Shiflett, 2006; Shiflett and Yokozeki, 2011; Shiflett and Yokozeki, 2007; Shiflett, Yokozeki and Knapp, 2011), concluding that the solubility is greater in ILs whose anion contains fluorinated groups (Dong et al., 2011; Shariati et al., 2005). While most studies primarily focused on assessing the phase equilibria of binary refrigerant/IL systems, Shiflett and Yokozeki initially proposed the separation of the R410A mixture using  $[C_4mim][PF_6]$  (Shiflett and Yokozeki, 2006d) and further described the utilization of ILs for separation, purification, and recycling of refrigerants and fluorinated monomers in several patents (Noelke and Shiflett, 2013; Shiflett et al., 2011; Shiflett, 2015; Shiflett and Yokozeki, 2014a, 2014b, 2012, 2011). Still with that, it is desirable to gain a deeper understanding of the feasibility of employing other fluorinated ILs to separate a refrigerant blend through evaluating the phase behavior of the ternary system formed by the IL and the HFCs mixture.

In literature, different theoretical approaches have been satisfactorily used to describe the phase behavior of IL/gas mixtures based on pure compound characteristics (Vega et al., 2010). Regarding IL/F-refrigerants, Shiflett and coworkers were the first to measure and model these mixtures in a series of papers published since 2006 using activity coefficient methods, namely, the Non-Random Two Liquid (NRTL) model (Shiflett et al., 2006a; Shiflett and Yokozeki, 2008, 2006e, 2006c) and the Redlich-Kwong (RK) cubic EoS (Shiflett and Yokozeki, 2006b). Its pioneering contributions included the description of VLE and also the VLLE line for systems involving common refrigerants in ILs with different anions, obtaining very good agreement when comparing to experimental data. The reader is referred to the review chapter published by these authors, where a summary of their work can be found (Shiflett and Yokozeki, 2009). Later, Kim and cowork-

ing by the end of the 21<sup>st</sup> century. Accordingly, some of the currently most employed HFC compounds in refrigeration and air conditioning, e.g., R134a (GWP = 1430), R404A (GWP = 3922) and R410A (GWP = 2088), must be replaced in the short-term by environment-friendly and energy-efficient alternative refrigerants (Mota-Babiloni et al., 2015).



**Table 1**  
Main properties of the refrigerant gases studied in this work (Honeywell Genetron Properties Suite, 2016).

Property	R32	R125	R410A
Molecular formula	CH <sub>2</sub> F <sub>2</sub>	C <sub>2</sub> HF <sub>5</sub>	CH <sub>2</sub> F <sub>2</sub> + C <sub>2</sub> HF <sub>5</sub> (69.8/30.2 mol%)
Molecular weight (g mol <sup>-1</sup> )	52.024	120.02	72.585
Normal boiling point (K)	221.50	225.06	~221.75
Critical temperature (K)	351.26	339.17	344.49
Critical pressure (MPa)	5.7820	3.6177	4.9013
GWP (CO <sub>2</sub> -eq., 100 yr) <sup>a</sup>	677	3170	2088

<sup>a</sup> Values taken from the IPCC fifth assessment report (IPCC – Intergovernmental Panel on Climate Change, 2015)

ers also used NRTL (Kim et al., 2012) and RK (Kim et al., 2013; Kim and Kohl, 2014) to thermodynamically evaluate the efficiency of the refrigerant- IL absorbent pairs. More recently, molecular-based methods such as the Statistical Associating Fluid Theory (SAFT) have also been used to assess these mixtures (Sujatha and Venkatarathnam, 2018).

The aim of this work is to assess the feasibility of the selective recovery of HFCs from common refrigerant mixtures contained in waste refrigeration equipment using ILs. By doing so, the recovered HFCs could be further reused to produce new HFC refrigerant mixtures, thus increasing their lifetime and minimizing the amount of new fluorinated gases placed into the market. We focus our attention on evaluating the technical viability of splitting into its individual components the refrigerant blend R410A that is going to be phased out in air conditioning applications. Refrigerant R410A is a near-azeotropic mixture formed by R32 and R125, whose main characteristics are summarized in Table 1. To that end, the phase behavior of the refrigerant gases R32 and R125, as well as that of their mixtures, will be described using the soft-SAFT EoS (Blas and Vega, 1998, 1997). Next, the solubility of these gases into different ILs will be evaluated with the same equation. Three fluorinated ILs are considered based on their potential use in novel separations and the availability of experimental HFCs solubility data: 1-butyl-3-methylimidazolium hexafluorophosphate ([C<sub>4</sub>mim][PF<sub>6</sub>]), 1-hexyl-3-methylimidazolium bis(trifluoromethylsulfonyl)imide ([C<sub>6</sub>mim][Tf<sub>2</sub>N]), and 1-ethyl-3-methylimidazolium bis(trifluoromethylsulfonyl)imide ([C<sub>2</sub>mim][Tf<sub>2</sub>N]). The possible interactions between the refrigerant gases and these ILs will be ascertained by predicting the high-pressure phase behavior of the ternary mixtures formed by the two HFCs and each IL, as well as the expected separation performance of the gas-liquid separation. Based on this study, a potential IL candidate is selected and a process simulation of the recovery unit is performed to estimate the approximate energy cost of the separation process.

## 2. Theory

### 2.1. soft-SAFT

The soft-SAFT EoS (Blas and Vega, 1997) is a successful variant of the original SAFT EoS (Chapman et al., 1990, 1989), which modifies the reference term of the original SAFT theory by a Lennard-Jones (LJ) dispersion term. The equation has already been proved to accurately reproduce the thermophysical properties of fluorinated refrigerants, such as hydrofluorocarbons (Llovel et al., 2013; Vilaseca et al., 2010) and hydrofluoroolefins (Albà et al., 2020), as well as the solubility of other greenhouse gases (CO<sub>2</sub>, SO<sub>2</sub>, N<sub>2</sub>O, CO) in many ILs (Andreu and Vega, 2008, 2007; Llovel et al., 2015; Oliveira et al., 2012; Pereira et al., 2016, 2014, 2013; Zarca et al., 2017a, 2017b).

Soft-SAFT is written in terms of the different microscopic contributions to the residual molar Helmholtz free energy

$$A^{res} = A - A^{id} = A^{ref} + A^{chain} + A^{assoc} \quad (1)$$

where the subscripts *id*, *ref*, *chain* and *assoc* refer to the ideal, reference, chain and association terms, respectively. These terms include a total of five molecular parameters defining the fluid: the chain length (*m*), the characteristic segment diameter ( $\sigma_{ii}$ ), the dispersive energy ( $\epsilon_{ii}/k_B$ ) and the volume ( $K_{\alpha\beta,ii}^{HB}$ ) and energy ( $\epsilon_{\alpha\beta,ii}^{HB}$ ) of association. For mixtures, the Lorentz-Berthelot combining rules are applied and two binary parameters,  $\eta_{ij}$  and  $\xi_{ij}$ , account for deviations in the crossed segment diameter and dispersive energy of the mixtures. Further details of the different terms of soft-SAFT are provided in the Supplementary Information (section A), while for a whole analysis of the equation the reader is referred to the original soft-SAFT contributions (Blas and Vega, 1998, 1997).

### 2.2. Molecular models

HFCs are considered homonuclear chainlike molecules modeled as several segments (*m*) of equal diameter ( $\sigma$ ) and dispersive energy ( $\epsilon/k_B$ ). The strong dipole moments due to the electronegativity of fluorine atoms (Costa Cabral et al., 2001) are considered through the association term by incorporating two associating sites of different nature (type A and B) and equal association energy ( $\epsilon^{HB}/k_B$ ) and volume ( $K^{HB}$ ). Both self-association (A-B interactions) between molecules of the same refrigerant and, for binary HFCs mixtures, cross-association (A-B' and A'-B interactions) between different refrigerant molecules are allowed.

Regarding ILs, molecular dynamics simulations have evidenced that this type of Coulombic fluids form ionic clusters in which cations and anions are coupled together (Del Pópolo and Voth, 2004; Urahata and Ribeiro, 2004). For this reason, ILs are typically modeled as Lennard-Jones chains with specific association sites describing the interactions between ions that derive from their ionic nature and the asymmetric charge distribution of molecular ions. In particular, the [C<sub>x</sub>mim][PF<sub>6</sub>] ILs have been modeled with a single associating site (type C) mimicking the strong cation-anion interactions (Andreu and Vega, 2007; Llovel et al., 2012). On the other hand, the model proposed for the [C<sub>x</sub>mim][Tf<sub>2</sub>N] ILs considers three association sites: one site (type D) represents the nitrogen atom interactions with the cation, and two sites (type E) take into account the delocalization of the anion electric charge due to the presence of the oxygen groups (Llovel et al., 2011). Both self-association interactions (C-C and D-E) between different molecules of the same IL and cross-association interactions with the refrigerant molecules (A-C, B-C, A-D and B-E) are considered to model the phase behavior of HFC + IL systems in this work.

The molecular parameters of HFCs and ILs used in this study are collected in Table 2. The optimized parameters of ILs were obtained from the abovementioned works (Andreu and Vega, 2007; Llovel et al., 2011), while the parameters for R32 and R125 have been reparametrized here. The main reason is that the original contribution (Vilaseca et al., 2010) included a renormalization group treatment for the critical region (Llovel et al., 2004), not used here. This slightly worsened the description of the vapor

**Table 2**  
Soft-SAFT molecular parameters of the HFCs and ILs investigated in this work.

Compound	$m$	$\sigma$ (Å)	$\epsilon/k_B$ (K)	$\epsilon^{HB}/k_B$ (K)	$\kappa^{HB}$ (Å <sup>3</sup> )	Range (K)	Reference
HFC-R32	1.321	3.529	144.4	1708	24050	180–333	This work
HFC-R125	1.392	4.242	148.8	1685	24050	180–333	This work
[C <sub>2</sub> mim][Tf <sub>2</sub> N]	6.023	4.069	394.6	3450	2250	-	(Llovel et al., 2011)
[C <sub>6</sub> mim][Tf <sub>2</sub> N]	6.338	4.334	404.2	3450	2250	-	(Llovel et al., 2011)
[C <sub>4</sub> mim][PF <sub>6</sub> ]	4.570	4.146	418.0	3450	2250	-	(Andreu and Vega, 2007)

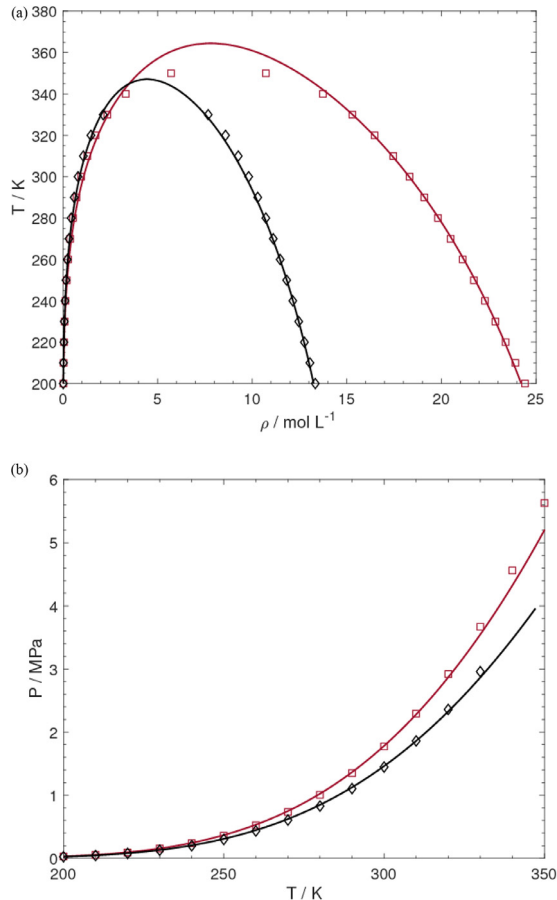


**Fig. 1.** Phase equilibria of R32 (red squares) and R125 (black diamonds). (a) Coexisting vapor and liquid densities and (b) vapor pressure vs. temperature. Symbols represent the correlated data from experimental measurements (Linstrom and Mallard, 2014) and solid lines are the soft-SAFT calculations.

pressure with the previous parameters, which were here refined by refitting the dispersive energy, as done for R125. Concerning R32, the original restriction forcing this molecule to be modeled as a sphere (so  $m=1$ ) was removed, based on the fact that the non-sphericity of this compound is evident from observation of its chemical structure geometry and acentric factor value ( $\omega=0.2769$ ). The new R32 parametrization provides a better overall description of the molecule in a wide range of temperatures, as it will be shown in the next section.

### 3. Results and discussion

#### 3.1. Phase behavior of HFCs

The phase envelope of both refrigerants calculated with the new molecular parameters is depicted in Fig. 1, where the temperature-density (Fig. 1a) and the pressure-temperature (Fig. 1b) diagrams are described with soft-SAFT and compared to

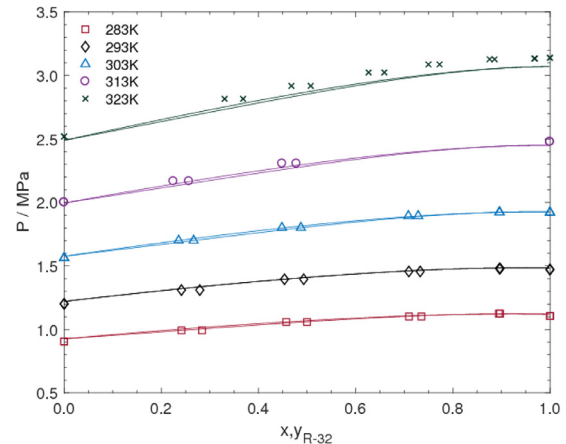


**Fig. 2.** Vapor-liquid equilibria for the system R32+R125 at 283.15 (red squares), 293.15 (black diamonds), 303.15 (blue triangles), 313.15 (violet circles) and 323.15 K (green crosses). Symbols represent the experimental data (Higashi, 1997) and solid lines are the soft-SAFT calculations obtained in the present study.

NIST correlated data (Linstrom and Mallard, 2014). An excellent description is found in a wide range of temperatures, from close to the triple point up to 95% of the critical point. The critical point is slightly overestimated due to the absence of the crossover treatment and this produces a slight underestimation of the vapor pressure of R32 at the highest temperatures. Nevertheless, the relative average deviation (AAD%) respect to the experimental data is very low for both the saturated liquid density calculations (AAD%) (1.13% and 0.21% for R125 and R32, respectively) and the vapor pressure (3.48% and 1.52% for R125 and R32, respectively).

The molecular models proposed for R32 and R125 are then used to calculate the phase behavior of their mixtures. The binary mixture R32+R125 is a near-azeotropic blend that forms a slightly positive pressure azeotrope at a composition of 91 mol % R32 (Higashi, 1997). The soft-SAFT description of the vapor-liquid equilibria (VLE) of this system at temperatures ranging between 283.15 and 323.15K is given in Fig. 2, where the model is compared to the available experimental data (Higashi, 1997). A temperature-independent energy binary parameter has been fitted to an intermediate isotherm at 303.15 K and transferred to predict the VLE of this system at the other temperatures. An accurate description of the phase equilibria is obtained in the whole composition range using a value of  $\xi=0.955$ . Minor deviations are found at the highest temperature ( $T=323.15$  K) because of the underprediction of the pure vapor pressures, affecting the performance of the binary model.

Once the interactions between R32 and R125 have been adequately characterized, the VLE of the refrigerant blend R410A is predicted with soft-SAFT by transferring the binary parameter previously fitted. The temperature-density and pressure-temperature diagrams of R410A, plotted in Figs. 3a and 3b, respectively, reveal an excellent agreement between the experimental (correlated) data (Honeywell Genetron Properties Suite, 2016) and the predicted values.

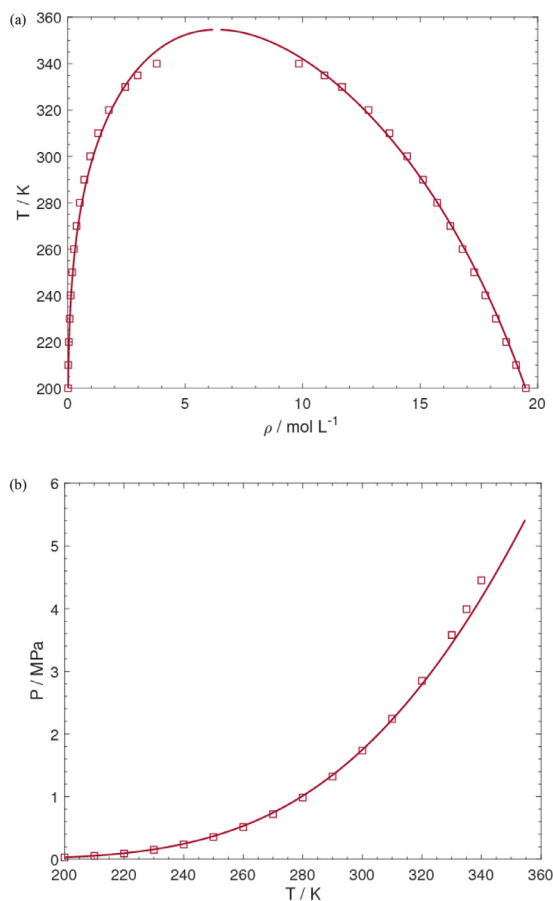


**Fig. 3.** Predicted vapor-liquid equilibria of blend R410A. a) Temperature-density, and b) pressure-temperature diagrams. Symbols represent correlated data from experimental measurements (Honeywell Genetron Properties Suite, 2016) and solid lines are the soft-SAFT calculations.

**Table 3**

Binary energy and size parameters for the studied HFCs + ionic liquid systems.

Ionic liquid	HFC	$\xi$	$\eta$
[C <sub>2</sub> mim][Tf <sub>2</sub> N]	R32	1.185	1.052
	R125	1.236	1.052
[C <sub>6</sub> mim][Tf <sub>2</sub> N]	R32	1.180	1.052
	R125	1.230	1.052
[C <sub>4</sub> mim][PF <sub>6</sub> ]	R32	1.238	1.052
	R125	1.266	1.070

### 3.2. Binary mixtures of HFCs and ILs

The following step consists in modeling the behavior of R32 and R125 in the presence of ILs. Fig. 4 and Figure 5 show the solubility of both refrigerants in [C<sub>2</sub>mim][Tf<sub>2</sub>N] and [C<sub>4</sub>mim][PF<sub>6</sub>], respectively. Results with [C<sub>6</sub>mim][Tf<sub>2</sub>N] are also provided as **Supplementary Information**, in Fig. S1. In all cases, the size and energy binary parameters were fitted to one isotherm (298.15 K) and used to predict the rest of them. The list of the optimized binary parameters is collected in Table 3.

The optimized binary parameters have similar values, regardless of the IL. In particular, the size binary parameter,  $\eta$ , is constant for all cases except for the R125 + [C<sub>4</sub>mim][PF<sub>6</sub>], whose value is slightly higher in order to capture the convex nature of the solubility curve at low temperatures. This means that the influence of the IL in the volume interactions (entropic effects) is almost negligible, allowing predictions of the solubility of these compounds

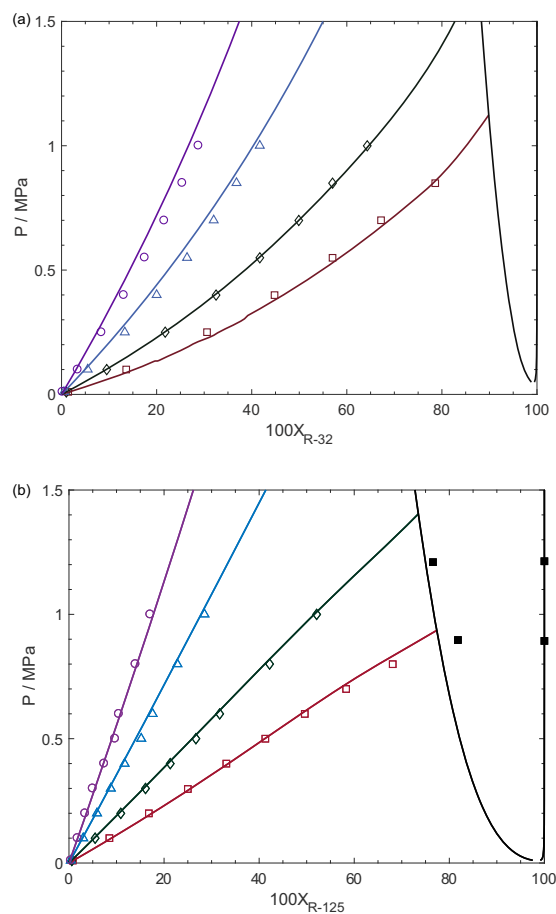


**Fig. 4.** Pressure-composition diagram of (a) R32 + [C<sub>2</sub>mim][Tf<sub>2</sub>N] and (b) R125 + [C<sub>2</sub>mim][Tf<sub>2</sub>N] at several temperatures: 283.15 (red squares), 298.15 (green diamonds), 323.15 (blue triangles) and 348.15 K (violet circles). Symbols represent the experimental data (Shiflett et al., 2006b; Shiflett and Yokozeki, 2008) and solid lines are the soft-SAFT calculations. The black curve represents the prediction of the VLL three-phase line.

in other ILs. The energy binary parameter,  $\xi$ , has similar values for the two [Tf<sub>2</sub>N]-based ILs, indicating that the effect of the alkyl chain in the cation is minor in the description of the association interactions. This information is useful to check the transferability of these parameters to other compounds when no experimental data are available. A final comment concerns the value of the  $\xi$  parameter which, in all cases, is remarkably higher than one, meaning the classical Lorentz-Berthelot combining rules underestimate the solubility of the refrigerant in the IL. This might be an indication that the model for the mixture is missing some interactions. Also, the size binary parameter is higher than one, increasing the miscibility of the refrigerant at high mole fractions.

Overall, the description of the solubility of these systems is very good at all temperatures, agreeing with the available experimental data (Shiflett et al., 2006b; Shiflett and Yokozeki, 2008; Yokozeki and Shiflett, 2006). Moreover, the soft-SAFT model predicts an immiscibility gap at very high concentrations of R32 and R125 for all ILs. The R125 gap is more significant and occurs around 80% of R125. The presence of an immiscible region was also found by Shiflett and Yokozeki (Shiflett and Yokozeki, 2008) in the mixture R125 + [C<sub>2</sub>mim][Tf<sub>2</sub>N]. These authors measured some VLE data, which is used here for comparison. Our predicted VLE is in good agreement with the previous data, although it is slightly larger. On the other hand, the same authors (Shiflett et al., 2006b) did not find any immiscibility gap for the mixtures with

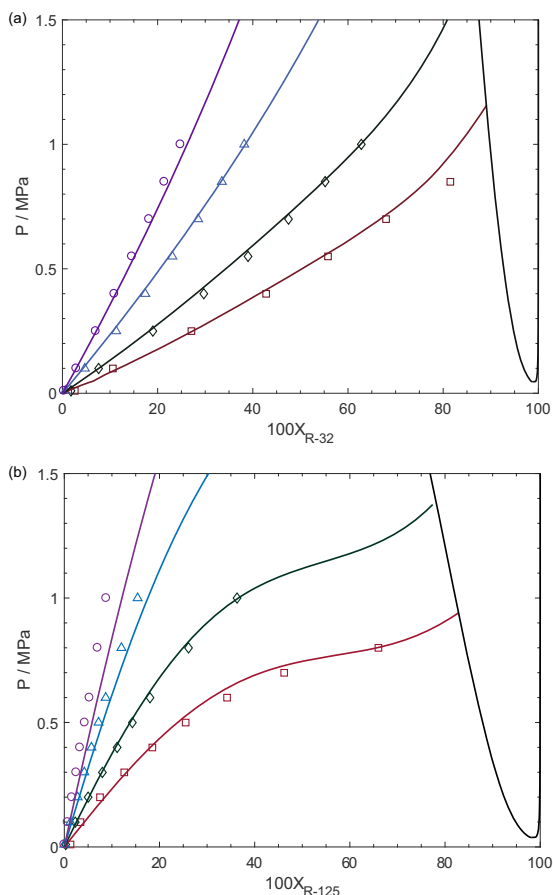


**Fig. 5.** Pressure-composition diagram of the G-L systems (a) R32 + [C<sub>4</sub>mim][PF<sub>6</sub>] and (b) R125 + [C<sub>4</sub>mim][PF<sub>6</sub>] at several temperatures: 283.15 (red squares), 298.15 (green diamonds), 323.15 (blue triangles) and 348.15 K (violet circles). Symbols represent the experimental data (Yokozeki and Shiflett, 2006) and solid lines are the soft-SAFT calculations. The black curve represents the prediction of the VLL three-phase line.

R32 + [C<sub>2</sub>mim][Tf<sub>2</sub>N], when they modeled their data using the nonrandom two-liquid (NRTL) activity coefficient model.

From the results discussed above, Henry's coefficients ( $k_H$ ), which relate the amount of gas dissolved in the liquid ( $x$ ) to the vapor phase fugacity of the solute in equilibrium with the solvent ( $f^V$ ) at infinite dilution and constant temperature, are calculated from the slope of the absorption isotherm at very low pressures.

$$k_H(T) = \lim_{x \rightarrow 0} \frac{f^V(P, T)}{x} \quad (2)$$

The temperature influence on the Henry's law constants is described following the expression (Liu et al., 2015a):

$$\ln k_H = \frac{A}{T} + B \quad (3)$$

where  $A$  and  $B$  are the experimental regression coefficients provided in **Table S1** of the **Supplementary Information**.

**Fig. 6** plots the calculated Henry's law constant of R32 and R125 in the ILs under study. As can be seen, the solubility of R32 is higher than that of R125 in all cases. Also, the ILs with the [Tf<sub>2</sub>N] anion exhibit slightly higher sorption capacities than [C<sub>4</sub>mim][PF<sub>6</sub>], as they have lower Henry's constants. In addition, the influence of temperature on the Henry's constants is very similar for R32 and R125 in each IL, as deduced from **Table S1**.

The theoretical performance of these ILs to separate R410A compounds is firstly approached by defining the ideal selectivity,

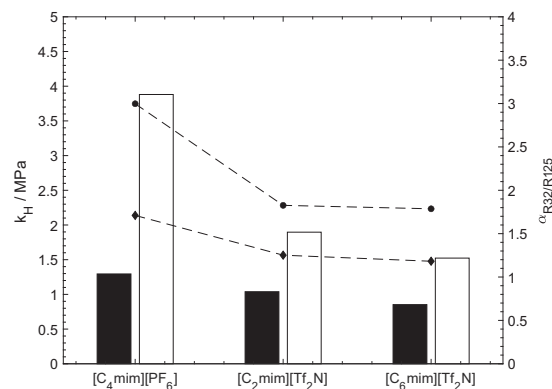


**Fig. 6.** Calculated Henry's law constants for R32 (black) and R125 (white) and ideal selectivity at infinite dilution (circles) and 1.0 MPa (diamonds) in [C<sub>4</sub>mim][PF<sub>6</sub>] and [C<sub>2</sub>mim][Tf<sub>2</sub>N] at 298.15 K and [C<sub>6</sub>mim][Tf<sub>2</sub>N] at 303.15 K.

$\alpha$ , calculated at infinite dilution as:

$$\alpha_{R32/R125} = \frac{k_H^{R125}}{k_H^{R32}} \quad (4)$$

The selectivity values, also plotted in **Fig. 6** for each IL, follow the opposite trend to that observed in gas solubility, as the ideal selectivity is higher for [C<sub>4</sub>mim][PF<sub>6</sub>] than for the [Tf<sub>2</sub>N]-based ILs. This is a consequence of the lower solubility of R125 at low compositions of [C<sub>4</sub>mim][PF<sub>6</sub>]. This difference decreases at higher pressures, as it is shown by additionally plotting the ideal selectivity at 1.0 MPa, calculated from the VLE modeled data (**Figs. 4, 5** and **S1**). At this pressure, which is likely to be employed in an extractive distillation process in order to increase gas sorption throughout and reduce the amount of IL to be used, all three ILs provide similar selectivity values. Consequently, selecting the best IL to perform the separation becomes difficult if the comparison is made only in terms of absorption capacity and selectivity, as there are no significant differences among them. Mass transfer is another key factor affecting the performance of gas separation processes (Mota-Martinez et al., 2018). Using [C<sub>2</sub>mim][Tf<sub>2</sub>N] would favor the separation because its viscosity (34 mPa s at 298 K) is twofold and tenfold lower than [C<sub>6</sub>mim][Tf<sub>2</sub>N] (71 mPa s at 298 K) and [C<sub>4</sub>mim][PF<sub>6</sub>] (329 mPa s at 298 K), respectively (Ahosseini and Scurto, 2008; Harris et al., 2005). Moreover, [PF<sub>6</sub>] anion is less stable as it can hydrolyze in the presence of water (Wasserscheid et al., 2002). Therefore, [C<sub>2</sub>mim][Tf<sub>2</sub>N] is selected in this work to further assess the separation of R32 from R125 using ILs.

Finally, the van't Hoff equation is used to obtain the enthalpy (Eq. (5)) and entropy (Eq. (6)) of dissolution of the mixtures (Blath et al., 2011) using the data obtained from soft-SAFT to evaluate the dependence of the solvation process on temperature.

$$\Delta H_{dis} = R \left( \frac{\partial \ln k_H}{\partial (1/T)} \right)_p \quad (5)$$

$$\Delta S_{dis} = -R \left( \frac{\partial \ln k_H}{\partial \ln T} \right)_p \quad (6)$$

The results of the calculation of solvation enthalpies and entropies are presented in **Table 4**. The magnitude of the solvation enthalpies of R32 and R125 are within the typical range of physical sorption and are just slightly higher than that found for CO<sub>2</sub> sorption in these ILs (Cadena et al., 2004).



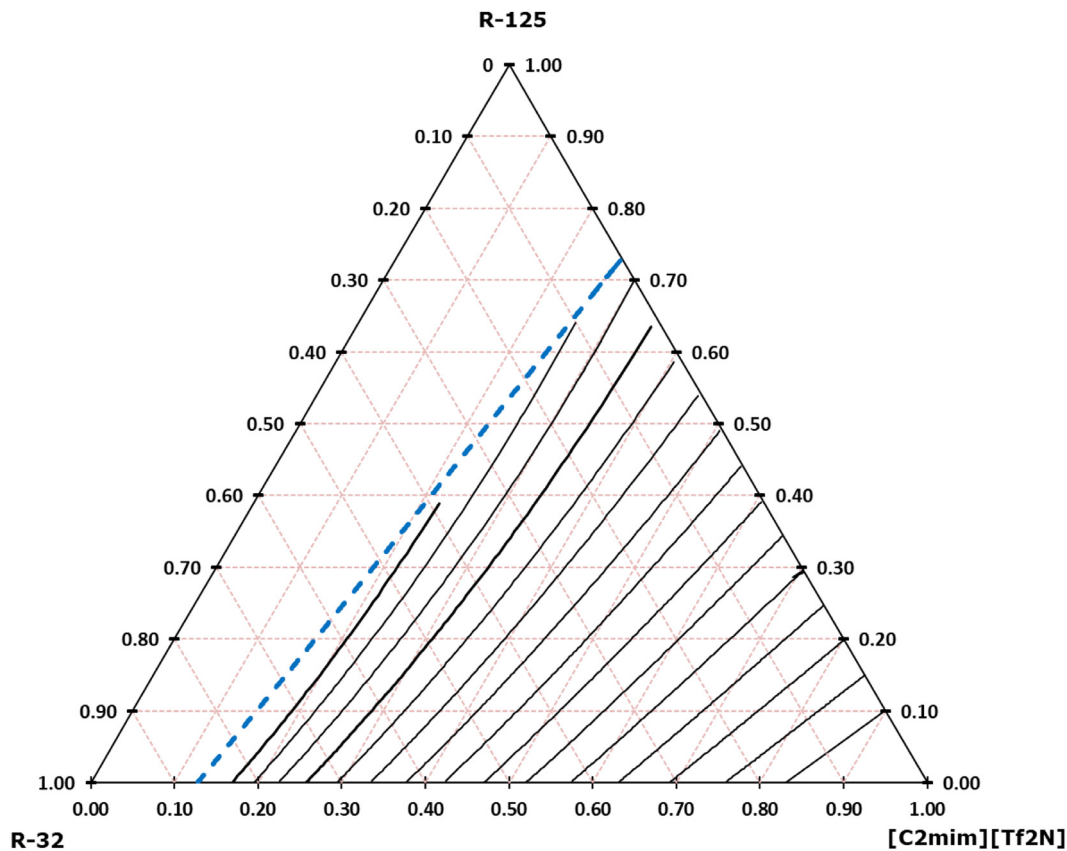


Fig. 7. Isothermal ternary phase diagram predicted with soft-SAFT for the system R32 + R125 + [C<sub>2</sub>mim][Tf<sub>2</sub>N] at 300 K. The different curves represent predicted isobars at pressures ranging from 0.2 (bottom line) to 1.6 MPa (upper line) at 0.1 MPa intervals. The dashed blue line corresponds to the VLE curve.

**Table 4**  
Enthalpy and entropy of solvation of R32 and R125 in selected ILs.

Ionic liquid	HFC	$\Delta H$ (kJ mol <sup>-1</sup> )	$\Delta S$ (J mol <sup>-1</sup> K <sup>-1</sup> )
[C <sub>2</sub> mim][Tf <sub>2</sub> N]	R32	-21.5	-68.3
	R125	-20.1	-63.8
[C <sub>6</sub> mim][Tf <sub>2</sub> N]	R32	-20.5	-63.5
	R125	-19.0	-59.0
[C <sub>4</sub> mim][PF <sub>6</sub> ]	R32	-18.8	-59.6
	R125	-16.0	-50.7

### 3.3. Phase behavior of ternary mixtures

The information gathered from the study of the binary systems is used to predict, in the absence of experimental data, the phase behavior of ternary mixtures formed by the two HFCs and the candidate IL, [C<sub>2</sub>mim][Tf<sub>2</sub>N], selected to perform the separation. The ternary diagram R32 + R125 + [C<sub>2</sub>mim][Tf<sub>2</sub>N] at 300 K is presented in Fig. 7. Several isobars were calculated to assess the influence of pressure on the phase behavior of the mixture, and the corresponding liquid composition is indicated in the diagram. A region of immiscibility, i.e., liquid-liquid equilibrium (LLE), is found at high compositions of both refrigerants above 1.4 MPa, as expected from the information gathered in the binary systems. The three VLE phase line has been estimated and indicated in the diagram as a dashed line. Similar diagrams have been reported for the absorption into ILs of very soluble gases such as CO<sub>2</sub> and SO<sub>2</sub> (Shiflett and Yokozeki, 2010; Yokozeki and Shiflett, 2009).

Using the ternary diagrams, the performance of the gas separation for a given inlet composition is reevaluated by defining the gaseous absorption selectivity,  $S$ , as follows (Yokozeki and Shi-

flett, 2007):

$$S_{R32/R125} = \frac{y_{R125}/x_{R125}}{y_{R32}/x_{R32}} \quad (7)$$

where  $x$  and  $y$  denote the molar composition of R32 and R125 in the solvent liquid and vapor phases, respectively. This is a more realistic value than that obtained from Eq. (4), as it includes the competition between the two HFCs. In Eq. (7), the vapor compositions in equilibrium with the liquid are calculated as a function of the IL concentration in the feed ( $z_{IL}$ ) and the operating pressure through an iterative process that involves solving the Rachford-Rice flash equation. The separation performance for the mixture R410A provided by [C<sub>2</sub>mim][Tf<sub>2</sub>N] at 300 K is presented in Fig. 8. The predicted value of separation performance tends to the calculated ideal selectivity at infinite dilution and decreases, as expected, with pressure. Moreover, although lower pressures yield higher separation performances (closer to the ideal selectivity), this occurs at the expense of lower sorption capacity and consequently, lower recovery. At higher pressures, the predicted LLE immiscibility region also limits the amount of gas that can be recovered. Nevertheless, very high-pressure operating conditions do not seem to be attractive because they incur in ~25% separation performance drops for a given IL feed composition.

## 4. Process Simulation

### 4.1. Configuration and implementation details

The thermodynamic characterization has been accompanied by a process simulation of the mixture separation of R32 and R125 at the proportions forming the R410A blend. The simulation is done through the design of an extractive distillation unit where the IL

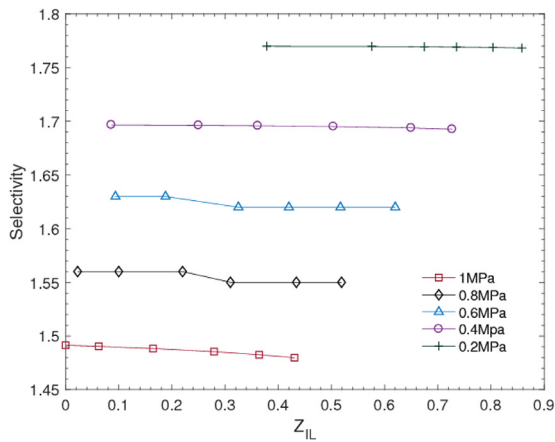


**Fig. 8.** Predicted separation performance (Selectivity calculated as Eq (7)) for the recovery of R32 from R410A as a function of the  $[C_2mim][Tf_2N]$  feed mole fraction ( $Z_{IL}$ ) at 300 K and several pressures: 0.2 (green crosses), 0.4 (violet circles), 0.6 (blue triangles), 0.8 (black diamonds) and 1 MPa (red squares).

selected in the previous section,  $[C_2mim][Tf_2N]$ , is used as entrainer. All simulations have been carried out with the Aspen Plus® v10 (36.0.0.249) simulator.

While the HFCs conforming R410A can be taken as conventional components from the Aspen Plus Database, the thermophysical properties of  $[C_2mim][Tf_2N]$  are required to be introduced in the system as no information was available in the ASPEN database. The critical properties of the IL were taken from the literature. (Shariati et al., 2013). The ideal heat gas capacity was estimated using the extended Joback method (Ge et al., 2008). The vapor pressure information was taken from the data presented by Heym et al. (Heym et al., 2015). The Clausius-Clapeyron equation was applied to predict the heat of vaporization with liquid vapor pressure data since the vapor phase is assumed as an ideal gas and the molar volume of the liquid is negligible compared to that of

the vapor. Finally, liquid viscosity data was obtained from the literature (Noda et al., 2001) and fitted to an Andrade-type equation, as the two-constant Arrhenius equation, suggested in by some authors (De Riva et al., 2014), was producing higher deviations. Further details on the numerical implementation of these properties into Aspen Plus, as well as the critical values, normal boiling point, acentric factor ( $\omega$ ) and all the optimized constants for the ideal heat capacity, vapor pressure, enthalpy of vaporization and liquid viscosity correlations, can be found in the **Supplementary Information, Section C**.

An extended version of the NRTL model is used to describe the non-ideal behavior in the liquid phase of the mixture (see the **Supplementary Information** for further details), as done by many researchers to model the behavior of mixtures containing ILs (Meindersma et al., 2006; Shiflett et al., 2011; Vatani et al., 2012), while an ideal gas model (IG) is kept for the gas phase. The extended NRTL parameters are fitted to experimental data (Higashi, 1997; Shiflett et al., 2006b; Shiflett and Yokozeki, 2008) by minimizing a least-squares function, including the calculated activity coefficients. The parameters obtained from the minimization are presented in **Table S4**.

Following the work of Shiflett and Yokozeki (Shiflett and Yokozeki, 2014b, 2006d), the process consisted of a main distillation column for the separation of R32 and R125 followed by two flash tanks for the regeneration of  $[C_2mim][Tf_2N]$  and an IL recirculation including a pump with a heat exchanger to cool the IL before returning to the main column (see Fig. 9).

The inlet flow of R410A introduced to the process was fixed to  $0.3 \text{ kg s}^{-1}$  and is considered an equimassic mixture of R125 and R32. Several configurations were tested to select the most appropriate column configuration to reach a purity of 99% mole for R125.

Several pre-calculations have shown that a column with 28 stages, including the reboiler and the partial condenser, is necessary to reach the purity requirements for R125. This column operates at 1 MPa, as in the publication of Shiflett and Yokozeki

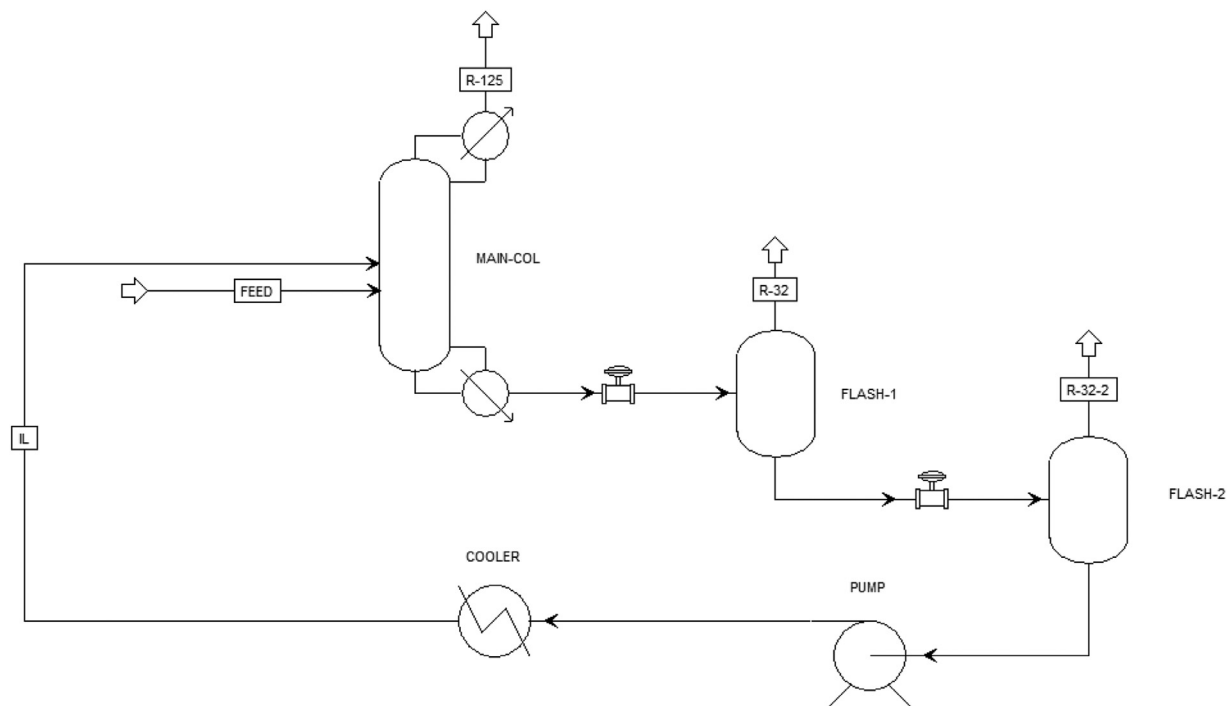


**Fig. 9.** Main process flowsheet of a separation unit of the R410A blend using  $[C_2mim][Tf_2N]$  as entrainer. The diagram contains a distillation column (MAIN-COL) for the removal of R125 followed by two flash tanks (FLASH-1 and FLASH-2) for the regeneration of the IL and removal of R32. The IL recirculation line includes a pump with a heat exchanger to cool the IL before returning to the main column.

**Table 5**  
ASPEN Plus simulation for the separation of R410A

Feed	
Flow rate (kg s <sup>-1</sup> )	0.3000
R32 flow rate (kg s <sup>-1</sup> )	0.1500
R125 flow rate (kg s <sup>-1</sup> )	0.1500
R410A inlet temperature (K)	303.15
[C <sub>2</sub> mim][Tf <sub>2</sub> N] flow rate (kg s <sup>-1</sup> )	4.2464
[C <sub>2</sub> mim][Tf <sub>2</sub> N] inlet temperature (K)	313.15
Main Column	
Condenser temperature (K)	286.3
Condenser heat duty (kW)	-29.11
Distillate rate (kg s <sup>-1</sup> )	0.1218
R125 overhead mole fraction	0.9900
Reboiler temperature (K)	353.7
Reboiler heat duty (kW)	1955
Bottoms rate (kg s <sup>-1</sup> )	4.425
Operating pressure (MPa)	1.000
Theoretical stages	28.00
R410A feed stage	22.00
[C <sub>2</sub> mim][Tf <sub>2</sub> N] feed stage	2.000
Flash Drum 1	
Outlet Pressure (MPa)	0.1000
Outlet temperature (K)	353.7
R32 overhead flow rate (kg s <sup>-1</sup> )	0.1354
R32 overhead mole fraction	0.9196
Flash Drum 2	
Outlet Pressure (MPa)	0.0100
Outlet temperature (K)	353.73
R32 overhead flow rate (kg s <sup>-1</sup> )	0.0139
R32 overhead mole fraction	0.9569
Cooler	
Heat duty (kW)	1957
Pump	
Net Work Required (kW)	6.834

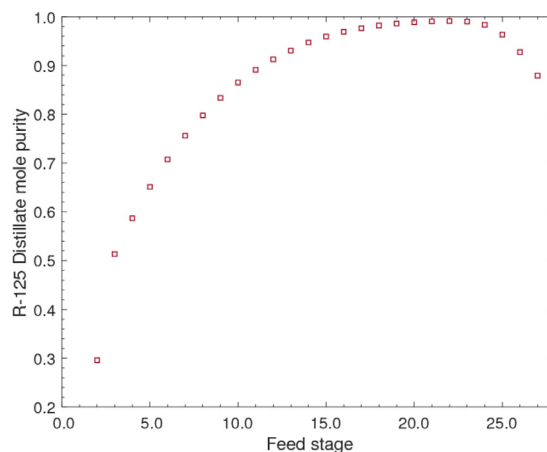
(Shiflett and Yokozeki, 2006d). The column has been modeled with the ASPEN RadFrac® module to account for the VLLE. Due to the non-ideal nature of the mixture, the column must be converged in two phases. In a first iteration, the highly non-ideal convergence method was selected and the key components of the three-phase equilibrium were established. To make the column numerically more robust, a second iteration comprises a custom convergence method that uses the Newton-Raphson algorithm. A maximum of 200 iterations have been considered along with Powell's algorithm to find local minimums of functions. The IL and the refrigerant mixture have been fed through stages 2 and 22, respectively, with a molar reflux ratio of 1.5 and a [C<sub>2</sub>mim][Tf<sub>2</sub>N] flow rate of 4.24 kg s<sup>-1</sup> in order to meet the specified separation requirement.

The flash drums have been modeled with ASPEN two-outlet flash module, and the operating temperature has been set equal to the reboiler temperature (353.73 K). The fluid is depressurized when passing through a throttling valve so that part of the fluid can be vaporized for further separation. No IL is vaporized and gaseous R32 is obtained through the flash drums heads. Both drums are connected in series and operated adiabatically. The pressure drop is set at 0 MPa, being the operating pressure the same as that obtained after the valve expansion i.e., 0.1 MPa and 0.01 MPa, respectively.

Due to the pressure changes that the IL undergoes during the separation process and the temperature changes that this entails, the solvent must be pressurized again, and its temperature must be lowered to the feed temperature. For this purpose, a pump and heat exchanger are provided to recirculate the entire solvent used in the separation.

#### 4.2. Analysis of the results

Table 5 shows the ASPEN Plus simulation results for the separation of R410A using [C<sub>2</sub>mim][Tf<sub>2</sub>N] as entrainer. A distillate flow

**Fig. 10.** Influence of the feed stage on the distillate (R125) mole purity.

rate of 0.1218 kg s<sup>-1</sup> with a mole fraction of R125 of 0.99 is obtained. This represents a 99.56 wt % with respect to the initial feed of R125. R32 is absorbed in the IL and later separated in the cascade system of flash separators, due to the pressure drop experienced by the mixture, obtaining a molar composition of 0.92 and 0.96 in the first and second flash separators, respectively. The IL is then recirculated to the column with minimal traces of R32 and R125.

The effect of the feeding stage of the HFC mixture on the purity of the distillate obtained in the first separation stage has been analyzed in order to select the adequate configuration to perform the extractive distillation of [C<sub>2</sub>mim][Tf<sub>2</sub>N] + R410A. While the IL must be introduced in the early stages of separation to ensure as much contact as possible between the extracting agent and the mixture, this is not the case for the feeding stage of the R410A blend.

Several simulations were carried out to find the most suitable combination of the solvent and feed stage location that will maximize the purity of R32 and R125. As can be seen from Fig. 10, the optimum feed location was estimated to be at stage 22.

## 5. Conclusions

In this work, the absorption and separation of R32 and R125, the two hydrofluorocarbons forming the R410A blend, using Ionic Liquids (ILs) has been theoretically addressed by means of the soft-SAFT molecular-based equation of state. For that purpose, three imidazolium ILs containing two fluorinated anions, [PF<sub>6</sub>]<sup>-</sup> and [Tf<sub>2</sub>N]<sup>-</sup>, have been selected and their capacity to absorb and selectively separate these HFCs has been evaluated. Using relatively simple coarse-grained molecular models for the HFCs and assuming a cation-anion pair with the charges represented by a certain number of associating sites, the solubility of R32 and R125 in the studied ILs has been characterized with soft-SAFT using two binary temperature-independent parameters. An excellent representation of the solubility curves is achieved at all compositions and temperature conditions. The immiscibility regions at high refrigerant compositions have been theoretically predicted. Also, the enthalpy and entropy of solvation, the Henry constants and the selectivity of these mixtures are evaluated and compared. Although results do not reveal significant differences from a thermodynamics perspective, [C<sub>2</sub>mim][Tf<sub>2</sub>N] is selected as the most promising solvent considering mass transfer and viscosity aspects. A ternary mixture is then predicted so as to build the thermodynamic diagram and evaluate the competitive selectivity. The results reveal low selectivity values in a range of values between 1 and 2 at 300 K. Even if the selectivity values are relatively low, a process simulation of the

whole recovery process has been performed in order to study the feasibility of the separation. The thermodynamic properties of the IL have been fitted to available experimental data and introduced into the process simulators. The results reveal that it is possible to obtain a high yield of separation (99.56% of the initial mass) using a column of 28 stages and a reasonable amount of energy. While the focus of this work is on the use of molecular modeling tools to provide thermophysical information on the separation process, the simulations allow a predesign of a future unit equipment.

### Declaration of Competing interest

The authors declare that they have no known competing financial interests or personal relationships that could have appeared to influence the work reported in this paper.

### Acknowledgments

This research is supported by Project KET4F-Gas – SOE2/P1/P0823, which is co-financed by the European Regional Development Fund within the framework of the Interreg SUDOE Program. Also, S. Asensio-Delgado would like to thank the FPU grant (18/03939) awarded by the Spanish Ministry of Science, Innovation and Universities.

### Supplementary materials

Supplementary material associated with this article can be found, in the online version, at [doi:10.1016/j.ijrefrig.2020.04.013](https://doi.org/10.1016/j.ijrefrig.2020.04.013).

### References

- Ahosseini, A., Scurto, A.M., 2008. Viscosity of imidazolium-based ionic liquids at elevated pressures: Cation and anion effects. *Int. J. Thermophys.* 29, 1222–1243. doi:10.1007/s10765-008-0497-7.
- Albà, C.G., Vega, L.F., Llovel, F., 2020. A consistent thermodynamic molecular model of n-hydrofluorolefins and blends for refrigeration applications. *Int. J. Refrig.* 113, 145–155. doi:10.1016/j.ijrefrig.2020.01.008.
- Andreu, J.S., Vega, L.F., 2008. Modeling the solubility behavior of CO<sub>2</sub>, H<sub>2</sub>, and Xe in [Cn-mim][Tf<sub>2</sub>N] ionic liquids. *J. Phys. Chem. B* 112, 15398–15406. doi:10.1021/jp807484g.
- Andreu, J.S., Vega, L.F., 2007. Capturing the solubility behavior of CO<sub>2</sub> in ionic liquids by a simple model. *J. Phys. Chem. C* 111, 16028–16034. doi:10.1021/jp074353x.
- Blas, F.J., Vega, L.F., 1998. Prediction of Binary and Ternary Diagrams Using the Statistical Associating Fluid Theory (SAFT) Equation of State. *Ind. Eng. Chem. Res.* 37, 660–674. doi:10.1021/ie970449+.
- Blas, F.J., Vega, L.F., 1997. Thermodynamic behaviour of homonuclear and heteronuclear Lennard-Jones chains with association sites from simulation and theory. *Mol. Phys.* 92, 135–150. doi:10.1080/002689797170707.
- Blath, J., Christ, M., Deubler, N., Hirth, T., Schiestel, T., 2011. Gas solubilities in room temperature ionic liquids - Correlation between RTIL-molar mass and Henry's law constant. *Chem. Eng. J.* 172, 167–176. doi:10.1016/j.cej.2011.05.084.
- Cadena, C., Anthony, J.L., Shah, J.K., Morrow, T.I., Brennecke, J.F., Maginn, E.J., 2004. Why is CO<sub>2</sub> so Soluble in Imidazolium-Based Ionic Liquids? *J. Am. Chem. Soc.* 126, 5300–5308. doi:10.1021/ja039615x.
- Chapman, W.G., Gubbins, K.E., Jackson, G., Radosz, M., 1990. New reference equation of state for associating liquids. *Ind. Eng. Chem. Res.* 29, 1709–1721. doi:10.1021/ie00104a021.
- Chapman, W.G., Gubbins, K.E., Jackson, G., Radosz, M., 1989. SAFT: Equation-of-state solution model for associating fluids. *Fluid Phase Equilib* 52, 31–38. doi:10.1016/0378-3812(89)80308-5.
- Costa Cabral, B.J., Guedes, R.C., Pai-Panandiker, R.S., Nieto de Castro, C.A., 2001. Hydrogen bonding and the dipole moment of hydrofluorocarbons by density functional theory. *Phys. Chem. Chem. Phys.* 3, 4200–4207. doi:10.1039/b102879k.
- De Riva, J., Ferro, V.R., Del Olmo, L., Ruiz, E., Lopez, R., Palomar, J., 2014. Statistical refinement and fitting of experimental viscosity-to-temperature data in ionic liquids. *Ind. Eng. Chem. Res.* 53, 10475–10484. doi:10.1021/ie5014426.
- Del Pópulo, M.G., Voth, G.A., 2004. On the structure and dynamics of ionic liquids. *J. Phys. Chem. B* 108, 1744–1752.
- Dong, L., Zheng, D., Sun, G., Wu, X., 2011. Vapor-liquid equilibrium measurements of difluoromethane + [Emim]OTf, difluoromethane + [Bmim]OTf, difluoroethane + [Emim]OTf, and difluoroethane + [Bmim]OTf systems. *J. Chem. Eng. Data* 56, 3663–3668. doi:10.1021/je2005566.
- European Parliament and Council, 2012. Directive 2012/19/EU of the European Parliament and of the Council of 4 July 2012 on waste electrical and electronic equipment (WEEE). *Off. J. Eur. Union L197*, 38–71.
- Ge, R., Hardacre, C., Jacquemin, J., Nancarrow, P., Rooney, D.W., 2008. Heat capacities of ionic liquids as a function of temperature at 0.1 MPa. Measurement and prediction. *J. Chem. Eng. Data* 53, 2148–2153. doi:10.1021/je800335v.
- Harris, K.R., Woolf, L.A., Kanakubo, M., 2005. Temperature and pressure dependence of the viscosity of the ionic liquid 1-butyl-3-methylimidazolium hexafluorophosphate. *J. Chem. Eng. Data*. doi:10.1021/je050147b.
- Heath, E.A., 2017. Amendment to the Montreal Protocol on Substances that Deplete the Ozone Layer (Kigali Amendment). *Int. Leg. Mater.* 56, 193–205. doi:10.1017/ilm.2016.2.
- Heym, F., Korth, W., Thiessen, J., Kern, C., Jess, A., 2015. Evaporation and decomposition behavior of pure and supported ionic liquids under thermal stress. *Chemie-Ingenieur-Technik* 87, 791–802. doi:10.1002/cite.201400139.
- Higashi, Y., 1997. Vapor-liquid equilibrium, coexistence curve, and critical locus for difluoromethane + pentafluoroethane (R-32 + R-125). *J. Chem. Eng. Data* 42, 1269–1273. doi:10.1021/je9701083.
- Honeywell Genetron Properties Suite, 2016. European Refrigerants. <https://www.honeywell-refrigerants.com/europe/genetron-properties-suite>.
- IPCC – Intergovernmental Panel on Climate Change, 2015. *Global Warming Potential Values*. Gas Protoc. Greenh.
- Kim, S., Kohl, P.A., 2014. Analysis of [hmim][PF<sub>6</sub>] and [hmim][Tf<sub>2</sub>N] ionic liquids as absorbents for an absorption refrigeration system. *Int. J. Refrig.* 48, 105–113. doi:10.1016/j.ijrefrig.2014.09.003.
- Kim, S., Patel, N., Kohl, P.A., 2013. Performance simulation of ionic liquid and hydrofluorocarbon working fluids for an absorption refrigeration system. *Ind. Eng. Chem. Res.* 52, 6329–6335. doi:10.1021/ie400261g.
- Kim, Y.J., Kim, S., Joshi, Y.K., Fedorov, A.G., Kohl, P.A., 2012. Thermodynamic analysis of an absorption refrigeration system with ionic-liquid/refrigerant mixture as a working fluid. *Energy* 44, 1005–1016. doi:10.1016/j.energy.2012.04.048.
- Lei, Z., Dai, C., Chen, B., 2014. Gas solubility in ionic liquids. *Chem. Rev.* doi:10.1021/cr300497a.
- Linström, P.J., Mallard, W.G., 2014. NIST Chemistry webBook, NIST Standard Reference Database Number 69. National Institute of Standards and Technology <https://doi.org/citeulike-article-id:3211271>.
- Liu, X., He, M., Lv, N., Qi, X., Su, C., 2015a. Solubilities of R-161 and R-143a in 1-Hexyl-3-methylimidazolium bis(trifluoromethylsulfonyl)imide. *Fluid Phase Equilib* 388, 37–42. doi:10.1016/j.fluid.2014.12.026.
- Liu, X., He, M., Lv, N., Qi, X., Su, C., 2015b. Vapor-liquid equilibrium of three hydrofluorocarbons with [HMIM][Tf<sub>2</sub>N]. *J. Chem. Eng. Data* 60, 1354–1361. doi:10.1021/je501069b.
- Liu, X., Pan, P., He, M., 2018. Vapor-liquid equilibrium and diffusion coefficients of R32 + [HMIM][FEP], R152a + [HMIM][FEP] and R161 + [HMIM][FEP]. *J. Mol. Liq.* 253, 28–35. doi:10.1016/j.molliq.2018.01.032.
- Liu, X., Qi, X., Lv, N., He, M., 2015c. Gaseous absorption of fluorinated ethanes by ionic liquids. *Fluid Phase Equilib* 405, 1–6. doi:10.1016/j.fluid.2015.07.001.
- Llovel, F., Marcos, R.M., Vega, L.F., 2013. Transport properties of mixtures by the soft-SAFT + Free-volume theory: Application to mixtures of n-alkanes and hydrofluorocarbons. *J. Phys. Chem. B* 117. doi:10.1021/jp401754r.
- Llovel, F., Oliveira, M.B., Coutinho, J.A.P., Vega, L.F., 2015. Solubility of greenhouse and acid gases on the [C<sub>4</sub>mim][MeSO<sub>2</sub>] ionic liquid for gas separation and CO<sub>2</sub> conversion. *Catal. Today* 255, 87–96. doi:10.1016/j.cattod.2014.12.049.
- Llovel, F., Pàmies, J.C., Vega, L.F., 2004. Thermodynamic properties of Lennard-Jones chain molecules: Renormalization-group corrections to a modified statistical associating fluid theory. *J. Chem. Phys.* 121, 10715–10724. doi:10.1063/1.1809112.
- Llovel, F., Valente, E., Vilaseca, O., Vega, L.F., 2011. Modeling complex associating mixtures with [C<sub>n</sub>mim][Tf<sub>2</sub>N] ionic liquids: Predictions from the soft-SAFT equation. *J. Phys. Chem. B* 115, 4387–4398. doi:10.1021/jp112315b.
- Llovel, F., Vilaseca, O., Vega, L.F., 2012. Thermodynamic Modeling of Imidazolium-Based Ionic Liquids with the [PF<sub>6</sub>]<sup>-</sup> Anion for Separation Purposes. *Sep. Sci. Technol.* 47, 399–410. doi:10.1080/01496395.2011.635625.
- Meindersma, G.W., Podt, A.J.G., de Haan, A.B., 2006. Ternary liquid-liquid equilibria for mixtures of toluene + n-heptane + an ionic liquid. *Fluid Phase Equilib* 247, 158–168. doi:10.1016/j.fluid.2006.07.002.
- Mota-Babiloni, A., Makhnatch, P., Khodabandeh, R., 2017. Recent investigations in HFCs substitution with lower GWP synthetic alternatives: Focus on energetic performance and environmental impact. *Int. J. Refrig.* 82, 288–301. doi:10.1016/j.ijrefrig.2017.06.026.
- Mota-Babiloni, A., Navarro-Esbrí, J., Barragán-Cervera, Á., Molés, F., Peris, B., 2015. Analysis based on EU Regulation No 517/2014 of new HFC/HFO mixtures as alternatives of high GWP refrigerants in refrigeration and HVAC systems. *Int. J. Refrig.* 52, 21–31. doi:10.1016/j.ijrefrig.2014.12.021.
- Mota-Martinez, M.T., Brandl, P., Hallett, J.P., Mac Dowell, N., 2018. Challenges and opportunities for the utilisation of ionic liquids as solvents for CO<sub>2</sub> capture. *Mol. Syst. Des. Eng.* 3, 560–571. doi:10.1039/c8me00009c.
- Noda, A., Hayamizu, K., Watanabe, M., 2001. Pulsed-gradient spin-echo 1H and 19F NMR ionic diffusion coefficient, viscosity, and ionic conductivity of non-chloroaluminate room-temperature ionic liquids. *J. Phys. Chem. B* 105, 4603–4610. doi:10.1021/jp004132q.
- Noelke, C.J., Shifflett, M.B., 2013. Capture of fluorinated vinyl monomers using ionic liquids. *US 2013/0296499 A1*.
- Oliveira, M.B., Llovel, F., Coutinho, J.A.P., Vega, L.F., 2012. Modeling the [NTf<sub>2</sub>]<sup>-</sup> pyridinium ionic liquids family and their mixtures with the soft statistical associating fluid theory equation of state. *J. Phys. Chem. B* 116, 9089–9100. doi:10.1021/jp303166f.
- Pardo, F., Zarca, G., Urriaga, A., 2020. Separation of Refrigerant Gas Mixtures Containing R32, R134a, and R1234yf through Poly(ether-block -amide) Membranes. *ACS Sustain. Chem. Eng.* 8, 2548–2556. doi:10.1021/acssuschemeng.9b07195.



- Pereira, L.M.C., Martins, V., Kurnia, K.A., Oliveira, M.B., Dias, A.M.A., Llovel, F., Vega, L.F., Carvalho, P.J., Coutinho, J.A.P., 2016. High pressure solubility of CH<sub>4</sub>, N<sub>2</sub>O and N<sub>2</sub> in 1-butyl-3-methylimidazolium dicyanamide: Solubilities, selectivities and soft-SAFT modeling. *J. Supercrit. Fluids* 110, 56–64. doi:10.1016/j.supflu.2015.12.006.
- Pereira, L.M.C., Oliveira, M.B., Dias, A.M.A., Llovel, F., Vega, L.F., Carvalho, P.J., Coutinho, J.A.P., 2013. High pressure separation of greenhouse gases from air with 1-ethyl-3-methylimidazolium methyl-phosphonate. *Int. J. Greenh. Gas Control* 19, 299–309. doi:10.1016/j.ijggc.2013.09.007.
- Pereira, L.M.C., Oliveira, M.B., Llovel, F., Vega, L.F., Coutinho, J.A.P., 2014. Assessing the N<sub>2</sub>O/CO<sub>2</sub> high pressure separation using ionic liquids with the soft-SAFT EoS. *J. Supercrit. Fluids* 92, 231–241. doi:10.1016/j.supflu.2014.06.005.
- Ren, W., Scurto, A.M., 2009. Phase equilibria of imidazolium ionic liquids and the refrigerant gas, 1,1,1,2-tetrafluoroethane (R-134a). *Fluid Phase Equilib* 286, 1–7. doi:10.1016/j.fluid.2009.07.007.
- Schulz, M., Kourkoulas, D., 2014. Regulation (EU) No 517/2014 of the European Parliament and of the Council of 16 April 2014 on fluorinated greenhouse gases and repealing Regulation (EC) No 842/2006. *Off. J. Eur. Union* doi:10.4271/1999-01-0874, 2014, L150/195-230https://doi.org/https://doi.org/.
- Shariati, A., Ashrafmansouri, S.S., Osbuei, M.H., Hooshdaran, B., 2013. Critical properties and acentric factors of ionic liquids. *Korean J. Chem. Eng.* 30, 187–193. doi:10.1007/s11814-012-0118-9.
- Shariati, A., Gutkowski, K., Peters, C.J., 2005. Comparison of the phase behavior of some selected binary systems with ionic liquids. *AIChE J* 51, 1532–1540. doi:10.1002/aic.10384.
- Shiflett, M.B., 2015. Capture of trifluoromethane using ionic liquids. *US 2015/082981 A1*.
- Shiflett, M.B., Harmer, M.A., Junk, C.P., Yokozeki, A., 2006a. Solubility and diffusivity of 1,1,1,2-tetrafluoroethane in room-temperature ionic liquids. *Fluid Phase Equilib* 242, 220–232. doi:10.1016/j.fluid.2006.01.026.
- Shiflett, M.B., Harmer, M.A., Junk, C.P., Yokozeki, A., 2006b. Solubility and diffusivity of difluoromethane in room-temperature ionic liquids. *J. Chem. Eng. Data* 51, 483–495. doi:10.1021/je050386z.
- Shiflett, M.B., Shiflett, A.D., Yokozeki, A., 2011. Separation of tetrafluoroethylene and carbon dioxide using ionic liquids. *Sep. Purif. Technol.* 79, 357–364. doi:10.1016/j.seppur.2011.03.023.
- Shiflett, M.B., Yokozeki, A., 2014a. Process for purifying perfluorinated products. *US 8,771,626 B2*.
- Shiflett, M.B., Yokozeki, A., 2014b. Utilizing ionic liquids for hydrofluorocarbon separation. *US 8,628,644 B2*.
- Shiflett, M.B., Yokozeki, A., 2012. Process for separation of tetrafluoroethylene from carbon dioxide using ionic liquids. *US 8,313,558 B2*.
- Shiflett, M.B., Yokozeki, A., 2011. Process for the separation of diastereomers. *US 8,075,777 B2*.
- Shiflett, M.B., Yokozeki, A., 2010. Separation of carbon dioxide and sulfur dioxide using room-temperature ionic liquid [bmim][MeSO<sub>4</sub>]. *Energy and Fuels* 24, 1001–1008. doi:10.1021/ef900997b.
- Shiflett, M.B., Yokozeki, A., 2009. Solubility of Fluorocarbons in Room Temperature Ionic Liquids, in: *Ionic Liquids: From Knowledge to Application*. ACS 21–42. doi:10.1021/bk-2009-1030.
- Shiflett, M.B., Yokozeki, A., 2008. Binary vapor-liquid and vapor-liquid-liquid equilibria of hydrofluorocarbons (HFC-125 and HFC-143a) and hydrofluoroethers (HFE-125 and HFE-143a) with ionic liquid [emim][Tf<sub>2</sub>N]. *J. Chem. Eng. Data* 53, 492–497. doi:10.1021/je700588d.
- Shiflett, M.B., Yokozeki, A., 2007. Solubility differences of halocarbon isomers in ionic liquid [emim][Tf<sub>2</sub>N]. *J. Chem. Eng. Data* 52, 2007–2015. doi:10.1021/je700295e.
- Shiflett, M.B., Yokozeki, A., 2006a. Vapor-liquid-liquid equilibria of pentafluoroethane and ionic liquid [bmim][PF<sub>6</sub>] mixtures studied with the volumetric method. *J. Phys. Chem. B* 110, 14436–14443. doi:10.1021/jp062437k.
- Shiflett, M.B., Yokozeki, A., 2006b. Vapor - Liquid - Liquid equilibria of hydrofluorocarbons + 1-butyl-3-methylimidazolium hexafluorophosphate. *J. Chem. Eng. Data* 51, 1931–1939. doi:10.1021/je060275f.
- Shiflett, M.B., Yokozeki, A., 2006c. Gaseous absorption of fluoromethane, fluoroethane, and 1,1,2,2-tetrafluoroethane in 1-butyl-3-methylimidazolium hexafluorophosphate. *Ind. Eng. Chem. Res* 45, 6375–6382. doi:10.1021/ie060192s.
- Shiflett, M.B., Yokozeki, A., 2006d. Separation of difluoromethane and pentafluoroethane by extractive distillation using ionic liquid. *Chim. Oggi* 24, 28–30.
- Shiflett, M.B., Yokozeki, A., 2006e. Solubility and diffusivity of hydrofluorocarbons in room-temperature ionic liquids. *AIChE J* 52, 1205–1219. doi:10.1002/aic.10685.
- Shiflett, M.B., Yokozeki, A., Knapp, J.P., 2011. Process for the separation of fluorocarbons using ionic liquids. *US 7,964,760 B2*.
- Sujatha, I., Venkatarathnam, G., 2018. Comparison of performance of a vapor absorption refrigeration system operating with some hydrofluorocarbons and hydrofluoroolefins as refrigerants along with ionic liquid [hmim][TF<sub>2</sub>N] as the absorbent. *Int. J. Refrig.* 88, 370–382. doi:10.1016/j.ijrefrig.2018.03.004.
- Urahata, S.M., Ribeiro, M.C.C., 2004. Structure of ionic liquids of 1-alkyl-3-methylimidazolium cations: A systematic computer simulation study. *J. Chem. Phys.* 120, 1855–1863. doi:10.1063/1.1635356.
- Vatani, M., Asghari, M., Vakili-Nezhaad, G., 2012. Application of Genetic Algorithm to the calculation of parameters for NRTL and Two-Suffix Margules models in ternary extraction ionic liquid systems. *J. Ind. Eng. Chem.* 18, 1715–1720. doi:10.1016/j.jiec.2012.03.008.
- Vega, L.F., Vilaseca, O., Llovel, F., Andreu, J.S., 2010. Modeling ionic liquids and the solubility of gases in them: Recent advances and perspectives. *Fluid Phase Equilib* 294, 15–30. doi:10.1016/j.fluid.2010.02.006.
- Vilaseca, O., Llovel, F., Yustos, J., Marcos, R.M., Vega, L.F., 2010. Phase equilibria, surface tensions and heat capacities of hydrofluorocarbons and their mixtures including the critical region. *J. Supercrit. Fluids* 55, 755–768. doi:10.1016/j.supflu.2010.10.015.
- Wasserscheid, P., Van Hal, R., Bösmann, A., 2002. 1-n-butyl-3-methylimidazolium ([bmim]) octylsulfate - An even “greener” ionic liquid. *Green Chem* 4, 400–404. doi:10.1039/b205425f.
- Yokozeki, A., Shiflett, M.B., 2009. Separation of carbon dioxide and sulfur dioxide gases using room-temperature ionic liquid [hmim][Tf<sub>2</sub>N]. *Energy and Fuels* 23, 4701–4708. doi:10.1021/ef900649c.
- Yokozeki, A., Shiflett, M.B., 2007. Vapor-liquid equilibria of ammonia + ionic liquid mixtures. *Appl. Energy* 84, 1258–1273. doi:10.1016/j.apenergy.2007.02.005.
- Yokozeki, A., Shiflett, M.B., 2006. Global phase behaviors of trifluoromethane in ionic liquid [bmim][PF<sub>6</sub>]. *AIChE J* 52, 3952–3957. doi:10.1002/aic.11007.
- Zarca, G., Ortiz, I., Urtiaga, A., 2018. Novel solvents based on thiocyanate ionic liquids doped with copper(I) with enhanced equilibrium selectivity for carbon monoxide separation from light gases. *Sep. Purif. Technol.* 196, 47–56. doi:10.1016/j.seppur.2017.06.069.
- Zarca, G., Ortiz, I., Urtiaga, A., Llovel, F., 2017a. Accurate thermodynamic modeling of ionic liquids/metal salt mixtures: Application to carbon monoxide reactive absorption. *AIChE J* 63, 3532–3543. doi:10.1002/aic.15790.
- Zarca, G., Ortiz, I., Urtiaga, A., Llovel, F., 2017b. Modelling the physical properties of ionic liquid/metal salt mixtures with the soft-SAFT equation of state: application to carbon monoxide reactive separation. *Comput. Aided Chem. Eng.* 40, 217–222. doi:10.1016/B978-0-444-63965-3.50038-6.
- Zhao, Y., Gani, R., Afzal, R.M., Zhang, X., Zhang, S., 2017. Ionic liquids for absorption and separation of gases: An extensive database and a systematic screening method. *AIChE J* 63, 1353–1367. doi:10.1002/aic.15618.

# **Thermodynamic and process modeling of the recovery of R410A compounds with ionic liquids**

**S. Asensio-Delgado<sup>1</sup>, D. Jovell<sup>2</sup>, G. Zarca<sup>1</sup>, A. Urtiaga<sup>1</sup>, F. Llovell\***

*<sup>1</sup>Dep. Chemical and Biomolecular Engineering, Universidad de Cantabria, Av. Los Castros s/n, Santander 39005, Spain.*

*<sup>2</sup>Dep. Chemical Engineering and Materials Science, IQS School of Engineering, Universitat Ramon Llull, Via Augusta 390, Barcelona 08017, Spain*

\*Corresponding author: [felix.llovell@iqs.edu](mailto:felix.llovell@iqs.edu)

## **Supplementary Information**

## A. Additional details on the soft-SAFT EoS

The soft-SAFT EoS is written in terms of the different microscopic contributions to the residual molar Helmholtz free energy (being the result of the total free energy,  $A$ , minus the ideal term,  $A^{id}$ ), according to Eq. (S1),

$$A^{res} = A - A^{id} = A^{ref} + A^{chain} + A^{assoc} \quad (S1)$$

The  $A^{ref}$  refers to the reference term (including the intermolecular attractive and repulsive contributions to the energy between each pair of segments using a spherical LJ potential), the chain term  $A^{chain}$  arises from the presence of covalent bonds between the different segments, while  $A^{assoc}$  contributes to the free energy according to the hydrogen-bonding association of the different segments through some defined association sites.

The LJ reference term is defined for each fluid by a characteristic segment diameter ( $\sigma_{ii}$ ) and depth of the potential well (i.e. the dispersive energy) ( $\varepsilon_{ii}/k_B$ ) between two segments. This contribution is calculated using a correlation equation fitted to LJ monomers simulation data (Johnson et al., 1993). The van der Waals one-fluid theory is applied with the modified Lorentz-Berthelot mixing rules (Eq. (S2) and Eq. (S3)) to extend this term to mixtures. Here,  $\eta_{ij}$  and  $\xi_{ij}$  (i.e.,  $i$  and  $j$  are different species) are the size and energy binary parameters, respectively. If both values are equal to one, the original Lorentz-Berthelot combining rules are recovered, and the LJ reference term for mixtures is calculated without any additional fitting.

$$\sigma_{ij} = \eta_{ij} \left( \frac{\sigma_{ii} + \sigma_{jj}}{2} \right) \quad (S2)$$

$$\varepsilon_{ij} = \xi_{ij} \sqrt{\varepsilon_{ii} \cdot \varepsilon_{jj}} \quad (S3)$$

The chain and association terms are directly expressed for mixtures as a function of the molar composition,  $x_i$ , and are formally equivalent in the different versions of SAFT.

$$A^{chain} = RT \sum_i x_i (1 - m_i) \ln g_{ij}^{LJ} \quad (S4)$$

$$A^{assoc} = RT \sum_i x_i \sum_{\alpha} \left( \ln X_{\alpha,i} - \frac{X_{\alpha,i}}{2} \right) + \frac{M_i}{2} \quad (S5)$$

where  $T$  is the temperature,  $R$  is the ideal gas constant. The chain term (Eq. (S4)) depends on the radial distribution function ( $g_{ij}^{LJ}$ ) of the fluid and the chain length parameter ( $m_i$ ) that describes the number of LJ spheres forming the chain. On the other hand, the association term (Eq. (S5)) depends on the total number of association sites of each

component ( $M_i$ ), and the fraction of molecules not bonded to the site  $\alpha$  ( $X_\alpha$ ). To calculate  $X_{\alpha,i}$  in Eq. (S5) one needs to adjust two parameters for each hydrogen bonding: the site-site bonding-volume of association  $K_{\alpha\beta,ii}^{HB}$  and the site-site association energy  $\varepsilon_{\alpha\beta,ii}^{HB}$ . These parameters are related to  $X_{\alpha,i}$  through a mass action balance (see Eq. (S6) and Eq. (S7)).

$$X_{\alpha,i} = \frac{1}{1 + \rho \sum_{j=1}^n x_j \sum_{\beta=1}^s X_{\beta,j} \Delta_{\alpha\beta,ij}} \quad (\text{S6})$$

$$\Delta_{\alpha\beta,ij} = K_{\alpha\beta,ij}^{HB} \left[ e^{(\varepsilon_{\alpha\beta,ij}^{HB}/k_B T)} - 1 \right] g_{ij}^{LJ} \quad (\text{S7})$$

$\alpha$  and  $\beta$  in Eqs. (S6) and (S7) refer to different association bonding sites, and  $\rho$  is the total density. The cross-association interaction for the site-bonding volume and site-site association energy can be obtained by means of equivalent Lorentz-Berthelot combining rules, without the addition of binary parameters.

$$K_{\alpha\beta,ij}^{HB} = \left( \frac{\sqrt[3]{K_{\alpha\beta,ii}^{HB}} + \sqrt[3]{K_{\alpha\beta,jj}^{HB}}}{2} \right)^3 \quad (\text{S8})$$

$$\varepsilon_{\alpha\beta,ij}^{HB} = \sqrt{\varepsilon_{\alpha\beta,ii}^{HB} \cdot \varepsilon_{\alpha\beta,jj}^{HB}} \quad (\text{S9})$$



## B. Binary mixtures of HFCs and ILs

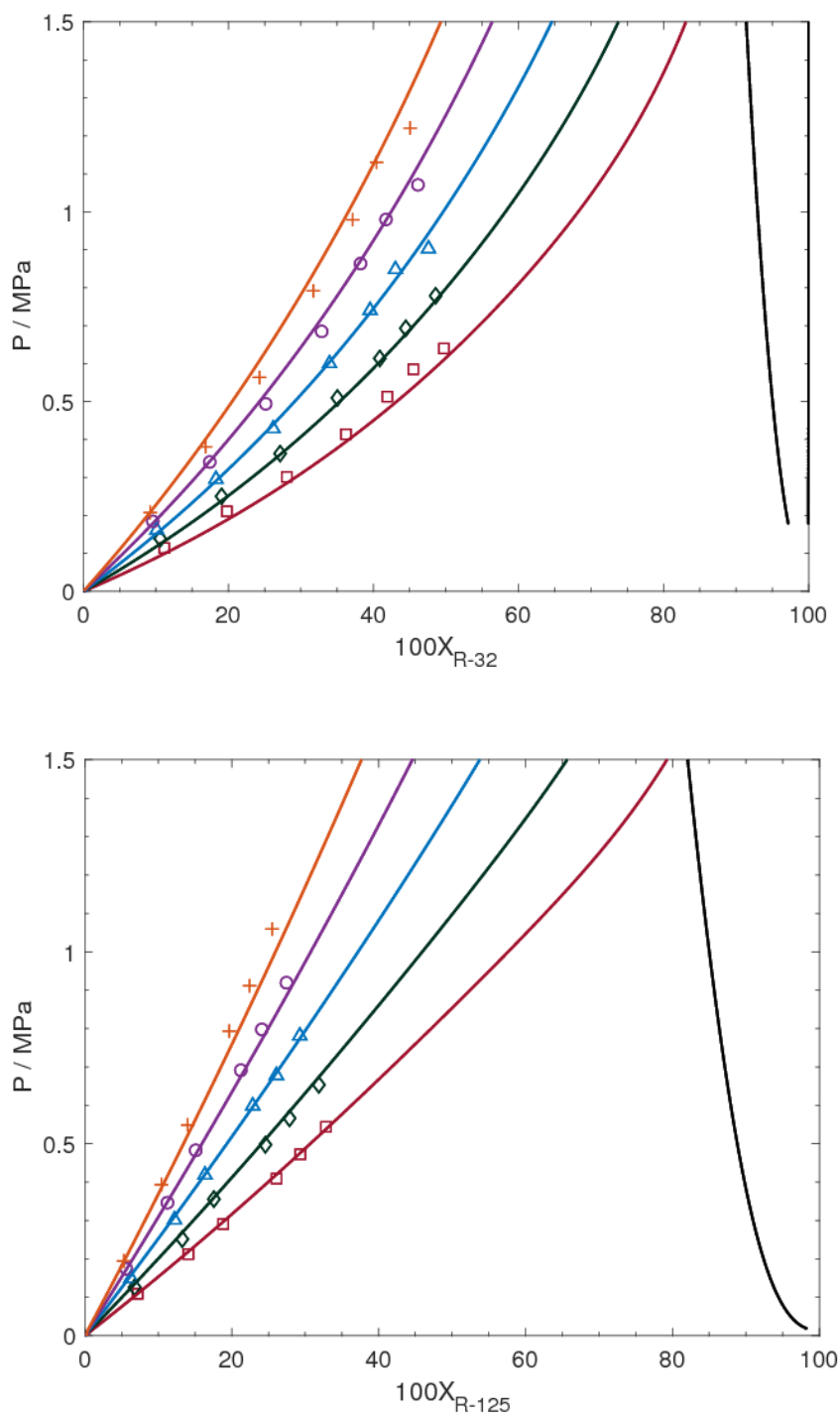


**Figure S1.** Pressure-composition diagram of the systems (a) R32 + [C<sub>6</sub>mim][Tf<sub>2</sub>N] and (b) R125 + [C<sub>6</sub>mim][Tf<sub>2</sub>N] at several temperatures: 303 (red squares), 313 (green diamonds), 323 (blue triangles), 333 (violet circles) and 343 K (orange crosses). Symbols represent the experimental data (Liu et al., 2015) and solid lines are the soft-SAFT calculations.

**Table S1.** Henry's law constant correlation parameters of Eq. (11).

Ionic liquid	HFC	<b>A</b>	<b>B</b>
[C <sub>2</sub> mim][Tf <sub>2</sub> N]	R32	-2581.02	8.652
	R125	-2411.84	8.681
[C <sub>6</sub> mim][Tf <sub>2</sub> N]	R32	-2462.40	7.987
	R125	-2287.55	7.986
[C <sub>4</sub> mim][PF <sub>6</sub> ]	R32	-2255.43	7.770
	R125	-1919.86	7.727

### C. Process simulation details: Implementation of the thermophysical properties of ILs

The critical properties of the IL were taken from the work of Shariati et al. (Shariati et al., 2013), who estimated the critical properties of ten ILs, including [C<sub>2</sub>mim][Tf<sub>2</sub>N], by making an optimum fit of the calculated VLE data of binary mixtures of CO<sub>2</sub>+IL to the experimental values found in literature using the Peng-Robinson EoS and a differential evolution optimization method.

The ideal heat gas capacity was estimated using the extended Joback method presented in the work of Ge et al. (Ge et al., 2008).. The data was used to fit a polynomial (CPIG in Aspen) of the form,

$$C_p^\circ = C_1 + C_2T + C_3T^2 + C_4T^3 + C_5T^4 + C_6T^5 \quad \text{for } 0 \leq T \leq 1000 \text{ K} \quad (\text{S10})$$

where  $C_p^\circ$  is the ideal gas heat capacity (J mol<sup>-1</sup> K<sup>-1</sup>).

The vapor pressure information was taken from the data presented by Heym et al. (Heym et al., 2015), who determined the vapor pressure of several ionic liquids, including in a magnetic suspension balance under HV condition. The results were then regressed into a simplified Antoine-like simplified equation assuming constant entropy term and enthalpy of vaporization,

$$\frac{P_{vap}}{P_{ref}} = C_{vap} \exp\left(\frac{-\Delta_{vap}H}{RT}\right) \quad \text{with } P_{ref} = 1 \text{ Pa} \quad (\text{S11})$$

where  $C_{vap}$  is the constant entropy term (Pa) and  $\Delta_{vap}H$  is the enthalpy of vaporization (kJ mol<sup>-1</sup>). The parameters of vaporization for [C<sub>2</sub>mim][Tf<sub>2</sub>N] are  $3.5 \times 10^{11}$  and 120.0 respectively. As in the previous case, the experimental data has been adjusted to the NIST-TDE Polynomial for Liquid Vapor Pressure (PLTDEP):

$$\ln(P_{vap}) = C_1 + \frac{C_2}{T} + C_3 \ln T + C_4T \quad \text{for } 256.91 \leq T \leq 723.13 \text{ K} \quad (\text{S12})$$

Since, to our knowledge, no experimental data has been published regarding the heat of vaporization of [C<sub>2</sub>mim][Tf<sub>2</sub>N], the Clausius-Clapeyron equation has been applied to predict the heat of vaporization with liquid vapor pressure data since the vapor phase is assumed as an ideal gas and the molar volume of the liquid is negligible against the molar volume of the vapor. The Clausius-Clapeyron equation is expressed as,

$$\Delta H_{vap} = -R \frac{d \ln P_{vap}}{d (1/T)} \quad (S13)$$

Being  $\Delta H_{vap}$  the enthalpy of vaporization (J mol<sup>-1</sup>) and R the ideal gas constant (J K<sup>-1</sup> mol<sup>-1</sup>).

The results were regressed, as in the work of Chen et al. (Chen et al., 2017), to the DHVLWT model: an ASPEN model based on the Watson equation (Eq. S14) used to calculate the heat of vaporization.

$$\Delta H_{vap} = C_1 \frac{1-T/T_c}{1-C_2/T_c}^{C_3+C_4(1-T/T_c)} \quad (S14)$$

Finally, liquid viscosity data,  $\eta$ , were obtained from the literature for all the components, including the ionic liquid, and fitted to an Andrade-like Aspen Model named MULAND. Although some authors suggested the use of a more simple two-constant Arrhenius equation (De Riva et al., 2014), the fitting to experimental data produced worse results in the range of operating conditions. Hence, the three-constant Andrade's model was kept.

$$\ln \eta = C_1 + \frac{C_2}{T} + C_3 \ln T \quad (S15)$$

The critical values, normal boiling point, acentric factor ( $\omega$ ) and all the optimized constants for the ideal heat capacity, vapor pressure, enthalpy of vaporization and liquid viscosity correlations can be found in Tables S2 and S3.

The nonrandom two-liquid model (NRTL) is used to describe the nonideal behavior in the liquid phase of the mixture, as done by many researchers to model the behavior of mixtures containing ILs (Meindersma et al., 2006; Shiflett et al., 2011; Vatani et al., 2012). An ideal gas model (IG) is used to describe the gas phase.

The NRTL-model calculates the activity coefficient from the parameters given in order to predict the VLE. Aspen plus provides an extended version of the basic NRTL model with theoretically a better representation of the temperature dependence of the activity coefficients. The equation is expressed as,

$$\ln \gamma_i = \frac{\sum_j \tau_{ji} G_{ji} x_{ji}}{\sum_k G_{ki} x_k} + \sum_j \frac{x_j G_{ij}}{\sum_k G_{kj} x_k} \left( \tau_{ij} - \frac{\sum_n x_n \tau_{nj} G_{nj}}{\sum_k G_{kj} x_k} \right) \quad (S16)$$

with  $\tau_{ij} = a_{ij} + \frac{b_{ij}}{T} + e_{ij} \ln T + f_{ij}T$ ,  $\tau_{jj} = 0$ ,  $G_{ij} = \exp(-\alpha_{ij}\tau_{ij})$ ,  $G_{jj} = 1$  and  $\alpha_{ij} = c_{ij} + d_{ij}(T - 273.15)$

In this work, only parameters a-c are used since this keeps the model closer to the original NRTL model. The parameters are provided in Table S4.

**Table S2.** Critical Properties of [C<sub>2</sub>mim][Tf<sub>2</sub>N]

Property	Value
T <sub>b</sub> (K)	805.930
T <sub>c</sub> (K)	1244.68
P <sub>c</sub> (bar)	32.6
V <sub>c</sub> (cm <sup>3</sup> /mol)	892.890
ω	0.182

**Table S3.** Summarized model parameters for [C<sub>2</sub>mim][Tf<sub>2</sub>N]

	C1	C2	C3	C4
CPIG	29.98	-1.333 x 10 <sup>5</sup>	0.000	0.000
PLTDEP	1388.3	-71662.4	-266.8	0.2015
DHVLWT	109.1	1074.49	3.1 x 10 <sup>-3</sup>	0.033
MULAND	-1293	8177.6	1730	-

**Table S4.** NRTL Parameters for the system R125 + R32 + [C<sub>2</sub>mim][Tf<sub>2</sub>N]

Component <i>i</i>	Component <i>j</i>	A <sub>ij</sub>	A <sub>ji</sub>	B <sub>ij</sub>	B <sub>ji</sub>	C <sub>ij</sub>
R32	R125	0.0363046	-0.23109	98.4229	12.6789	0.5
R32	[C <sub>2</sub> mim][Tf <sub>2</sub> N]	1.01304	-1.41622	-88.1006	142.254	0.5
R125	[C <sub>2</sub> mim][Tf <sub>2</sub> N]	4.46939	-0.030298	-108.64	-277.433	0.298343

## Bibliography

- Chen, H.H., Chen, M.K., Chen, B.C., Chien, I.L., 2017. Critical Assessment of Using an Ionic Liquid as Entrainer via Extractive Distillation. *Ind. Eng. Chem. Res.* 56, 7768–7782.  
<https://doi.org/10.1021/acs.iecr.7b01223>
- De Riva, J., Ferro, V.R., Del Olmo, L., Ruiz, E., Lopez, R., Palomar, J., 2014. Statistical refinement and fitting of experimental viscosity-to-temperature data in ionic liquids.

- Ind. Eng. Chem. Res. 53, 10475–10484. <https://doi.org/10.1021/ie5014426>
- Ge, R., Hardacre, C., Jacquemin, J., Nancarrow, P., Rooney, D.W., 2008. Heat capacities of ionic liquids as a function of temperature at 0.1 MPa. Measurement and prediction. J. Chem. Eng. Data 53, 2148–2153. <https://doi.org/10.1021/je800335v>
- Heym, F., Korth, W., Thiessen, J., Kern, C., Jess, A., 2015. Evaporation and decomposition behavior of pure and supported ionic liquids under thermal stress. Chemie-Ingenieur-Technik 87, 791–802. <https://doi.org/10.1002/cite.201400139>
- Johnson, J.K., Zollweg, J.A., Gubbins, K.E., 1993. The Lennard-Jones equation of state revisited. Mol. Phys. 78, 591–618. <https://doi.org/10.1080/00268979300100411>
- Liu, X., He, M., Lv, N., Qi, X., Su, C., 2015. Vapor-liquid equilibrium of three hydrofluorocarbons with [HMIM][Tf2N]. J. Chem. Eng. Data 60, 1354–1361. <https://doi.org/10.1021/je501069b>
- Meindersma, G.W., Podt, A.J.G., de Haan, A.B., 2006. Ternary liquid-liquid equilibria for mixtures of toluene + n-heptane + an ionic liquid. Fluid Phase Equilib. 247, 158–168. <https://doi.org/10.1016/j.fluid.2006.07.002>
- Shariati, A., Ashrafmansouri, S.S., Osbuei, M.H., Hooshdaran, B., 2013. Critical properties and acentric factors of ionic liquids. Korean J. Chem. Eng. 30, 187–193. <https://doi.org/10.1007/s11814-012-0118-9>
- Shiflett, M.B., Shiflett, A.D., Yokozeki, A., 2011. Separation of tetrafluoroethylene and carbon dioxide using ionic liquids. Sep. Purif. Technol. 79, 357–364. <https://doi.org/10.1016/j.seppur.2011.03.023>
- Vatani, M., Asghari, M., Vakili-Nezhaad, G., 2012. Application of Genetic Algorithm to the calculation of parameters for NRTL and Two-Suffix Margules models in ternary extraction ionic liquid systems. J. Ind. Eng. Chem. 18, 1715–1720. <https://doi.org/10.1016/j.jiec.2012.03.008>

**3.3. Scientific publication 3. “Vapor-liquid equilibria and diffusion coefficients of difluoromethane, 1,1,1,2-tetrafluoroethane, and 2,3,3,3-tetrafluoropropene in low-viscosity ionic liquids”, Salvador Asensio-Delgado, Fernando Pardo, Gabriel Zarca, Ane Urtiaga, Journal of Chemical & Engineering Data, 65 (2020) 4242-4251**

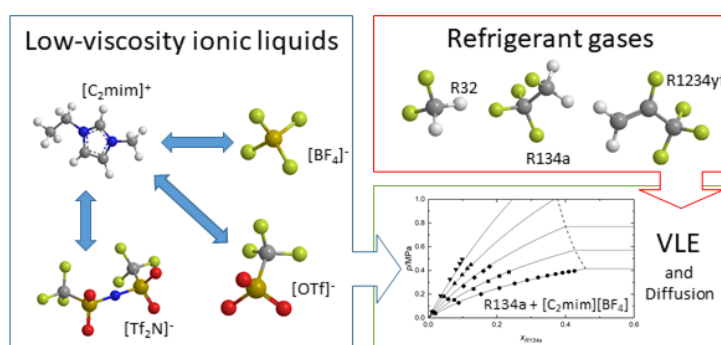


Figure 17. Graphical abstract of the article “Vapor-liquid equilibria and diffusion coefficients of difluoromethane, 1,1,1,2-tetrafluoroethane, and 2,3,3,3-tetrafluoropropene in low-viscosity ionic liquids”

This article is the beginning of the experimental part of the thesis. Here, the objective was to fill the gaps in the missing information on the absorption of F-gases in ILs to be able to analyze the data and infer trends. The article focuses in the three most important refrigerant gases nowadays, R32, R134a, and R1234yf, and in low-viscosity ILs, as their use in industrial scale processes requires low viscosity to favor pumping and mass transfer. Then, five systems that had not been studied before were addressed as Table 6 depicts with question marks. The Henry’s law constants presented in Table 6 were calculated from published data [1]–[4].

The results showed that low molar volume ILs with few fluorine atoms increased the selectivity for the separation of F-gases, which aided in the selection of the ILs used in the following articles. Figure 17 shows the graphical abstract available in the online version and in the first page of the article.

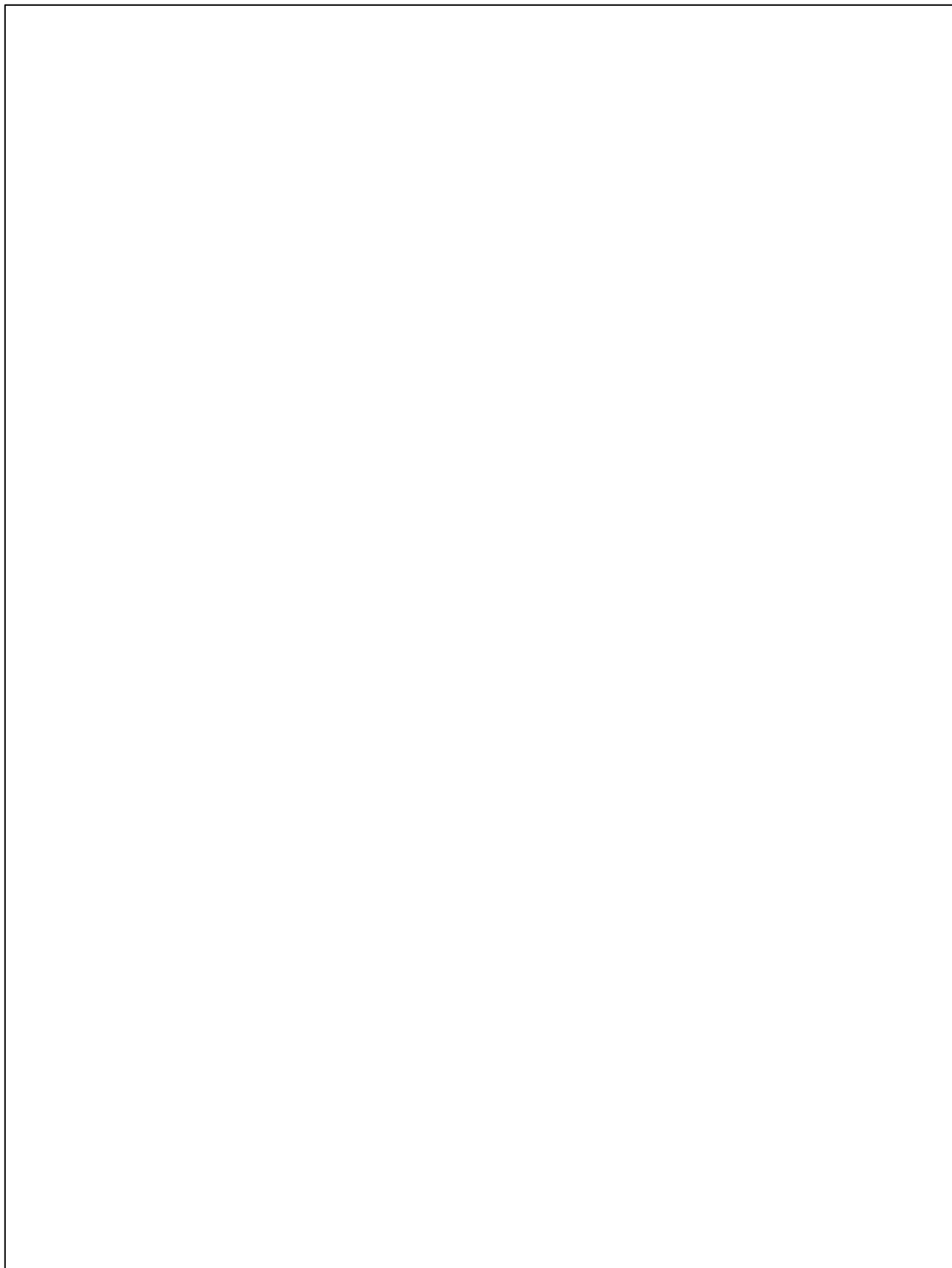
Table 6. Systems studied in the scientific publication 3.

Ionic liquid		Henry's law constants (MPa)				
Anion	Cation	Molar volume (cm <sup>3</sup> mol <sup>-1</sup> )	Viscosity (mPa s)	Most used refrigerants in the newest generation		
				HFC-R32	HFC-R134a	HFO-R1234yf
[BF <sub>4</sub> ]	[C <sub>2</sub> mim]	154.4	38.8	?	?	15.56
[OTf]	[C <sub>2</sub> mim]	189.9	42.9	1.83	?	?
[Tf <sub>2</sub> N]	[C <sub>2</sub> mim]	257.7	31.3	0.96	0.73	?

## References

- [1] L. Dong, D. Zheng, G. Sun, and X. Wu, "Vapor-Liquid Equilibrium Measurements of Difluoromethane + [Emim]OTf, Difluoromethane + [Bmim]OTf, Difluoroethane + [Emim]OTf, and Difluoroethane + [Bmim]OTf Systems," *J. Chem. Eng. Data*, vol. 56, pp. 3663–3668, 2011, doi: 10.1021/je2005566.
- [2] M. B. Shiflett, M. A. Harmer, C. P. Junk, and A. Yokozeki, "Solubility and Diffusivity of Difluoromethane in Room-Temperature Ionic Liquids," *J. Chem. Eng. Data*, vol. 51, pp. 483–495, 2006, doi: 10.1021/je050386z.
- [3] M. B. Shiflett and A. Yokozeki, "Solubility Differences of Halocarbon Isomers in Ionic Liquid [emim][Tf<sub>2</sub>N]," *J. Chem. Eng. Data*, vol. 52, pp. 2007–2015, 2007, doi: 10.1021/je700295e.
- [4] Y. Sun, Y. Zhang, X. Wang, J. M. Prausnitz, and L. Jin, "Gaseous absorption of 2,3,3,3-tetrafluoroprop-1-ene in three imidazolium-based ionic liquids," *Fluid Phase Equilib.*, vol. 450, pp. 65–74, 2017, doi: 10.1016/j.fluid.2017.07.013.

The graphical abstract of publication 3 was featured in the cover page of the 9<sup>th</sup> issue of volume 65 of the Journal of Chemical & Engineering Data





1  
2  
3  
4  
5  
6  
7 Vapor-liquid equilibria and diffusion coefficients of  
8  
9  
10 difluoromethane, 1,1,1,2-tetrafluoroethane and 2,3,3,3-  
11  
12  
13 tetrafluoropropene in low-viscosity ionic liquids  
14  
15  
16  
17  
18  
19  
20  
21  
22  
23

24 **Authors:**

25  
26  
27 **Salvador Asensio-Delgado, Fernando Pardo, Gabriel Zarca\*, Ane Urtiaga**

28  
29  
30 Department of Chemical and Biomolecular Engineering, Universidad de Cantabria,

31  
32  
33 Av. Los Castros 46, Santander 39005, Spain.

34  
35  
36  
37 \*Corresponding author e-mail address: [zarcag@unican.es](mailto:zarcag@unican.es)  
38  
39  
40  
41  
42  
43  
44  
45  
46  
47  
48  
49  
50  
51  
52  
53  
54  
55  
56  
57  
58  
59  
60

**Abstract**

The phase-down of hydrofluorocarbons (HFCs) established by the Kigali Amendment to the Montreal Protocol is leading to the formulation and commercialization of new refrigerant blends containing hydrofluoroolefins (HFOs), such as 2,3,3,3-tetrafluoropropene (R1234yf), and HFCs with moderate global warming potential, namely, difluoromethane (R32) and 1,1,1,2-tetrafluoroethane (R134a). Moreover, the recycling of refrigerants is attracting attention as a means to reduce the amount of new HFCs produced and their release to the environment. To that end, the use of ionic liquids has been proposed as entrainers to separate refrigerants with close-boiling points or azeotropic blends. Thus, the vapor-liquid equilibria and diffusion coefficients of the refrigerant-ionic liquid pairs formed by R32 + [C<sub>2</sub>mim][BF<sub>4</sub>], R134a + [C<sub>2</sub>mim][BF<sub>4</sub>], R134a + [C<sub>2</sub>mim][OTf], R1234yf + [C<sub>2</sub>mim][OTf] and R1234yf + [C<sub>2</sub>mim][Tf<sub>2</sub>N] are studied using an isochoric saturation method at temperatures ranging from 283.15 to 323.15 K and pressures up to 0.9 MPa. In addition, the solubility behavior is successfully modeled using the non-random two-liquid activity coefficient method, and the Henry's law constants at infinite dilution, solvation energies and infinite dilution activity coefficients are calculated.

## 1. Introduction

Hydrofluorocarbons (HFCs) are fluorinated gases widely used in refrigeration and air conditioning (RAC) as substitutes for the ozone-depleting substances that were phased out under the Montreal Protocol (MP).<sup>1,2</sup> Despite their zero ozone depletion potential (ODP), HFCs still exhibit high global warming potential (GWP), which makes them environmentally concerning greenhouse gases<sup>3</sup> to be phased out under the Kigali Amendment to the MP. In contrast, hydrofluoroolefins (HFOs) have been proposed as a new generation of refrigerants because of their zero ODP, low GWP, and short atmospheric lifetime.<sup>4</sup> One of the most common HFOs is 2,3,3,3-tetrafluoropropene (R1234yf, GWP = 4), which is being currently used in pure form in mobile air conditioning systems by the automotive sector. However, HFOs are mildly flammable (ASHRAE category A2L) and their use is constraint to a limited set of temperatures, thus affecting the refrigeration efficiency in refrigerators and freezers of commercial use when used as pure compounds.<sup>5-7</sup> For these reasons, HFOs are usually blended with HFCs such as difluoromethane (R32, GWP = 675) and 1,1,1,2-tetrafluoroethane (R134a, GWP = 1430), which are very well-known refrigerants with a strong penetration in the RAC market. These HFC/HFO blends (e.g., R513A, R454C, R449A) are being commercialized as environmentally friendly drop-in replacements of typical HFC-only mixtures (e.g., R410A, R404A, R407 series).

Ionic liquids (ILs) are a family of compounds that has attracted attention in several fields because of their interesting properties, namely, extremely low vapor pressure, chemical and thermal stability, wide liquid temperature range or non-flammability, among others.<sup>8-10</sup> The use of ILs as entrainers has been proposed to allow for the separation of azeotropic or close-boiling point blends of refrigerant gases,<sup>10-24</sup> and as working fluids in absorption refrigeration systems.<sup>25-34</sup> The efficient separation of refrigerant blends would promote a more circular economy in the RAC sector, whereby HFCs and HFOs recovered from end-of-life equipment are used to formulate novel low GWP blends.<sup>35</sup> In this sense, ILs provide several benefits over conventional

1  
2  
3 molecular solvents in the design of separation processes because solvent evaporation is  
4 avoided, and they are not flammable nor corrosive and do not release toxic vapors.<sup>36</sup>  
5  
6 Furthermore, the separation of some HFC/HFO refrigerant mixtures by conventional methods is  
7  
8 challenging because these blends typically have very small temperature glide, i.e., small  
9  
10 difference between the refrigerant blend dew point and bubble point at constant pressure (e.g.,  
11  
12 system R32 + R1234yf) or present azeotropic behavior (e.g., system R134a + R1234yf),<sup>37–39</sup> which  
13  
14 makes necessary the use of a mass separation agent to improve the purification process.  
15  
16  
17

18  
19 Thus, this work focuses on increasing current knowledge on the ability of ILs to perform the  
20  
21 separation of new HFC/HFO refrigerant blends. We are particularly interested in examining the  
22  
23 absorption of common HFCs and HFOs into low-viscosity ILs. The interest in low-viscosity ILs  
24  
25 arises as a means to overcome scale-up problems associated to low mass transfer rates and high  
26  
27 pumping costs of highly viscous ILs.<sup>36,40</sup> Moreover, the absorption process in ILs is reported to  
28  
29 be kinetically controlled so that using low-viscosity ILs would enhance gas diffusion coefficients  
30  
31 and, consequently, lead to higher recoveries and more energy-efficient separations.<sup>41</sup> Thus, we  
32  
33 present the experimental gas solubility and diffusion coefficients of refrigerants R32, R134a and  
34  
35 R1234yf in 1-ethyl-3-methylimidazolium tetrafluoroborate ( $[\text{C}_2\text{mim}][\text{BF}_4]$ ), 1-ethyl-3-  
36  
37 methylimidazolium trifluoromethanesulfonate ( $[\text{C}_2\text{mim}][\text{OTf}]$ ) and 1-ethyl-3-methylimidazolium  
38  
39 bis(trifluoromethylsulfonyl)imide ( $[\text{C}_2\text{mim}][\text{Tf}_2\text{N}]$ ) for the binary systems that have not been  
40  
41 previously reported in the literature, at temperatures ranging from 283.15 to 323.15 K and  
42  
43 pressures up to 0.9 MPa. In addition, the solubility behavior is modeled using the non-random  
44  
45 two-liquid activity coefficient model (NRTL).  
46  
47  
48  
49  
50  
51  
52  
53

## 54 **2. Experimental section**

### 55 **2.1. Materials.**

56  
57  
58  
59  
60

R32 (99.9%) was purchased from Coproven Climatización (Gas Servei licensed supplier, Spain). R134a (99.8%) and R1234yf (99.9%) were supplied by Carbueros Metálicos (Air Products group, Spain). The ILs [C<sub>2</sub>mim][BF<sub>4</sub>], [C<sub>2</sub>mim][OTf] and [C<sub>2</sub>mim][Tf<sub>2</sub>N] were purchased from Sigma-Aldrich. Before use, the three ILs were vacuum dried at 333 K for 24 h and their water content was measured using the Karl Fischer titration. The purity of all compounds and the viscosity and water content of ILs are specified in Table 1.

Table 1. Chemical samples used in this work

Chemical	CAS No.	Supplier	Fraction purity	$\mu\text{mPa}\cdot\text{s}$	Purification method	Water content (ppm)
[C <sub>2</sub> mim][BF <sub>4</sub> ]	143314-16-3	Sigma-Aldrich, Inc.	>98 wt %	32.31 <sup>42</sup>	Vacuum drying	15
[C <sub>2</sub> mim][OTf]	145022-44-2	Sigma-Aldrich, Inc.	>98 wt %	35.98 <sup>43</sup>	Vacuum drying	10
[C <sub>2</sub> mim][Tf <sub>2</sub> N]	174899-82-2	Sigma-Aldrich, Inc.	>98 wt %	26.9 <sup>44</sup>	Vacuum drying	10
R32	75-10-5	Gas Servei, S.A.	>99.9 vol %			
R134a	811-97-2	Air Products and Chemicals, Inc.	>99.8 vol %			
R1234yf	754-12-1	Air Products and Chemicals, Inc.	>99.9 vol %			

## 2.2. Experimental apparatus and procedure.

An isochoric saturation method was used to measure the absorption of gases in the selected ILs. The experimental system, described in detail in previous works,<sup>8,9,36</sup> consists of an absorption chamber and a storage cylinder connected by a valve. The absorption chamber is a jacketed stirred tank reactor (Buchi, model Picoclave, 170 mL), equipped with a pressure transducer (Aplisens, model PCE-28,  $\pm 0.001$  bar) and a Pt-100 temperature sensor, connected to a cryothermostatic bath (Julabo, model F25-ME,  $\pm 0.01$  K). The storage cylinder (140 mL) is equipped with an absolute digital manometer (Keller, model Leo 2,  $\pm 0.001$  bar). The absorption chamber was loaded with  $\sim 35$  g ( $\pm 0.0001$  g) of the vacuum dried IL. The difference between the total available volume and loaded IL volume is large enough to ensure that the measurements are independent of IL volumetric expansion as will be shown by the validation experiments in

Figure 1. Before each experiment, the IL was degassed at 333 K for a minimum of 6 h. This experimental system allows for the determination of both solubility and diffusivity in a single experiment. First, the temperature and pressure of the gas-filled storage cylinder were recorded. Then, the valve connecting both sections was opened and the absorption process was allowed to proceed spontaneously for the first 20 minutes for diffusivity measurements.<sup>45</sup> After that, the stirrer was set to 500 rpm and gas absorption proceeded until the system reached equilibrium conditions, this is, when pressure remained constant for more than 20 minutes.

### 2.3. Solubility measurement

Solubility is derived from temperature and pressure data as follows. The molar fraction of refrigerant gas dissolved in the IL is defined as:

$$x = \frac{n_{abs}}{n_l + n_{abs}} \quad (1)$$

where  $n_l$  are moles of IL and  $n_{abs}$  are the total dissolved moles of refrigerant. The isochoric saturation method was applied in several steps so that  $n_{abs}$  is calculated from the amount of gas dissolved in each step,  $n_i$ , plus the amount dissolved in the previous  $k$  steps:

$$n_{abs} = n_i + \sum_{k=1}^{i-1} n_k \quad (2)$$

where  $n_i$  is calculated as the difference between the initial and final moles in the vapor phase as follows:

$$n_i = \rho_{(i,s)} \cdot V_s + \rho_{(i-1,c)} \cdot (V_c - V_l) - \rho_{(i,eq)} \cdot (V_s + V_c - V_l) \quad (3)$$

In Eq. (3),  $V_s$ ,  $V_c$  and  $V_l$  are the storage cylinder, sorption chamber and loaded IL volumes (L), respectively, and  $\rho_{i,s}$ ,  $\rho_{i-1,c}$  and  $\rho_{i,eq}$  are the gas molar densities ( $\text{mol} \cdot \text{L}^{-1}$ ) in the storage cylinder, the sorption chamber and at equilibrium conditions, respectively. Molar densities were

calculated from pressure and temperature data using the cubic Peng-Robinson equation of state to account for deviations from ideal behavior.<sup>13,18,19</sup>

The uncertainty in molar fraction values was calculated using the quadratic propagation of errors:

$$u(x) = \sqrt{\left(\frac{\partial x}{\partial n_{abs}}\right)^2 \cdot u(n_{abs})^2 + \left(\frac{\partial x}{\partial n_l}\right)^2 \cdot u(n_l)^2} \quad (4)$$

where  $u$  is standard uncertainty. The uncertainty in  $n_l$  is derived from the mass of IL, and the uncertainty in  $n_{abs}$  is:

$$u(n_{abs}) = \sqrt{\left(\frac{\partial n_{abs}}{\partial n_i}\right)^2 \cdot u(n_i)^2 + \sum_k \left(\frac{\partial n_{abs}}{\partial n_k}\right)^2 \cdot u(n_k)^2} \quad (5)$$

The uncertainty in dissolved moles in each step,  $u(n_i)$ , is calculated following the same principles from the uncertainty in each of the variables of Eq. (3).

#### 2.4. Diffusivity calculation

Gas diffusion coefficients in the ILs at infinite dilution were calculated using the semi-infinite volume model, derived from the expression of Fickian diffusion:<sup>45,46</sup>

$$\frac{\partial C}{\partial t} = D \frac{\partial^2 C}{\partial y^2} \quad (6)$$

Here,  $C$  expresses the concentration of gas in the solution ( $\text{mol}\cdot\text{m}^{-3}$ ),  $t$  is time (s),  $D$  is diffusivity ( $\text{m}^2\cdot\text{s}^{-1}$ ) and  $y$  is the depth into the IL (m). Integration of Eq. (6) leads to the accumulated dissolved moles per unit area  $M_t$  from which diffusion coefficients are obtained:

$$M_t = \int_0^t \left( D \left( \frac{\partial C}{\partial y} \right)_{y=0} \right) dt = \sqrt{D} \left( 2C_{y=t=0} \sqrt{\frac{t}{\pi}} - \frac{1}{2} m t \sqrt{\pi} \right) = \sqrt{D} \varepsilon \quad (7)$$

where  $C_{y=t=0}$  is the initial concentration of gas in the surface and  $m$  is a mass transfer coefficient expressed in  $\text{mol}\cdot\text{m}^{-3}\cdot\text{s}^{-1/2}$ , both of them calculated according to:

$$C_{y=0} = C_{y=t=0} + m\sqrt{t} \quad (8)$$

with  $C_{y=0}$  being the surface concentration defined as:<sup>47</sup>

$$C_{y=0} = \frac{\rho_{IL}}{M_{IL} \cdot \left( \frac{k_H}{f} - 1 \right)} \quad (9)$$

In Eq. (9),  $\rho_{IL}$  and  $M_{IL}$  are the IL density ( $\text{kg}\cdot\text{m}^{-3}$ ) and molar mass ( $\text{kg}\cdot\text{mol}^{-1}$ ), respectively, and  $k_H$  is the Henry's law constant (MPa) calculated from solubility data:

$$k_H(T) = \lim_{x \rightarrow 0} \frac{f(P, T)}{x} \quad (10)$$

where  $f$  is the refrigerant fugacity (MPa) calculated using the Peng-Robinson equation of state.

As Henry's law constants are defined at infinite dilution, Eq. (10) can be simplified to:<sup>10,23</sup>

$$k_H \approx \left( \frac{df}{dx} \right)_{x=0} \quad (11)$$

Thus, diffusivity calculation involves three least squares adjustments in Eqs. (7, 8, and 11) to determine the regression parameters  $D$ ,  $m$ ,  $C_{y=t=0}$ , and  $k_H$ . The uncertainties in these parameters was derived by rigorous statistical treatment of least squares adjustment to account for the uncertainties present in both the independent and dependent variables.<sup>48</sup>

### 3. Results and discussion

To validate the reliability and accuracy of our experimental system, the solubility of R1234yf in  $[\text{C}_2\text{mim}][\text{BF}_4]$  at 303.15 K, and R32 in  $[\text{C}_2\text{mim}][\text{OTf}]$  at 298.15 K was measured and compared with available data. Table 2 presents the results of the validation experiments and Figure 1 shows the excellent agreement with published data.<sup>25,34</sup>



Table 2. Mole-fraction solubility of R1234yf in  $[\text{C}_2\text{mim}][\text{BF}_4]$  and R32 in  $[\text{C}_2\text{mim}][\text{OTf}]$ 

R1234yf + $[\text{C}_2\text{mim}][\text{BF}_4]$				R32 + $[\text{C}_2\text{mim}][\text{OTf}]$			
$T/\text{K}$	$p/\text{MPa}$	$x$	$u(x)$	$T/\text{K}$	$p/\text{MPa}$	$x$	$u(x)$
303.15	0.0607	0.0038	0.0002	298.15	0.0492	0.0296	0.0004
303.15	0.1411	0.0087	0.0003	298.15	0.0561	0.0336	0.0004
303.15	0.2323	0.0147	0.0004	298.15	0.1729	0.1007	0.0008
303.15	0.3263	0.0207	0.0006	298.15	0.2522	0.1481	0.0010
303.15	0.4223	0.0277	0.0009	298.15	0.3015	0.1679	0.0012
				298.15	0.4404	0.2469	0.0014

Standard uncertainties are  $u(T) = 0.01$  K and  $u(p) = 0.001$  bar. The standard uncertainties for molar fraction  $u(x)$  are given in the table.

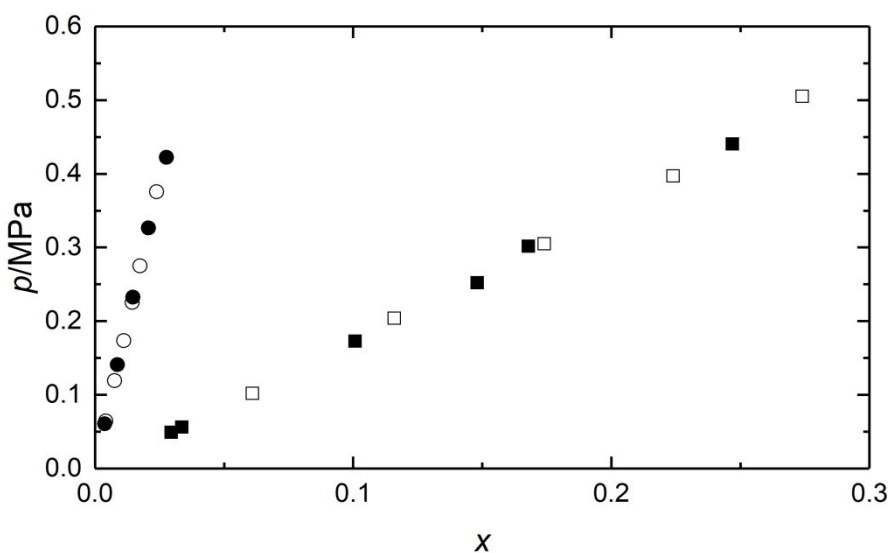


Figure 1. Solubility of refrigerant gases in ILs and comparison with literature data: system R1234yf +  $[\text{C}_2\text{mim}][\text{BF}_4]$  ( $\bullet$ ), and system R32 +  $[\text{C}_2\text{mim}][\text{OTf}]$  ( $\blacksquare$ ). Hollow symbols are the literature data.<sup>25,34</sup>

The experimental data for the solubility of R32 and R134a in  $[\text{C}_2\text{mim}][\text{BF}_4]$ , R134a and R1234yf in  $[\text{C}_2\text{mim}][\text{OTf}]$  and R1234yf in  $[\text{C}_2\text{mim}][\text{Tf}_2\text{N}]$  determined at temperatures between 283.15 and 323.15 K and pressures up to 0.9 MPa, are presented in Tables 3-7. In addition, Figures 2-6 show the experimental and calculated solubility isotherms for each of the refrigerant-IL pairs. As expected, the molar fraction of gas absorbed in the IL increases when temperature decreases and pressure increases.

Table 3. Mole-fraction solubility of R32 in [C<sub>2</sub>mim][BF<sub>4</sub>]

<i>T</i> /K	<i>p</i> /MPa	<i>x</i>	<i>u</i> ( <i>x</i> )
283.15	0.0379	0.0260	0.0003
283.15	0.2510	0.1837	0.0013
283.15	0.3993	0.2869	0.0013
283.15	0.5031	0.3573	0.0014
283.15	0.5883	0.4155	0.0017
283.15	0.6549	0.4600	0.0020
283.15	0.7079	0.4962	0.0025
283.15	0.7509	0.5245	0.0031
293.15	0.0369	0.0212	0.0002
293.15	0.1769	0.1012	0.0008
293.15	0.3770	0.2099	0.0012
293.15	0.5156	0.2817	0.0013
293.15	0.6391	0.3443	0.0015
293.15	0.7524	0.3993	0.0018
293.15	0.8753	0.4582	0.0021
303.15	0.0459	0.0164	0.0002
303.15	0.2353	0.0961	0.0009
303.15	0.4500	0.1831	0.0012
303.15	0.6267	0.2499	0.0013
303.15	0.7504	0.2950	0.0016
303.15	0.8305	0.3262	0.0021
313.15	0.0482	0.0132	0.0002
313.15	0.1367	0.0409	0.0004
313.15	0.2502	0.0767	0.0006
313.15	0.4126	0.1262	0.0009
313.15	0.6648	0.1972	0.0013
313.15	0.8307	0.2423	0.0015
323.15	0.0552	0.0140	0.0002
323.15	0.2468	0.0617	0.0007
323.15	0.4939	0.1162	0.0010
323.15	0.6768	0.1551	0.0013
323.15	0.8639	0.1926	0.0016

Standard uncertainties are  $u(T) = 0.01$  K and  $u(p) = 0.001$  bar. The standard uncertainties for molar fraction,  $u(x)$ , are given in the table.

Table 4. Mole-fraction solubility of R134a in [C<sub>2</sub>mim][BF<sub>4</sub>]

<i>T</i> /K	<i>p</i> /MPa	<i>x</i>	<i>u</i> ( <i>x</i> )
283.15	0.0374	0.0213	0.0002
283.15	0.1261	0.0888	0.0007
283.15	0.1994	0.1538	0.0008
283.15	0.2517	0.2073	0.0010
283.15	0.2899	0.2519	0.0012
283.15	0.3182	0.2885	0.0016
283.15	0.3400	0.3204	0.0020
283.15	0.3567	0.3473	0.0026
283.15	0.3697	0.3713	0.0034
283.15	0.3806	0.3915	0.0046
283.15	0.3890	0.4096	0.0061
283.15	0.3956	0.4266	0.0081
293.15	0.0430	0.0185	0.0002
293.15	0.1511	0.0761	0.0006
293.15	0.2439	0.1323	0.0008
293.15	0.3083	0.1750	0.0010
293.15	0.3525	0.2076	0.0013
293.15	0.3866	0.2352	0.0017
303.15	0.0473	0.0168	0.0002
303.15	0.1574	0.0583	0.0005
303.15	0.2685	0.1029	0.0007
303.15	0.3402	0.1343	0.0009
303.15	0.3952	0.1607	0.0012
303.15	0.4335	0.1788	0.0016
313.15	0.0520	0.0127	0.0002
313.15	0.1800	0.0462	0.0005
313.15	0.2905	0.0770	0.0007
313.15	0.3639	0.0988	0.0009
313.15	0.4161	0.1139	0.0012
313.15	0.4496	0.1245	0.0016
323.15	0.0520	0.0104	0.0002
323.15	0.1856	0.0361	0.0005
323.15	0.3257	0.0634	0.0007
323.15	0.4084	0.0805	0.0009
323.15	0.4590	0.0918	0.0012
323.15	0.4946	0.0986	0.0016

Standard uncertainties are  $u(T) = 0.01$  K and  $u(p) = 0.001$  bar. The standard uncertainties for molar fraction,  $u(x)$ , are given in the table.

Table 5. Mole-fraction solubility of R134a in [C<sub>2</sub>mim][OTf]

<i>T</i> /K	<i>p</i> /MPa	<i>x</i>	<i>u</i> ( <i>x</i> )
283.15	0.0308	0.0381	0.0004
283.15	0.0902	0.1151	0.0007
283.15	0.1639	0.2133	0.0010
283.15	0.2149	0.2842	0.0011
283.15	0.2522	0.3392	0.0013
283.15	0.2804	0.3833	0.0016
283.15	0.3027	0.4208	0.0020
293.15	0.0347	0.0298	0.0003
293.15	0.1018	0.0910	0.0006
293.15	0.1921	0.1747	0.0009
293.15	0.2557	0.2353	0.0011
293.15	0.3029	0.2818	0.0013
293.15	0.3369	0.3176	0.0017
293.15	0.3653	0.3483	0.0022
303.15	0.0396	0.0256	0.0003
303.15	0.1109	0.0720	0.0006
303.15	0.2178	0.1403	0.0009
303.15	0.2922	0.1891	0.0010
303.15	0.3457	0.2254	0.0013
303.15	0.3828	0.2513	0.0017
313.15	0.0422	0.0193	0.0003
313.15	0.1247	0.0574	0.0005
313.15	0.2396	0.1096	0.0008
313.15	0.3137	0.1440	0.0010
313.15	0.3674	0.1691	0.0013
313.15	0.4049	0.1869	0.0018
323.15	0.0513	0.0185	0.0003
323.15	0.1392	0.0500	0.0005
323.15	0.2662	0.0942	0.0008
323.15	0.3583	0.1257	0.0010
323.15	0.4216	0.1475	0.0013

Standard uncertainties are  $u(T) = 0.01$  K and  $u(p) = 0.001$  bar. The standard uncertainties for molar fraction,  $u(x)$ , are given in the table.

Table 6. Mole-fraction solubility of R1234yf in [C<sub>2</sub>mim][OTf]

<i>T</i> /K	<i>p</i> /MPa	<i>x</i>	<i>u</i> ( <i>x</i> )
283.15	0.0511	0.0163	0.0003
283.15	0.1430	0.0471	0.0006
283.15	0.2804	0.0972	0.0009
283.15	0.3731	0.1333	0.0011
283.15	0.4298	0.1577	0.0015
293.15	0.0550	0.0129	0.0003
293.15	0.1520	0.0357	0.0005
293.15	0.2898	0.0699	0.0009
293.15	0.3846	0.0961	0.0011
293.15	0.4481	0.1115	0.0014
303.15	0.0579	0.0103	0.0003
303.15	0.1633	0.0284	0.0005
303.15	0.3039	0.0536	0.0008
303.15	0.4188	0.0718	0.0011
303.15	0.4825	0.0839	0.0014
313.15	0.0609	0.0078	0.0003
313.15	0.1665	0.0211	0.0005
313.15	0.2927	0.0348	0.0007
313.15	0.4127	0.0459	0.0010
313.15	0.4801	0.0535	0.0013
323.15	0.0641	0.0051	0.0002
323.15	0.1756	0.0139	0.0005
323.15	0.3441	0.0240	0.0008
323.15	0.4319	0.0296	0.0010
323.15	0.4810	0.0344	0.0014

Standard uncertainties are  $u(T) = 0.01$  K and  $u(p) = 0.001$  bar. The standard uncertainties for molar fraction,  $u(x)$ , are given in the table.

Table 7. Mole-fraction solubility of R1234yf in [C<sub>2</sub>mim][Tf<sub>2</sub>N]

<i>T</i> /K	<i>p</i> /MPa	<i>x</i>	<i>u</i> ( <i>x</i> )
283.15	0.1368	0.0985	0.0009
283.15	0.2644	0.2009	0.0013
283.15	0.3467	0.2725	0.0014
283.15	0.3983	0.3222	0.0017
283.15	0.4335	0.3602	0.0021
293.15	0.0499	0.0241	0.0004
293.15	0.1491	0.0758	0.0008
293.15	0.2860	0.1503	0.0012
293.15	0.3698	0.1978	0.0014
293.15	0.4257	0.2311	0.0018
303.15	0.0550	0.0194	0.0004
303.15	0.1555	0.0581	0.0008
303.15	0.2912	0.1099	0.0011
303.15	0.3853	0.1464	0.0014
303.15	0.4462	0.1710	0.0018
313.15	0.0566	0.0162	0.0004
313.15	0.1700	0.0497	0.0008
313.15	0.2816	0.0817	0.0010
313.15	0.4026	0.1148	0.0014
313.15	0.4796	0.1366	0.0018
323.15	0.0581	0.0134	0.0004
323.15	0.1605	0.0359	0.0007
323.15	0.3259	0.0702	0.0011
323.15	0.4213	0.0901	0.0014
323.15	0.4767	0.0996	0.0019

Standard uncertainties are  $u(T) = 0.01$  K and  $u(p) = 0.001$  bar. The standard uncertainties for molar fraction,  $u(x)$ , are given in the table.

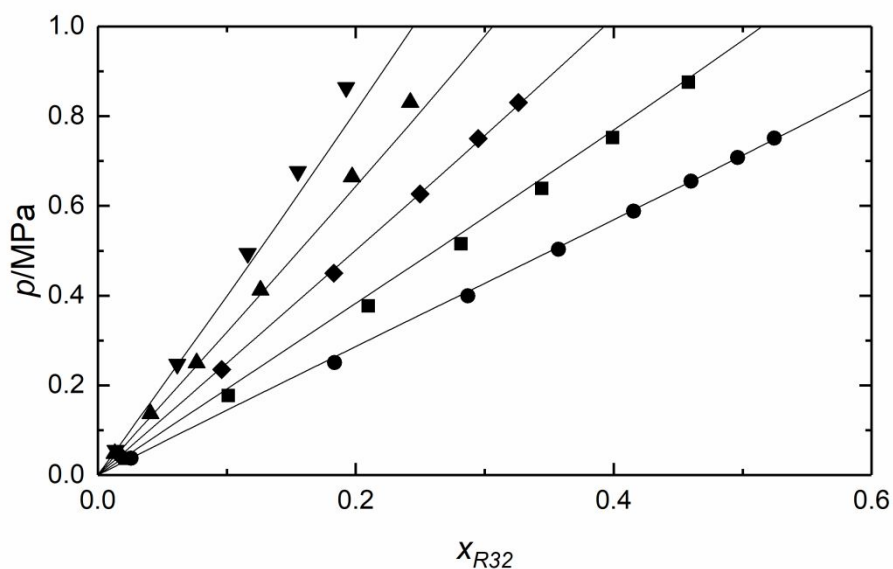


Figure 2. Solubility of R32 in  $[\text{C}_2\text{mim}][\text{BF}_4]$  at various temperatures: 283.15 (●), 293.15 (■), 303.15 (◆), 313.15 (▲) and 323.15 K (▼). Solid lines represent NRTL model calculations.

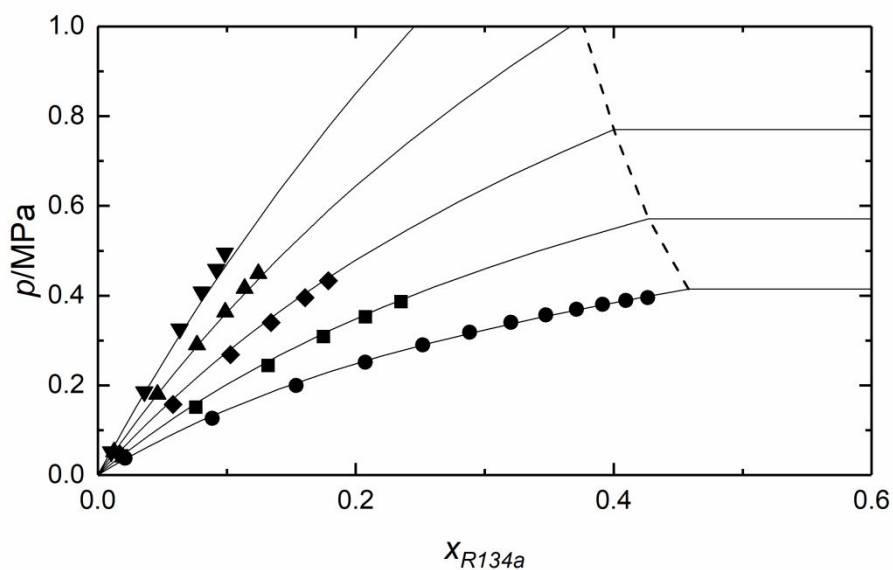


Figure 3. Solubility of R134a in  $[\text{C}_2\text{mim}][\text{BF}_4]$  at various temperatures: 283.15 (●), 293.15 (■), 303.15 (◆), 313.15 (▲) and 323.15 K (▼). Solid lines represent NRTL model calculations and dashed lines represent the NRTL VLLE prediction.

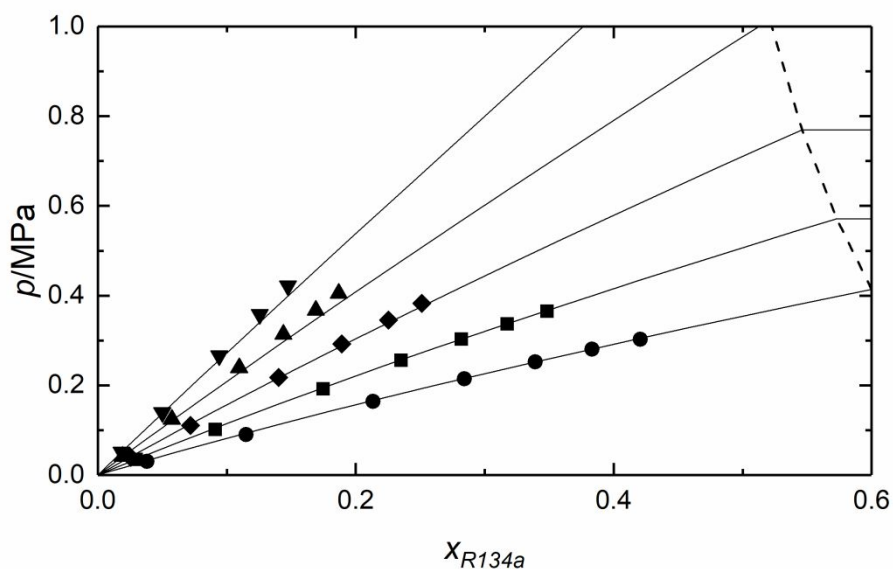


Figure 4. Solubility of R134a in [C<sub>2</sub>mim][OTf] at various temperatures: 283.15 (●), 293.15 (■), 303.15 (◆), 313.15 (▲) and 323.15 K (▼). Solid lines represent NRTL model calculations and dashed lines represent the NRTL VLLE prediction.

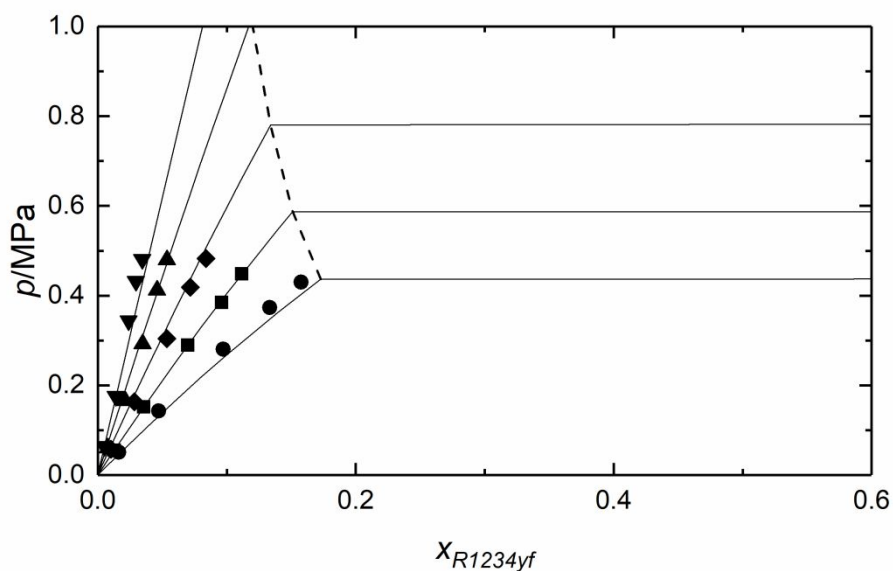


Figure 5. Solubility of R1234yf in [C<sub>2</sub>mim][OTf] at various temperatures: 283.15 (●), 293.15 (■), 303.15 (◆), 313.15 (▲) and 323.15 K (▼). Solid lines represent NRTL model calculations and dashed lines represent the NRTL VLLE prediction.



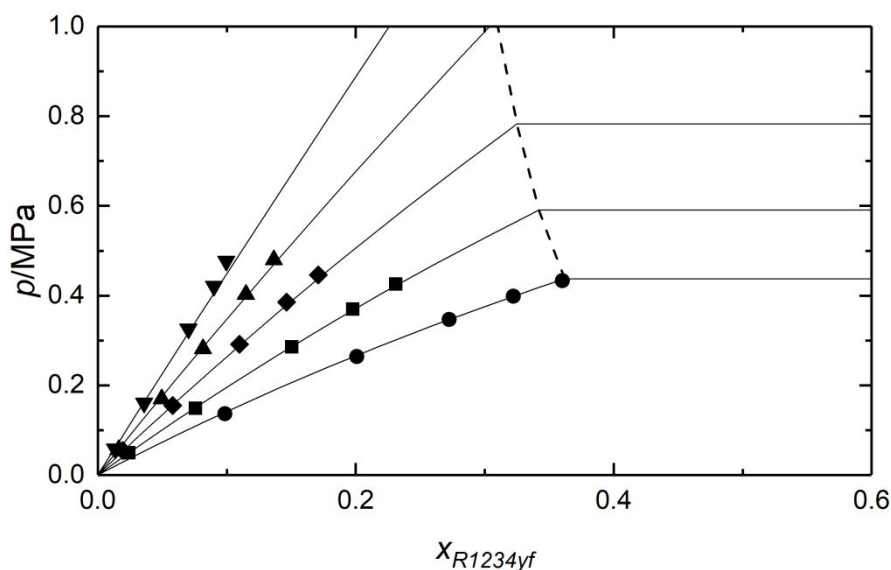


Figure 6. Solubility of R1234yf in [C<sub>2</sub>mim][Tf<sub>2</sub>N] at various temperatures: 283.15 (●), 293.15 (■), 303.15 (◆), 313.15 (▲) and 323.15 K (▼). Solid lines represent NRTL model calculations and dashed lines represent the NRTL VLLE prediction.

Experimental solubility data were modeled using the non-random two-liquid model (NRTL), an activity-coefficient model widely applied to this type of systems.<sup>10,34,49</sup> The vapor-liquid equilibria for each component of a mixture can be described by:

$$y_i p \Phi_i = x_i \gamma_i p_i^S \quad (i \in \mathbb{Z} [1, N]) \quad (12)$$

where  $y_i$  and  $x_i$  are molar fractions of the  $i$  species in vapor and liquid phases, respectively, and  $\gamma_i$  and  $p_i^S$  are the activity coefficient and vapor pressure, respectively.

The correction factor,  $\Phi_i$ , is calculated as:

$$\Phi_i = \exp \left[ \frac{(B_i - V_i^L)(p - p_i^S)}{RT} \right] \quad (13)$$

where  $R$  is the ideal gas constant,  $B_i$  is the second virial coefficient and  $V_i^L$  is the saturated liquid molar volume.  $p_i^S$ ,  $B_i$  and  $V_i^L$  were calculated using CoolProp 6.3.0 software.<sup>50</sup> CoolProp is a powerful tool that calculates physical properties of refrigerant gases from multiparameter

Helmholtz-energy-explicit-type equations of state specifically developed for each individual compound.<sup>50–53</sup> Combination of Eqs. (12) and (13) leads to the following expression of the activity coefficients:

$$\gamma_1 = \frac{p}{x_1 p_1^S} \exp \left[ \frac{(B_1 - V_1^L)(p - p_1^S)}{RT} \right] \quad (14)$$

In addition, the following expression is used to calculate the activity coefficients according to the NRTL model:

$$\ln \gamma_1 = x_2^2 \left[ \tau_{21} \left( \frac{G_{21}}{x_1 + x_2 G_{21}} \right)^2 + \frac{\tau_{12} G_{12}}{(x_2 + x_1 G_{12})^2} \right] \quad (15)$$

where

$$G_{12} = \exp(-\alpha \tau_{12}), \quad G_{21} = \exp(-\alpha \tau_{21}) \quad (16)$$

$$\tau_{12} = \tau_{12}^0 + \frac{\tau_{12}^1}{T}, \quad \tau_{21} = \tau_{21}^0 + \frac{\tau_{21}^1}{T} \quad (17)$$

The tendency of two species to distribute in an organized way is characterized by the parameter  $\alpha$ . Although  $\alpha$  can be treated as an adjustable parameter, for the case of hydrocarbons and fluorocarbons  $\alpha$  is usually assumed constant and equal to 0.2, a convention that we followed for consistency with previous works.<sup>10,49,54</sup> Thus, only the temperature-dependent binary interaction parameters  $\tau_{12}$  and  $\tau_{21}$  were optimized in this work. Out of them,  $\tau_{12}^1$  and  $\tau_{21}^1$  represent the excess free energy of Gibbs divided by the ideal gas constant, while  $\tau_{12}^0$  and  $\tau_{21}^0$  lack a physical interpretation and are only used to model systems with a behavior far from ideal. Nevertheless, in the present work, the equilibria of most of the systems were accurately described using two adjustable parameters, and only the absorption of R1234yf in [C<sub>2</sub>mim][OTf] required all four parameters due to its very low solubility. Accordingly, the NRTL model parameters, tabulated for each system in Table 8, were optimized by minimizing the average absolute relative deviation (AARD) in activity coefficients:

$$AARD = \frac{100}{N} \sum_{i=1}^N \frac{|\gamma_{exp} - \gamma_{calc}|}{\gamma_{exp}} \quad (18)$$

Table 8. Determined parameters for the NRTL activity-coefficient model

System	R32 + [C <sub>2</sub> mim][BF <sub>4</sub> ]	R134a + [C <sub>2</sub> mim][BF <sub>4</sub> ]	R134a + [C <sub>2</sub> mim][OTf]	R1234yf + [C <sub>2</sub> mim][OTf]	R1234yf + [C <sub>2</sub> mim][Tf <sub>2</sub> N]
$\alpha$	0.2	0.2	0.2	0.2	0.2
$\tau_{12}^0$	0	0	0	6.226	0
$\tau_{12}^1$	6148.1	4794.7	5076.4	414.6	3844.6
$\tau_{21}^0$	0	0	0	4.338	0
$\tau_{21}^1$	51.99	278.9	99.29	-1126.1	135.2
AARD/%	3.64	2.56	2.20	5.97	1.68

Interestingly, NRTL is an activity-coefficient model that has also been successfully applied to predict liquid-liquid equilibrium (LLE) of refrigerant + IL mixtures.<sup>10</sup> NRTL parameters presented in this work enable the prediction of immiscibility regions, defined in Figures 2-6 with dashed lines, where three phases (gas + IL with gas dissolved + liquefied gas) coexist at pressures above  $p_i^S$ .

The calculated Henry's law constants that describe the solubility behavior of the refrigerant gases at infinite dilution are presented in Table 9. As it can be seen, R32 is slightly more soluble than R134a in [C<sub>2</sub>mim][BF<sub>4</sub>], and R1234yf is the least soluble gas. Regarding the solubility trend for each IL, it can be observed that R134a is less soluble in [C<sub>2</sub>mim][BF<sub>4</sub>] than in [C<sub>2</sub>mim][OTf], which may be related to the bigger molar volume of [C<sub>2</sub>mim][OTf].<sup>23,24</sup> This hypothesis would also explain the higher solubility of R1234yf in [C<sub>2</sub>mim][Tf<sub>2</sub>N] than in [C<sub>2</sub>mim][OTf]. In fact, the comparison of the Henry's law constants for R134a obtained in this work with available data, shown in Figure 7, reveals that R134a is less soluble in [C<sub>2</sub>mim][BF<sub>4</sub>] than in [C<sub>2</sub>mim][OTf], and exhibits the highest solubility in [C<sub>2</sub>mim][Tf<sub>2</sub>N]. The same trend is also observed for R32 and R1234yf in these ILs.

Table 9. Henry's law constants (MPa) of R32, R134a and R1234yf

T/K	R32 + [C <sub>2</sub> mim][BF <sub>4</sub> ]	R134a + [C <sub>2</sub> mim][BF <sub>4</sub> ]	R134a + [C <sub>2</sub> mim][OTf]	R1234yf + [C <sub>2</sub> mim][OTf]	R1234yf + [C <sub>2</sub> mim][Tf <sub>2</sub> N]
283.15	1.328 ± 0.009	1.374 ± 0.010	0.811 ± 0.008	2.481 ± 0.107	1.015 ± 0.045
293.15	1.713 ± 0.005	1.996 ± 0.012	1.133 ± 0.009	3.650 ± 0.130	1.676 ± 0.048
303.15	2.297 ± 0.019	2.802 ± 0.016	1.576 ± 0.020	5.268 ± 0.091	2.378 ± 0.043
313.15	3.072 ± 0.031	3.956 ± 0.034	2.188 ± 0.017	8.203 ± 0.221	3.207 ± 0.020
323.15	3.822 ± 0.071	5.393 ± 0.059	2.759 ± 0.018	13.430 ± 0.505	4.396 ± 0.022

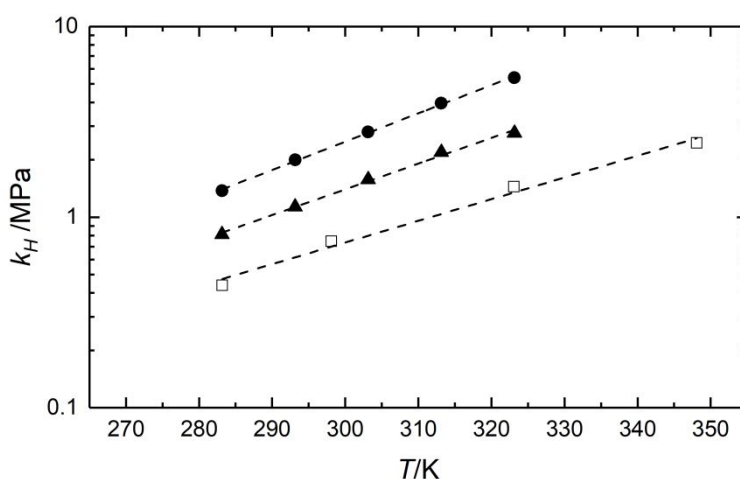


Figure 7. Henry's law constants dependence of temperature of R134a in [C<sub>2</sub>mim][BF<sub>4</sub>] (●), [C<sub>2</sub>mim][OTf] (▲), and [C<sub>2</sub>mim][Tf<sub>2</sub>N] (■). Solid symbols represent the refrigerant-IL pairs studied in this work and hollow symbols are calculated from published data.<sup>19</sup> Dashed lines represent Arrhenius least-square regressions.

Eventually, the solvation enthalpy,  $\Delta H_{sol}$ , and entropy,  $\Delta S_{sol}$ , are calculated from Henry's law constants at infinite dilution using van't Hoff equation<sup>55</sup>:

$$\Delta H_{sol} = R \left( \frac{\partial \ln k_H}{\partial (1/T)} \right)_p \quad (19)$$

$$\Delta S_{sol} = -R \left( \frac{\partial \ln k_H}{\partial \ln T} \right)_p \quad (20)$$

The thermodynamic properties of solvation presented in Table 10 evidence that the absorption of refrigerants is exothermic and enthalpically favorable, which can be related to the gas-IL interactions (H-bonding capability, permanent dipole moment and van der Waals forces). Yet the entropic effects are unfavorable due to the large molecule size of refrigerant gases that makes it difficult to accommodate large molecules within the IL free volume. These results are consistent with those found for similar systems in other works.<sup>14,17</sup>

Table 10. Thermodynamic properties of solvation

System	$\Delta H/(\text{kJ}\cdot\text{mol}^{-1})$	$\Delta S/(\text{J}\cdot\text{mol}^{-1}\cdot\text{K}^{-1})$
R32 + [C <sub>2</sub> mim][BF <sub>4</sub> ]	-20.479 ± 0.012	-68.4 ± 3.2
R134a + [C <sub>2</sub> mim][BF <sub>4</sub> ]	-25.919 ± 0.003	-86.2 ± 0.9
R134a + [C <sub>2</sub> mim][OTf]	-23.547 ± 0.006	-77.5 ± 2.8
R1234yf + [C <sub>2</sub> mim][OTf]	-32.005 ± 0.029	-105.9 ± 7.8
R1234yf + [C <sub>2</sub> mim][Tf <sub>2</sub> N]	-27.011 ± 0.009	-88.1 ± 4.1

Last, solubility differences can be qualitatively explained regarding the activity coefficients at infinite dilution ( $\gamma_1^\infty$ ), which are calculated from Eq. (17) when  $x_1 = 0$  and  $x_2 = 1$ .

$$\ln \gamma_1^\infty = \tau_{21} + \tau_{12}G_{12} \quad (21)$$

A certain compound is more soluble than ideal if  $\gamma_1^\infty < 1$  and vice versa. Table 11 shows the calculated  $\gamma_1^\infty$  for the systems under study. As can be observed, higher values of  $\gamma_1^\infty$  are obtained for the least soluble pairs, and with increasing temperature.

Table 11. Fugacity coefficients at infinite dilution calculated with NRTL at various temperatures

T/K	R32 + [C <sub>2</sub> mim][BF <sub>4</sub> ]	R134a + [C <sub>2</sub> mim][BF <sub>4</sub> ]	R134a + [C <sub>2</sub> mim][OTf]	R1234yf + [C <sub>2</sub> mim][OTf]	R1234yf + [C <sub>2</sub> mim][Tf <sub>2</sub> N]
283.15	1.593	4.747	2.334	7.485	3.959
293.15	1.638	4.817	2.414	8.622	4.109
303.15	1.687	4.897	2.498	9.839	4.262
313.15	1.738	4.987	2.587	11.133	4.417
323.15	1.794	5.084	2.680	12.501	4.573

Regarding mass transfer rates, the diffusion coefficients at infinite dilution of R32 and R134a in [C<sub>2</sub>mim][BF<sub>4</sub>], R134a and R1234yf in [C<sub>2</sub>mim][OTf] and R1234yf in [C<sub>2</sub>mim][Tf<sub>2</sub>N] are presented in Table 12 at temperatures between 283.15 and 323.15 K. The highest diffusion coefficients are

obtained in [C<sub>2</sub>mim][BF<sub>4</sub>] for the smallest molecule R32 (Chung diameter<sup>56</sup> is 4.02 Å). On the other hand, R134a and R1234yf have similar values of diffusion coefficient in ILs, as their molecular size is comparable (Chung diameter is 4.73 and 5.02 Å, respectively). Figure 8 shows the dependence of the diffusivity with temperature and the Arrhenius regression from which the activation energy of diffusion is calculated (Eq. (22)) and presented in Table 13:

$$D = A \exp\left(-\frac{E_D}{RT}\right) \quad (22)$$

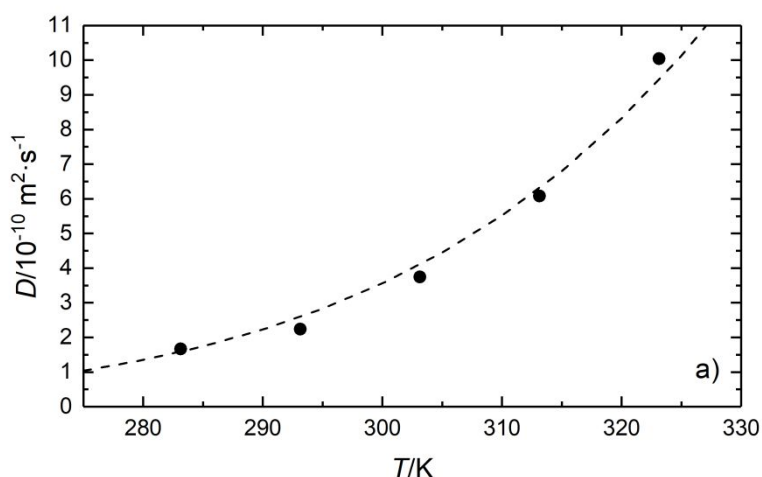
Table 12. Binary diffusion coefficients at infinite dilution for the refrigerant-IL pairs at various temperatures

System	R32 + [C <sub>2</sub> mim][BF <sub>4</sub> ]	R134a + [C <sub>2</sub> mim][BF <sub>4</sub> ]	R134a + [C <sub>2</sub> mim][OTf]	R1234yf + [C <sub>2</sub> mim][OTf]	R1234yf + [C <sub>2</sub> mim][Tf <sub>2</sub> N]
<i>T/K</i>	<i>D/10<sup>-10</sup> m<sup>2</sup>·s<sup>-1</sup></i>	<i>D/10<sup>-10</sup> m<sup>2</sup>·s<sup>-1</sup></i>	<i>D/10<sup>-10</sup> m<sup>2</sup>·s<sup>-1</sup></i>	<i>D/10<sup>-10</sup> m<sup>2</sup>·s<sup>-1</sup></i>	<i>D/10<sup>-10</sup> m<sup>2</sup>·s<sup>-1</sup></i>
283.15	1.67 ± 0.02	1.27 ± 0.03	1.06 ± 0.06	0.97 ± 0.06	0.36 ± 0.02
293.15	2.24 ± 0.04	1.67 ± 0.04	1.28 ± 0.02	1.26 ± 0.08	0.65 ± 0.03
303.15	3.75 ± 0.07	3.08 ± 0.06	1.85 ± 0.03	3.54 ± 0.21	1.46 ± 0.09
313.15	6.08 ± 0.10	6.40 ± 0.18	2.86 ± 0.05	4.17 ± 0.69	2.48 ± 0.31
323.15	10.04 ± 0.13	9.57 ± 0.20	5.42 ± 0.12	8.01 ± 0.88	5.14 ± 0.31

Standard uncertainty of temperature is  $u(T) = 0.01$  K. The standard uncertainties for binary diffusion coefficients at infinite dilution are given in the table.

Table 13. Arrhenius regression of diffusion coefficients for the refrigerant-IL pairs

System	$A/(10^{-3} \text{ m}^2 \cdot \text{s}^{-1})$	$E_D/(\text{kJ} \cdot \text{mol}^{-1})$	AARD/%
R32 + [C <sub>2</sub> mim][BF <sub>4</sub> ]	0.28	33.9	8.01
R134a + [C <sub>2</sub> mim][BF <sub>4</sub> ]	2.32	39.6	11.9
R134a + [C <sub>2</sub> mim][OTf]	0.19	34.7	12.2
R1234yf + [C <sub>2</sub> mim][OTf]	8.00	43.2	16.5
R1234yf + [C <sub>2</sub> mim][Tf <sub>2</sub> N]	81	50.8	6.16



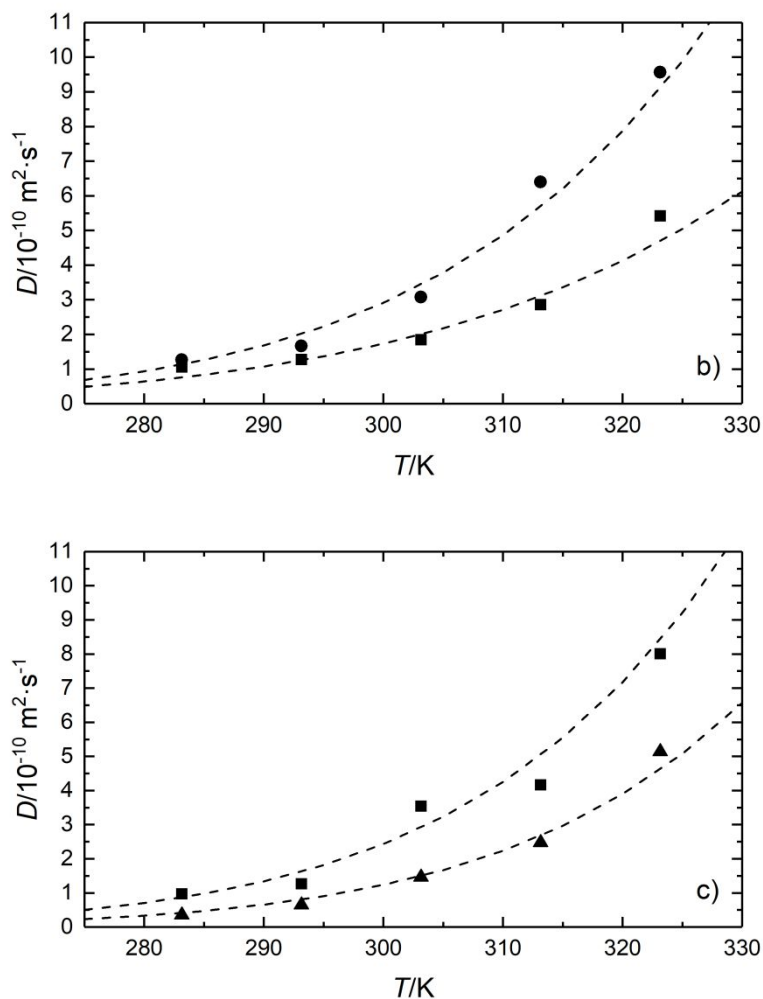


Figure 8. Diffusion coefficients dependence of temperature of a) R32, b) R134a and c) R1234yf in [C<sub>2</sub>mim][BF<sub>4</sub>] (●), [C<sub>2</sub>mim][OTf] (■), and [C<sub>2</sub>mim][Tf<sub>2</sub>N] (▲). Dashed lines represent Arrhenius least-square regressions.

#### 4. Conclusions

The solubility and diffusivity of HFC-32, HFC-134a, and HFO-1234yf, three important compounds present in new commercial refrigerant mixtures, was measured in the low-viscosity ILs [C<sub>2</sub>mim][BF<sub>4</sub>], [C<sub>2</sub>mim][OTf] and [C<sub>2</sub>mim][Tf<sub>2</sub>N]. Moreover, the phase behavior of the refrigerant-IL binary systems has been successfully modeled using the NRTL activity-coefficient method with only two adjustable parameters and average deviation below 4% AARD, with the sole exception of the system R1234yf + [C<sub>2</sub>mim][OTf], that exhibits a very low solubility and required four adjustable parameters to be accurately described (6% AARD). The Henry's law constants at

1  
2  
3 infinite dilution were calculated and used to evaluate the enthalpy and entropy of solvation,  
4  
5 which show that the absorption of large refrigerant molecules into ILs is enthalpically favorable  
6  
7 and exhibits unfavorable entropic contributions. In addition, the diffusion coefficients of  
8  
9 refrigerants in ILs have been obtained using the semi-infinite volume model. As expected, the  
10  
11 use of low-viscosity ionic liquids results in higher diffusion coefficients ( $10^{-10} - 10^{-9} \text{ m}^2\cdot\text{s}^{-1}$ ) than  
12  
13 those found in more viscous ILs. Overall, solubility differences observed among studied systems  
14  
15 are significant in the field of separation, and therefore, these low-viscosity ILs could be used to  
16  
17 separate HFCs and HFOs by means of extractive distillations with enhanced mass transfer rates.  
18  
19

## 20 21 **Acknowledgements**

22  
23  
24 This research is supported by Project KET4F-Gas – SOE2/P1/P0823, which is co-financed by the  
25  
26 European Regional Development Fund within the framework of Interreg Sudoe Programme. S.  
27  
28 A-D. and F.P acknowledge the FPU grant (18/03939) and the post-doctoral fellowship (FJCI-2017-  
29  
30 32884 Juan de la Cierva Formación), respectively, awarded by the Spanish Ministry of Science,  
31  
32 Innovation and Universities.  
33  
34  
35  
36  
37  
38  
39  
40  
41  
42  
43  
44  
45  
46  
47  
48  
49  
50  
51  
52  
53  
54  
55  
56  
57  
58  
59  
60



## References

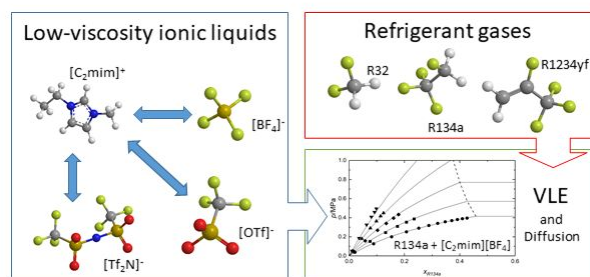
- (1) Graziosi, F.; Arduini, J.; Furlani, F.; Giostra, U.; Cristofanelli, P.; Fang, X.; Hermanssen, O.; Lunder, C.; Maenhout, G.; O'Doherty, S.; Reimann, S.; Schmidbauer, N.; Vollmer, M. K.; Young, D.; Maione, M. European Emissions of the Powerful Greenhouse Gases Hydrofluorocarbons Inferred from Atmospheric Measurements and Their Comparison with Annual National Reports to UNFCCC. *Atmos. Environ.* 2017, *158*, 85–97.
- (2) Vilaseca, O.; Llovel, F.; Yustos, J.; Marcos, R. M.; Vega, L. F. Phase Equilibria, Surface Tensions and Heat Capacities of Hydrofluorocarbons and Their Mixtures Including the Critical Region. *J. Supercrit. Fluids* 2010, *55*, 755–768.
- (3) Abas, N.; Kalair, A. R.; Khan, N.; Haider, A.; Saleem, Z.; Saleem, M. S. Natural and Synthetic Refrigerants, Global Warming: A Review. *Renew. Sustain. Energy Rev.* 2018, *90*, 557–569.
- (4) Nielsen, O. J.; Javadi, M. S.; Sulbaek Andersen, M. P.; Hurley, M. D.; Wallington, T. J.; Singh, R. Atmospheric Chemistry of CF<sub>3</sub>CF<sub>2</sub>CH<sub>2</sub>: Kinetics and Mechanisms of Gas-Phase Reactions with Cl Atoms, OH Radicals, and O<sub>3</sub>. *Chem. Phys. Lett.* 2007, *439*, 18–22.
- (5) Mota-Babiloni, A.; Makhnatch, P.; Khodabandeh, R. Recent Investigations in HFCs Substitution with Lower GWP Synthetic Alternatives: Focus on Energetic Performance and Environmental Impact. *Int. J. Refrig.* 2017, *82*, 288–301.
- (6) Mota-Babiloni, A.; Navarro-Esbrí, J.; Barragán-Cervera, Á.; Molés, F.; Peris, B. Analysis Based on EU Regulation No 517/2014 of New HFC/HFO Mixtures as Alternatives of High GWP Refrigerants in Refrigeration and HVAC Systems. *Int. J. Refrig.* 2015, *52*, 21–31.
- (7) Albà, C. G.; Vega, L. F.; Llovel, F. A Consistent Thermodynamic Molecular Model of N-Hydrofluorolefins and Blends for Refrigeration Applications. *Int. J. Refrig.* 2020, *113*, 145–155.
- (8) Zarca, G.; Ortiz, I.; Urriaga, A. Recovery of Carbon Monoxide from Flue Gases by Reactive Absorption in Ionic Liquid Imidazolium Chlorocuprate(I): Mass Transfer Coefficients. *Chinese J. Chem. Eng.* 2015, *23*, 769–774.
- (9) Zarca, G.; Ortiz, I.; Urriaga, A. Kinetics of the Carbon Monoxide Reactive Uptake by an Imidazolium Chlorocuprate(I) Ionic Liquid. *Chem. Eng. J.* 2014, *252*, 298–304.
- (10) Shiflett, M. B.; Yokozeki, A. Solubility and Diffusivity of Hydrofluorocarbons in Room-Temperature Ionic Liquids. *AIChE J.* 2006, *52*, 1205–1219.
- (11) Asensio-Delgado, S.; Jovell, D.; Zarca, G.; Urriaga, A.; Llovel, F. Thermodynamic and Process Modeling of the Recovery of R410A Compounds with Ionic Liquids. *Int. J. Refrig.* In press 2020.
- (12) Noelke, C. J.; Shiflett, M. B. Capture of Fluorinated Vinyl Monomers Using Ionic Liquids. US Patent 8,779,220 B2, 2014.
- (13) Shiflett, M. B.; Yokozeki, A. Vapor-Liquid-Liquid Equilibria of Hydrofluorocarbons + 1-Butyl-3-Methylimidazolium Hexafluorophosphate. *J. Chem. Eng. Data* 2006, *51*, 1931–1939.
- (14) Shiflett, M. B.; Yokozeki, A. Gaseous Absorption of Fluoromethane, Fluoroethane, and 1,1,2,2-Tetrafluoroethane in 1-Butyl-3-Methylimidazolium Hexafluorophosphate. *Ind. Eng. Chem. Res.* 2006, *45*, 6375–6382.
- (15) Shiflett, M. B.; Harmer, M. A.; Junk, C. P.; Yokozeki, A. Solubility and Diffusivity of

- 1  
2  
3 Difluoromethane in Room-Temperature Ionic Liquids. *J. Chem. Eng. Data* 2006, 51, 483–  
4 495.  
5
- 6 (16) Shiflett, M. B.; Harmer, M. A.; Junk, C. P.; Yokozeki, A. Solubility and Diffusivity of 1,1,1,2-  
7 Tetrafluoroethane in Room-Temperature Ionic Liquids. *Fluid Phase Equilib.* 2006, 242,  
8 220–232.  
9
- 10 (17) Minnick, D. L.; Shiflett, M. B. Solubility and Diffusivity of Chlorodifluoromethane in  
11 Imidazolium Ionic Liquids: [Emim][Tf2N], [Bmim][BF4], [Bmim][PF6], and [Emim][TFES].  
12 *Ind. Eng. Chem. Res.* 2019, 58, 11072–11081.  
13
- 14 (18) Shiflett, M. B.; Yokozeki, A. Binary Vapor–Liquid and Vapor–Liquid–Liquid Equilibria of  
15 Hydrofluorocarbons (HFC-125 and HFC-143a) and Hydrofluoroethers (HFE-125 and HFE-  
16 143a) with Ionic Liquid [Emim][Tf2N]. *J. Chem. Eng. Data* 2008, 53, 492–497.  
17
- 18 (19) Shiflett, M. B.; Yokozeki, A. Solubility Differences of Halocarbon Isomers in Ionic Liquid  
19 [Emim][Tf2N]. *J. Chem. Eng. Data* 2007, 52, 2007–2015.  
20
- 21 (20) Shiflett, M. B.; Yokozeki, A. Absorption Cycle Utilizing Ionic Liquid as Working Fluid. US  
22 Patent 8715521 B2, 2014.  
23
- 24 (21) Shiflett, M. B. Capture of Trifluoromethane Using Ionic Liquids. US Patent Application  
25 Publication 2015/0082981 A1, 2015.  
26
- 27 (22) Shiflett, M. B.; Yokozeki, A. Utilizing Ionic Liquids for Hydrofluorocarbon Separation. US  
28 Patent 9,628,644 B2, 2014.  
29
- 30 (23) Lepre, L. F.; Andre, D.; Denis-Quanquin, S.; Gautier, A.; Pádua, A. A. H.; Costa Gomes, M.  
31 F. Ionic Liquids Can Enable the Recycling of Fluorinated Greenhouse Gases. *ACS Sustain.*  
32 *Chem. Eng.* 2019, 7, 16900–16906.  
33
- 34 (24) Sosa, J. E.; Ribeiro, R. P. P. L.; Castro, P. J.; Mota, J. P. B.; Araújo, J. M. M.; Pereiro, A. B.  
35 Absorption of Fluorinated Greenhouse Gases Using Fluorinated Ionic Liquids. *Ind. Eng.*  
36 *Chem. Res.* 2019, 58, 20769–20778.  
37
- 38 (25) Sun, Y.; Zhang, Y.; Wang, X.; Prausnitz, J. M.; Jin, L. Gaseous Absorption of 2,3,3,3-  
39 Tetrafluoroprop-1-Ene in Three Imidazolium-Based Ionic Liquids. *Fluid Phase Equilib.*  
40 2017, 450, 65–74.  
41
- 42 (26) Zhang, Y.; Yin, J.; Wang, X. Vapor-Liquid Equilibrium of 2,3,3,3-Tetrafluoroprop-1-Ene  
43 with 1-Butyl-3-Methylimidazolium Hexafluorophosphate, 1-Hexyl-3-Methyl Imidazolium  
44 Hexafluorophosphate, and 1-Octyl-3-Methylimidazolium Hexafluorophosphate. *J. Mol.*  
45 *Liq.* 2018, 260, 203–208.  
46
- 47 (27) Liu, X.; Ye, Z.; Bai, L.; He, M. Performance Comparison of Two Absorption-Compression  
48 Hybrid Refrigeration Systems Using R1234yf/Ionic Liquid as Working Pair. *Energy*  
49 *Convers. Manag.* 2019, 181, 319–330.  
50
- 51 (28) Liu, X.; Lv, N.; Su, C.; He, M. Solubilities of R32, R245fa, R227ea and R236fa in a  
52 Phosphonium-Based Ionic Liquid. *J. Mol. Liq.* 2016, 218, 525–530.  
53
- 54 (29) Liu, X.; Bai, L.; Liu, S.; He, M. Vapor–Liquid Equilibrium of R1234yf/[HMIM][Tf2N] and  
55 R1234ze (E)/[HMIM][Tf2N] Working Pairs for the Absorption Refrigeration Cycle. *J. Chem.*  
56 *Eng. Data* 2016, 61, 3952–3957.  
57
- 58 (30) Liu, X.; Nguyen, M. Q.; Xue, S.; Song, C.; He, M. Vapor-Liquid Equilibria and Inter-Diffusion  
59 Coefficients for Working Pairs for Absorption Refrigeration Systems Composed of  
60 [HMIM][BF4] and Fluorinated Propanes. *Int. J. Refrig.* 2019, 104, 34–41.

- 1  
2  
3 (31) He, M.; Pan, P.; Yang, F.; Wang, T.; Liu, X. Gaseous Absorption of Trans-1-Chloro-3,3,3-  
4 Trifluoropropene in Three Imidazolium-Based Ionic Liquids. *J. Chem. Eng. Data* 2018,  
5 63, 1780–1788.  
6  
7 (32) Liu, X.; Qi, X.; Lv, N.; He, M. Gaseous Absorption of Fluorinated Ethanes by Ionic Liquids.  
8 *Fluid Phase Equilib.* 2015, 405, 1–6.  
9  
10 (33) Liu, X.; Pan, P.; Yang, F.; He, M. Solubilities and Diffusivities of R227ea, R236fa and R245fa  
11 in 1-Hexyl-3-Methylimidazolium Bis(Trifluoromethylsulfonyl)Imide. *J. Chem. Thermodyn.*  
12 2018, 123, 158–164.  
13  
14 (34) Dong, L.; Zheng, D.; Sun, G.; Wu, X. Vapor-Liquid Equilibrium Measurements of  
15 Difluoromethane + [Emim]OTf, Difluoromethane + [Bmim]OTf, Difluoroethane +  
16 [Emim]OTf, and Difluoroethane + [Bmim]OTf Systems. *J. Chem. Eng. Data* 2011, 56,  
17 3663–3668.  
18  
19 (35) Pardo, F.; Zarca, G.; Urriaga, A. Separation of Refrigerant Gas Mixtures Containing R32,  
20 R134a, and R1234yf through Poly(Ether- Block -Amide) Membranes. *ACS Sustain. Chem.*  
21 *Eng.* 2020, 8, 2548–2556.  
22  
23 (36) Zarca, G.; Ortiz, I.; Urriaga, A. Novel Solvents Based on Thiocyanate Ionic Liquids Doped  
24 with Copper(I) with Enhanced Equilibrium Selectivity for Carbon Monoxide Separation  
25 from Light Gases. *Sep. Purif. Technol.* 2018, 196, 47–56.  
26  
27 (37) Hu, X.; Meng, X.; Wu, J. Isothermal Vapor Liquid Equilibrium Measurements for  
28 Difluoromethane (R32) + Trans-1,3,3,3-Tetrafluoropropene (R1234ze(E)). *Fluid Phase*  
29 *Equilib.* 2017, 431, 58–65.  
30  
31 (38) Dong, X.; Guo, H.; Gong, M.; Yang, Z.; Wu, J. Measurements of Isothermal (Vapour +  
32 Liquid) Equilibria Data for {1,1,2,2-Tetrafluoroethane (R134) + Trans-1,3,3,3-  
33 Tetrafluoropropene (R1234ze(E))} at T = (258.150 to 288.150) K. *J. Chem. Thermodyn.*  
34 2013, 60, 25–28.  
35  
36 (39) Kamiaka, T.; Dang, C.; Hihara, E. Vapor-Liquid Equilibrium Measurements for Binary  
37 Mixtures of R1234yf with R32, R125, and R134a. *Int. J. Refrig.* 2013, 36, 965–971.  
38  
39 (40) Zarca, G.; Urriaga, A.; Ortiz, I.; Cañizares, P.; Rodrigo, M. A. Carbon Monoxide Reactive  
40 Separation with Basic 1-Hexyl-3-Methylimidazolium Chlorocuprate (I) Ionic Liquid :  
41 Electrochemical Determination of Mass Transport Properties. *Sep. Purif. Technol.* 2015,  
42 141, 31–37.  
43  
44 (41) Palomar, J.; Larriba, M.; Lemus, J.; Moreno, D.; Santiago, R.; Moya, C.; de Riva, J.; Pedrosa,  
45 G. Demonstrating the Key Role of Kinetics over Thermodynamics in the Selection of Ionic  
46 Liquids for CO<sub>2</sub> Physical Absorption. *Sep. Purif. Technol.* 2019, 213, 578–586.  
47  
48 (42) Neves, C. M. S. S.; Kurnia, K. A.; Coutinho, J. A. P.; Marrucho, I. M.; Lopes, J. N. C.; Freire,  
49 M. G.; Rebelo, L. P. N. Systematic Study of the Thermophysical Properties of Imidazolium-  
50 Based Ionic Liquids with Cyano-Functionalized Anions. *J. Phys. Chem. B* 2013, 117, 10271–  
51 10283.  
52  
53 (43) Freire, M. G.; Teles, A. R. R.; Rocha, M. A. A.; Schröder, B.; Neves, C. M. S. S.; Carvalho, P.  
54 J.; Evtuguin, D. V.; Santos, L. M. N. B. F.; Coutinho, J. A. P. Thermophysical  
55 Characterization of Ionic Liquids Able To Dissolve Biomass. *J. Chem. Eng. Data* 2011, 56,  
56 4813–4822.  
57  
58 (44) Atilhan, M.; Jacquemin, J.; Rooney, D.; Khraisheh, M.; Aparicio, S. Viscous Behavior of  
59 Imidazolium-Based Ionic Liquids. *Ind. Eng. Chem. Res.* 2013, 52, 16774–16785.  
60

- 1  
2  
3 (45) Camper, D.; Becker, C.; Koval, C.; Noble, R. Diffusion and Solubility Measurements in  
4 Room Temperature Ionic Liquids. *Ind. Eng. Chem. Res.* 2006, *45*, 445–450.  
5  
6 (46) Crank, J. *The Mathematics of Diffusion*, 2nd ed.; Clarendon Press: Oxford, UK, 1975.  
7  
8 (47) He, M.; Peng, S.; Liu, X.; Pan, P.; He, Y. Diffusion Coefficients and Henry's Constants of  
9 Hydrofluorocarbons in [HMIM][Tf2N], [HMIM][TfO], and [HMIM][BF4]. *J. Chem.*  
10 *Thermodyn.* 2017, *112*, 43–51.  
11  
12 (48) Wentworth, W. E. Rigorous Least Squares Adjustment: Application to Some Non-Linear  
13 Equations, I. *J. Chem. Educ.* 1965, *42*, 96–103.  
14  
15 (49) Seader, J. D.; Henley, E. J.; Roper, D. K. *Separation Process Principles*, 3rd ed.; John Wiley  
16 & Sons, Ltd: New Jersey, USA, 2010.  
17  
18 (50) Bell, I. H.; Wronski, J.; Quoilin, S.; Lemort, V. Pure and Pseudo-Pure Fluid Thermophysical  
19 Property Evaluation and the Open-Source Thermophysical Property Library CoolProp.  
20 *Ind. Eng. Chem. Res.* 2014, *53*, 2498–2508.  
21  
22 (51) Tillner-Roth, R.; Baehr, H. D. An International Standard Formulation for the  
23 Thermodynamic Properties of 1,1,1,2-Tetrafluoroethane (HFC-134a) for Temperatures  
24 from 170 K to 455 K and Pressures up to 70 MPa. *J. Phys. Chem. Ref. Data* 1994, *23*, 657–  
25 729.  
26  
27 (52) Tillner-Roth, R.; Yokozeki, A. An International Standard Equation of State for  
28 Difluoromethane (R-32) for Temperatures from the Triple Point at 136.34 K to 435 K and  
29 Pressures up to 70 MPa. *J. Phys. Chem. Ref. Data* 1997, *26*, 1273–1328.  
30  
31 (53) Richter, M.; McLinden, M. O.; Lemmon, E. W. Thermodynamic Properties of 2,3,3,3-  
32 Tetrafluoroprop-1-Ene (R1234yf): Vapor Pressure and  $p - \phi - T$  Measurements and an  
33 Equation of State. *J. Chem. Eng. Data* 2011, *56*, 3254–3264.  
34  
35 (54) Sun, Y.; Zhang, Y.; Di, G.; Wang, X.; Prausnitz, J. M.; Jin, L. Vapor-Liquid Equilibria for  
36 R1234ze(E) and Three Imidazolium-Based Ionic Liquids as Working Pairs in Absorption-  
37 Refrigeration Cycle. *J. Chem. Eng. Data* 2018, *63*, 3053–3060.  
38  
39 (55) Blath, J.; Christ, M.; Deubler, N.; Hirth, T.; Schiestel, T. Gas Solubilities in Room  
40 Temperature Ionic Liquids - Correlation between RTiL-Molar Mass and Henry's Law  
41 Constant. *Chem. Eng. J.* 2011, *172*, 167–176.  
42  
43 (56) Chung, T.-H.; Ajlan, M.; Lee, L. L.; Starling, K. E. Generalized Multiparameter Correlation  
44 for Nonpolar and Polar Fluid Transport Properties. *Ind. Eng. Chem. Res.* 1988, *27*, 671–  
45 679.  
46  
47  
48  
49  
50  
51  
52  
53  
54  
55  
56  
57  
58  
59  
60

## For Table of Contents use only



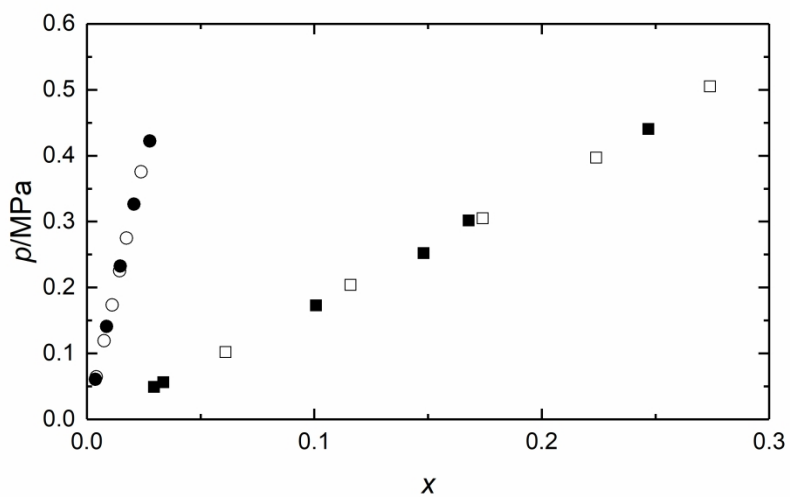


Figure 1

272x149mm (300 x 300 DPI)

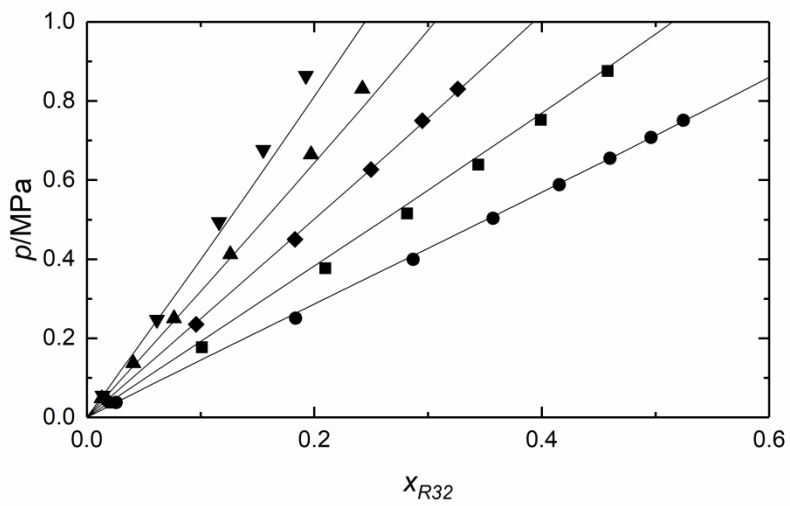


Figure 2

272x149mm (300 x 300 DPI)

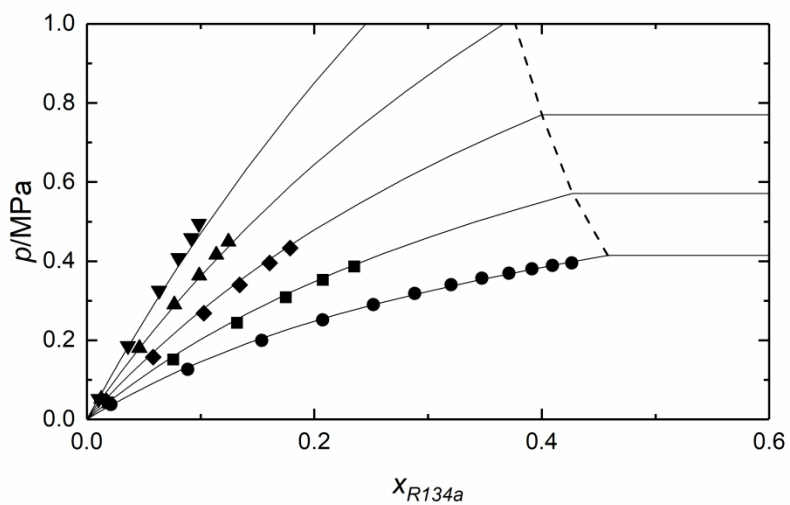


Figure 3

272x149mm (300 x 300 DPI)



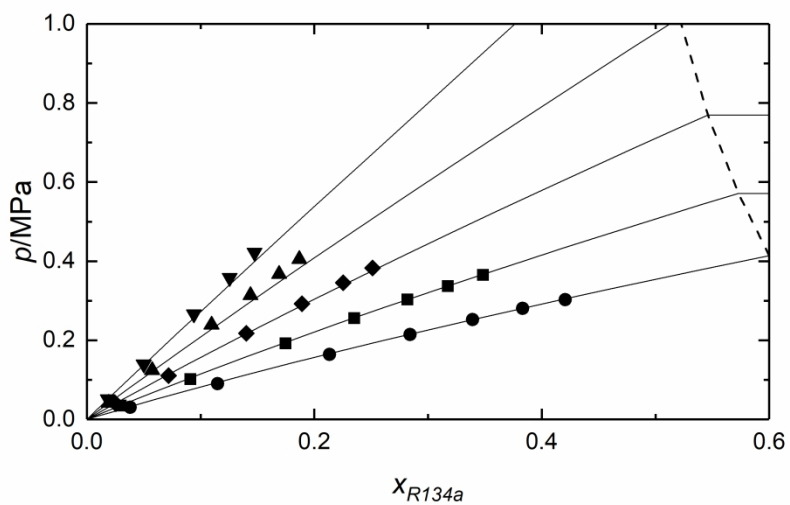


Figure 4

272x149mm (300 x 300 DPI)

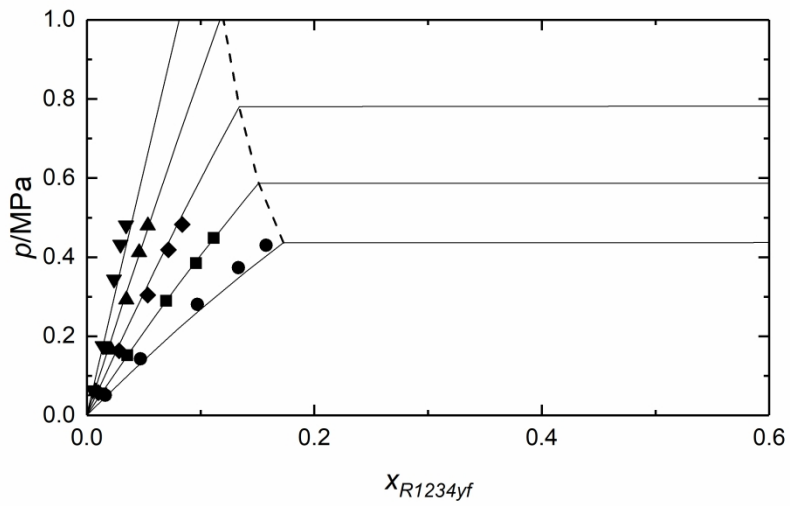


Figure 5

272x149mm (300 x 300 DPI)

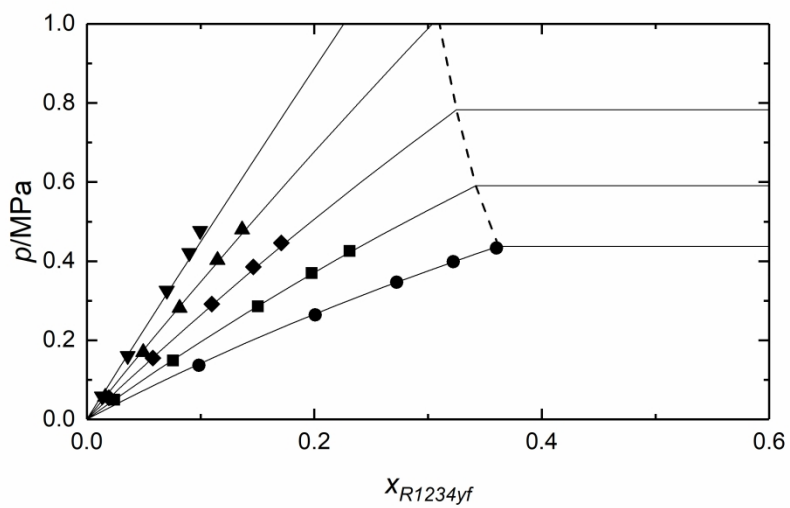


Figure 6

272x149mm (300 x 300 DPI)

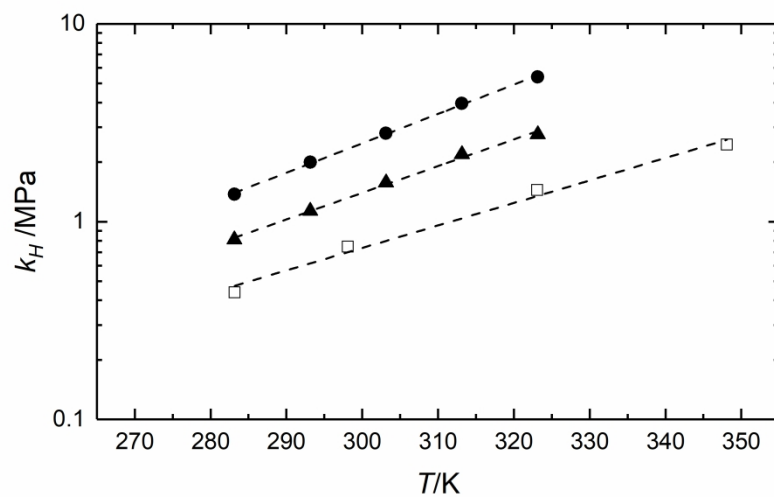


Figure 7

272x149mm (300 x 300 DPI)

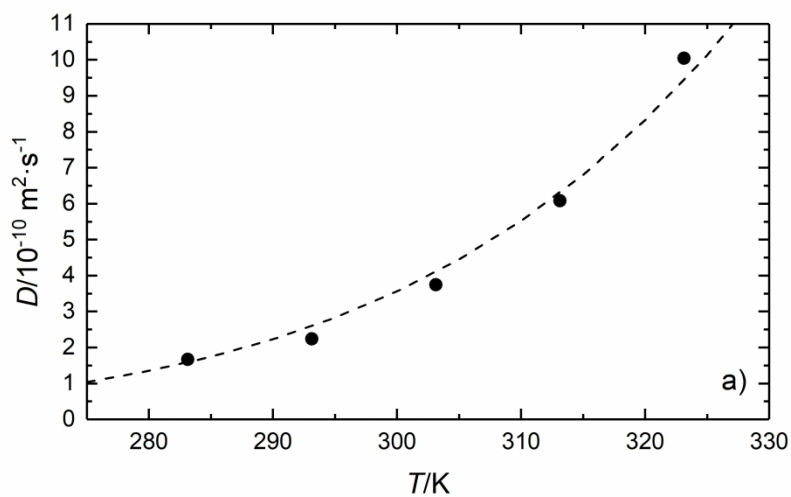


Figure 8a

272x149mm (300 x 300 DPI)

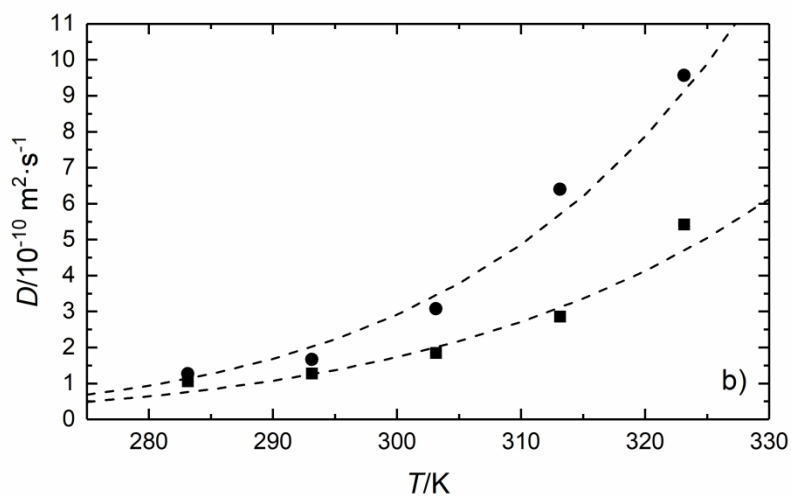


Figure 8b

272x149mm (300 x 300 DPI)

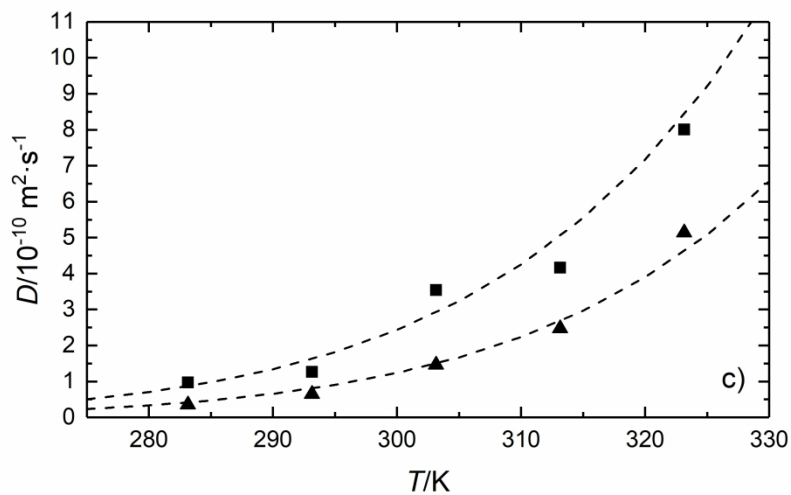
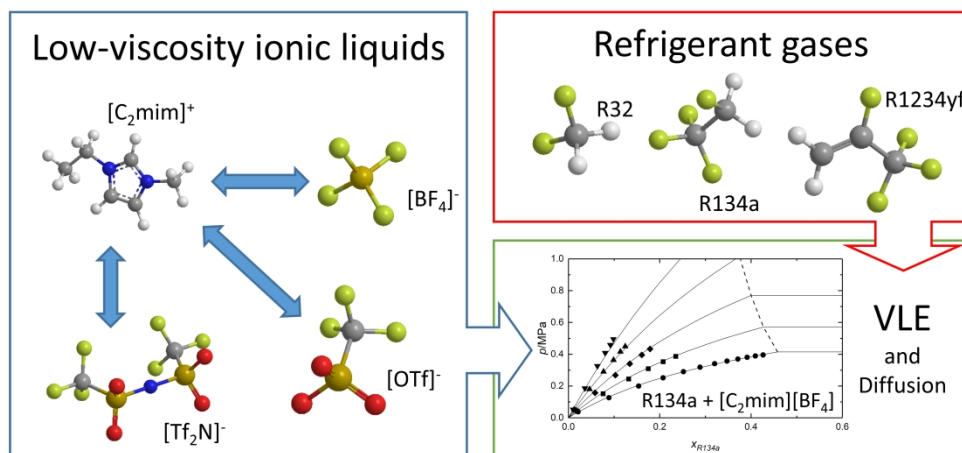


Figure 8c

272x149mm (300 x 300 DPI)



TOC graphic

159x80mm (768 x 768 DPI)





**3.4. Scientific publication 4. “Enhanced absorption separation of hydrofluorocarbon/hydrofluoroolefin refrigerant blends using ionic liquids”, Salvador Asensio-Delgado, Fernando Pardo, Gabriel Zarca, Ane Urtiaga, *Separation and Purification Technology*, 249 (2020) 117136**

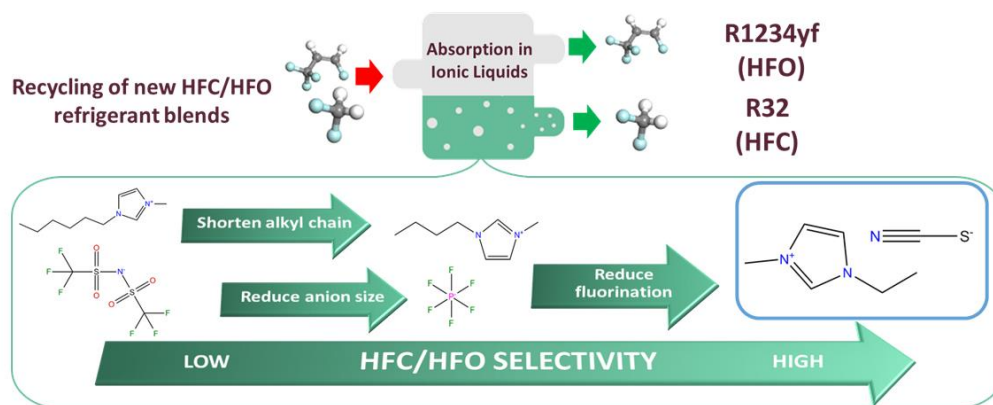


Figure 18. Graphical abstract of the article “Enhanced absorption separation of hydrofluorocarbon/hydrofluoroolefin refrigerant blends using ionic liquids”

This is the second article related to the experimental studies that aim to find ILs with high selectivity for the separation of F-gases using ILs. The previous publication concluded that low IL molar volumes and reduced solvent fluorination achieved better selectivity values for the separation of refrigerant mixtures. Here, the reduction in molar volume was performed through the selection of an imidazolium cation with a short alkyl chain and a small anion. Additionally, the fluorination was reduced to zero selecting as a solvent the IL [C<sub>2</sub>mim][SCN]. The results in this article show that [C<sub>2</sub>mim][SCN] gives the highest selectivity for the separation of F-gases among all ILs studied to date. Figure 18 shows the graphical abstract available in the online version of the article.



## Enhanced absorption separation of hydrofluorocarbon/hydrofluoroolefin refrigerant blends using ionic liquids



Salvador Asensio-Delgado, Fernando Pardo, Gabriel Zarca\*, Ane Urriaga

Department of Chemical and Biomolecular Engineering, Universidad de Cantabria, Av. Los Castros 46, Santander 39005, Spain

### ARTICLE INFO

#### Keywords:

Difluoromethane  
Ionic liquid  
NRTL model  
Solubility selectivity  
1,1,1,2-tetrafluoroethane  
2,3,3,3-tetrafluoropropene

### ABSTRACT

The separation of hydrofluorocarbons (HFCs) and hydrofluoroolefins (HFOs) from novel refrigerant blends will become essential to boost the recycling of these compounds and drastically reduce the emission of HFCs, which are powerful greenhouse gases. In this work, the use of ionic liquids (ILs) as solvent media is explored to perform the selective separation of HFC/HFO refrigerant mixtures composed of the HFCs R32 (difluoromethane) and R134a (1,1,1,2-tetrafluoroethane) and the HFO R1234yf (2,3,3,3-tetrafluoropropene). The low-viscosity IL 1-ethyl-3-methylimidazolium thiocyanate, [C<sub>2</sub>mim][SCN], is selected as separation agent to prove that small and non-fluorinated ILs, with lower hydrogen bonding capability than other ILs, can provide enhanced solubility selectivity and mass transport properties for the selective separation of HFC/HFO refrigerant blends. The phase behavior of IL-refrigerant systems is determined at temperatures between 283.15 and 313.15 K and pressures up to 0.7 MPa. Results are parametrized according to the NRTL activity model and the separation selectivity is assessed in terms of Henry's law constants, solvation enthalpies and entropies, infinite dilution coefficients, Gibbs free energy of mixing, and ideal and noncompetitive selectivity. Results show superior HFC/HFO solubility selectivity in [C<sub>2</sub>mim][SCN] compared to other ILs due to unfavorable entropic effects that difficult the solvation of large molecules such as R1234yf.

### 1. Introduction

Hydrofluorocarbons (HFCs) are a family of compounds with excellent refrigerant properties that substituted ozone-depleting substances, namely, chlorofluorocarbons (CFCs) and hydrochlorofluorocarbons (HCFCs), whose production and use were phased out under the Montreal Protocol. Therefore, the concentration of HFCs in the atmosphere has raised more than twofold since 1990 as a consequence of their massive introduction to the market as refrigerants, fire retardants, foam blowing agents and propellants [1]. Once established on the market, emissions of HFCs are steadily increasing due to fugitive emissions, the lack or non-application of end-of-life recovery protocols, and the low share of refrigerant recycling [2]. However, despite having negligible ozone depletion potentials (ODPs), HFCs are still concerning greenhouse gases with extremely high global warming potentials (GWPs), up to several orders of magnitude higher than that of the reference CO<sub>2</sub> (GWP = 1) [3,4]. For this reason, new legislation and international agreements have recently entered into force. Mainly, Regulation EU 517/2014 in Europe has scheduled the progressive HFCs phase-down, and the Kigali Amendment to Montreal Protocol, already adopted by 93 parties, aims at reducing HFCs emissions by 80% with

respect to 1990 levels by 2045 [5–7].

Accordingly, there are several HFC blends commercialized as refrigerants that will be phased-out due to their high GWP (e.g., R404A, R407C, R410A, and R507C). To meet current legislation requirements, new refrigerant mixtures containing hydrofluoroolefins (HFOs), unsaturated hydrofluorocarbons that exhibit very low GWP, are being formulated and incorporated into the refrigerant market as environmentally friendly alternatives (e.g., R448A, R449A, R454A, R455A, and R513A). The composition of the aforementioned mixtures and their GWP is provided in Table S1 as [Supplementary Information](#). In addition, [Table 1](#) presents relevant properties of the main HFCs and HFOs that are being used in new HFC/HFO blends [2,3,8].

The current legal framework provides an excellent opportunity to focus technological innovations on the design of refrigerant recovery processes to shift the refrigeration and air conditioning (RAC) industry towards a more circular economy [9]. To promote the recycling of refrigerants, blend components must be recovered as pure compounds so they can be then reused in the formulation of new more environmentally friendly commercial blends. However, some relevant HFC + HFO systems behave almost like pure fluids with virtually no variation of composition between the vapor and liquid phases and

\* Corresponding author.

E-mail address: [zarca@unican.es](mailto:zarca@unican.es) (G. Zarca).

<https://doi.org/10.1016/j.seppur.2020.117136>

Received 3 January 2020; Received in revised form 24 March 2020; Accepted 19 May 2020

Available online 22 May 2020

1383-5866/ © 2020 Elsevier B.V. All rights reserved.

**Table 1**  
Properties of common HFCs and HFOs contained in new refrigerant blends [8].

Properties	HFCs			HFOs	
	R32	R125	R134a	R1234yf	R1234ze(E)
Molecular formula	CH <sub>2</sub> F <sub>2</sub>	C <sub>2</sub> HF <sub>5</sub>	C <sub>2</sub> H <sub>2</sub> F <sub>4</sub>	C <sub>3</sub> H <sub>2</sub> F <sub>4</sub>	C <sub>3</sub> H <sub>2</sub> F <sub>4</sub>
GWP	675	3500	1430	4	6
Molar mass (g mol <sup>-1</sup> )	52.02	120.02	102.03	114.04	114.04
Critical temperature (K)	351.26	339.17	374.21	367.85	382.52
Critical pressure (bar)	57.82	36.18	40.59	33.82	36.35
Critical volume (cm <sup>3</sup> mol <sup>-1</sup> )	122.70	209.25	199.32	239.81	233.10
Acentric factor	0.2769	0.3052	0.3268	0.2760	0.3131
Normal boiling point (°C)	-51.65	-48.09	-26.07	-29.45	-18.95
ASHRAE-34 flammability	A2L	A1	A1	A2L	A2L

almost constant evaporation/condensation temperature at a given pressure (i.e., the temperature glide is lower than 1 K). This is for instance the case of systems R134a + R1234yf, R134a + R1234ze(E) and R134 + R1234ze(E). Other important systems also exhibit near-azeotropic behavior at some point, e.g., system R32 + R1234yf, and therefore, it may be difficult to recover their individual components at the high purity needed for reuse [10–13]. These reasons make the separation of those refrigerant systems by means of conventional distillation very challenging or even impossible [14].

In contrast, the development of extractive distillation processes for the separation of HFCs/HFOs based on gas solubility differences appears as a more effective alternative [15,72]. Moreover, ionic liquids (ILs) have been proposed as a novel solvent platform in new gas separation processes owing to their unique features, e.g., extremely low vapor pressure, high thermal and chemical stability, liquid state in a wide temperature range, and enhanced solvation properties, among others [16–18]. Several studies have been conducted to assess the phase equilibria of binary systems of fluorinated refrigerants and ILs [14,19–33,73]. However, the design of novel gas separation processes for the recovery of refrigerants requires a deep understanding of both the refrigerant-IL phase behavior and mass transport phenomena, which can severely affect the process efficiency [34]. In this sense, a preliminary assessment of published data is performed in Table 2, which shows the Henry's law constants at infinite dilution of the gases studied in this work in several ILs, along with the IL molar volume and viscosity. As can be seen, for a given solute, solubility increases with IL molar volume and fluorination of the anion. Moreover, these trends are particularly significant for the HFO R1234yf, whose solubility is consistently lower than that of R32 and R134a. In addition, to date, solubility data for all these refrigerant gases in low viscosity ILs have not been reported. Consequently, it is expected that an IL that combines a small non-fluorinated anion and a cation with a short alkyl chain would significantly decrease the HFO solubility and provide enhanced HFC/HFO selectivity and improved mass transfer rates. Therefore, the IL 1-

**Table 2**  
Henry's law constants of R32, R134a and R1234yf in several ILs at 300 K [18,19,26–28,32,37–49].

Ionic liquid			Henry's law constants (MPa)			
Anion	Cation	Molar volume (cm <sup>3</sup> mol <sup>-1</sup> )	Viscosity (mPa s)	HFC-R32	HFC-R134a	HFO-R1234yf
[BF <sub>4</sub> ]	[C <sub>2</sub> mim]	154.27	38.8			15.56
	[C <sub>4</sub> mim]	188.10	103.5	1.32		
	[C <sub>6</sub> mim]	222.08	206		0.90	4.57
[PF <sub>6</sub> ]	[C <sub>4</sub> mim]	207.82	282	1.21	1.22	5.24
	[C <sub>6</sub> mim]	241.26	483		0.96	4.30
[Tf <sub>2</sub> N]	[C <sub>2</sub> mim]	257.70	33.9	0.96	0.73	
	[C <sub>6</sub> mim]	326.20	70.1	0.72	0.63	1.65

ethyl-3-methylimidazolium thiocyanate, [C<sub>2</sub>mim][SCN], is selected in the present work because of its low molar volume (151.52 cm<sup>3</sup> mol<sup>-1</sup>), the absence of fluorine atoms and its very low viscosity compared to other ILs (24.5 mPa s at 298 K) [35,36]. The thermodynamic absorption equilibria of R32, R134a and R1234yf in [C<sub>2</sub>mim][SCN] are assessed and modeled using the NRTL activity method to allow simulation of an extractive distillation separation process in a further stage. Moreover, the diffusion coefficients of each refrigerant gas are evaluated at several temperatures and compared to those found in other systems. Finally, a thermodynamic assessment is performed to gain a deeper understanding on the refrigerant solvation in ILs and the importance of adequate IL selection for designing novel separation processes.

## 2. Experimental

### 2.1. Materials

The IL [C<sub>2</sub>mim][SCN] (98%) was purchased from IoLiTec and dried under vacuum during 48 h before used. The water content of [C<sub>2</sub>mim][SCN] was determined using Karl Fischer titration to be < 200 ppm. R32 (99.9%) was purchased from Coproven Climatización (Gas Servei licensed supplier, Spain). R134a (99.8%) and R1234yf (99.9%) were supplied by Carbueros Metálicos (Air Products).

### 2.2. Procedure

Gas absorption into ILs was measured using an isochoric saturation method, which relies on gas-phase measurements. The experimental system was described in detail in our previous works [16,17,35]. It consists of a jacketed stirred tank reactor (Buchi, model Picoclave type 1/100 mL) equipped with a pressure transducer (Aplisens, model PCE-28, 0.2% accuracy) and a Pt-100 temperature sensor connected to a cryothermostatic bath (Julabo, model F25-ME, ± 0.01 K). A storage cylinder of known volume equipped with an absolute digital manometer (Keller, model Leo 2, 0.1% accuracy at full scale) is used as gas reservoir. The reactor was loaded with ~10 g (± 0.0001 g) of IL and degassed at 333 K applying vacuum for 4–6 h before each absorption experiment. Initially, absorption was allowed to proceed without stirring for the first 20 min for diffusivity measurements. After that, the stirrer was set to 500 rpm and gas absorption proceeded until the system reached equilibrium conditions. It was assumed that equilibrium was reached when pressure remained constant for more than 20 min. The amount of gas absorbed in each step ( $n_i$ ) and the accumulated absorbed amount ( $n_{abs}$ ) were calculated as follows:

$$n_i = \rho_{(i,s)} \cdot V_s + \rho_{(i-1,r)} \cdot (V_r - V_i) - \rho_{(i,eq)} \cdot (V_s + V_r - V_i) \quad (1)$$

$$n_{abs} = n_i + \sum_{k=1}^{i-1} n_k \quad (2)$$

where  $V_s$ ,  $V_r$  and  $V_i$  are the storage, reactor and loaded IL volumes, respectively, and  $\rho_{i,s}$ ,  $\rho_{i-1,r}$  and  $\rho_{i,eq}$  are the gas molar densities in the storage cylinder, in the reactor and at equilibrium conditions, respectively. Molar densities were calculated from pressure and temperature data using the Peng-Robinson equation of state to account for deviations from ideal behavior. The molar fraction of gas dissolved in the IL is defined as:

$$x = \frac{n_{abs}}{n_i + n_{abs}} \quad (3)$$

where  $n_i$  are the moles of IL. To validate the accuracy of our system, we performed absorption experiments of R1234yf in [C<sub>2</sub>mim][BF<sub>4</sub>] achieving excellent agreement with data available in literature [19] as shown in Figure S1 of the Supplementary Information.

### 2.3. Modeling

Modeling the absorption equilibria is essential for the simulation of absorption systems with computer tools used for process design. We present here the model parameters of the absorption equilibria of the three hydrofluorocarbon gases in [C<sub>2</sub>mim][SCN] using the non-random two-liquid (NRTL) model [18,50,51]. According to this activity coefficient based model, vapor–liquid equilibria is calculated as

$$y_i p \Phi_i = x_i \gamma_i p_i^S \quad (i \in \mathbb{Z}[1, N]) \quad (4)$$

where  $y_i$  and  $x_i$  are molar fractions of the  $i$  species in vapor and liquid phases, respectively, and  $\gamma_i$  and  $p_i^S$  are the activity coefficient and vapor pressure, respectively. The correction factor  $\Phi_i$  is calculated as follows:

$$\Phi_i = \exp \left[ \frac{(B_i - V_i^L)(p - p_i^S)}{RT} \right] \quad (5)$$

where  $R$  is the ideal gas constant,  $B_i$  is the second virial coefficient and  $V_i^L$  is the saturated liquid molar volume.  $p_i^S$ ,  $B_i$  and  $V_i^L$  were calculated using CoolProp 6.3.0 software [8]. Combination of Eqs. (4) and (5) leads to the following expression of the activity coefficients:

$$\gamma_i = \frac{p}{x_i p_i^S} \exp \left[ \frac{(B_i - V_i^L)(p - p_i^S)}{RT} \right] \quad (6)$$

NRTL minimizes the difference between this experimental activity coefficient and the calculated as

$$\ln \gamma_i = x_2^2 \left[ \tau_{21} \left( \frac{G_{21}}{x_1 + x_2 G_{21}} \right)^2 + \frac{\tau_{12} G_{12}}{(x_2 + x_1 G_{12})^2} \right] \quad (7)$$

where  $G_{12} = \exp(-\alpha \tau_{12})$ ,  $G_{21} = \exp(-\alpha \tau_{21})$ ,  $\tau_{12} = \tau_{12}^0 + \tau_{12}^1/T$  and  $\tau_{21} = \tau_{21}^0 + \tau_{21}^1/T$ . Thus, the model parameters to be optimized are  $\alpha$ ,  $\tau_{12}^0$ ,  $\tau_{12}^1$ ,  $\tau_{21}^0$  and  $\tau_{21}^1$ .

### 2.4. Diffusivity

Diffusion coefficients were calculated using the semi-infinite volume model [52,53].

$$\frac{\partial C}{\partial t} = D \frac{\partial^2 C}{\partial y^2} \quad (8)$$

where  $C$  expresses the concentration of gas in solution,  $t$  is time,  $D$  is the diffusion coefficient and  $y$  is the depth into the IL. Integration of Eq. (8) leads to the accumulated dissolved moles per unit area from which diffusion coefficients are obtained:

$$M_t = \int_0^t \left( D \left( \frac{\partial C}{\partial y} \right)_{y=0} \right) dt = \sqrt{D} \left( 2C_{y=t=0} \sqrt{\frac{t}{\pi}} - \frac{1}{2} m t \sqrt{\pi} \right) = \sqrt{D} \varepsilon \quad (9)$$

where  $C_{y=t=0}$  is the initial concentration in the surface and  $m$  is a mass transfer coefficient, both of them calculated according to

$$C_{y=0} = C_{y=t=0} + m \sqrt{t} \quad (10)$$

where  $C_{y=0}$  is the surface concentration defined as [54]

$$C_{y=0} = \frac{\rho_{IL}}{M_{IL} \left( \frac{k_H}{f} - 1 \right)} \quad (11)$$

where  $\rho_{IL}$  and  $M_{IL}$  are density and molar mass of the IL, respectively.

### 2.5. Separation assessment

The Henry's law constants ( $k_H$ ) are calculated from the experimental data as follows:

$$k_H(T) = \lim_{x \rightarrow 0} \frac{f(P, T)}{x} \quad (12)$$

where  $f$  is the refrigerant fugacity calculated using PR-EoS. As Henry's law constants are defined at infinite dilution, Eq. (12) can be simplified to [18,25]

$$k_H \approx \left( \frac{df}{dx} \right)_{x=0} \quad (13)$$

Solvation enthalpy,  $\Delta H_{sol}$ , and entropy,  $\Delta S_{sol}$ , provide information regarding the strength of interaction between the IL and gas and the ordering in the mixture [55,56]. Henry's law constants allow calculation of solvation enthalpies and entropies at infinite dilution using the van't Hoff equation [57]:

$$\Delta H_{sol} = R \left( \frac{\partial \ln k_H}{\partial \left( \frac{1}{T} \right)} \right)_p \quad (14)$$

$$\Delta S_{sol} = -R \left( \frac{\partial \ln k_H}{\partial \ln T} \right)_p \quad (15)$$

The comparison of solvation energies gives information regarding solubility differences between gases that is very useful for an initial assessment of the expected selectivity provided by a certain IL. Besides, Henry's law constants can be used to calculate the ideal selectivity at infinite dilution,  $S_{1/2}$ , defined as [55]

$$S_{1/2} = \frac{1/k_{H,1}}{1/k_{H,2}} = \frac{k_{H,2}}{k_{H,1}} \quad (16)$$

At higher pressures, a non-competitive selectivity can be defined from VLE data as

$$S_{1/2}^P = \frac{y_2/x_2}{y_1/x_1} = \frac{x_1}{x_2} \quad (17)$$

where the vapor phase,  $y_i = 1$ , owing to the negligible vapor pressure of ILs.

Further understanding of the separation mechanism involves the analysis of thermodynamic properties related to solute and solvent interactions. NRTL model allows for the calculation of these interaction parameters. Activity coefficients at infinite dilution ( $\gamma_i^\infty$ ) are calculated from Eq. (7) when  $x_1 = 0$  and  $x_2 = 1$ .

$$\ln \gamma_1^\infty = \tau_{21} + \tau_{12} G_{12} \quad (18)$$

Finally, Gibbs free energy of mixing is derived as the sum of the ideal contribution and the excess energy:

$$\Delta g^{mix} = \Delta g^{id} + \Delta g^{ex} \quad (19)$$

where both contributions are calculated as follows:

$$\Delta g^{id} = RT (x_1 \ln x_1 + x_2 \ln x_2) \quad (20)$$

$$\Delta g^{ex} = RT (x_1 \ln \gamma_1 + x_2 \ln \gamma_2) \quad (21)$$

## 3. Results and discussion

### 3.1. Gas solubility

In this section, the absorption of R32, R134a and R1234yf in [C<sub>2</sub>mim][SCN] is presented. The solubility data were measured at temperatures between 283.15 and 313.15 K and pressures up to 0.7 MPa. The results are plotted in Fig. 1. Also, Tables S2-S4 of the Supplementary information present the solubility data of each system expressed as molar fraction and molality, which is a more adequate unit for process design [58], along with the related uncertainties calculated by the propagation-of-errors method. As can be seen, the molar fraction of gas absorbed in the IL increases, as expected, when temperature decreases and pressure increases. The comparison between refrigerants reveals that the HFCs R32 and R134a exhibit much higher solubility in

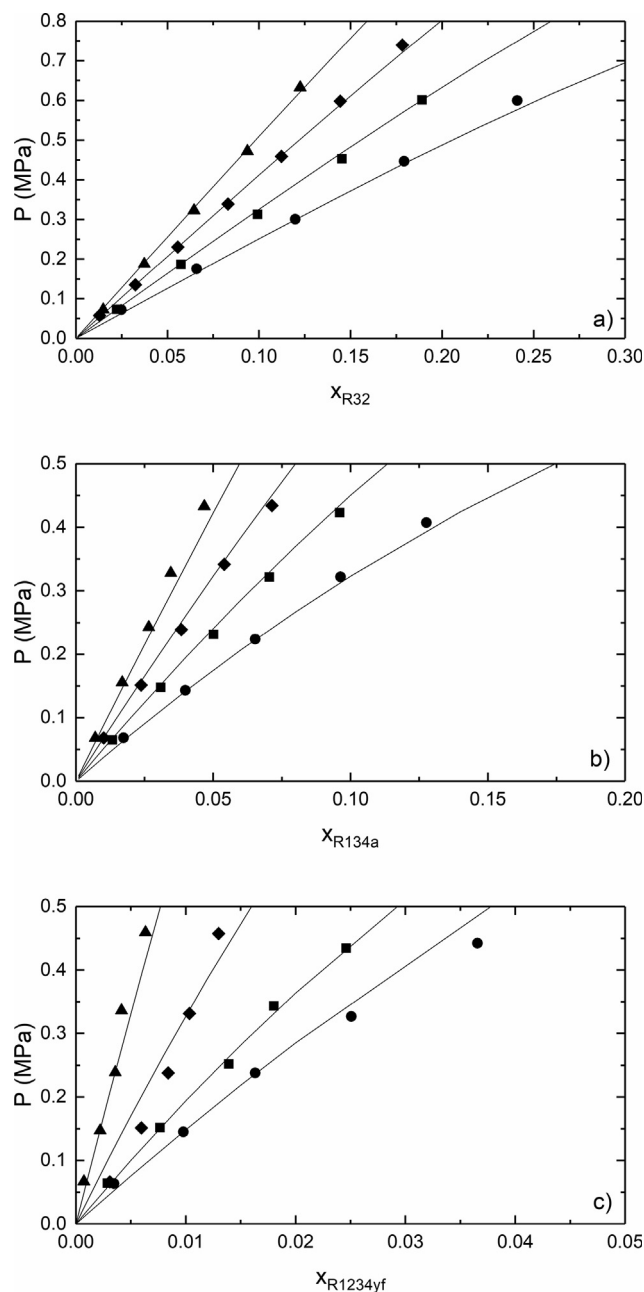


Fig. 1. Solubility of common refrigerant gases in [C<sub>2</sub>mim][SCN] at several temperatures: 283.15 (●), 293.15 (■), 303.15 (◆) and 313.15 K (▲). a) R32, b) R134a and c) R1234yf. Solid lines represent NRTL model calculations.

[C<sub>2</sub>mim][SCN] than the HFO R1234yf. This solubility difference is of great relevance to design selective absorption processes in which R32, or R134a, is preferentially absorbed into the IL while the HFO primarily remains in the gas phase.

Fig. 1 shows that the phase equilibria of HFC/HFO + IL systems are correlated with very good accuracy using the conventional NRTL activity model for nonelectrolyte solutions, which is in good agreement with previous works that also treated ILs as undissociated species [18]. Table 3 presents the model parameters, the calculated absolute average relative deviation in activity coefficients ( $AARD_\gamma$ ) and the root-mean-square deviation in pressure (RMSD) for each system. The parameter  $\alpha$  characterizes the tendency of two species to distribute in an organized way, where the system is ordered if  $\alpha = 0$  and immiscibility is predicted if  $\alpha > 0.426$ . Although  $\alpha$  can be treated as an adjustable parameter, for the case of fluorocarbons and hydrocarbons  $\alpha$  is usually assumed

constant and equal to 0.2 [18,50,59], and therefore, we decided to follow this approach for consistency with previous works. The parameters  $\tau_{12}^1$  and  $\tau_{21}^1$  represent the excess free energy of Gibbs divided by the ideal gas constant, while  $\tau_{12}^0$  and  $\tau_{21}^0$  lack physical meaning and are used to correct deviations from the ideal behavior [18]. In this way, the absorption of R32 and R134a was modeled using only two adjustable parameters ( $\tau_{12}^1$  and  $\tau_{21}^1$ ), while the absorption of R1234yf required all four adjustable parameters to be accurately modeled.

Fig. 2 shows the calculated Henry's law constants of R32, R134a and R1234yf in [C<sub>2</sub>mim][SCN] as a function of temperature, which are well-correlated with an Arrhenius type expression.

$$\ln k_H = \frac{A}{T} + B \quad (22)$$

These results are also provided as Supplementary Information in Table S5 and S6. According to Eq. (12), Henry's law constants increase with increasing temperature as solubility decreases. As can be seen, Fig. 2 indicates that the effect of temperature on the solubility of R1234yf is larger than for the other two refrigerant gases. Accordingly, the solubility selectivity of R32 and R134a towards the HFO R1234yf is enhanced with temperature.

### 3.2. Gas diffusivity

Regarding gas diffusivity, Fig. 3 presents the value of diffusion coefficients at infinite dilution of the three refrigerants in [C<sub>2</sub>mim][SCN] between 283.15 and 313.15 K. In addition, data are provided in Table S7 as Supplementary Information. As can be seen, diffusivity in [C<sub>2</sub>mim][SCN] increases with temperature and the influence of temperature on the diffusion coefficients is well correlated with an Arrhenius type expression. Besides, selecting a low-viscosity IL such as [C<sub>2</sub>mim][SCN] enhances diffusivity of the gases as expected, so the diffusion coefficients of hydrofluorocarbons in [C<sub>2</sub>mim][SCN] obtained in this work are higher than those found in more viscous ILs [54,60], which is extremely important to reduce mass transfer resistance in this type of viscous fluids. Moreover, the activation energy of diffusion,  $E_D$ , derived from diffusivity data at infinite dilution is presented in Fig. 4 as a function of the penetrant size. As expected, a strong influence is found between  $E_D$  and the molecular diameter of the refrigerants [61,62].

### 3.3. Thermodynamic separation assessment

The IL [C<sub>2</sub>mim][SCN] presents significantly different absorption capacity for the three fluorinated compounds assessed (R32, R134a and R1234yf), which differs from other ILs in which higher and very similar absorption capacities for these gases are observed [18,26,28,46,49]. It is generally accepted that the high solubility of hydrofluorocarbons in ILs is associated with their H-bonding capability (H-F-H) [18,51,56,64]. In the present work, selecting the [SCN] anion moiety, without neither fluorine nor hydrogen atoms, is aimed at avoiding hydrogen bonding between the refrigerant gas and the IL anion, thus limiting the penetrant-IL interactions in order to increase the typically low HFC/HFO solubility selectivity found in other ILs. In this regard, solubility differences observed among hydrofluorocarbon gases in [C<sub>2</sub>mim][SCN] could be related to their polar nature. However, the electric dipole moments of R32, R134a and R1234yf (1.649, 1.563 and 2.24 D, respectively [18,65]) do not correlate the observed solubility trend (R32 > R134a > R1234yf), a fact that is in good agreement with previous works [18]. Moreover, it has been reported that the effective dipolar moment of HFCs increases due to clusters formed by molecular associations between the gas molecules [18,66–68]. On the other hand, the electron-rich double bond of the R1234yf molecule may weaken the possibility of forming these clusters due to shielding effects of the C-H bonds that eventually reduce their potential to act as H-bond donors [69]. Thus, the formation of HFC molecular associations might contribute to the higher solubility of HFCs R32 and R134a with respect to



**Table 3**  
NRTL activity model parameters for the absorption of fluorinated gases in [C<sub>2</sub>mim][SCN].

	R32 + [C <sub>2</sub> mim] [SCN]	R134a + [C <sub>2</sub> mim] [SCN]	R1234yf + [C <sub>2</sub> mim] [SCN]
$\alpha$	0.2	0.2	0.2
$\tau_{12}^0$	0	0	179.52
$\tau_{12}^1$	1025.6	2682.6	-47781
$\tau_{21}^0$	0	0	21.89
$\tau_{21}^1$	-210.04	254.58	-5506.8
RMSE (MPa)	0.009	0.013	0.029
AARD <sub><math>\gamma</math></sub> (%)	2.45	3.63	10.92

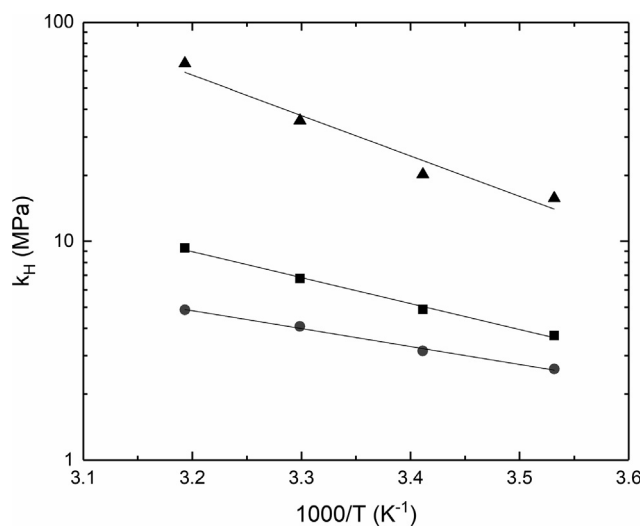


**Fig. 2.** Henry's law constants for the absorption of R32 (●), R134a (■) and R1234yf (▲) in [C<sub>2</sub>mim][SCN] as a function of temperature. Solid lines represent the linear least-squares regressions.

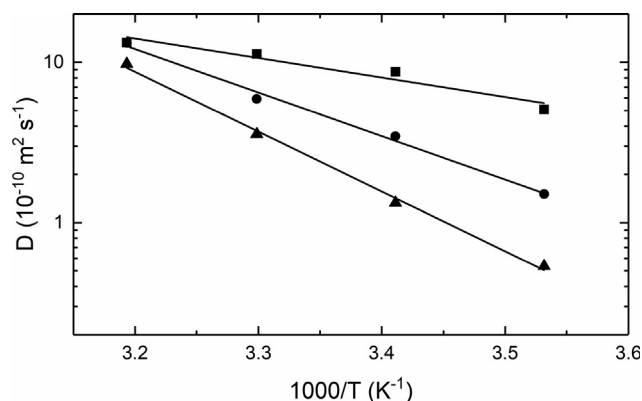


**Fig. 3.** Influence of temperature on the diffusion coefficients at infinite dilution of refrigerant gases in [C<sub>2</sub>mim][SCN]: R32 (■), R134a (●) and R1234yf (▲). Solid lines are the linear least-squares regressions.

the HFO R1234yf.

A deeper understanding of refrigerants solvation into ILs is gained by assessing the solvation enthalpy and entropy at infinite dilution, which are presented in Table S8 as [Supplementary Information](#) and in [Fig. 5](#). Solvation enthalpy reflects the energy of gas-IL interactions (hydrogen bonds, dipoles, Van der Waals forces), and solvation entropy is a measure of the degree of ordering of solvent molecules around the solute [55]. [Fig. 5](#) also shows a comparison between solvation energies of the three fluorinated gases in [C<sub>2</sub>mim][SCN] calculated in this work and in other ILs, which were derived from available absorption data in the literature [18,26,28,46,48,49]. As can be seen, there are larger

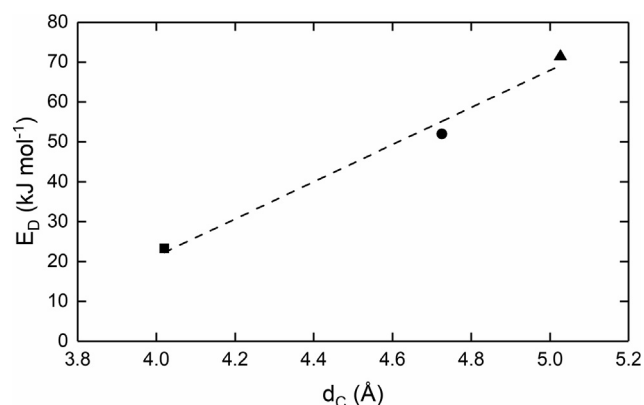


**Fig. 4.** Relationship between the activation energy of diffusion and refrigerant Chung diameter [63] of R32 (■), R134a (●) and R1234yf (▲). Dashed line is a guide to the eye.

differences between the solvation energies of R32, R134a and R1234yf in [C<sub>2</sub>mim][SCN] than in the other two ILs, which are consistent with the larger solubility differences observed between refrigerants in [C<sub>2</sub>mim][SCN]. Apart from the enthalpic effects discussed above, entropic effects can also play an important role regarding the solubility differences between hydrofluorocarbons in ILs [25]. In [C<sub>2</sub>mim][SCN], the biggest molecule R1234yf yields a less-ordered structure in solution, as evidenced by its more negative solvation entropy, what eventually leads to notably lower gas solubility [55]. Therefore, the comparison shown in [Fig. 5](#) also confirms the initial hypothesis that decreasing cation alkyl chain length and anion size and avoiding fluorine substitution allows [C<sub>2</sub>mim][SCN] to improve the selective separation of HFCs from HFOs with respect to other ILs. In summary, the reduction in size and limiting fluorine substitution contribute to reducing the IL free volume, which hampers the accommodation of larger molecules such as the HFO R1234yf [24,70,71].

Activity coefficients at infinite dilution and Gibbs free energy of mixing can be used to rationalize the solubility differences between these refrigerants. A certain compound is more soluble than ideal if  $\gamma_1^\infty < 1$ , and less soluble than ideal if  $\gamma_1^\infty > 1$ . [Table 4](#) presents the results of  $\gamma_1^\infty$  at several temperatures, showing that the three gases are less soluble than ideal. Particularly, R1234yf is much less soluble than ideal, which is in accordance with the observed behavior. Likewise, the Gibbs free energy of mixing calculated with NRTL is presented in [Figure S2](#) as [Supplementary Information](#). The more negative the  $\Delta g^{mix}$ , the higher the sorption capacity, so the trends observed in [Figure S2](#) are also consistent with experimental observations.

The observed solubility differences are promising for the design of absorption or extractive distillation processes aimed towards the selective separation and recovery of refrigerant fluorinated gases. Mixtures of R32 or R134a, both HFC refrigerant gases, with R1234yf, an HFO, are gaining importance as replacement for high GWP HFC mixtures affected by legislation. The recovery of these refrigerants employing advanced regeneration technologies will be key for

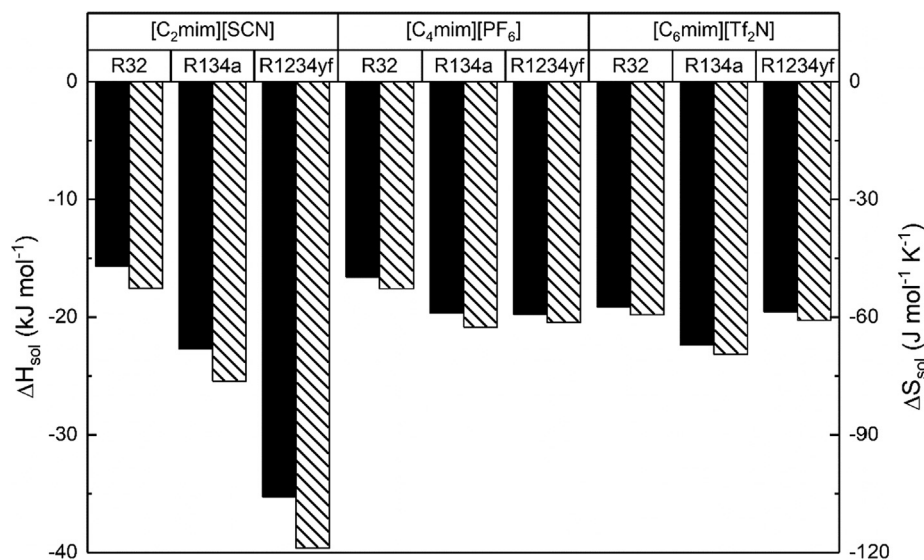


Fig. 5. Comparison of solvation enthalpies (solid column) and entropies (striped column) of refrigerant gases in [C<sub>2</sub>mim][SCN] and other ILs [18,26,28,46,48,49].

Table 4

Activity coefficients at infinite dilution of R32, R134a and R1234yf in [C<sub>2</sub>mim][SCN].

T (K)	$\gamma_{R32}^{\infty}$	$\gamma_{R134a}^{\infty}$	$\gamma_{R1234yf}^{\infty}$
283.15	2.76	10.21	40.06
293.15	2.78	10.34	40.88
303.15	2.79	10.46	54.49
313.15	2.80	10.56	83.70

Table 5

Ideal selectivity ( $S_{1/2}$ ) and noncompetitive absorption selectivity at 0.5 MPa ( $S_{1/2}^p$ ) in [C<sub>2</sub>mim][SCN].

T (K)	283.15	293.15	303.15	313.15
$S_{R32/R1234yf}$	6.0	6.4	8.7	13.3
$S_{R32/R1234yf}^p$	5.1	5.5	7.5	14.2
$S_{R134a/R1234yf}$	4.2	4.0	5.3	7.0
$S_{R134a/R1234yf}^p$	4.5	4.0	4.9	8.6

companies in their adaptation to the new regulations. For a preliminary assessment of IL candidates, the ideal separation factors are a useful measure to determine theoretical separation performances of absorption systems [57]. Table 5 presents both the ideal selectivity at infinite dilution and the noncompetitive selectivity calculated at 0.5 MPa in the temperature range 283.15–313.15 K. R32/R1234yf and R134a/R1234yf selectivity are in the range 5–14 and 4–9, respectively, and increase with temperature. Therefore, further stages of process design will have to focus on analyzing the optimal separation conditions to reach a trade-off between the amount of solvent and the number of equilibrium stages required for a certain degree of separation.

Finally, the selectivity achieved with [C<sub>2</sub>mim][SCN] is compared to that of other ILs in Fig. 6 [18,19,26–28,46,48,49]. The comparison shows that the solubility selectivity of [C<sub>2</sub>mim][SCN] for R32/R1234yf separation is at least twofold higher than in any other system. On the other hand, for the case of R134a/R1234yf separation, selectivity differences among ILs are smaller. Only [C<sub>6</sub>mim][BF<sub>4</sub>] at infinite dilution and [C<sub>4</sub>mim][PF<sub>6</sub>] at 0.5 MPa exhibit comparable selectivity to [C<sub>2</sub>mim][SCN], yet their viscosity is one order of magnitude higher (Table 2).

## 4. Conclusions

This work is directed towards the development of innovative technologies for the separation and recycling of hydrofluorocarbon refrigerant gases. Specifically, we have studied the absorption separation using ILs of the HFCs R32 and R134a, and the HFO R1234yf, which are among the main components of most of the new commercial refrigerant blends. The results obtained reveal that [C<sub>2</sub>mim][SCN], with a small and non-fluorinated anion, provides higher HFC/HFO sorption selectivity than ILs with bigger molar volume and fluorinated anions. This fact can be ascribed to unfavorable entropic solvation effects that hinder the solvation of large molecules such as the HFO R1234yf in [C<sub>2</sub>mim][SCN]. In particular, for the gas pair R32/R1234yf, the solubility selectivity found in [C<sub>2</sub>mim][SCN] is 2–6 times higher (at 0.5 MPa) than that previously reported in any other IL, and up to twofold higher for the pair R134a/R1234yf. In addition, the phase behavior of the refrigerant-IL binary systems has been accurately modeled using the NRTL activity-coefficient method. Moreover, the diffusion coefficients of R32, R134a and R1234yf in [C<sub>2</sub>mim][SCN], in the range 10<sup>-9</sup>-10<sup>-10</sup> m<sup>2</sup> s<sup>-1</sup>, are also higher than those found in more viscous ILs, which is extremely important to overcome mass transfer limitations in kinetically controlled separation processes using ILs.

## CRedit authorship contribution statement

**Salvador Asensio-Delgado:** Investigation, Visualization, Writing - original draft. **Fernando Pardo:** Supervision, Writing - review & editing. **Gabriel Zarca:** Conceptualization, Writing - review & editing, Funding acquisition. **Ane Urriaga:** Conceptualization, Writing - review & editing, Funding acquisition.

## Declaration of Competing Interest

The authors declared that there is no conflict of interest.

## Acknowledgements

This research is supported by Project KET4F-Gas – SOE2/P1/P0823, which is co-financed by the European Regional Development Fund within the framework of Interreg Sudoe Programme. S. A-D. and F.P acknowledge the FPU grant (18/03939) and the post-doctoral fellowship (FJCI-2017-32884 Juan de la Cierva Formación), respectively, awarded by the Spanish Ministry of Science, Innovation and



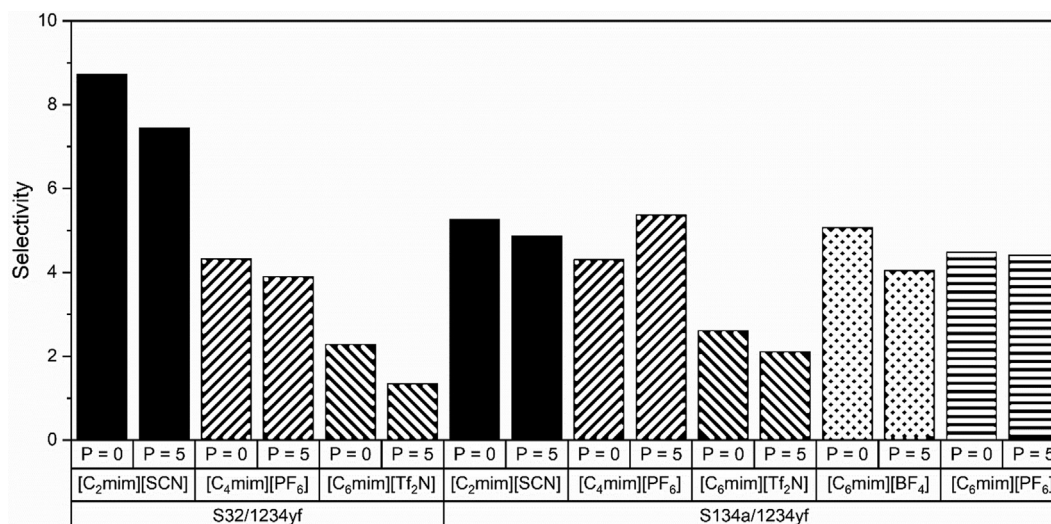


Fig. 6. Comparison of R32/R1234yf and R134a/1234yf ideal selectivity at infinite dilution ( $P = 0$ ) and non-competitive selectivity at 0.5 MPa ( $P = 5$ ) in [C<sub>2</sub>mim][SCN] (data from this work) and in other ILs ([18,19,26–28,46,48,49]).

Universities.

## Appendix A. Supplementary material

Supplementary data to this article can be found online at <https://doi.org/10.1016/j.seppur.2020.117136>.

## References

- [1] F. Graziosi, J. Arduini, F. Furlani, U. Giostra, P. Cristofanelli, X. Fang, O. Hermanssen, C. Lunder, G. Maenhout, S. O'Doherty, S. Reimann, N. Schmidbauer, M.K. Vollmer, D. Young, M. Maione, European emissions of the powerful greenhouse gases hydrofluorocarbons inferred from atmospheric measurements and their comparison with annual national reports to UNFCCC, *Atmos. Environ.* 158 (2017) 85–97, <https://doi.org/10.1016/j.atmosenv.2017.03.029>.
- [2] A. Mota-Babiloni, P. Makhnatch, R. Khodabandeh, Recent investigations in HFCs substitution with lower GWP synthetic alternatives: Focus on energetic performance and environmental impact, *Int. J. Refrig* 82 (2017) 288–301, <https://doi.org/10.1016/j.ijrefrig.2017.06.026>.
- [3] A. Mota-Babiloni, J. Navarro-Esbrí, Á. Barragán-Cervera, F. Molés, B. Peris, Analysis based on EU Regulation No 517/2014 of new HFC/HFO mixtures as alternatives of high GWP refrigerants in refrigeration and HVAC systems, *Int. J. Refrig* 52 (2015) 21–31, <https://doi.org/10.1016/j.ijrefrig.2014.12.021>.
- [4] N. Abas, A.R. Kalair, N. Khan, A. Haider, Z. Saleem, M.S. Saleem, Natural and synthetic refrigerants, global warming: A review, *Renew. Sustain. Energy Rev.* 90 (2018) 557–569, <https://doi.org/10.1016/j.rser.2018.03.099>.
- [5] European Parliament and Council, Regulation EU 517/2014, (2014) 195–230.
- [6] United Nations Environment Programme, Ratification of the Kigali Amendment, Ozone Secr. (2017).
- [7] United Nations, Amendment to the Montreal protocol on substances that deplete the ozone layer, (2016).
- [8] I.H. Bell, J. Wronski, S. Quoilin, V. Lemort, Pure and Pseudo-pure Fluid Thermophysical Property Evaluation and the Open-Source Thermophysical Property Library CoolProp, *Ind. Eng. Chem. Res.* 53 (2014) 2498–2508, <https://doi.org/10.1021/ie4033999>.
- [9] F. Pardo, G. Zarca, A. Urriaga, Separation of Refrigerant Gas Mixtures Containing R32, R134a, and R1234yf through Poly(ether-block-amide) Membranes, *ACS Sustain. Chem. Eng.* 8 (2020) 2548–2556, <https://doi.org/10.1021/acssuschemeng.9b07195>.
- [10] X. Hu, X. Meng, J. Wu, Isothermal vapor liquid equilibrium measurements for difluoromethane (R32) + trans-1,3,3,3-tetrafluoropropene (R1234ze(E)), *Fluid Phase Equilib.* 431 (2017) 58–65, <https://doi.org/10.1016/j.fluid.2016.10.011>.
- [11] X. Dong, H. Guo, M. Gong, Z. Yang, J. Wu, Measurements of isothermal (vapour + liquid) equilibria data for 1,1,2,2-Tetrafluoroethane (R134) + trans-1,3,3,3-tetrafluoropropene (R1234ze(E)) at  $T = (258.150 \text{ to } 288.150) \text{ K}$ , *J. Chem. Thermodyn.* 60 (2013) 25–28, <https://doi.org/10.1016/j.jct.2012.12.026>.
- [12] T. Kamiaka, C. Dang, E. Hihara, Vapor-liquid equilibrium measurements for binary mixtures of R1234yf with R32, R125, and R134a, *Int. J. Refrig* 36 (2013) 965–971, <https://doi.org/10.1016/j.ijrefrig.2012.08.016>.
- [13] L. Kou, Z. Yang, X. Tang, W. Zhang, J. Lu, Experimental measurements and correlation of isothermal vapor-liquid equilibria for HFC-32 + HFO-1234ze (E) and HFC-134a + HFO-1234ze (E) binary systems, *J. Chem. Thermodyn.* 139 (2019) 105798, <https://doi.org/10.1016/j.jct.2019.04.020>.
- [14] M.B. Shiflett, A. Yokozeki, Separation of difluoromethane and pentafluoroethane by extractive distillation using ionic liquid, *Chem. Today.* 24 (2006) 28–30.
- [15] M.B. Shiflett, A.D. Shiflett, A. Yokozeki, Separation of tetrafluoroethylene and carbon dioxide using ionic liquids, *Sep. Purif. Technol.* 79 (2011) 357–364, <https://doi.org/10.1016/j.seppur.2011.03.023>.
- [16] G. Zarca, I. Ortiz, A. Urriaga, Recovery of carbon monoxide from flue gases by reactive absorption in ionic liquid imidazolium chlorocuprate(I): Mass transfer coefficients, *Chinese J. Chem. Eng.* 23 (2015) 769–774, <https://doi.org/10.1016/j.cjche.2014.06.040>.
- [17] G. Zarca, I. Ortiz, A. Urriaga, Kinetics of the carbon monoxide reactive uptake by an imidazolium chlorocuprate(I) ionic liquid, *Chem. Eng. J.* 252 (2014) 298–304, <https://doi.org/10.1016/j.cej.2014.05.011>.
- [18] M.B. Shiflett, A. Yokozeki, Solubility and Diffusivity of Hydrofluorocarbons in Room-Temperature Ionic Liquids, *AIChE J.* 52 (2006) 1205–1219, <https://doi.org/10.1002/aic.10685>.
- [19] Y. Sun, Y. Zhang, X. Wang, J.M. Prausnitz, L. Jin, Gaseous absorption of 2,3,3,3-tetrafluoroprop-1-ene in three imidazolium-based ionic liquids, *Fluid Phase Equilib.* 450 (2017) 65–74, <https://doi.org/10.1016/j.fluid.2017.07.013>.
- [20] M.B. Shiflett, A. Yokozeki, Absorption cycle utilizing ionic liquid as working fluid, *US 8715521 B2* (2014).
- [21] C.J. Noelle, M.B. Shiflett, Capture of fluorinated vinyl monomers using ionic liquids, *US 8,779,220 B2*, 2014.
- [22] M.B. Shiflett, Capture of trifluoromethane using ionic liquids, *US Patent Application 2015/0082981 A1*, 2015.
- [23] D.L. Minnick, M.B. Shiflett, Solubility and Diffusivity of Chlorodifluoromethane in Imidazolium Ionic Liquids: [emim][Tf<sub>2</sub>N], [bmim][BF<sub>4</sub>], [bmim][PF<sub>6</sub>], and [emim][TfES], *Ind. Eng. Chem. Res.* 58 (2019) 11072–11081, <https://doi.org/10.1021/acs.iecr.9b02419>.
- [24] J.E. Sosa, R.P.P.L. Ribeiro, P.J. Castro, J.P.B. Mota, J.M.M. Araújo, A.B. Pereira, Absorption of Fluorinated Greenhouse Gases Using Fluorinated Ionic Liquids, *Ind. Eng. Chem. Res.* 58 (2019) 20769–20778, <https://doi.org/10.1021/acs.iecr.9b04648>.
- [25] L.F. Lepre, D. Andre, S. Denis-Quanquin, A. Gautier, A.A.H. Pádua, M.F. Costa Gomes, Ionic liquids can enable the recycling of fluorinated greenhouse gases, *ACS Sustain. Chem. Eng.* 7 (2019) 16900–16906, <https://doi.org/10.1021/acssuschemeng.9b04214>.
- [26] Y. Zhang, J. Yin, X. Wang, Vapor-liquid equilibrium of 2,3,3,3-tetrafluoroprop-1-ene with 1-butyl-3-methylimidazolium hexafluorophosphate, 1-hexyl-3-methylimidazolium hexafluorophosphate, and 1-octyl-3-methylimidazolium hexafluorophosphate, *J. Mol. Liq.* 260 (2018) 203–208, <https://doi.org/10.1016/j.molliq.2018.03.112>.
- [27] X. Liu, Z. Ye, L. Bai, M. He, Performance comparison of two absorption-compression hybrid refrigeration systems using R1234yf/ionic liquid as working pair, *Energy Convers. Manag.* 181 (2019) 319–330, <https://doi.org/10.1016/j.enconman.2018.12.030>.
- [28] X. Liu, M. He, N. Lv, X. Qi, C. Su, Vapor-Liquid Equilibrium of Three Hydrofluorocarbons with [HMIM][Tf<sub>2</sub>N], *J. Chem. Eng. Data* 60 (2015) 1354–1361, <https://doi.org/10.1021/je060275f>.
- [29] M.B. Shiflett, A. Yokozeki, Vapor-Liquid-Liquid Equilibria of Hydrofluorocarbons + 1-Butyl-3-methylimidazolium Hexafluorophosphate, *J. Chem. Eng. Data* 51 (2006) 1931–1939, <https://doi.org/10.1021/je060275f>.
- [30] M.B. Shiflett, A. Yokozeki, Gaseous Absorption of Fluoromethane, Fluoroethane, and 1,1,2,2-Tetrafluoroethane in 1-Butyl-3-Methylimidazolium Hexafluorophosphate, *Ind. Eng. Chem. Res.* 45 (2006) 6375–6382, <https://doi.org/10.1021/ie060192s>.
- [31] M.B. Shiflett, M.A. Harmer, C.P. Junk, A. Yokozeki, Solubility and diffusivity of 1,1,1,2-tetrafluoroethane in room-temperature ionic liquids, *Fluid Phase Equilib.*

- 242 (2006) 220–232, <https://doi.org/10.1016/j.fluid.2006.01.026>.
- [32] M.B. Shiflett, A. Yokozeki, Solubility Differences of Halocarbon Isomers in Ionic Liquid [emim][Tf2N], *J. Chem. Eng. Data* 52 (2007) 2007–2015, <https://doi.org/10.1021/jc700295e>.
- [33] M.B. Shiflett, A. Yokozeki, Utilizing ionic liquids for hydrofluorocarbon separation, *US 9,628,644 B2* (2014).
- [34] J. Palomar, M. Larriba, J. Lemus, D. Moreno, R. Santiago, C. Moya, J. de Riva, G. Pedrosa, Demonstrating the key role of kinetics over thermodynamics in the selection of ionic liquids for CO<sub>2</sub> physical absorption, *Sep. Purif. Technol.* 213 (2019) 578–586, <https://doi.org/10.1016/j.seppur.2018.12.059>.
- [35] G. Zarca, I. Ortiz, A. Urriaga, Novel solvents based on thiocyanate ionic liquids doped with copper(I) with enhanced equilibrium selectivity for carbon monoxide separation from light gases, *Sep. Purif. Technol.* 196 (2018) 47–56, <https://doi.org/10.1016/j.seppur.2017.06.069>.
- [36] M.G. Freire, A.R.R. Teles, M.A.A. Rocha, B. Schröder, C.M.S.S. Neves, P.J. Carvalho, D.V. Evtuguin, L.M.N.B.F. Santos, J.A.P. Coutinho, Thermophysical Characterization of Ionic Liquids Able To Dissolve Biomass, *J. Chem. Eng. Data* 56 (2011) 4813–4822, <https://doi.org/10.1021/jc200790q>.
- [37] D. Song, J. Chen, Density and viscosity data for mixtures of ionic liquids with a common anion, *J. Chem. Eng. Data* 59 (2014) 257–262, <https://doi.org/10.1021/jc400332j>.
- [38] J.A. Widegren, J.W. Magee, Density, viscosity, speed of sound, and electrolytic conductivity for the ionic liquid 1-hexyl-3-methylimidazolium bis(trifluoromethylsulfonyl)imide and its mixtures with water, *J. Chem. Eng. Data* 52 (2007) 2331–2338, <https://doi.org/10.1021/jc700329a>.
- [39] K.R. Harris, M. Kanakubo, L.A. Woolf, Temperature and pressure dependence of the viscosity of the ionic liquid 1-butyl-3-methylimidazolium tetrafluoroborate: Viscosity and density relationships in ionic liquids, *J. Chem. Eng. Data* 52 (2007) 2425–2430, <https://doi.org/10.1021/jc700370z>.
- [40] W. Fan, Q. Zhou, J. Sun, S. Zhang, Density, excess molar volume, and viscosity for the methyl methacrylate + 1-butyl-3-methylimidazolium hexafluorophosphate ionic liquid binary system at atmospheric pressure, *J. Chem. Eng. Data* 54 (2009) 2307–2311, <https://doi.org/10.1021/jc900091b>.
- [41] C.M.S.S. Neves, K.A. Kurnia, J.A.P. Coutinho, I.M. Marrucho, J.N.C. Lopes, M.G. Freire, L.P.N. Rebelo, Systematic study of the thermophysical properties of imidazolium-based ionic liquids with cyano-functionalized anions, *J. Phys. Chem. B* 117 (2013) 10271–10283, <https://doi.org/10.1021/jp405913b>.
- [42] B. Hasse, J. Lehmann, D. Assenbaum, P. Wasserscheid, A. Leipertz, A.P. Fröba, Viscosity, Interfacial Tension, Density, and Refractive Index of Ionic Liquids [EMIM][MeSO<sub>3</sub>], [EMIM][MeOHPO<sub>2</sub>], [EMIM][OeSO<sub>4</sub>], and [BBIM][NTf<sub>2</sub>] in Dependence on Temperature at Atmospheric Pressure, *J. Chem. Eng. Data* 54 (2009) 2576–2583, <https://doi.org/10.1021/jc900134z>.
- [43] Y.A. Sanmamed, D. González-Salgado, J. Troncoso, L. Romani, A. Baylaucq, C. Boned, Experimental methodology for precise determination of density of RTILs as a function of temperature and pressure using vibrating tube densimeters, *J. Chem. Thermodyn.* 42 (2010) 553–563, <https://doi.org/10.1016/j.jct.2009.11.014>.
- [44] M.A.A. Rocha, F.M.S. Ribeiro, A.I.M.C.L. Ferreira, J.A.P. Coutinho, L.M.N.B.F. Santos, Thermophysical properties of [CN - 1Clim][PF 6] ionic liquids, *J. Mol. Liq.* 188 (2013) 196–202, <https://doi.org/10.1016/j.molliq.2013.09.031>.
- [45] A. Hofmann, M. Migeot, T. Hanemann, Investigation of Binary Mixtures Containing 1-Ethyl-3-methylimidazolium Bis(trifluoromethanesulfonyl)azanide and Ethylene Carbonate, *J. Chem. Eng. Data* 61 (2016) 114–123, <https://doi.org/10.1021/acs.jced.5b00338>.
- [46] W. Ren, A.M. Scurto, Phase equilibria of imidazolium ionic liquids and the refrigerant gas, 1,1,1,2-tetrafluoroethane (R-134a), *Fluid Phase Equilib.* 286 (2009) 1–7, <https://doi.org/10.1016/j.fluid.2009.07.007>.
- [47] M.B. Shiflett, M.A. Harmer, C.P. Junk, A. Yokozeki, Solubility and Diffusivity of Difluoromethane in Room-Temperature Ionic Liquids, *J. Chem. Eng. Data* 51 (2006) 483–495, <https://doi.org/10.1021/jc050386z>.
- [48] A. Ahoosseini, W. Ren, L.R. Weatherly, A.M. Scurto, Viscosity and self-diffusivity of ionic liquids with compressed hydrofluorocarbons: 1-Hexyl-3-methyl-imidazolium bis(trifluoromethylsulfonyl)amide and 1,1,1,2-tetrafluoroethane, *Fluid Phase Equilib.* 437 (2017) 34–42, <https://doi.org/10.1016/j.fluid.2016.11.022>.
- [49] X. Liu, L. Bai, S. Liu, M. He, Vapor – Liquid Equilibrium of R1234yf/[HMIM][Tf<sub>2</sub>N] and R1234ze (E)/[HMIM][Tf<sub>2</sub>N] Working Pairs for the Absorption Refrigeration Cycle, *J. Chem. Eng. Data* 61 (2016) 3952–3957, <https://doi.org/10.1021/acs.jced.6b00731>.
- [50] J.D. Seader, E.J. Henley, D.K. Roper, *Separation process principles*, 3rd ed, John Wiley & Sons Ltd, New Jersey, USA, 2010.
- [51] L. Dong, D. Zheng, G. Sun, X. Wu, Vapor-Liquid Equilibrium Measurements of Difluoromethane + [Emim]OTf, Difluoromethane + [Bmim]OTf, Difluoroethane + [Emim]OTf, and Difluoroethane + [Bmim]OTf Systems, *J. Chem. Eng. Data* 56 (2011) 3663–3668.
- [52] J. Crank, *The Mathematics of Diffusion*, 2nd ed, Clarendon Press, Oxford, UK, 1975. [https://doi.org/10.1016/0306-4549\(77\)90072-X](https://doi.org/10.1016/0306-4549(77)90072-X).
- [53] D. Camper, C. Becker, C. Koval, R. Noble, Diffusion and solubility measurements in room temperature ionic liquids, *Ind. Eng. Chem. Res.* 45 (2006) 445–450, <https://doi.org/10.1021/ie0506668>.
- [54] M. He, S. Peng, X. Liu, P. Pan, Y. He, Diffusion coefficients and Henry's constants of hydrofluorocarbons in [HMIM][Tf<sub>2</sub>N], [HMIM][TfO], and [HMIM][BF<sub>4</sub>], *J. Chem. Thermodyn.* 112 (2017) 43–51, <https://doi.org/10.1016/j.jct.2017.04.009>.
- [55] L. Moura, W. Darwich, C.C. Santini, M.F. Costa Gomes, Imidazolium-based ionic liquids with cyano groups for the selective absorption of ethane and ethylene, *Chem. Eng. J.* 280 (2015) 755–762, <https://doi.org/10.1016/j.cej.2015.06.034>.
- [56] D. Almantariotis, T. Gefflaut, A.A.H. Pádua, J.-Y. Coxam, M.F. Costa Gomes, Effect of fluorination and size of the alkyl side-Chain on the solubility of carbon dioxide in 1-alkyl-3-methylimidazolium bis(trifluoromethylsulfonyl) amide ionic liquids, *J. Phys. Chem. B* 114 (2010) 3608–3617, <https://doi.org/10.1021/jp912176m>.
- [57] J. Blath, M. Christ, N. Deubler, T. Hirth, T. Schiestel, Gas solubilities in room temperature ionic liquids - Correlation between RTIL-molar mass and Henry's law constant, *Chem. Eng. J.* 172 (2011) 167–176, <https://doi.org/10.1016/j.cej.2011.05.084>.
- [58] P.J. Carvalho, K.A. Kurnia, J.A.P. Coutinho, Dispelling some myths about the CO<sub>2</sub> solubility in ionic liquids, *PCCP* 18 (2016) 14757–14771, <https://doi.org/10.1039/c6cp01896c>.
- [59] Y. Sun, Y. Zhang, G. Di, X. Wang, J.M. Prausnitz, L. Jin, Vapor-Liquid Equilibria for R1234ze(E) and Three Imidazolium-Based Ionic Liquids as Working Pairs in Absorption-Refrigeration Cycle, *J. Chem. Eng. Data* 63 (2018) 3053–3060, <https://doi.org/10.1021/acs.jced.8b00314>.
- [60] X. Liu, P. Pan, M. He, Vapor-liquid equilibrium and diffusion coefficients of R32 + [HMIM][FEP], R152a + [HMIM][FEP] and R161 + [HMIM][FEP], *J. Mol. Liq.* 253 (2018) 28–35, <https://doi.org/10.1016/j.molliq.2018.01.032>.
- [61] R. Condemarin, P. Scovazzo, Gas permeabilities, solubilities, diffusivities, and diffusivity correlations for ammonium-based room temperature ionic liquids with comparison to imidazolium and phosphonium RTIL data, *Chem. Eng. J.* 147 (2009) 51–57, <https://doi.org/10.1016/j.cej.2008.11.015>.
- [62] Y. Yampolskii, I. Pinnau, B. Freeman, *Materials science of membranes for gas and vapor separation*, John Wiley & Sons Ltd, West Sussex, 2006.
- [63] T.-H. Chung, M. Ajlan, L.L. Lee, K.E. Starling, Generalized Multiparameter Correlation for Nonpolar and Polar Fluid Transport Properties, *Ind. Eng. Chem. Res.* 27 (1988) 671–679, <https://doi.org/10.1021/ie00076a024>.
- [64] X. Liu, M.Q. Nguyen, S. Xue, C. Song, M. He, Vapor-Liquid Equilibria and Inter-Diffusion Coefficients for Working Pairs for Absorption Refrigeration Systems Composed of [HMIM][BF<sub>4</sub>] and Fluorinated Propanes, *Int. J. Refrig* 104 (2019) 34–41, <https://doi.org/10.1016/j.ijrefrig.2019.04.023>.
- [65] C.C. Sampson, M. Kamson, M.G. Hopkins, P.L. Stanwix, E.F. May, Dielectric permittivity, polarizability and dipole moment of refrigerants R1234ze(E) and R1234yf determined using a microwave re-entrant cavity resonator, *J. Chem. Thermodyn.* 128 (2019) 148–158, <https://doi.org/10.1016/j.jct.2018.07.011>.
- [66] B.J. Costa Cabral, R.C. Guedes, R.S. Pai-Panandiker, C.A. Nieto de Castro, Hydrogen bonding and the dipole moment of hydrofluorocarbons by density functional theory, *Phys. Chem. Chem. Phys.* 3 (2001) 4200–4207, <https://doi.org/10.1039/b102879k>.
- [67] E. Kryachko, S. Scheiner, CH–F hydrogen bonds. Dimers of fluoromethanes, *J. Phys. Chem. A* 108 (2004) 2527–2535, <https://doi.org/10.1021/jp0365108>.
- [68] M. Karamoddin, F. Varaminian, Solubility of R22, R23, R32, R134a, R152a, R125 and R744 refrigerants in water by using equations of state, *Int. J. Refrig* 36 (2013) 1681–1688, <https://doi.org/10.1016/j.ijrefrig.2013.04.013>.
- [69] I. Skarmoutsos, P.A. Hunt, Structural and dynamic properties of the new alternative refrigerant 2,3,3,3-tetrafluoro-1-propene (HFO-1234yf) in the liquid state, *J. Phys. Chem. B* 114 (2010) 17120–17127, <https://doi.org/10.1021/jp108647p>.
- [70] M.L. Ferreira, J.M.M. Araújo, A.B. Pereira, L.F. Vega, Insights into the influence of the molecular structures of fluorinated ionic liquids on their thermophysical properties. A soft-SAFT based approach, *PCCP* 21 (2019) 6362–6380, <https://doi.org/10.1039/c8cp07522k>.
- [71] T. Endo, Y. Nishisaka, Y. Kin, Y. Kimura, Systematic estimation and interpretation of fractional free volume in 1-alkyl-3-methylimidazolium-based ionic liquids, *Fluid Phase Equilib.* 498 (2019) 144–150, <https://doi.org/10.1016/j.fluid.2019.06.027>.
- [72] S. Asensio-Delgado, D. Jovell, G. Zarca, A. Urriaga, F. Llovel, Thermodynamic and process modeling of the recovery of R410A compounds with ionic liquids, *Int. J. Refrig.* (2020) 10.1016/j.ijrefrig.2020.04.013 In press.
- [73] S. Asensio-Delgado, F. Pardo, G. Zarca, A. Urriaga, Vapor-liquid equilibria and diffusion coefficients of difluoromethane, 1,1,1,2-tetrafluoroethane and 2,3,3,3-tetrafluoropropene in low-viscosity ionic liquids, *J. Chem. Eng. Data* (2020), <https://doi.org/10.1021/acs.jced.0c00224> In press.

## Supplementary Information

Enhanced absorption separation of  
hydrofluorocarbon/hydrofluoroolefin refrigerant blends using  
ionic liquids

### Authors:

**Salvador Asensio-Delgado, Fernando Pardo, Gabriel Zarca\*, Ane Urtiaga**

Department of Chemical and Biomolecular Engineering, Universidad de Cantabria,

Av. Los Castros 46, Santander 39005, Spain.

\*Corresponding author e-mail address: [zarcag@unican.es](mailto:zarcag@unican.es)

Table S1. Examples of HFC blends and new HFC+HFO blends. HFOs are R1234yf and R1234ze(E).

System	Mixture	Composition* (Mass %)	GWP
HFCs-only	R404A	R125/R143a/R134a (44.0/52.0/4.0)	3922
	R407C	R32/R125/R134a (23.0/25.0/52.0)	1774
	R410A	R32/R125 (50.0/50.0)	2088
	R507C	R125/R143a (50.0/50.0)	2465
	HFCs+HFOs	R448A	R32/R125/R1234yf/R134a/R1234ze(E) (26.0/26.0/20.0/21.0/7.0)
R449A		R32/R125/R1234yf/R134a (24.3/24.7/25.3/25.7)	1397
R454A		R32/R1234yf (35.0/65.0)	239
R455A		CO <sub>2</sub> /R32/R1234yf (3.0/21.5/75.5)	148
R513A		R1234yf/R134a (56.0/44.0)	631

\*R32: difluoromethane, R143a: 1,1,1-trifluoroethane, R134a: 1,1,1,2-tetrafluoroethane, R125: pentafluoroethane, R1234yf: 2,3,3,3-tetrafluoropropene, R1234ze(E): trans-1,3,3,3-tetrafluoropropene

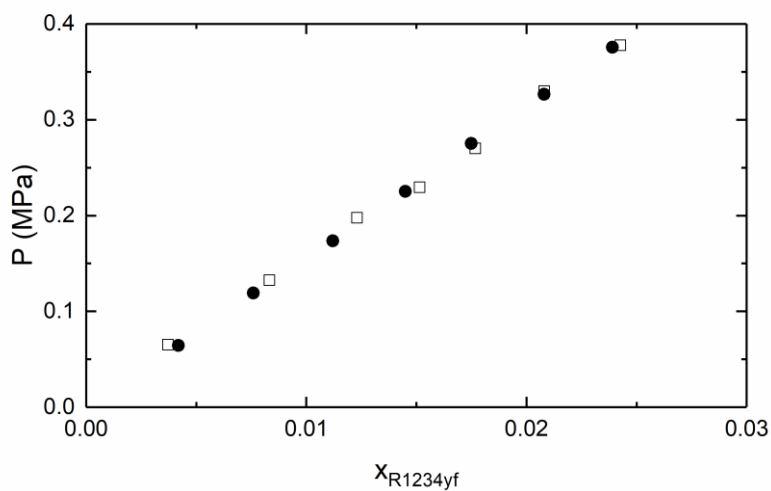


Figure S1. Solubility of R1234yf in [C<sub>2</sub>mim][BF<sub>4</sub>] at 303.15 K. This work (□) and Sun et al. [1] (●).

Table S2. Experimental solubility data of R32 in [C<sub>2</sub>mim][SCN].

T (K)	P (MPa)	x	u(x)	m (mol/kg)	u(m)
283.15	0.0719	0.0248	0.0007	0.150	0.004
283.15	0.1752	0.0660	0.0011	0.418	0.008
283.15	0.3009	0.1198	0.0016	0.804	0.012
283.15	0.4467	0.1793	0.0021	1.291	0.018
283.15	0.5994	0.2411	0.0026	1.877	0.026
293.15	0.0730	0.0223	0.0007	0.135	0.004
293.15	0.1861	0.0575	0.0012	0.361	0.008
293.15	0.3130	0.0993	0.0016	0.651	0.012
293.15	0.4527	0.1454	0.0021	1.005	0.017
293.15	0.6012	0.1892	0.0027	1.378	0.025
303.15	0.0578	0.0130	0.0005	0.078	0.003
303.15	0.1353	0.0325	0.0009	0.199	0.005
303.15	0.2303	0.0557	0.0012	0.348	0.008
303.15	0.3392	0.0831	0.0017	0.536	0.012
303.15	0.4589	0.1123	0.0023	0.747	0.017
303.15	0.5976	0.1445	0.0031	0.998	0.025
303.15	0.7396	0.1783	0.0041	1.282	0.036
313.15	0.0726	0.0150	0.0006	0.090	0.004
313.15	0.1876	0.0374	0.0011	0.229	0.007
313.15	0.3231	0.0645	0.0016	0.407	0.011
313.15	0.4722	0.0937	0.0022	0.611	0.016
313.15	0.6322	0.1225	0.0029	0.825	0.022

Table S3. Experimental solubility data of R134a in [C<sub>2</sub>mim][SCN].

T (K)	P (MPa)	x	u(x)	m (mol/kg)	u(m)
283.15	0.0683	0.0174	0.0006	0.104	0.004
283.15	0.1430	0.0399	0.0009	0.245	0.006
283.15	0.2237	0.0653	0.0013	0.413	0.009
283.15	0.3218	0.0964	0.0018	0.631	0.013
283.15	0.4072	0.1276	0.0023	0.864	0.018
293.15	0.0648	0.0133	0.0006	0.080	0.004
293.15	0.1476	0.0309	0.0009	0.188	0.006
293.15	0.2314	0.0501	0.0013	0.312	0.008
293.15	0.3217	0.0705	0.0018	0.448	0.012
293.15	0.4230	0.0961	0.0024	0.628	0.017
303.15	0.0683	0.0102	0.0006	0.061	0.004
303.15	0.1513	0.0228	0.0009	0.144	0.006
303.15	0.2387	0.0375	0.0013	0.236	0.008
303.15	0.3418	0.0532	0.0018	0.338	0.012
303.15	0.4342	0.0705	0.0025	0.454	0.017
313.15	0.0683	0.0071	0.0006	0.042	0.003
313.15	0.1556	0.0169	0.0009	0.101	0.006
313.15	0.2429	0.0266	0.0013	0.161	0.008
313.15	0.3279	0.0346	0.0018	0.212	0.011
313.15	0.4329	0.0468	0.0025	0.290	0.016

Table S4. Experimental solubility data of R1234yf in [C<sub>2</sub>mim][SCN].

T (K)	P (MPa)	x	u(x)	m (mol/kg)	u(m)
283.15	0.0635	0.0035	0.0005	0.021	0.003
283.15	0.1452	0.0098	0.0009	0.058	0.005
283.15	0.2379	0.0163	0.0013	0.098	0.008
283.15	0.3265	0.0251	0.0018	0.152	0.011
283.15	0.4421	0.0366	0.0026	0.224	0.016
293.15	0.0643	0.0029	0.0005	0.017	0.003
293.15	0.1514	0.0077	0.0009	0.046	0.005
293.15	0.2519	0.0139	0.0013	0.083	0.008
293.15	0.3435	0.0180	0.0018	0.108	0.011
293.15	0.4346	0.0246	0.0026	0.149	0.016
303.15	0.0665	0.0031	0.0005	0.018	0.003
303.15	0.1514	0.0060	0.0009	0.035	0.005
303.15	0.2378	0.0084	0.0012	0.050	0.007
303.15	0.3313	0.0103	0.0018	0.062	0.011
303.15	0.4576	0.0130	0.0026	0.078	0.016
313.15	0.0671	0.0007	0.0005	0.004	0.003
313.15	0.1470	0.0022	0.0008	0.013	0.005
313.15	0.2388	0.0036	0.0012	0.021	0.007
313.15	0.3364	0.0042	0.0017	0.025	0.010
313.15	0.4593	0.0063	0.0026	0.038	0.015

Table S5. Henry's law constants for the absorption of R32, R134a and R1234yf in [C<sub>2</sub>mim][SCN].

System	T = 283.15 K	T = 293.15 K	T = 303.15 K	T = 313.15 K
<b>R32 + [C<sub>2</sub>mim][SCN]</b>	2.61	3.16	4.08	4.86
<b>R134a + [C<sub>2</sub>mim][SCN]</b>	3.72	4.88	6.76	9.32
<b>R1234yf + [C<sub>2</sub>mim][SCN]</b>	15.72	20.22	35.56	64.75

Table S6. Parameters of Eq. (22) to describe the influence of temperature on the Henry's law constant of R32, R134a and R1234yf in [C<sub>2</sub>mim][SCN].

	<b>R32 + [C<sub>2</sub>mim][SCN]</b>	<b>R134a + [C<sub>2</sub>mim][SCN]</b>	<b>R1234yf + [C<sub>2</sub>mim][SCN]</b>
<b>A</b>	-1883.4	-2729.1	-4241.9
<b>B</b>	7.6	10.9	17.6
<b>R<sup>2</sup></b>	0.995	0.995	0.961

Table S7. Diffusion coefficients at infinite dilution, Eq. (9), of R32, R134a and R1234yf in [C<sub>2</sub>mim][SCN].

$T$ (K)	$D \cdot 10^{10}$ (m <sup>2</sup> /s)		
	R32 + [C <sub>2</sub> mim][SCN]	R134a + [C <sub>2</sub> mim][SCN]	R1234yf + [C <sub>2</sub> mim][SCN]
283.15	5.1 ± 0.3	1.5 ± 0.1	0.5 ± 0.2
293.15	8.7 ± 0.3	3.5 ± 0.2	1.3 ± 0.7
303.15	11.3 ± 0.3	5.9 ± 0.3	3.6 ± 2.5
313.15	13.3 ± 0.4	13.2 ± 0.7	9.8 ± 8.3*

\*High uncertainty due to very low solubility at this temperature

Table S8. Solvation enthalpies and entropies for the absorption of R32, R134a and R1234yf in [C<sub>2</sub>mim][SCN] at infinite dilution.

$T$ (K)	$\Delta H_{sol}$ ( $\frac{kJ}{mol}$ )	$\Delta S_{sol}$ ( $\frac{J}{mol \cdot K}$ )
R32 + [C <sub>2</sub> mim][SCN]	-15.76	-52
R134a + [C <sub>2</sub> mim][SCN]	-23.27	-78
R1234yf + [C <sub>2</sub> mim][SCN]	-29.78	-101

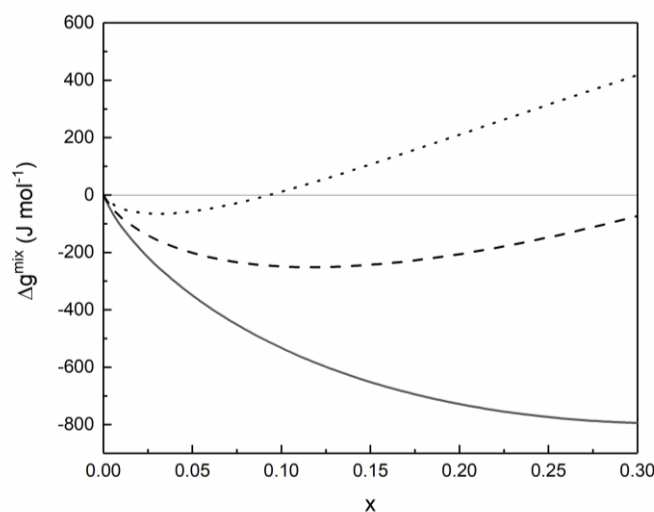


Figure S2. Predicted mixing free energy of Gibbs, Eqs. (19-21), at 283.15 K of refrigerant gases in [C<sub>2</sub>mim][SCN]: R32 (solid line), R134a (dashed line) and R1234yf (dotted line).

## References

- [1] Y. Sun, Y. Zhang, X. Wang, J.M. Prausnitz, L. Jin, Gaseous absorption of 2,3,3,3-tetrafluoroprop-1-ene in three imidazolium-based ionic liquids, *Fluid Phase Equilib.* 450 (2017) 65–74.

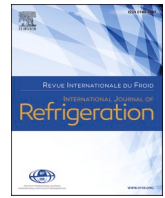




---

**3.5. Scientific publication 5. “Analysis of hybrid compression absorption refrigeration using low-GWP HFC or HFO/ionic liquid working pairs”, José M. Asensio-Delgado, Salvador Asensio-Delgado, Gabriel Zarca, Ane Urtiaga, International Journal of Refrigeration, 134 (2022) 232-241**

This article presents two sections. The first part continues the experimental assessment of the absorption of F-gases using ILs, this time for the refrigerant R1234ze(E), an HFO which is steadily gaining importance in the RACHP market. The study showed that the solubility of R1234ze(E) in ILs was much higher than that of its isomer R1234yf that we had studied in previous publications, so we wanted to test and compare its behavior with other refrigerant gases in absorption refrigeration systems. To that end, in the second section we did the process design for absorption refrigeration and hybrid compression absorption refrigeration systems and studied their performances in terms of solvent consumption and energy efficiency (*COP*, coefficient of performance). The results show that the compression assisted version is more interesting if the amount of low-grade thermal energy available is not excessive. The best system was the one formed by the working pair R32/[C<sub>2</sub>mim][Tf<sub>2</sub>N] because the solubility of the gas was high, giving *COP* values competitive with respect to the classical pairs H<sub>2</sub>O/LiBr and NH<sub>3</sub>/H<sub>2</sub>O. However, if enough thermal energy is available and the use of low-GWP refrigerants is favored, R1234ze(E) working pairs with [C<sub>2</sub>mim][Tf<sub>2</sub>N] or [C<sub>2</sub>mim][OTf] could be interesting. Contrary to what is observed in separation applications, absorption refrigeration systems improve their performance with highly fluorinated and high molar volumes ILs, so further improvement of the results of this work should look in this direction.



# Analysis of hybrid compression absorption refrigeration using low-GWP HFC or HFO/ionic liquid working pairs

## Analyse du froid hybride à absorption-compression utilisant des couples de travail HFC ou HFO/liquide ionique à faible PRP

José M. Asensio-Delgado, Salvador Asensio-Delgado, Gabriel Zarca, Ane Urtiaga\*

Department of Chemical and Biomolecular Engineering, University of Cantabria, Av. Los Castros 46, Santander 39005, Spain

### ARTICLE INFO

#### Keywords:

Hydrofluorocarbon  
Hydrofluoroolefin  
Absorption refrigeration  
Thermodynamic modeling  
R1234ze(E)  
Ionic liquid

#### Mots clés:

Hydrofluorocarbure  
Hydrofluoroléfine  
Froid à absorption  
Modélisation thermodynamique  
R1234ze(E)  
Liquide ionique

### ABSTRACT

Absorption refrigeration systems (ARS) are the leading alternative for reducing the electricity costs associated with compression refrigeration systems. However, classical pairs based on  $\text{NH}_3/\text{H}_2\text{O}$  and  $\text{H}_2\text{O}/\text{LiBr}$  have drawbacks that limit their practical application. In this work, we analyze 16 pairs of refrigerant gases and ionic liquid sorbents based on two low global warming potential (GWP) hydrofluorocarbons (HFCs), R32 and R134a, and two novel hydrofluoroolefins (HFOs), R1234ze(E) and R1234yf, using the low-viscosity ionic liquids  $[\text{C}_2\text{mim}][\text{BF}_4]$ ,  $[\text{C}_2\text{mim}][\text{OTf}]$ ,  $[\text{C}_2\text{mim}][\text{SCN}]$ , and  $[\text{C}_2\text{mim}][\text{Tf}_2\text{N}]$ . We provide new data and modeling of the vapor-liquid equilibria of R1234ze(E) with  $[\text{C}_2\text{mim}][\text{OTf}]$ ,  $[\text{C}_2\text{mim}][\text{SCN}]$  and  $[\text{C}_2\text{mim}][\text{Tf}_2\text{N}]$ . ARS performance in single-effect (SE-ARS) and compression-assisted absorption refrigeration (CA-ARS), in terms of coefficient of performance (COP, ECOP), solution circulation factor ( $f$ ), and the thermal and electrical contribution to the total COP, is evaluated through energy and exergy analyses. The results showed that CA-ARS performs better even at lower generator temperatures. In addition, HFCs returned a better performance than HFOs because of their higher solubility in ILs. The working pair R32/ $[\text{C}_2\text{mim}][\text{Tf}_2\text{N}]$  gave the best results,  $\text{COP} = 0.74$  and  $f = 5.4$  at 328 K in the desorber, and a maximum ECOP of 0.41 at 318 K. Furthermore, the HFO R1234ze(E), with a lower working pressure and negligible GWP, is also a promising option for CA-ARS. In conclusion, we consider that ARS with the HFC or HFO/IL pairs examined in this study shows outstanding potential as a more energy efficient system compared to compression systems, when an inexpensive energy source is available.

### 1. Introduction

Modern global challenges encourage our society to develop a clean and carbon-neutral economy. In this context, the heating and cooling sector accounted for 51% of the total final energy consumption in the EU in 2012 and 27% of total greenhouse gas (GHG) emissions in Europe in 2018, making it the highest contributor ahead of road transportation (European Environment Agency, 2020; European Commission, 2020). Current refrigeration technology is mostly based on compression refrigeration systems (CRS), which have high power consumptions, e.g., up to 15% of the total electricity consumption in developed countries

such as Germany (Seiler et al., 2013). To meet climate change objectives and reduce atmospheric pollution, more innovation and further research into energy-saving cooling technologies are required (Seiler et al., 2013; Garcia et al., 2021).

Absorption refrigeration systems (ARS) are alternatives to conventional compression refrigeration systems (CRS). ARS are powered by thermal energy rather than electricity, so the objective is to use low-grade energy from renewable sources, such as solar or geothermal energy, or from waste heat. Classical ARS use ammonia/water ( $\text{NH}_3/\text{H}_2\text{O}$ ) and water/lithium bromide ( $\text{H}_2\text{O}/\text{LiBr}$ ) as working pairs, although they have several disadvantages, namely, toxicity, flammability, the need for a rectifier to separate the  $\text{NH}_3$  from the  $\text{H}_2\text{O}$ , high-temperature

**Abbreviations:** ARS, Absorption Refrigeration Systems; CA-ARS, Compression-Assisted Absorption Refrigeration Systems; CRS, Compression Refrigeration Systems; COP, Coefficient of Performance; ECOP, Exergy efficiency; GHG, Greenhouse Gas; GWP, Global Warming Potential; HFC, Hydrofluorocarbons; HFO, Hydrofluoroolefins; IL, Ionic liquids; NRTL, NonRandom Two-Liquid model; SE-ARS, Single-Effect Absorption Refrigeration Systems; VLE, Vapor-Liquid Equilibria.

\* Corresponding author.

E-mail address: [urtiaga@unican.es](mailto:urtiaga@unican.es) (A. Urtiaga).

<https://doi.org/10.1016/j.ijrefrig.2021.11.013>

Received 2 July 2021; Received in revised form 20 October 2021; Accepted 22 November 2021

Available online 24 November 2021

0140-7007/© 2021 The Author(s). Published by Elsevier Ltd. This is an open access article under the CC BY-NC-ND license (<http://creativecommons.org/licenses/by-nc-nd/4.0/>).

Nomenclature		$\rho$	Molar density, mol·L <sup>-1</sup>
$B$	Second virial coefficient, m <sup>3</sup> ·mol <sup>-1</sup>	$\Phi$	Fugacity correction factor
$C$	Gas concentration, mol·m <sup>-3</sup>	<i>Subscripts</i>	
$D$	Diffusivity, m <sup>2</sup> ·s <sup>-1</sup>	c	condenser
$f$	Circulation factor,	comp	compressor
$\bar{f}$	Fugacity, MPa	con	IL-concentrated solution
$h$	Specific enthalpy, kJ·kg <sup>-1</sup> or kJ·mol <sup>-1</sup>	d	desorber or generator
$k_H$	Henry's law constant, MPa	dil	IL-diluted solution
$m$	Mass flow rate, kg·s <sup>-1</sup>	e	evaporator
$M_m$	Molecular mass, kg·mol <sup>-1</sup>	el	electrical
$p$	Pressure, MPa	ex	excess
$Q$	Heat duty, kW	hx	heat exchanger
$R$	Ideal gas constant, J·mol <sup>-1</sup> ·K <sup>-1</sup>	i, 1, 2...	component
$T$	Temperature, K	p	pump
$V$	Volume, L	r	refrigerant
$w$	Mass fraction,	ref	reference
$W$	Power, kW	th	thermal
$x, y$	Mole fraction,	v	expansion valve
<i>Greek letters</i>		<i>Superscripts</i>	
$\alpha, \tau_{12}^0, \tau_{12}^1, \tau_{21}^0, \tau_{21}^1$	NRTL adjustable parameters	L	saturated liquid
$\gamma$	Activity coefficient, -	S	saturated vapor
$\mu$	Dynamic viscosity, mPa·s	s	isentropic
$\eta_{hx}$	Heat exchanger efficiency, -		

corrosion, and operation at subatmospheric pressures or crystallization in the case of H<sub>2</sub>O/LiBr (Seiler et al., 2013).

There are various approaches to overcome the main drawbacks of classical ARS including the application of new absorbents and hydrofluorocarbon refrigerants. Regarding the absorbents, some recent studies have analyzed the use of organic solvents, such as TEGDME (triethylene glycol dimethyl ether) or the synthetic polyolester oil PZ46M (Gao et al., 2019; Zhang et al., 2021). The use of ionic liquids (ILs) is also attracting attention thanks to their interesting properties, including an extremely low vapor pressure, high thermal and chemical stability, liquid stability over a wide temperature range, non-flammability and excellent solvation properties, among others (Asensio-Delgado et al., 2021a). Some of these new IL absorbents have been studied in absorption pairs with NH<sub>3</sub> and H<sub>2</sub>O (Yokozeki and Shiflett, 2010; Kim et al., 2012; Wang and Infante Ferreira, 2017; Moreno et al., 2018). However, the pairs containing NH<sub>3</sub> are still toxic, flammable, and corrosive, and the use of H<sub>2</sub>O is limited at low evaporator temperatures. In this regard, the use of hydrofluorocarbon (HFC) refrigerants is expected to increase the range of viable operating temperatures and reduce the toxicity of ARS. Nontoxic HFCs are noted for their low or negligible flammability, stability and good thermodynamic properties (Asensio-Delgado et al., 2020a). However, some HFCs act as greenhouse gasses (GHGs) with a high global warming potential (GWP). This factor is driving the refrigeration sector towards the use of hydrofluoroolefins (HFOs), a group of compounds with a much lower GWP than HFCs and harmless to the ozone layer (McLinden and Huber, 2020). To date, only the performance of some fluorinated refrigerant/IL working pairs has been assessed in absorption refrigeration using, among others, R134a, R32, R152a, R161, R1234ze(E), or R1234yf refrigerants combined with [C<sub>4</sub>mim][PF<sub>6</sub>], [C<sub>6</sub>mim][PF<sub>6</sub>], [C<sub>6</sub>mim][Tf<sub>2</sub>N], [C<sub>6</sub>mim][BF<sub>4</sub>], or [C<sub>6</sub>mim][OTf] ILs (Kim et al., 2012; Wu et al., 2018; Y. Sun et al., 2020; Y. Sun et al., 2020; Liu et al., 2019; Wu et al., 2020; W. Wu et al., 2017; W. Wu et al., 2017). However, with the exception of [C<sub>6</sub>mim][Tf<sub>2</sub>N], the ILs studied so far have viscosities higher than 100 mPa·s at 303.15 K. The high viscosity of the absorbents may reduce mass and energy transfer rates and increase pumping costs, thereby reducing the system's energy efficiency (Zarca et al., 2014;

Zarca et al., 2015). So, we still need to learn more about ARS performance when using low-viscosity ILs together with HFCs and HFOs as working fluids.

ARS involve replacing the compressor of a CRS with an absorption—desorption cycle in which the refrigerant is first dissolved and then pressurized in liquid state, which is a more energy-efficient process than vapor compression given the lower specific volume (Seiler et al., 2013). After pumping, the refrigerant is released from the absorbent by heating the solution. This cycle is known as Single-Effect Absorption Refrigeration System (SE-ARS) and is shown schematically in Fig. 1a. Additionally, a solution heat exchanger is placed between the absorber and desorber to increase the cycle's thermal efficiency. However, the system may underperform if the heat source is too cool or the pressure in the absorber too low. To expand the range of viable operating conditions, the Compression-Assisted Absorption Refrigeration System (CA-ARS), a hybrid between CRS and SE-ARS, has also been proposed (Fig. 1b). In CA-ARS, the compressor is installed after the evaporator to increase the solubility in the absorber thanks to the higher inlet pressure. Consequently, CA-ARS does not eliminate the use of a compressor but substantially reduces its energy requirements.

In this work, we aimed to characterize the behavior of 16 working pairs formed from HFCs or HFOs with different low-viscosity ILs and analyze their refrigeration performance in SE-ARS and CA-ARS, which is a more demanding application than air conditioning for these thermally driven systems. We focused on two of the most widely used HFCs, R134a and R32, and the two HFOs that are attracting the most attention at the moment, R1234ze(E) and R1234yf. Table 1 contains their chemical names, molar masses and GWPs. The very low-viscosity ILs [C<sub>2</sub>mim][BF<sub>4</sub>], [C<sub>2</sub>mim][OTf], [C<sub>2</sub>mim][SCN], and [C<sub>2</sub>mim][Tf<sub>2</sub>N] were selected over more viscous ILs because it was expected their real performances would approach those predicted by the equilibrium analyses considering the higher heat and mass transfer rates. This hypothesis has already been tested for IL-based separation processes analyzed in rate-based models (Mota-Martinez et al., 2018; Palomar et al., 2019). We also assess the influence of the anion structure on ARS cycle performance. Table 2 presents the chemical names of these ILs as well as some properties of interest. The vapor-liquid equilibria (VLE) required for

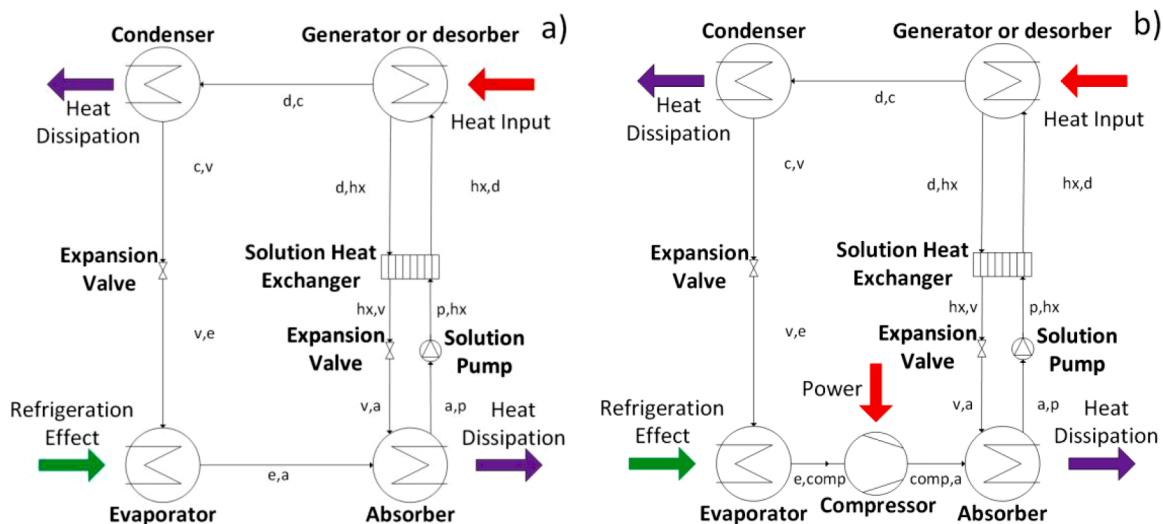


Fig. 1. Schematics of (a) a Single-Effect Absorption Refrigeration System (SE-ARS) and (b) a Compression-Assisted Absorption Refrigeration System (CA-ARS).

Table 1.  
Refrigerants studied.

Type	Code	Name	$M_m$ ( $\text{g}\cdot\text{mol}^{-1}$ )	GWP	$T_c$ (K)
HFC	R134a	1,1,1,2-Tetrafluoroethane	102.03	1430	374.21
HFC	R32	Difluoromethane	52.02	675	351.26
HFO	R1234ze(E)	Trans-1,3,3,3-tetrafluoropropene	114.04	1	382.52
HFO	R1234yf	2,3,3,3-Tetrafluoropropene	114.04	1	367.85

Table 2.  
Ionic liquids studied. Density and viscosity at 303.15 K (Sanmamed et al., 2010; Neves et al., 2013; Gardas et al., 2008; Freire et al., 2011; Součková et al., 2014; Atilhan et al., 2013).

Abbreviation	Name	$M_m$ ( $\text{g}\cdot\text{mol}^{-1}$ )	$\rho$ ( $\text{kg}\cdot\text{m}^{-3}$ )	$\mu$ ( $\text{mPa}\cdot\text{s}$ )
[C <sub>2</sub> mim][BF <sub>4</sub> ]	1-Ethyl-3-methylimidazolium tetrafluoroborate	197.97	1281.7	32.31
[C <sub>2</sub> mim][OTf]	1-Ethyl-3-methylimidazolium trifluoromethanesulfonate	260.23	1370.0	35.98
[C <sub>2</sub> mim][SCN]	1-Ethyl-3-methylimidazolium thiocyanate	169.24	1113.9	20.79
[C <sub>2</sub> mim][Tf <sub>2</sub> N]	1-Ethyl-3-methylimidazolium bis(trifluoromethylsulfonyl) imide	391.31	1514.3	26.9

some of these systems have been studied previously, but there is no information available in the literature on the absorption of R1234ze(E) in [C<sub>2</sub>mim][OTf], [C<sub>2</sub>mim][SCN] or [C<sub>2</sub>mim][Tf<sub>2</sub>N]. To solve this gap, we experimentally determined the VLE of these systems. We used the nonrandom two-liquid (NRTL) model to describe the VLE of each absorption pair and then used it in the thermodynamic modeling of the cycles. Overall, this study provides insights into the performance of new refrigerant/IL pairs in SE-ARS and CA-ARS systems working with a wide range of low-grade heat sources (generator temperature of between 313 and 373 K) for refrigeration purposes (evaporator temperature of 278 K).

## 2. Experimental section

### 2.1. Materials

R1234ze(E) (99.9%) was supplied by Coproven Climatización (Gas Servei licensed supplier, Spain). The IL [C<sub>2</sub>mim][SCN] (98 wt%) was purchased from IoLiTec, and ILs [C<sub>2</sub>mim][OTf] (98 wt%) and [C<sub>2</sub>mim][Tf<sub>2</sub>N] (98 wt%) were purchased from Sigma-Aldrich. Before use, the three ILs were vacuum dried and their water content measured using the Karl Fischer titration and found to be < 100 ppm.

### 2.2. Experimental apparatus and procedure

We used an isochoric saturation method to quantify the absorption of R1234ze(E) in the selected ILs. The description and validation of the experimental system is detailed in previous works (Asensio-Delgado et al., 2020b). In brief, it consisted of a jacketed stirred tank reactor (Buchi, model Picoclave, 170 mL) fitted with a temperature and pressure transducer (Keller, series PAA-33X, 0.01% accuracy) and a Pt-100 temperature sensor connected to a cryothermostatic bath (Julabo, model F25-ME,  $\pm 0.01$  K). This chamber was connected to a storage cylinder of known volume (146 mL) with another temperature and pressure transducer.

The gas chamber was loaded with 30 to 40 g ( $\pm 0.0001$  g) of IL and degassed by applying a vacuum for a minimum of 6 h at 333 K. In this setup, both gas solubility and diffusivity were obtained in a single experiment. After measuring the initial pressure and temperature of the gas-filled storage, the absorption process was allowed to proceed spontaneously for 20 min in order to make the diffusivity data calculation. It was then stirred at 500 rpm and gas absorption proceeded until it reached equilibrium conditions, i.e., when the pressure remained constant for more than 20 min. Section S1 of the Supplementary Information explains the data treatment used to calculate the solubility and diffusivity.

## 3. Modeling

### 3.1. Process simulation

The single-effect (SE-ARS) and the hybrid compression assisted (CA-ARS) systems were simulated using Matlab. The evaporator temperature was set at 278.15 K and the dissipation temperature (condenser and absorber) at 303 K, representing conditions found in a refrigeration system. The following assumptions were considered in this work:

- 1 The system operates at steady state.
- 2 The absorber and generator outlet solutions are in equilibrium.
- 3 Heat losses, flow resistance, and pressure drops are not considered.
- 4 The expansion valves produce isenthalpic pressure decrements.
- 5 The liquid and vapor phases are in the saturated state.
- 6 The efficiency of the solution heat exchanger is set at 0.8.
- 7 Following ASHRAE considerations (ASHRAE, 2013), the temperature of the refrigerant leaving the generator ( $d,c$ ) is the same as that of the solution inlet ( $hx,d$ ).
- 8 The compressor isentropic efficiency and compression ratio (CR) are set at 0.7 and 1.5, respectively (Wu et al., 2018).

The mass and energy balances Eqs. (1) to (9) must be solved simultaneously for each element in the system to determine the thermodynamic performance. The enthalpy subscripts indicate the equipment a stream comes from and goes to, e.g.,  $h_{d,c}$  represents the specific enthalpy of the stream that comes from the desorber and goes to the condenser. In addition,  $h_{(comp,a),s}$  is the ideal enthalpy of the stream leaving the compressor.

$$Q_g + m_r f h_{hx,d} = m_r h_{d,c} + m_r (f - 1) h_{d,hx} \quad (1)$$

$$Q_a + m_r f h_{a,p} = m_r h_{comp,a} + m_r (f - 1) h_{v,a} \quad (2)$$

$$Q_c - m_r h_{c,v} = m_r h_{d,c} \quad (3)$$

$$Q_e - m_r h_{v,e} = m_r h_{e,comp} \quad (4)$$

$$m_r f h_{p,hx} = m_r f h_{a,p} + W_p \Rightarrow h_{b,hx} = h_{a,b} \quad (5)$$

$$W_{comp} = m_r (h_{comp,a} - h_{e,a}) = \frac{m_r (h_{(comp,a),s} - h_{e,a})}{\eta_i} \quad (6)$$

$$p_a = p_e \quad CR \quad (7)$$

$$Q_{hx} = m_r (f - 1) (h_{d,hx} - h_{hx,v}) = m_r (f - 1) (h_{hx,d} - h_{b,hx}) \quad (8)$$

$$\eta_{hx} = \frac{T_{hx,d} - T_{b,hx}}{T_{d,hx} - T_{b,hx}} \quad (9)$$

The thermodynamic properties of the refrigerants were obtained using CoolProp 6.4.0 software (Bell et al., 2014). The specific enthalpy of the solution can be calculated from:

$$h = x_1 h_1 + x_2 h_2 + h_{ex} \quad (10)$$

where  $x_1$  and  $x_2$  are the refrigerant and absorbent molar fractions, and  $h_{ex}$  is the excess enthalpy of the mixture calculated from the NRTL parameters:

$$h_{ex} = -RT^2 \left[ x_1 \left( \frac{\partial \ln \gamma_1}{\partial T} \right)_{p,x} + x_2 \left( \frac{\partial \ln \gamma_2}{\partial T} \right)_{p,x} \right] \quad (11)$$

The enthalpies of the ILs were obtained from their heat capacities, which were fitted to a quadratic expression from experimental data (Waliszewski et al., 2005; Diedrichs and Gmehling, 2006; Zorębski et al., 2018) as shown in Section S2 of the Supplementary Information.

ARS performance is based on the refrigerant mass fraction difference ( $\Delta w$ ) between the absorber ( $w_{dil}$ ) and desorber ( $w_{con}$ ). To study this effect, the circulation factor ( $f$ ) is defined as the ratio between the solution mass flow leaving the absorber ( $m_{dil}$ ) and the refrigerant mass flow used in the evaporator ( $m_r$ ). This parameter is calculated from the mass balance on the refrigerant.

$$f = \frac{m_{dil}}{m_r} = \frac{1 - w_{con}}{\Delta w} = \frac{1 - w_{con}}{w_{dil} - w_{con}} \quad (12)$$

In addition to the circulation factor, other metrics can be used to evaluate the efficiency of these systems, namely, the coefficients of

performance (COPs). COPs are defined as the amount of heat removed divided by the sum of the required energy and power input.

$$COP = \frac{Q_e}{Q_g + W_{comp}} \quad (13)$$

In CA-ARS, it is recommendable to evaluate partial COPs that consider the efficiency in function of the energy source, i.e., the electrical or mechanical  $COP_{el}$  that analyzes the power used in the compressor and pump, and the thermal  $COP_{th}$  that is used to compare absorption cycle thermodynamics and calculate the heat needed in the generator.

$$COP_{el} = \frac{Q_e}{W_{comp}} \quad (14)$$

$$COP_{th} = \frac{Q_e}{Q_g} \quad (15)$$

In addition, the efficiency of energy usage according to the second law of thermodynamics is measured with the exergy coefficient of performance (ECOP). Exergy is defined as the maximum useful power that can be produced by a system or flow (Takalkar et al., 2019). A reference ambient temperature is set (298.15 K in this work) and the exergy is measured as the system's deviation from equilibrium within this environment. For an ARS, the ECOP is defined as the ratio between the evaporator exergy and the exergy inputs.

$$ECOP = \frac{Q_e \left| 1 - \frac{T_{ref}}{T_e} \right|}{Q_g \left( 1 - \frac{T_{ref}}{T_g} \right) + W_{comp}} \quad (16)$$

To verify the accuracy of the thermodynamic model's description of ARS, we compared our results for the working pair R1234ze(E)/[C<sub>2</sub>mim][BF<sub>4</sub>] with those published in the literature under the same conditions (Wu et al., 2018). Fig. S2 in the Supplementary Information shows that both SE-ARS and CA-ARS were reproduced to a high accuracy.

### 3.2. NRTL solubility model

An accurate absorption model is a crucial tool in the design of ARS. This study calculates the parameters for the nonrandom two-liquid (NRTL) model for the VLE of R1234ze(E) with [C<sub>2</sub>mim][OTf], [C<sub>2</sub>mim][SCN] and [C<sub>2</sub>mim][Tf<sub>2</sub>N]. The model is based on the use of activity coefficients and the VLE expression is given by

$$y_i \Phi p = x_i \gamma_i p_i^s \quad (i \in \mathbb{Z} [1, N]) \quad (17)$$

where  $\gamma_i$  is the activity coefficient,  $p_i^s$  the saturation pressure and  $\Phi$  the correction factor, which is obtained from:

$$\Phi = \exp \left[ \frac{(B_i - V_i^L)(p - p_i^s)}{RT} \right] \quad (18)$$

where  $B_i$  is the second virial coefficient and  $V_i^L$  is the saturated liquid molar volume, both obtained using CoolProp 6.4.0 software (Bell et al., 2014). Combining Eqs. (17) and (18), and as  $y_i = 0$  due to the non-volatile character of ILs, the activity coefficient is:

$$\gamma_1 = \frac{p}{x_1 p_1^s} \exp \left[ \frac{(B_1 - V_1^L)(p - p_1^s)}{RT} \right] \quad (19)$$

The optimized model parameters were obtained by minimizing the difference between the experimental activity coefficients and the values calculated with the NRTL model:

$$\ln \gamma_1 = x_2^2 \left[ \tau_{21} \left( \frac{G_{21}}{x_1 + x_2 G_{21}} \right)^2 + \frac{\tau_{12} G_{12}}{(x_2 + x_1 G_{12})^2} \right] \quad (20)$$



The  $G_{12}$ ,  $G_{21}$ ,  $\tau_{12}$  and  $\tau_{21}$  parameters are expressed as

$$G_{12} = \exp(-\alpha\tau_{12}) \quad G_{21} = \exp(-\alpha\tau_{21}) \quad (21)$$

$$\tau_{12} = \tau_{12}^0 + \frac{\tau_{12}^1}{T} \quad \tau_{21} = \tau_{21}^0 + \frac{\tau_{21}^1}{T} \quad (22)$$

where  $\alpha$ ,  $\tau_{12}^0$ ,  $\tau_{12}^1$ ,  $\tau_{21}^0$  and  $\tau_{21}^1$  are the model adjustable parameters.

## 4. Results and discussion

### 4.1. Experimental VLE, NRTL modeling and diffusivity

This section addresses the absorption of R1234ze(E) in [C<sub>2</sub>mim][Tf<sub>2</sub>N], [C<sub>2</sub>mim][OTf], and [C<sub>2</sub>mim][SCN]. The solubility data, measured at temperatures of between 283.15 and 323.15 K and pressures up to 0.35 MPa, are compiled in Tables S2-S4 of the Supplementary Information and plotted in Fig. 2. As can be seen, the amount of dissolved R1234ze(E) is much higher in [C<sub>2</sub>mim][Tf<sub>2</sub>N] and [C<sub>2</sub>mim][OTf] than in [C<sub>2</sub>mim][SCN] at the same temperature and pressure. The very low solubility of R1234ze(E) in [C<sub>2</sub>mim][SCN] can be ascribed to the absence of fluorine moieties and weaker molecular interactions between R1234ze(E) and the [SCN]<sup>-</sup> anion.

The results also show that the NRTL model accurately described the VLE of mixtures of R1234ze(E) with ILs, where the absolute average relative deviations between experimental and calculated activity coefficients were 5.00%, 2.41%, and 5.95% for [C<sub>2</sub>mim][Tf<sub>2</sub>N], [C<sub>2</sub>mim][OTf], and [C<sub>2</sub>mim][SCN], respectively. The optimized binary interaction parameters are presented in Table 3, as well as the parameters for every other absorption pair studied in this work. The NRTL model was

unavailable for some systems, denoted by an asterisk in Table 3, so we fitted experimental data from the literature to find the NRTL parameters.

The gas diffusion coefficients for R1234ze(E) at infinite dilution from 283.15 to 323.15 K are provided in Table 4. The gas diffusivity increases at higher temperatures and was very similar for [C<sub>2</sub>mim][Tf<sub>2</sub>N] and [C<sub>2</sub>mim][OTf], while the diffusion coefficients for [C<sub>2</sub>mim][SCN] were higher. These values are consistent with diffusion coefficients published for R134a and R1234yf in the same ILs; (Asensio-Delgado et al., 2021b; Asensio-Delgado et al., 2020c). These are the first values for R1234ze(E) diffusivity reported in this type of solvent, so the results cannot be compared to the diffusion coefficients in more viscous ILs, but the use of these low-viscosity ILs is expected to provide higher mass transfer rates. For example, the diffusion coefficient for R1234yf in [C<sub>2</sub>mim][OTf] is twice the diffusion coefficient in the more viscous [C<sub>6</sub>mim][OTf] (S. Asensio-Delgado et al., 2020; He et al., 2017). Low viscosity helps decrease the resistance to flow (Asensio-Delgado et al., 2021b), so low-viscosity ILs should perform better than other ILs because of both increased mass transfer rates and reduced pump power consumption. The need for experimental diffusion coefficients has been brought up previously (Kühn et al., 2020), as these parameters would help us develop more accurate models that consider mass transfer resistances in the absorber and desorber.

### 4.2. Performance of refrigerant/IL working pairs in SE-ARS

This section looks at the performance of the 16 refrigerant/low-viscosity IL working pairs in SE-ARS. Fig. 3 shows the COP calculated for each working pair as a function of generator temperature, which ranged between 333 K and 373 K, except for refrigerants with a lower

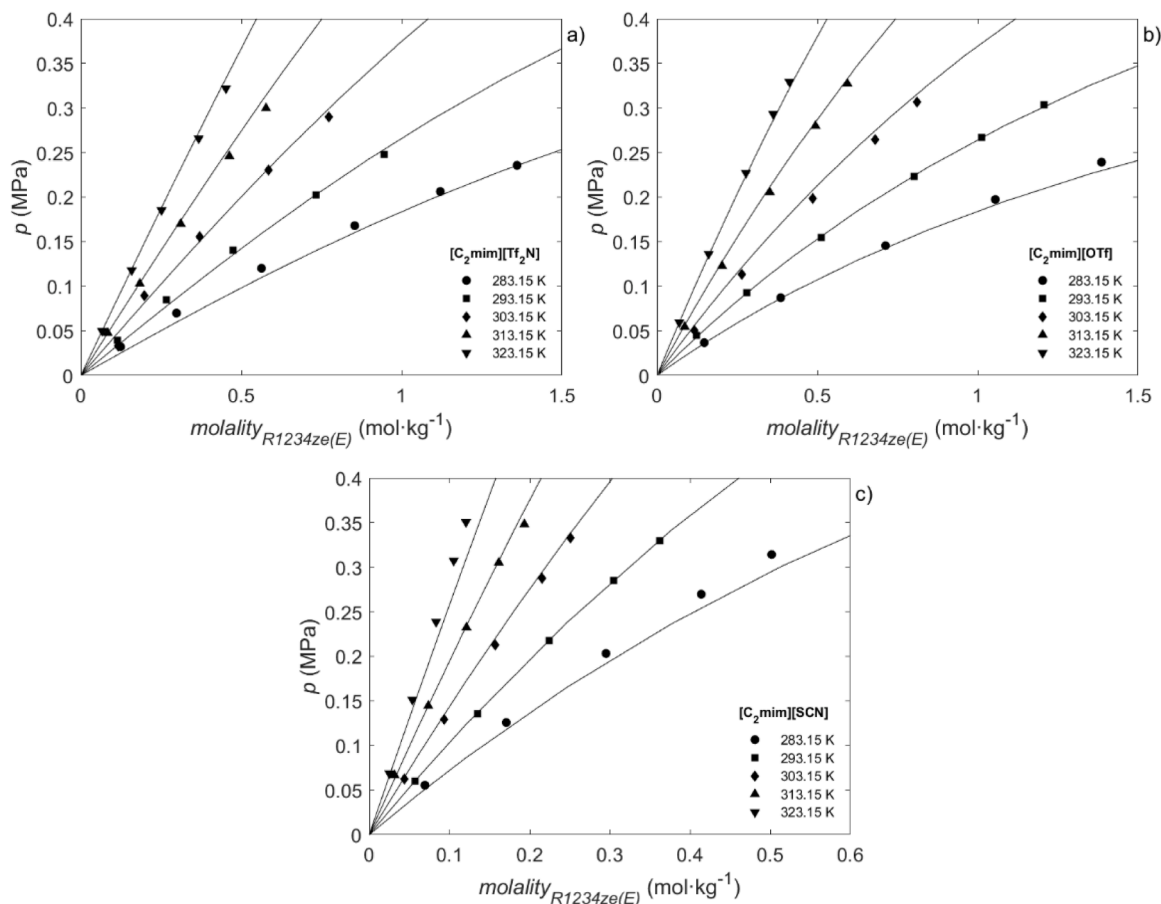


Fig. 2. Solubility of R1234ze(E) in (a) [C<sub>2</sub>mim][Tf<sub>2</sub>N], (b) [C<sub>2</sub>mim][OTf] and (c) [C<sub>2</sub>mim][SCN] at various temperatures: 283.15 (●), 293.15 (■), 303.15 (◆), 313.15 (▲), and 323.15 K (▼). Solid lines represent NRTL model calculations.

**Table 3.**  
NRTL model parameters for each refrigerant/IL working pair.

Refrigerant	IL	$\alpha$	$\tau_{12}^0$	$\tau_{12}^1$	$\tau_{21}^0$	$\tau_{21}^1$	Source
R134a	[C <sub>2</sub> mim][BF <sub>4</sub> ]	0.2	0	4794.7	0	278.9	(Asensio-Delgado et al., 2020b)
	[C <sub>2</sub> mim][OTf]	0.2	0	5076.4	0	99.29	(Asensio-Delgado et al., 2020b)
	[C <sub>2</sub> mim][SCN]	0.2	0	2682.6	0	254.58	(Asensio-Delgado et al., 2020c)
	[C <sub>2</sub> mim][Tf <sub>2</sub> N]*	0.2	0	969.496	0	-443.388	(Shiflett and Yokozeki, 2007)
R32	[C <sub>2</sub> mim][BF <sub>4</sub> ]	0.2	0	6148.1	0	51.99	(Asensio-Delgado et al., 2020b)
	[C <sub>2</sub> mim][OTf]	0.24	-0.32	1259.4	-0.912	-145.71	(Dong et al., 2011)
	[C <sub>2</sub> mim][SCN]	0.2	0	1025.6	0	-210.04	(Asensio-Delgado et al., 2020c)
	[C <sub>2</sub> mim][Tf <sub>2</sub> N]	0.2	0	959.31	0	-621.18	(Shiflett et al., 2006)
R1234ze(E)	[C <sub>2</sub> mim][BF <sub>4</sub> ]	0.22	44.33	-10,698.57	6.8	-1805.14	(Wu et al., 2018)
	[C <sub>2</sub> mim][OTf]	0.2	0	3782.794	0	97.713	This work
	[C <sub>2</sub> mim][SCN]	0.2	4.056	372.699	2.458	-428.676	This work
	[C <sub>2</sub> mim][Tf <sub>2</sub> N]	0.2	0	3083.775	0	-175.027	This work
R1234yf	[C <sub>2</sub> mim][BF <sub>4</sub> ]*	0.2	0	3238.731	0	596.401	(Sun et al., 2017)
	[C <sub>2</sub> mim][OTf]	0.2	6.226	414.6	4.338	-1126.1	(Asensio-Delgado et al., 2020b)
	[C <sub>2</sub> mim][SCN]	0.2	179.52	-47,781	21.89	-5506.8	(Asensio-Delgado et al., 2020c)
	[C <sub>2</sub> mim][Tf <sub>2</sub> N]	0.2	0	3844.6	0	135.2	(Asensio-Delgado et al., 2020b)

\*NRTL model parameters optimized in this work.

**Table 4.**  
R1234ze(E) diffusion coefficients (10<sup>-10</sup> m<sup>2</sup>.s<sup>-1</sup>) at infinite dilution.

T (K)	[C <sub>2</sub> mim][Tf <sub>2</sub> N]	[C <sub>2</sub> mim][OTf]	[C <sub>2</sub> mim][SCN]
283.15	0.42 ± 0.01	0.48 ± 0.01	1.2 ± 0.1
293.15	0.55 ± 0.02	0.60 ± 0.02	2.0 ± 0.2
303.15	1.05 ± 0.03	1.03 ± 0.03	2.6 ± 0.2
313.15	2.21 ± 0.06	2.18 ± 0.06	4.8 ± 0.4
323.15	4.0 ± 0.1	3.3 ± 0.1	11.3 ± 1.1

critical temperature (see Table 1). The COP behavior was very similar for almost every pair, with an initial increase in the COP at low temperatures thanks to a rapid decrease in refrigerant solubility in the generator, followed by a sluggish decrease due to the asymptotic value of the mass fraction difference between the generator and absorber observed at high generator temperatures. The exception was R1234yf in [C<sub>2</sub>mim][SCN], owing to its very low solubility at all generator temperatures.

The best performances in SE-ARS were achieved using R32 with [C<sub>2</sub>mim][BF<sub>4</sub>], reaching a COP slightly over 0.4 with a generator temperature of around 350 K, similar to the values obtained in other studies for R32, R152a and R161 with [C<sub>6</sub>mim][Tf<sub>2</sub>N] (Wu et al., 2020). The next best IL was [C<sub>2</sub>mim][Tf<sub>2</sub>N], for which the highest COPs were 0.4 for R32 at 350 K and 0.35 for R134a at 360 K. In contrast, the COPs obtained with [C<sub>2</sub>mim][SCN] were considerably lower. Between the two HFCs,

R32 exhibited higher COPs than R134a except in [C<sub>2</sub>mim][OTf], an IL that stands out as a R134a solvent, thus providing a stable working pair resilient to generator temperatures variations and with COP values of between 0.25 and 0.31 from 335 to 370 K. On the other hand, HFCs clearly outperformed the HFOs pairs. The HFO R1234ze(E) yielded better results than R1234yf for all the HFOs/ILs pairs at almost every generator temperature. The HFO pairs with the best performances were R1234ze(E)/[C<sub>2</sub>mim][Tf<sub>2</sub>N] and R1234ze(E)/[C<sub>2</sub>mim][OTf], yet with COP values of just slightly over 0.2.

The complete assessment of SE-ARS is presented in Section S5 of the Supplementary Information, including the exergy analysis, circulation factors, mass fraction increments, and a comparison of the performance of the 16 working pairs under the same operating conditions. Overall, the refrigerant/IL pairs did not perform very well in SE-ARS, so their practical use is limited for such low-temperature refrigeration purposes. In contrast, SE-ARS may be a suitable option when thermal energy is abundant and relatively inexpensive, and for applications requiring higher evaporator temperatures, such as air conditioning, where the COP is twice as high with the evaporator at 18 °C instead of 5 °C as shown in Fig. S7 if the Supplementary Information. However, for cases with low-temperature energy sources or when limited heat is available the use of more efficient configurations such as CA-ARS should be encouraged.

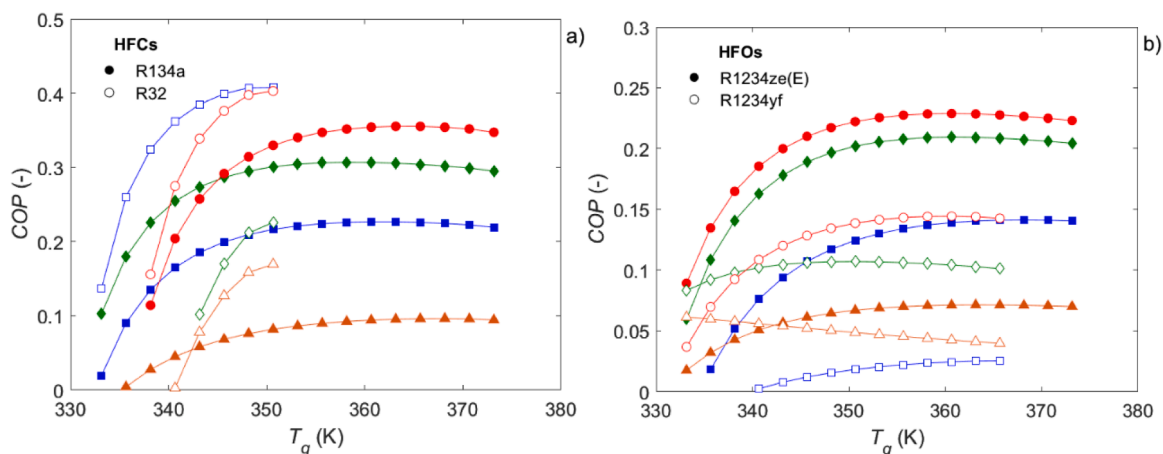


**Fig. 3.** COP of the SE-ARS systems as a function of generator temperature ( $T_g$ ). (a) HFCs/IL: R134a (filled symbols) and R32 (empty symbols), and (b) HFOs/IL: R1234ze(E) (filled symbols) and R1234yf (empty symbols). Symbols represent the different ILs: [C<sub>2</sub>mim][BF<sub>4</sub>] (■), [C<sub>2</sub>mim][OTf] (◆), [C<sub>2</sub>mim][SCN] (▲), and [C<sub>2</sub>mim][Tf<sub>2</sub>N] (●).  $T_e = 278$  K,  $T_c = T_a = 303$  K.



### 4.3. Performance of refrigerant/IL working pairs in CA-ARS

In CA-ARS, three *COPs* can be assessed in terms of the electricity input, the heat input, or both at the same time. As heat extraction in the evaporator does not vary with generator temperature, the electrical *COP* is constant for each refrigerant in all the working conditions studied regardless of the IL used, as it only depends on the vapor pressures of pure refrigerants at the operating temperatures, which are shown in Table S7 in the Supplementary Information. The electrical *COPs* are given in Table 5, which shows that the highest  $COP_{el}$  was that of R1234ze(E), followed by R134a, R1234yf, and R32.

As electrical usage was around ten times lower than the heat requirement, the thermal and total *COP* shared a similar variation with generator temperature, as shown in Fig. 4 and Fig. S8 in the Supplementary Information, in which the generator temperature ranged between 313 K and either 373 K or the refrigerant critical temperature (see Table 1). The working pair with the best performance was R32/[C<sub>2</sub>mim][Tf<sub>2</sub>N] with a  $COP_{th}$  of 0.79 and *COP* of 0.74 at 328 K. Out of the four ILs studied, [C<sub>2</sub>mim][Tf<sub>2</sub>N] stands out as the best absorbent for every refrigerant thanks to its high absorption capacity. In CA-ARS, HFCs again outperformed HFOs, but the combination of R1234ze(E) with [C<sub>2</sub>mim][Tf<sub>2</sub>N] or [C<sub>2</sub>mim][OTf] may still hold some promise if enough waste heat is available at around 330 K. The working pairs studied in CA-ARS in this work performed better than HFC/IL working pairs assessed previously. For example, in the present study the pairs formed by R32 with [C<sub>2</sub>mim][Tf<sub>2</sub>N] and [C<sub>2</sub>mim][OTf] yielded maximum *COP* values of over 0.7 at 328 K, while published pairs of R32, R152a and R161 with [C<sub>6</sub>mim][Tf<sub>2</sub>N] have peak performances below 0.68 at 328 K (Wu et al., 2020).

The *ECOP* calculated for the CA-ARS is shown in Fig. 5. For the HFO/IL pairs studied here, the maximum *ECOP* was approximately 0.24 at 323 K for the systems R1234ze(E)/[C<sub>2</sub>mim][Tf<sub>2</sub>N] and R1234ze(E)/[C<sub>2</sub>mim][OTf], which is similar to literature data; for instance, the system R1234ze(E)/[C<sub>6</sub>mim][Tf<sub>2</sub>N] has been reported with a slightly higher *ECOP* of 0.26 (Wu et al., 2018). For the HFC/IL working pairs, the *ECOPs* obtained in this study are higher; for instance, the R32/IL and R134a/[C<sub>2</sub>mim][Tf<sub>2</sub>N] pairs reached peak values at between 0.41 and 0.3 in the temperature range 323–333 K.

The behavior of *COP* and *ECOP* was similar in SE-ARS and CA-ARS; it rose with increasing generator temperature up to a maximum value and then decreased. In CA-ARS, this increment was steeper and occurred at a lower generator temperature. The rationale behind this behavior can be found in the circulation ratio (*f*) plotted in Fig. 6, which shows an initial sharp decrease within a small range of generator temperatures, before stabilizing at an asymptotic value equal to the inverse of  $w_{dil}$  (i.e., when  $w_{con} = 0$  in Eq. (18)). As the circulation ratio is derived from the dissolved mass fractions, the different changes in the *COP* values can be ascribed to the VLE, where ILs that absorb large amounts of refrigerant at low temperature and small amounts at high temperatures will afford the best performances. For CA-ARS, the lowest circulation factors reach values of 4–5 for both HFCs (R134a and R32) and values slightly over 10 for R1234ze(E) (the HFO that returned the best results in this study). The increase in *COP* with generator temperature is due to the reduction in the mass flow of the concentrated solution that needs to be heated. Once *f* stabilizes, an increase in generator temperature implies a reduction in the concentrated flow rate to be heated, but this does not

compensate for the greater energy required to reach higher temperatures. In other words, the system becomes slightly less efficient as the generator temperature rises. In the case of CA-ARS, the compressor helps achieve an asymptotic value at lower generator temperatures, resulting in a better performance. Hence, CA-ARS clearly outperformed SE-ARS at low generator temperatures and the efficiency loss at high generator temperatures was still not enough to translate into a worse performance than SE-ARS.

Fig. 7 shows the mass fraction increment between the absorber and desorber in CA-ARS and Table S8 in the Supplementary Information compiles the mass fraction of refrigerant in the absorber. As can be seen, ARS presented some operational limits at low generator temperatures corresponding to unfeasible situations in which the pressure and temperature conditions resulted in a lower refrigerant solubility in the absorber than the desorber (i.e., when  $\Delta w \leq 0$ ). This restricts the ARS' correct operation when only very low-grade thermal energy is available. Moreover, a comparison between the mass fraction increments in CA-ARS and SE-ARS (Table S5) highlights the improvement achieved with CA-ARS compared to SE-ARS. For example, for the R32/[C<sub>2</sub>mim][Tf<sub>2</sub>N] pair, the mass fraction in the absorber of the SE-ARS configuration was 0.147, whereas the maximum mass fraction increment of CA-ARS was over 0.2. The pressurization of the refrigerant before entering the absorber increases the amount of refrigerant absorbed and, therefore, improves system performance.

If we compare ILs to organic solvents as absorbents, better results were reported with TEGDME in terms of circulation factors, with values of around 3, and mass fraction increments over 0.3 at temperatures above 373 K with refrigerants such as R32, R152 and R161 (Zhang et al., 2021). However, the overall maximum *COP* was slightly higher with the system R32/[C<sub>2</sub>mim][Tf<sub>2</sub>N] studied in this work. This contrast is because the generator temperature for the optimal working point is lower for ILs. The *ECOP* underlines this difference, as the maximum *ECOP* was lower than 0.25 for TEGDME systems and higher than 0.35 for the systems in this study. This difference translates directly into one of the key advantages of IL-based CA-ARS proposed in this work, the possibility of using low-grade waste heat.

Table 6 shows a comparative assessment of CA-ARS performances (*COP*, circulation factor, compressor power, and energy in each element) for the 16 pairs analyzed in this study for a refrigerant mass flow rate of 1 kg·s<sup>-1</sup> and a low-grade heat source at 333 K. HFC-R32 pairs gave the best overall performances in terms of *COP* and *f*, whereas HFO-R1234yf based pairs were the poorest performers. Although the HFO R1234ze(E) exhibited lower *COPs* than R32, this very-low-GWP refrigerant significantly reduces the compressor power and has a similar refrigeration capacity ( $Q_e$ ) as R134a, thus making it an attractive refrigerant in a low-cost IL production scenario.

## 5. Conclusion

Here we have presented the thermodynamic modeling and analysis of the performance of 16 novel working pairs formed from low-GWP HFC and very-low-GWP HFO refrigerant gasses combined with low-viscosity ILs. Additionally, we provide new experimental data on the solubility of R1234ze(E) in [C<sub>2</sub>mim][Tf<sub>2</sub>N], [C<sub>2</sub>mim][OTf], and [C<sub>2</sub>mim][SCN]. After comparing the results for single effect and compression assisted refrigeration systems, we conclude that:

- (1) The solubility of R1234ze(E) in the selected ILs is significantly higher than that of previously studied HFOs, being much higher than its isomer R1234yf, and similar to the solubility of R134a. This makes R1234ze(E) an interesting refrigerant for absorption machines as its GWP is 1000 times lower.
- (2) SE-ARS have medium to low performances and limitations in cooling with low-grade thermal energy. The best results are achieved with R32/[C<sub>2</sub>mim][BF<sub>4</sub>] with *COP* = 0.41 and *f* = 21.3 at a generator temperature of 348 K.

**Table 5.**  
Electrical *COP* for the different refrigerant gases.

Gas	$COP_{el}$
R32	11.86
R134a	13.39
R1234ze(E)	13.53
R1234yf	12.10

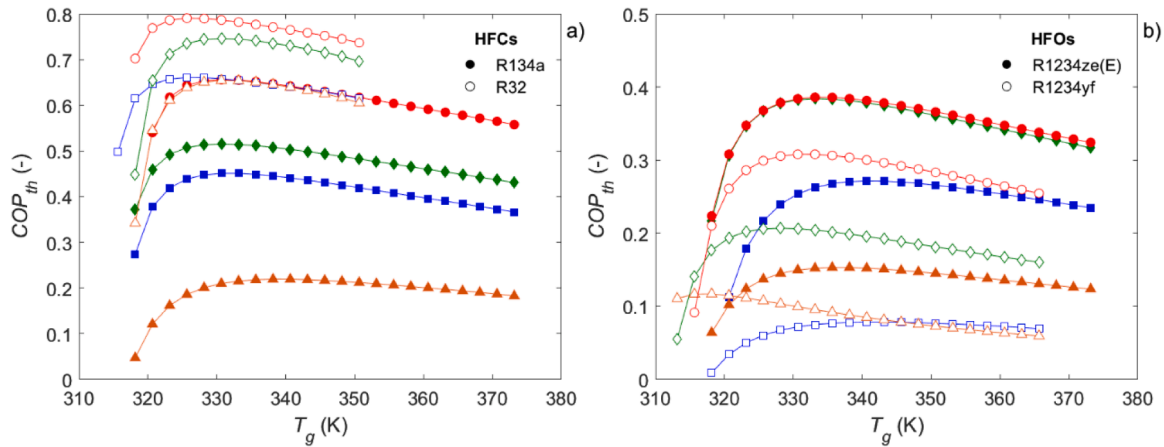


**Fig. 4.** Thermal COP of the CA-ARS systems as a function of generator temperature ( $T_g$ ). (a) HFCs/IL: R134a (filled symbols) and R32 (empty symbols), and (b) HFOs/IL: R1234ze(E) (filled symbols) and R1234yf (empty symbols). Symbols represent the different ILs:  $[C_2mim][BF_4]$  (■),  $[C_2mim][OTf]$  (◆),  $[C_2mim][SCN]$  (▲), and  $[C_2mim][Tf_2N]$  (●).  $T_e = 278$  K,  $T_c = T_a = 303$  K.

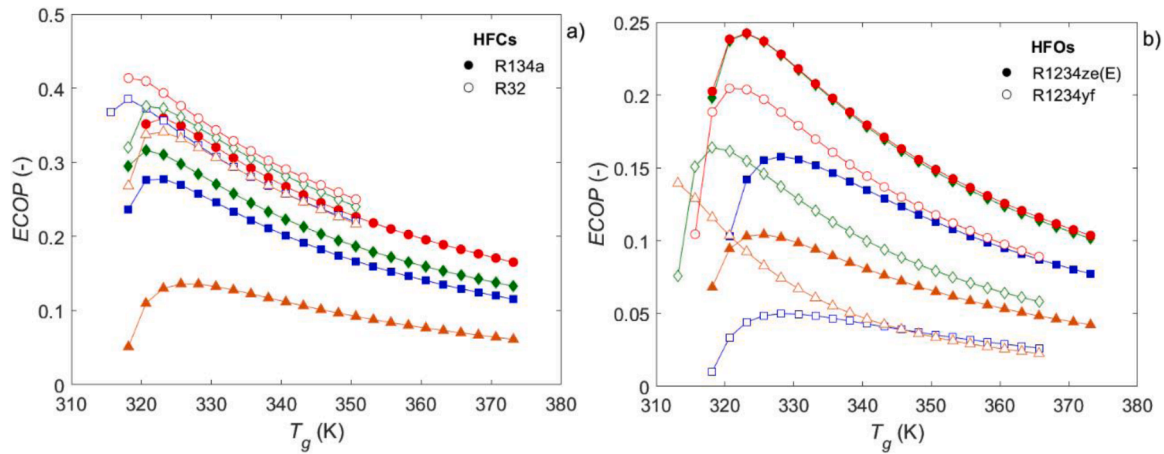


**Fig. 5.** ECOP of the CA-ARS systems as a function of generator temperature ( $T_g$ ). (a) HFCs/IL: R134a (filled symbols) and R32 (empty symbols), and (b) HFOs/IL: R1234ze(E) (filled symbols) and R1234yf (empty symbols). Symbols represent the different ILs:  $[C_2mim][BF_4]$  (■),  $[C_2mim][OTf]$  (◆),  $[C_2mim][SCN]$  (▲), and  $[C_2mim][Tf_2N]$  (●).  $T_e = 278$  K,  $T_c = T_a = 303$  K.

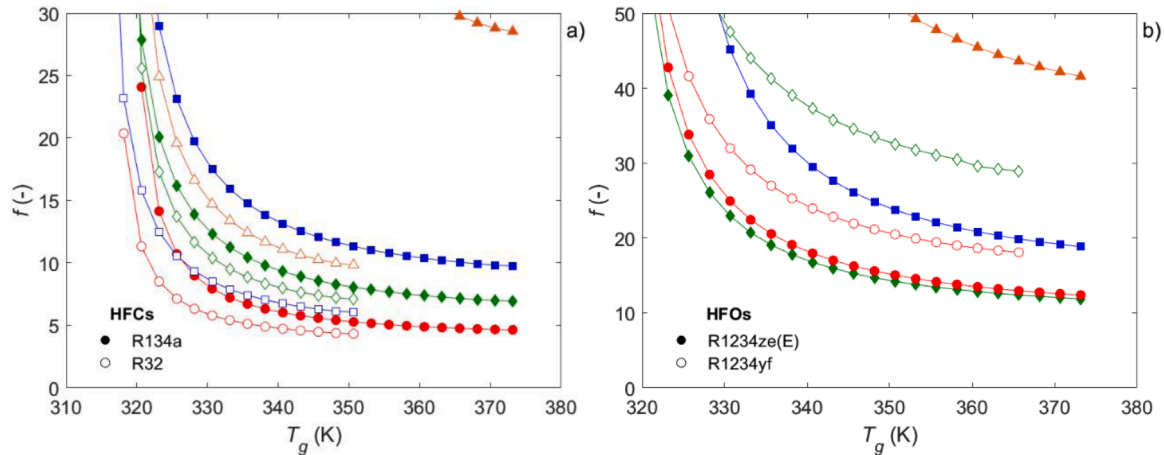


**Fig. 6.** Circulation factor ( $f$ ) of the CA-ARS systems as a function of generator temperature ( $T_g$ ). (a) HFCs/IL: R134a (filled symbols) and R32 (empty symbols), and (b) HFOs/IL: R1234ze(E) (filled symbols) and R1234yf (empty symbols). Symbols represent the different ILs:  $[C_2mim][BF_4]$  (■),  $[C_2mim][OTf]$  (◆),  $[C_2mim][SCN]$  (▲), and  $[C_2mim][Tf_2N]$  (●).  $T_e = 278$  K,  $T_c = T_a = 303$  K.

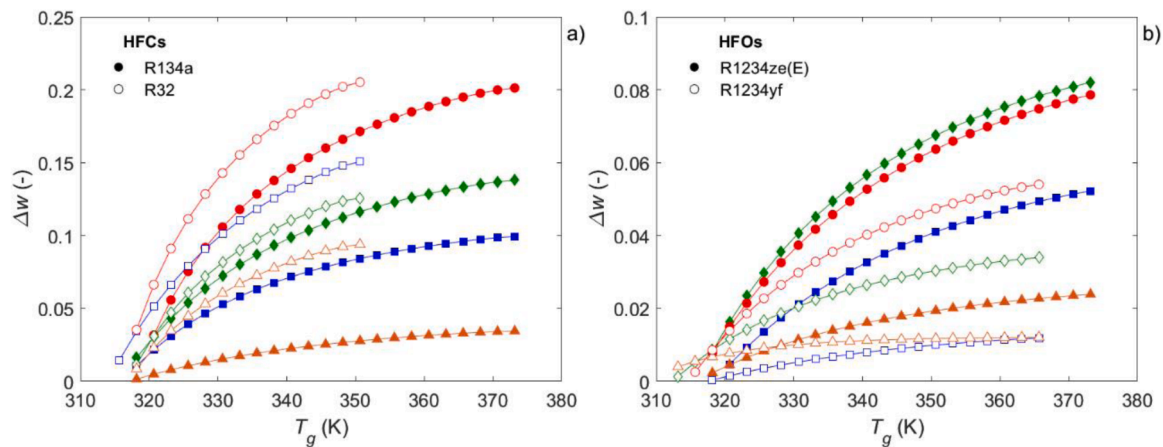


**Fig. 7.** Mass fraction increment ( $\Delta w$ ) of the CA-ARS systems as a function of generator temperature ( $T_g$ ). (a) HFCs/IL: R134a (filled symbols) and R32 (empty symbols), and (b) HFOs/IL: R1234ze(E) (filled symbols) and R1234yf (empty symbols). Symbols represent the different ILs: [C<sub>2</sub>mim][BF<sub>4</sub>] (■), [C<sub>2</sub>mim][OTf] (◆), [C<sub>2</sub>mim][SCN] (▲), and [C<sub>2</sub>mim][Tf<sub>2</sub>N] (●).  $T_e = 278$  K,  $T_c = T_a = 303$  K.

**Table 6.**

Performance of the CA-ARS under the same conditions ( $T_e = 278$  K,  $T_c = T_a = 303$  K,  $T_g = 333$  K,  $CR = 1.5$ ,  $m_r = 1$  kg·s<sup>-1</sup>).

Working Pair	$f$	$Q_g$ (kW)	$Q_e$ (kW)	$Q_a$ (kW)	$Q_c$ (kW)	$W_{comp}$ (kW)	$COP$
R134a/[C <sub>2</sub> mim][BF <sub>4</sub> ]	15.9	354.4	159.8	-329.5	-196.6	11.9	0.436
R134a/[C <sub>2</sub> mim][OTf]	11.2	310.6	159.8	-286.5	-195.9	11.9	0.495
R134a/[C <sub>2</sub> mim][SCN]	55.4	742.4	159.8	-716.7	-197.5	11.9	0.212
R134a/[C <sub>2</sub> mim][Tf <sub>2</sub> N]	7.2	243.9	159.8	-221.4	-194.2	11.9	0.624
R32/[C <sub>2</sub> mim][BF <sub>4</sub> ]	7.9	398.5	260.8	-390.1	-291.1	22.0	0.620
R32/[C <sub>2</sub> mim][OTf]	9.5	350.2	260.8	-341.7	-291.2	22.0	0.701
R32/[C <sub>2</sub> mim][SCN]	13.4	398.9	260.8	-389.1	-292.5	22.0	0.620
R32/[C <sub>2</sub> mim][Tf <sub>2</sub> N]	5.4	333.4	260.8	-328.5	-287.8	22.0	0.734
R1234ze(E)/[C <sub>2</sub> mim][BF <sub>4</sub> ]	39.2	559.1	146.8	-530.4	-186.4	10.9	0.258
R1234ze(E)/[C <sub>2</sub> mim][OTf]	20.7	382.2	146.8	-353.9	-186.0	10.9	0.374
R1234ze(E)/[C <sub>2</sub> mim][SCN]	76.9	965.4	146.8	-936.2	-186.9	10.9	0.150
R1234ze(E)/[C <sub>2</sub> mim][Tf <sub>2</sub> N]	22.4	380.4	146.8	-352.2	-185.9	10.9	0.375
R1234yf/[C <sub>2</sub> mim][BF <sub>4</sub> ]	162.9	1681.8	126.0	-1651.4	-166.9	10.4	0.075
R1234yf/[C <sub>2</sub> mim][OTf]	44.0	616.9	126.0	-586.9	-166.4	10.4	0.201
R1234yf/[C <sub>2</sub> mim][SCN]	95.5	1320.2	126.0	-1289.1	-167.6	10.4	0.095
R1234yf/[C <sub>2</sub> mim][Tf <sub>2</sub> N]	29.1	409.2	126.0	-379.6	-166.1	10.4	0.300

(3) CA-ARS represents an important improvement in  $COP$  and expands the range of working temperatures compared to SE-ARS, which has cooling limitations using low-grade thermal energy in the generator. In CA-ARS, the increased absorber solubility leads to significant improvements in the circulation factor, even with low generator temperatures.

(4) High refrigerant solubility at ambient temperatures is the key consideration in ARS to minimize the amount of solvent used, as such, new working pairs with very-low-GWP HFOs, such as R1234ze(E), and ILs with higher absorption capacities and low viscosities should be examined further for their use in cooling applications.

Moreover, promising results have been obtained in CA-ARS. The most remarkable results with CA-ARS were:

- (1) The pair R32/[C<sub>2</sub>mim][Tf<sub>2</sub>N] outperformed pairs reported previously, and it is competitive with the classic pairs of NH<sub>3</sub>/H<sub>2</sub>O and H<sub>2</sub>O/LiBr. R32/[C<sub>2</sub>mim][Tf<sub>2</sub>N] presents a  $COP$  of 0.74, a circulation factor of 5.4 at 328 K in the desorber, and a maximum  $ECOP$  of 0.41 at 318 K. This pair is the most promising alternative of all the HFC or HFO/ionic liquid mixtures published to date for energy efficient cooling by absorption refrigeration technology.
- (2) If we focus on using refrigerants with a negligible GWP, the HFO R1234ze(E) ( $GWP = 1$ ) shows promising results in its pairs with [C<sub>2</sub>mim][Tf<sub>2</sub>N] and [C<sub>2</sub>mim][OTf], with  $COPs$  of 0.37. They do

not perform as well as HFC-based pairs, but they can be used when significant amounts of waste heat are available. In addition, the lower working pressure of R1234ze(E) compared to that of R32 reduces the compressor electricity demand.

**Author contribution**

**José M. Asensio-Delgado:** Investigation, Visualization, Writing - original draft. **Salvador Asensio-Delgado:** Investigation, conceptualization, Supervision, Writing - review & editing, original draft. **Gabriel Zarca:** Conceptualization, Writing - review & editing, Funding acquisition. **Ane Urriaga:** Conceptualization, Writing - review & editing, Funding acquisition (Eq.10, Eq.11, Eq.12, Eq.13, Eq.14, Eq.15, Eq.16, Eq.19, Eq.20, Eq.21, Eq.22, Eq.2, Eq.3, Eq.4, Eq.5, Eq.6, Eq.7, Eq.8)

**Declaration of Competing Interest**

The authors declare no competing financial interest.

**Acknowledgments**

We gratefully acknowledge the support from projects KET4F-Gas-SOE2/P1/P0823 (Interreg SUDOE) and PID2019-105827RB-I00 (MCIN/AEI/10.13039/501100011033). S. A-D. acknowledges the FPU grant (18/03939) awarded by the Spanish MSIU.



## References

- Annual European Union Greenhouse Gas Inventory 1990-2018 and Inventory Report 2020, 2020. European Environment Agency, Brussels. <https://www.eea.europa.eu/publications/european-union-greenhouse-gas-inventory-2020>.
- Seiler, M., Kühn, A., Ziegler, F., Wang, X., 2013. Sustainable cooling strategies using new chemical system solutions. *Ind. Eng. Chem. Res.* 52, 16519–16546. <https://doi.org/10.1021/ie401297u>.
- García, E.J., Bahamon, D., Vega, L.F., 2021. Systematic Search of Suitable Metal-Organic Frameworks for Thermal Energy-Storage Applications with Low Global Warming Potential Refrigerants. *ACS Sustain. Chem. Eng.* 9, 3157–3171. <https://doi.org/10.1021/acssuschemeng.0c07797>.
- Gao, Y., He, G., Chen, P., Zhao, X., Cai, D., 2019. Energy and exergy analysis of an air-cooled waste heat-driven absorption refrigeration cycle using R290/oil as working fluid. *Energy* 173, 820–832. <https://doi.org/10.1016/j.energy.2019.02.117>.
- Zhang, X., Cai, L., Chen, T., Qiao, J., Zhang, X., 2021. Vapor-Liquid Equilibrium Measurements and Assessments of Low-GWP Absorption Working Pairs (R32+DMETEG, R152a+DMETEG, and R161+DMETEG) for Absorption Refrigeration Systems. *Energy* 224, 120082. <https://doi.org/10.1016/j.energy.2021.120082>.
- Asensio-Delgado, S., Viar, M., Pardo, F., Zarca, G., Urriaga, A., 2021a. Gas solubility and diffusivity of hydrofluorocarbons and hydrofluoroolefins in cyanide-based ionic liquids for the separation of refrigerant mixtures. *Fluid Phase Equilib* 549, 113210. <https://doi.org/10.1016/j.fluid.2021.113210>.
- Yokozeki, A., Shiflett, M.B., 2010. Water solubility in ionic liquids and application to absorption cycles. *Ind. Eng. Chem. Res.* 49, 9496–9503. <https://doi.org/10.1021/ie101143z>.
- Kim, Y.J., Kim, S., Joshi, Y.K., Fedorov, A.G., Kohl, P.A., 2012. Thermodynamic analysis of an absorption refrigeration system with ionic-liquid/refrigerant mixture as a working fluid. *Energy* 44, 1005–1016. <https://doi.org/10.1016/j.energy.2012.04.048>.
- Wang, M., Infante Ferreira, C.A., 2017. Absorption heat pump cycles with NH<sub>3</sub> – ionic liquid working pairs. *Appl. Energy* 204, 819–830. <https://doi.org/10.1016/j.apenergy.2017.07.074>.
- Moreno, D., Ferro, V.R., de Riva, J., Santiago, R., Moya, C., Larriba, M., Palomar, J., 2018. Absorption refrigeration cycles based on ionic liquids: refrigerant/absorbent selection by thermodynamic and process analysis. *Appl. Energy* 213, 179–194. <https://doi.org/10.1016/j.apenergy.2018.01.034>.
- Asensio-Delgado, S., Jovell, D., Zarca, G., Urriaga, A., Llovel, F., 2020a. Thermodynamic and process modeling of the recovery of R410A compounds with ionic liquids. *Int. J. Refrig.* 118, 365–375. <https://doi.org/10.1016/j.ijrefrig.2020.04.013>.
- McLinden, M.O., Huber, M.L., 2020. (R)Evolution of Refrigerants. *J. Chem. Eng. Data* 65, 4176–4193. <https://doi.org/10.1021/acs.jced.0c00338>.
- Wu, W., You, T., Zhang, H., Li, X., 2018. Comparisons of different ionic liquids combined with trans-1,3,3,3-tetrafluoropropene (R1234ze(E)) as absorption working fluids. *Int. J. Refrig.* 88, 45–57. <https://doi.org/10.1016/j.ijrefrig.2017.12.011>.
- Sun, Y., Di, G., Wang, J., Hu, Y., Wang, X., He, M., 2020a. Gaseous solubility and thermodynamic performance of absorption system using R1234yf /IL working pairs. *Appl. Therm. Eng.* 172, 115161 <https://doi.org/10.1016/j.applthermaleng.2020.115161>.
- Sun, Y., Di, G., Wang, J., Wang, X., Wu, W., 2020b. Performance analysis of R1234yf/ionic liquid working fluids for single-effect and compression-assisted absorption refrigeration systems. *Int. J. Refrig.* 109, 25–36. <https://doi.org/10.1016/j.ijrefrig.2019.10.007>.
- Liu, X., Ye, Z., Bai, L., He, M., 2019. Performance comparison of two absorption-compression hybrid refrigeration systems using R1234yf/ionic liquid as working pair. *Energy Convers. Manag.* 181, 319–330. <https://doi.org/10.1016/j.enconman.2018.12.030>.
- Wu, W., Leung, M., Ding, Z., Huang, H., Bai, Y., Deng, L., 2020. Comparative analysis of conventional and low-GWP refrigerants with ionic liquid used for compression-assisted absorption cooling cycles. *Appl. Therm. Eng.* 172, 115145 <https://doi.org/10.1016/j.applthermaleng.2020.115145>.
- Wu, W., Zhang, H., You, T., Li, X., 2017a. Performance comparison of absorption heating cycles using various low-GWP and natural refrigerants. *Int. J. Refrig.* 82, 56–70. <https://doi.org/10.1016/j.ijrefrig.2017.07.004>.
- Wu, W., Zhang, H., You, T., Li, X., 2017b. Thermodynamic Investigation and Comparison of Absorption Cycles Using Hydrofluoroolefins and Ionic Liquid. *Ind. Eng. Chem. Res.* 56, 9906–9916. <https://doi.org/10.1021/acs.iecr.7b02343>.
- Zarca, G., Ortiz, I., Urriaga, A., 2014. Kinetics of the carbon monoxide reactive uptake by an imidazolium chlorocuprate(I) ionic liquid. *Chem. Eng. J.* 252, 298–304. <https://doi.org/10.1016/j.cej.2014.05.011>.
- Zarca, G., Ortiz, I., Urriaga, A., 2015. Recovery of carbon monoxide from flue gases by reactive absorption in ionic liquid imidazolium chlorocuprate(I): mass transfer coefficients. *Chinese J. Chem. Eng.* 23, 769–774. <https://doi.org/10.1016/j.cjche.2014.06.040>.
- Mota-Martinez, M.T., Brandl, P., Hallett, J.P., Dowell, N.M., 2018. Challenges and opportunities for the utilisation of ionic liquids as solvents for CO<sub>2</sub> capture. *Mol. Syst. Des. Eng.* 3, 560–571. <https://doi.org/10.1039/c8me00009c>.
- Palomar, J., Larriba, M., Lemus, J., Moreno, D., Santiago, R., Moya, C., de Riva, J., Pedrosa, G., 2019. Demonstrating the key role of kinetics over thermodynamics in the selection of ionic liquids for CO<sub>2</sub> physical absorption. *Sep. Purif. Technol.* 213, 578–586. <https://doi.org/10.1016/j.seppur.2018.12.059>.
- Sanmamed, Y.A., González-Salgado, D., Troncoso, J., Romani, L., Baylaucq, A., Boned, C., 2010. Experimental methodology for precise determination of density of RTILs as a function of temperature and pressure using vibrating tube densimeters. *J. Chem. Thermodyn.* 42, 553–563. <https://doi.org/10.1016/j.jct.2009.11.014>.
- Neves, C.M.S.S., Kurnia, K.A., Coutinho, J.A.P., Marrucho, I.M., Canongia Lopes, J.N., Freire, M.G., Rebelo, L.P.N., 2013. Systematic study of the thermophysical properties of imidazolium-based ionic liquids with cyano-functionalized anions. *J. Phys. Chem. B.* 117, 10271–10283. <https://doi.org/10.1021/jp405913b>.
- Gardas, R.L., Costa, H.F., Freire, M.G., Carvalho, P.J., Marrucho, I.M., Fonseca, I.M.A., Ferreira, A.G.M., Coutinho, J.A.P., 2008. Densities and derived thermodynamic properties of imidazolium-, pyridinium-, pyrrolidinium-, and piperidinium-based ionic liquids. *J. Chem. Eng. Data* 53, 805–811. <https://doi.org/10.1021/je700670k>.
- European Commission, 2020. Mapping and analyses of the current and future (2020–2030) heating/cooling fuel deployment (fossil/renewables). European Commission. [https://ec.europa.eu/energy/studies\\_main/final\\_studiesmapping-and-analyses-current-and-future-2020-2030-heating-cooling-fuel](https://ec.europa.eu/energy/studies_main/final_studiesmapping-and-analyses-current-and-future-2020-2030-heating-cooling-fuel).
- Freire, M.G., Teles, A.R.R., Rocha, M.A.A., Schröder, B., Neves, C.M.S.S., Carvalho, P.J., Evtuguin, D.V., Santos, L.M.N.B.F., Coutinho, J.A.P., 2011. Thermophysical Characterization of Ionic Liquids Able To Dissolve Biomass. *J. Chem. Eng. Data* 56, 4813–4822. <https://doi.org/10.1021/je200790q>.
- Součková, M., Klomfar, J., Pátek, J., 2014. Measurements and group contribution analysis of 0.1 MPa densities for still poorly studied ionic liquids with the [PF<sub>6</sub>] and [NTf<sub>2</sub>] anions. *J. Chem. Thermodyn.* 77, 31–39. <https://doi.org/10.1016/j.jct.2014.04.017>.
- ASHRAE, 2013. *ASHRAE Handbook—Fundamentals*. 2013 ASHRAE Handbook—Fundamentals.
- Atilhan, M., Jacquemin, J., Rooney, D., Khraisheh, M., Aparicio, S., 2013. Viscous behavior of imidazolium-based ionic liquids. *Ind. Eng. Chem. Res.* 52, 16774–16785. <https://doi.org/10.1021/ie403065u>.
- Asensio-Delgado, S., Pardo, F., Zarca, G., Urriaga, A., 2020b. Vapor–Liquid Equilibria and Diffusion Coefficients of Difluoromethane, 1,1,1,2-Tetrafluoroethane, and 2,3,3,3-Tetrafluoropropene in Low-Viscosity Ionic Liquids. *J. Chem. Eng. Data* 65, 4242–4251. <https://doi.org/10.1021/acs.jced.0c00224>.
- Bell, I.H., Wronski, J., Quoilin, S., Lemort, V., 2014. Pure and Pseudo-pure Fluid Thermophysical Property Evaluation and the Open-Source Thermophysical Property Library CoolProp. *Ind. Eng. Chem. Res.* 53, 2498–2508. <https://doi.org/10.1021/ie4033999>.
- Waliszewski, D., Stępnia, I., Piekarski, H., Lewandowski, A., 2005. Heat capacities of ionic liquids and their heats of solution in molecular liquids. *Thermochim. Acta* 433, 149–152. <https://doi.org/10.1016/j.tca.2005.03.001>.
- Diedrichs, A., Gmehling, J., 2006. Measurement of heat capacities of ionic liquids by differential scanning calorimetry. *Fluid Phase Equilib* 244, 68–77. <https://doi.org/10.1016/j.fluid.2006.03.015>.
- Zorębski, E., Musiał, M., Batuszyńska, K., Zorębski, M., Dzida, M., 2018. Isochoric and Isochoric Heat Capacities as Well as Isentropic and Isothermal Compressibilities of Di- and Trisubstituted Imidazolium-Based Ionic Liquids as a Function of Temperature. *Ind. Eng. Chem. Res.* 57, 5161–5172. <https://doi.org/10.1021/acs.iecr.8b00506>.
- Takalkar, G.D., Bhosale, R.R., Mali, N.A., Bhagwat, S.S., 2019. Thermodynamic analysis of EMISE–Water as a working pair for absorption refrigeration system. *Appl. Therm. Eng.* 148, 787–795. <https://doi.org/10.1016/j.applthermaleng.2018.11.092>.
- Asensio-Delgado, S., Pardo, F., Zarca, G., Urriaga, A., 2020c. Enhanced absorption separation of hydrofluorocarbon/hydrofluoroolefin refrigerant blends using ionic liquids. *Sep. Purif. Technol.* 249, 117136 <https://doi.org/10.1016/j.seppur.2020.117136>.
- Shiflett, M.B., Yokozeki, A., 2007. Solubility Differences of Halocarbon Isomers in Ionic Liquid [emim][Tf<sub>2</sub>N]. *J. Chem. Eng. Data* 52, 2007–2015. <https://doi.org/10.1021/je700295e>.
- Dong, L., Zheng, D., Sun, G., Wu, X., 2011. Vapor-Liquid Equilibrium Measurements of Difluoromethane + [Emim]OTf, Difluoromethane + [Bmim]OTf, Difluoroethane + [Emim]OTf, and Difluoroethane + [Bmim]OTf Systems. *J. Chem. Eng. Data* 56, 3663–3668. <https://doi.org/10.1021/je2005566>.
- Shiflett, M.B., Harmer, M.A., Junk, C.P., Yokozeki, A., 2006. Solubility and Diffusivity of Difluoromethane in Room-Temperature Ionic Liquids. *J. Chem. Eng. Data* 51, 483–495. <https://doi.org/10.1021/je050386z>.
- Sun, Y., Zhang, Y., Wang, X., Prausnitz, J.M., Jin, L., 2017. Gaseous absorption of 2,3,3,3-tetrafluoroprop-1-ene in three imidazolium-based ionic liquids. *Fluid Phase Equilib* 450, 65–74. <https://doi.org/10.1016/j.fluid.2017.07.013>.
- He, M., Peng, S., Liu, X., Pan, P., He, Y., 2017. Diffusion coefficients and Henry's constants of hydrofluorocarbons in [HMIM][Tf<sub>2</sub>N], [HMIM][TfO], and [HMIM][BF<sub>4</sub>]. *J. Chem. Thermodyn.* 112, 43–51. <https://doi.org/10.1016/j.jct.2017.04.009>.
- Asensio-Delgado, S., Pardo, F., Zarca, G., Urriaga, A., 2021b. Absorption separation of fluorinated refrigerant gases with ionic liquids: equilibrium, mass transport, and process design. *Sep. Purif. Technol.* 276, 119363 <https://doi.org/10.1016/j.seppur.2021.119363>.
- Kühn, R., Meyer, T., Ziegler, F., 2020. Experimental investigation of ionic liquids as substitute for lithium bromide in water absorption chillers. *Energy* 205, 117990. <https://doi.org/10.1016/j.energy.2020.117990>.

## Supplementary Information

### **Analysis of hybrid compression absorption refrigeration using low-GWP HFC or HFO/ionic liquid working pairs**

#### **Authors:**

**José M. Asensio-Delgado, Salvador Asensio-Delgado, Gabriel Zarca, Ane Urtiaga\***

Department of Chemical and Biomolecular Engineering, Universidad de Cantabria,

Av. Los Castros 46, Santander 39005, Spain.

\*Corresponding author e-mail address: [urtiaga@unican.es](mailto:urtiaga@unican.es)

## Nomenclature

$C_p$	Heat capacity, $\text{J}\cdot\text{mol}^{-1}\cdot\text{K}^{-1}$
$D$	Diffusivity, $\text{m}^2\cdot\text{s}^{-1}$
$f$	Circulation factor, -
$h$	Specific enthalpy, $\text{kJ}\cdot\text{kg}^{-1}$ or $\text{kJ}\cdot\text{mol}^{-1}$
$n$	<i>mol</i>
$p$	Pressure, MPa
$Q$	Heat duty, kW
$R$	Ideal gas constant, $\text{J}\cdot\text{mol}^{-1}\cdot\text{K}^{-1}$
$SD$	<i>Standard deviation</i> , -
$\Delta S$	Entropy, $\text{kJ}\cdot\text{kg}^{-1}\cdot\text{K}^{-1}$
$T$	Temperature, K
$u$	<i>Uncertainty</i> , -
$w$	Mass fraction, -
$W$	Power, kW
$x, y$	Mole fraction, -
$z$	Depth, m

## Greek letters

$\rho$	Molar density, $\text{mol}\cdot\text{L}^{-1}$
--------	---

## Subscripts

abs	absorbed moles
c	condenser
comp	compressor

con	IL-concentrated solution
d	desorber or generator
dil	IL-diluted solution
e	evaporator
el	electrical
ex	excess
hx	heat exchanger
p	pump
r	refrigerant
th	thermal
v	expansion valve

### **Abbreviations**

ARS Absorption Refrigeration Systems

CA-ARS Compression-Assisted Absorption Refrigeration Systems

*COP* Coefficient of Performance

*ECOP* Exergy efficiency

HFC Hydrofluorocarbons

HFO Hydrofluoroolefins

IL Ionic liquids

NRTL NonRandom Two-Liquid model

SE-ARS Single-Effect Absorption Refrigeration Systems

VLE Vapor—Liquid Equilibria

## S1. Experimental measurements. Calculation procedure.

The molar fraction of gas dissolved in the liquid phase is defined as:

$$x = \frac{n_{abs}}{n_l + n_{abs}} \quad (S1)$$

where  $n_l$  are the moles of IL and  $n_{abs}$  the total dissolved moles of refrigerant. Several steps are performed in the isochoric saturation method. The amount of gas absorbed in each step ( $n_i$ ) is calculated as follows:

$$n_i = \rho_{(i,s)} \cdot V_S + \rho_{(i-1,c)} \cdot (V_c - V_l) - \rho_{(i,eq)} \cdot (V_S + V_c - V_l) \quad (S2)$$

where  $V_S$ ,  $V_c$ , and  $V_l$  are the storage cylinder, sorption chamber, and loaded IL volumes (L), and  $\rho_s$ ,  $\rho_c$ , and  $\rho_{eq}$  are the gas molar densities ( $\text{mol}\cdot\text{L}^{-1}$ ) in the storage cylinder, in the sorption chamber, and in the whole system at equilibrium conditions, respectively. Molar densities were calculated from pressure and temperature data using the cubic Peng–Robinson equation of state to account for deviations from ideal behavior [1]. The dissolved moles are calculated as the moles dissolved in one step plus the moles dissolved in the previous steps:

$$n_{abs} = n_i + \sum_{k=1}^{i-1} n_k \quad (S3)$$

Uncertainties were calculated using the quadratic propagation of errors:

$$u(x) = \sqrt{\left(\frac{\partial x}{\partial n_{abs}}\right)^2 \cdot u(n_{abs})^2 + \left(\frac{\partial x}{\partial n_l}\right)^2 \cdot u(n_l)^2} \quad (S4)$$

where  $u$  is the standard uncertainty.  $u(n_l)$  is derived from the mass of IL, and  $u(n_{abs})$  is:

$$u(n_{abs}) = \sqrt{\left(\frac{\partial n_{abs}}{\partial n_i}\right)^2 \cdot u(n_i)^2 + \sum_k \left(\frac{\partial n_{abs}}{\partial n_k}\right)^2 \cdot u(n_k)^2} \quad (S5)$$

The uncertainty in dissolved moles in each step,  $u(n_i)$  is calculated following the same methodology from the uncertainty in each of the variables.

R1234ze(E) diffusion coefficients at infinite dilution were calculated using the semi-infinite volume model, derived from the expression of Fickian diffusion [2,3]:

$$\frac{\partial C}{\partial t} = D \frac{\partial^2 C}{\partial z^2} \quad (S6)$$



where  $C$  is the gas concentration;  $t$ , time;  $D$ , diffusivity; and  $z$ , depth into the IL. The accumulated dissolved moles per unit area,  $M_t$ , are calculated integrating Eq. (S6), and the diffusion coefficients are calculated from the slope of the fitting:

$$M_t = \int_0^t \left( D \left( \frac{\partial C}{\partial z} \right)_{z=0} \right) dt = \sqrt{D} \left( 2C_{z=t=0} \sqrt{\frac{t}{\pi}} - \frac{1}{2} m t \sqrt{\pi} \right) = \sqrt{D} \varepsilon \quad (S7)$$

where  $C_{z=t=0}$  is the initial concentration in the surface and  $m$  is a mass transfer coefficient, both of them calculated according to

$$C_{z=0} = C_{z=t=0} + m\sqrt{t} \quad (S8)$$

where  $C_{z=0}$  is the surface concentration defined as [4]

$$C_{y=0} = \frac{\rho_{IL}}{M_{IL} \cdot \left( \frac{k_H}{f} - 1 \right)} \quad (S9)$$

where  $\rho_{IL}$  and  $M_{IL}$  are density and molar mass of the IL, respectively and  $k_H$  is the Henry's law constant (MPa) obtained from solubility data:

$$k_H(T) = \lim_{x \rightarrow 0} \frac{\bar{f}(p, T)}{x} \quad (S10)$$

where  $\bar{f}$  is the refrigerant fugacity (MPa) calculated using the Peng–Robinson equation of state.

As Henry's law constants are defined at infinite dilution, Eq. (S10) can be simplified to [5,6]:

$$k_H \approx \left( \frac{d\bar{f}}{dx} \right)_{x=0} \quad (S11)$$

## S2. Heat capacities of Ionic Liquids

The enthalpies of ILs are obtained from their heat capacities, which are fitted to a quadratic expression from experimental data [7–9].

$$h_2 = \int_{T_0}^T C_{p,IL} dT + h_0 \quad (S12)$$

$$C_{p,IL} = C_0 + C_1T + C_2T^2 \quad (S13)$$

$$SD = \sqrt{\frac{1}{N-1} \sum (x_i - \bar{x})^2} \quad (S14)$$

The fitting parameters are collected in Table S1 altogether with their standard deviation. Figure S1 presents the experimental and calculated IL heat capacities.

**Table S1**

Coefficients and standard deviation of the IL heat capacities (mass-based).

Parameters of Eq. S13	Ionic Liquid			
	[C <sub>2</sub> mim][Tf <sub>2</sub> N]	[C <sub>2</sub> mim][OTf]	[C <sub>2</sub> mim][BF <sub>4</sub> ]	[C <sub>2</sub> mim][SCN]
$C_0 (J \cdot kg^{-1} K^{-1})$	1.026	0.953	1.261	1.343
$C_1 (J \cdot kg^{-1} K^{-2})$	$6.704 \times 10^{-4}$	$1.939 \times 10^{-3}$	$2.505 \times 10^{-4}$	$2.818 \times 10^{-4}$
$C_2 (J \cdot kg^{-1} K^{-3})$	$8.487 \times 10^{-7}$	$-7.990 \times 10^{-7}$	$2.479 \times 10^{-6}$	$2.376 \times 10^{-6}$
$SD (J \cdot kg^{-1} K^{-1})$	$6.847 \times 10^{-5}$	$8.197 \times 10^{-4}$	$7.863 \times 10^{-4}$	$8.012 \times 10^{-4}$

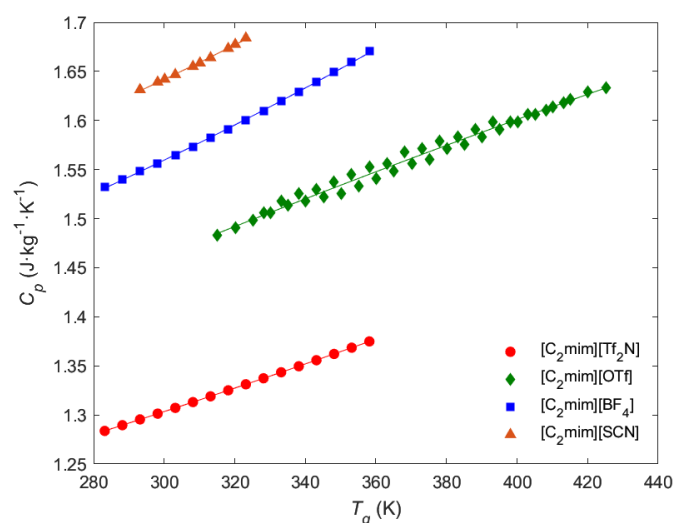


**Figure S1.** Experimental values (points) and quadratic fitting (solid lines) of the IL heat capacities.

### S3. Model validation

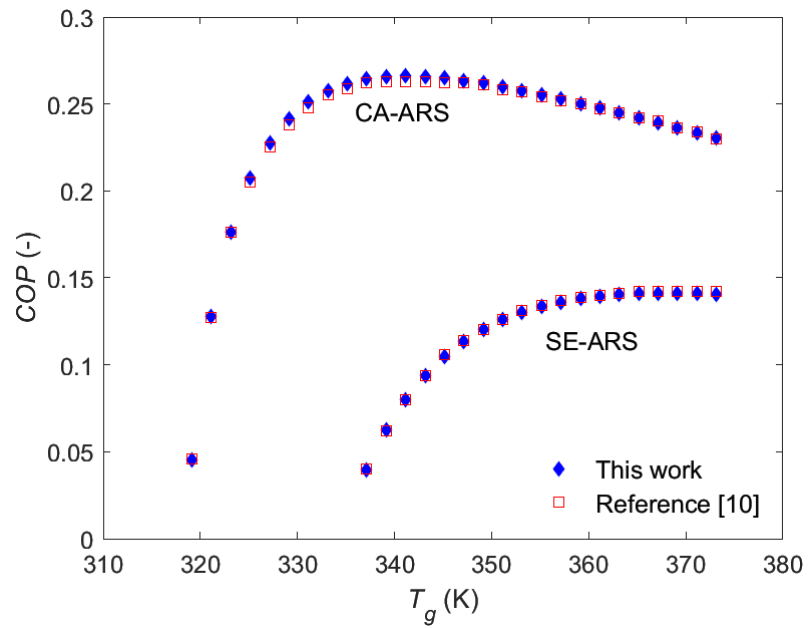


**Figure S2.** Model validation for the working pair R1234ze(E)/[C<sub>2</sub>mim][BF<sub>4</sub>] in a SE-ARS and a CA-ARS as a function of generator temperature [10]. Evaporator temperature at 278 K, dissipation (condenser and absorber) at 303 K and CA-ARS with a compression ratio of 1.5.

## S4. Experimental and modeling results

**Table S2**

Mole-fraction solubility and molality of R1234ze(E) in [C<sub>2</sub>mim][Tf<sub>2</sub>N].

$T$ (K)	$p$ (MPa)	$x$	$u(x)$	$m$ (mol·kg <sup>-1</sup> )	$u(m)$ (mol·kg <sup>-1</sup> )
283.15	0.0321	0.0462	0.0004	0.124	0.001
283.15	0.0699	0.1045	0.0005	0.298	0.002
283.15	0.1201	0.1806	0.0007	0.563	0.003
283.15	0.1679	0.2505	0.0008	0.854	0.004
283.15	0.2062	0.3049	0.0009	1.121	0.005
283.15	0.2356	0.3474	0.0012	1.360	0.007
293.15	0.0393	0.0430	0.0004	0.115	0.001
293.15	0.0845	0.0946	0.0005	0.267	0.002
293.15	0.1407	0.1568	0.0007	0.475	0.003
293.15	0.2027	0.2232	0.0008	0.734	0.003
293.15	0.2477	0.2702	0.0010	0.946	0.005
303.15	0.0434	0.0333	0.0004	0.116	0.001
303.15	0.0894	0.0722	0.0006	0.199	0.002
303.15	0.1553	0.1265	0.0007	0.370	0.002
303.15	0.2306	0.1863	0.0009	0.585	0.004
303.15	0.2899	0.2325	0.0012	0.774	0.005
313.15	0.0475	0.0317	0.0004	0.084	0.001
313.15	0.1029	0.0671	0.0006	0.184	0.002
313.15	0.1700	0.1086	0.0008	0.311	0.003
313.15	0.2458	0.1534	0.0010	0.463	0.004
313.15	0.2996	0.1843	0.0013	0.577	0.005
323.15	0.0499	0.0252	0.0004	0.066	0.001
323.15	0.1179	0.0584	0.0006	0.159	0.002
323.15	0.1853	0.0896	0.0008	0.252	0.003
323.15	0.2657	0.1257	0.0011	0.367	0.004
323.15	0.3218	0.1504	0.0014	0.452	0.005

**Table S3**Mole-fraction solubility and molality of R1234ze(E) in [C<sub>2</sub>mim][OTf].

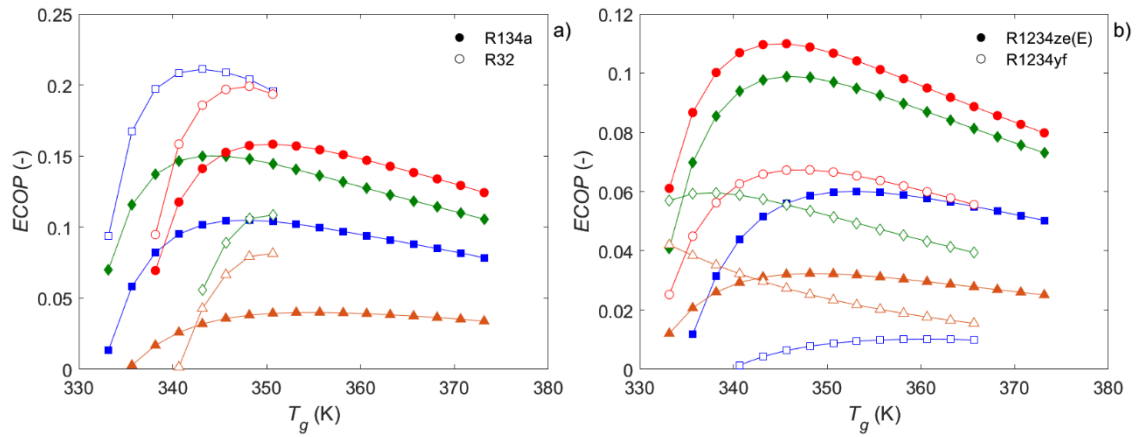
$T$ (K)	$p$ (MPa)	$x$	$u(x)$	$m$ (mol·kg <sup>-1</sup> )	$u(m)$ (mol·kg <sup>-1</sup> )
283.15	0.0367	0.0369	0.0004	0.147	0.002
283.15	0.0871	0.0912	0.0005	0.386	0.002
283.15	0.1455	0.1564	0.0006	0.712	0.003
283.15	0.1973	0.2154	0.0008	1.055	0.005
283.15	0.2391	0.2651	0.0010	1.386	0.007
293.15	0.0449	0.0312	0.0004	0.124	0.002
293.15	0.0926	0.0681	0.0005	0.281	0.002
293.15	0.1546	0.1174	0.0007	0.511	0.004
293.15	0.2230	0.1726	0.0009	0.802	0.005
293.15	0.2669	0.2086	0.0011	1.013	0.007
293.15	0.3032	0.2389	0.0015	1.206	0.010
303.15	0.0508	0.0291	0.0004	0.115	0.002
303.15	0.1131	0.0643	0.0005	0.264	0.002
303.15	0.1981	0.1123	0.0007	0.486	0.003
303.15	0.2645	0.1506	0.0009	0.681	0.005
303.15	0.3062	0.1744	0.0013	0.812	0.007
313.15	0.0545	0.0219	0.0004	0.086	0.002
313.15	0.1228	0.0501	0.0006	0.203	0.003
313.15	0.2054	0.0838	0.0008	0.352	0.004
313.15	0.2798	0.1139	0.0010	0.494	0.005
313.15	0.3271	0.1338	0.0014	0.594	0.007
323.15	0.0595	0.0177	0.0004	0.069	0.002
323.15	0.1362	0.0402	0.0006	0.161	0.003
323.15	0.2270	0.0673	0.0008	0.277	0.004
323.15	0.2931	0.0862	0.0011	0.363	0.005
323.15	0.3292	0.0970	0.0015	0.413	0.007

**Table S4**Mole-fraction solubility and molality of R1234ze(E) in [C<sub>2</sub>mim][SCN].

$T$ (K)	$p$ (MPa)	$x$	$u(x)$	$m$ (mol·kg <sup>-1</sup> )	$u(m)$ (mol·kg <sup>-1</sup> )
283.15	0.0554	0.0116	0.0002	0.069	0.001
283.15	0.1257	0.0281	0.0003	0.171	0.002
283.15	0.2032	0.0476	0.0005	0.295	0.003
283.15	0.2696	0.0655	0.0006	0.414	0.004
283.15	0.3141	0.0783	0.0009	0.502	0.006
293.15	0.0599	0.0095	0.0002	0.057	0.001
293.15	0.1359	0.0223	0.0003	0.135	0.002
293.15	0.2171	0.0366	0.0005	0.225	0.003
293.15	0.2849	0.0491	0.0007	0.305	0.005
293.15	0.3300	0.0578	0.0009	0.363	0.006
303.15	0.0622	0.0074	0.0002	0.044	0.001
303.15	0.1289	0.0156	0.0003	0.094	0.002
303.15	0.2126	0.0259	0.0005	0.157	0.003
303.15	0.2873	0.0352	0.0007	0.216	0.004
303.15	0.3332	0.0407	0.0010	0.251	0.006
313.15	0.0666	0.0053	0.0002	0.032	0.001
313.15	0.1445	0.0123	0.0004	0.074	0.002
313.15	0.2322	0.0201	0.0005	0.121	0.003
313.15	0.3049	0.0266	0.0007	0.162	0.004
313.15	0.348	0.0317	0.0010	0.193	0.006
323.15	0.0687	0.0042	0.0002	0.025	0.001
323.15	0.1513	0.0090	0.0004	0.054	0.002
323.15	0.2386	0.0139	0.0005	0.083	0.003
323.15	0.3072	0.0175	0.0007	0.105	0.004
323.15	0.3505	0.0200	0.0010	0.121	0.006

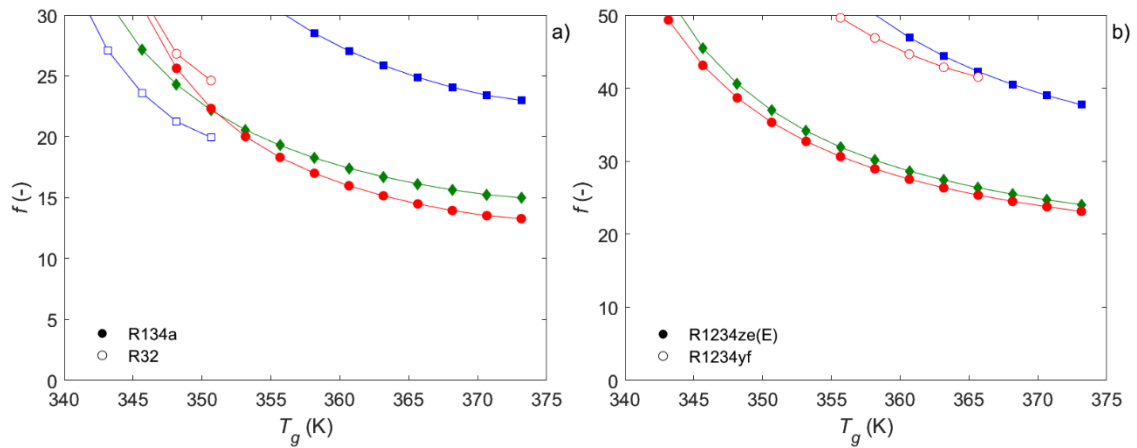
## S5. ARS model. Results

Figure S3 presents the results of the exergy analysis of the SE-ARS. The highest  $ECOP$  of HFC/IL pairs is achieved with R32/[C<sub>2</sub>mim][Tf<sub>2</sub>N] at 343 K with a value of 0.21. In the case of HFO/IL pairs, the best exergy efficiency is 0.11, obtained with R1234ze(E)/[C<sub>2</sub>mim][Tf<sub>2</sub>N] at 343 K.



**Figure S3.**  $ECOP$  of the SE-ARS systems as a function of generator temperature ( $T_g$ ). (a) HFCs/IL: R134a (filled symbols) and R32 (empty symbols), and (b) HFOs/IL: R1234ze(E) (filled symbols) and R1234yf (empty symbols). Symbols represent the different ILs: [C<sub>2</sub>mim][BF<sub>4</sub>] (■), [C<sub>2</sub>mim][OTf] (◆), [C<sub>2</sub>mim][SCN] (▲), and [C<sub>2</sub>mim][Tf<sub>2</sub>N] (●).  $T_e = 278$  K,  $T_c = T_o = 303$  K.

The behavior of the circulation ratio is the opposite to that of the  $COP$  and therefore, the systems with higher  $COPs$  also present the lowest circulation factors. Figure S4 presents the variation in circulation factor for the SE-ARS depending on the generator temperature, where  $f$  sharply decreases with increasing generator temperature and reaching an asymptotic value that is equal to the inverse of  $w_{dil}$  (i.e., when  $w_{con} = 0$  in Eq. (12) of the main article). The values of  $f$  for R1234yf/[C<sub>2</sub>mim][BF<sub>4</sub>] and every [C<sub>2</sub>mim][SCN]-based working pair are not presented because they are higher than 50 at every generator temperature. These high mass circulation ratios incur in high electric and thermal energy consumptions that make them not suitable for ARS.



**Figure S4.** Circulation factor ( $f$ ) of the SE-ARS systems as a function of generator temperature ( $T_g$ ). (a) HFCs/IL: R134a (filled symbols) and R32 (empty symbols), and (b) HFOs/IL: R1234ze(E) (filled symbols) and R1234yf (empty symbols). Symbols represent the different ILs:  $[\text{C}_2\text{mim}][\text{BF}_4]$  ( $\blacksquare$ ),  $[\text{C}_2\text{mim}][\text{OTf}]$  ( $\blacklozenge$ ),  $[\text{C}_2\text{mim}][\text{SCN}]$  ( $\blacktriangle$ ), and  $[\text{C}_2\text{mim}][\text{Tf}_2\text{N}]$  ( $\bullet$ ).  $T_e = 278$  K,  $T_c = T_a = 303$  K.

The difference between the mass fraction of the streams leaving the absorber and desorber ( $\Delta w$ ) is shown in Figure S5 and Table S5 collects the values of the IL-diluted stream mass fraction ( $w_{aii}$ ). In all cases, the mass fraction difference is narrow, the largest value is 0.070 for the system R134a/ $[\text{C}_2\text{mim}][\text{Tf}_2\text{N}]$  at 373 K. Generator low-temperature limitation is evident as all curves leave the viable operating conditions ( $\Delta w > 0$ ) at temperatures between 330 and 340 K.

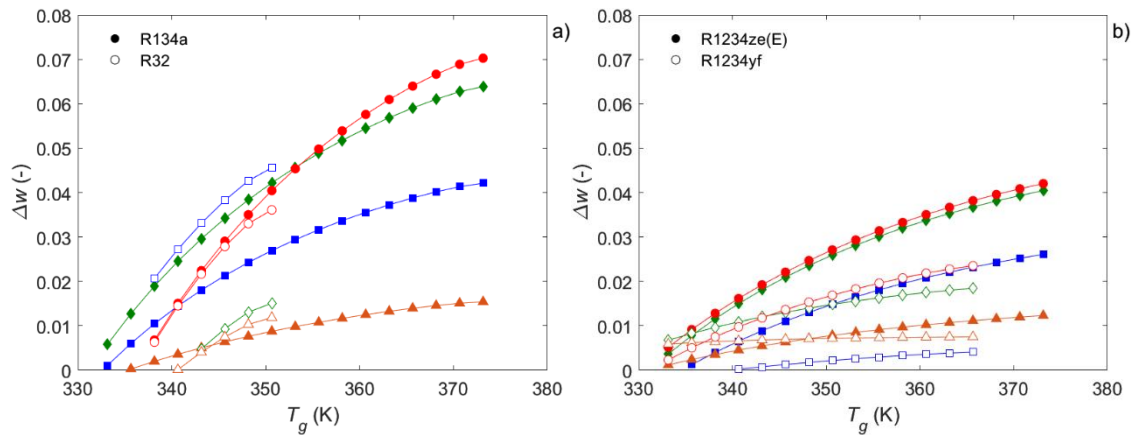


**Figure S5.** Mass fraction increment ( $\Delta w$ ) of the SE-ARS systems as a function of generator temperature ( $T_g$ ). (a) HFCs/IL: R134a (filled symbols) and R32 (empty symbols), and (b) HFOs/IL: R1234ze(E) (filled symbols) and R1234yf (empty symbols). Symbols represent the different ILs:  $[\text{C}_2\text{mim}][\text{BF}_4]$  ( $\blacksquare$ ),  $[\text{C}_2\text{mim}][\text{OTf}]$  ( $\blacklozenge$ ),  $[\text{C}_2\text{mim}][\text{SCN}]$  ( $\blacktriangle$ ), and  $[\text{C}_2\text{mim}][\text{Tf}_2\text{N}]$  ( $\bullet$ ).  $T_e = 278$  K,  $T_c = T_a = 303$  K.



**Table S5**Absorber mass fractions ( $w_{dil}$ ) in SE-ARS ( $T_e=278$  K,  $T_c=303$  K, CR=1.5).

	[C <sub>2</sub> mim][BF <sub>4</sub> ]	[C <sub>2</sub> mim][OTf]	[C <sub>2</sub> mim][SCN]	[C <sub>2</sub> mim][Tf <sub>2</sub> N]
<b>R134a</b>	0.0738	0.1061	0.0335	0.1370
<b>R32</b>	0.1359	0.1224	0.0889	0.1473
<b>R1234ze(E)</b>	0.0424	0.0674	0.0209	0.0700
<b>R1234yf</b>	0.0140	0.0276	0.0078	0.0467

The whole picture of the performances of the SE-ARS with the studied pairs evaluated for a refrigerant mass flow rate of 1 kg·s<sup>-1</sup> and a low-grade heat source at 348 K.

**Table S6**Performance of different SE-ARS under the same conditions ( $T_e = 278$  K,  $T_c = T_a = 303$  K,  $T_g = 348$  K,  $m_r = 1$  kg·s<sup>-1</sup>)

Working Pair	$f$	$Q_g$ (kW)	$Q_e$ (kW)	$Q_a$ (kW)	$Q_c$ (kW)	$COP$
R134a/[C <sub>2</sub> mim][BF <sub>4</sub> ]	39.2	762.7	159.8	-713.1	-209.4	0.210
R134a/[C <sub>2</sub> mim][OTf]	24.3	541.3	159.8	-492.3	-208.7	0.295
R134a/[C <sub>2</sub> mim][SCN]	127.9	2103.9	159.8	-2053.8	-209.8	0.076
R134a/[C <sub>2</sub> mim][Tf <sub>2</sub> N]	25.6	508.3	159.8	-459.5	-208.5	0.314
R32/[C <sub>2</sub> mim][BF <sub>4</sub> ]	21.3	640.4	260.8	-592.2	-309.0	0.407
R32/[C <sub>2</sub> mim][OTf]	68.2	1232.7	260.8	-1183.1	-310.4	0.212
R32/[C <sub>2</sub> mim][SCN]	89.4	1646.2	260.8	-1596.6	-310.4	0.158
R32/[C <sub>2</sub> mim][Tf <sub>2</sub> N]	26.8	655.8	260.8	-607.6	-309.0	0.398
R1234ze(E)/[C <sub>2</sub> mim][BF <sub>4</sub> ]	74.6	1254.0	146.8	-1201.9	-198.9	0.117
R1234ze(E)/[C <sub>2</sub> mim][OTf]	40.6	746.4	146.8	-694.7	-198.5	0.197
R1234ze(E)/[C <sub>2</sub> mim][SCN]	138.6	2274.0	-146.8	-2221.7	199.1	0.065
R1234ze(E)/[C <sub>2</sub> mim][Tf <sub>2</sub> N]	38.7	675.7	146.8	-624.3	-198.2	0.217
R1234yf/[C <sub>2</sub> mim][BF <sub>4</sub> ]	563.2	8121.2	126.0	-8067.4	-179.9	0.016
R1234yf/[C <sub>2</sub> mim][OTf]	70.6	1178.3	126.0	-1125.0	-179.3	0.107
R1234yf/[C <sub>2</sub> mim][SCN]	141.4	2500.7	126.0	-2446.5	-180.2	0.050
R1234yf/[C <sub>2</sub> mim][Tf <sub>2</sub> N]	63.2	937.1	126.0	-883.9	-179.2	0.135

These results were calculated for refrigeration applications with evaporator temperatures of 278 K, which are demanding for a SE-ARS because the absorber operates at the same pressure as the evaporator. In air conditioning applications, the refrigerant leaves the evaporator at its vapor pressure at a higher temperature. As this pressure is higher, the solubility of the

refrigerant is higher at the same absorber temperature and the circulation ratio  $f$  is therefore much lower than for refrigeration applications as shown in Figure S6.

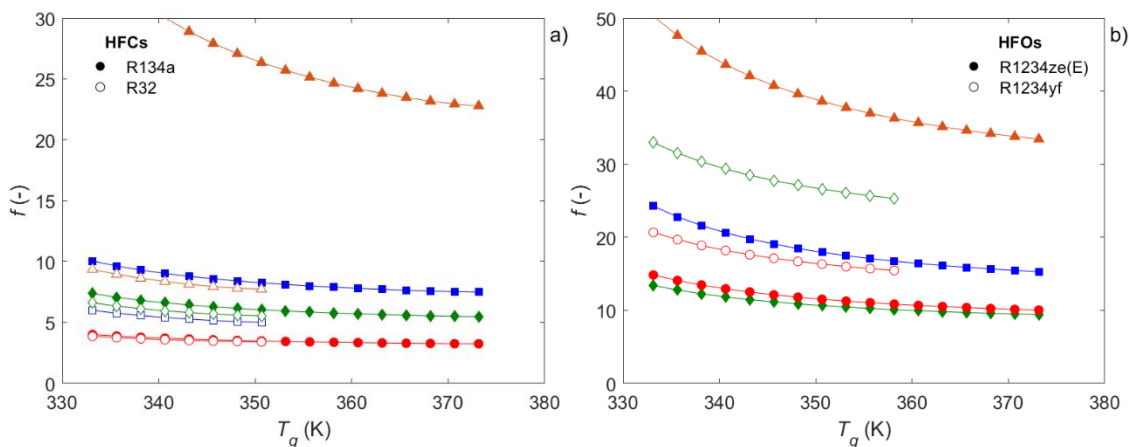


**Figure S6.** Circulation factor ( $f$ ) of the SE-ARS systems as a function of generator temperature ( $T_g$ ). (a) HFCs/IL: R134a (filled symbols) and R32 (empty symbols), and (b) HFOs/IL: R1234ze(E) (filled symbols) and R1234yf (empty symbols). Symbols represent the different ILs: [C<sub>2</sub>mim][BF<sub>4</sub>] (■), [C<sub>2</sub>mim][OTf] (◆), [C<sub>2</sub>mim][SCN] (▲), and [C<sub>2</sub>mim][Tf<sub>2</sub>N] (●).  $T_e = 291$  K,  $T_c = T_a = 300$  K.

Figure S7 shows the calculated  $COP$  for each working-pair as a function of the generator temperature, which ranged between 333 K and 373 K, with an evaporator temperature of 291 K. As it can be seen, the  $COP$  does not increase initially, but it is in the decreasing zone from very low generator temperatures. Most interestingly, the  $COP$  values at every generator temperature are more than twice as high as the maximum  $COP$  value of the refrigeration ( $T_e = 278$  K) application. The best performances in air conditioning are achieved using R32 with [C<sub>2</sub>mim][Tf<sub>2</sub>N] and [C<sub>2</sub>mim][OTf], with  $COP$  values around 0.8, and R134a with [C<sub>2</sub>mim][Tf<sub>2</sub>N], with the  $COP$  just below 0.8, which are at the same level than those achieved with H<sub>2</sub>O/LiBr and NH<sub>3</sub>/H<sub>2</sub>O. In fact, the working pairs using R32 have competitive performances with the  $COP$  always higher than 0.65. Compared to HFOs, HFCs still present clearly better performances for air conditioning as it happened for refrigeration. However, the  $COP$  of R1234ze(E) with [C<sub>2</sub>mim][Tf<sub>2</sub>N] and [C<sub>2</sub>mim][OTf] is close to 0.5, so they could be used as working pairs if a waste heat source was available.

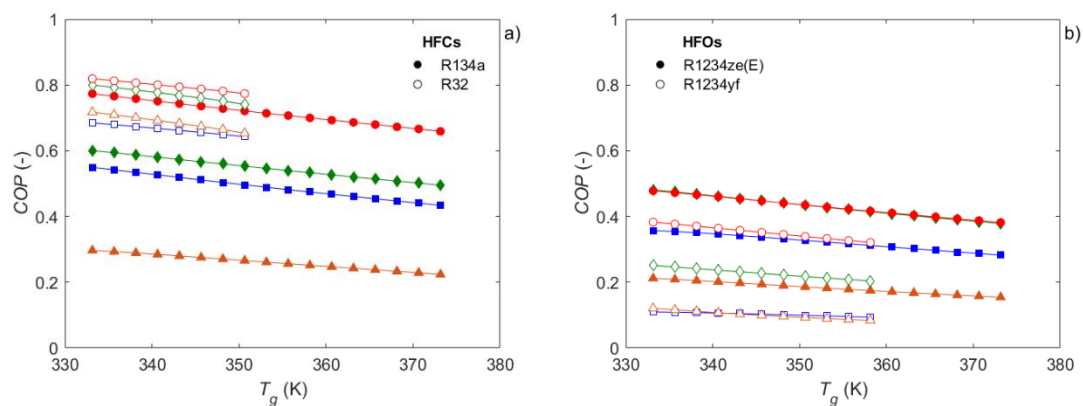


**Figure S7.** COP of the SE-ARS systems as a function of generator temperature ( $T_g$ ). (a) HFCs/IL: R134a (filled symbols) and R32 (empty symbols), and (b) HFOs/IL: R1234ze(E) (filled symbols) and R1234yf (empty symbols). Symbols represent the different ILs: [C<sub>2</sub>mim][BF<sub>4</sub>] (■), [C<sub>2</sub>mim][OTf] (◆), [C<sub>2</sub>mim][SCN] (▲), and [C<sub>2</sub>mim][Tf<sub>2</sub>N] (●).  $T_e = 291$  K,  $T_c = T_a = 300$  K.

**Table S7**

Operating pressures of SE-ARS and CA-ARS systems ( $T_e = 278$  K,  $T_c = 303$  K, CR = 1.5)

Refrigerant	$p_e$ (kPa)	$p_a^*$ (kPa)	$p_g$ (kPa)
R134a	349.7	524.5	770.2
R32	951.4	1427.2	1927.5
R1234ze(E)	259.3	389.0	578.2
R1234yf	372.9	559.4	783.5

\*In SE-ARS,  $p_a$  is equal to  $p_e$ .

**Table S8**

Absorber mass fractions ( $w_{dil}$ ) in CA-ARS ( $T_e = 278$  K,  $T_c = 303$  K, CR = 1.5)

	[C <sub>2</sub> mim][BF <sub>4</sub> ]	[C <sub>2</sub> mim][OTf]	[C <sub>2</sub> mim][SCN]	[C <sub>2</sub> mim][Tf <sub>2</sub> N]
R134a	0.1310	0.1803	0.0525	0.2679
R32	0.2409	0.2330	0.1709	0.3164
R1234ze(E)	0.0685	0.1090	0.0324	0.1066
R1234yf	0.0218	0.0431	0.0123	0.0772

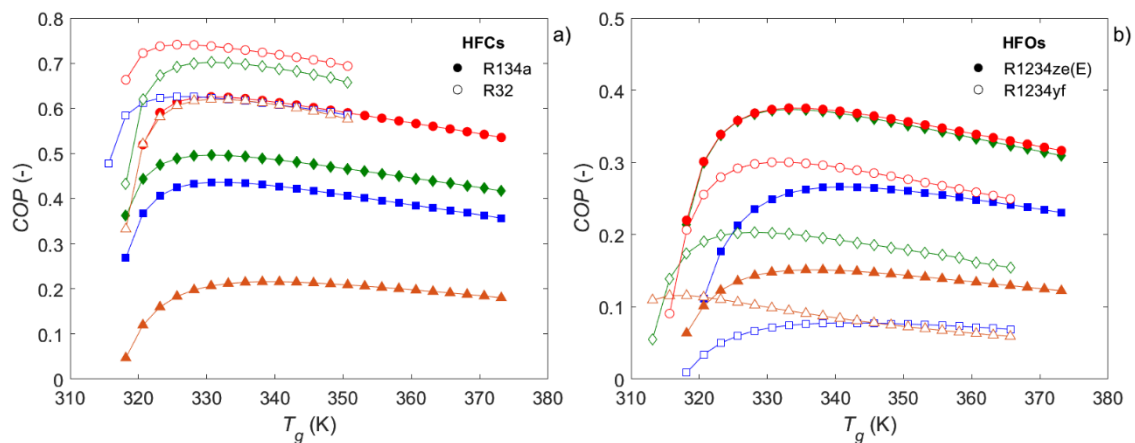


**Figure S8.** COP of the CA-ARS systems as a function of generator temperature ( $T_g$ ). (a) HFCs/IL: R134a (filled symbols) and R32 (empty symbols), and (b) HFOs/IL: R1234ze(E) (filled symbols) and R1234yf (empty symbols). Symbols represent the different ILs: [C<sub>2</sub>mim][BF<sub>4</sub>] (■), [C<sub>2</sub>mim][OTf] (◆), [C<sub>2</sub>mim][SCN] (▲), and [C<sub>2</sub>mim][Tf<sub>2</sub>N] (●).  $T_e = 278$  K,  $T_c = T_a = 303$  K.

## REFERENCES

- [1] M.B. Shiflett, A. Yokozeki, Gaseous Absorption of Fluoromethane, Fluoroethane, and 1,1,2,2-Tetrafluoroethane in 1-Butyl-3-Methylimidazolium Hexafluorophosphate, *Ind. Eng. Chem. Res.* 45 (2006) 6375–6382. <https://doi.org/10.1021/ie060192s>.
- [2] J. Crank, *The Mathematics of Diffusion*, 2nd ed, Clarendon Press, Oxford, UK, 1975. [https://doi.org/10.1016/0306-4549\(77\)90072-X](https://doi.org/10.1016/0306-4549(77)90072-X).
- [3] D. Camper, C. Becker, C. Koval, R.D. Noble, Diffusion and solubility measurements in room temperature ionic liquids, *Ind. Eng. Chem. Res.* 45 (2006) 445–450. <https://doi.org/10.1021/ie0506668>.
- [4] M. He, S. Peng, X. Liu, P. Pan, Y. He, Diffusion coefficients and Henry's constants of hydrofluorocarbons in [HMIM][Tf2N], [HMIM][TfO], and [HMIM][BF4], *J. Chem. Thermodyn.* 112 (2017) 43–51. <https://doi.org/10.1016/j.jct.2017.04.009>.
- [5] M.B. Shiflett, A. Yokozeki, Solubility and Diffusivity of Hydrofluorocarbons in Room-Temperature Ionic Liquids, *AIChE J.* 52 (2006) 1205–1219. <https://doi.org/10.1002/aic.10685>.
- [6] L.F. Lepre, D. Andre, S. Denis-Quanquin, A. Gautier, A.A.H. Pádua, M.F. Costa Gomes, Ionic liquids can enable the recycling of fluorinated greenhouse gases, *ACS Sustain. Chem. Eng.* 7 (2019) 16900–16906. <https://doi.org/10.1021/acssuschemeng.9b04214>.
- [7] D. Waliszewski, I. Stępnia, H. Piekarski, A. Lewandowski, Heat capacities of ionic liquids and their heats of solution in molecular liquids, *Thermochim. Acta.* 433 (2005) 149–152. <https://doi.org/10.1016/j.tca.2005.03.001>.
- [8] A. Diedrichs, J. Gmehling, Measurement of heat capacities of ionic liquids by differential scanning calorimetry, *Fluid Phase Equilib.* 244 (2006) 68–77. <https://doi.org/10.1016/j.fluid.2006.03.015>.
- [9] E. Zorębski, M. Musiał, K. Bałuszyńska, M. Zorębski, M. Dzida, Isobaric and Isochoric Heat Capacities as Well as Isentropic and Isothermal Compressibilities of Di- and Trisubstituted Imidazolium-Based Ionic Liquids as a Function of Temperature, *Ind. Eng. Chem. Res.* 57 (2018) 5161–5172. <https://doi.org/10.1021/acs.iecr.8b00506>.
- [10] W. Wu, T. You, H. Zhang, X. Li, Comparisons of different ionic liquids combined with trans-1,3,3,3-tetrafluoropropene (R1234ze(E)) as absorption working fluids, *Int. J. Refrig.* 88 (2018) 45–57. <https://doi.org/10.1016/j.ijrefrig.2017.12.011>.

---

**3.6. Scientific publication 6. “Gas solubility and diffusivity of hydrofluorocarbons and hydrofluoroolefins in cyanide-based ionic liquids for the separation of refrigerant mixtures”, Salvador Asensio-Delgado, Miguel Viar, Fernando Pardo, Gabriel Zarca, Ane Urtiaga, Fluid Phase Equilibria, 549 (2021) 113210**

The scientific publication 4 showed that the IL [C<sub>2</sub>mim][SCN] provided the best selectivity to date to separate R1234yf from R32 and R134a. However, we observed that the solubility of the most soluble compounds decreased a little despite the great increase in selectivity. For that reason, we tested the absorption of refrigerant gases in additional ILs with cyanide groups in the anion, in this case [C<sub>2</sub>mim][dca] and [C<sub>4</sub>mim][dca]. The F-gases studied were R32, R134a, R1234yf, R1234ze(E), and, for the first time in this thesis, R125, which we had just acquired because it is no longer sold as a pure compound due to its high GWP and needs to be custom made by the suppliers. As we had the R125, we studied its solubility in [C<sub>2</sub>mim][SCN] and complete our assessment of this IL. Once the vapor liquid-equilibria were determined, ternary mixtures were predicted using the NRTL activity-coefficient model and the Rachford-Rice equation was used as in Publication 2 for the design of a flash evaporator to separate binary refrigerant mixtures. This way, separation factors considering the interaction between refrigerants in the gas phase were calculated and compared to the selectivity calculated as the ratio of the Henry's law constants of the binary F-gas/IL systems. The ILs with the [dca]<sup>-</sup> anion showed an increase in solubility for all the F-gases with respect to [C<sub>2</sub>mim][SCN], but it was still lower than in other ILs such as [C<sub>2</sub>mim][Tf<sub>2</sub>N], which allowed it to maintain high selectivity values. The selectivity was still higher using [C<sub>2</sub>mim][SCN] to separate R32 from R125 and R1234yf, but [C<sub>2</sub>mim][dca] showed higher selectivity in the separation of R134a from R1234yf in the single-stage separator. The higher solubility in conjunction with the higher selectivity should decrease the solvent needs and the energy used in solvent regeneration in an industrial size process.



# Gas solubility and diffusivity of hydrofluorocarbons and hydrofluoroolefins in cyanide-based ionic liquids for the separation of refrigerant mixtures

Salvador Asensio-Delgado, Miguel Viar, Fernando Pardo, Gabriel Zarca, Ane Urriaga\*

Department of Chemical and Biomolecular Engineering, Universidad de Cantabria, Av. Los Castros 46, Santander 39005, Spain

## ARTICLE INFO

### Article history:

Received 22 July 2021

Revised 27 August 2021

Accepted 31 August 2021

Available online 2 September 2021

### Keywords:

Vapor-liquid equilibria

Diffusion

Solubility selectivity

1-ethyl-3-methylimidazolium dicyanamide

Flash separation

## ABSTRACT

Ionic liquids (ILs) have been extensively studied for their use as solvents in separation processes. In this work, we determine the vapor-liquid equilibria (VLE) and diffusion coefficients at infinite dilution of three hydrofluorocarbons (R32 – difluoromethane, R125 – pentafluoroethane, and R134a – 1,1,1,2-tetrafluoroethane) and two hydrofluoroolefins (R1234yf – 2,3,3,3-tetrafluoropropene, and R1234ze(E) – trans-1,3,3,3-tetrafluoropropene) and the ILs 1-ethyl-3-methylimidazolium and 1-butyl-3-methylimidazolium dicyanamide ([C<sub>2</sub>mim][dca] and [C<sub>4</sub>mim][dca]). Additionally, we study the VLE of R125 and [C<sub>2</sub>mim][SCN] (thiocyanate) to complete the previous studies with this liquid. These ILs have been selected because other ILs with cyanide moieties in the anion have shown good selectivity to separate fluorinated refrigerant gases and their low viscosity would improve the mass transfer and reduce the pumping costs in a separation process. The experimental data have been determined at temperatures from 283.15 K to 323.15 K and pressures up to 1 MPa, and the nonrandom two-liquid model (NRTL) has been used to fit the VLE. The non-competitive ideal selectivity and the separation factor achieved in an isothermal flash operating at 303.15 K and 5 bar have been evaluated for target mixtures of interest. The use of dicyanamide based ILs leads to the best selectivity results to date, concluding that the studied ILs are promising for the design of separation processes that selectively recover fluorinated refrigerant gases.

© 2021 The Author(s). Published by Elsevier B.V.

This is an open access article under the CC BY-NC-ND license (<http://creativecommons.org/licenses/by-nc-nd/4.0/>)

## 1. Introduction

Refrigeration is essential in modern society, as it allows to preserve food and medicines, and condition inner spaces to bear high ambient temperatures. As a result of the population growth, wealth increase, and the temperature raise consequence of global warming, the refrigeration requirements are increasing such that nearly 20% of the energy consumed worldwide is due to the demand for refrigeration and air conditioning [1,2]. Current refrigerants are mostly based on a few hydrofluorocarbons (HFCs) and hydrofluoroolefins (HFOs), namely, the HFCs difluoromethane (R32), pentafluoroethane (R125), and 1,1,1,2-tetrafluoroethane (R134a), and the HFOs 2,3,3,3- and trans-1,3,3,3-tetrafluoropropene (R1234yf and R1234ze(E), respectively),

and their mixtures with hydrocarbons and carbon dioxide. However, some HFCs are molecules of high global warming potential (GWP) and are to be phased down, so their content in refrigerant mixtures must be progressively reduced. Unfortunately, refrigerant mixtures often form azeotropes or close-boiling mixtures that hinder the separation and purification of their components with conventional separation techniques [53]. In particular, the mixtures formed by R134a with the HFOs R1234yf and R1234ze(E) present azeotropic behavior in their whole range of composition, with temperature glides (or difference between the bubble and dew point temperature) always below 0.2 K [3,4]; and the mixture formed by R32 and R125 presents an azeotrope at around 92% of R32 in molar fraction [5,6]. In some other cases, such as for the mixtures of R32 and R1234yf, the compounds can be separated by distillation up to some composition after which the vapor and liquid lines pinch, hindering their complete purification beyond that composition [3].

The use of ionic liquids (ILs), liquid salts composed of asymmetric organic cations and organic or inorganic anions, have been proposed for the design of novel absorption-based separation processes because of their fascinating properties, e.g., extremely low

Abbreviations: GHG, Greenhouse Gas; GWP, Global Warming Potential; HFC, Hydrofluorocarbons; HFO, Hydrofluoroolefins; IL, Ionic liquids; NRTL, Nonrandom two-liquid model; VLE, Vapor-liquid equilibria.

\* Corresponding author at: Universidad de Cantabria, Spain.

E-mail address: [urriaga@unican.es](mailto:urriaga@unican.es) (A. Urriaga).

## Nomenclature

$B$	Second virial coefficient, $\text{m}^3 \cdot \text{mol}^{-1}$
$C$	Gas concentration, $\text{mol} \cdot \text{m}^{-3}$
$D$	Diffusivity, $\text{m}^2 \cdot \text{s}^{-1}$
$E_D$	Activation energy of diffusion, $\text{kJ} \cdot \text{mol}^{-1}$
$f$	Circulation factor, -
$\bar{f}$	Fugacity, MPa
$k_H$	Henry's law constant, MPa
$m$	mass transfer coefficient, $\text{mol} \cdot \text{m}^{-3} \cdot \text{s}^{-1/2}$
$M_{IL}$	Molecular mass of the IL, $\text{kg} \cdot \text{mol}^{-1}$
$M_t$	Accumulated moles per unit area, $\text{mol} \cdot \text{m}^{-2}$
$n$	mol
$p$	Pressure, MPa
$R$	Ideal gas constant, $\text{J} \cdot \text{mol}^{-1} \cdot \text{K}^{-1}$
$S$	Ideal selectivity, -
SF	Separation factor, -
$T$	Temperature, K
$t$	Time, s
$u$	Uncertainty, -
$V$	Volume, L
$x, y$	Mole fraction, -
$z$	Depth, m

### Greek letters

$\alpha, \tau_{12}^0, \tau_{12}^1, \tau_{21}^0, \tau_{21}^1$	NRTL adjustable parameters
$\gamma$	Activity coefficient, -
$\Delta H_{sol}$	Solvation enthalpy, $\text{kJ} \cdot \text{mol}^{-1}$
$\Delta S_{sol}$	Solvation entropy, $\text{J} \cdot \text{mol}^{-1} \cdot \text{K}^{-1}$
$\rho$	Molar density, $\text{mol} \cdot \text{L}^{-1}$
$\Phi$	Fugacity correction factor

### Subscripts

$abs$	absorbed moles
$c$	sorption chamber
$eq$	equilibrium
$l$	liquid
$s$	storage cylinder

### Superscripts

$L$	Saturated liquid
$S$	Saturated vapor

volatility, high chemical and thermal stability, non-flammability, large liquid range, and tunable polarity [7–9]. In particular, ILs appear as very promising mass separation agents to perform the separation of binary systems of fluorinated refrigerants [10–24]. However, the analysis of the solubility data of fluorinated gases in ILs reveals that common ILs provide somewhat low solubility-selectivity for the abovementioned systems of interest, which arises the need to assess the impact of the IL chemical structure on the solubility selectivity [25].

In our previous works, we have observed that using ILs with the thiocyanate anion  $[\text{SCN}]^-$  leads to great improvements in the selectivity of the separation of the mixtures  $\text{R32} + \text{R1234yf}$  and  $\text{R134a} + \text{R1234yf}$ , at the cost of a slight decrease in gas solubility [11]. Interestingly, using cyanide anion-based ILs also decreases the fluid viscosity, an interesting property for enhancing the absorption rates [26–29]. Altogether, further studies assessing other ILs containing cyanide groups would provide novel and highly valuable results to comprehend the solubility/selectivity trade-off towards the selective separation of fluorinated refrigerants with ILs. For that reason, in this article we explore the possibility of using ILs with the dicyanamide anion  $[\text{dca}]^-$  and two imidazolium-based cations with differ-

ent radical alkyl chains, 1-ethyl-3-methylimidazolium and 1-butyl-3-methylimidazolium ( $[\text{C}_2\text{mim}]^+$  and  $[\text{C}_4\text{mim}]^+$ , respectively), to separate fluorinated refrigerant gases. Table S1 presents some properties of interest of the studied ILs, which present outstandingly low viscosities [30–32].

Thus, we present the experimental gas solubility of the most common refrigerant gases R32, R125, R134a, R1234yf, and R1234ze(E) at temperatures ranging from 283.15 to 323.15 K and pressures up to 1 MPa, and their diffusion coefficients at infinite dilution. Also, we present the solubility of R125 in  $[\text{C}_2\text{mim}][\text{SCN}]$  to complete the absorption data of fluorinated refrigerants with this IL [11]. The nonrandom two-liquid (NRTL) activity-coefficient model is applied to describe the vapor-liquid equilibria. Then, we use the solubility data to calculate thermodynamic properties of interest such as the Henry's law constants, and the solvation enthalpies and entropies. Finally, we assess the separation potential of ILs to recover the refrigerant gases from the target mixtures of interest comparing the ideal selectivity with the NRTL predictions for the ternary systems.

## 2. Methods

### 2.1. Materials

Table 1 lists the specifications of the materials used in this work. The refrigerant gases were used as received and the ILs were vacuum dried to remove any traces of water. The final water content was measured using the Karl Fischer coulometric method.

### 2.2. Experimental apparatus and procedure

The solubility and diffusion coefficients of fluorinated gases in ILs are determined using the same equipment described and validated in our previous publications [10,11]. It consists of a jacketed stirred tank reactor (Buchi, model Picoclave, 170 mL) equipped with a temperature and pressure transducer (Keller, series PAA-33X, 0.01% accuracy) and a Pt-100 temperature sensor connected to a cryothermostatic bath (Julabo, model F25-ME,  $\pm 0.01$  K). The absorption chamber is connected to a storage cylinder of known volume (146 mL) that is also equipped with a temperature and pressure transducer. Therefore, the total volume of the absorption system is 316 mL. Approximately 30 g ( $\pm 0.0001$  g) of IL are loaded and, before each experiment, the sample is degassed applying vacuum for a minimum of 6 h at 333 K. The solubility and diffusivity are obtained in a single experiment. To that end, the absorption process is initially allowed to proceed spontaneously for 20 min for diffusivity data calculation. Then, the stirring rate is set to 500 rpm and gas absorption proceeds until the equilibrium conditions are achieved, i.e., when pressure remains constant for more than 20 min.

The molar fraction of gas dissolved in the liquid phase is defined as:

$$x = \frac{n_{abs}}{n_l + n_{abs}} \quad (1)$$

where  $n_l$  are the moles of IL and  $n_{abs}$ , the total dissolved moles of refrigerant. To obtain an absorption isotherm, several absorption steps are performed sequentially increasing the gas feed pressure, and the amount of gas absorbed in each step ( $n_i$ ) is calculated with the isochoric saturation method:

$$n_i = \rho_{(i,s)} \cdot V_S + \rho_{(i-1,c)} \cdot (V_C - V_I) - \rho_{(i,eq)} \cdot (V_S + V_C - V_I) \quad (2)$$

where  $V_S$ ,  $V_C$ , and  $V_I$  are the storage cylinder, sorption chamber, and loaded IL volumes (L), and  $\rho_s$ ,  $\rho_c$ , and  $\rho_{eq}$  are the gas molar densities ( $\text{mol} \cdot \text{L}^{-1}$ ) in the storage cylinder, in the sorption chamber, and in the whole system at equilibrium conditions, respectively.



**Table 1**  
Chemicals used in this work.

Chemical	CAS No.	Supplier	Fraction purity	Purification method	Water content/ppm
[C <sub>2</sub> mim][dca]	370865-89-7	IoLiTec	>98 wt %	Vacuum drying	<100
[C <sub>4</sub> mim][dca]	448245-52-1	IoLiTec	>98 wt %	Vacuum drying	<100
[C <sub>2</sub> mim][SCN]	331717-63-6	IoLiTec	>98 wt %	Vacuum drying	<100
R32	75-10-5	Gas Servei, S.A.	>99.9 vol %		
R125	354-33-6	Gas Servei, S.A.	>99.9 vol %		
R134a	811-97-2	Air Products and Chemicals, Inc.	>99.8 vol %		
R1234yf	754-12-1	Air Products and Chemicals, Inc.	>99.9 vol %		
R1234ze(E)	29118-24-9	Gas Servei, S.A.	>99.9 vol %		

The experimental system is designed to have a much larger gas volume than IL volume to minimize the effect of the IL volumetric expansion during gas absorption. In this way, taking it into account the swelling effect results in a variation of molar fraction lower than the experimental uncertainty, even for systems with unfavorable volumetric expansion such as the one reported in this study or any of those reported by Aki et al. [33]. The molar densities are calculated from the pressure and temperature data using the cubic Peng–Robinson equation of state to account for deviations from ideal behavior. The dissolved moles are calculated as the moles absorbed in one step ( $n_i$ ) plus the moles dissolved in the previous steps ( $n_k$ ):

$$n_{abs} = n_i + \sum_{k=1}^{i-1} n_k \quad (3)$$

The diffusion coefficients at infinite dilution are calculated using the semi-infinite volume model [34]. The surface concentration is calculated as [35]:

$$C_{z=0} = \frac{\rho_{IL}}{M_{IL} \cdot \left(\frac{k_H}{\bar{f}} - 1\right)} \quad (4)$$

where  $\rho_{IL}$  and  $M_{IL}$  are the density and molar mass of the IL, respectively and  $k_H$  is the Henry's law constant (MPa) obtained from the solubility data:

$$k_H(T) = \lim_{x \rightarrow 0} \frac{\bar{f}(P, T)}{x} \quad (5)$$

where  $\bar{f}$  is the refrigerant fugacity (MPa) calculated using the Peng–Robinson equation of state. The surface concentration is used to calculate the initial concentration in the surface ( $C_{z=t=0}$ ) and the mass transfer coefficient ( $m$ ) from a linear fitting of the absorption data to Eq. (6):

$$C_{z=0} = C_{z=t=0} + m\sqrt{t} \quad (6)$$

Then, these parameters are used to calculate the accumulated dissolved moles per unit area ( $M_t$ ) by integrating the Fickian diffusion expression (Eq. (7)), and the diffusion coefficient is calculated from the slope of the linear fitting:

$$M_t = \int_0^t \left( D \left( \frac{\partial C}{\partial z} \right)_{z=0} \right) dt = \sqrt{D} \left( 2C_{z=t=0} \sqrt{\frac{t}{\pi}} - \frac{1}{2} m t \sqrt{\pi} \right) = \sqrt{D} \varepsilon \quad (7)$$

### 2.3. Modeling

The experimental solubility data are modeled using the nonrandom two-liquid activity-coefficient model (NRTL), which has been widely used to model the vapor-liquid equilibria (VLE) of fluorinated refrigerant gases in ILs. The experimental VLE can be described by:

$$y_i p \Phi = x_i \gamma_i p_i^s \quad (i \in \mathbb{Z} [1, N]) \quad (8)$$

where  $y_i$  and  $x_i$  are the molar fractions of the  $i$  species in the vapor and liquid phases, respectively, and  $\gamma_i$  and  $p_i^s$  are the activity coefficient and the vapor pressure, respectively.

The correction factor  $\Phi$  is calculated as

$$\Phi = \exp \left[ \frac{(B_i - V_i^L)(p - p_i^s)}{RT} \right] \quad (9)$$

where  $R$  is the ideal gas constant,  $B_i$  is the second virial coefficient and  $V_i^L$  is the saturated liquid molar volume.  $p_i^s$ ,  $B_i$  and  $V_i^L$  were calculated using the advanced equations of state based on Helmholtz energy formulations that are implemented in CoolProp 6.4.0 [36–41]. Substitution of Eq. (9) in Eq. (8) leads to the following expression of the activity coefficients:

$$\gamma_1 = \frac{p}{x_1 p_1^s} \exp \left[ \frac{(B_1 - V_1^L)(p - p_1^s)}{RT} \right] \quad (10)$$

For a binary mixture, the NRTL activity coefficients are expressed according to Eq. (11):

$$\ln \gamma_1 = x_2^2 \left[ \tau_{21} \left( \frac{G_{21}}{x_1 + x_2 G_{21}} \right)^2 + \frac{\tau_{12} G_{12}}{(x_2 + x_1 G_{12})^2} \right] \quad (11)$$

where

$$G_{12} = \exp(-\alpha \tau_{12}), \quad G_{21} = \exp(-\alpha \tau_{21}) \quad (12)$$

$$\tau_{12} = \tau_{12}^0 + \frac{\tau_{12}^1}{T}, \quad \tau_{21} = \tau_{21}^0 + \frac{\tau_{21}^1}{T} \quad (13)$$

The parameter  $\alpha$  can be treated as an adjustable parameter, but it is usually assumed constant and equal to 0.2 for fluorocarbons, a convention that we followed for consistency with our previous works. Thus, only the temperature-dependent binary interaction parameters  $\tau_{12}$  and  $\tau_{21}$  are optimized in this work. In Eq. (13),  $\tau_{12}^1$  and  $\tau_{21}^1$  represent the excess free energy of Gibbs divided by the ideal gas constant, while  $\tau_{12}^0$  and  $\tau_{21}^0$  are used in this work to model systems with large deviations from the ideal behavior. The NRTL activity coefficients are modeled to fit the experimental activity coefficients using the average absolute relative deviation (AARD), and we also provide the deviation in pressure (AARD<sub>p</sub>).

$$AARD = \frac{100}{N} \sum_{i=1}^N \left| \frac{\gamma_{exp} - \gamma_{calc}}{\gamma_{exp}} \right| \quad (14)$$

$$AARD_p = \frac{100}{N} \sum_{i=1}^N \left| \frac{P_{exp} - P_{calc}}{P_{exp}} \right| \quad (15)$$

## 3. Results and discussion

### 3.1. Solubility

The experimental and modeling results for the solubility of R32, R125, R134a, R1234yf, and R1234ze(E) in the cyanide-based ILs at

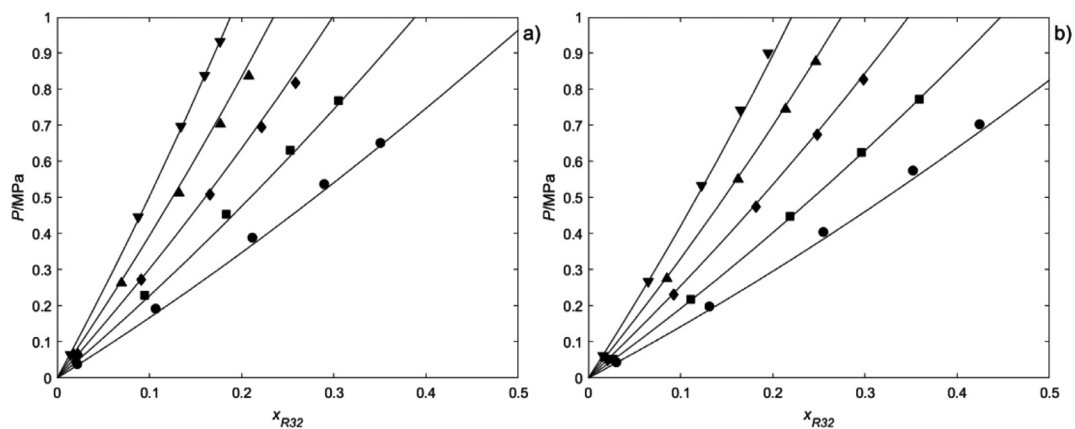


**Fig. 1.** Solubility of R32 in a)  $[C_2mim][dca]$  and b)  $[C_4mim][dca]$  at various temperatures: 283.15 (●), 293.15 (■), 303.15 (◆), 313.15 (▲) and 323.15 K (▼). Solid lines represent NRTL model calculations.

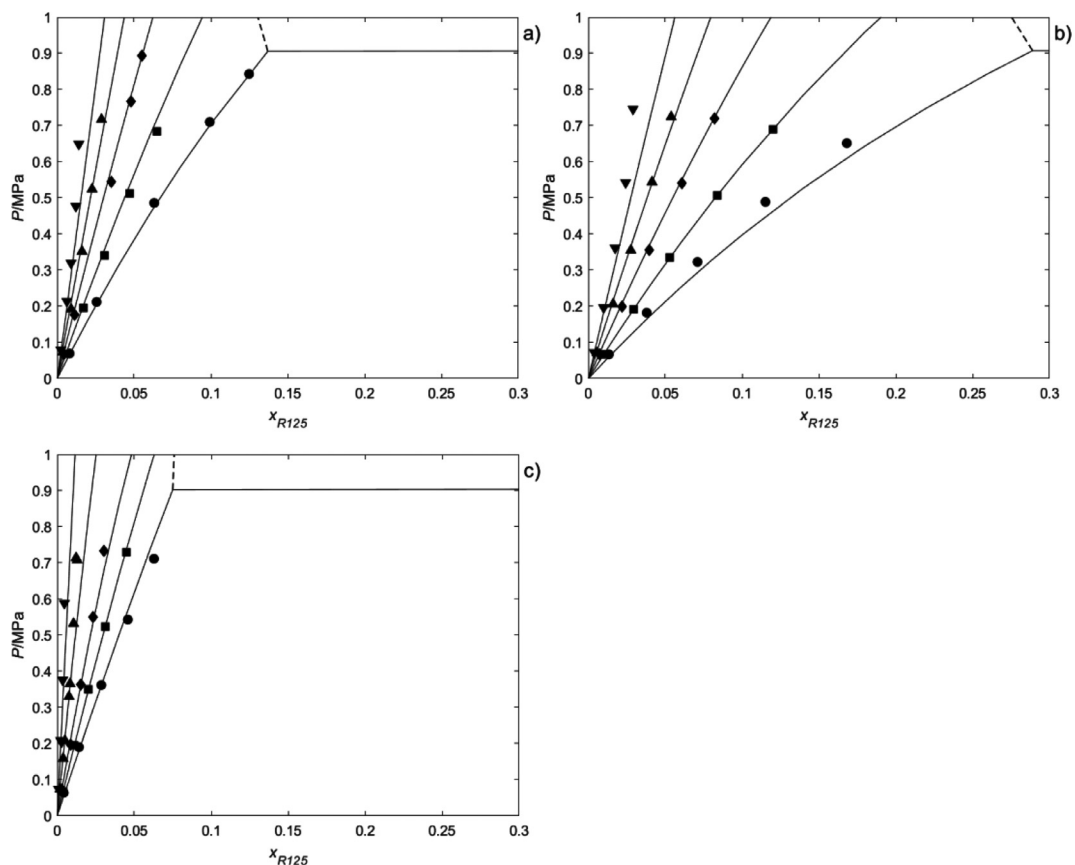


**Fig. 2.** Solubility of R125 in a)  $[C_2mim][dca]$ , b)  $[C_4mim][dca]$  and c)  $[C_2mim][SCN]$  at various temperatures: 283.15 (●), 293.15 (■), 303.15 (◆), 313.15 (▲) and 323.15 K (▼). Solid lines represent NRTL model calculations and dashed lines represent the NRTL VLE prediction.

temperatures ranging from 283.15 to 323.15 K and pressures up to 1 MPa are presented in Figs. 1-5. In addition, Tables S2 and S3 in the Supplementary Information present the solubility as a function of temperature and pressure together with the experimental uncertainty. As expected, the gas solubility increases as the pressure increases and the temperature decreases in all cases. The absorption capacity of  $[C_4mim][dca]$  is slightly higher than that of  $[C_2mim][dca]$  for every gas. The most soluble gas is R32, followed by R134a and R1234ze(E), whereas the least soluble gases are R125 and R1234yf. From this solubility trend, it is remarkable that the two HFO isomers have extremely different solubility in ILs, which

may be related to the differences in their dipole moments (1.27 and 2.48 D for R1234ze(E) and R1234yf, respectively [42]).

Figs. 1-5 also show the NRTL modeling of the vapor-liquid equilibria of refrigerant gases in ILs and the VLE region predicted with the NRTL model. The  $\alpha$  parameter was set at 0.2 for every absorption pair following previous works, and the rest of the NRTL parameters were optimized minimizing the AARD in the activity coefficients. The results are presented in Table 2, in which we also show the average deviation between the experimental and calculated pressure ( $AARD_p$ ). The overall AARD and  $AARD_p$  are 4.8% and 5.1%, respectively, showing that NRTL is an accurate model for the description of VLE of fluorinated refrigerant gases with ILs. It is

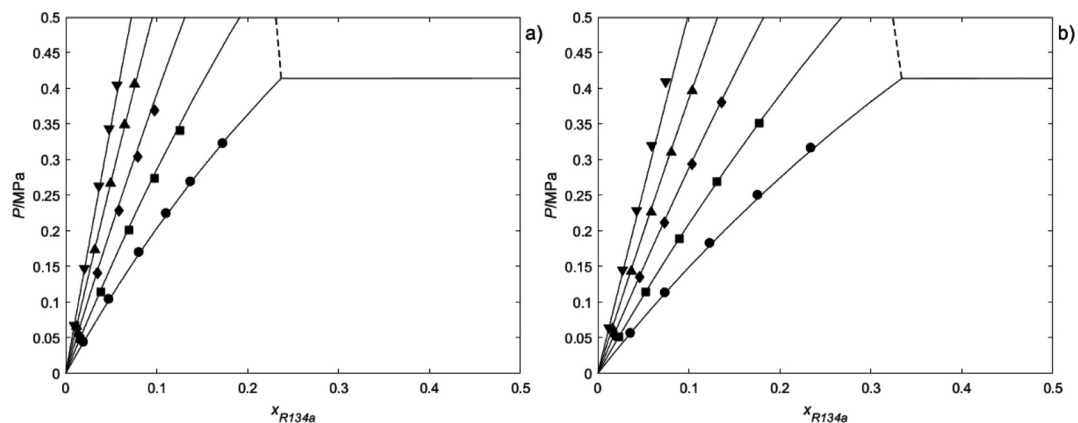


**Fig. 3.** Solubility of R134a in a) [C<sub>2</sub>mim][dca] and b) [C<sub>4</sub>mim][dca] at various temperatures: 283.15 (●), 293.15 (■), 303.15 (◆), 313.15 (▲) and 323.15 K (▼). Solid lines represent NRTL model calculations and dashed lines represent the NRTL VLE prediction.

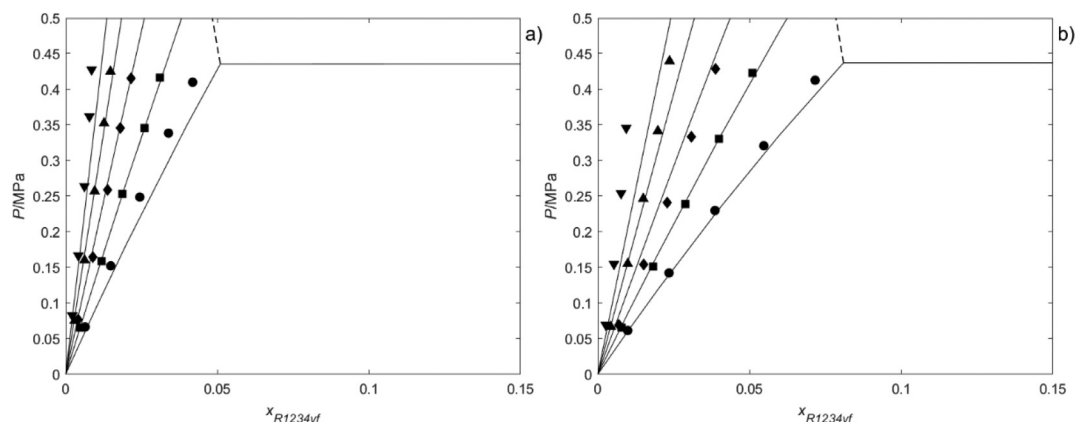


**Fig. 4.** Solubility of R1234yf in a) [C<sub>2</sub>mim][dca] and b) [C<sub>4</sub>mim][dca] at various temperatures: 283.15 (●), 293.15 (■), 303.15 (◆), 313.15 (▲) and 323.15 K (▼). Solid lines represent NRTL model calculations and dashed lines represent the NRTL VLE prediction.

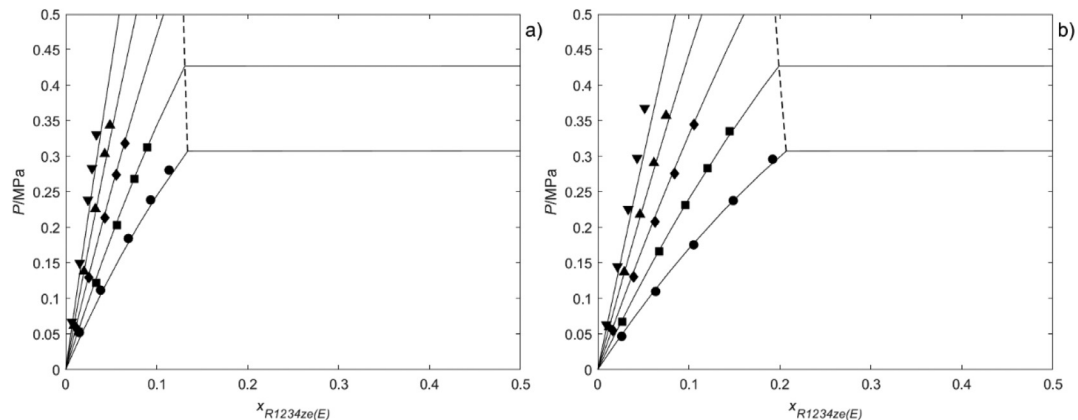


**Fig. 5.** Solubility of R1234ze(E) in a) [C<sub>2</sub>mim][dca] and b) [C<sub>4</sub>mim][dca] at various temperatures: 283.15 (●), 293.15 (■), 303.15 (◆), 313.15 (▲) and 323.15 K (▼). Solid lines represent NRTL model calculations and dashed lines represent the NRTL VLE prediction.

worth noticing that the NRTL model provides a better description of the VLE of highly soluble gases such as R32, R134a and R1234ze(E). Accordingly, only two parameters ( $\tau_{12}^1$  and  $\tau_{21}^1$ ) were used to model the equilibrium of these gases, while the least soluble gases (R125 and R1234yf) required the fitting of the additional parameters  $\tau_{12}^0$  and  $\tau_{21}^0$ .

Fig. 6 shows the Henry's law constants for the absorption of fluorinated gases in the cyanide anion-based ILs at 303.15 K. As previously noted, the solubility of R32, R134a, and R1234ze(E) is much higher than the solubility of R125 and R1234yf. Regarding

the influence of the IL chemical structure, the Henry's law constants decrease, as expected, with increasing IL molar volume, that is, the solubility is higher in [C<sub>4</sub>mim][dca] than in [C<sub>2</sub>mim][dca], and lower in the [SCN]<sup>-</sup> IL. Additionally, all the Henry's law constants at every temperature and the enthalpies and entropies at infinite dilution calculated using the van't Hoff equation are listed in Table S4 and Table S5, respectively, of the Supplementary Information.

$$\Delta H_{sol} = R \left( \frac{\partial \ln k_H}{\partial (1/T)} \right)_p \quad (16)$$

**Table 2**  
NRTL model parameters for the absorption of fluorinated gases in [dca]<sup>-</sup> ILs.

System	$\tau_{12}^0$	$\tau_{12}^1/K$	$\tau_{21}^0$	$\tau_{21}^1/K$	AARD/%	AARD <sub>p</sub> /%
R32 + [C <sub>2</sub> mim][dca]	0	4524.4	0	-27.312	3.10	3.27
R32 + [C <sub>4</sub> mim][dca]	0	5061.3	0	-29.548	1.94	2.05
R125 + [C <sub>2</sub> mim][dca]	2.015	2739.8	3.877	-731.37	6.56	6.96
R125 + [C <sub>4</sub> mim][dca]	-0.58	4144.8	3.84	-812.88	5.64	6.00
R125 + [C <sub>2</sub> mim][SCN]	187.11	-51435	23.863	-6466.3	7.32	7.82
R134a + [C <sub>2</sub> mim][dca]	0	3322.5	0	198.32	1.98	2.08
R134a + [C <sub>4</sub> mim][dca]	0	3760.7	0	155.39	1.75	1.84
R1234yf + [C <sub>2</sub> mim][dca]	4.893	399.13	4.400	-843.39	6.32	6.70
R1234yf + [C <sub>4</sub> mim][dca]	10.127	-906.24	3.420	-671.41	9.77	10.21
R1234ze(E) + [C <sub>2</sub> mim][dca]	0	2848.5	0	286.69	4.66	4.86
R1234ze(E) + [C <sub>4</sub> mim][dca]	0	3136.7	0	206.22	4.08	4.32

**Table 3**  
Binary diffusion coefficients at infinite dilution ( $\cdot 10^{-10}$  m<sup>2</sup>·s<sup>-1</sup>) for refrigerants in [C<sub>2</sub>mim][dca] and [C<sub>4</sub>mim][dca].

T/K	R32	R125	R134a	R1234yf	R1234ze(E)
	[C <sub>2</sub> mim][dca]				
283.15	3.31 ± 0.06	1.2 ± 0.2	2.81 ± 0.09	2.4 ± 0.5	1.7 ± 0.1
293.15	4.67 ± 0.09	2.7 ± 0.3	4.10 ± 0.13	4.2 ± 0.5	3.5 ± 0.2
303.15	7.00 ± 0.14	4.4 ± 0.7	6.14 ± 0.26	6.4 ± 0.7	5.0 ± 0.3
313.15	10.16 ± 0.22	6.3 ± 0.8	10.10 ± 0.49	8.4 ± 1.1	8.9 ± 0.6
323.15	18.70 ± 0.49	12.4 ± 1.4	15.31 ± 0.75	14 ± 2.6	14.9 ± 1
	[C <sub>4</sub> mim][dca]				
283.15	1.65 ± 0.05	0.8 ± 0.1	1.09 ± 0.05	1.5 ± 0.3	1.25 ± 0.05
293.15	2.99 ± 0.07	1.2 ± 0.2	1.56 ± 0.07	2.2 ± 0.3	2.28 ± 0.08
303.15	4.00 ± 0.09	3.3 ± 0.4	2.38 ± 0.12	2.7 ± 0.5	3.40 ± 0.14
313.15	7.57 ± 0.16	5.2 ± 0.6	4.75 ± 0.19	3.3 ± 0.6	5.85 ± 0.24
323.15	12.35 ± 0.44	10.5 ± 1.4	8.25 ± 0.46	4.9 ± 0.9	11.97 ± 0.56

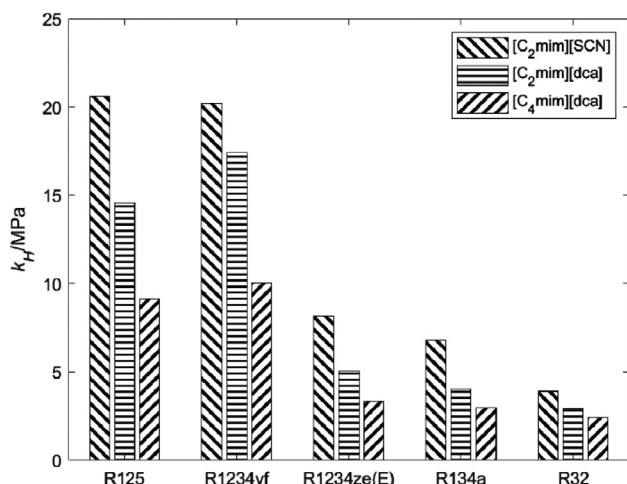


**Fig. 6.** Henry's law constants for the studied systems at 303.15 K. Values for [SCN]<sup>-</sup> from reference [11].

$$\Delta S_{sol} = -R \left( \frac{\partial \ln k_H}{\partial \ln T} \right)_p \quad (17)$$

### 3.2. Diffusivity

The diffusion coefficients at infinite dilution were calculated applying the semi-infinite volume method [34]. The diffusion coefficients, compiled in Table 3 are very similar for all gases and relatively high (in the range from  $10^{-10}$  to  $10^{-9}$  m<sup>2</sup>·s<sup>-1</sup>) compared to those found in ILs with anions such as [BF<sub>4</sub>]<sup>-</sup>, [OTf]<sup>-</sup>, and [Tf<sub>2</sub>N]<sup>-</sup> [10,35], which is consistent with the low viscosity of the cyanide-based ILs. For each gas, the diffusivity is higher in [C<sub>2</sub>mim][dca] than in [C<sub>4</sub>mim][dca], which may also be attributed

to the viscosity difference; despite being a very fluid IL, the viscosity of [C<sub>4</sub>mim][dca] is twice that of [C<sub>2</sub>mim][dca] (25.27 and 13.92 mPa·s, respectively, at 303.15 K [30,32]).

$$E_D = -R \left( \frac{\partial \ln D}{\partial (1/T)} \right)_p \quad (18)$$

### 3.3. Separation analysis

This work focuses on measuring the VLE of refrigerant gases for the design of separation processes based on the selective absorption into ILs. The five fluorinated gases studied in this work are commonly blended in mixtures that are difficult to separate. Here, we focus our attention on three systems of interest formed by the mixture of (1) R32 + R125 (R410 blend), (2) R32 + R1234yf (R454 blend), and (3) R134a + R1234yf (R513 blend). Unfortunately, the refrigerants R134a and R1234ze(E) that form another system of interest (R450 blend) have very similar solubility in ILs (see Fig. 6) and therefore, this system is not further considered in this work. To that end, we modeled the vapor-liquid equilibria of mixtures of R32 + R125, R32 + R1234yf, and R134a + R1234yf using data available in the literature [3,5,6,43,44]. The resulting parameters of the NRTL model are compiled in Table S6 of the Supplementary Information. Then, we used the NRTL model to predict the phase equilibria of the ternary mixtures of R32 + R125, R32 + R1234yf, and R134a + R1234yf with each IL. The compositions of each constituent of the multicomponent systems are calculated using the following expression [45]:

$$\ln \gamma_i = \frac{\sum_j \tau_{ji} G_{ji} x_j}{\sum_k G_{ki} x_k} + \sum_j \left[ \frac{x_j G_{ij}}{\sum_k G_{kj} x_k} \left( \tau_{ij} - \frac{\sum_k x_k \tau_{kj} G_{kj}}{\sum_k G_{kj} x_k} \right) \right] \quad (19)$$

Once predicted the phase equilibria of the ternary mixtures, which are showed in Fig. 7 at 303 K and 5 bar for R32 + R125 and in Figure S1 and S2 in the Supplementary Information for the other mixtures, we solved the mass balance for an isothermal flash

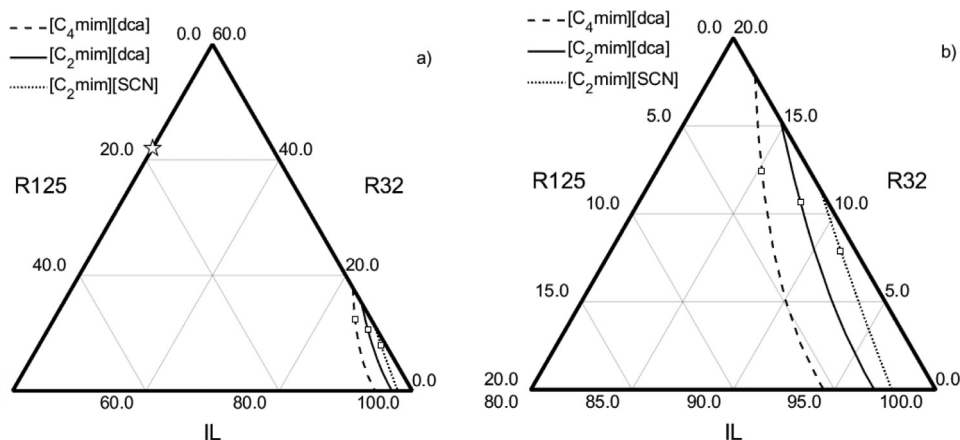


**Fig. 7.** Predicted equilibrium ternary mixtures at 303 K and 5 bar for the mixture of R32 and R125 (70:30 in moles) with the ILs  $[C_2mim][dca]$ ,  $[C_4mim][dca]$ , and  $[C_2mim][SCN]$ . In a), the star represents the feed composition of the system, IL:R32:R125 feed ratio equal to 0.4:0.42:0.18, and b) zooms in the equilibrium lines. The hollow squares represent the liquid composition of an isothermal flash outlet stream for each IL.

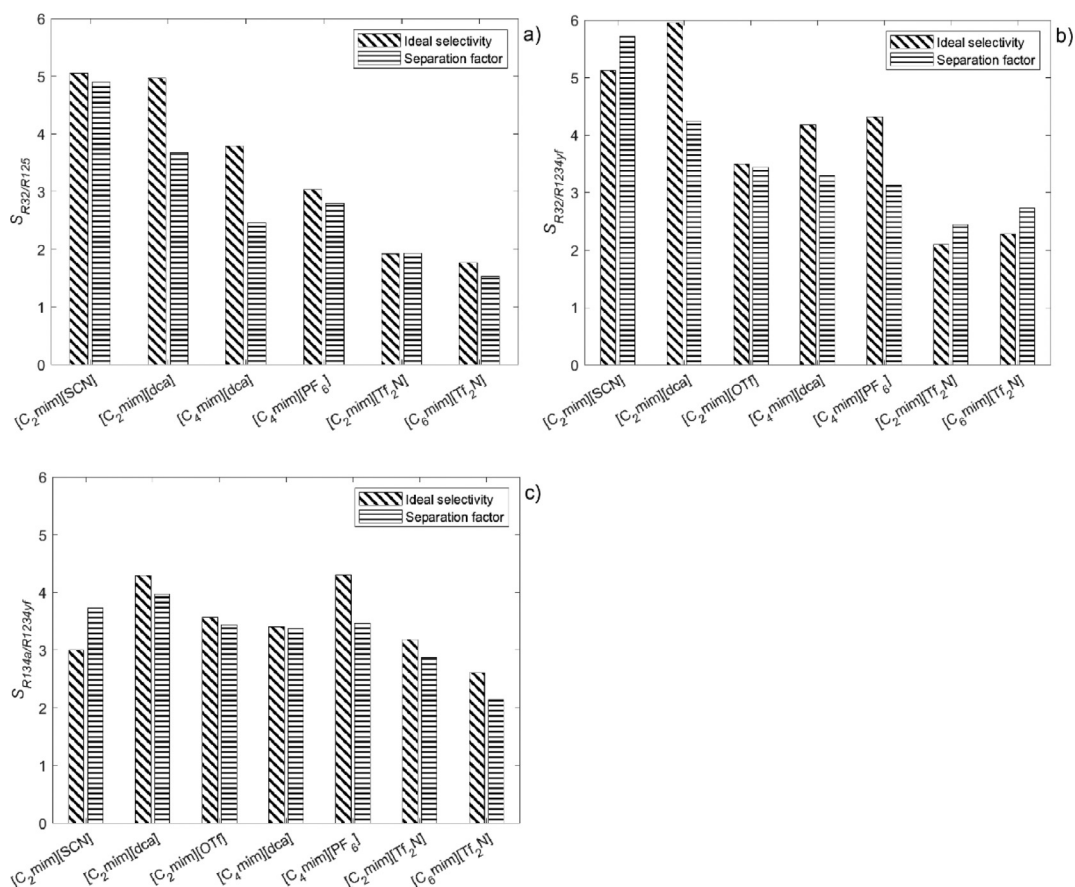


**Fig. 8.** Ideal selectivity and separation factor from a flash at 303 K and 5 bar for the separation of mixtures of a) R32 + R125 (70:30 vol %), b) R32 + R1234yf (80:20 vol %), and c) R134a + R1234yf (50:50 vol %). The IL to gas feed ratio is 2:3 in moles.

operating at 5 bar applying the Rachford-Rice equation [25]. To this purpose, we fixed the feed ratio of the IL to the gas mixture to 2:3 in moles. Additionally, the molar composition of the gas feed was set to 70:30 for R32/R125 (approximately the composition of R410A commercial mixture), 50:50 for the R134a/R1234yf (i.e., the azeotropic composition), and 80:20 for R32/R1234yf (i.e., the approximate composition at which the vapor and liquid equilibrium shows pinch behavior). The results of the equilibrium liquid phase composition of the flash outlet stream are also depicted in Fig. 7 (hollow squares) for each system.

Finally, the separation factor was calculated (Eq. (20)) and compared to the non-competitive ideal solubility selectivity in Fig. 8, which also includes the results calculated for other common ILs, namely,  $[C_2mim][OTf]$ ,  $[C_2mim][Tf_2N]$ ,  $[C_4mim][PF_6]$ , and  $[C_6mim][Tf_2N]$ . For these systems, the experimental data were compiled from the literature [10–12,16,23,46–52] and the NRTL parameters used are provided in Table S7 of the Supplementary Information. The ideal selectivity was obtained as the ratio of the Henry's law constants, while the separation factor was calculated from the equilibrium molar fraction of the two refrigerants (1 and



2) in the vapor ( $y_i$ ) and liquid ( $x_i$ ) streams abandoning the flash according to the expression:

$$SF_{1/2} = \frac{y_2/x_2}{y_1/x_1} \quad (20)$$

As can be seen in Fig. 8, the ideal solubility selectivity calculated at infinite dilution can be used as a simple screening tool for the selection of an IL candidate, but the competitive separation factor calculated at higher pressures may slightly differ from the calculated ideal selectivity, as the absorption isotherms do not show a linear behavior. Interestingly, the cyanide anion-based ILs yield the best separation factors for the three mixtures studied, for instance, [C<sub>2</sub>mim][SCN] presents a separation factor of almost 5 for the separation of R410A and [C<sub>2</sub>mim][dca] separates R32 and R134a from R1234yf with a separation factor of 4. Therefore, the combination of a separation factor higher than other ILs and their lower viscosities make cyanide-based ILs suitable for the design of separation processes based on solubility differences, which should be the next step towards the separation and recovery of fluorinated refrigerant gases.

#### 4. Conclusions

This article presents the experimental solubility and diffusivity of HFCs R32, R125 and R134a, and HFOs R1234yf and R1234ze(E) in ILs containing cyanide in the anion. Moreover, the VLE are modeled using the NRTL model with two to four adjustable parameters and deviations lower than 10% in activity coefficients. Henry's law constants are calculated, and it is observed that the solubility of R125 and R1234yf are much lower than the solubility of the other three gases, which is beneficial to separate these gases from common refrigerant gas mixtures (e.g., R410A and R454B blends) by preferential absorption of the more soluble gases R32 and R134a. The diffusion coefficients of refrigerant gases in ILs are higher in [C<sub>2</sub>mim][dca] than in [C<sub>4</sub>mim][dca], which is related to the lower viscosity of the first one, and the diffusion coefficients in both of them are high compared to other ILs previously studied such as [C<sub>6</sub>mim][BF<sub>4</sub>] and [C<sub>6</sub>mim][OTf]. Finally, the ideal selectivity and the separation factor in a flash separator were calculated showing that the results are promising to separate mixtures of hydrofluorocarbon and hydrofluoroolefin refrigerant gases. However, the separation of R1234ze(E) from R134a by means of gas-liquid absorption is still difficult because the solubility of R1234ze(E) in ILs is much higher than that of its isomer R1234yf.

#### Declaration of Competing Interest

The authors declare that they have no known competing financial interests or personal relationships that could have appeared to influence the work reported in this paper.

#### CRedit authorship contribution statement

**Salvador Asensio-Delgado:** Methodology, Investigation, Validation, Formal analysis, Writing – original draft. **Miguel Viar:** Investigation. **Fernando Pardo:** Investigation. **Gabriel Zarca:** Conceptualization, Methodology, Writing – review & editing, Funding acquisition, Project administration. **Ane Urriaga:** Supervision, Conceptualization, Funding acquisition, Writing – review & editing.

#### Acknowledgements

The authors fully acknowledge the financial support received from Project KET4F-Gas-SOE2/P1/P0823, which is co-financed by the European Regional Development Fund within the framework of Interreg Sudoe Programme, and project PID2019-105827RB-I00 –

Agencia Estatal de Investigación, Spain. S. A-D. and F.P acknowledge the FPU grant (18/03939) and the post-doctoral fellowship (FJCI-2017-32884 Juan de la Cierva Formación), respectively, awarded by the Spanish Ministry of Science and Innovation. M.V. acknowledges the Collaboration Grant awarded by the Spanish Ministry of Education and Professional Formation.

#### Supplementary materials

Supplementary material associated with this article can be found, in the online version, at doi:10.1016/j.fluid.2021.113210.

#### References

- [1] M.O. McLinden, M.L. Huber, (R)Evolution of refrigerants, *J. Chem. Eng. Data* 65 (2020) 4176–4193, doi:10.1021/acs.jced.0c00338.
- [2] M.O. McLinden, C.J. Seaton, A. Pearson, New refrigerants and system configurations for vapor-compression refrigeration, *Science* 370 (2020) 791–796, doi:10.1126/science.abe3692.
- [3] T. Kamiaka, C. Dang, E. Hihara, Vapor-liquid equilibrium measurements for binary mixtures of R1234yf with R32, R125, and R134a, *Int. J. Refrig.* 36 (2013) 965–971, doi:10.1016/j.ijrefrig.2012.08.016.
- [4] L. Kou, Z. Yang, X. Tang, W. Zhang, J. Lu, Experimental measurements and correlation of isothermal vapor-liquid equilibria for HFC-32 + HFO-1234ze(E) and HFC-134a + HFO-1234ze(E) binary systems, *J. Chem. Thermodyn.* 139 (2019) 105798, doi:10.1016/j.jct.2019.04.020.
- [5] Y. Higashi, Vapor-liquid equilibrium, coexistence curve, and critical locus for difluoromethane + pentafluoroethane (R-32 + R-125), *J. Chem. Eng. Data* 42 (1997) 1269–1273, doi:10.1021/je9701083.
- [6] M. Kobayashi, H. Nishiumi, Vapor-liquid equilibria for the pure, binary and ternary systems containing HFC32, HFC125 and HFC134a, *Fluid Phase Equilib.* 144 (1998) 191–202, doi:10.1016/S0378-3812(97)00257-4.
- [7] G. Zarca, A. Urriaga, I. Ortiz, P. Cañizares, M.A. Rodrigo, Carbon monoxide reactive separation with basic 1-hexyl-3-methylimidazolium chlorocuprate (I) ionic liquid : Electrochemical determination of mass transport properties, *Sep. Purif. Technol.* 141 (2015) 31–37, doi:10.1016/j.seppur.2014.11.027.
- [8] B. Wang, L. Qin, T. Mu, Z. Xue, G. Gao, Are ionic liquids chemically stable? *Chem. Rev.* 117 (2017) 7113–7131, doi:10.1021/acs.chemrev.6b00594.
- [9] A. Podgoršek, J. Jacquemin, A.A.H. Pádua, M.F. Costa Gomes, Mixing enthalpy for binary mixtures containing ionic liquids, *Chem. Rev.* 116 (2016) 6075–6106, doi:10.1021/acs.chemrev.5b00379.
- [10] S. Asensio-Delgado, F. Pardo, G. Zarca, A. Urriaga, Vapor-liquid equilibria and diffusion coefficients of difluoromethane, 1,1,2-tetrafluoroethane, and 2,3,3,3-tetrafluoropropene in low-viscosity ionic liquids, *J. Chem. Eng. Data* 65 (2020) 4242–4251, doi:10.1021/acs.jced.0c00224.
- [11] S. Asensio-Delgado, F. Pardo, G. Zarca, A. Urriaga, Enhanced absorption separation of hydrofluorocarbon/hydrofluoroolefin refrigerant blends using ionic liquids, *Sep. Purif. Technol.* 249 (2020) 117136, doi:10.1016/j.seppur.2020.117136.
- [12] X. Liu, M. He, N. Lv, X. Qi, C. Su, Vapor-liquid equilibrium of three hydrofluorocarbons with [HMIM][TF<sub>2</sub>N], *J. Chem. Eng. Data* 60 (2015) 1354–1361, doi:10.1021/je501069b.
- [13] M.B. Shiflett, A. Yokozeki, Vapor-liquid-liquid equilibria of hydrofluorocarbons + 1-butyl-3-methylimidazolium hexafluorophosphate, *J. Chem. Eng. Data* 51 (2006) 1931–1939, doi:10.1021/je060275f.
- [14] M.B. Shiflett, A. Yokozeki, Gaseous absorption of fluoromethane, fluoroethane, and 1,1,2,2-tetrafluoroethane in 1-butyl-3-methylimidazolium hexafluorophosphate, *Ind. Eng. Chem. Res.* 45 (2006) 6375–6382, doi:10.1021/je060192s.
- [15] M.B. Shiflett, M.A. Harmer, C.P. Junk, A. Yokozeki, Solubility and diffusivity of 1,1,1,2-tetrafluoroethane in room-temperature ionic liquids, *Fluid Phase Equilib.* 242 (2006) 220–232, doi:10.1016/j.fluid.2006.01.026.
- [16] M.B. Shiflett, A. Yokozeki, Solubility differences of halocarbon isomers in ionic liquid [emim][TF<sub>2</sub>N], *J. Chem. Eng. Data* 52 (2007) 2007–2015, doi:10.1021/je700295e.
- [17] D.L. Minnick, M.B. Shiflett, Solubility and diffusivity of bromodifluoromethane (Halon-1201) in imidazolium ionic liquids: [C<sub>2</sub>C<sub>1</sub>m][TF<sub>2</sub>N], [C<sub>4</sub>C<sub>1</sub>m][BF<sub>4</sub>], and [C<sub>4</sub>C<sub>1</sub>m][PF<sub>6</sub>], *J. Chem. Eng. Data* 65 (2020) 3277–3286, doi:10.1021/acs.jced.0c00022.
- [18] D.L. Minnick, M.B. Shiflett, Solubility and diffusivity of chlorodifluoromethane in imidazolium ionic liquids: [emim][TF<sub>2</sub>N], [bmim][BF<sub>4</sub>], [bmim][PF<sub>6</sub>], and [emim][TFES], *Ind. Eng. Chem. Res.* 58 (2019) 11072–11081, doi:10.1021/acs.iecr.9b02419.
- [19] Y. Sun, Y. Zhang, X. Wang, J.M. Prausnitz, L. Jin, Gaseous absorption of 2,3,3,3-tetrafluoroprop-1-ene in three imidazolium-based ionic liquids, *Fluid Phase Equilib.* 450 (2017) 65–74, doi:10.1016/j.fluid.2017.07.013.
- [20] J.E. Sosa, R.P.P.L. Ribeiro, P.J. Castro, J.P.B. Mota, J.M.M. Araújo, A.B. Pereira, Absorption of fluorinated greenhouse gases using fluorinated ionic liquids, *Ind. Eng. Chem. Res.* 58 (2019) 20769–20778, doi:10.1021/acs.iecr.9b04648.
- [21] L.F. Lepre, D. Andre, S. Denis-Quanquin, A. Gautier, A.A.H. Pádua, M.F. Costa Gomes, Ionic liquids can enable the recycling of fluorinated greenhouse gases, *ACS Sustain. Chem. Eng.* 7 (2019) 16900–16906, doi:10.1021/acssuschemeng.9b04214.
- [22] L.F. Lepre, L. Pison, I. Otero, A. Gautier, J. Dévény, P. Husson, A.A.H. Pádua, M.F. Costa Gomes, Using hydrogenated and perfluorinated gases to probe the

- interactions and structure of fluorinated ionic liquids, *Phys. Chem. Chem. Phys.* 21 (2019) 8865–8873, doi:[10.1039/c9cp00593e](https://doi.org/10.1039/c9cp00593e).
- [23] Y. Zhang, J. Yin, X. Wang, Vapor-liquid equilibrium of 2,3,3,3-tetrafluoroprop-1-ene with 1-butyl-3-methylimidazolium hexafluorophosphate, 1-hexyl-3-methylimidazolium hexafluorophosphate, and 1-octyl-3-methylimidazolium hexafluorophosphate, *J. Mol. Liq.* 260 (2018) 203–208, doi:[10.1016/j.molliq.2018.03.112](https://doi.org/10.1016/j.molliq.2018.03.112).
- [24] X. Liu, Z. Ye, L. Bai, M. He, Performance comparison of two absorption-compression hybrid refrigeration systems using R1234yf/ionic liquid as working pair, *Energy Convers. Manag.* 181 (2019) 319–330, doi:[10.1016/j.enconman.2018.12.030](https://doi.org/10.1016/j.enconman.2018.12.030).
- [25] S. Asensio-Delgado, D. Jovell, G. Zarca, A. Urriaga, F. Llovel, Thermodynamic and process modeling of the recovery of R410A compounds with ionic liquids, *Int. J. Refrig.* 118 (2020) 365–375, doi:[10.1016/j.jrefrig.2020.04.013](https://doi.org/10.1016/j.jrefrig.2020.04.013).
- [26] L. Moura, W. Darwich, C.C. Santini, M.F. Costa Gomes, Imidazolium-based ionic liquids with cyano groups for the selective absorption of ethane and ethylene, *Chem. Eng. J.* 280 (2015) 755–762, doi:[10.1016/j.cej.2015.06.034](https://doi.org/10.1016/j.cej.2015.06.034).
- [27] L.F. Lepre, J. Szala-Bilnik, L. Pison, M. Traïkia, A.A.H. Pádua, R.A. Ando, M.F. Costa Gomes, Can the tricyanomethanide anion improve CO<sub>2</sub> absorption by acetate-based ionic liquids? *Phys. Chem. Chem. Phys.* 19 (2017) 12431–12440, doi:[10.1039/c7cp01559c](https://doi.org/10.1039/c7cp01559c).
- [28] P.J. Carvalho, K.A. Kurnia, J.A.P. Coutinho, Dispelling some myths about the CO<sub>2</sub> solubility in ionic liquids, *Phys. Chem. Chem. Phys.* 18 (2016) 14757–14771, doi:[10.1039/c6cp01896c](https://doi.org/10.1039/c6cp01896c).
- [29] M. Ayuso, P. Navarro, A.M. Palma, M. Larriba, N. Delgado-Mellado, J. García, F. Rodríguez, J.A.P. Coutinho, P.J. Carvalho, Separation of benzene from methylcycloalkanes by extractive distillation with cyano-based ionic liquids: experimental and CPA EoS modelling, *Sep. Purif. Technol.* 234 (2020) 116128, doi:[10.1016/j.seppur.2019.116128](https://doi.org/10.1016/j.seppur.2019.116128).
- [30] M.G. Freire, A.R.R. Teles, M.A.A. Rocha, B. Schröder, C.M.S.S. Neves, P.J. Carvalho, D.V. Evtuguin, L.M.N.B.F. Santos, J.A.P. Coutinho, Thermophysical characterization of ionic liquids able to dissolve biomass, *J. Chem. Eng. Data.* 56 (2011) 4813–4822, doi:[10.1021/jc200790q](https://doi.org/10.1021/jc200790q).
- [31] C.A. Nieto de Castro, E. Langa, A.L. Morais, M.L. Matos Lopes, M.J.V. Lourenço, F.J.V. Santos, M.S.C.S. Santos, J.N. Canongia Lopes, H.I.M. Veiga, M. Macatrão, J.M.S.S. Esperança, C.S. Marques, L.P.N. Rebelo, C.A.M. Afonso, Studies on the density, heat capacity, surface tension and infinite dilution diffusion with the ionic liquids [C4mim][NTf<sub>2</sub>], [C4mim][dca], [C2mim][EtOSO<sub>3</sub>] and [Aliquat][dca], *Fluid Phase Equilib.* 294 (2010) 157–179, doi:[10.1016/j.fluid.2010.03.010](https://doi.org/10.1016/j.fluid.2010.03.010).
- [32] C.M.S.S. Neves, K.A. Kurnia, J.A.P. Coutinho, I.M. Marrucho, J.N. Canongia Lopes, M.G. Freire, L.P.N. Rebelo, Systematic study of the thermophysical properties of imidazolium-based ionic liquids with cyano-functionalized anions, *J. Phys. Chem. B.* 117 (2013) 10271–10283, doi:[10.1021/jp405913b](https://doi.org/10.1021/jp405913b).
- [33] S.N.V.K. Aki, B.R. Mellein, E.M. Saurer, J.F. Brennecke, High-pressure phase behavior of carbon dioxide with imidazolium-based ionic liquids, *J. Phys. Chem. B.* 108 (2004) 20355–20365, doi:[10.1021/jc8000443](https://doi.org/10.1021/jc8000443).
- [34] D. Camper, C. Becker, C. Koval, R.D. Noble, Diffusion and solubility measurements in room temperature ionic liquids, *Ind. Eng. Chem. Res.* 45 (2006) 445–450, doi:[10.1021/ie0506668](https://doi.org/10.1021/ie0506668).
- [35] M. He, S. Peng, X. Liu, P. Pan, Y. He, Diffusion coefficients and Henry's constants of hydrofluorocarbons in [HMIM][Tf<sub>2</sub>N], [HMIM][TfO], and [HMIM][BF<sub>4</sub>], *J. Chem. Thermodyn.* 112 (2017) 43–51, doi:[10.1016/j.jct.2017.04.009](https://doi.org/10.1016/j.jct.2017.04.009).
- [36] I.H. Bell, J. Wronski, S. Quoilin, V. Lemort, Pure and Pseudo-pure Fluid Thermophysical Property Evaluation and the Open-Source Thermophysical Property Library CoolProp, *Ind. Eng. Chem. Res.* 53 (2014) 2498–2508, doi:[10.1021/ie4033999](https://doi.org/10.1021/ie4033999).
- [37] R. Tillner-Roth, A. Yokozeki, An international standard equation of state for difluoromethane (R-32) for temperatures from the triple point at 136.34 K to 435 K and pressures up to 70 MPa, *J. Phys. Chem. Ref. Data.* 26 (1997) 1273–1328, doi:[10.1063/1.556002](https://doi.org/10.1063/1.556002).
- [38] R. Tillner-Roth, H.D. Baehr, An International Standard Formulation for the Thermodynamic Properties of 1,1,1,2-Tetrafluoroethane (HFC-134a) for Temperatures from 170 K to 455 K and Pressures up to 70 MPa, *J. Phys. Chem. Ref. Data.* 23 (1994) 657–729, doi:[10.1063/1.555958](https://doi.org/10.1063/1.555958).
- [39] M. Richter, M.O. McLinden, E.W. Lemmon, Thermodynamic properties of 2,3,3,3-tetrafluoroprop-1-ene (R1234yf): Vapor pressure and p -  $\phi$  - T Measurements and an Equation of State, *J. Chem. Eng. Data.* 56 (2011) 3254–3264, doi:[10.1021/jc200369m](https://doi.org/10.1021/jc200369m).
- [40] E.W. Lemmon, R.T. Jacobsen, A new functional form and new fitting techniques for equations of state with application to pentafluoroethane (HFC-125), *J. Phys. Chem. Ref. Data.* 34 (2005) 69–108, doi:[10.1063/1.1797813](https://doi.org/10.1063/1.1797813).
- [41] M. Thol, E.W. Lemmon, Equation of State for the Thermodynamic Properties of trans-1,3,3,3-Tetrafluoropropene [R-1234ze(E)], *Int. J. Thermophys.* 37 (2016) 1–16, doi:[10.1007/s10765-016-2040-6](https://doi.org/10.1007/s10765-016-2040-6).
- [42] C.C. Sampson, M. Kamson, M.G. Hopkins, P.L. Stanwix, E.F. May, Dielectric permittivity, polarizability and dipole moment of refrigerants R1234ze(E) and R1234yf determined using a microwave re-entrant cavity resonator, *J. Chem. Thermodyn.* 128 (2019) 148–158, doi:[10.1016/j.jct.2018.07.011](https://doi.org/10.1016/j.jct.2018.07.011).
- [43] M.Y. Jung, C.N. Kim, Y.M. Park, J.S. Yoo, Vapor-Liquid Equilibria for the Difluoromethane (HFC-32) + Pentafluoroethane (HFC-125) System, *J. Chem. Eng. Data.* 46 (2001) 750–753.
- [44] X. Hu, T. Yang, X. Meng, S. Bi, J. Wu, Vapor liquid equilibrium measurements for difluoromethane (R32) + 2,3,3,3-tetrafluoroprop-1-ene (R1234yf) and fluoroethane (R161) + 2,3,3,3-tetrafluoroprop-1-ene (R1234yf), *Fluid Phase Equilib.* 438 (2017) 10–17, doi:[10.1016/j.fluid.2017.01.024](https://doi.org/10.1016/j.fluid.2017.01.024).
- [45] J.D. Seader, E.J. Henley, D.K. Roper, *Separation Process Principles*, 3rd ed, John Wiley & Sons, Ltd, New Jersey, USA, 2010.
- [46] W. Ren, A.M. Scurto, Phase equilibria of imidazolium ionic liquids and the refrigerant gas, 1,1,1,2-tetrafluoroethane (R-134a), *Fluid Phase Equilib.* 286 (2009) 1–7, doi:[10.1016/j.fluid.2009.07.007](https://doi.org/10.1016/j.fluid.2009.07.007).
- [47] X. Liu, L. Bai, S. Liu, M. He, Vapor-liquid equilibrium of R1234yf/[HMIM][Tf<sub>2</sub>N] and R1234ze (E)/[HMIM][Tf<sub>2</sub>N] working pairs for the absorption refrigeration cycle, *J. Chem. Eng. Data.* 61 (2016) 3952–3957, doi:[10.1021/acs.jced.6b00731](https://doi.org/10.1021/acs.jced.6b00731).
- [48] L. Dong, D. Zheng, G. Sun, X. Wu, Vapor-Liquid Equilibrium Measurements of Difluoromethane + [Emim]OTf, Difluoromethane + [Bmim]OTf, Difluoroethane + [Emim]OTf, and Difluoroethane + [Bmim]OTf Systems, *J. Chem. Eng. Data.* 56 (2011) 3663–3668, doi:[10.1021/jc2005566](https://doi.org/10.1021/jc2005566).
- [49] M.B. Shiflett, M.A. Harmer, C.P. Junk, A. Yokozeki, Solubility and diffusivity of difluoromethane in room-temperature ionic liquids, *J. Chem. Eng. Data.* 51 (2006) 483–495, doi:[10.1021/jc050386z](https://doi.org/10.1021/jc050386z).
- [50] M.B. Shiflett, A. Yokozeki, Binary vapor-liquid and vapor-liquid-liquid equilibria of hydrofluorocarbons (HFC-125 and HFC-143a) and hydrofluoroethers (HFE-125 and HFE-143a) with ionic liquid [emim][Tf<sub>2</sub>N], *J. Chem. Eng. Data.* 53 (2008) 492–497, doi:[10.1021/jc700588d](https://doi.org/10.1021/jc700588d).
- [51] M.B. Shiflett, A. Yokozeki, Solubility and diffusivity of hydrofluorocarbons in room-temperature ionic liquids, *AIChE J.* 52 (2006) 1205–1219, doi:[10.1002/aic.10685](https://doi.org/10.1002/aic.10685).
- [52] A. Aghosseini, W. Ren, L.R. Weatherley, A.M. Scurto, Viscosity and self-diffusivity of ionic liquids with compressed hydrofluorocarbons: 1-Hexyl-3-methylimidazolium bis(trifluoromethylsulfonyl)amide and 1,1,1,2-tetrafluoroethane, *Fluid Phase Equilib.* 437 (2017) 34–42, doi:[10.1016/j.fluid.2016.11.022](https://doi.org/10.1016/j.fluid.2016.11.022).
- [53] Salvador Asensio-Delgado, Fernando Pardo, Gabriel Zarca, Ane Urriaga, Absorption separation of fluorinated refrigerant gases with ionic liquids: Equilibrium, mass transport, and process design, *Separation and Purification Technology* 276 (2021) 119363, doi:[10.1016/j.seppur.2021.119363](https://doi.org/10.1016/j.seppur.2021.119363).

## Supplementary Information

Gas solubility and diffusivity of hydrofluorocarbons and hydrofluoroolefins in cyanide-based ionic liquids for the separation of refrigerant mixtures

### Authors:

Salvador Asensio-Delgado, Miguel Viar-Fernandez, Fernando Pardo, Gabriel Zarca, Ane Urriaga\*

Department of Chemical and Biomolecular Engineering, Universidad de Cantabria,

Av. Los Castros 46, Santander 39005, Spain.

\*Corresponding author e-mail address: [urriaga@unican.es](mailto:urriaga@unican.es)



Table S1. Properties of the cyanide-based ILs. Density and viscosity at 303.15 K [1–3].

<b>Ionic liquid</b>	<b>Molar mass/g·mol<sup>-1</sup></b>	<b>Density/kg·m<sup>3</sup></b>	<b>Viscosity/mPa·s</b>
[C <sub>2</sub> mim][dca]	177.2	1100.6	13.92
[C <sub>4</sub> mim][dca]	205.3	1057.3	25.27
[C <sub>2</sub> mim][SCN]	169.2	1113.9	20.79

Table S2. Vapor-liquid equilibrium of HFCs in [C<sub>2</sub>mim][dca], [C<sub>4</sub>mim][dca], and [C<sub>2</sub>mim][SCN].

<b>T/K</b>	<b>p/MPa</b>	<b>x</b>	<b>u(x)</b>	<b>T/K</b>	<b>p/MPa</b>	<b>x</b>	<b>u(x)</b>
<i>R32 + [C<sub>2</sub>mim][dca]</i>							
283.15	0.0384	0.0216	0.0002	313.15	0.0653	0.0177	0.0003
	0.1920	0.1067	0.0004		0.2632	0.0697	0.0005
	0.3890	0.2116	0.0005		0.5123	0.1321	0.0006
	0.5374	0.2895	0.0006		0.7039	0.1768	0.0008
	0.6517	0.3505	0.0007		0.8369	0.2077	0.0010
293.15	0.0495	0.0205	0.0003	323.15	0.0651	0.0141	0.0003
	0.2296	0.0946	0.0004		0.4463	0.0877	0.0007
	0.4535	0.1832	0.0006		0.6975	0.1340	0.0008
	0.6317	0.2524	0.0007		0.8387	0.1598	0.0010
	0.7680	0.3049	0.0008		0.9329	0.1765	0.0014
303.15	0.0650	0.0223	0.0003				
	0.2717	0.0908	0.0005				
	0.5090	0.1659	0.0006				
	0.6946	0.2216	0.0007				
	0.8182	0.2587	0.0009				
<i>R125 + [C<sub>2</sub>mim][dca]</i>							
283.15	0.0694	0.0080	0.0003	313.15	0.0730	0.0035	0.0003
	0.2120	0.0256	0.0004		0.1922	0.0090	0.0004
	0.4859	0.0631	0.0007		0.3520	0.0161	0.0006
	0.7100	0.0992	0.0010		0.5241	0.0226	0.0009
	0.8429	0.1248	0.0013		0.7172	0.0288	0.0013
293.15	0.0693	0.0057	0.0003	323.15	0.0791	0.0024	0.0003
	0.1953	0.0171	0.0004		0.2139	0.0063	0.0004
	0.3413	0.0309	0.0006		0.3196	0.0090	0.0006
	0.5132	0.0472	0.0009		0.4771	0.0121	0.0009

<i>T/K</i>	<i>p/MPa</i>	<i>x</i>	<i>u(x)</i>	<i>T/K</i>	<i>p/MPa</i>	<i>x</i>	<i>u(x)</i>
	0.6848	0.0647	0.0012		0.6487	0.0140	0.0013
303.15	0.0679	0.0043	0.0003				
	0.1764	0.0114	0.0004				
	0.5441	0.0353	0.0009				
	0.7668	0.0481	0.0012				
	0.8940	0.0552	0.0016				
<i>R134a + [C<sub>2</sub>mim][dca]</i>							
283.15	0.0447	0.0192	0.0003	313.15	0.0658	0.0121	0.0003
	0.1049	0.0471	0.0004		0.1736	0.0321	0.0004
	0.1706	0.0801	0.0005		0.2669	0.0494	0.0006
	0.2252	0.1102	0.0006		0.3492	0.0648	0.0008
	0.2698	0.1368	0.0008		0.4061	0.0758	0.0011
	0.3235	0.1724	0.0011	323.15	0.0678	0.0094	0.0003
293.15	0.0489	0.0158	0.0003		0.1475	0.0205	0.0004
	0.1148	0.0385	0.0004		0.2631	0.0364	0.0006
	0.2012	0.0696	0.0005		0.3436	0.0477	0.0008
	0.2737	0.0976	0.0007		0.4049	0.0565	0.0011
	0.3409	0.1257	0.0009				
303.15	0.0556	0.0136	0.0003				
	0.1412	0.0354	0.0004				
	0.2288	0.0584	0.0005				
	0.3044	0.0793	0.0007				
	0.3695	0.0978	0.0010				
<i>R32 + [C<sub>4</sub>mim][dca]</i>							
283.15	0.0435	0.0303	0.0004	313.15	0.0558	0.0179	0.0004
	0.1984	0.1312	0.0006		0.2755	0.0852	0.0007
	0.4046	0.2547	0.0007		0.5507	0.1624	0.0010
	0.5749	0.3519	0.0008		0.7454	0.2138	0.0012
	0.7033	0.4242	0.0008		0.8768	0.2465	0.0016
293.15	0.0512	0.0271	0.0004	323.15	0.0617	0.0158	0.0004
	0.2173	0.1108	0.0006		0.2676	0.0649	0.0007
	0.4489	0.2186	0.0008		0.5335	0.1227	0.0010
	0.6261	0.2964	0.0009		0.7429	0.1649	0.0013

<i>T/K</i>	<i>p/MPa</i>	<i>x</i>	<i>u(x)</i>	<i>T/K</i>	<i>p/MPa</i>	<i>x</i>	<i>u(x)</i>
	0.7734	0.3588	0.0011		0.9008	0.1948	0.0017
303.15	0.0504	0.0213	0.0004				
	0.2305	0.0926	0.0007				
	0.4754	0.1819	0.0009				
	0.6748	0.2480	0.0010				
	0.8273	0.2980	0.0013				
<i>R125 + [C<sub>4</sub>mim][dca]</i>							
283.15	0.0670	0.0133	0.0004	313.15	0.0710	0.0055	0.0004
	0.1820	0.0380	0.0006		0.2059	0.0161	0.0007
	0.3227	0.0710	0.0009		0.3551	0.0276	0.0010
	0.4889	0.1152	0.0012		0.5437	0.0414	0.0015
	0.6515	0.1681	0.0015		0.7241	0.0538	0.0020
293.15	0.0677	0.0100	0.0004	323.15	0.0722	0.0038	0.0004
	0.1910	0.0293	0.0007		0.1962	0.0099	0.0007
	0.3340	0.0530	0.0009		0.3614	0.0174	0.0010
	0.5066	0.0837	0.0013		0.5423	0.0242	0.0015
	0.6890	0.1202	0.0017		0.7460	0.0290	0.0022
303.15	0.0674	0.0074	0.0004				
	0.1997	0.0221	0.0007				
	0.3548	0.0394	0.0010				
	0.5406	0.0610	0.0014				
	0.7190	0.0821	0.0019				
<i>R134a + [C<sub>4</sub>mim][dca]</i>							
283.15	0.0570	0.0356	0.0004	313.15	0.0630	0.0162	0.0004
	0.1140	0.0735	0.0005		0.1433	0.0370	0.0006
	0.1834	0.1228	0.0007		0.2263	0.0588	0.0008
	0.2510	0.1755	0.0009		0.3101	0.0809	0.0011
	0.3170	0.2337	0.0011		0.3968	0.1039	0.0015
293.15	0.0514	0.0230	0.0004	323.15	0.0644	0.0122	0.0004
	0.1146	0.0527	0.0006		0.1453	0.0273	0.0006
	0.1892	0.0896	0.0008		0.2289	0.0427	0.0009
	0.2695	0.1312	0.0010		0.3202	0.0592	0.0012
	0.3518	0.1771	0.0013		0.4095	0.0746	0.0016

$T/K$	$p/\text{MPa}$	$x$	$u(x)$	$T/K$	$p/\text{MPa}$	$x$	$u(x)$
303.15	0.0545	0.0182	0.0004				
	0.1354	0.0462	0.0006				
	0.2122	0.0735	0.0008				
	0.2937	0.1033	0.0011				
	0.3803	0.1358	0.0014				
<i>R125 + [C<sub>2</sub>mim][SCN]</i>							
283.15	0.0638	0.0042	0.0003	313.15	0.0734	0.0017	0.0003
	0.1900	0.0141	0.0004		0.1585	0.0038	0.0004
	0.3617	0.0286	0.0006		0.2082	0.0050	0.0004
	0.5431	0.0458	0.0009		0.3301	0.0076	0.0005
	0.7113	0.0628	0.0013		0.3653	0.0083	0.0007
293.15	0.0672	0.0036	0.0003		0.5321	0.0105	0.0010
	0.1951	0.0110	0.0004		0.7076	0.0129	0.0011
	0.3502	0.0203	0.0006		0.7138	0.0122	0.0014
	0.5239	0.0312	0.0009	323.15	0.0742	0.0008	0.0003
	0.7300	0.0447	0.0013		0.2088	0.0023	0.0004
303.15	0.0728	0.0027	0.0003		0.3759	0.0035	0.0007
	0.1977	0.0086	0.0004		0.5885	0.0046	0.0009
	0.3623	0.0154	0.0006				
	0.5500	0.0230	0.0009				
	0.7337	0.0302	0.0013				

Standard uncertainties are  $u(T) = 0.01$  K and  $u(p) = 0.0003$  MPa. The standard uncertainties for molar fraction,  $u(x)$ , are given in the table.

Table S3. Vapor-liquid equilibrium of HFOs in [C<sub>2</sub>mim][dca], and [C<sub>4</sub>mim][dca].

<i>T/K</i>	<i>p/MPa</i>	<i>x</i>	<i>u(x)</i>	<i>T/K</i>	<i>p/MPa</i>	<i>x</i>	<i>u(x)</i>
<i>R1234yf + [C<sub>2</sub>mim][dca]</i>							
283.15	0.0666	0.0064	0.0003	313.15	0.0753	0.0030	0.0003
	0.1523	0.0149	0.0004		0.1604	0.0062	0.0004
	0.2488	0.0245	0.0006		0.2571	0.0096	0.0006
	0.3387	0.0339	0.0008		0.3526	0.0127	0.0008
	0.4101	0.0419	0.0011		0.4250	0.0148	0.0011
293.15	0.0658	0.0048	0.0003	323.15	0.0826	0.0022	0.0003
	0.1586	0.0117	0.0004		0.1667	0.0042	0.0004
	0.2535	0.0188	0.0006		0.2640	0.0062	0.0006
	0.3456	0.0259	0.0008		0.3619	0.0078	0.0008
	0.4163	0.0312	0.0011		0.4277	0.0086	0.0012
303.15	0.0767	0.0041	0.0003				
	0.1643	0.0089	0.0004				
	0.2591	0.0138	0.0006				
	0.3456	0.0181	0.0008				
	0.4154	0.0215	0.0011				
<i>R1234ze(E) + [C<sub>2</sub>mim][dca]</i>							
283.15	0.0523	0.0150	0.0003	313.15	0.0620	0.0090	0.0003
	0.1119	0.0384	0.0004		0.1382	0.0202	0.0004
	0.1846	0.0689	0.0005		0.2261	0.0327	0.0005
	0.2388	0.0934	0.0007		0.3034	0.0429	0.0008
	0.2807	0.1137	0.0009		0.3438	0.0487	0.0011
293.15	0.0536	0.0144	0.0003	323.15	0.0672	0.0068	0.0003
	0.1224	0.0333	0.0004		0.1500	0.0155	0.0004
	0.2033	0.0565	0.0005		0.2388	0.0245	0.0006
	0.2684	0.0759	0.0007		0.2833	0.0290	0.0008
	0.3126	0.0895	0.0010		0.3308	0.0338	0.0011
303.15	0.0586	0.0112	0.0003				
	0.1298	0.0255	0.0004				
	0.2138	0.0428	0.0005				
	0.2741	0.0554	0.0007				
	0.3181	0.0649	0.0010				
<i>R1234yf + [C<sub>4</sub>mim][dca]</i>							

<i>T</i> /K	<i>p</i> /MPa	<i>x</i>	<i>u</i> ( <i>x</i> )	<i>T</i> /K	<i>p</i> /MPa	<i>x</i>	<i>u</i> ( <i>x</i> )
283.15	0.0615	0.0099	0.0004	313.15	0.0668	0.0043	0.0004
	0.1424	0.0235	0.0006		0.1553	0.0099	0.0006
	0.2300	0.0386	0.0009		0.2465	0.0150	0.0009
	0.3209	0.0547	0.0012		0.3416	0.0198	0.0013
	0.4128	0.0717	0.0017		0.4397	0.0237	0.0018
293.15	0.0660	0.0080	0.0004	323.15	0.0696	0.0026	0.0004
	0.1511	0.0183	0.0006		0.1548	0.0053	0.0006
	0.2390	0.0288	0.0009		0.2540	0.0077	0.0009
	0.3310	0.0400	0.0013		0.3458	0.0094	0.0013
	0.4232	0.0510	0.0018				
303.15	0.0695	0.0070	0.0004				
	0.1545	0.0151	0.0006				
	0.2414	0.0228	0.0009				
	0.3333	0.0309	0.0013				
	0.4287	0.0388	0.0018				
<i>R1234ze(E) + [C<sub>4</sub>mim][dca]</i>							
283.15	0.0470	0.0263	0.0004	313.15	0.0599	0.0125	0.0004
	0.1100	0.0637	0.0006		0.1374	0.0292	0.0006
	0.1757	0.1054	0.0007		0.2182	0.0464	0.0008
	0.2378	0.1488	0.0009		0.2908	0.0617	0.0012
	0.2961	0.1922	0.0012		0.3575	0.0751	0.0016
293.15	0.0676	0.0268	0.0004	323.15	0.0635	0.0095	0.0004
	0.1669	0.0678	0.0006		0.1451	0.0217	0.0006
	0.2312	0.0963	0.0008		0.2258	0.0334	0.0009
	0.2838	0.1207	0.0011		0.2977	0.0433	0.0012
	0.3353	0.1449	0.0014		0.3679	0.0515	0.0017
303.15	0.0555	0.0166	0.0004				
	0.1310	0.0395	0.0006				
	0.2081	0.0631	0.0008				
	0.2764	0.0845	0.0011				
	0.3446	0.1057	0.0015				

Standard uncertainties are  $u(T) = 0.01$  K and  $u(p) = 0.0003$  MPa. The standard uncertainties for molar fraction,  $u(x)$ , are given in the table.

Table S4. Henry's law constant (MPa) for the absorption of refrigerant gases in ILs

	<b>R125</b>	<b>R32</b>	<b>R134a</b>	<b>R1234yf</b>	<b>R1234ze(E)</b>
<i>T/K</i>	<b>[C<sub>2</sub>mim][dca]</b>				
283.15	8.27 ± 0.08	1.81 ± 0.02	2.276 ± 0.011	10.59 ± 0.11	2.663 ± 0.006
293.15	11.14 ± 0.10	2.41 ± 0.02	3.057 ± 0.009	13.55 ± 0.13	3.768 ± 0.01
303.15	14.55 ± 0.36	2.93 ± 0.02	4.061 ± 0.013	17.42 ± 0.37	5.073 ± 0.021
313.15	18.86 ± 0.78	3.66 ± 0.03	5.451 ± 0.039	23.01 ± 0.28	6.516 ± 0.125
323.15	21.85 ± 4.73	5.03 ± 0.02	7.235 ± 0.102	27.01 ± 3.71	9.413 ± 0.055
	<b>[C<sub>4</sub>mim][dca]</b>				
283.15	4.83 ± 0.04	1.51 ± 0.03	1.614 ± 0.001	6.051 ± 0.009	1.78 ± 0.02
293.15	6.59 ± 0.03	1.92 ± 0.02	2.206 ± 0.007	8.248 ± 0.050	2.55 ± 0.03
303.15	9.12 ± 0.05	2.4 ± 0.03	2.946 ± 0.008	10.039 ± 0.149	3.33 ± 0.02
313.15	12.29 ± 0.14	3.1 ± 0.02	3.871 ± 0.011	12.998 ± 0.671	4.54 ± 0.05
323.15	15.96 ± 2.01	3.94 ± 0.02	5.188 ± 0.046	14.886 ± 0.939	6.06 ± 0.23
	<b>[C<sub>2</sub>mim][SCN]</b>				
283.15	12.9 ± 0.2				
293.15	17.6 ± 0.1				
303.15	20.6 ± 0.7				
313.15	28.4 ± 3.8				
323.15	41.8 ± 4.2				

Table S5. Solvation enthalpy, solvation entropy and activation energy of diffusion for the absorption of refrigerant gases in ILs

<b>IL</b>	<b>Gas</b>	<b><math>\Delta H_{sol}/\text{kJ}\cdot\text{mol}^{-1}</math></b>	<b><math>\Delta S_{sol}/\text{J}\cdot\text{mol}^{-1}\cdot\text{K}^{-1}</math></b>
<b>[C<sub>2</sub>mim][dca]</b>	R125	-20.285 ± 0.003	-69 ± 2
	R32	-19.739 ± 0.016	-64 ± 5
	R134a	-21.463 ± 0.006	-72 ± 1
	R1234yf	-19.040 ± 0.007	-64 ± 2
	R1234ze(E)	-23.722 ± 0.006	-79 ± 2
<b>[C<sub>4</sub>mim][dca]</b>	R125	-23.120 ± 0.006	-78 ± 1
	R32	-18.848 ± 0.006	-62 ± 1
	R134a	-21.648 ± 0.003	-73 ± 1
	R1234yf	-19.528 ± 0.013	-67 ± 5
	R1234ze(E)	-22.700 ± 0.008	-76 ± 3
<b>[C<sub>2</sub>mim][SCN]</b>	R125	-19.616 ± 0.025	-67 ± 9

Table S6. NRTL model parameters for the fluorinated gases mixtures.

System	$\tau_{12}^1/K$	$\tau_{21}^1/K$	AARD/%	AARD <sub>p</sub> /%
<b>R32 + R125</b>	213.83	-152.50	5.95	0.83
<b>R32 + R1234yf</b>	264.44	-138.69	6.05	1.43
<b>R134a + R1234yf</b>	16.305	-2.173	6.36	2.00

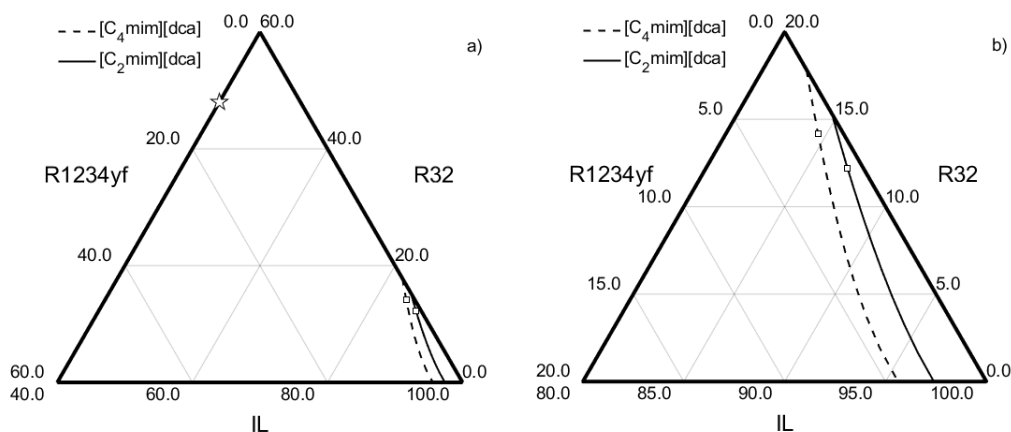


Figure S1. Predicted equilibrium ternary mixtures at 303 K and 5 bar for the mixture of R32 and R1234yf (80:20 in moles) with the ILs  $[C_2mim][dca]$  and  $[C_4mim][dca]$ . In a), the star represents the feed composition of the system, IL: R134a:R1234yf feed ratio equal to 0.4:0.48:0.12, and b) zooms in the equilibrium lines. The hollow squares represent the liquid composition of an isothermal flash outlet stream for each IL.

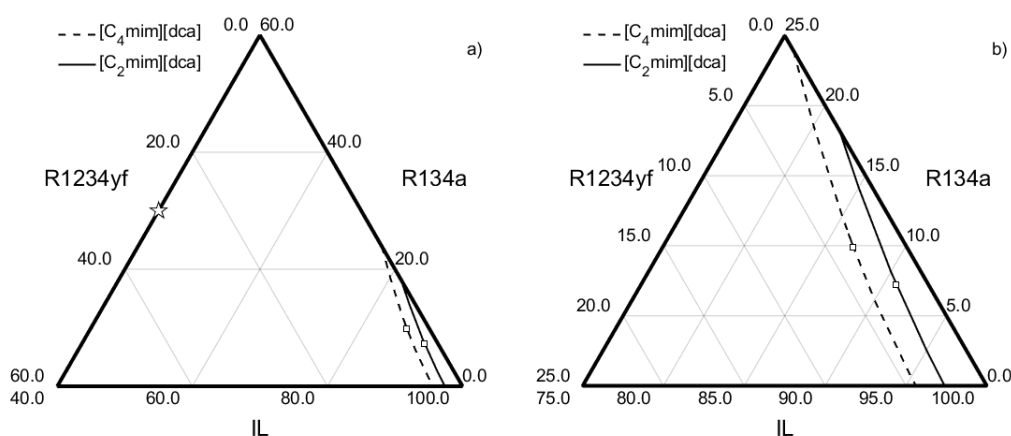


Figure S2. Predicted equilibrium ternary mixtures at 303 K and 5 bar for the mixture of R134a and R1234yf (50:50 in moles)  $[C_2mim][dca]$  and  $[C_4mim][dca]$ . In a), the star represents the feed composition of the system, IL: R134a:R1234yf feed ratio equal to 0.4:0.3:0.3, and b) zooms in the equilibrium lines. The hollow squares represent the liquid composition of an isothermal flash outlet stream for each IL.



Table S7. NRTL model parameters for the fluorinated gases + IL mixtures used for the flash calculation.

System	$\tau_{12}^0$	$\tau_{12}^1/K$	$\tau_{21}^0$	$\tau_{21}^1/K$	AARD/%	AARD <sub>p</sub> /%	Source
R32 + [C <sub>2</sub> mim][SCN]	0	1025.6	0	-210.04	2.45	2.54	[4]
R134a + [C <sub>2</sub> mim][SCN]	0	2682.6	0	254.58	3.63	3.82	[4]
R1234yf + [C <sub>2</sub> mim][SCN]	179.52	-47781	21.89	-5506.8	10.92	11.59	[4]
R32 + [C <sub>2</sub> mim][OTf]	0	1214.9	0	-515.69	5.77	6.05	This work
R134a + [C <sub>2</sub> mim][OTf]	0	5076.4	0	99.29	2.20	2.31	[5]
R1234yf + [C <sub>2</sub> mim][OTf]	6.226	414.6	4.338	-1126.1	5.97	6.35	[5]
R32 + [C <sub>4</sub> mim][PF <sub>6</sub> ]	4.408	-565.89	-1.0275	-199.06	15.51	15.95	[6]
R125 + [C <sub>4</sub> mim][PF <sub>6</sub> ]	2.788	-78.28	1.2041	-422.79	15.57	15.80	[6]
R134a + [C <sub>4</sub> mim][PF <sub>6</sub> ]	-3.001	1699.2	2.5102	-1000	10.06	10.14	[6]
R1234yf + [C <sub>4</sub> mim][PF <sub>6</sub> ]	7.024	2.898	0.331	26.581	1.68	1.76	[7]
R32 + [C <sub>2</sub> mim][Tf <sub>2</sub> N]	0	959.31	0	-621.18	5.11	5.20	[8]
R125 + [C <sub>2</sub> mim][Tf <sub>2</sub> N]	0	1041.3	0	-371.00	5.09	5.46	This work
R134a + [C <sub>2</sub> mim][Tf <sub>2</sub> N]	0	969.496	0	-443.388	7.41	7.54	This work
R1234yf + [C <sub>2</sub> mim][Tf <sub>2</sub> N]	0	3844.6	0	135.2	1.68	1.79	[5]
R32 + [C <sub>6</sub> mim][Tf <sub>2</sub> N]	0	101.29	0	-273.40	3.67	3.85	This work
R125 + [C <sub>6</sub> mim][Tf <sub>2</sub> N]	0	6206.9	0	-42.520	2.68	2.89	This work
R134a + [C <sub>6</sub> mim][Tf <sub>2</sub> N]	0	8178.9	0	50.859	7.19	8.24	This work
R1234yf + [C <sub>6</sub> mim][Tf <sub>2</sub> N]	8.692	1565.6	33.166	-1413.4	1.81	1.98	This work

## References

- [1] M.G. Freire, A.R.R. Teles, M.A.A. Rocha, B. Schröder, C.M.S.S. Neves, P.J. Carvalho, D. V. Evtuguin, L.M.N.B.F. Santos, J.A.P. Coutinho, Thermophysical Characterization of Ionic Liquids Able To Dissolve Biomass, *J. Chem. Eng. Data.* 56 (2011) 4813–4822. <https://doi.org/10.1021/je200790q>.
- [2] C.A. Nieto de Castro, E. Langa, A.L. Morais, M.L. Matos Lopes, M.J.V. Lourenço, F.J.V. Santos, M.S.C.S. Santos, J.N. Canongia Lopes, H.I.M. Veiga, M. Macatrão, J.M.S.S. Esperança, C.S. Marques, L.P.N. Rebelo, C.A.M. Afonso, Studies on the density, heat capacity, surface tension and infinite dilution diffusion with the ionic liquids [C4mim][NTf2], [C4mim][dca], [C2mim][EtOSO3] and [Aliquat][dca], *Fluid Phase Equilib.* 294 (2010) 157–179. <https://doi.org/10.1016/j.fluid.2010.03.010>.
- [3] C.M.S.S. Neves, K.A. Kurnia, J.A.P. Coutinho, I.M. Marrucho, J.N. Canongia Lopes, M.G. Freire, L.P.N. Rebelo, Systematic study of the thermophysical properties of imidazolium-based ionic liquids with cyano-functionalized anions, *J. Phys. Chem. B.* 117 (2013) 10271–10283. <https://doi.org/10.1021/jp405913b>.
- [4] S. Asensio-Delgado, F. Pardo, G. Zarca, A. Urtiaga, Enhanced absorption separation of hydrofluorocarbon/hydrofluoroolefin refrigerant blends using ionic liquids, *Sep. Purif. Technol.* 249 (2020) 117136. <https://doi.org/10.1016/j.seppur.2020.117136>.
- [5] S. Asensio-Delgado, F. Pardo, G. Zarca, A. Urtiaga, Vapor–Liquid Equilibria and Diffusion Coefficients of Difluoromethane, 1,1,1,2-Tetrafluoroethane, and 2,3,3,3-Tetrafluoropropene in Low-Viscosity Ionic Liquids, *J. Chem. Eng. Data.* 65 (2020) 4242–4251. <https://doi.org/10.1021/acs.jced.0c00224>.
- [6] M.B. Shiflett, A. Yokozeki, Solubility and Diffusivity of Hydrofluorocarbons in Room-Temperature Ionic Liquids, *AIChE J.* 52 (2006) 1205–1219. <https://doi.org/10.1002/aic.10685>.
- [7] Y. Zhang, J. Yin, X. Wang, Vapor-liquid equilibrium of 2,3,3,3-tetrafluoroprop-1-ene with 1-butyl-3-methylimidazolium hexafluorophosphate, 1-hexyl-3-methyl imidazolium hexafluorophosphate, and 1-octyl-3-methylimidazolium hexafluorophosphate, *J. Mol. Liq.* 260 (2018) 203–208. <https://doi.org/10.1016/j.molliq.2018.03.112>.
- [8] M.B. Shiflett, M.A. Harmer, C.P. Junk, A. Yokozeki, Solubility and Diffusivity of Difluoromethane in Room-Temperature Ionic Liquids, *J. Chem. Eng. Data.* 51 (2006) 483–495. <https://doi.org/10.1021/je050386z>.

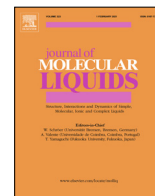


---

**3.7. Scientific publication 7. “Machine learning for predicting the solubility of high-GWP fluorinated refrigerants in ionic liquids”, Salvador Asensio-Delgado, Fernando Pardo, Gabriel Zarca, Ane Urtiaga, *Journal of Molecular Liquids*, 367 (2022) 120472**

At best, one experiment for the determination of an absorption isotherm using the isochoric saturation method takes 5 hours. The full characterization of the absorption of F-gases in ILs requires the study of the solubility at several temperatures to know the temperature effect on the solubility. Also, random repetition of some of the experiments is required to ensure that the data are correct. Additionally, the IL must be correctly degassed before charging it in the system and between every isotherm determination. Then, all the procedure must be repeated for each F-gas in each IL, leading to the use of a huge amount of time.

This article explores the use of one of current megatrends, artificial intelligence, and develops a machine learning tool based on artificial neural networks (ANNs) to decrease the time needed for the experimental studies, allowing a fast prescreening of the absorption of several F-gases in several ILs to test experimentally only those that were shown as promising candidates in the ANN predictions. Using the UC-RAIL database from Publication 1, an ANN was trained to accurately predict the VLE of F-gases and ILs based on pure component properties, namely, the IL molar mass, molar volume and fluorine atoms, and the F-gas critical properties, acentric factor, molar mass, fluorine atoms and vapor pressure. The results were very successful with accurate predictions of data that were published after the compilation of the UC-RAIL database, being able to even predict the solubility of a new HFO that had not yet been studied, the R1243zf, with a relative error lower than 10%. The predictive tool was provided as Supplementary Material for its use by the scientific community and is contained in the electronic version of the article.



# Machine learning for predicting the solubility of high-GWP fluorinated refrigerants in ionic liquids



Salvador Asensio-Delgado, Fernando Pardo, Gabriel Zarca, Ane Urtiaga\*

Department of Chemical and Biomolecular Engineering, Universidad de Cantabria. Av. Los Castros 46, Santander 39005, Spain

## ARTICLE INFO

### Article history:

Received 30 May 2022

Revised 12 September 2022

Accepted 22 September 2022

Available online 28 September 2022

### Keywords:

Artificial neural network

ionic liquids

Refrigerant gases

Predictive tool

GWP mitigation

## ABSTRACT

The development of technology to reduce the environmental impact of fluorinated refrigerant gases (F-gases) is currently of utmost importance. The capture of F-gases in ionic liquids (ILs) is envisaged as a solution to avoid emissions of F-gases to the atmosphere, and many studies have been devoted to the experimental determination of the vapor-liquid equilibrium of F-gas/IL mixtures. However, this is an expensive and time-consuming task, so finding prescreening options that can reduce the experimental load would pose a significant advantage in the development of new industrial-scale processes. Here, we develop a prescreening tool based on the use of artificial neural networks (ANNs) to predict the solubility of F-gases in ILs from easily accessible properties of the pure compounds, such as the critical properties of the gases or the molar mass and volume of the IL. We have used the UC-RAIL database with more than 4300 solubility data of 24 F-gases in 52 ILs. The ANN resulting from this study is capable to predict the fed dataset with an average absolute relative deviation (AARD) and mean absolute error (MAE) of 10.93% and 0.014, respectively, and we further demonstrate its predictive capabilities showing the very accurate prediction of a system including R-1243zf, an F-gas that was not present in the training set because it had not been previously studied. Finally, the developed ANN is implemented in an easy-to-use spreadsheet that will allow to extend its use in the prescreening of ILs towards the abatement and recovery of high environmental impact refrigerant gases.

© 2022 The Author(s). Published by Elsevier B.V.

## 1. Introduction

Refrigeration is considered one of the greatest engineering achievements of the 20th century, with applications that span from the preservation of fresh food and pharmaceutical compounds to providing air conditioning comfort in domestic, industrial, and transport environments [1]. Currently, a majority of refrigeration and air conditioning (RAC) equipment apply compression assisted evaporation and condensation cycles that use hydrofluorocarbons (HFCs) as refrigeration fluids. HFCs are synthetic fluorinated gases that were created to substitute the ozone-depleting chlorofluorocarbons (CFCs) and hydrochlorofluorocarbons (HCFCs) previously applied. However, HFCs are still powerful greenhouse gases. At present, a new class of related compounds, the hydrofluoroolefins (HFOs), with very low global warming potential (GWP), are gaining market share as a strategy for climate change mitigation [2]. As a result, commercial refrigerant blends are transitioning from HFC-only to low-GWP HFC/HFO mixtures containing mainly the HFCs R-32 (difluoromethane) and R-134a (1,1,1,2-tetrafluoroethane),

and the HFOs R-1234yf (2,3,3,3-tetrafluoropropene) and R-1234ze(E) (trans-1,3,3,3-tetrafluoropropene) [3].

The emissions of HFCs contributed to global greenhouse gas emissions as 0.73 and 1.1 Gt CO<sub>2</sub>-eq in 2010 and 2015, respectively, and only a small fraction of the HFCs in waste equipment are recovered or sent to incineration [4]. New regulations aim to stop this steady-rise scenario, among which the Kigali Amendment (2016) to the Montreal Protocol stands out, by defining a schedule for phasing down the production and consumption of HFCs by 85% by the late 2040s [5–7]. Thus, apart from the search for new low-GWP working fluids [8,9], the current context presents the opportunity of creating new abatement and regeneration technologies to recover and purify the HFCs from waste refrigerant mixtures, allowing their reuse in the formulation of the new HFC/HFO blends. Additionally, some mid-GWP HFC/HFO blends will only be used in the interim between emission reduction steps in international F-gas regulations, so recovering the HFOs to reuse them in low-GWP blends is of the utmost interest [10].

Different technologies have been proposed to perform the recovery of refrigerants from mixtures that usually exhibit azeotropic or near-azeotropic behavior [10]. These are, namely, membrane separation [11–15], adsorption on porous materials [16–

\* Corresponding author.

E-mail address: [urtiaga@umican.es](mailto:urtiaga@umican.es) (A. Urtiaga).

18], and absorption-based extractive distillation processes [19–21], in which ionic liquids (ILs) have attracted the most attention as entrainers. ILs are compounds preferentially composed of bulky organic ions that are liquid near room temperature [22] and exhibit unique properties, namely, nonvolatility, nonflammability, existence in liquid state over a wide range of temperatures, chemical and thermal stability, and ability to solubilize both polar and nonpolar compounds [23]. In particular, the high solubility of HFCs in ILs is related to hydrogen bonding and polar interactions between the solute and solvent molecules in the liquid mixture, and to favorable entropic effects in ILs featuring large free volume [24].

For developing F-gas reclamation processes, ILs need to be tested to find those that preferentially absorb some refrigerants over others, providing high solubility selectivity. In this regard, imidazolium ILs with thiocyanate and dicyanamide anions [23,25], as well as the combination of these anions with pyridinium cations [26], have shown high solubility selectivity for key F-gas separations, which can be related to the small molar volume and no fluorination of the anions [10]. In addition, the favorable solubility of HFCs and HFOs in ILs is encouraging the design of more energy efficient absorption refrigeration systems, in which the gas compressor is substituted by an absorber and a desorber [27]. In this field, the interest lies in finding low-viscosity ILs capable of dissolving large quantities of refrigerant gases of low-GWP so as to reduce the amount of solvent used and minimize the pumping costs.

In any case, knowledge on the vapor-liquid equilibrium (VLE) at several temperatures and pressures is crucial for the development of both applications. However, the experimental VLE determination is expensive and time-consuming and there are so many different fluorinated refrigerants, and even more possible ILs, that testing all the combinations becomes an unattainable goal. For this reason, developing a screening tool that allows the user to test the solubility behavior of F-gases in different ILs has a great interest, including systems for which there are not experimental information available [26].

In this sense, artificial intelligence approaches have shown excellent prediction capability in the field of chemical and process engineering, including their use in the design of new more sustainable refrigerants (HFCs, HFOs, and HCFOs) [28]. Machine learning are superior versus classical data analysis techniques in two main aspects, data classification and prediction; consequently, their predictive ability is being investigated in depth in ILs research [29]. For example, an Artificial Neural Network (ANN) and a Supported-Vector Machine (SVM) were trained to predict the viscosity of ILs using 1079 experimental data points from 45 ILs [30], and the melting point of ILs was predicted using a SVM trained using 22268 data points of 2068 ILs [31]. Some studies also developed machine learning methods to predict the solubility in ILs of CO<sub>2</sub> [32–36] and H<sub>2</sub>S [36–38], where ANNs showed improved prediction accuracy compared to cubic equations of state. In the field of refrigerant gases, previous attempts of developing ANNs to predict their solubility in ILs are limited to the works of Faúndez et al. [39], who used 254 data points of the solubility of the R-32 refrigerant in different ILs to train an ANN, and later extended the database to 642 data points to include one- and two-carbons HFCs [40]. However, training machine learning tools is not straightforward and requires strategies to overcome the difficulty in finding a global minimum, avoid overfitting and obtain a meaningfully predictive model [41]. As it will be detailed in section 2, several approaches are applied in this work to overcome these shortcomings, namely, applying multi-start initialization, using early-stopping methods to avoid overfitting, and using a large dataset as input for the training.

In this work, we use the recently published UC-RAIL database containing over 4000 solubility data of 24 fluorinated refrigerant gases (F-gases) in 52 ILs [10] to train an ANN to predict the molar fraction of F-gas absorbed from pure component data, namely, critical properties and vapor pressure of the gas, molecular weights and number of fluorine atoms of the gas and the IL, and IL density. We have trained the ANN with different F-gas families that include HFCs, HFOs, hydrochlorofluoroolefins (HCFOs), CFCs, HCFCs, and perfluorocarbons (PFCs). Furthermore, the trained ANN has been used to predict recently published VLE data that were not included in the UC-RAIL database. The ANN also describes the phase behavior at several pressures and temperatures. The developed tool will be useful in the initial stages of F-gas capture processes to make fast screenings of several ILs.

## 2. Methodology

### 2.1. Dataset

The VLE data recently compiled in the UC-RAIL database were used for developing the ANN to predict the solubility of fluorinated refrigerant gases in ILs [10]. This database contains experimental data for the solubility of 24 F-gases in 52 ILs that were randomly divided in training, validation, and test sets in the proportion 70/15/15. Out of the 4444 experimental data points available, 1% of the information (48 points) was removed. These points correspond to the solubility of fluorobutenes in ILs, for which there are not enough data available to make a meaningful network training, and to F-gas/IL systems that deal with the solubility of R-134a in [C<sub>2</sub>mim][Ac] and R-125 in [C<sub>2</sub>mim][Ac], [C<sub>4</sub>mim][Ac], and [C<sub>6</sub>mim][Cl]. The latter four systems could not be predicted accurately, even if they were purposely included in the training set. This can be considered a new proof of the unexpectedly strong interactions found between carboxylate and chloride anions with R-134a and R-125 gases [42,43]. As reported by Morais et al. [42], these interactions could be of chemical nature, like those of CO<sub>2</sub> absorption [44]. The list of IL cations and anions and F-gases considered in this work is presented in Table 1.

### 2.2. Artificial neural networks

An ANN is formed by processing units called neurons that are organized in layers [45]. The first layer of the network is the input layer, through which the input data is fed to the ANN. The input data provides useful and relevant information, the so-called features, to the network. These features are then fed to the hidden layers, where they undergo a series of transformations. Next, the information is sent from the last hidden layer to the output layer, which provides the results [46,47]. Each of the hidden layers communicates with their adjacent layers, this is, the ones that are immediately before and after. To that end, each neuron  $j$  in layer  $i$  receives  $k$  inputs ( $u_{i-1,k}$ ) from the previous layer ( $k$  is the number of neurons in the previous layer), multiplies them by their corresponding weights ( $w_{ijk}$ ) and adds the bias ( $b_{ij}$ ):

$$y_{ij} = b_{ij} + \sum_k w_{ijk} u_{i-1,k} \quad (1)$$

The calculated value of each neuron ( $y_{ij}$ ), normalized with a transfer function, represents the input to the neurons of the next layer. In this work, we have used the hyperbolic tangent sigmoid function (*tansig*) to normalize the neuron output [48]:

$$u_{ij} = \frac{2}{1 + \exp(-2y_{ij})} - 1 \quad (2)$$

where  $u_{ij}$  is the normalized neuron output which will be used as an input for the following layer.

**Table 1**  
List of IL cations and anions and F-gases included in the UC-RAIL database.

Ionic Liquids			
Cation	Cation name	Anion	Anion name
[C <sub>2</sub> mim] <sup>+</sup>	1-ethyl-3-methylimidazolium	[Ac] <sup>-</sup>	acetate
[C <sub>4</sub> mim] <sup>+</sup>	1-butyl-3-methylimidazolium	[BEI] <sup>-</sup>	bis(pentafluoroethylsulfonyl)imide
[C <sub>6</sub> mim] <sup>+</sup>	1-hexyl-3-methylimidazolium	[BF <sub>4</sub> ] <sup>-</sup>	tetrafluoroborate
[C <sub>7</sub> mim] <sup>+</sup>	1-heptyl-3-methylimidazolium	[Cl] <sup>-</sup>	chloride
[C <sub>8</sub> mim] <sup>+</sup>	3-octyl-1-methylimidazolium	[Et <sub>2</sub> PO <sub>4</sub> ] <sup>-</sup>	diethylphosphate
[(C <sub>8</sub> ) <sub>2</sub> im] <sup>+</sup>	1,3-dioctylimidazolium	[FEP] <sup>-</sup>	tris(pentafluoroethyl)trifluorophosphate
[C <sub>8</sub> H <sub>4</sub> F <sub>13</sub> mim] <sup>+</sup>	1-(3,3,4,4,5,5,6,6,7,7,8,8,8-tridecafluorooctyl)-3-methylimidazolium	[FS] <sup>-</sup>	2-(1,2,2,2-tetrafluoroethoxy)-1,1,2,2-tetrafluoroethanesulfonate
[C <sub>12</sub> mim] <sup>+</sup>	1-dodecyl-3-methylimidazolium	[HFPS] <sup>-</sup>	1,1,2,3,3,3-hexafluoropropanesulfonate
[(C <sub>1</sub> ) <sub>2</sub> C <sub>3</sub> im] <sup>+</sup>	1,2-dimethyl-3-propylimidazolium	[I] <sup>-</sup>	iodide
[C <sub>2</sub> mpy] <sup>+</sup>	1-ethyl-3-methylpyridinium	[MeSO <sub>4</sub> ] <sup>-</sup>	methylsulfate
[C <sub>3</sub> mpy] <sup>+</sup>	3-methyl-1-propylpyridinium	[OTf] <sup>-</sup>	trifluoromethanesulfonate
[C <sub>4</sub> mpy] <sup>+</sup>	1-butyl-3-methylpyridinium	[Pe] <sup>-</sup>	pentanoate
[P <sub>4441</sub> ] <sup>+</sup>	tributyl(methyl)phosphonium	[PF <sub>6</sub> ] <sup>-</sup>	hexafluorophosphate
[P <sub>4442</sub> ] <sup>+</sup>	tributyl(ethyl)phosphonium	[Pr] <sup>-</sup>	propionate
[P <sub>44414</sub> ] <sup>+</sup>	tributyl(tetradecyl)phosphonium	[PFBS] <sup>-</sup>	perfluorobutanesulfonate
[P <sub>66614</sub> ] <sup>+</sup>	trihexyl(tetradecyl)phosphonium	[PPF] <sup>-</sup>	perfluoropentanoate
[m-2-HEA] <sup>+</sup>	N-methyl-2-hydroxyethylammonium	[SCN] <sup>-</sup>	thiocyanate
		[TF <sub>2</sub> N] <sup>-</sup>	bis(trifluoromethylsulfonyl)imide
		[TFES] <sup>-</sup>	1,1,2,2-tetrafluoroethanesulfonate
		[TMeM] <sup>-</sup>	tris(trifluoromethylsulfonyl)methide
		[TMPP] <sup>-</sup>	bis(2,4,4-trimethylpentyl)phosphinate
		[TPES] <sup>-</sup>	1,1,2-trifluoro-2-(perfluoroethoxy)ethanesulfonate
		[TTES] <sup>-</sup>	1,1,2-trifluoro-2-(trifluoromethoxy)ethanesulfonate
Fluorinated refrigerants			
HFCs	Chemical name	HFOs/ HCFOs	Chemical name
R-41	fluoromethane	R-1234yf	2,3,3,3-tetrafluoropropene
R-32	difluoromethane	R-1234ze(E)	trans-1,3,3,3-tetrafluoropropene
R-23	trifluoromethane	R-1233zd(E)	trans-1-chloro-3,3,3-trifluoropropene
R-161	fluoroethane	R-1243zf	3,3,3-trifluoropropene
R-152a	1,1-difluoroethane	<b>PFCs</b>	<b>Chemical name</b>
R-143a	1,1,1-trifluoroethane	R-14	tetrafluoromethane
R-134	1,1,2,2-tetrafluoroethane	R-116	hexafluoroethane
R-134a	1,1,1,2-tetrafluoroethane	R-218	octafluoropropane
R-125	pentafluoroethane	<b>Phased out</b>	<b>Chemical name</b>
R-245fa	1,1,1,3,3-pentafluoropropane	R-114	1,2-dichloro-1,1,2,2-tetrafluoroethane
R-236fa	1,1,1,3,3,3-hexafluoropropane	R-114a	1,1-dichloro-1,2,2,2-tetrafluoroethane
R-227ea	1,1,1,2,3,3,3-heptafluoropropane	R-124	2-chloro-1,1,1,2-tetrafluoroethane
		R-124a	2-chloro-1,1,2,2-tetrafluoroethane
		R-22	chlorodifluoromethane
		R-22B1	bromodifluoromethane

After the last hidden layer, the normalized outputs are multiplied by the output layer weights and summed using the *purelin* function [48]. A developed explanation of the ANN calculation can be found in the [Supplementary Material](#).

To develop the ANN, all the weights,  $w_{ijk}$ , and biases,  $b_{ij}$ , are parametrized for every neuron in every layer. Unfortunately, there is not an explicit rule that determines the number of hidden layers or the number of neurons in each layer, so they must be selected by trial and error [39]. In this work, we focused in three-hidden-layers structures containing between 1 and 10 neurons in each layer. This decision was made after checking that the structures containing only one or two hidden layers resulted in much worse performances. For each possible combination, 50 different networks were trained to overcome the main shortcoming of the ANN regarding initialization and only the best one was kept. The training was made using the Neural Network Toolbox of MATLAB R2021a software using the BFGS Quasi-Newton training function (*trainbfg*). The maximum number of epochs was set to 10000, but the maximum number of fails was kept at 50 to avoid overfitting, so that the final network was only trained for 1544 epochs.

We used the average absolute relative deviation (AARD) as the performance function, Eq. (3), because minimizing the AARD allowed the accurate prediction of the solubility of low-sorbing

gases, while it also provided low absolute errors for the prediction of highly soluble gases. However, the root mean square error (RMSE) and mean absolute error (MAE) were also evaluated as performance indicators of the ANN.

$$\begin{aligned}
 AARD &= \frac{100}{N} \sum_i \left| \frac{x_{calc,i} - x_{exp,i}}{x_{exp,i}} \right| \\
 RMSE &= \sqrt{\frac{1}{N} \sum_i (x_{calc,i} - x_{exp,i})^2} \\
 MAE &= \frac{1}{N} \sum_i |x_{calc,i} - x_{exp,i}|
 \end{aligned} \tag{3}$$

### 3. Results

#### 3.1. Feature selection

The ANN was trained to predict the solubility of F-gases in ILs as a function of the equilibrium temperature and pressure using easily accessible and well-known properties of the pure solvents and solutes. The properties used to describe the IL solvents are the molar mass of the cation and the anion ( $M_{cat}$  and  $M_{an}$ ), the IL molar volume ( $V_{m,IL}$ ), and the number of fluorine atoms in the IL ( $F_{at,IL}$ ). The selection of these properties was based on our previous review on the topic [10], where we showed that all of them had a

relevant effect on the solubility of F-gases in ILs. For the F-gases, we used as features the critical properties of pressure, temperature, and volume ( $T_c$ ,  $P_c$ , and  $V_c$ ), the acentric factor ( $\omega$ ), the vapor pressure ( $P_{vap}$ ), the molar mass ( $M_{gas}$ ), and the number of fluorine atoms ( $F_{at, gas}$ ). The thermophysical properties database and equations of state library Coolprop 6.4.0 [49] was used to calculate the vapor pressures of all the compounds available and the rest were calculated using the correlations available in the book by Poling and Prausnitz [50]. The input properties for each IL and F-gas are compiled in the **Supplementary Material**.

**Fig. 1a** presents the correlation coefficients of the selected input variables with the molar fraction of gas absorbed ( $x$ ). The numeric values of the correlation coefficients as well as the regression lines and individual histograms for the variables are presented in **Figure S1** in the **Supplementary Information**. As can be observed, the correlation coefficient between each descriptor and the solubility ( $x$ ), that can be read in the bottom line of **Fig. 1a**, are lower than  $\pm 0.25$ , except for the equilibrium temperature,  $T$ , and the refrigerant critical pressure,  $P_c$ . These moderate correlation coefficients indicate that all of them should have a very similar importance

on the solubility prediction. Among the IL features, the anion molar mass,  $M_{an}$ , presents the best correlation to the solubility ( $x$ ) with a correlation coefficient of 0.23. Additionally, **Fig. 1a** also provides information regarding the positive or negative correlation between the descriptor variables. For instance, the molar mass of the gas ( $M_{gas}$ ), is positively correlated with its critical molar volume ( $V_c$ ), and degree of fluorination ( $F_{at, gas}$ ), as the most fluorinated gases are bigger and have higher molar mass than those hydrofluorocarbon gases with more hydrogen atoms than fluorine atoms bonded to the carbon chain. In addition, it is possible to infer whether there is a significant contribution of one input variable on the prediction of the output variable by assessing its fractional variance, which is calculated as the variance of each variable over the cumulative variance of all the input variables [51]. Thus, **Fig. 1b** shows the fractional variance of each of the descriptors of the ILs and F-gases, which ranges between 5 and 15% of the total cumulative variance in all cases. Therefore, we can infer that all the input variables have a similar importance in the prediction of F-gas solubility *a priori*.

### 3.2. Neural network training and performance

The ANNs were trained following the methodology described in section 2.2. The considered structures consisted of three-layer networks with 1 to 10 neurons in each layer ( $10^3$  possible combinations), and 50 networks were trained for each structure, given a total number of trained networks equal to 50000. **Fig. 2** shows the overall AARD of the best ANN out of each 50 ANNs trained with the same structure. As can be seen, increasing the number of neurons in the first and third layers reduces the AARD significantly, while the number of neurons in the second layer has a lower effect on the performance function.

The final structure of the ANN was selected in a point where increasing the number of neurons did not improve the performance significantly. Although it is possible to further reduce the AARD of the ANN, it may incur in overfitting derived from using too many parameters. The resulting ANN has a structure of 10, 4, and 5 neurons in the first, second, and third layer, respectively. Observing **Fig. 2**, it can be seen that increasing the number of neurons in the first layer has an important effect on the resulting AARD, so using the maximum limit of neurons allowed in this layer was expected. For the second and third layers, the AARD surface flattens, so there is no significant advantage in using more than 4 and 5 neurons, respectively, to obtain accurate results. **Table 2** shows the performance indicators for the test set using this net-

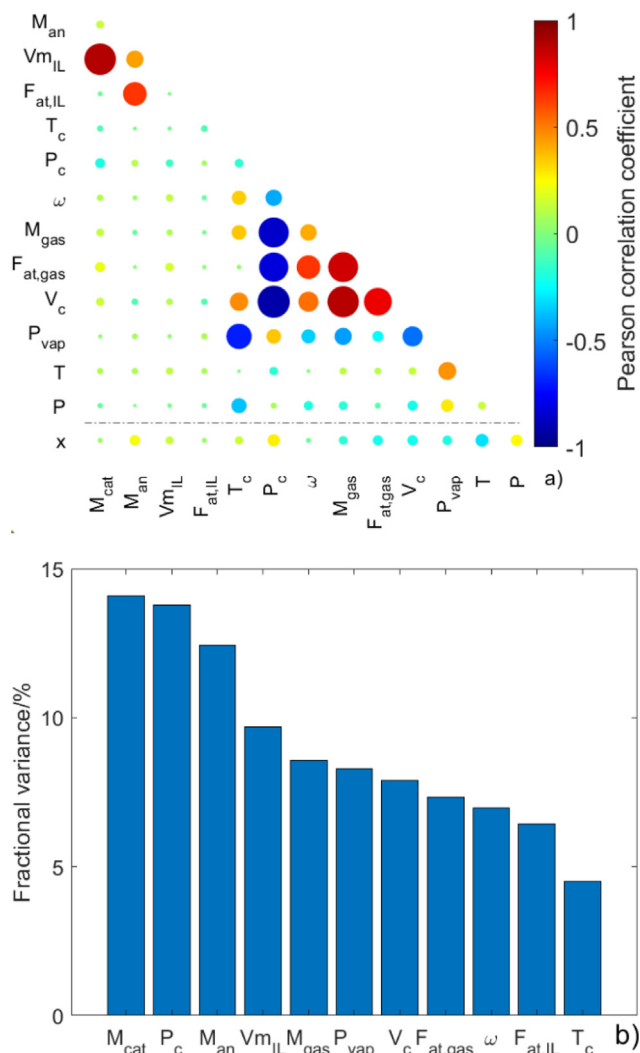


**Fig. 1.** (a) Pearson correlation coefficients between the input variables and the output variable ( $x$ , molar fraction of gas absorbed in the IL). The color code and the point size are related to the magnitude of the correlation coefficient according to the scale of the right-hand side of the y-axis. (b) Fractional variance of the ILs and F-gases descriptors presented as percentage of the total variance of the input variables.

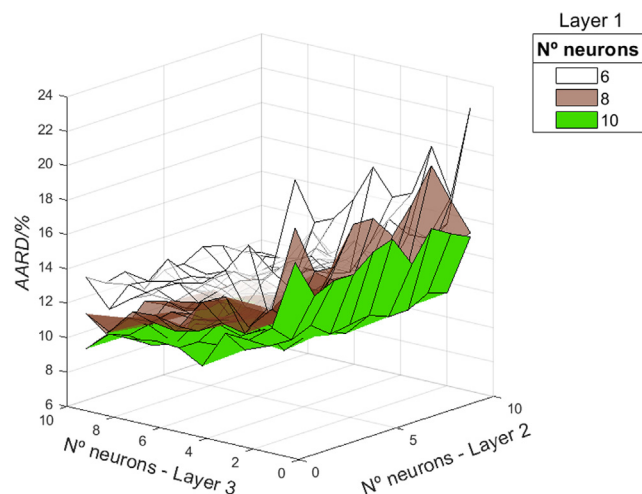


**Fig. 2.** Minimum AARD achieved for different number of neurons in each of the three layers of the ANN.



**Table 2**

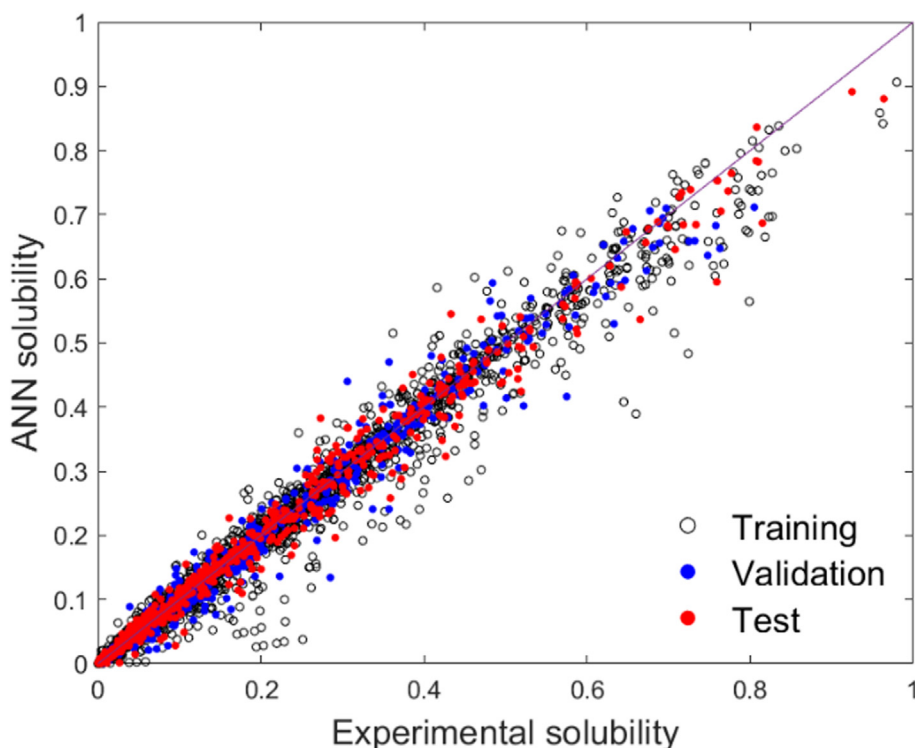
Performance indicators for the neural network trained to predict the solubility of F-gases in ILs.

Indicator	Database	Train set	Validation set	Test set
AARD/%	10.93	10.39	10.98	13.41
MAE	0.014	0.014	0.014	0.015
RMSE	0.028	0.028	0.026	0.028

work. As expected, minimizing the AARD performance function was a useful strategy to obtain errors below 15% for the train, validation, and test sets and achieve an overall AARD of 10.93%, while the MAE and RMSE are very low and kept almost constant for every set. The comparison between experimental and ANN solubilities is shown in Fig. 3, showing that most of the data can be well reproduced using the developed model.

An analysis *a posteriori* of the influence of the variables on the output provides meaningful insights of the systems subject to study. To that end, we present here an analysis performed using the Partial Derivatives (PaD) method, as it was found to be the most useful approach to study the contribution of the inputs to the ANN output [52]. As its name indicates, the PaD method consists in calculating the partial derivatives of the output with respect to the input variables. The resulting relative contribution (%) of each input on the F-gas solubility is presented in Fig. 4. Moreover, this method yields a set of graphs that enables direct access to the influence of the input variable on the output, which are presented in Figures S2 (relating the derivatives to their corresponding input) and Figure S3 (relating the derivatives to the resulting molar fraction of absorbed gas in the IL solvent) in the Supplementary Information. Figure S2 and S3 show that the derivatives with respect to every variable take both positive and negative values where linear relationships between the derivatives and the molar fraction can be seen, although they are fuzzy, and no obvious trends can be inferred.

Fig. 4 shows that the critical temperature of the gas is the input variable having the highest impact (61.2%) on the calculated absorbed gas molar fraction. This result reinforces the importance of the empirical trend found in previous works pointing to the strong relationship observed between the Henry's law constants for the absorption of different F-gases in a certain IL and the critical temperature of the F-gas being absorbed [10,53]. The following two variables in order of importance are also gas-related properties: the critical volume and the number of fluorine atoms. The relevance of the critical volume of the gas (13.3%) shows that the size of the solute is a determining factor in the prediction of the solubility, i.e., the lower the critical volume, the higher the solubility (for that reason, in Figures S2 and S3, the derivative of the output with respect to critical volume is mostly negative). Similarly, there is an important contribution (6.4%) of the number of fluorine atoms of the gas molecule (Fig. 4) that indicates that it is a relevant descriptor for the prediction of the molar fraction of F-gas absorbed in ILs. Interestingly, the relative contribution of the critical pressure (3.7%) only represents the fourth most important gas feature, whereas this property exhibited one of the highest correlation coefficients to the solubility and was ranked as the gas feature with the highest importance in Fig. 1. This fact clearly shows that an analysis of the correlation coefficients is not enough to infer the influence of the input variables on the ANN output, and highlights the importance of evaluating the relative contribution of each input variable after obtaining the parameters of the final ANN.

**Fig. 3.** Comparison between the experimental and ANN solubilities for the training, validation and test sets.

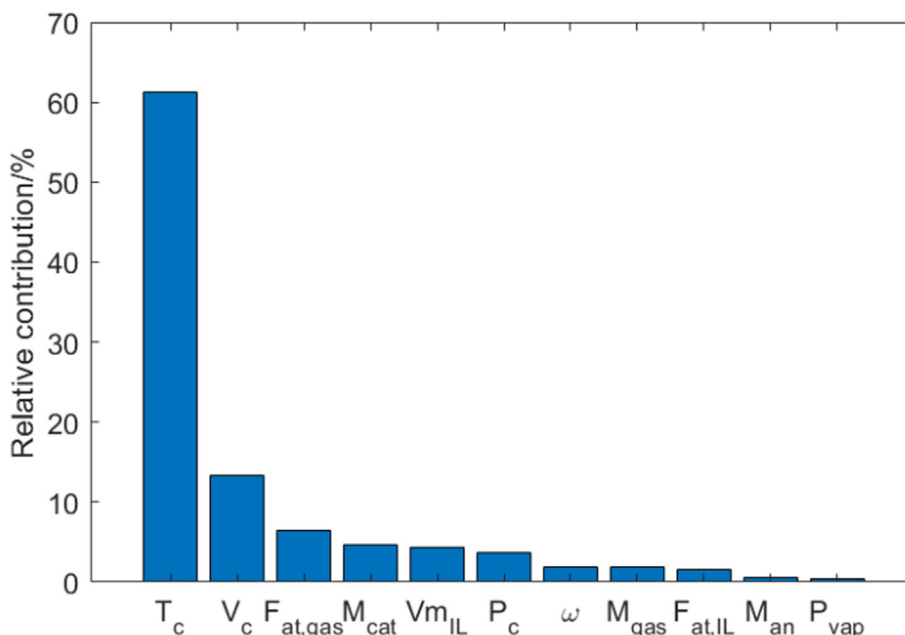


Fig. 4. Contribution of the input variables to the F-gas solubility in ILs for the three-layer 10-4-5 ANN calculated with the PaD method.

Regarding the IL features, the two properties with the highest importance are the cation molar mass (4.7%) and the IL molar volume (4.4%). This result also confirms our previous analysis of the F-gas solubility using the Regular Solution Theory [10], according to which the ILs with lower molar volume have lower absorption capacities towards F-gases. The rest of the variables related to the IL properties do not have strong contributions on the F-gas solubility, as shown in Fig. 4.

Future extensions of this ANN to expand its domain of application should consider mainly the gas critical properties and the number of fluorine atoms in the gas molecule, as well as the IL molar mass and volume. A successful extension should also include properties related to polarity. For example, including the dipole moment of the gases could be beneficial to allow the ANN to distinguish the behavior of F-gases from apolar molecules like hydrocarbons. However, including information on the polarity of the ILs would be more difficult, as IL solvents are segregated in polar and apolar domains [54,55]. Maybe using solvatochromic properties like the Kamlet-Taft parameters would help in this regard as they describe the dipolarity/polarizability, and hydrogen bond acidity and basicity [56], but currently there are not enough data available to cover all the ILs considered in this database. Additionally, molecular modeling and machine learning can be modeled by using advanced molecular models and equations of state to generate descriptors of the molecules to be fed to the machine learning algorithms [8,28]. For example, the newly proposed quantum chemical parameters referred to as ionic polarity index could be applied to describe IL polarity based on the ion charge and average surface potential [57].

Fig. 5 presents the performance of the ANN to predict the solubility in ILs of each of the 24 F-gases included in the network training in terms of both the AARD and MAE. The F-gases in Fig. 5 are grouped in four families: first, the gases that cannot be used in current equipment because they were phased out, second, the PFCs, used in ultra-low temperature applications and characterized because they do not contain hydrogen atoms, third, the HFCs that are currently predominant in installed RAC equipment, and last, the HFOs that are now entering the RAC market. As can be seen, the ANN results are accurate for predicting the solubility in ILs of

the HFCs R-32, R-134a, and the HFOs R-1234yf, and R-1234ze(E), the most extended gases in current refrigerant mixtures, with AARD < 10% except for R-134a, for which the AARD is 12%. Also, the HCFC R-22, that is present in end-of-life RAC equipment, is predicted accurately by the ANN. The high error observed in the prediction of R-23 and R-41 solubilities may be due to the fact that these F-gases are the only ones studied with ammonium-based ILs that contain carboxylate anions. As mentioned earlier, carboxylate anions are suspected to have strong polar interactions with R-134a and R-125, and they may be interacting with R-41 and R-23 too, but there is not enough empirical information available in this regard. The training of an enhanced predictive model would need expanding the dataset to include more examples of these ILs and studying the nature of the interaction between them and F-gases. With respect to R-125, a low sorbing gas, the prediction is good despite the high AARD value observed. This value is related to some experimental points with very low solubility of this gas, so that the relative error is magnified as a result of dividing by near-zero values. In the case of R-125, the good performance of the ANN is depicted by the MAE, which is only 0.020, very similar to the MAE of the calculated solubilities of a highly soluble gas like R-32.

### 3.3. Predictive capabilities

To show the predictive capabilities of the ANN, we present in this section the VLE of several F-gas/IL systems that were not included the UC-RAIL database as they have been recently published. Therefore, these data were not used for training the ANN. These data correspond mostly to HFOs, which are the new compounds of the fourth generation of refrigerants whose use is steadily increasing in the formulation of new refrigerant blends with the objective of reducing the impact of the RAC sector in the global warming. Table 3 shows that the network is predicting accurately the absorption of R-134a and R-1234ze(E), while it shows higher deviations for R-1233zd(E), for which the available dataset is small. Remarkably, the influence of the principal operation variables, temperature and pressure, are well predicted. This fact is of particular relevance for the usefulness of the ANN model, as temperature

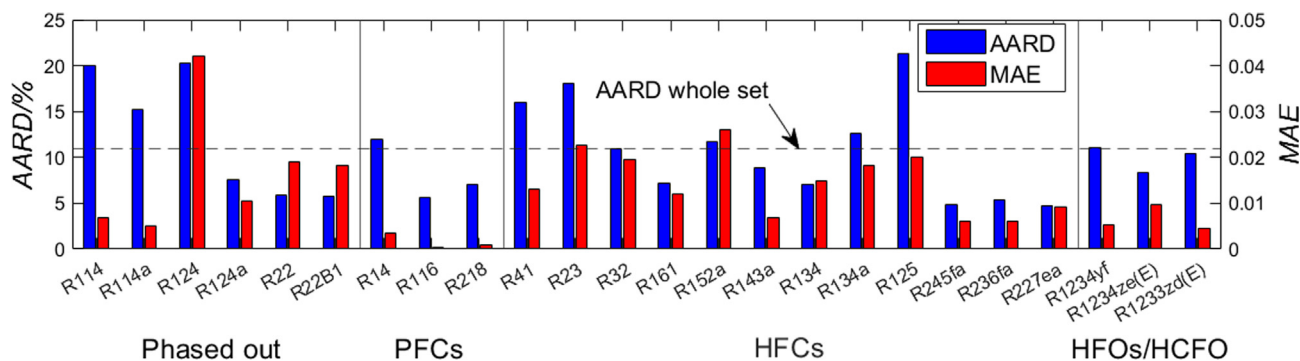


Fig. 5. AARD and MAE of the ANN as a function of the F-gas considered.

Table 3

VLE prediction of systems not included in the database. Experimental data from [58–61].

Gas + IL	AARD/%	MAE	RMSE
R-134a + [C <sub>4</sub> mim][Tf <sub>2</sub> N]	13.25	0.030	0.038
R-1234ze(E) + [P <sub>66614</sub> ][Cl]	10.73	0.050	0.056
R-1233zd(E) + [P <sub>66614</sub> ][Cl]	29.97	0.076	0.108
R-1243zf + [C <sub>4</sub> mim][Ac]	8.49	0.007	0.009
R-1243zf + [C <sub>4</sub> mim][OTf]	18.63	0.027	0.035
R-1243zf + [C <sub>4</sub> mim][PF <sub>6</sub> ]	4.93	0.006	0.012

and pressure are relevant variables during the process design procedures. In fact, the chloride anion of the IL increases its solubility as mentioned in section 2.1, which results in the underprediction of the ANN. Very interestingly, the ANN predicts very accurately the solubility of R-1243zf in [C<sub>4</sub>mim][Ac], [C<sub>4</sub>mim][OTf], and [C<sub>4</sub>mim][PF<sub>6</sub>], in an ample temperature range from 283 to 343 K, as shown in Fig. 6 and Figure S4. R-1243zf is an HFO that had not been previously studied, and therefore completely unknown to the ANN, combined in the case of Fig. 6 with an IL that contains the carboxylate group. Considering the low deviation between the experimental data and predicted VLE results, the ANN proves a useful *in silico* tool to infer solubility differences between F-gases in a certain IL, thus avoiding time-consuming experimental work for the selection of task-specific ILs.

These highly accurate predictions show that the developed ANN can be reliably integrated in process design. This ANN can provide the solubility of F-gases in ILs, which can then be used to calculate Henry's law constants and ideal selectivity values for separations based in solubility differences. Furthermore, it can be included in the process design of extractive distillation columns and of new absorption refrigeration cycles where the VLE of the mixtures in the process can be calculated with this matrix multiplication procedure, easier to converge than the activity-coefficient models like NRTL.

### 3.4. Network parameters and easy-to-use tool

With the aim of facilitating the widespread use of the ANN presented in this work, we provide as [Supplementary Material](#) a spreadsheet containing all the ANN parameters and a calculator of F-gas solubility in ILs that implements the ANN (Fig. 7). The user simply needs to provide the 13 input parameters and the software will automatically calculate the F-gas solubility predicted by the ANN. In case the user wants to predict whole isotherms or many systems at the same time, the parameters are available in the same excel file and the formulas can be seen, so that the calculation can be easily replicated. With this, we hope to improve the user experience and favor the widespread use of the results of this article as

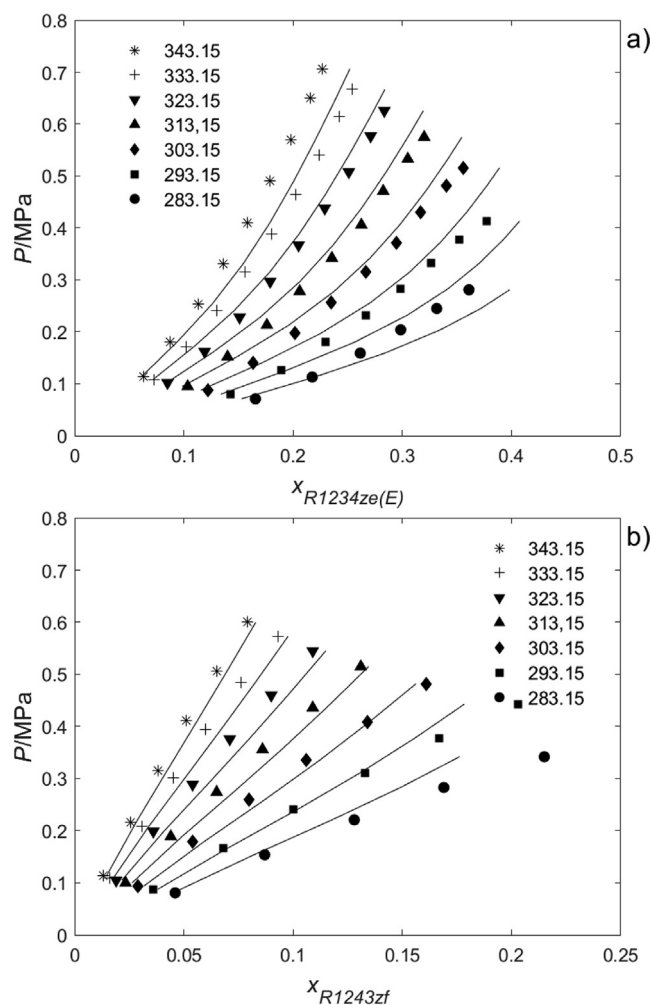


Fig. 6. Comparison between the experimental data (symbols) from references [59,60] and the ANN predictions (lines) for the systems (a) R-1234ze(E) + [P<sub>66614</sub>][Cl], and (b) R-1243zf + [C<sub>4</sub>mim][Ac].

an effective prescreening method for the abatement of high-GWP fluorinated gases using ionic liquids.

## 4. Conclusions

The UC-RAIL database has been used to prepare a predictive tool for the prescreening of ionic liquids for the absorption of fluorinated refrigerant gases. This tool is based on the use of an ANN that

Introduce here the input variables			Prediction result	
Ionic liquid properties	$M_{cat}/g \cdot mol^{-1}$	195.32	$x_{pred}$	0.0693
	$M_{an}/g \cdot mol^{-1}$	144.97		
	$Vm_{il}/cm^3 \cdot mol^{-1}$	282.91		
	$F_{at,il}$	6		
F-gas properties	$T_c/K$	367.85		
	$P_c/bar$	33.822		
	$\omega$	0.276		
	$M_{gas}/g \cdot mol^{-1}$	114.04		
	$F_{at,gas}$	4		
	$V_c/cm^3 \cdot mol^{-1}$	239.81		
	$P_{vap}/bar$	20.45		
Equilibrium conditions	$T/K$	343.15		
	$P/MPa$	0.4377		

Fig. 7. Implementation of the ANN to predict the F-gas solubility in ILs.

is fed with easily accessible pure compound properties of the solvent and solute, as well as the VLE equilibrium conditions. A total of 4396 experimental VLE points for the solubility of 24 F-gases in 52 ILs were randomly divided in training, validation, and test sets in the proportion 70/15/15 to train 50000 three-hidden-layer ANNs varying the number of neurons on each layer. Out of all the trained networks, an ANN with 10, 4, and 5 neurons in each layer was selected due to its satisfying accuracy and good predictive properties, with an overall AARD of 10.93%, and low values for the MAE and RMSE (0.014 and 0.028, respectively). Using the AARD as the objective function made possible obtaining good predictions for both high- and low-soluble refrigerant gases. Also, the relative importance of the selected inputs in the final predicted molar fraction value was evaluated, showing that the critical temperature and volume and the number of fluorine atoms of the gas have the highest contributions, followed by the IL molar volume and cation molar mass. Further refinements of this ANN to predict not only the solubility of fluorinated refrigerant gases, but also other compounds such as hydrocarbons should include information on the polarity of the solutes and solvents to improve the information introduced to the network and be able to distinguish between solute families. Nevertheless, for the purpose of fluorinated refrigerant gases, the ANN proposed in this contribution is very reliable and highly useful, as we have demonstrated predicting the vapor-liquid equilibrium of systems that are not present in the UC-RAIL database, including the gas R-1243zf, which was not present in the training whatsoever.

To facilitate the use of this ANN screening tool, we provide as [Supplementary Material](#) an easy-to-use datasheet to predict the solubility of new systems that can be applied to the design of novel separation processes aimed at the recovery of fluorinated refrigerants, with the final double purpose of increasing the share of reclaimed refrigerants in RAC equipment and contributing to the development of climate change mitigation technologies, by avoiding the release to the atmosphere of high global warming potential fluorinated gases.

#### CRediT authorship contribution statement

**Salvador Asensio-Delgado:** Conceptualization, Methodology, Software, Validation, Writing – original draft. **Fernando Pardo:** Resources, Investigation. **Gabriel Zarca:** Conceptualization, Supervision, Writing – review & editing. **Ane Urriaga:** Conceptualization,

Supervision, Writing – review & editing, Funding acquisition, Project administration.

#### Data availability

We have shared the data file as [Supplementary Material](#)

#### Declaration of Competing Interest

The authors declare that they have no known competing financial interests or personal relationships that could have appeared to influence the work reported in this paper.

#### Acknowledgements

This publication is a result of project PID2019-105827RB-I00 funded by MCIN/AEI/10.1039/501100011033. S. A.-D. acknowledges the FPU18/03939 grant and F.P. acknowledges the post-doctoral fellowship (FJCI-2017-32884 Juan de la Cierva Formación) awarded by the Spanish Ministry of Science and Innovation (MCIN/AEI/10.1039/501100011033).

#### Appendix A. Supplementary data

Supplementary data to this article can be found online at <https://doi.org/10.1016/j.molliq.2022.120472>.

#### References

- [1] M.O. McLinden, C.J. Seeton, A. Pearson, New refrigerants and system configurations for vapor-compression refrigeration, *Science* 370 (6518) (2020) 791–796.
- [2] M.O. McLinden, M.L. Huber, (R)Evolution of Refrigerants, *J. Chem. Eng. Data* 65 (2020) 4176–4193, <https://doi.org/10.1021/acs.jced.0c00338>.
- [3] Y. Heredia-Aricapa, J.M. Belman-Flores, A. Mota-Babiloni, J. Serrano-Arellano, J. J. García-Pabón, Overview of low GWP mixtures for the replacement of HFC refrigerants: R134a, R404A and R410A, *Int. J. Refrig.* 111 (2020) 113–123, <https://doi.org/10.1016/j.ijrefrig.2019.11.012>.
- [4] P. Purohit, L. Höglund-Isaksson, J. Dulac, N. Shah, M. Wei, P. Rafaj, W. Schöpp, Electricity savings and greenhouse gas emission reductions from global phase-down of hydrofluorocarbons, *Atmos. Chem. Phys.* 20 (2020) 11305–11327, <https://doi.org/10.5194/acp-20-11305-2020>.
- [5] United Nations, Amendment to the Montreal protocol on substances that deplete the ozone layer, (2016).
- [6] E.A. Heath, Amendment to the Montreal Protocol on Substances that Deplete the Ozone Layer (Kigali Amendment), *Int. Leg. Mater.* 56 (2017) 193–205, <https://doi.org/10.1017/ilm.2016.2>.
- [7] European Parliament and Council, EU 517/2014, (2014) 195–230.
- [8] D. Jovell, R. Gonzalez-Olmos, F. Llovel, A computational drop-in assessment of hydrofluoroethers in Organic Rankine Cycles, *Energy* 254 (2022) 124319.
- [9] C.G. Albà, I.I.I. Alkhatib, F. Llovel, L.F. Vega, Assessment of Low Global Warming Potential Refrigerants for Drop-In Replacement by Connecting their Molecular Features to Their Performance, *ACS Sustain. Chem. Eng.* 9 (2021) 17034–17048, <https://doi.org/10.1021/acssuschemeng.1c05985>.
- [10] S. Asensio-Delgado, F. Pardo, G. Zarca, A. Urriaga, Absorption separation of fluorinated refrigerant gases with ionic liquids: Equilibrium, mass transport, and process design, *Sep. Purif. Technol.* 276 (2021), <https://doi.org/10.1016/j.seppur.2021.119363> 119363.
- [11] F. Pardo, G. Zarca, A. Urriaga, Effect of feed pressure and long-term separation performance of Pebax-ionic liquid membranes for the recovery of difluoromethane (R32) from refrigerant mixture R410A, *J. Memb. Sci.* 618 (2021), <https://doi.org/10.1016/j.memsci.2020.118744> 118744.
- [12] C. Hermida-Merino, F. Pardo, G. Zarca, J.M.M. Araújo, A. Urriaga, M.M. Piñero, A.B. Pereiro, Integration of stable ionic liquid-based nanofluids into polymer membranes. Part I: Membrane synthesis and characterization, *Nanomaterials* 11 (2021), <https://doi.org/10.3390/nano11030607> 607.
- [13] F. Pardo, S. Gutiérrez-Hernández, C. Hermida-Merino, J.M.M. Araújo, M.M. Piñero, A.B. Pereiro, G. Zarca, A. Urriaga, Integration of Stable Ionic Liquid-Based Nanofluids into Polymer Membranes. Part II: Gas Separation Properties toward Fluorinated Greenhouse Gases, *Nanomaterials* 11 (2021), <https://doi.org/10.3390/nano11030607> 582.
- [14] F. Pardo, S. Gutiérrez-Hernández, G. Zarca, A. Urriaga, Toward the recycling of low-GWP hydrofluorocarbon/hydrofluoroolefin refrigerant mixtures using composite ionic liquid-polymer membranes, *ACS Sustain. Chem. Eng.* 9 (2021) 7012–7021, <https://doi.org/10.1021/acssuschemeng.1c00668>.
- [15] F. Pardo, G. Zarca, A. Urriaga, Separation of Refrigerant Gas Mixtures Containing R32, R134a, and R1234yf through Poly(ether- block -amide)



- Membranes, *ACS Sustain. Chem. Eng.* 8 (2020) 2548–2556, <https://doi.org/10.1021/acssuschemeng.9b07195>.
- [16] J.E. Sosa, C. Malheiro, R.P. Ribeiro, P.J. Castro, M.M. Piñeiro, J.M.M. Araújo, F. Plantier, J.P.B. Mota, A.B. Pereiro, Adsorption of Fluorinated Greenhouse Gases on Activated Carbons: Evaluation of their Potential for Gas Separation, *J. Chem. Technol. Biotechnol.* 95 (7) (2020) 1892–1905.
- [17] A.D. Yancey, S.J. Terian, B.J. Shaw, T.M. Bish, D.R. Corbin, M.B. Shiflett, A review of fluorocarbon sorption on porous materials, *Microporous Mesoporous Mater.* 331 (2022), <https://doi.org/10.1016/j.micromeso.2021.111654> 111654.
- [18] D.K.J.A. Wanigarathna, J. Gao, B. Liu, Metal organic frameworks for adsorption-based separation of fluorocompounds: a review, *Mater. Adv.* 1 (2020) 310–320, <https://doi.org/10.1039/d0ma00083c>.
- [19] E.A. Finberg, M.B. Shiflett, Process Designs for Separating R-410A, R-404A, and R-407C Using Extractive Distillation and Ionic Liquid Entrainers, *Ind. Eng. Chem. Res.* 60 (44) (2021) 16054–16067.
- [20] D. Jovell, J.O. Pou, F. Llovel, R. Gonzalez-Olmos, Life Cycle Assessment of the Separation and Recycling of Fluorinated Gases Using Ionic Liquids in a Circular Economy Framework, *ACS Sustain. Chem. Eng.* 10 (2022) 71–80, <https://doi.org/10.1021/acssuschemeng.1c04723>.
- [21] S. Asensio-Delgado, D. Jovell, G. Zarca, A. Urriaga, F. Llovel, Thermodynamic and process modeling of the recovery of R410A compounds with ionic liquids, *Int. J. Refrig.* 118 (2020) 365–375, <https://doi.org/10.1016/j.ijrefrig.2020.04.013>.
- [22] A. Podgoršek, J. Jacquemin, A.A.H. Pádua, M.F. Costa Gomes, Mixing Enthalpy for Binary Mixtures Containing Ionic Liquids, *Chem. Rev.* 116 (2016) 6075–6106, <https://doi.org/10.1021/acs.chemrev.5b00379>.
- [23] S. Asensio-Delgado, F. Pardo, G. Zarca, A. Urriaga, Enhanced absorption separation of hydrofluorocarbon/hydrofluoroolefin refrigerant blends using ionic liquids, *Sep. Purif. Technol.* 249 (2020), <https://doi.org/10.1016/j.seppur.2020.117136> 117136.
- [24] J.E. Sosa, R. Santiago, A.E. Redondo, J. Avila, L.F. Lepre, M.F. Costa Gomes, J.M.M. Araújo, J. Palomar, A.B. Pereiro, Design of Ionic Liquids for Fluorinated Gas Absorption: COSMO-RS Selection and Solubility Experiments, *Environ. Sci. Technol.* 56 (2022) 5898–5909, <https://doi.org/10.1021/acs.est.2c00051>.
- [25] S. Asensio-Delgado, M. Viar, F. Pardo, G. Zarca, A. Urriaga, Gas solubility and diffusivity of hydrofluorocarbons and hydrofluoroolefins in cyanide-based ionic liquids for the separation of refrigerant mixtures, *Fluid Phase Equilib.* 549 (2021), <https://doi.org/10.1016/j.fluid.2021.113210> 113210.
- [26] H. Qin, J. Cheng, H. Yu, T. Zhou, Z. Song, Hierarchical Ionic Liquid Screening Integrating COSMO-RS and Aspen Plus for Selective Recovery of Hydrofluorocarbons and Hydrofluoroolefins from a Refrigerant Blend, *Ind. Eng. Chem. Res.* 61 (11) (2022) 4083–4094.
- [27] J.M. Asensio-Delgado, S. Asensio-Delgado, G. Zarca, A. Urriaga, Analysis of hybrid compression absorption refrigeration using low-GWP HFC or HFO/ionic liquid working pairs, *Int. J. Refrig.* 134 (2022) 232–241, <https://doi.org/10.1016/j.ijrefrig.2021.11.013>.
- [28] I.I. Alkhatib, C.G. Albà, A.S. Darwish, F. Llovel, L.F. Vega, Searching for Sustainable Refrigerants by Bridging Molecular Modeling with Machine Learning, *Ind. Eng. Chem. Res.* 61 (21) (2022) 7414–7429.
- [29] S. Koutsoukos, F. Philippi, F. Malaret, T. Welton, A review on machine learning algorithms for the ionic liquid chemical space, *Chem. Sci.* 12 (2021) 6820–6843, <https://doi.org/10.1039/d1sc01000j>.
- [30] Y. Zhao, X. Zhang, L. Deng, S. Zhang, Prediction of viscosity of imidazolium-based ionic liquids using MLR and SVM algorithms, *Comput. Chem. Eng.* 92 (2016) 37–42, <https://doi.org/10.1016/j.compchemeng.2016.04.035>.
- [31] K. Wang, H. Xu, C. Yang, T. Qiu, Machine learning-based ionic liquids design and process simulation for CO<sub>2</sub> separation from flue gas, *Green, Energy Environ.* 6 (2021) 432–443, <https://doi.org/10.1016/j.gee.2020.12.019>.
- [32] M. Mesbah, S. Shahsavari, E. Soroush, N. Rahaei, M. Rezakazemi, Accurate prediction of miscibility of CO<sub>2</sub> and supercritical CO<sub>2</sub> in ionic liquids using machine learning, *J. CO<sub>2</sub> Util.* 25 (2018) 99–107, <https://doi.org/10.1016/j.jcou.2018.03.004>.
- [33] A. Baghban, M.A. Ahmadi, B.H. Shahraki, Prediction carbon dioxide solubility in presence of various ionic liquids using computational intelligence approaches, *J. Supercrit. Fluids.* 98 (2015) 50–64, <https://doi.org/10.1016/j.supflu.2015.01.002>.
- [34] I. Mehraein, S. Riahi, The QSPR models to predict the solubility of CO<sub>2</sub> in ionic liquids based on least-squares support vector machines and genetic algorithm-multi linear regression, *J. Mol. Liq.* 225 (2017) 521–530, <https://doi.org/10.1016/j.molliq.2016.10.133>.
- [35] Z. Song, H. Shi, X. Zhang, T. Zhou, Prediction of CO<sub>2</sub> solubility in ionic liquids using machine learning methods, *Chem. Eng. Sci.* 223 (2020), <https://doi.org/10.1016/j.ces.2020.115752> 115752.
- [36] H. Feng, P. Zhang, W. Qin, W. Wang, H. Wang, Estimation of solubility of acid gases in ionic liquids using different machine learning methods, *J. Mol. Liq.* 349 (2022), <https://doi.org/10.1016/j.molliq.2021.118413> 118413.
- [37] M. Nait Amar, M.A. Ghriga, H. Ouaer, On the evaluation of solubility of hydrogen sulfide in ionic liquids using advanced committee machine intelligent systems, *J. Taiwan Inst. Chem. Eng.* 118 (2021) 159–168, <https://doi.org/10.1016/j.jtice.2021.01.007>.
- [38] Y. Zhao, J. Gao, Y. Huang, R.M. Afzal, X. Zhang, S. Zhang, Predicting H<sub>2</sub>S solubility in ionic liquids by the quantitative structure-property relationship method using:  $\sigma$  profile molecular descriptors, *RSC Adv.* 6 (2016) 70405–70413, <https://doi.org/10.1039/c6ra15429h>.
- [39] C.A. Faúndez, R.A. Campusano, J.O. Valderrama, Misleading results on the use of artificial neural networks for correlating and predicting properties of fluids. A case on the solubility of refrigerant R-32 in ionic liquids, *J. Mol. Liq.* 298 (2020) 112009.
- [40] E.N. Fierro, C.A. Faúndez, A.S. Muñoz, Influence of thermodynamically inconsistent data on modeling the solubilities of refrigerants in ionic liquids using an artificial neural network, *J. Mol. Liq.* 337 (2021), <https://doi.org/10.1016/j.molliq.2021.116417> 116417.
- [41] C.C. Aggarwal, *Neural Networks and Deep Learning*, 2018. <https://doi.org/10.1007/978-3-319-94463-0>.
- [42] A.R.C. Morais, A.N. Harders, K.R. Baca, G.M. Olson, B. Befort, A.W. Dowling, E.J. Maginn, M.B. Shiflett, Phase Equilibria, Diffusivities, and Equation of State Modeling of HFC-32 and HFC-125 in Imidazolium-based Ionic Liquids for the Separation of R-410A, *Ind. Eng. Chem. Res.* 59 (2020) 18222–18235, <https://doi.org/10.1021/acs.iecr.0c02820>.
- [43] J.E. Sosa, R.P.P.L. Ribeiro, P.J. Castro, J.P.B. Mota, J.M.M. Araújo, A.B. Pereiro, Absorption of Fluorinated Greenhouse Gases Using Fluorinated Ionic Liquids, *Ind. Eng. Chem. Res.* 58 (2019) 20769–20778, <https://doi.org/10.1021/acs.iecr.9b04648>.
- [44] M.S. Shannon, J.E. Bara, Reactive and Reversible Ionic Liquids for CO<sub>2</sub> Capture and Acid Gas Removal, *Sep. Sci. Technol.* 47 (2012) 178–188, <https://doi.org/10.1080/01496395.2011.630055>.
- [45] M. Kuhn, K. Johnson, *Applied predictive modeling*, Springer Science+Business Media, New York (2013), <https://doi.org/10.1007/978-1-4614-6849-3>.
- [46] J. Li, L. Pan, M. Suvama, X. Wang, Machine learning aided supercritical water gasification for H<sub>2</sub>-rich syngas production with process optimization and catalyst screening, *Chem. Eng. J.* 426 (2021), <https://doi.org/10.1016/j.cej.2021.131285> 131285.
- [47] D. Serrano, D. Castelló, Tar prediction in bubbling fluidized bed gasification through artificial neural networks, *Chem. Eng. J.* 402 (2020) 126229.
- [48] A. Tarafdar, N.C. Shahi, A. Singh, R. Sirohi, Artificial Neural Network Modeling of Water Activity: a Low Energy Approach to Freeze Drying, *Food Bioprocess Technol.* 11 (2018) 164–171, <https://doi.org/10.1007/s11947-017-2002-4>.
- [49] I.H. Bell, J. Wronski, S. Quoilin, V. Lemort, Pure and Pseudo-pure Fluid Thermophysical Property Evaluation and the Open-Source Thermophysical Property Library CoolProp, *Ind. Eng. Chem. Res.* 53 (2014) 2498–2508, <https://doi.org/10.1021/ie4033999>.
- [50] B.E. Poling, J.M. Prausnitz, J.P. O'Connell, *The Properties of Gases and Liquids*, fifth ed., McGraw-Hill Education, New York, USA, 2001.
- [51] C. Albon, *Machine Learning with Python Cookbook*, O'Reilly Media Inc, Sebastopol, CA, 2018.
- [52] M. Gevrey, I. Dimopoulos, S. Lek, Review and comparison of methods to study the contribution of variables in artificial neural network models, *Ecol. Modell.* 160 (2003) 249–264, [https://doi.org/10.1016/S0304-3800\(02\)00257-0](https://doi.org/10.1016/S0304-3800(02)00257-0).
- [53] M.B. Shiflett, A. Yokozeki, Gaseous Absorption of Fluoromethane, Fluoroethane, and 1,1,2,2-Tetrafluoroethane in 1-Butyl-3-Methylimidazolium Hexafluorophosphate, *Ind. Eng. Chem. Res.* 45 (2006) 6375–6382, <https://doi.org/10.1021/ie060192s>.
- [54] K. Shimizu, M.F. Costa Gomes, A.A.H. Pádua, L.P.N. Rebelo, J.N. Canongia Lopes, Three commentaries on the nano-segregated structure of ionic liquids, *J. Mol. Struct. THEOCHEM.* 946 (2010) 70–76, <https://doi.org/10.1016/j.theochem.2009.11.034>.
- [55] M.L. Ferreira, J.M.M. Araújo, A.B. Pereiro, L.F. Vega, Insights into the influence of the molecular structures of fluorinated ionic liquids on their thermophysical properties. A soft-SAFT based approach, *Phys. Chem. Chem. Phys.* 21 (2019) 6362–6380, <https://doi.org/10.1039/c8cp07522k>.
- [56] S. Spange, R. Lungwitz, A. Schade, Correlation of molecular structure and polarity of ionic liquids, *J. Mol. Liq.* 192 (2014) 137–143, <https://doi.org/10.1016/j.molliq.2013.06.016>.
- [57] X. Liu, K.E. O'Hara, J.E. Bara, C.H. Turner, Solubility Behavior of CO<sub>2</sub> in Ionic Liquids Based on Ionic Polarity Index Analyses, *J. Phys. Chem. B.* 125 (2021) 3665–3676, <https://doi.org/10.1021/acs.jpcc.1c01508>.
- [58] T. Esaki, N. Kobayashi, H. Uchiyama, Y. Matsukuma, Characteristics of Absorption Equilibrium with HFC-134a and an Ionic Liquid Pair, *J. Mater. Sci. Chem. Eng.* 07 (2019) 65–78, <https://doi.org/10.4236/msce.2019.73006>.
- [59] X. Jia, H. Wang, X. Wang, Solubility measurement, modeling and mixing thermodynamic properties of R1243zf and R600a in [BMIM][Ac], *J. Chem. Thermodyn.* 164 (2022), <https://doi.org/10.1016/j.jct.2021.106637> 106637.
- [60] T. Jiang, X. Meng, Y. Sun, L. Jin, Q. Wei, J. Wang, X. Wang, M. He, Absorption behavior for R1234ze(E) and R1233zd(E) in [P66614][Cl] as Working Fluids in Absorption Refrigeration Systems, *Int. J. Refrig.* In press 131 (2021) 178–185.
- [61] X. Jia, W. Dou, X. Wang, Solubility determination and mixing thermodynamic properties of R1243zf in two 1-butyl-3-methyl-imidazolium based ionic liquids, *J. Mol. Liq.* 364 (2022), <https://doi.org/10.1016/j.molliq.2022.120031> 120031.

## Supplementary Information

### Machine learning for predicting the solubility of high-GWP fluorinated refrigerants in ionic liquids

#### Authors:

Salvador Asensio-Delgado, Fernando Pardo, Gabriel Zarca, Ane Urtiaga\*

Department of Chemical and Biomolecular Engineering, Universidad de Cantabria,

Av. Los Castros 46, Santander 39005, Spain.

\*Corresponding author e-mail address: [urtiaga@unican.es](mailto:urtiaga@unican.es)

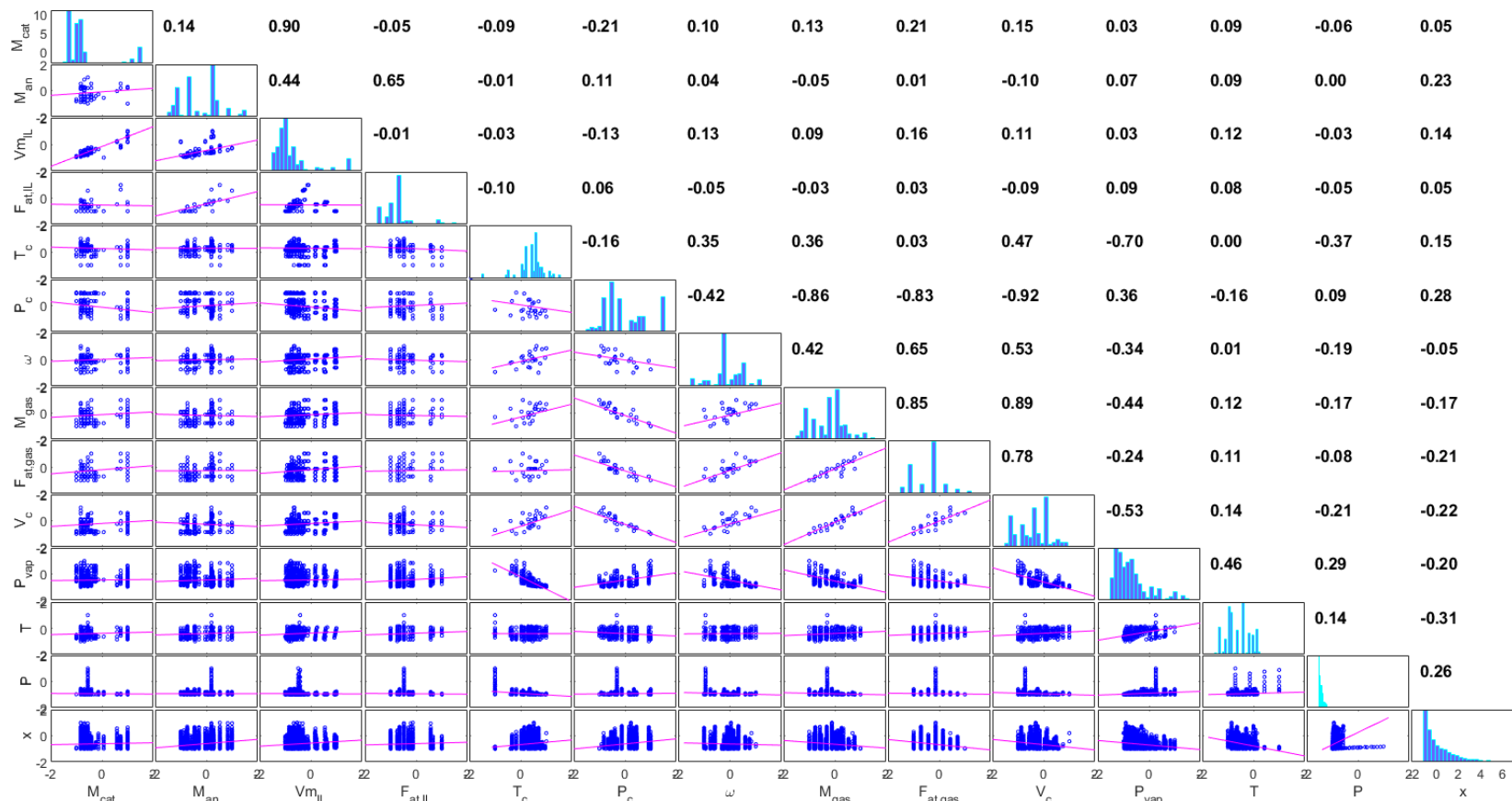


Figure S1. Correlation between the input variables and the output variable ( $x$ ). The lower half presents the regression lines explaining the relation to each other and the upper half presents the Pearson correlation coefficients. The diagonal shows the histograms of each independent variable.

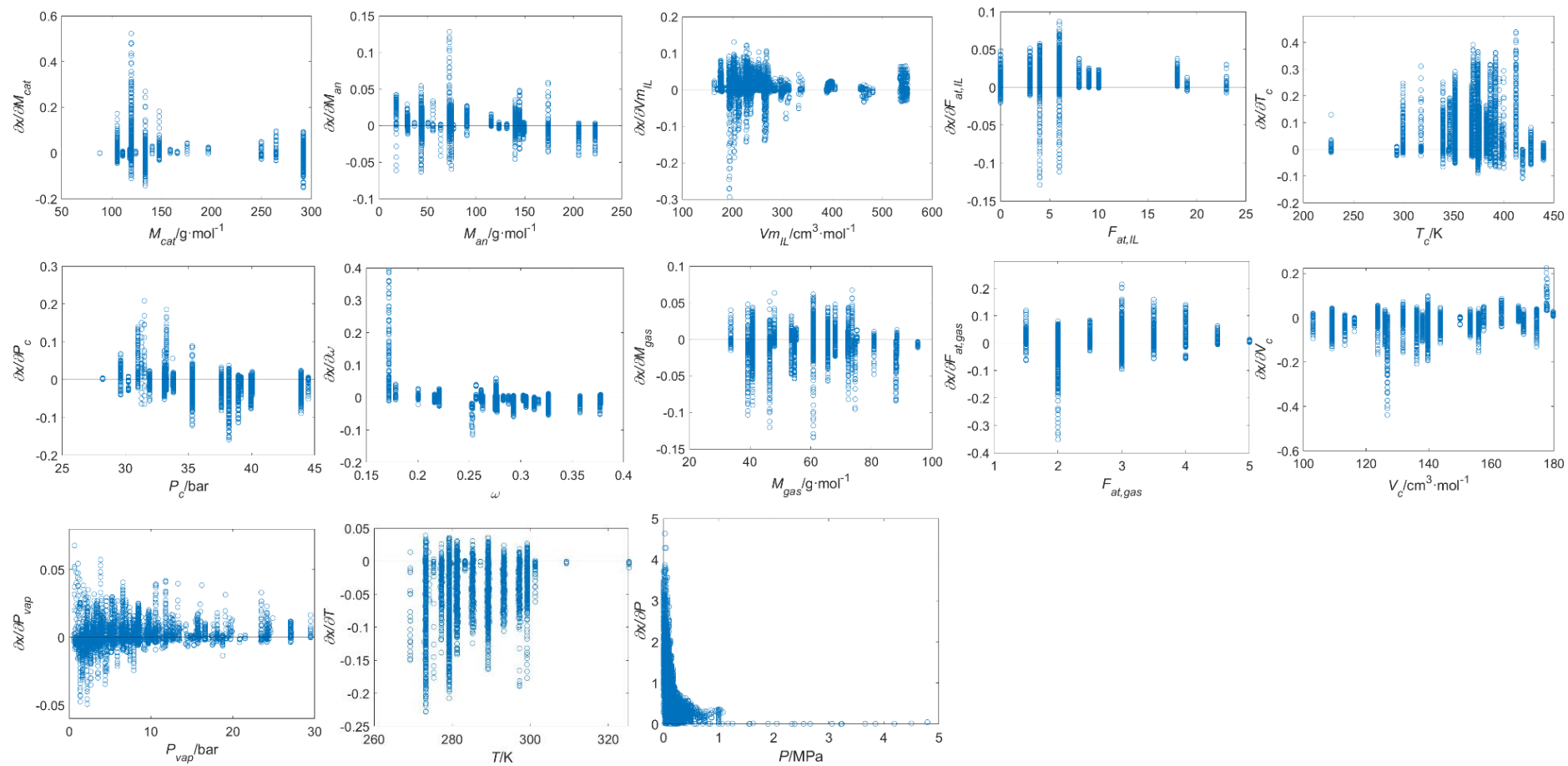


Figure S2. Partial derivatives of the absorbed gas molar fraction ( $x$ ) with respect to each input variable represented against its corresponding input variable.



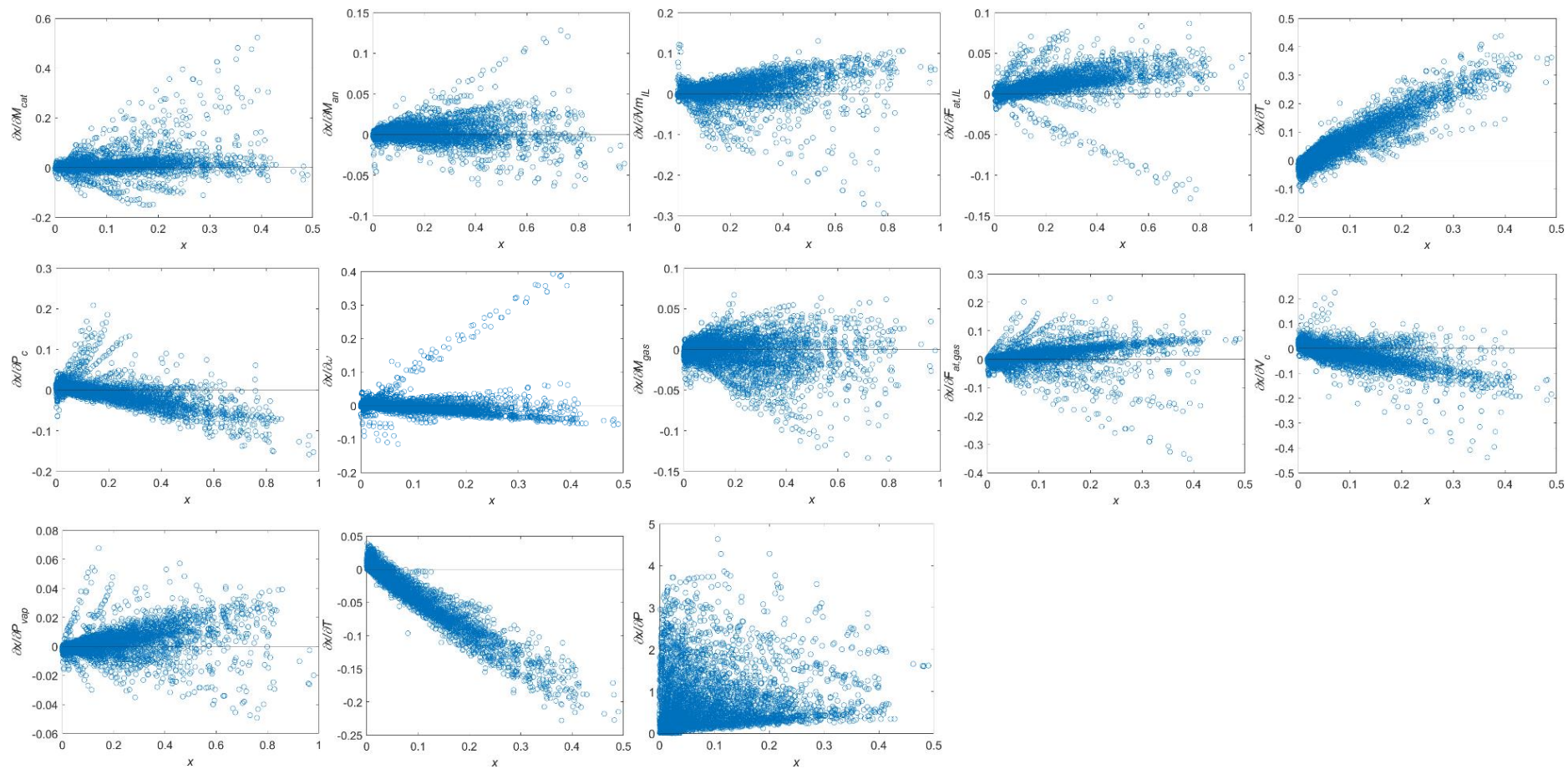
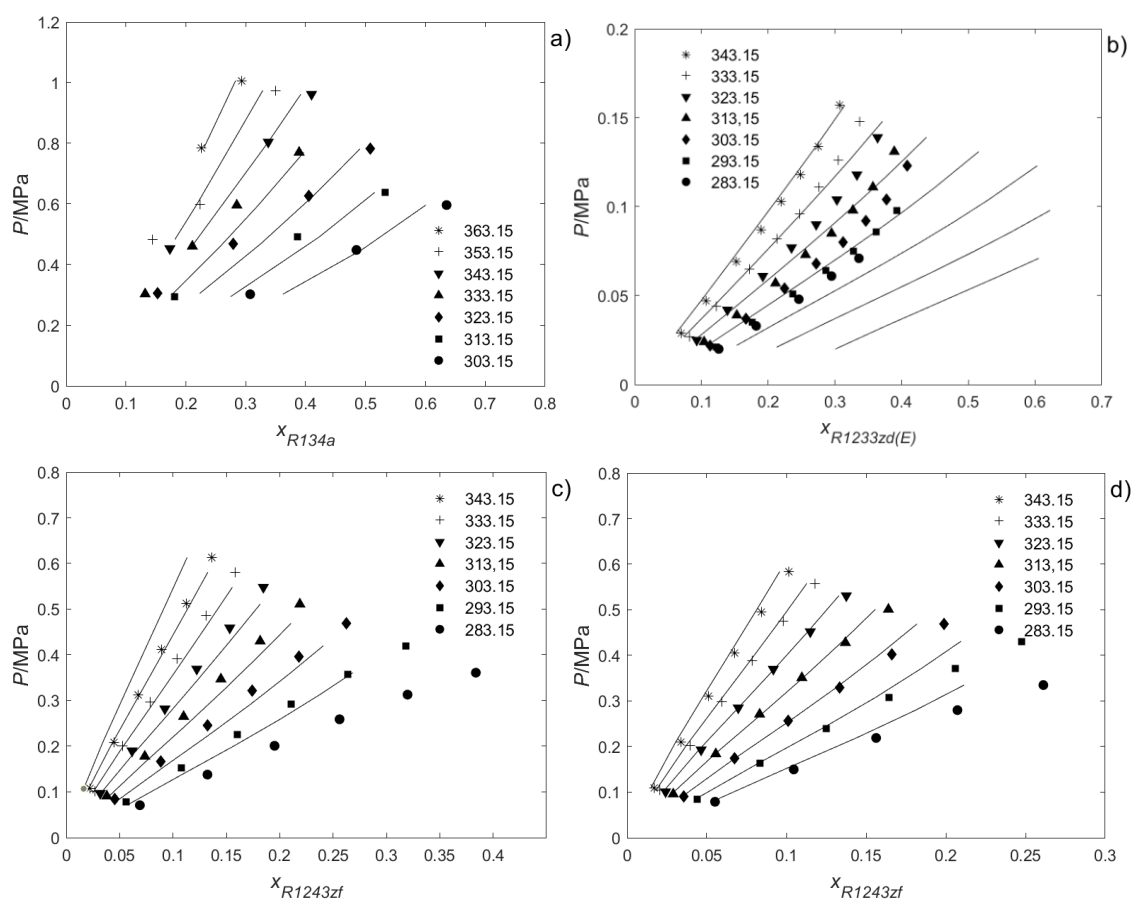


Figure S3. Partial derivatives of the calculated output variable ( $x$ , absorbed gas molar fraction) with respect to each input variable represented against the experimental absorbed molar fraction.



**Figure S4.** Comparison between the experimental data (symbols) from references [1–3] and the ANN predictions (lines) for the systems (a) R134a + [C<sub>4</sub>mim][Tf<sub>2</sub>N], (b) R1233zd(E) + [P<sub>66614</sub>][Cl], (c) R1243zf + [C<sub>4</sub>mim][OTf], and (d) R1243zf + [C<sub>4</sub>mim][PF<sub>6</sub>].

## References

- [1] T. Esaki, N. Kobayashi, H. Uchiyama, Y. Matsukuma, Characteristics of Absorption Equilibrium with HFC-134a and an Ionic Liquid Pair, *J. Mater. Sci. Chem. Eng.* 07 (2019) 65–78. <https://doi.org/10.4236/msce.2019.73006>.
- [2] T. Jiang, X. Meng, Y. Sun, L. Jin, Q. Wei, J. Wang, X. Wang, M. He, Absorption behavior for R1234ze(E) and R1233zd(E) in [P66614][Cl] as Working Fluids in Absorption Refrigeration Systems, *Int. J. Refrig.* In press (2021). <https://doi.org/10.1016/j.ijrefrig.2021.07.020>.
- [3] X. Jia, W. Dou, X. Wang, Solubility determination and mixing thermodynamic properties of R1243zf in two 1-butyl-3-methyl-imidazolium based ionic liquids, *J. Mol. Liq.* 364 (2022) 120031. <https://doi.org/10.1016/j.molliq.2022.120031>.



**3.8. Scientific publication 8. “Understanding the molecular features controlling the solubility differences of R-134a, R-1234ze(E) and R-1234yf in 1-alkyl-3-methylimidazolium tricyanomethanide ionic liquids”, Salvador Asensio-Delgado, Miguel Viar, Agílio A.H. Pádua, Gabriel Zarca, Ane Urriaga, *ACS Sustainable Chemistry & Engineering*, 10 (2022), 15124-15134.**

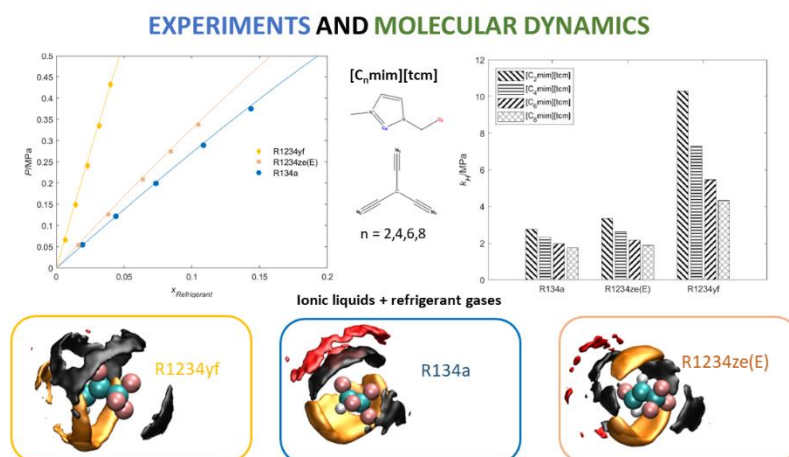


Figure 19. Graphical abstract of the article “Experimental and molecular dynamics study on the absorption of R134a, R1234ze(E), and R1234yf in 1-alkyl-3-methylimidazolium tricyanomethanide ionic liquids”.

The previous experimental studies showed that the solubility of R1234ze(E) in ILs was much higher than that of its isomer R1234yf, and similar to the solubility of R134a. Even though this high solubility is positive for the design of absorption refrigeration systems, it hinders the design of separation processes such as extractive distillation able to separate the azeotropic mixture of R134a and R1234ze(E). The analysis of trends in Publication 1 did not find any way to increase the selectivity, so that advanced methods are necessary to understand the solvation behavior and interactions between the solutes and solvents. To that end, I visited the Ionic Liquids group of the Laboratoire de Chimie of the ENS de Lyon and learned, under the supervision of Professor Agílio Pádua, the basics on how to use molecular dynamics simulations to study the interactions between F-gases and ILs. This methodology allows the study of the microscale of properties that cannot be observed in the mesoscale, giving useful information on solute-solvent interactions for the design of solvents and entrainers, among other applications. Resulting from this experience, this article is published as a combination of a series of experiments made at the University of Cantabria and simulations made at the ENS de Lyon. To continue with cyanide based ILs, the solubility of R134a, R1234ze(E), and R1234yf in  $[C_n\text{mim}][\text{tcm}]$  ILs with  $n = 2, 4, 6$ , and 8 was determined experimentally. Then, the data were used to validate the force fields used

for the simulations, and the solvation environments were studied combining the CL&Pol force field for ILs with some fixed-charge force fields for the gases adapted to make them polarizable. This combined experimental and simulation study showed that the interactions between F-gases and  $[C_n\text{mim}][\text{tcm}]$  ILs occurs mainly through interactions of the IL cation alkyl chain with the fluorinated parts of the refrigerants in the form of nonpolar-nonpolar interactions. Therefore, the future selection of a suitable solvent to separate R134a and R1234ze(E) should aim to modify the IL cation alkyl chains in a way such that they interact differently with each of the gases. Figure 19 shows the graphical abstract available in the online version and in the first page of the article.

# Understanding the Molecular Features Controlling the Solubility Differences of R-134a, R-1234ze(E), and R-1234yf in 1-Alkyl-3-methylimidazolium Tricyanomethanide Ionic Liquids

Salvador Asensio-Delgado, Miguel Viar, Agílio A.H. Pádua,\* Gabriel Zarca, and Ane Urriaga\*

Cite This: *ACS Sustainable Chem. Eng.* 2022, 10, 15124–15134

Read Online

ACCESS |

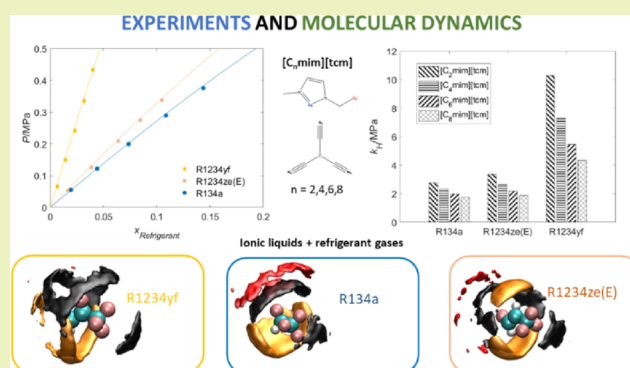
Metrics &amp; More

Article Recommendations

Supporting Information

**ABSTRACT:** This work reports a study of the absorption of fluorinated refrigerant gases in ionic liquids (ILs) from a combined experimental and computational approach to gain insights into the solvation of these greenhouse gases. The results allow the selection of solvents for fluorinated gas recovery, based on molecular characteristics, and improve the recyclability of these high-value-added compounds. The solubility of R-134a, R-1234yf, and R-1234ze(E) was measured experimentally in 1-alkyl-3-methylimidazolium tricyanomethanide ILs at 283.15–323.15 K and up to 5 bar to investigate the influence of the alkyl side chain length of the cations in the ILs. Molecular dynamics was used to study solvation environments around refrigerant molecules in terms of radial distribution functions, coordination numbers, and spatial distribution functions. Simulations were carried out with the recent CL&Pol polarizable force field for ILs, which includes polarization effects explicitly. The force field was validated against experimental solubility through free-energy perturbation calculations. The main effects influencing the solubility of fluorinated refrigerants in ILs result from interactions with the anions and with the cation head group alkyl chain, setting a basis for a rational selection and design of ILs for processes to recover and recycle refrigerants in a circular economy model.

**KEYWORDS:** ionic liquids, fluorinated refrigerant gases, absorption, recovery, experimental thermodynamics, computational chemistry, molecular dynamics simulations, polarizable force field



## INTRODUCTION

The sector of refrigeration and air conditioning (RAC) is shifting toward the use of more environmentally friendly working fluids. Hydrofluorocarbon (HFC) mixtures have been used since the early 2000s as an alternative to the concerning ozone-depleting chlorofluorocarbons (CFCs) and hydrochlorofluorocarbons (HCFCs) because HFCs do not affect the atmospheric ozone layer.<sup>1</sup> However, HFCs are powerful, persistent greenhouse gases, with global warming potentials (GWP) several orders of magnitude higher than those of CO<sub>2</sub>, the reference substance. Driven by new legislation aiming at reducing greenhouse gas emissions,<sup>2,3</sup> refrigerant manufacturers developed hydrofluoroolefins (HFOs), a new class of fluorinated gases (F-gases). HFO molecules include carbon-carbon double bonds that greatly reduce their atmospheric lifetimes and, therefore, their GWP.<sup>1</sup> Nevertheless, there is no quintessential alternative compound able to fully substitute HFCs in every operating condition, as new proposed refrigerants with lower GWP present trade-offs, such as increased flammability or low volumetric capacities, that lead to larger RAC equipment.<sup>4,5</sup> Therefore, the new refrigerant mixtures that appear consist of low-GWP, slightly flammable

HFOs, for example, R-1234yf or R-1234ze(E) (2,3,3,3- and trans-1,3,3,3-tetrafluoropropene, respectively), with moderate-GWP and nonflammable HFCs such as R-134a (1,1,1,2-tetrafluoroethane).<sup>6,7</sup>

Despite these developments, the RAC industry still needs to adapt to a more sustainable model aligned with a circular and low-carbon economy.<sup>8</sup> In this sense, new F-gas legislation established a new paradigm in the RAC sector by including the term “reclamation”, defined as the reprocessing of a fluorinated greenhouse gas recovered during maintenance or prior to disposal, to match the equivalent performance of a virgin substance.<sup>2</sup> At present, different technologies have been proposed for the separation of close-boiling and azeotropic refrigerant mixtures, such as membrane separation,<sup>9–12</sup>

Received: July 30, 2022

Revised: October 24, 2022

Published: November 8, 2022

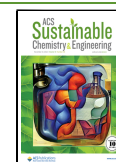




Table 1. Properties of the Refrigerant Gases Studied in This Work<sup>43–45</sup>

refrigerant	R-134a	R-1234yf	R-1234ze(E)
chemical name	1,1,1,2-tetrafluoroethane	2,3,3,3-tetrafluoropropene	trans-1,3,3,3-tetrafluoropropene
formula	C <sub>2</sub> H <sub>2</sub> F <sub>4</sub>	C <sub>3</sub> H <sub>2</sub> F <sub>4</sub>	C <sub>3</sub> H <sub>2</sub> F <sub>4</sub>
molecular weight (g·mol <sup>-1</sup> )	102	114	114
boiling point at atmospheric pressure (K)	247.08	243.67	254.19
critical temperature (K)	374.21	367.85	382.52
critical pressure (MPa)	4.06	3.38	3.63
critical volume (cm <sup>3</sup> ·mol <sup>-1</sup> )	199	240	233
dipole moment (D)	1.56	2.24	1.13

adsorption on porous materials,<sup>13–18</sup> or absorption-based extractive distillation processes.<sup>6,19–29</sup> This last application is where ionic liquids (ILs) have attracted the most attention because of their unique properties, among which their nonvolatility and the ability to solubilize large amounts of F-gases stand out, related to the objective of the present study.<sup>30,31</sup>

Our extensive analysis of the information available on F-gas absorption in ILs showed that the solubility selectivity for separation of HFC and HFO mixtures could be enhanced using ILs with low molar volume (which is linked to higher charge density in the ions).<sup>6</sup> Using this knowledge, we previously studied the absorption of HFCs and HFOs in ILs with thiocyanate and dicyanamide anions and obtained the highest selectivity values to date for the separation of R-32 (difluoromethane) and R-134a from R-125 (pentafluoroethane) and R-1234yf, calculated in terms of the ratio of Henry's law constants at infinite dilution and equilibrium flash separations at 5 bar based on NRTL model calculations.<sup>30,32,33</sup> These statements should be validated by means of experimental ternary data as in the recent article by Baca et al.<sup>34,35</sup> However, the separation of R-134a from R-1234ze(E) was still found to be difficult because the HFO R-1234ze(E) is more soluble than its isomer R-1234yf. The rationale behind this difference in solubility is not completely clear because of their very similar physical properties. Table 1 shows a summary of properties of the F-gases considered in this work, which are very similar except for the dipole moment. As can be seen, the higher value of the dipole of R-1234yf compared to that of R-134a and R-1234ze(E) would suggest stronger solute-IL interactions, which is the opposite trend to the observed experimental solubility. Therefore, advanced studies based not only on experimental observations but also on theoretical studies from different perspectives can help understand the interactions between F-gases and ILs, and to select or design the optimal ILs to act as entrainers in solubility-based separation processes.<sup>36</sup> In this regard, advanced molecular equations of state like soft-SAFT,<sup>8,22,37–39</sup> quantum chemistry calculations such as those from COSMO-RS,<sup>23,40</sup> or molecular dynamics (MD) simulations,<sup>41,42</sup> can help characterize the interactions between F-gases and ILs suitable for separations.

MD proved an essential tool for the study of the physical chemistry of ILs. The main advantage of MD is the possibility of modeling systems consisting of tens of thousands of atoms for several tens of nanoseconds with a high level of detail at the atomistic scale on specific site-site interactions, being at an intermediate level between quantum chemistry calculations (electronic structure level) and coarse-grained simulations (in which atomic-level details are sacrificed).<sup>46</sup> Thus, the use of atomistic force fields presents a reasonable compromise between the necessary computational cost and the level of

detail that can be attained to represent the interactions and the resulting local structure, medium-range ordering, and dynamic properties of ILs.<sup>47</sup> To our knowledge, three MD studies of mixtures of F-gases and ILs have been reported. One of them analyzes the interaction of [C<sub>4</sub>C<sub>1</sub>im][Tf<sub>2</sub>N] with R-1234yf, concluding that both the anion and the cation play an important role in the absorption of the HFO.<sup>48</sup> The other two studies concern imidazolium ILs where the alkyl chains have been fluorinated, showing that fluorination increases the solubility because of entropic effects related to larger free volumes.<sup>41,42</sup> During the revision process of this article, another study was published studying the structure and dynamics of absorption of HFCs in ILs.<sup>49</sup>

The studies in the literature were performed using fixed-charge force fields, which have drawbacks for ILs, namely, shortcomings when representing both structural and dynamic properties. Nonpolarizable models with ionic charges can give good structural properties and density but lead to slow dynamics (overestimating viscosity and underestimating diffusion by one order of magnitude). Attempts to remediate this by scaling down ionic charges (to 0.8 instead of 1 for example) improve dynamics, but the loss of cohesive energy leads to underestimation of density. The CL&Pol polarizable force field for ILs was recently developed for the simulation of systems containing aprotic and protic ILs and deep eutectic solvents.<sup>50</sup> CL&Pol includes explicitly polarization effects through placing Drude-induced dipoles on the atomic sites to realistically account for induction (polarization) effects in ionic systems, enabling a correct description of their structure and dynamics.<sup>51</sup> The CL&Pol model is also transferable and extendable, including the capability to generate polarizable parameters from fixed-charge force fields following a procedure detailed since its conception.<sup>47</sup>

Hence, in this work, we take advantage of already available fixed-charge force fields<sup>52–54</sup> for the F-gases of interest and create a polarizable version of them, compatible with the CL&Pol force field for the solvents. We study the solubility of the HFC R-134a and the HFOs R-1234yf and R-1234ze(E) in ILs with the tricyanomethanide anion, to complete the information on the absorption of F-gases in ILs with cyano-based anions and gain more insight into the differences in solubility between the very similar HFOs. To do so, we start by determining experimentally the solubility of the three F-gases in four 1-alkyl-3-methylimidazolium tricyanomethanide ILs ([C<sub>n</sub>C<sub>1</sub>im][tcm]), considering alkyl chains with 2, 4, 6, and 8 carbon atoms. We compare these with previous data on the absorption of the three gases in other ILs and obtain thermodynamic properties, namely, the Henry's law constants. We then use MD simulations with the recently developed CL&Pol polarizable force field to analyze the solvation environments around the F-gases and gain insight into the

absorption mechanisms of the refrigerants in ILs. We check the validity of the simulation methodology by means of free-energy perturbation (FEP) calculations of the solubility, which we compare with the experimental data.

## METHODS

**Materials.** The refrigerant gases R-134a, R-1234ze(E), and R-1234yf were purchased from Gas Servei, S.A. (Spain) with a purity of 99.9 vol % and used as received. The ILs  $[C_nC_1im][tcm]$  ( $n = 2, 4, 6, 8$ ) were purchased from IoLiTec (Germany) with a purity of 98 wt % and vacuum dried to remove any traces of water. The final water content was measured to be lower than 50 ppm using the Karl Fischer coulometric method.

**Experimental Apparatus and Procedure.** The solubility of F-gases in ILs was measured using the isochoric saturation in the same equipment described and validated in our previous publications<sup>30,31</sup> and summarized in the Supporting Information of this article.

**Thermodynamic Modeling.** The experimental solubility data are modeled using the nonrandom two-liquid activity-coefficient model (NRTL), which has been widely used<sup>30–33,45,55–59</sup> to model the vapor–liquid equilibria (VLE) of fluorinated refrigerant gases in ILs. The thermodynamic modeling methodology is the same used in our previous studies<sup>30–33</sup> and is summarized in Section II of the Supporting Information.

**MD Simulations.** MD simulations were performed in large-scale atomic/molecular massively parallel Simulator (LAMMPS) software using the CL&Pol polarizable force field for the ILs.<sup>47,50,51</sup> The F-gases were described using available sets of parameters<sup>52–54</sup> in compatible functional forms, that is, Lennard–Jones (LJ) sites with point charges. In the CL&Pol force field, the explicit polarization effects are represented by Drude-induced dipoles, where each atomic site holds a positively charged Drude core and a negatively charged Drude particle with mass equal to 0.4 atomic units, attached by a harmonic spring of constant  $k_D$  equal to 4184 kJ·mol<sup>-1</sup>. The polarization procedure presented in the study of Goloviznina et al.<sup>47</sup> was followed here to obtain a polarizable version of the original fixed-charge force fields of the gases, of which a short summary follows. This procedure uses the *polarizer* and *scaleLJ* tools available in Pádúa's group repositories.<sup>60</sup>

The partial charges of the Drude particles were evaluated from atomic polarizabilities according to  $\alpha = q_D^2/k_D$  using the atomic polarizabilities from the work of Heid et al.<sup>61</sup> Heavy atoms are considered as polarizable, while the polarizability of the H atoms was merged into those of the atoms they are attached to. The Thole damping function<sup>62</sup> with the  $a$  parameter set to 2.6 was used to screen (or smear) the interactions between induced dipoles at a short range, to avoid instabilities. The temperature of the degrees of freedom of the Drude particles with respect to their cores was kept at 1 K to approximate the dynamics to those of the self-consistent regime.<sup>47</sup> The LJ potential from the nonpolarizable CL&P force field was scaled down to avoid double counting the induction effect, which is present in the initial fixed-charge force field implicitly.<sup>47</sup> The cut-off radius for LJ interactions was set to 12 Å, applying tail correction to energy and pressure. The electrostatic interactions were calculated up to a long range using the particle–particle–particle–mesh method with a relative accuracy of 10<sup>-5</sup>. The bond lengths involving H atoms were constrained using the SHAKE algorithm to allow simulations with a time step of 1 fs. Periodic cubic boxes containing 300 IL ion pairs with 12 molecules of F-gas were prepared using the *Packmol*<sup>63</sup> and *fftool*<sup>64</sup> utilities. Then, they were equilibrated for 5 ns at 343 K and 1 bar using a Nosé–Hoover thermostat and barostat, followed by 10 ns production runs, from which the local structure was analyzed. The simulations have been performed using 100 fs as temperature time constant, 1 ps as pressure time constant, and 20 fs for the thermostat of the Drude particle motion.

For validation of the simulations, the residual chemical potential ( $\mu^{res}$ ) of 1 molecule of F-gas in cubic boxes of 35 Å of side length with 100 IL ion pairs was calculated using the free-energy perturbation (FEP) method. First, the LJ interaction was progressively activated

followed by the Coulomb interactions and the induced dipoles, passing from a molecule of gas present in the box but not interacting with the solvent to a final state with the molecule fully interacting with the solvent, through a sequence of equilibrium intermediate states of 1000 ps each. The full procedure for the FEP method is explained in the Supporting Information.

## RESULTS AND DISCUSSION

**Experimental Solubility.** The solubility of R-134a, R-1234yf, and R-1234ze(E) in  $[C_nC_1im][tcm]$  ILs was measured at temperatures from 283.15 to 323.15 K and pressures up to 5 bar. Figure 1 shows the solubility of R-134a, R-1234yf, and R-1234ze(E) in  $[C_2C_1im][tcm]$ , and all the experimental data and figures for the remaining systems are presented in Tables S1 to S12 and Figures S1 to S3 of the Supporting information. In addition, Table S13 lists the NRTL parameters for the 12 F-gas/IL pairs considered in this study. Additionally, the solid lines in Figure 1 present the solubility obtained from NRTL modeling and the dashed lines represent the immiscibility region predicted by the NRTL model.

Figure 1 shows that the solubility is higher at lower temperatures and that the solubility of R-1234yf is much lower than that of the other two F-gases, which is consistent with the solubility trend observed in other ILs.<sup>6</sup> These solubility trends are also followed by the other three ILs, as shown in the Supporting Information. In addition, a comparison of the solubility of each F-gas and IL pair is made in Figure 2, which clearly shows that R-1234yf has larger values of the Henry's law constants, so a much lower solubility. On the other hand, the Henry's law constants of R-1234ze(E) are similar to those of R-134a, showing that the separation of these two gases would be difficult by means of solubility differences in ILs. Figure 2 also shows that, for the three gases, increasing the length of the cation alkyl chain decreases the Henry's law constant and increases the solubility, which is attributed to the higher free volume available in the ILs with longer chains (smaller cohesive energy density because of smaller contribution from the ionic groups). Furthermore, the solubility of R-1234yf increases more steadily with the alkyl chain length than that of the other two F-gases, and therefore, the use of ILs with short cation alkyl chains will provide enhanced solubility selectivity for the separation of this HFO from refrigerant mixtures. In summary,  $[C_2C_1im][tcm]$  would be the most suitable of the four ILs studied in this work for the separation and recovery of R-1234yf from its azeotropic mixtures with R-134a.

**MD Simulation. Validation of the Force Fields through FEP Calculations.** The solubility behavior of the two tetrafluoropropene isomers, R-1234yf and R-1234ze(E), considered in this work is striking because they have very different solubilities in ILs despite similar physical properties. While some ILs have been identified as potential candidates for the separation of the azeotropic mixture of R-134a with R-1234yf (including the  $[C_2C_1im][tcm]$  IL studied in this work), there are still no suitable candidates for the separation of the also azeotropic mixture of R-134a with R-1234ze(E), which is a binary mixture present, for example, in the R-448A or R-450A commercial refrigerants. For this particular separation using absorption media, the highest solubility selectivity values in ILs are lower than 1.2 as of today.<sup>6</sup> Thus, studying the mechanisms that rule the solvation of the F-gases in ILs becomes necessary to aid in the selection of suitable solvents for the separation of R-1234ze(E) from R-134a.



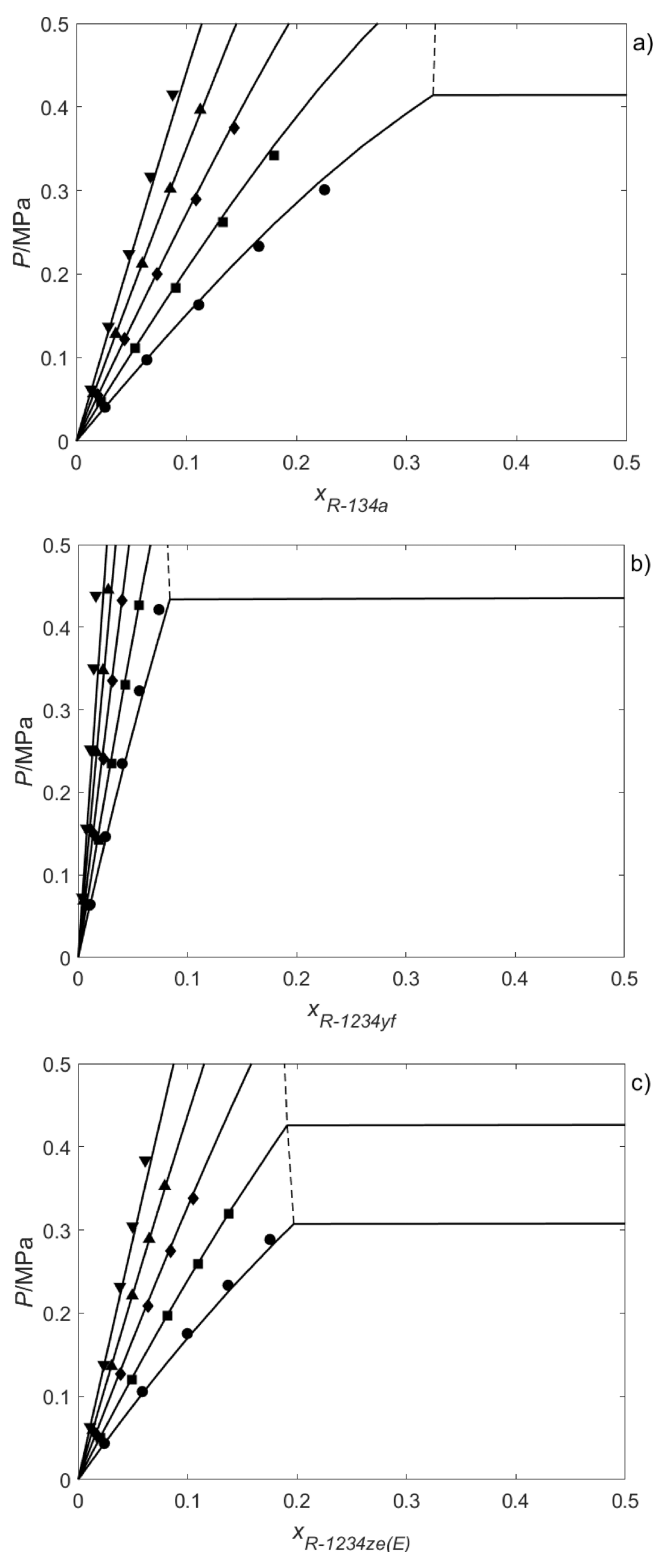


**Figure 1.** Solubility of the refrigerant gases (a) R-134a, (b) R-1234yf, and (c) R-1234ze(E) in  $[C_2C_1im][tcm]$  at various temperatures: 283.15 (●), 293.15 (■), 303.15 (◆), 313.15 (▲), and 323.15 K (▼). Solid lines represent calculations using the NRTL model and dashed lines represent the immiscibility region predicted by the NRTL model.

In order to check the ability of the polarizable force field to reproduce the interactions of the F-gases with the ILs, the solubility of the polarized version of the F-gases was computed

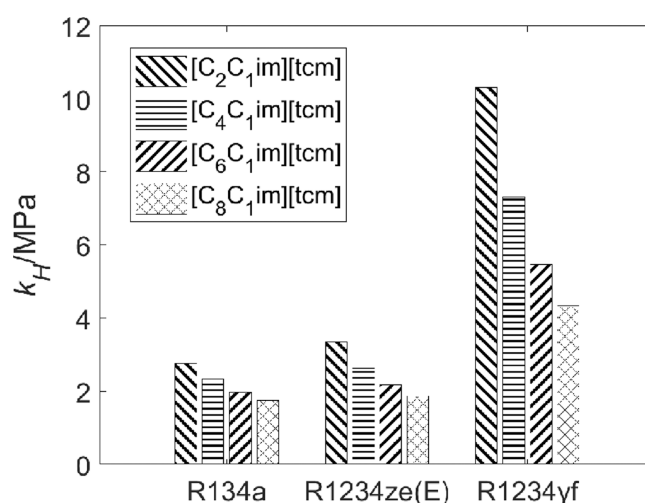


**Figure 2.** Henry's law constants for the solubility of R-134a, R-1234ze(E), and R-1234yf in  $[C_nC_1im][tcm]$  ILs at 303.15 K.

in  $[C_2C_1im][tcm]$ . These solubilities were determined as Henry's law constants from the residual chemical potentials calculated using the FEP method, as explained in Section 2.4. Figure 3 shows the simulation results at 343 and 353 K as

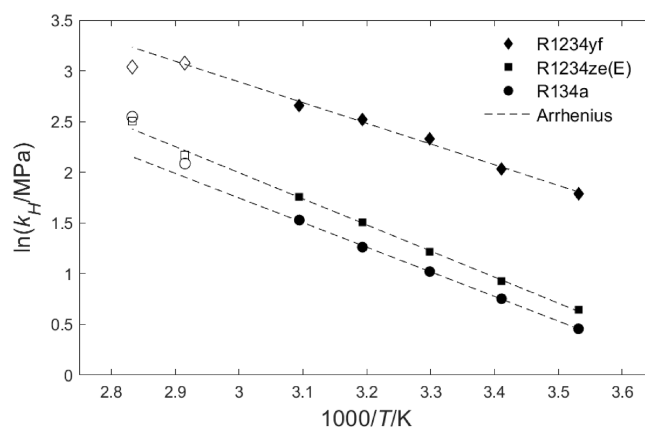


**Figure 3.** Henry's law constants for the solubility of F-gases in  $[C_2C_1im][tcm]$ . Filled symbols are the experimental solubility data, while the hollow symbols result from the FEP calculations. Lines are the van't Hoff regressions calculated using only the experimental datapoints and extended to 353 K.

hollow symbols, together with the experimental Henry's law constant (filled symbols) previously determined in the temperature range 283.15–323.15 K, from which a van't Hoff extrapolation was done up to 353 K. The FEP calculations were carried out at higher temperature than the experimental range because the lower viscosity of the ILs reduces enormously the time required for the trajectories. As can be seen, the Henry's constants predicted by FEP are in quantitative agreement at 343 K with the van't Hoff extrapolations, especially for the two HFOs. R-134a shows a slightly higher deviation, but still with the correct qualitative trend. The results at 353 K are still in good agreement with the Arrhenius extrapolation for R-1234ze(E), but they are more deviated for the other two gases. These solubility calculations are very sensitive to solute–solvent interactions, so the level of agreement obtained means the force field model represents

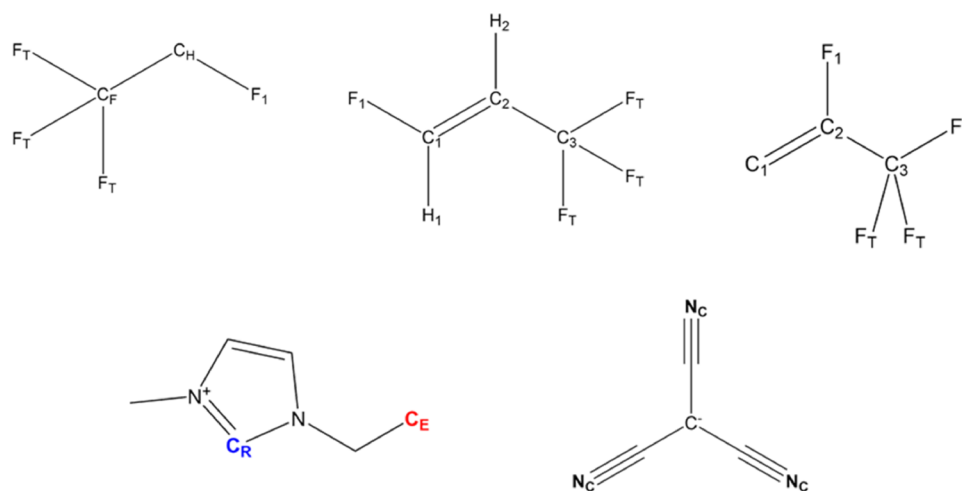


**Figure 4.** Names attributed to the atoms of the F-gases and ILs. From left to right and top to bottom, the structures are R-134a, R-1234ze(E), R-1234yf, and [C<sub>2</sub>C<sub>1</sub>im][tcm].

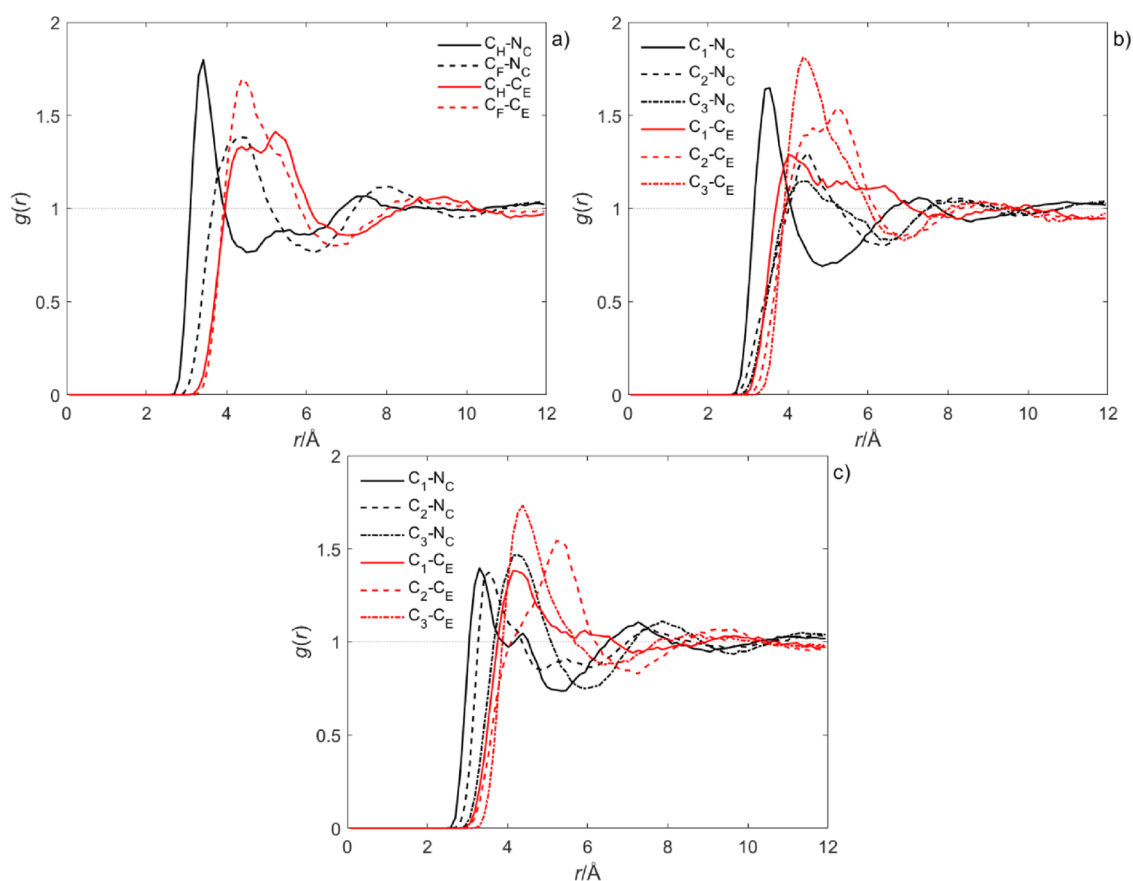


**Figure 5.** Radial distributions function between representative atoms of (a) R-134a, (b) R-1234yf, and (c) R-1234ze(E) and [C<sub>2</sub>C<sub>1</sub>im][tcm].

well those interactions and allows the study of the absorption of F-gases in the [C<sub>n</sub>C<sub>1</sub>im][tcm] ILs.

**Analysis of the Solvation Environments with [C<sub>2</sub>C<sub>1</sub>im][tcm].** Thus, MD simulations can be used to study the solvation environments around F-gases to investigate the solvation behavior. We focused the study of the F-gas interactions with the anion on the terminal N nitrogen atoms of the anion, denoted as N<sub>C</sub> in the CL&Pol force field. For the cation, we focused on the F-gas interactions with the terminal C atoms of the alkyl chains—C<sub>E</sub> for [C<sub>2</sub>C<sub>1</sub>im]<sup>+</sup> and

C<sub>T</sub> for longer alkyl chains—because these represent the nonpolar domain of the IL. In addition, we also considered the F-gas interactions with the acidic carbon placed between the two N atoms of the imidazolium ring of the cations, named C<sub>R</sub>, which presents a positive charge. The R-134a molecular formula is CH<sub>2</sub>F–CF<sub>3</sub>, and we use C<sub>H</sub> to refer to the C atom connected to two H and C<sub>F</sub> to refer to the perfluorinated carbon atom. The carbon atoms of R-1234yf and R-1234ze(E) are referred to as C<sub>1</sub>, C<sub>2</sub>, and C<sub>3</sub> for the CH<sub>2</sub>=CF–CF<sub>3</sub> and

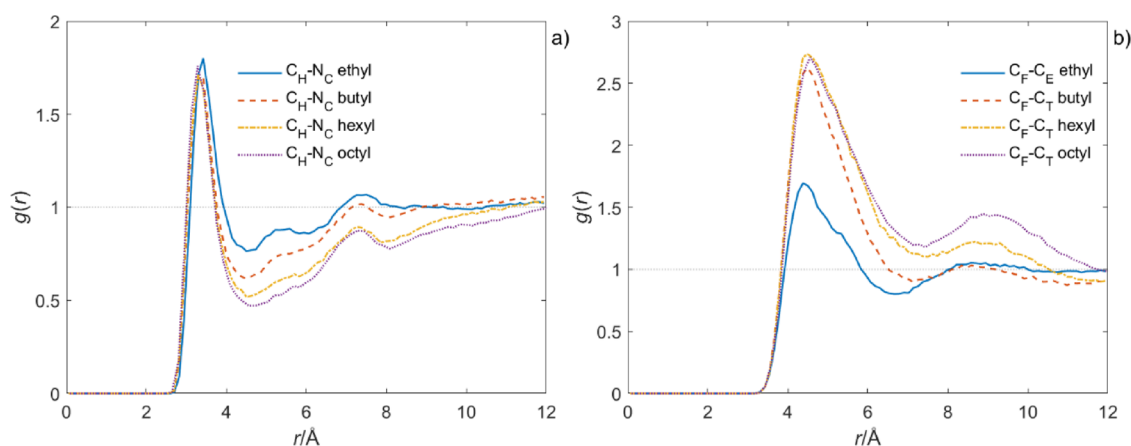


**Figure 6.** Analysis of the local environments around R-134a in  $[C_nC_1im][tcm]$  ILs depending on the cation alkyl chain length. Radial distribution function for (a) the  $C_H-N_C$  interaction and (b) the  $C_F-C_{E/T}$  interaction.

$CHF=CH-CF_3$ , respectively. The molecular structures of the F-gases with the atom nomenclature are shown in Figure 4.

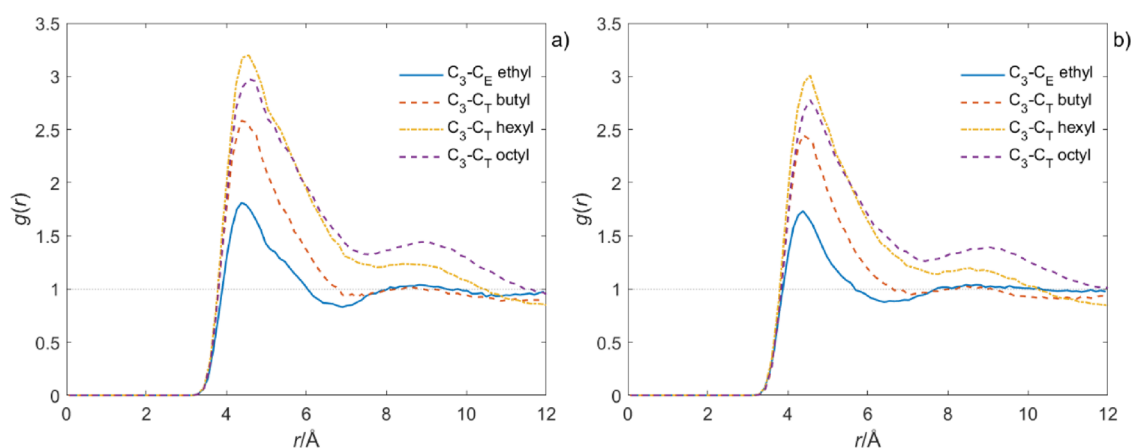
All the simulations were initially equilibrated ensuring convergence of density, as shown in Figure S6a of the Supporting Information. Then, the production trajectories of 10 ns sample the ILs well into the diffusive regime, as shown by the linear plot of mean-squared displacement of the ions as a function of time in Figure S6b of the Supporting Information.<sup>65</sup> Using mean-squared displacement data, the diffusion coefficients of the solvent ions were calculated, and they are presented in Figure S7 of the Supporting Information. Diffusion coefficients characterize the dynamics of the liquid phases and are valuable quantities for process calculations in a number of unit operations. As it can be observed, diffusion coefficients are higher for less viscous ILs (shorter alkyl chains). Also, the ratio between the cation and anion diffusion coefficient decreases for longer cation alkyl chains, which is logical considering that the cation would suffer more collisions decreasing its mobility.

Figure 5 shows the radial distribution functions for the interaction of selected atomic sites of the F-gases R-134a, R-1234yf, and R-1234ze(E), with those of the IL  $[C_2C_1im][tcm]$ , which shows that the F-gases interact both with the cations and the anions. The spatial correlations of every F-gas with the  $C_R$  of the cation ring are weak (peaks of low intensity), so they will not be analyzed further because it does not have an important influence on the differences in solubility and are only depicted in the Supporting Information in Figure S8. The strongest and closest interaction between R134a and  $[C_2C_1im][tcm]$  occurs between the  $N_C$  atoms of the anion and the  $C_H$  atom of the refrigerant, at a distance of 3.42 Å, where the local density of  $N_C$  atoms is 1.8 times the average density, and the coordination number (calculated by integrating the radial distribution function up to the first minimum) equals 0.94, meaning that each  $C_H$  has roughly one  $N_C$  atom close, maybe as a result of a hydrogen bond between the gas and the anion. This happens because the  $N_C$  atoms represent the negative domain of the IL, and the  $C_H$  is where the positive charge of R-134a is localized because of the presence of the two H atoms. The next stronger correlation occurs between the  $C_F$  and the alkyl chain of the cation ( $C_E$ ), at 4.38 Å with a local density 1.7 times the average density and a coordination number equal to 2.86, which represents the nonpolar domain of the IL. This same behavior is observed for

the terminal  $-CF_3$  groups of the HFO molecules ( $C_3-C_E$  interactions), which present even stronger peaks than for the anion interaction ( $N_C$ ) with the carbon atoms of the F-gas. The most likely distance of  $C_3-C_E$  interactions is also 4.38 Å for the HFOs, which is interesting because it shows that the three refrigerant gases interact through van der Waals interactions with the ILs despite being polar molecules. In fact, to confirm this, we made quantum chemistry calculations in Gaussian using the CHelpG method with MP2/cc-pVTZ(-f) densities (Table S14) that showed that the  $-CF_3$  group of the F-gases has a small net charge, making it suitable for dispersion-dominated interactions.

Regarding the solubility differences between the HFO isomers, Figure 5 shows a remarkable difference between R-1234yf and R-1234ze(E), which is that only the  $C_1$  of the former interacts in the first solvation shell with the  $N_C$  of the IL anion, while both the  $C_1$  and  $C_2$  of the latter show this kind of interaction. This is due to all the positive charge (the H atoms) of R-1234yf being placed around the  $C_1$ , while in R-1234ze(E), both the  $C_1$  and  $C_2$  have one H atom each, creating two positive sites that can bind to the negative  $N_C$  atoms. Another effect of this isomer difference can be seen in the atomic charges listed in Table S14, where the  $CH_2=$  and  $=CF-$  groups of R-1234yf present almost no charge because the charge on these C compensates those of their substituents, whereas the  $CHF-$  and  $-CH-$  groups of R-1234ze(E) present local positive and negative charges, respectively. Therefore, this difference in partial charges of the atomic sites may be the reason why the solubility of R-1234ze(E) is always larger than that of R-1234yf despite its lower dipole moment, that is, the local structure of R-1234ze(E) allows stronger interactions between both the  $C_1$  and  $C_2$  atoms and the anion.

**Influence of the Cation Alkyl Chain.** The solvation environments around the F-gas molecules vary depending on the length of the cation alkyl chain. Figure 6 shows how the radial distribution functions for the interaction of R-134a with the anion and the cation vary depending on the alkyl chain length of the IL. As it can be seen, for the interaction of the hydrogenated carbon  $C_H$  of R-134a with the  $N_C$  of the anion, the peak is in every case almost at the same distance of 3.3–3.4 Å and exhibits a similar peak intensity. However, the coordination numbers shown in Figure S9a decrease with increasing cation alkyl chain, which can be related to a less



**Figure 7.** Analysis of the local environment of HFOs in  $[C_n C_1 im][tcm]$  ILs depending on the cation alkyl chain length. Radial distribution function for (a) the R-1234yf  $C_F-C_{E/T}$  interaction and (b) the R-1234ze(E)  $C_F-C_{E/T}$  interaction.

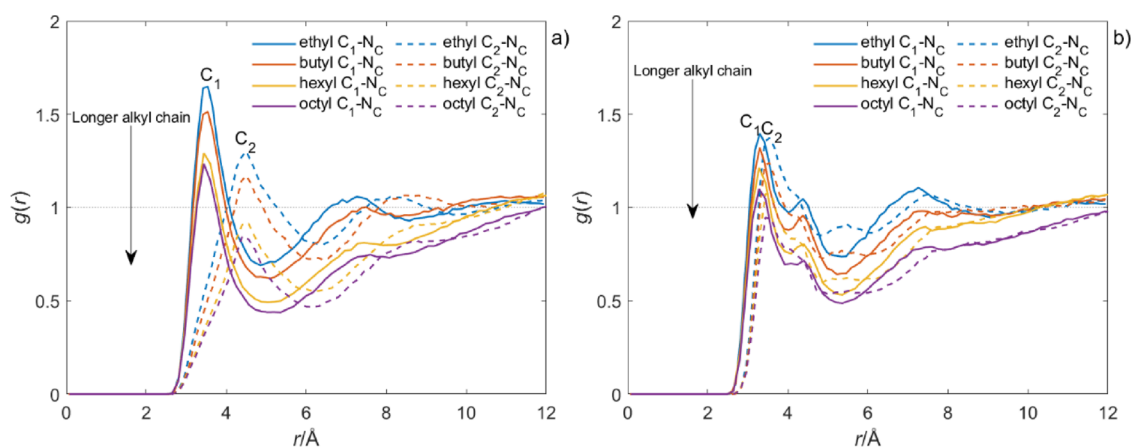


**Figure 8.** Analysis of the local environments of HFOs in  $[C_n C_1 im][tcm]$  ILs depending on the cation alkyl chain length. Radial distribution function for (a) the R-1234yf  $C_{1/2}-N_C$  interaction and (b) the R-1234ze(E)  $C_{1/2}-N_C$  interaction.



**Figure 9.** Spatial distribution functions for selected atoms of  $[C_2 C_1 im][tcm]$  around R-134a (left), R-1234yf (middle), and R-1234ze(E) (right). Gray surface corresponds to  $C_E$  atoms (isodensity contour at 2.6 times the average density), the orange surface corresponds to  $N_C$  atoms (isodensity contour at 2.6 times the average density), and the red surface corresponds to  $C_R$  atoms (isodensity contour at 1.8 times the average density). Figure prepared using TRAVIS.<sup>66,67</sup>

structured packing. For the interaction with the end-carbon of the alkyl chain, the interaction of  $C_F$  with the  $C_E$  of  $[C_2 C_1 im]^+$  behaves a little different than that with the  $C_T$  of the longer-chain ILs. In this way, the  $C_F-C_E$  interaction takes place at a slightly closer distance (4.38 Å vs 4.5–4.58 Å) and with a maximum intensity lower than that for the  $C_F-C_T$  interactions. Accordingly, comparing the coordination numbers in Figure S9b, the same decreasing trend as for the  $C_H-N_C$  interactions can be seen for the butyl, hexyl, and octyl chains; however, the coordination number is smaller for the  $C_F-C_E$  interaction because of closer IL packing that may result from lesser steric impediments that can explain the lowest solubility of F-gases in

the smaller IL, as shown in Figure 2 above in terms of experimental Henry's law constants. The same difference between the  $C_E$  and  $C_T$  interactions are observed for the two HFOs in Figures 7 and S10.

For the interaction of the HFOs with the anion, the behavior is markedly different than that for R-134a. In R-134a, the main peak has the same height and is at the same distance for the 4 ILs, but for the HFOs, the first peak is at a slightly closer distance and exhibits a somewhat lower intensity when the alkyl chain is smaller, as shown in Figure 8. The coordination numbers of anions in Figure S11, nevertheless, follow the same trend as for R-134a, that is, they decrease for longer cation



alkyl chains. This behavior of the HFOs can be explained because the longer alkyl chains may shield the anions and hinder their interactions with the refrigerants, while they also incur in a less ordered packing that enhances the solubility so that the main driving force of the solubility is the interactions with the alkyl chains. However, the difference in solubility between R-1234yf and R-1234ze(E) has to be explained by the interactions with the anion because, as commented earlier, both the  $C_1$  and  $C_2$  of the R-1234ze(E) are able to interact with the  $N_C$ , while this interaction only happens with the  $C_1$  of the R-1234yf, as evidenced by the very similar peaks for  $C_1$  and  $C_2$  in Figure 8b, clearly different from Figure 8a. This can be demonstrated further by looking at the spatial distribution functions that we calculated using the TRAVIS trajectory analyzer.<sup>66,67</sup> Figure 9 presents the spatial density isosurfaces for the F-gases in  $[C_2C_1im][tcm]$ , and the remaining are presented as Figures S12 to S14 of the Supporting Information. They were prepared using TRAVIS Trajectory Analyzer and Visualizer.<sup>66,67</sup>

The spatial distribution functions show that the interactions of the F-gases with the cation alkyl chains (gray) are similar for all of them, where the  $C_E$  or  $C_T$  are placed around the F atoms of the solute and along axially near the  $-CF_3$  group. A significant difference comes from the interactions with the anion (orange), where it can be seen that for R-134a and R-1234ze(E), these present thick regions opposed to the H atoms (two of them in R-1234ze(E) forming a sort of anion "ring" around the  $C_1$  and  $C_2$ ), whereas the anionic regions around the H atoms of R-1234yf are thinner or almost nonexistent as in  $[C_8C_1im][tcm]$ , Figure S14. The spatial distribution functions also show the interactions with the acidic carbon  $C_R$  of the cation ring (red), as a low, noisy signal that always occurs in the second solvation shell.

Therefore, for the ILs studied in this work, we can conclude that the main difference in solubility between R-134a and R-1234ze(E) against R-1234yf comes from the different interactions that they undergo with the anions, as the interactions with the cations are similar. Then, to find an IL able to separate mixtures of R-1234ze(E) with R-134a, the ILs should be selected so that they act in one of two domains. The first one would be finding an anion that interacts differently with R-134a than with R-1234ze(E). As the main interaction with the anions in this work occurs through H-bonds to the  $N_C$  atoms, the selected anion should not be able to form this kind of bond, but it should still be capable of interacting strongly with only one of the refrigerants. Finding an anion with these characteristics may be difficult, so an IL acting on the other domain might be a better option. This second domain consists of changing the way in which the cation alkyl chain interacts with the gases. Doping the alkyl chains with double or triple bonds, or including O or other types of atoms, will perturb the IL nonpolar domain, and then, the interactions with  $-CF_3$  groups of the refrigerants will change. Further theoretical and experimental studies should be carried out in this regard to find or design a suitable solvent for this separation.

## CONCLUSIONS

We studied the absorption of R-134a, R-1234yf, and R-1234ze(E) in  $[C_nC_1im][tcm]$  ( $n = 2, 4, 6, 8$ ) ILs from a combined experimental and computational approach in order to gain insights into the mechanisms of absorption of the hydrofluorocarbon and hydrofluoroolefin refrigerant gases in ILs.

The experimental study showed that the solubility of the fluorinated refrigerant gases increases in ILs of higher molecular weight, for the three gases studied. Additionally, the solubility of R-1234yf is lower than those of the other two gases so that its separation could be easily done in extractive processes using ILs as entrainers. However, the separation of R-1234ze(E) from its mixtures with R-134a remains a difficulty because of the low solubility differences of these two gases.

Using MD simulations with the CL&Pol polarizable force field, here parameterized for the F-gases, we first showed that the solvation of refrigerant gases in ILs is predicted in qualitative agreement by FEP calculations. From this model validation, we then analyzed the solvation environments around solvated molecules of R-134a, R-1234yf, and R-1234ze(E) and concluded that the strongest interaction between these gases and the ILs happens through dispersion interactions between the cation alkyl chains and the low-polarity  $-CF_3$  groups of the refrigerants. However, the main difference between the interactions of the two isomers R-1234yf and R-1234ze(E) with the ILs is that the former interacts weakly with the anion, whereas the latter can interact more strongly through the two H atomic sites in its  $C_1$  and  $C_2$  carbon atoms.

Finding or designing an IL able to separate R-134a and R-1234ze(E) should focus on modifying either the interaction with the cation alkyl chain or with the anions, as neither of the two F-gases has a significant interaction with the acidic carbon of the imidazolium ring.

In general, through experiments and advanced computational techniques, this work has contributed to increase the knowledge on the absorption of refrigerant gases with ILs, providing new experimental information and useful insights into the solvation behavior that will promote separation, recovery, and recycling of refrigerants and shift the refrigeration industry toward a more circular economy.

## ASSOCIATED CONTENT

### Supporting Information

The Supporting Information is available free of charge at <https://pubs.acs.org/doi/10.1021/acssuschemeng.2c04561>.

Section I of the SI includes the description of the experimental methods used to measure the solubility of F-gases in ILs and the experimental solubility data of R-134a, R-1234yf, and R-1234ze (E) in  $[C_2C_1im][tcm]$ ,  $[C_4C_1im][tcm]$ ,  $[C_6C_1im][tcm]$ , and  $[C_8C_1im][tcm]$  in the temperature range 283.15 to 323.15 K, at different pressures. Section II includes the description of the NRTL model, how the triphasic equilibrium regions were calculated, and the regressed binary interaction parameters for the systems studied in this work. Section III includes the description of the FEP methodology used to calculate solubility by means of MD simulations, the density and mean-squared displacement showing the correct equilibration of the systems, ion diffusion coefficients, coordination numbers, radial and spatial distribution coefficients for the F-gas + IL systems, and the Gaussian calculations of refrigerant atomic charges (PDF)

## AUTHOR INFORMATION

## Corresponding Authors

Agílio A.H. Pádua – *Laboratoire de Chimie, École Normale Supérieure de Lyon de Lyon & CNRS, 69364 Lyon, France;* [orcid.org/0000-0002-7641-6526](https://orcid.org/0000-0002-7641-6526); Email: [agilio.padua@ens-lyon.fr](mailto:agilio.padua@ens-lyon.fr)

Ane Urriaga – *Department of Chemical and Biomolecular Engineering, Universidad de Cantabria, Santander 39005, Spain;* [orcid.org/0000-0002-8189-9171](https://orcid.org/0000-0002-8189-9171); Email: [urriaga@unican.es](mailto:urriaga@unican.es)

## Authors

Salvador Asensio-Delgado – *Department of Chemical and Biomolecular Engineering, Universidad de Cantabria, Santander 39005, Spain;* [orcid.org/0000-0002-0722-6139](https://orcid.org/0000-0002-0722-6139)

Miguel Viar – *Department of Chemical and Biomolecular Engineering, Universidad de Cantabria, Santander 39005, Spain*

Gabriel Zarca – *Department of Chemical and Biomolecular Engineering, Universidad de Cantabria, Santander 39005, Spain;* [orcid.org/0000-0002-4072-4252](https://orcid.org/0000-0002-4072-4252)

Complete contact information is available at: <https://pubs.acs.org/10.1021/acssuschemeng.2c04561>

## Notes

The authors declare no competing financial interest.

## ACKNOWLEDGMENTS

This publication is a result of project PID2019-105827RB-I00 funded by MCIN/AEI/10.1039/S01100011033 (Spain). S. A.-D. acknowledges the FPU18/03939 grant funded by MCIN/AEI/10.1039/S01100011033 and the funding for the research stay EST21/00100. MD simulations were performed on the computer clusters of the Pôle Scientifique de Modélisation Numérique (PSMN) at the ENS de Lyon (France). S. A.-D. thanks Agílio Pádua and Margarida Costa Gomes for hosting him as a visiting researcher at the Ionic Liquids group of Laboratoire de Chimie of the ENS de Lyon.

## REFERENCES

- (1) McLinden, M. O.; Huber, M. L. (R)Evolution of Refrigerants. *J. Chem. Eng. Data* **2020**, *65*, 4176–4193.
- (2) European Parliament and Council. *EU 517/2014*; European Parliament and Council, 2014; pp 195–230.
- (3) United Nations. Amendment to the Montreal Protocol on Substances That Deplete the Ozone Layer. [https://treaties.un.org/Pages/ViewDetails.aspx?src=IND&mtmsg\\_no=XXVII-2-f&chapter=27&clang=\\_en](https://treaties.un.org/Pages/ViewDetails.aspx?src=IND&mtmsg_no=XXVII-2-f&chapter=27&clang=_en), **2016**.
- (4) McLinden, M. O.; Brown, J. S.; Brignoli, R.; Kazakov, A. F.; Domanski, P. A. Limited Options for Low-Global-Warming-Potential Refrigerants. *Nat. Commun.* **2017**, *8*, 14476.
- (5) Albà, C. G.; Alkhatib, I. I.; Llovel, F.; Vega, L. F. Assessment of Low Global Warming Potential Refrigerants for Drop-In Replacement by Connecting Their Molecular Features to Their Performance. *ACS Sustainable Chem. Eng.* **2021**, *9*, 17034–17048.
- (6) Asensio-Delgado, S.; Pardo, F.; Zarca, G.; Urriaga, A. Absorption Separation of Fluorinated Refrigerant Gases with Ionic Liquids: Equilibrium, Mass Transport, and Process Design. *Sep. Purif. Technol.* **2021**, *276*, No. 119363.
- (7) Mota-Babiloni, A.; Makhnatch, P.; Khodabandeh, R. Recent Investigations in HFCs Substitution with Lower GWP Synthetic Alternatives: Focus on Energetic Performance and Environmental Impact. *Int. J. Refrig.* **2017**, *82*, 288–301.
- (8) Jovell, D.; Pou, J. O.; Llovel, F.; Gonzalez-Olmos, R. Life Cycle Assessment of the Separation and Recycling of Fluorinated Gases Using Ionic Liquids in a Circular Economy Framework. *ACS Sustainable Chem. Eng.* **2022**, *10*, 71–80.
- (9) Pardo, F.; Zarca, G.; Urriaga, A. Separation of Refrigerant Gas Mixtures Containing R32, R134a, and R1234yf through Poly(Ether-Block -Amide) Membranes. *ACS Sustainable Chem. Eng.* **2020**, *8*, 2548–2556.
- (10) Pardo, F.; Gutiérrez-Hernández, S.; Zarca, G.; Urriaga, A. Toward the Recycling of Low-GWP Hydrofluorocarbon/Hydrofluoroolefin Refrigerant Mixtures Using Composite Ionic Liquid-Polymer Membranes. *ACS Sustainable Chem. Eng.* **2021**, *9*, 7012–7021.
- (11) Pardo, F.; Zarca, G.; Urriaga, A. Effect of Feed Pressure and Long-Term Separation Performance of Pebax-Ionic Liquid Membranes for the Recovery of Difluoromethane (R32) from Refrigerant Mixture R410A. *J. Membr. Sci.* **2021**, *618*, No. 118744.
- (12) Harders, A. N.; Sturd, E. R.; Vallier, J. E.; Corbin, D. R.; White, W. R.; Junk, C. P.; Shiflett, M. B. Selective Separation of HFC-32 from R-410A Using Poly(Dimethylsiloxane) and a Copolymer of Perfluoro(Butenyl Vinyl Ether) and Perfluoro(2,2-Dimethyl-1,3-Dioxole). *J. Membr. Sci.* **2022**, *652*, No. 120467.
- (13) Yancey, A. D.; Terian, S. J.; Shaw, B. J.; Bish, T. M.; Corbin, D. R.; Shiflett, M. B. A Review of Fluorocarbon Sorption on Porous Materials. *Microporous Mesoporous Mater.* **2022**, *2022*, No. 111654.
- (14) Wanigarathna, D. K. J. A.; Liu, B.; Gao, J. Adsorption Separation of R134a, R125, and R143a Fluorocarbon Mixtures Using 13X and Surface Modified 5A Zeolites. *AIChE J.* **2018**, *64*, 640–648.
- (15) Wanigarathna, D. K. J. A.; Gao, J.; Liu, B. Fluorocarbon Separation in a Thermally Robust Zirconium Carboxylate Metal–Organic Framework. *Chem. –Asian J.* **2018**, *13*, 977–981.
- (16) Motkuri, R. K.; Annapureddy, H. V. R.; Vijaykumar, M.; Schaeff, H. T.; Martin, P. F.; McGrail, B. P.; Dang, L. X.; Krishna, R.; Thallapally, P. K. Fluorocarbon Adsorption in Hierarchical Porous Frameworks. *Nat. Commun.* **2014**, *5*, 1–6.
- (17) Yancey, A. D.; Broom, D. P.; Roper, M. G.; Benham, M. J.; Corbin, D. R.; Shiflett, M. B. Separation of Azeotropic Hydrofluorocarbon Refrigerant Mixtures: Thermodynamic and Kinetic Modeling for Binary Adsorption of HFC-32 and HFC-125 on Zeolite 5A. *Langmuir* **2022**, *38*, 10836–10853.
- (18) Yancey, A. D.; Corbin, D. R.; Shiflett, M. B. Difluoromethane (HFC-32) and Pentafluoroethane (HFC-125) Sorption on Linde Type A (LTA) Zeolites for the Separation of Azeotropic Hydrofluorocarbon Refrigerant Mixtures. *Langmuir* **2022**, *38*, 1937–1953.
- (19) Asensio-Delgado, S.; Jovell, D.; Zarca, G.; Urriaga, A.; Llovel, F. Thermodynamic and Process Modeling of the Recovery of R410A Compounds with Ionic Liquids. *Int. J. Refrig.* **2020**, *118*, 365–375.
- (20) Garcadiago, A.; Mazumder, M.; Befort, B. J.; Dowling, A. W. Modeling and Optimization of Ionic Liquid Enabled Extractive Distillation of Ternary Azeotrope Mixtures. *Comput. Aided Chem. Eng.* **2022**, *49*, 307–312.
- (21) Monjur, M. S.; Iftakher, A.; Hasan, M. M. F. Sustainable Process Intensification of Refrigerant Mixture Separation and Management: A Multiscale Material Screening and Process Design Approach. *Comput. Aided Chem. Eng.* **2022**, *49*, 661–666.
- (22) Jovell, D.; Gómez, S. B.; Zakrzewska, M. E.; Nunes, A. V. M.; Araújo, J. M. M.; Pereiro, A. B.; Llovel, F. Insight on the Solubility of R134a in Fluorinated Ionic Liquids and Deep Eutectic Solvents. *J. Chem. Eng. Data* **2020**, *65*, 4956–4969.
- (23) Sosa, J. E.; Santiago, R.; Redondo, A. E.; Avila, J.; Lepre, L. F.; Costa Gomes, M. F.; Araújo, J. M. M.; Palomar, J.; Pereiro, A. B. Design of Ionic Liquids for Fluorinated Gas Absorption: COSMO-RS Selection and Solubility Experiments. *Environ. Sci. Technol.* **2022**, *56*, 5898–5909.
- (24) Finberg, E. A.; Shiflett, M. B. Process Designs for Separating R-410A, R-404A, and R-407C Using Extractive Distillation and Ionic Liquid Entrainers. *Ind. Eng. Chem. Res.* **2021**, *60*, 16054.

- (25) Finberg, E. A.; May, T. L.; Shiflett, M. B. Multicomponent Refrigerant Separation Using Extractive Distillation with Ionic Liquids. *Ind. Eng. Chem. Res.* **2022**, *61*, 9795–9812.
- (26) Morais, A. R. C.; Harders, A. N.; Baca, K. R.; Olson, G. M.; Befort, B.; Dowling, A. W.; Maginn, E. J.; Shiflett, M. B. Phase Equilibria, Diffusivities, and Equation of State Modeling of HFC-32 and HFC-125 in Imidazolium-Based Ionic Liquids for the Separation of R-410A. *Ind. Eng. Chem. Res.* **2020**, *59*, 18222–18235.
- (27) Baca, K. R.; Olsen, G. M.; Matamoros Valenciano, L.; Bennett, M. G.; Haggard, D. M.; Befort, B. J.; Garciadiego, A.; Dowling, A. W.; Maginn, E. J.; Shiflett, M. B. Phase Equilibria and Diffusivities of HFC-32 and HFC-125 in Ionic Liquids for the Separation of R-410A. *ACS Sustainable Chem. Eng.* **2022**, *10*, 816–830.
- (28) Monjur, M. S.; Iftakher, A.; Hasan, M. M. F. Separation Process Synthesis for High-GWP Refrigerant Mixtures: Extractive Distillation Using Ionic Liquids. *Ind. Eng. Chem. Res.* **2022**, *61*, 4390–4406.
- (29) Sosa, J. E.; Ribeiro, R. P. P. L.; Castro, P. J.; Mota, J. P. B.; Araújo, J. M. M.; Pereira, A. B. Absorption of Fluorinated Greenhouse Gases Using Fluorinated Ionic Liquids. *Ind. Eng. Chem. Res.* **2019**, *58*, 20769–20778.
- (30) Asensio-Delgado, J. M.; Asensio-Delgado, S.; Zarca, G.; Urriaga, A. Analysis of Hybrid Compression Absorption Refrigeration Using Low-GWP HFC or HFO/Ionic Liquid Working Pairs. *Int. J. Refrig.* **2022**, *134*, 232–241.
- (31) Asensio-Delgado, S.; Pardo, F.; Zarca, G.; Urriaga, A. Vapor-Liquid Equilibria and Diffusion Coefficients of Difluoromethane, 1,1,1,2-Tetrafluoroethane, and 2,3,3,3-Tetrafluoropropene in Low-Viscosity Ionic Liquids. *J. Chem. Eng. Data* **2020**, *65*, 4242–4251.
- (32) Asensio-Delgado, S.; Pardo, F.; Zarca, G.; Urriaga, A. Enhanced Absorption Separation of Hydrofluorocarbon/Hydrofluoroolefin Refrigerant Blends Using Ionic Liquids. *Sep. Purif. Technol.* **2020**, *249*, No. 117136.
- (33) Asensio-Delgado, S.; Viar, M.; Pardo, F.; Zarca, G.; Urriaga, A. Gas Solubility and Diffusivity of Hydrofluorocarbons and Hydrofluoroolefins in Cyanide-Based Ionic Liquids for the Separation of Refrigerant Mixtures. *Fluid Phase Equilib.* **2021**, *549*, No. 113210.
- (34) Baca, K. R.; Broom, D. P.; Roper, M. G.; Benham, M. J.; Shiflett, M. B. First Measurements for the Simultaneous Sorption of Difluoromethane and Pentafluoroethane Mixtures in Ionic Liquids Using the Integral Mass Balance Method. *Ind. Eng. Chem. Res.* **2022**, *61*, 9774–9784.
- (35) Garciadiego, A.; Befort, B. J.; Franco, G.; Dowling, A. W. What Data Are Most Valuable to Screen Ionic Liquid Entrainers for Hydrofluorocarbon Refrigerant Reuse and Recycling? *ChemRxiv*, DOI: 10.26434/chemrxiv-2022-b60nn.
- (36) Asensio-delgado, S.; Pardo, F.; Zarca, G.; Urriaga, A. Machine Learning for Predicting the Solubility of High-GWP Fluorinated Refrigerants in Ionic Liquids. *J. Mol. Liq.* **2022**, *367*, No. 120472.
- (37) Albà, C. G.; Vega, L. F.; Llovel, F. A Consistent Thermodynamic Molecular Model of N-Hydrofluoroolefins and Blends for Refrigeration Applications. *Int. J. Refrig.* **2020**, *113*, 145–155.
- (38) Alkhatib, I. I. I.; Albà, C. G.; Darwish, A. S.; Llovel, F.; Vega, L. F. Searching for Sustainable Refrigerants by Bridging Molecular Modeling with Machine Learning. *Ind. Eng. Chem. Res.* **2022**, *61*, 7414.
- (39) Albà, C. G.; Vega, L. F.; Llovel, F. Assessment on Separating Hydrofluoroolefins from Hydrofluorocarbons at the Azeotropic Mixture R513A by Using Fluorinated Ionic Liquids: A Soft-SAFT Study. *Ind. Eng. Chem. Res.* **2020**, *59*, 13315–13324.
- (40) Sosa, J. E.; Santiago, R.; Hospital-Benito, D.; Costa Gomes, M. F.; Araújo, J. M. M.; Pereira, A. B.; Palomar, J. Process Evaluation of Fluorinated Ionic Liquids as F-Gases Absorbents. *Environ. Sci. Technol.* **2020**, *54*, 12784.
- (41) Lepre, L. F.; Pison, L.; Otero, I.; Gautier, A.; Dévemy, J.; Husson, P.; Pádua, A. A. H.; Costa Gomes, M. F. Using Hydrogenated and Perfluorinated Gases to Probe the Interactions and Structure of Fluorinated Ionic Liquids. *Phys. Chem. Chem. Phys.* **2019**, *21*, 8865–8873.
- (42) Lepre, L. F.; Andre, D.; Denis-Quanquin, S.; Gautier, A.; Pádua, A. A. H.; Costa Gomes, M. F. Ionic Liquids Can Enable the Recycling of Fluorinated Greenhouse Gases. *ACS Sustainable Chem. Eng.* **2019**, *7*, 16900–16906.
- (43) Bell, I. H.; Wronski, J.; Quoilin, S.; Lemort, V. Pure and Pseudo-Pure Fluid Thermophysical Property Evaluation and the Open-Source Thermophysical Property Library CoolProp. *Ind. Eng. Chem. Res.* **2014**, *53*, 2498–2508.
- (44) Sampson, C. C.; Kamson, M.; Hopkins, M. G.; Stanwix, P. L.; May, E. F. Dielectric Permittivity, Polarizability and Dipole Moment of Refrigerants R1234ze(E) and R1234yf Determined Using a Microwave Re-Entrant Cavity Resonator. *J. Chem. Thermodyn.* **2019**, *128*, 148–158.
- (45) Shiflett, M. B.; Yokozeki, A. Solubility and Diffusivity of Hydrofluorocarbons in Room-Temperature Ionic Liquids. *AIChE J.* **2006**, *52*, 1205–1219.
- (46) Goloviznina, K.; Lepre, L. F.; Sabelle, S.; Pádua, A. A. H.; Costa Gomes, M. F. Enhancement of the Solubility of Organic Dyes in Aqueous Ionic Solvents Doped with Surfactants. *J. Mol. Liq.* **2022**, *357*, No. 118958.
- (47) Goloviznina, K.; Canongia Lopes, J. N.; Costa Gomes, M. F.; Pádua, A. A. H. Transferable, Polarizable Force Field for Ionic Liquids. *J. Chem. Theory Comput.* **2019**, *15*, 5858–5871.
- (48) Wang, T.; Liu, X.; Chu, J.; Shi, Y.; Li, J.; He, M. Molecular Dynamics Simulation of Diffusion and Interaction of [Bmim][Tf2N] + HFO-1234yf Mixture. *J. Mol. Liq.* **2020**, *312*, No. 113390.
- (49) Wang, N.; Zhang, Y.; Al-Barghouti, K. S.; Kore, R.; Scurto, A. M.; Maginn, E. J. Structure and Dynamics of Hydrofluorocarbon/Ionic Liquid Mixtures: An Experimental and Molecular Dynamics Study. *J. Phys. Chem. B* **2022**, *126*, 8309–8321.
- (50) Goloviznina, K.; Gong, Z.; Pádua, A. A. H. The CL&Pol Polarizable Force Field for the Simulation of Ionic Liquids and Eutectic Solvents. *Wiley Interdiscip. Rev.: Comput. Mol. Sci.* **2022**, *12*, No. e1572.
- (51) Goloviznina, K.; Gong, Z.; Costa Gomes, M. F.; Pádua, A. A. H. Extension of the CL&Pol Polarizable Force Field to Electrolytes, Protic Ionic Liquids, and Deep Eutectic Solvents. *J. Chem. Theory Comput.* **2021**, *17*, 1606.
- (52) Peguin, R. P. S.; Kamath, G.; Potoff, J. J.; da Rocha, S. R. P. All-Atom Force Field for the Prediction of Vapor-Liquid Equilibria and Interfacial Properties of HFA134a. *J. Phys. Chem. B* **2009**, *113*, 178–187.
- (53) Raabe, G.; Maginn, E. J. A Force Field for 3,3,3-Fluoro-1-Propenes, Including HFO-1234yf. *J. Phys. Chem. B* **2010**, *114*, 10133–10142.
- (54) Raabe, G. Molecular Modeling of Fluoropropene Refrigerants. *J. Phys. Chem. B* **2012**, *116*, 5744–5751.
- (55) Shiflett, M. B.; Harmer, M. A.; Junk, C. P.; Yokozeki, A. Solubility and Diffusivity of Difluoromethane in Room-Temperature Ionic Liquids. *J. Chem. Eng. Data* **2006**, *51*, 483–495.
- (56) Shiflett, M. B.; Harmer, M. A.; Junk, C. P.; Yokozeki, A. Solubility and Diffusivity of 1,1,1,2-Tetrafluoroethane in Room-Temperature Ionic Liquids. *Fluid Phase Equilib.* **2006**, *242*, 220–232.
- (57) Liu, X.; Nguyen, M. Q.; Xue, S.; Song, C.; He, M. Vapor-Liquid Equilibria and Inter-Diffusion Coefficients for Working Pairs for Absorption Refrigeration Systems Composed of [HMIM][BF4] and Fluorinated Propanes. *Int. J. Refrig.* **2019**, *104*, 34–41.
- (58) Liu, X.; Pan, P.; He, M. Vapor-Liquid Equilibrium and Diffusion Coefficients of R32 + [HMIM][FEP], R152a + [HMIM][FEP] and R161 + [HMIM][FEP]. *J. Mol. Liq.* **2018**, *253*, 28–35.
- (59) Minnick, D. L.; Shiflett, M. B. Solubility and Diffusivity of Bromodifluoromethane (Halon-1201) in Imidazolium Ionic Liquids: [C2C1im][Tf2N], [C4C1im][BF4], and [C4C1im][PF6]. *J. Chem. Eng. Data* **2020**, *65*, 3277–3286.
- (60) Goloviznina, K.; Pádua, A. A. H. clandpol <https://github.com/paduaGROUP/clandpol> (accessed September 25, 2022).
- (61) Heid, E.; Szabadi, A.; Schröder, C. Quantum Mechanical Determination of Atomic Polarizabilities of Ionic Liquids. *Phys. Chem. Chem. Phys.* **2018**, *20*, 10992–10996.



(62) Dequidt, A.; Devémy, J.; Pádua, A. A. H. Thermalized Drude Oscillators with the LAMMPS Molecular Dynamics Simulator. *J. Chem. Inf. Model.* **2016**, *56*, 260–268.

(63) Martínez, L.; Andrade, R.; Birgin, E. G.; Martínez, J. M. PACKMOL: A Package for Building Initial Configurations for Molecular Dynamics Simulation. *J. Comput. Chem.* **2009**, *30*, 2157–2164.

(64) Pádua, A. A. H. *fftool* <https://github.com/paduagroup/fftool> (accessed September 25, 2022).

(65) Maginn, E. J.; Messerly, R. A.; Carlson, D. J.; Roe, D. R.; Elliot, J. R. Best Practices for Computing Transport Properties 1. Self-Diffusivity and Viscosity from Equilibrium Molecular Dynamics [Article v1.0]. *Living J. Comput. Mol. Sci.* **2020**, *1*, 6324.

(66) Brehm, M.; Thomas, M.; Gehrke, S.; Kirchner, B. TRAVIS—A Free Analyzer for Trajectories from Molecular Simulation. *J. Chem. Phys.* **2020**, *152*, 164105.

(67) Brehm, M.; Kirchner, B. TRAVIS - A Free Analyzer and Visualizer for Monte Carlo and Molecular Dynamics Trajectories. *J. Chem. Inf. Model.* **2011**, *51*, 2007–2023.

## Recommended by ACS

### Thermal Conductivity of 1-Alkyl-3-methylimidazolium [Tf<sub>2</sub>N] Ionic Liquids and Compressed 1,1,1,2-Tetrafluoroethane (R-134a)

Karim S. Al-Barghouti and Aaron M. Scurto

JULY 26, 2022

JOURNAL OF CHEMICAL & ENGINEERING DATA

READ 

### Ionic Liquid Mixtures for Direct Air Capture: High CO<sub>2</sub> Permeation Driven by Superior CO<sub>2</sub> Absorption with Lower Absolute Enthalpy

Yuki Kohno, Takashi Makino, *et al.*

NOVEMBER 11, 2022

ACS OMEGA

READ 

### Diffusivities in Binary Mixtures of [AMIM][NTf<sub>2</sub>] Ionic Liquids with the Dissolved Gases H<sub>2</sub>, He, N<sub>2</sub>, CO, CO<sub>2</sub>, or Kr Close to Infinite Dilution

Tobias Klein, Andreas P. Fröba, *et al.*

JULY 06, 2020

JOURNAL OF CHEMICAL & ENGINEERING DATA

READ 

### Solubility for Propane and Isobutane in [P<sub>66614</sub>]Cl from 278.15 to 348.15 K

YanJun Sun, Xiaopo Wang, *et al.*

FEBRUARY 05, 2021

JOURNAL OF CHEMICAL & ENGINEERING DATA

READ 

Get More Suggestions >



## Supplementary Information

### Understanding the molecular features controlling the solubility differences of R-134a, R-1234ze(E) and R-1234yf in 1-alkyl-3-methylimidazolium tricyanomethanide ionic liquids

#### Authors:

Salvador Asensio-Delgado<sup>1</sup>, Miguel Viar<sup>1</sup>, Agílio A.H. Pádua<sup>2,\*</sup>,

Gabriel Zarca<sup>1</sup>, Ane Urriaga<sup>1,\*</sup>

<sup>1</sup>Department of Chemical and Biomolecular Engineering, Universidad de Cantabria. Av. Los Castros 46, Santander 39005, Spain.

Laboratoire de Chimie, École Normale Supérieure de Lyon de Lyon & CNRS, 46 allée d'Italie, 69364 Lyon, France

\*Corresponding author e-mail address: [urriaga@unican.es](mailto:urriaga@unican.es), [agilio.padua@ens-lyon.fr](mailto:agilio.padua@ens-lyon.fr)

#### Supporting information consists of:

- Number of pages: 28
- Number of tables: 14
- Number of figures: 14

## Section I. Experimental results

The experimental systems used for determining gas solubility in ILs consists of a jacketed stirred-tank reactor (Buchi, model Picoclave, 170 mL) equipped with a temperature and pressure transducer (Keller, series PAA-33X, 0.01% accuracy) and a Pt-100 temperature sensor connected to a cryothermostatic bath (Julabo, model F25–ME,  $\pm 0.01$  K). The absorption chamber is connected to a storage cylinder of known volume (146 mL) that is also equipped with a temperature and pressure transducer. Approximately 30 g ( $\pm 0.0001$  g) of IL are loaded and, before each experiment, the sample is degassed applying vacuum for a minimum of 6 h at 333 K. The stirring rate is set at 500 rpm and gas absorption proceeds until the equilibrium conditions are achieved, i.e., when the pressure remains constant for more than 20 min.

The mole fraction of gas dissolved in the liquid phase is:

$$x = \frac{n_{abs}}{n_l + n_{abs}} \quad (1)$$

where  $n_l$  is the amount of substance of IL and  $n_{abs}$  the amount of refrigerant dissolved. An absorption isotherm is the result of several consecutive absorption steps with increasing feed gas pressure, where the amount of gas absorbed in each step ( $n_i$ ) is calculated using the isochoric saturation method:

$$n_i = \rho_{(i,s)} \cdot V_S + \rho_{(i-1,c)} \cdot (V_C - V_l) - \rho_{(i,eq)} \cdot (V_S + V_C - V_l) \quad (2)$$

where  $V_S$ ,  $V_C$ , and  $V_l$  are the volumes of the storage cylinder, the sorption chamber, and loaded IL (L), and  $\rho_S$ ,  $\rho_C$ , and  $\rho_{eq}$  are the gas molar densities ( $\text{mol}\cdot\text{L}^{-1}$ ) in the storage cylinder, in the sorption chamber, and at equilibrium, respectively. The experimental setup is designed to minimize the effect of the IL volumetric expansion during gas absorption, by using a much larger volume of gas phase than IL. The molar densities are calculated from the pressure and temperature values using the Peng–Robinson cubic equation of state, to account for deviations from ideal gas behavior. The amounts of substance dissolved are calculated as the amount absorbed in one step ( $n_i$ ) plus the amount dissolved in the previous steps ( $n_k$ ):

$$n_{abs} = n_i + \sum_{k=1}^{i-1} n_k \quad (3)$$

Using the solubility data, Henry's law constants  $k_H$  are calculated from:

$$k_H(T) = \lim_{x \rightarrow 0} \frac{\bar{f}(P, T)}{x} \quad (4)$$

where  $\bar{f}$  is the refrigerant fugacity calculated using the Peng–Robinson equation of state. The limit at low solubility is approximated using a second order polynomial to fit the experimental solubilities.<sup>1,2</sup>

The uncertainty is calculated using the quadratic expansion of error and each value was expanded until considering the basic properties we measured, i.e., temperature, pressure, and mass. For example, for the case of molar fraction, the uncertainty is calculated as follows:

$$u(x) = \sqrt{\left(\frac{\partial x}{\partial n_{abs}}\right)^2 \cdot (u(n_{abs}))^2 + \left(\frac{\partial x}{\partial n_l}\right)^2 \cdot (u(n_l))^2} \quad (5)$$

For properties that are obtained as the regression coefficients of a regression, the error was calculated following the rigorous least squares adjustment as explained by Wentworth.<sup>3</sup>

If the function to be adjusted is expressed as  $F = 0$ , where  $F = w - a - bv - cv^2$ , the regression is made iteratively in a matrix form:

$$\mathbf{B} \cdot \Delta = \mathbf{C} \quad (6)$$

where

$$\mathbf{B} = \begin{bmatrix} \sum \frac{F_{ai} \cdot F_{ai}}{L_i} & \sum \frac{F_{ai} \cdot F_{bi}}{L_i} & \sum \frac{F_{ai} \cdot F_{ci}}{L_i} \\ \sum \frac{F_{bi} \cdot F_{ai}}{L_i} & \sum \frac{F_{bi} \cdot F_{bi}}{L_i} & \sum \frac{F_{bi} \cdot F_{ci}}{L_i} \\ \sum \frac{F_{ci} \cdot F_{ai}}{L_i} & \sum \frac{F_{ci} \cdot F_{bi}}{L_i} & \sum \frac{F_{ci} \cdot F_{ci}}{L_i} \end{bmatrix} \quad (7)$$

$$\mathbf{C} = \begin{bmatrix} \sum \frac{F_{ai} \cdot F_i^0}{L_i} \\ \sum \frac{F_{bi} \cdot F_i^0}{L_i} \\ \sum \frac{F_{ci} \cdot F_i^0}{L_i} \end{bmatrix} \quad (8)$$

Here,  $F_i^0$  is the value of the function with the initial guessed parameters ( $a_0, b_0, c_0$ ) in each experimental point  $i$ , formed by two values  $v_i$  and  $w_i$ .  $F_{ai}$  is the derivative of the function with respect to parameter  $a$  evaluated at point  $i$ ,  $F_{bi}$  is the derivative of the function with respect to parameter  $b$  evaluated at point  $i$ , and  $F_{ci}$  is the derivative of the function with respect to

parameter  $c$  evaluated at point  $i$ .  $L_i$  is a variable of variance inherent to each experimental point that includes the uncertainty ponderation:

$$L_i = (u(v_i))^2 \cdot F_{v_i}^2 + (u(w_i))^2 \cdot F_{w_i}^2 \quad (9)$$

Here, the derivative is made with respect to the variables instead of the parameters, so that  $F_{v_i}$  and  $F_{w_i}$  are the derivatives of the function with respect to  $v$  and  $w$ , respectively, in each experimental point.

The matrix  $\Delta$  is a vertical vector of the form:

$$\Delta = \begin{bmatrix} \Delta a \\ \Delta b \\ \Delta c \end{bmatrix} \quad (10)$$

Where  $\Delta a$ ,  $\Delta b$ , and  $\Delta c$  are the difference between the initial value of the parameters and the value estimated using least squares regression. Once converged, the uncertainty of the parameters is the square root of the main diagonal of the inverse matrix of the coefficient matrix ***B***.

Table S1. Solubility of R-134a in [C<sub>2</sub>C<sub>1</sub>im][tcm].

<i>T/K</i>	<i>p/MPa</i>	<i>x</i>	<i>u(x)</i>	<i>m/mol·kg<sup>-1</sup></i>	<i>u(m)</i>
283.15	0.0406	0.0261	0.0003	0.133	0.002
283.15	0.0973	0.0640	0.0004	0.340	0.002
283.15	0.1631	0.1111	0.0006	0.621	0.003
283.15	0.2332	0.1658	0.0007	0.987	0.005
283.15	0.3008	0.2254	0.0009	1.446	0.007
293.15	0.0472	0.0222	0.0003	0.113	0.002
293.15	0.1118	0.0538	0.0004	0.283	0.002
293.15	0.1835	0.0905	0.0006	0.495	0.003
293.15	0.2618	0.1332	0.0008	0.764	0.005
293.15	0.3420	0.1797	0.0010	1.089	0.007
303.15	0.0551	0.0194	0.0003	0.098	0.002
303.15	0.1220	0.0440	0.0004	0.229	0.002
303.15	0.1996	0.0735	0.0006	0.394	0.004
303.15	0.2894	0.1085	0.0008	0.605	0.005
303.15	0.3754	0.1437	0.0011	0.834	0.007
313.15	0.0571	0.0156	0.0003	0.079	0.002
313.15	0.1282	0.0358	0.0005	0.184	0.002
313.15	0.2122	0.0599	0.0006	0.316	0.004
313.15	0.3020	0.0853	0.0009	0.464	0.005
313.15	0.3963	0.1126	0.0011	0.631	0.007
323.15	0.0620	0.0133	0.0003	0.067	0.002
323.15	0.1371	0.0293	0.0005	0.150	0.002
323.15	0.2241	0.0479	0.0007	0.250	0.004
323.15	0.3169	0.0674	0.0009	0.359	0.005
323.15	0.4151	0.0875	0.0012	0.477	0.007

Table S2. Solubility of R-1234yf in [C<sub>2</sub>C<sub>1</sub>im][tcm].

<i>T/K</i>	<i>p/MPa</i>	<i>x</i>	<i>u(x)</i>	<i>m/mol·kg<sup>-1</sup></i>	<i>u(m)</i>
283.15	0.0643	0.0110	0.0003	0.055	0.002
283.15	0.1463	0.0250	0.0005	0.127	0.003
283.15	0.2348	0.0403	0.0007	0.208	0.004
283.15	0.3230	0.0560	0.0009	0.295	0.005
283.15	0.4213	0.0739	0.0013	0.397	0.007
293.15	0.0632	0.0084	0.0003	0.042	0.002
293.15	0.1427	0.0188	0.0005	0.095	0.002
293.15	0.2345	0.0306	0.0007	0.157	0.004
293.15	0.3304	0.0431	0.0010	0.224	0.005
293.15	0.4262	0.0554	0.0013	0.292	0.007
303.15	0.0662	0.0066	0.0003	0.033	0.002
303.15	0.1493	0.0144	0.0005	0.073	0.003
303.15	0.2410	0.0230	0.0007	0.117	0.004
303.15	0.3356	0.0317	0.0010	0.162	0.005
303.15	0.4327	0.0401	0.0014	0.208	0.007
313.15	0.0687	0.0051	0.0003	0.025	0.002
313.15	0.1553	0.0111	0.0005	0.056	0.003
313.15	0.2483	0.0170	0.0007	0.086	0.004
313.15	0.3476	0.0227	0.0010	0.116	0.005
313.15	0.4449	0.0275	0.0014	0.141	0.008
323.15	0.0728	0.0037	0.0003	0.019	0.002
323.15	0.1563	0.0075	0.0005	0.038	0.003
323.15	0.2522	0.0112	0.0007	0.056	0.004
323.15	0.3503	0.0142	0.0010	0.072	0.005
323.15	0.4382	0.0162	0.0015	0.082	0.007

Table S3. Solubility of R-1234ze(E) in [C<sub>2</sub>C<sub>1</sub>im][tcm].

<i>T/K</i>	<i>p/MPa</i>	<i>x</i>	<i>u(x)</i>	<i>m/mol·kg<sup>-1</sup></i>	<i>u(m)</i>
283.15	0.0435	0.0238	0.0003	0.121	0.002
283.15	0.1058	0.0585	0.0004	0.309	0.002
283.15	0.1755	0.0997	0.0006	0.550	0.004
283.15	0.2336	0.1369	0.0007	0.788	0.005
283.15	0.2886	0.1748	0.0010	1.055	0.007
293.15	0.0503	0.0204	0.0003	0.103	0.002
293.15	0.1198	0.0489	0.0004	0.255	0.002
293.15	0.1967	0.0816	0.0006	0.441	0.004
293.15	0.2591	0.1093	0.0008	0.610	0.005
293.15	0.3199	0.1374	0.0011	0.791	0.007
303.15	0.0543	0.0165	0.0003	0.083	0.002
303.15	0.1265	0.0384	0.0005	0.198	0.002
303.15	0.2090	0.0638	0.0006	0.339	0.004
303.15	0.2747	0.0847	0.0009	0.460	0.005
303.15	0.3378	0.1048	0.0012	0.582	0.007
313.15	0.0594	0.0131	0.0003	0.067	0.002
313.15	0.1362	0.0303	0.0005	0.156	0.002
313.15	0.2211	0.0492	0.0007	0.258	0.004
313.15	0.2891	0.0646	0.0009	0.344	0.005
313.15	0.3528	0.0787	0.0012	0.427	0.007
323.15	0.0632	0.0108	0.0003	0.054	0.002
323.15	0.1380	0.0232	0.0005	0.118	0.002
323.15	0.2320	0.0381	0.0007	0.197	0.004
323.15	0.3045	0.0496	0.0009	0.260	0.005
323.15	0.3837	0.0612	0.0013	0.324	0.007

Table S4. Solubility of R-134a in [C<sub>4</sub>C<sub>1</sub>im][tcm].

<i>T/K</i>	<i>p/MPa</i>	<i>x</i>	<i>u(x)</i>	<i>m/mol·kg<sup>-1</sup></i>	<i>u(m)</i>
283.15	0.0432	0.0326	0.0004	0.147	0.002
283.15	0.1006	0.0780	0.0005	0.369	0.003
283.15	0.1663	0.1325	0.0007	0.666	0.004
283.15	0.2346	0.1940	0.0008	1.050	0.006
283.15	0.3017	0.2613	0.0010	1.542	0.008
293.15	0.0495	0.0273	0.0004	0.123	0.002
293.15	0.1132	0.0640	0.0005	0.298	0.003
293.15	0.1962	0.1137	0.0007	0.559	0.004
293.15	0.2687	0.1592	0.0009	0.826	0.006
293.15	0.3488	0.2120	0.0012	1.173	0.008
303.15	0.0515	0.0218	0.0004	0.097	0.002
303.15	0.1235	0.0532	0.0006	0.245	0.003
303.15	0.2010	0.0875	0.0008	0.418	0.004
303.15	0.2884	0.1269	0.0010	0.634	0.006
303.15	0.3764	0.1678	0.0013	0.879	0.008
313.15	0.0608	0.0198	0.0004	0.088	0.002
313.15	0.1313	0.0430	0.0006	0.196	0.003
313.15	0.2165	0.0709	0.0008	0.333	0.004
313.15	0.3032	0.0992	0.0011	0.480	0.006
313.15	0.3970	0.1296	0.0014	0.649	0.008
323.15	0.0631	0.0159	0.0004	0.070	0.002
323.15	0.1381	0.0345	0.0006	0.156	0.003
323.15	0.2225	0.0553	0.0008	0.255	0.004
323.15	0.3136	0.0772	0.0011	0.365	0.006
323.15	0.4077	0.0994	0.0015	0.481	0.008



Table S5. Solubility of R-1234yf in [C<sub>4</sub>C<sub>1</sub>im][tcm].

<i>T/K</i>	<i>p/MPa</i>	<i>x</i>	<i>u(x)</i>	<i>m/mol·kg<sup>-1</sup></i>	<i>u(m)</i>
283.15	0.0598	0.0135	0.0004	0.060	0.002
283.15	0.1382	0.0320	0.0006	0.144	0.003
283.15	0.2259	0.0535	0.0008	0.247	0.004
283.15	0.314	0.0737	0.0011	0.347	0.006
283.15	0.4151	0.0983	0.0015	0.475	0.008
293.15	0.0676	0.0120	0.0004	0.053	0.002
293.15	0.1469	0.0261	0.0006	0.117	0.003
293.15	0.2366	0.0421	0.0009	0.192	0.004
293.15	0.3285	0.0584	0.0012	0.271	0.006
293.15	0.4212	0.0746	0.0016	0.351	0.008
303.15	0.0662	0.0086	0.0004	0.038	0.002
303.15	0.1494	0.0195	0.0006	0.087	0.003
303.15	0.2387	0.0312	0.0009	0.140	0.004
303.15	0.3315	0.0430	0.0012	0.196	0.006
303.15	0.4318	0.0550	0.0017	0.254	0.008
313.15	0.0701	0.0069	0.0004	0.030	0.002
313.15	0.1591	0.0153	0.0006	0.068	0.003
313.15	0.2466	0.0233	0.0009	0.104	0.004
313.15	0.3415	0.0311	0.0013	0.140	0.006
313.15	0.4365	0.0380	0.0018	0.172	0.008
323.15	0.0748	0.0047	0.0004	0.021	0.002
323.15	0.1603	0.0097	0.0006	0.043	0.003
323.15	0.2566	0.0141	0.0009	0.062	0.004
323.15	0.3506	0.0178	0.0013	0.079	0.006

Table S6. Solubility of R-1234ze(E) in [C<sub>4</sub>C<sub>1</sub>im][tcm].

<i>T/K</i>	<i>p/MPa</i>	<i>x</i>	<i>u(x)</i>	<i>m/mol·kg<sup>-1</sup></i>	<i>u(m)</i>
283.15	0.0447	0.0285	0.0004	0.128	0.002
283.15	0.1052	0.0713	0.0005	0.335	0.003
283.15	0.1744	0.1233	0.0007	0.613	0.004
283.15	0.2312	0.1694	0.0009	0.890	0.006
283.15	0.2837	0.2158	0.0011	1.200	0.008
293.15	0.0491	0.0250	0.0004	0.112	0.002
293.15	0.1163	0.0599	0.0006	0.278	0.003
293.15	0.1928	0.1007	0.0007	0.488	0.004
293.15	0.2552	0.1355	0.0010	0.684	0.006
293.15	0.3144	0.1702	0.0013	0.895	0.008
303.15	0.0545	0.0200	0.0004	0.089	0.002
303.15	0.1260	0.0476	0.0006	0.218	0.003
303.15	0.2084	0.0798	0.0008	0.378	0.004
303.15	0.2738	0.1061	0.0010	0.517	0.006
303.15	0.3364	0.1313	0.0014	0.659	0.008
313.15	0.0611	0.0123	0.0004	0.054	0.002
313.15	0.1353	0.0334	0.0006	0.151	0.003
313.15	0.2201	0.0577	0.0008	0.267	0.004
313.15	0.2870	0.0769	0.0011	0.364	0.006
313.15	0.3504	0.0955	0.0015	0.460	0.008
323.15	0.0626	0.0117	0.0004	0.052	0.002
323.15	0.1415	0.0276	0.0006	0.124	0.003
323.15	0.2300	0.0453	0.0009	0.207	0.004
323.15	0.2995	0.0591	0.0012	0.274	0.006
323.15	0.3633	0.0715	0.0016	0.336	0.008

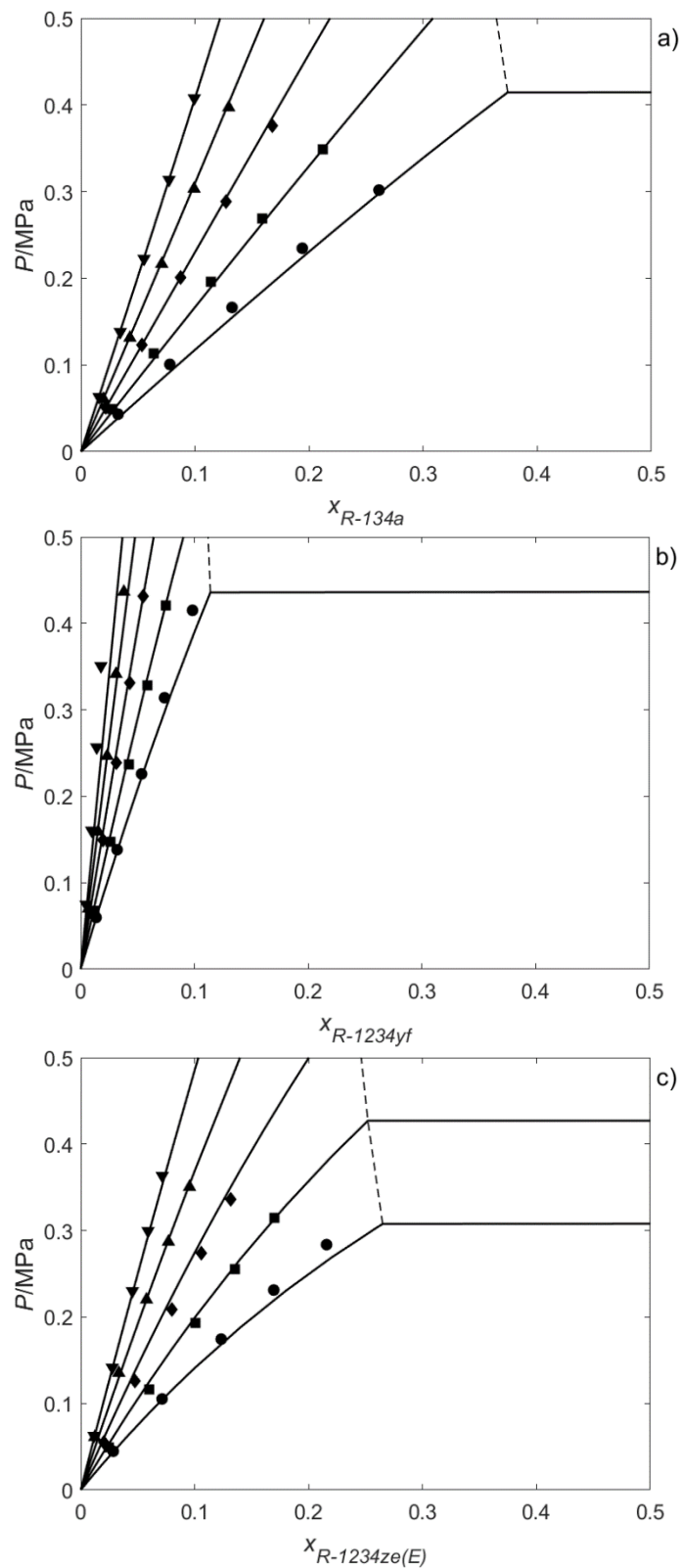


Figure S1. Solubility of the refrigerant gases (a) R-134a, (b) R-1234yf, and (c) R-1234ze(E) in [C<sub>4</sub>C<sub>1</sub>im][tcm] at various temperatures: 283.15 (●), 293.15 (■), 303.15 (◆), 313.15 (▲), and 323.15 K (▼). Solid lines represent NRTL model calculations and dashed lines represent the immiscibility region predicted by the NRTL model.

Table S7. Solubility of R-134a in [C<sub>6</sub>C<sub>1</sub>im][tcm].

<i>T/K</i>	<i>p/MPa</i>	<i>x</i>	<i>u(x)</i>	<i>m/mol·kg<sup>-1</sup></i>	<i>u(m)</i>
283.15	0.0401	0.0353	0.0004	0.142	0.002
283.15	0.0945	0.0846	0.0005	0.359	0.002
283.15	0.1563	0.1427	0.0006	0.647	0.003
283.15	0.2241	0.2105	0.0008	1.036	0.005
283.15	0.2885	0.2809	0.0009	1.518	0.007
293.15	0.0464	0.0302	0.0004	0.121	0.002
293.15	0.1109	0.0739	0.0005	0.310	0.002
293.15	0.1817	0.1228	0.0007	0.544	0.003
293.15	0.2867	0.1968	0.0008	0.952	0.005
293.15	0.3564	0.2501	0.0010	1.296	0.007
303.15	0.0533	0.0267	0.0004	0.106	0.002
303.15	0.1184	0.0598	0.0005	0.247	0.002
303.15	0.1949	0.0991	0.0007	0.427	0.003
303.15	0.2788	0.1418	0.0009	0.642	0.005
303.15	0.3630	0.1858	0.0012	0.887	0.007
313.15	0.0586	0.0227	0.0004	0.090	0.002
313.15	0.1292	0.0502	0.0006	0.205	0.002
313.15	0.2093	0.0815	0.0007	0.345	0.003
313.15	0.2963	0.1152	0.0010	0.506	0.005
313.15	0.4006	0.1540	0.0013	0.708	0.007
323.15	0.0601	0.0180	0.0004	0.071	0.002
323.15	0.1345	0.0400	0.0006	0.162	0.002
323.15	0.2193	0.0648	0.0008	0.269	0.003
323.15	0.3105	0.0910	0.0010	0.389	0.005
323.15	0.4085	0.1185	0.0014	0.522	0.007

Table S8. Solubility of R-1234yf in [C<sub>6</sub>C<sub>1</sub>im][tcm].

<i>T/K</i>	<i>p/MPa</i>	<i>x</i>	<i>u(x)</i>	<i>m/mol·kg<sup>-1</sup></i>	<i>u(m)</i>
283.15	0.0594	0.0164	0.0004	0.065	0.002
283.15	0.1342	0.0393	0.0006	0.159	0.002
283.15	0.2185	0.0658	0.0008	0.274	0.003
283.15	0.3085	0.0948	0.0010	0.407	0.005
283.15	0.4006	0.1260	0.0014	0.560	0.007
293.15	0.0605	0.0142	0.0004	0.056	0.002
293.15	0.1392	0.0326	0.0006	0.131	0.002
293.15	0.2266	0.0532	0.0008	0.218	0.003
293.15	0.3200	0.0751	0.0011	0.315	0.005
293.15	0.4165	0.0980	0.0015	0.422	0.007
303.15	0.0640	0.0112	0.0004	0.044	0.002
303.15	0.1472	0.0260	0.0006	0.104	0.002
303.15	0.2353	0.0415	0.0008	0.168	0.003
303.15	0.3301	0.0574	0.0011	0.237	0.005
303.15	0.4272	0.0737	0.0016	0.309	0.007
313.15	0.0664	0.0088	0.0004	0.035	0.002
313.15	0.1487	0.0199	0.0006	0.079	0.002
313.15	0.2412	0.0318	0.0008	0.128	0.004
313.15	0.3368	0.0433	0.0012	0.176	0.005
313.15	0.4375	0.0548	0.0017	0.225	0.007
323.15	0.0684	0.0070	0.0004	0.028	0.002
323.15	0.1527	0.0152	0.0006	0.060	0.002
323.15	0.2450	0.0232	0.0009	0.092	0.004
323.15	0.3411	0.0307	0.0012	0.123	0.005
323.15	0.4427	0.0374	0.0017	0.151	0.007

Table S9. Solubility of R-1234ze(E) in [C<sub>6</sub>C<sub>1</sub>im][tcm].

<i>T/K</i>	<i>p/MPa</i>	<i>x</i>	<i>u(x)</i>	<i>m/mol·kg<sup>-1</sup></i>	<i>u(m)</i>
283.15	0.0404	0.0335	0.0004	0.135	0.002
283.15	0.0979	0.0819	0.0005	0.346	0.002
283.15	0.1628	0.1388	0.0006	0.626	0.003
283.15	0.2171	0.1891	0.0008	0.906	0.005
283.15	0.2682	0.2394	0.0010	1.223	0.007
293.15	0.0464	0.0281	0.0004	0.112	0.002
293.15	0.1102	0.0673	0.0005	0.280	0.002
293.15	0.1835	0.1132	0.0007	0.496	0.003
293.15	0.2441	0.1523	0.0009	0.698	0.005
293.15	0.3024	0.1902	0.0012	0.913	0.007
303.15	0.0512	0.0238	0.0004	0.095	0.002
303.15	0.1208	0.0557	0.0005	0.229	0.002
303.15	0.2000	0.0917	0.0007	0.392	0.003
303.15	0.2660	0.1221	0.0010	0.540	0.005
303.15	0.3276	0.1498	0.0013	0.685	0.007
313.15	0.0556	0.0190	0.0004	0.075	0.002
313.15	0.1297	0.0443	0.0006	0.180	0.002
313.15	0.2137	0.0726	0.0008	0.304	0.003
313.15	0.2814	0.0950	0.0010	0.408	0.005
313.15	0.3457	0.1154	0.0014	0.507	0.007
323.15	0.0616	0.0164	0.0004	0.065	0.002
323.15	0.1388	0.0362	0.0006	0.146	0.002
323.15	0.2261	0.0580	0.0008	0.239	0.003
323.15	0.2918	0.0737	0.0011	0.309	0.005
323.15	0.3572	0.0883	0.0015	0.376	0.007

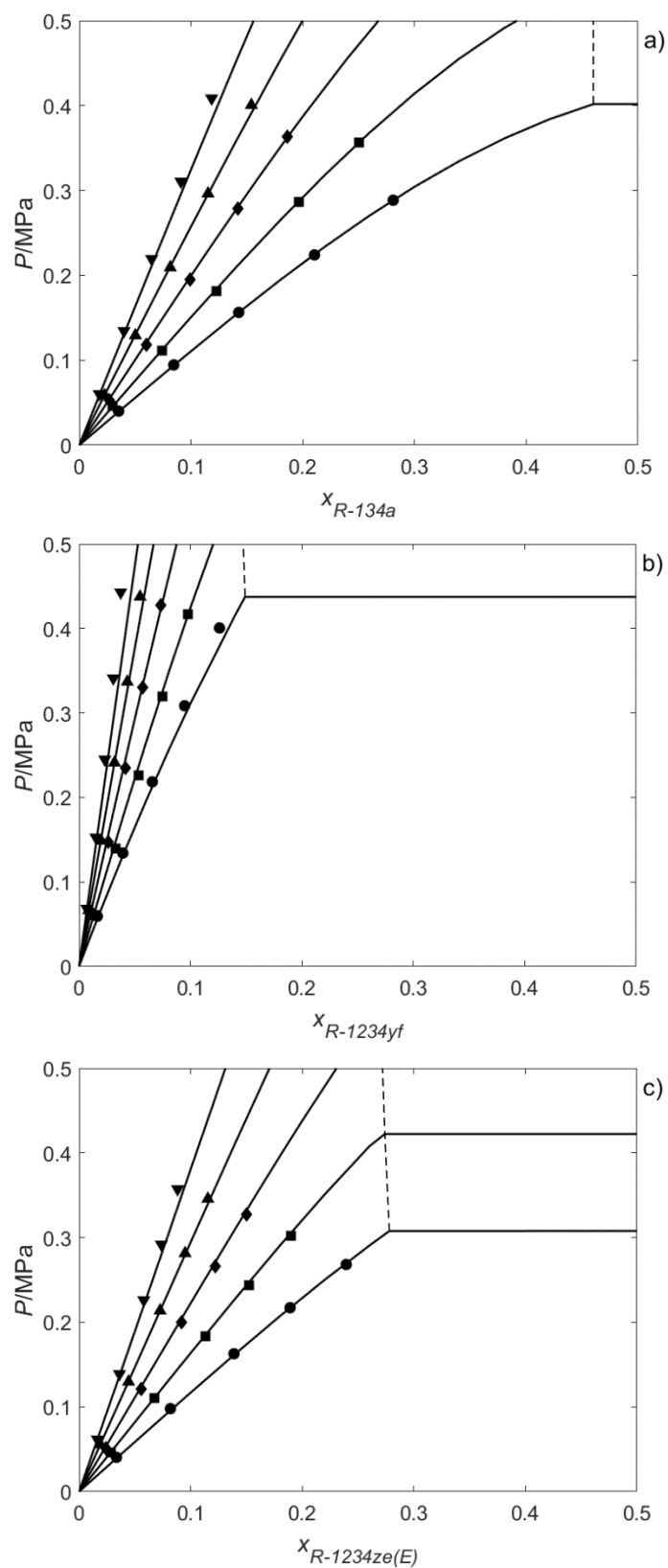


Figure S2. Solubility of the refrigerant gases (a) R-134a, (b) R-1234yf, and (c) R-1234ze(E) in [C<sub>6</sub>C<sub>1</sub>im][tcm] at various temperatures: 283.15 (●), 293.15 (■), 303.15 (◆), 313.15 (▲), and 323.15 K (▼). Solid lines represent NRTL model calculations and dashed lines represent the immiscibility region predicted by the NRTL model.

Table S10. Solubility of R-134a in [C<sub>8</sub>C<sub>1</sub>im][tcm].

<i>T/K</i>	<i>p/MPa</i>	<i>x</i>	<i>u(x)</i>	<i>m/mol·kg<sup>-1</sup></i>	<i>u(m)</i>
283.15	0.0417	0.0407	0.0005	0.149	0.002
283.15	0.1001	0.0999	0.0006	0.389	0.003
283.15	0.1629	0.1652	0.0008	0.693	0.004
283.15	0.2300	0.2384	0.0009	1.097	0.005
283.15	0.2939	0.3152	0.0010	1.613	0.008
293.15	0.0471	0.0342	0.0005	0.124	0.002
293.15	0.1150	0.0851	0.0006	0.326	0.003
293.15	0.1841	0.1379	0.0008	0.561	0.004
293.15	0.2628	0.1995	0.0010	0.873	0.006
293.15	0.3374	0.2606	0.0012	1.235	0.008
303.15	0.0506	0.0290	0.0005	0.105	0.002
303.15	0.1196	0.0688	0.0007	0.259	0.003
303.15	0.1979	0.1139	0.0009	0.450	0.004
303.15	0.2816	0.1626	0.0011	0.680	0.006
303.15	0.3677	0.2133	0.0014	0.950	0.008
313.15	0.0599	0.0226	0.0005	0.081	0.002
313.15	0.1310	0.0543	0.0007	0.201	0.003
313.15	0.2134	0.0905	0.0009	0.349	0.004
313.15	0.3023	0.1295	0.0012	0.521	0.006
313.15	0.3899	0.1678	0.0016	0.706	0.008
323.15	0.0607	0.0167	0.0005	0.060	0.002
323.15	0.1349	0.0404	0.0007	0.148	0.003
323.15	0.2228	0.0688	0.0010	0.259	0.004
323.15	0.3136	0.0978	0.0013	0.380	0.006
323.15	0.4079	0.1273	0.0017	0.511	0.008



Table S11. Solubility of R-1234yf in [C<sub>8</sub>C<sub>1</sub>im][tcm].

<i>T/K</i>	<i>p/MPa</i>	<i>x</i>	<i>u(x)</i>	<i>m/mol·kg<sup>-1</sup></i>	<i>u(m)</i>
283.15	0.0580	0.0207	0.0005	0.074	0.002
283.15	0.1316	0.0497	0.0007	0.183	0.003
283.15	0.2143	0.0831	0.0009	0.318	0.004
283.15	0.3061	0.1220	0.0012	0.487	0.006
283.15	0.3956	0.1625	0.0016	0.680	0.008
293.15	0.0612	0.0181	0.0005	0.065	0.002
293.15	0.1376	0.0406	0.0007	0.148	0.003
293.15	0.2255	0.0675	0.0010	0.254	0.004
293.15	0.3171	0.0955	0.0013	0.370	0.006
293.15	0.4132	0.1254	0.0018	0.503	0.008
303.15	0.0662	0.0146	0.0005	0.052	0.002
303.15	0.1444	0.0325	0.0007	0.118	0.003
303.15	0.2325	0.0523	0.0010	0.194	0.004
303.15	0.3265	0.0731	0.0014	0.276	0.006
303.15	0.4236	0.0945	0.0019	0.366	0.008
313.15	0.0815	0.0141	0.0005	0.050	0.002
313.15	0.1552	0.0267	0.0007	0.096	0.003
313.15	0.2429	0.0413	0.0011	0.151	0.004
313.15	0.3367	0.0558	0.0015	0.207	0.006
313.15	0.4309	0.0685	0.0020	0.258	0.008
323.15	0.0698	0.0088	0.0005	0.031	0.002
323.15	0.1523	0.0186	0.0008	0.066	0.003
323.15	0.2433	0.0286	0.0011	0.103	0.004
323.15	0.3394	0.0384	0.0015	0.140	0.006
323.15	0.4402	0.0480	0.0021	0.177	0.008

Table S12. Solubility of R-1234ze(E) in [C<sub>8</sub>C<sub>1</sub>im][tcm].

<i>T/K</i>	<i>p/MPa</i>	<i>x</i>	<i>u(x)</i>	<i>m/mol·kg<sup>-1</sup></i>	<i>u(m)</i>
283.15	0.0408	0.0403	0.0005	0.147	0.002
283.15	0.0983	0.0972	0.0006	0.377	0.003
283.15	0.1637	0.1644	0.0008	0.690	0.004
283.15	0.2179	0.2223	0.0009	1.002	0.005
283.15	0.2675	0.2793	0.0011	1.358	0.008
293.15	0.0475	0.0333	0.0005	0.121	0.002
293.15	0.1127	0.0804	0.0006	0.306	0.003
293.15	0.1860	0.1344	0.0008	0.544	0.004
293.15	0.2446	0.1784	0.0011	0.761	0.005
293.15	0.3022	0.2234	0.0013	1.008	0.008
303.15	0.0527	0.0265	0.0005	0.095	0.002
303.15	0.1221	0.0637	0.0007	0.238	0.003
303.15	0.2018	0.1068	0.0009	0.419	0.004
303.15	0.2660	0.1416	0.0012	0.578	0.006
303.15	0.3276	0.1757	0.0015	0.747	0.008
313.15	0.0563	0.0226	0.0005	0.081	0.002
313.15	0.1295	0.0524	0.0007	0.194	0.003
313.15	0.2137	0.0863	0.0009	0.331	0.004
313.15	0.2804	0.1128	0.0012	0.446	0.006
313.15	0.3437	0.1375	0.0017	0.558	0.008
323.15	0.0599	0.0190	0.0005	0.068	0.002
323.15	0.1373	0.0430	0.0007	0.157	0.003
323.15	0.2240	0.0693	0.0010	0.261	0.004
323.15	0.2913	0.0894	0.0013	0.344	0.006
323.15	0.3546	0.1078	0.0018	0.424	0.008

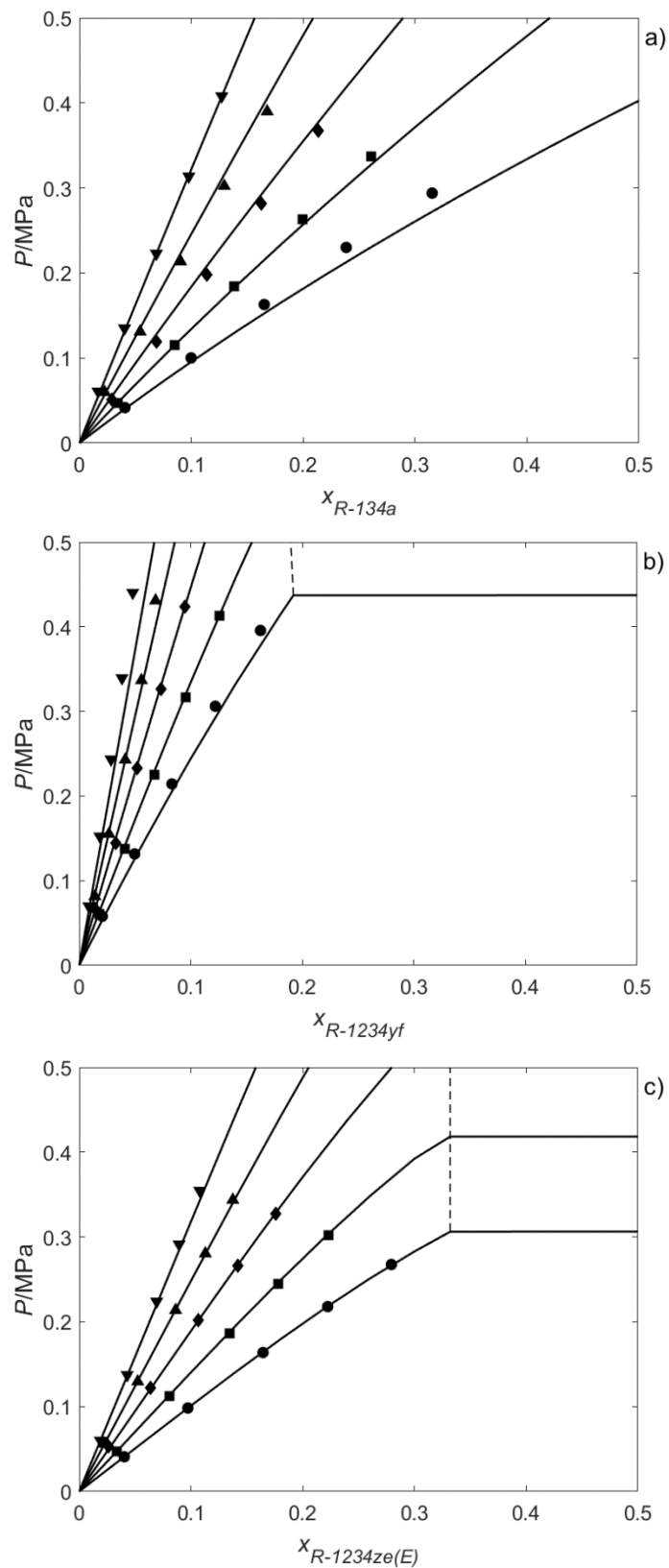


Figure S3. Solubility of the refrigerant gases (a) R-134a, (b) R-1234yf, and (c) R-1234ze(E) in  $[C_8C_1im][tcm]$  at various temperatures: 283.15 (●), 293.15 (■), 303.15 (◆), 313.15 (▲), and 323.15 K (▼). Solid lines represent NRTL model calculations and dashed lines represent the immiscibility region predicted by the NRTL model.

## Section II. Thermodynamic modeling using the NRTL activity coefficient model

The experimental solubility data are modeled using the nonrandom two-liquid activity-coefficient model (NRTL), which has been widely used to model the vapor-liquid equilibria (VLE) of fluorinated refrigerant gases in ILs. The experimental VLE can be described by:

$$y_i p \Phi = x_i \gamma_i p_i^S \quad (i \in \mathbb{Z} [1, N]) \quad (11)$$

where  $y_i$  and  $x_i$  are the molar fractions of the  $i$  species in the vapor and liquid phases, respectively, and  $\gamma_i$  and  $p_i^S$  are the activity coefficient and the vapor pressure, respectively.

The correction factor  $\Phi$  is calculated as

$$\Phi = \exp \left[ \frac{(B_i - V_i^L)(p - p_i^S)}{RT} \right] \quad (12)$$

where  $R$  is the ideal gas constant,  $B_i$  is the second virial coefficient and  $V_i^L$  is the saturated liquid molar volume.  $p_i^S$ ,  $B_i$  and  $V_i^L$  were calculated using the advanced equations of state based on Helmholtz energy formulations that are implemented in CoolProp 6.4.0.<sup>4</sup> Substitution of Eq. (12) in Eq. (11) leads to the following expression of the activity coefficients:

$$\gamma_1 = \frac{p}{x_1 p_1^S} \exp \left[ \frac{(B_1 - V_1^L)(p - p_1^S)}{RT} \right] \quad (13)$$

For a binary mixture, the NRTL activity coefficients are expressed according to Eq. (14):

$$\ln \gamma_1 = x_2^2 \left[ \tau_{21} \left( \frac{G_{21}}{x_1 + x_2 G_{21}} \right)^2 + \frac{\tau_{12} G_{12}}{(x_2 + x_1 G_{12})^2} \right] \quad (14)$$

where

$$G_{12} = \exp(-\alpha \tau_{12}), \quad G_{21} = \exp(-\alpha \tau_{21}) \quad (15)$$

$$\tau_{12} = \tau_{12}^0 + \frac{\tau_{12}^1}{T}, \quad \tau_{21} = \tau_{21}^0 + \frac{\tau_{21}^1}{T} \quad (16)$$

The parameter  $\alpha$  can be treated as an adjustable parameter, but it is usually assumed constant and equal to 0.2 for fluorocarbons, a convention that we followed for consistency with our previous works. Thus, only the temperature-dependent binary interaction parameters  $\tau_{12}$  and  $\tau_{21}$  are optimized in this work. In Eq. (13),  $\tau_{12}^1$  and  $\tau_{21}^1$  represent the excess free energy of Gibbs divided by the ideal gas constant, while  $\tau_{12}^0$  and  $\tau_{21}^0$  are used in this work to model systems with

large deviations from the ideal behavior. The NRTL activity coefficients are modeled to fit the experimental activity coefficients using the average absolute relative deviation (AARD), and we also provide the deviation in pressure (AARD<sub>p</sub>).

$$AARD = \frac{100}{N} \sum_{i=1}^N \left| \frac{\gamma_{exp} - \gamma_{calc}}{\gamma_{exp}} \right| \quad (17)$$

$$AARD_p = \frac{100}{N} \sum_{i=1}^N \left| \frac{P_{exp} - P_{calc}}{P_{exp}} \right| \quad (18)$$

Once regressed the parameters using the experimental binary data, immiscibility regions at high pressure were predicted based on minimum Gibbs energy calculations. The composition of phases in equilibrium is found as follows. The Gibbs free energy of the mixture is calculated as:

$$G = \sum x_i G_i = RT \sum x_i \ln(\gamma_i x_i) \quad (19)$$

If Gibbs free energy is represented against composition, some instable nodes can appear. These instable nodes are maxima in the  $G$  curve as presented in Figure XX and they are mathematically described as:

$$\frac{\partial G}{\partial x} = 0 \quad (20)$$

$$\frac{\partial^2 G}{\partial x^2} > 0 \quad (21)$$

In that case, the system can assume a lower value of Gibbs energy (“Minimum energy” in the graph) by splitting into two phases in equilibrium with each other with compositions given by the points where the common tangent line touches the  $G$  curve. These points are also called double-tangent points and every mixture composition between these two points will split into two phases of composition equal to each of the two double-tangent points. The condition of double tangency is expressed mathematically as:

$$\frac{G_2 - G_1}{x_2 - x_1} = \left. \frac{\partial G}{\partial x} \right|_{x_1} = \left. \frac{\partial G}{\partial x} \right|_{x_2} \quad (22)$$

Further information on the calculation of phase splitting can be found in the books by Tassios and Walas.<sup>5,6</sup>

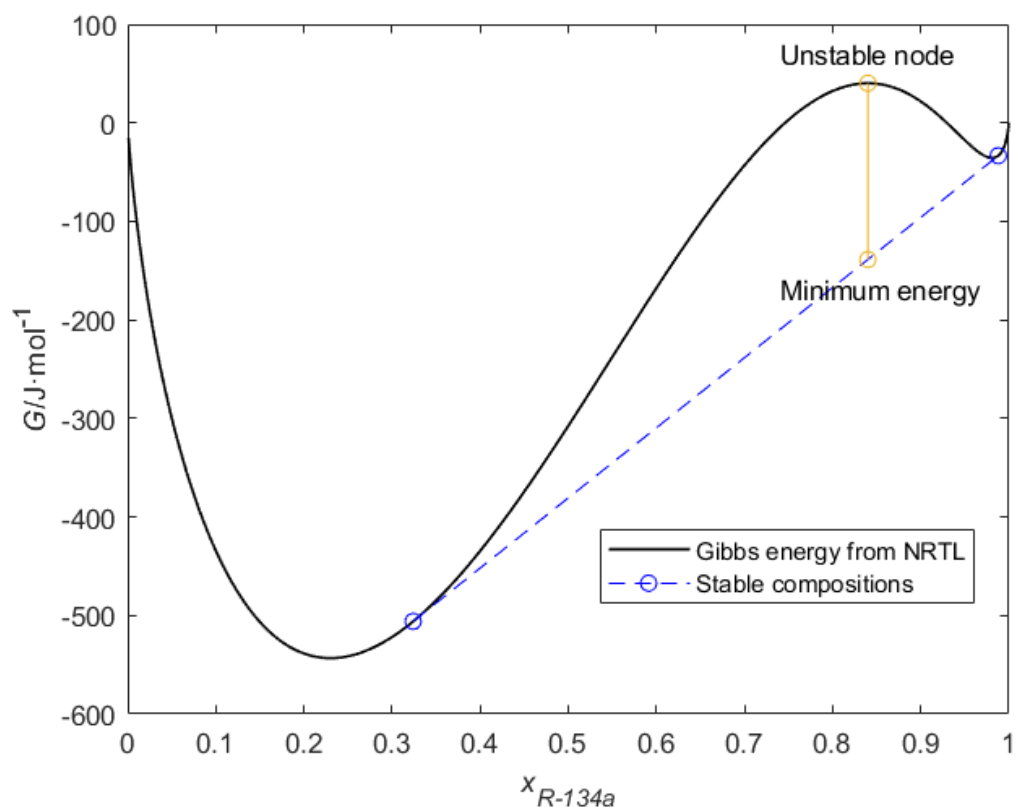


Figure S4. Determination of the phase separation using the NRTL model.

Table S13. NRTL parameters for the solubility of refrigerant gases in  $[C_nC_1im][tcm]$  ILs. The parameter  $\alpha$  was set to 0.2 for all the systems.

System	$\tau_{12}^0$	$\tau_{12}^1/K$	$\tau_{21}^0$	$\tau_{21}^1/K$	AARD/%	AARD <sub>p</sub> /%
R-134a + $[C_2C_1im][tcm]$	0	1360.3	0	-111.37	2.17	2.29
R-1234yf + $[C_2C_1im][tcm]$	6.252	121.84	2.670	-477.81	6.57	6.95
R-1234ze(E) + $[C_2C_1im][tcm]$	0	2579.7	0	117.56	2.15	2.27
R-134a + $[C_4C_1im][tcm]$	0	3569.7	0	45.063	2.52	2.61
R-1234yf + $[C_4C_1im][tcm]$	8.004	-341.56	2.213	-428.00	6.43	6.75
R-1234ze(E) + $[C_4C_1im][tcm]$	0	3540.7	0	203.68	4.34	4.52
R-134a + $[C_6C_1im][tcm]$	0	1222.9	0	-202.9	1.34	1.40
R-1234yf + $[C_6C_1im][tcm]$	0	2521.7	0	199.54	4.52	4.78
R-1234ze(E) + $[C_6C_1im][tcm]$	0	1954.3	0	-86.481	1.48	1.56
R-134a + $[C_8C_1im][tcm]$	0	4618.6	0	107.52	3.75	3.91
R-1234yf + $[C_8C_1im][tcm]$	0	2535.2	0	119.92	4.50	4.75
R-1234ze(E) + $[C_8C_1im][tcm]$	0	1604.04	0	-153.53	0.86	0.90

### Section III. Molecular dynamics and analysis of the solvation environments

During the FEP method calculation, the progressive activation of the interactions was done increasing a coupling parameter  $\lambda$  from 0 to 1 in steps of 0.05 for the Lennard-Jones interaction and 0.1 for the other two, and also decreased from 1 to 0 to confirm that hysteresis is negligible. The chemical potential is then obtained from the difference between the free energies initial and final states calculated as:

$$\Delta\mu = -kT \sum_{i=0}^{i-1} \ln \frac{\langle V \exp\left(-\frac{U_{\lambda_{i+1}} - U_{\lambda_i}}{kT}\right) \rangle_{\lambda_i}}{\langle V \rangle_{\lambda_i}} \quad (23)$$

The  $\mu^{res}$  is calculated subtracting the  $\Delta\mu$  for the F-gas in vacuum to the  $\Delta\mu$  for the F-gas in the IL to avoid counting the intramolecular terms as shown in Figure S4. Then, the Henry's law constants were evaluated according to:

$$k_H = \rho_{solvent} RT \ln \left( \frac{\mu^{res}}{RT} \right) \quad (24)$$

where  $\rho_{solvent}$  is the density of the IL. For the FEP calculations, the Langevin thermostat was used to improve the stability of the trajectories.

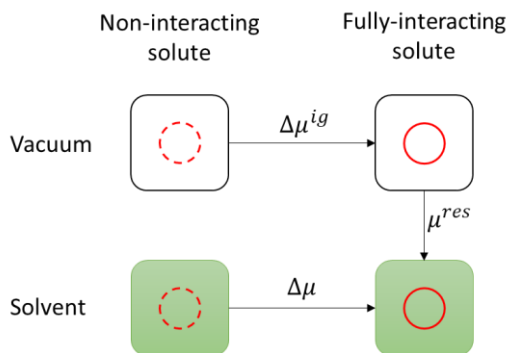


Figure S5. Scheme of the FEP calculation

To ensure the convergence of density, all systems were initially equilibrated during 5 ns as shown in Figure S6a for the system R-1234ze(E) + [C<sub>8</sub>C<sub>1</sub>im][tcm]. Then, the production trajectories of 10 ns sample the ILs well into the diffusive regime, as shown by the linear plot of the logarithm of mean-squared displacement of ions as a function of the logarithm of time as shown in Figure S6b for the same system. In this case with the most viscous IL of the four considered, the plot of mean-squared displacement becomes linear at 4.5 ns. Then, diffusion

coefficients and radial distribution functions were computed with the last 5 ns of the production trajectories.

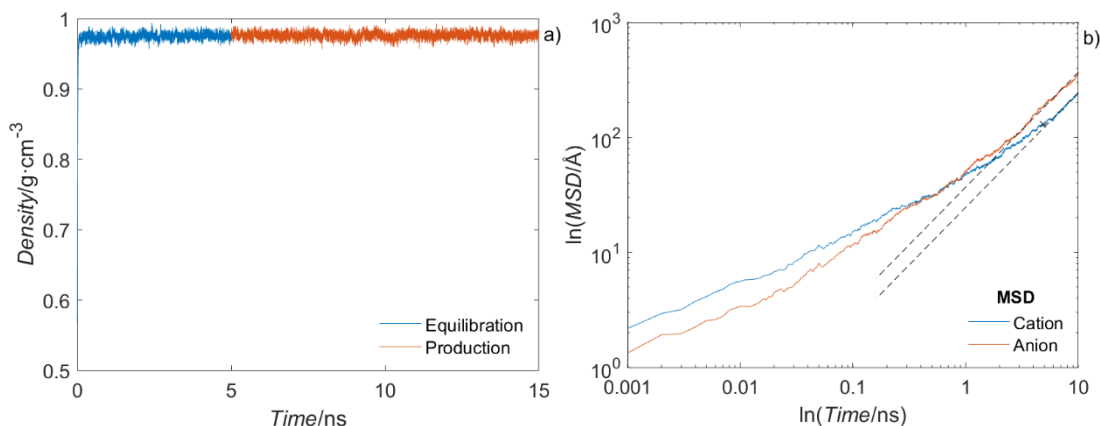


Figure S6. Equilibration of the trajectory for R-1234ze(E) in  $[\text{C}_8\text{C}_1\text{im}][\text{tcm}]$ . (a) Stabilization of density for the equilibration and production runs. (b) Arrival of the system to the diffusive regime after 4.5 ns of the production run, shown by the linear relation between  $\ln(\text{MSD})$  and  $\ln(\text{time})$ .

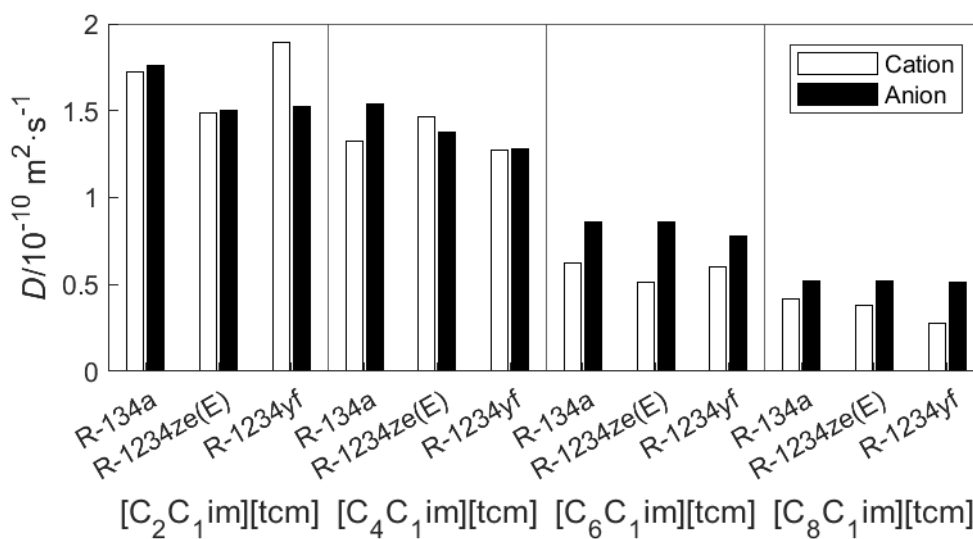


Figure S7. Diffusion coefficient of the ions calculated from molecular dynamics trajectories in each of the systems studied.



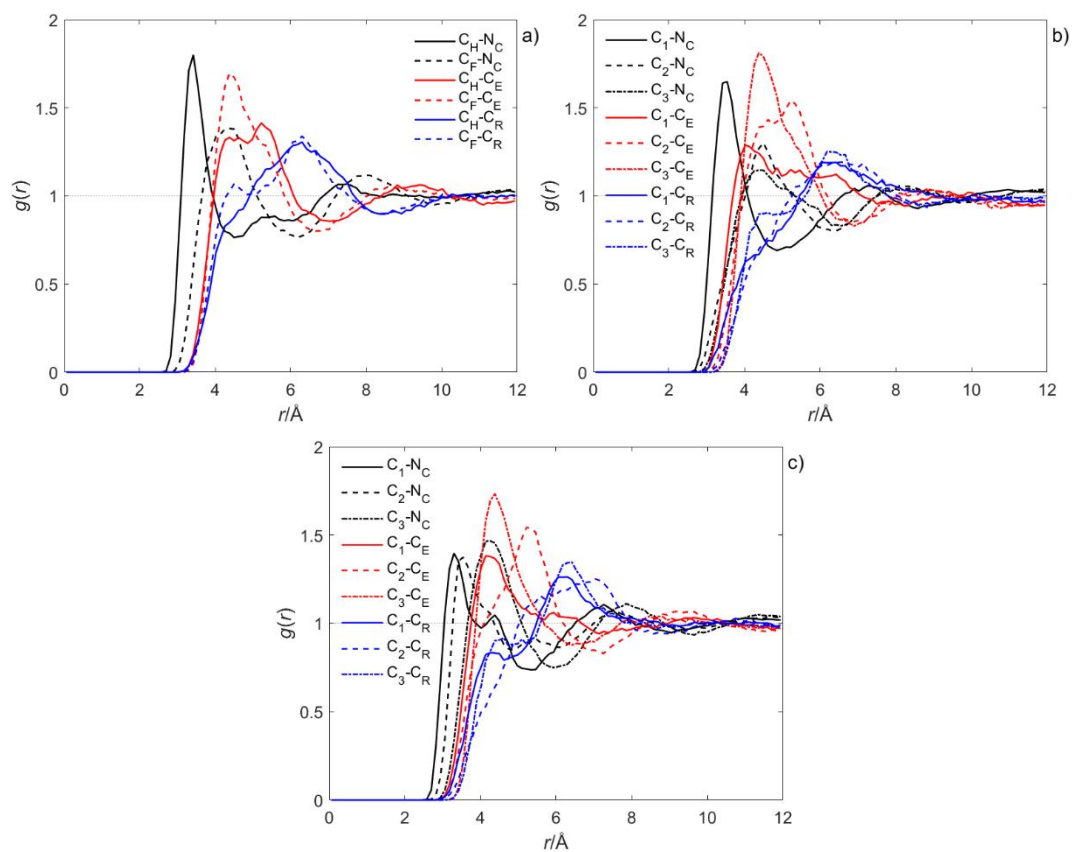


Figure S8. Radial distributions function between representative atoms of (a) R-134a, (b) R-1234yf, and (c) R-1234ze(E), and  $[C_2C_{1im}][tcm]$ . Same figure as Figure 5 but including the interactions with the  $C_R$  of the cation.

Table S14. Results of the quantum calculations using the CHelpG method with MP2/cc-pVTZ(-f) densities.

R-134a		R-1234yf		R-1234ze(E)	
<b>Dipole</b>	2.3002		2.5733		1.2833
<b>Atom</b>	<b>Charge</b>	<b>Atom</b>	<b>Charge</b>	<b>Atom</b>	<b>Charge</b>
C <sub>F</sub>	0.622180	C <sub>1</sub>	-0.405555	C <sub>1</sub>	0.237788
F <sub>T</sub>	-0.203814	H	0.187182	H <sub>1</sub>	0.139028
F <sub>T</sub>	-0.203815	H	0.220635	F <sub>1</sub>	-0.191375
F <sub>T</sub>	-0.241359	C <sub>2</sub>	0.186021	C <sub>2</sub>	-0.465722
C <sub>H</sub>	0.016181	F <sub>1</sub>	-0.177845	H <sub>2</sub>	0.247622
F <sub>1</sub>	-0.223336	C <sub>3</sub>	0.615976	C <sub>3</sub>	0.755143
H	0.116981	F <sub>T</sub>	-0.214413	F <sub>T</sub>	-0.245595
H	0.116981	F <sub>T</sub>	-0.206001	F <sub>T</sub>	-0.238444
		F <sub>T</sub>	-0.206001	F <sub>T</sub>	-0.238444
<b>Grouping the atoms connected to the C atoms</b>					
CF <sub>3</sub> -	-0.026808	CH <sub>2</sub> -	0.002262	CHF-	0.185441
-CH <sub>2</sub> F	0.026807	-CF-	0.008176	-CH-	-0.2181
		-CF <sub>3</sub>	-0.010439	-CF <sub>3</sub>	0.03266

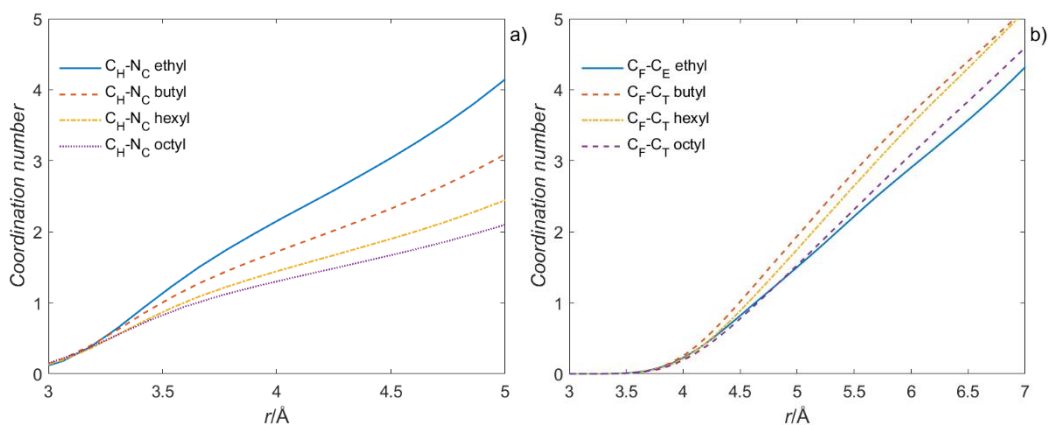


Figure S9. Analysis of the local environments around R-134a in  $[C_nC_{1im}][tcm]$  ILs depending on the cation alkyl chain length. Coordination number for (a) the  $C_H-N_C$  interaction, and (b) the  $C_F-C_{E/T}$  interaction.

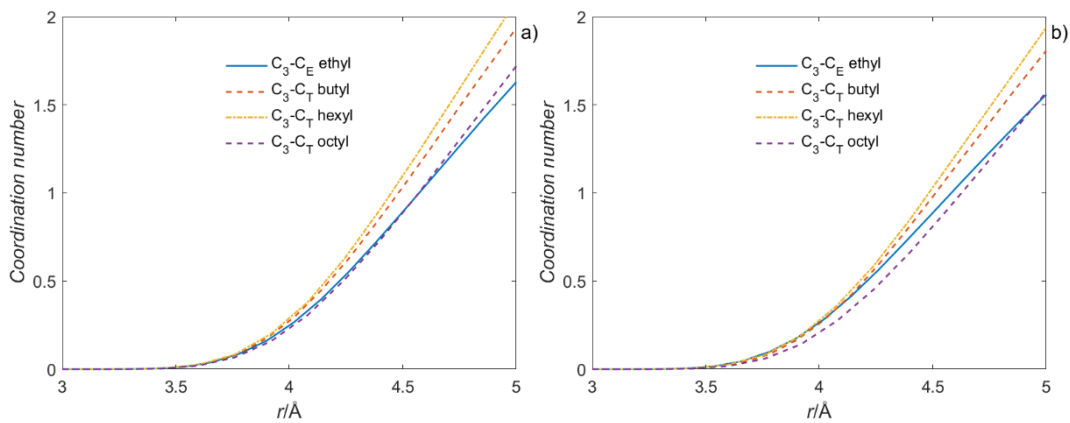


Figure S10. Analysis of the local environment of HFOs in  $[C_nC_{1im}][tcm]$  ILs depending on the cation alkyl chain length. Coordination number for (a) the R-1234yf  $C_F-C_{E/T}$  interaction, and (b) the R-1234ze(E)  $C_F-C_{E/T}$  interaction.

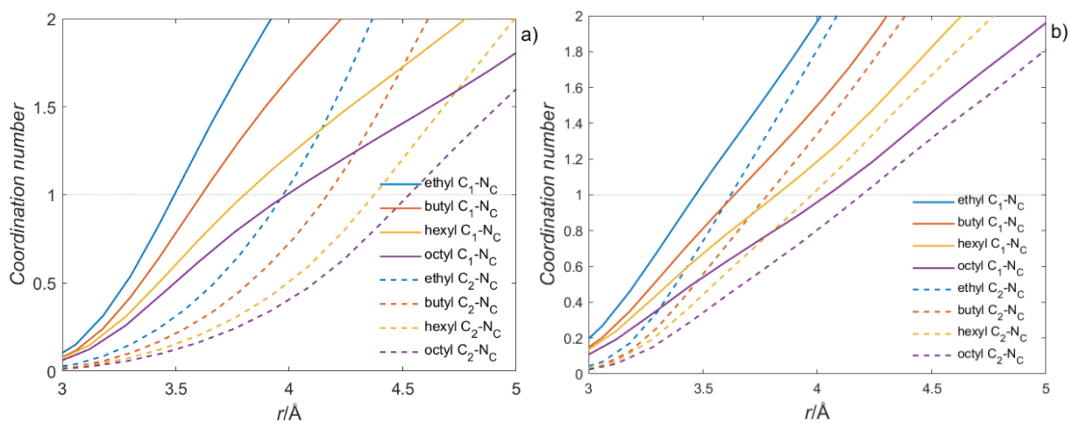


Figure S11. Analysis of the local environments of HFOs in  $[C_nC_{1im}][tcm]$  ILs depending on the cation alkyl chain length. Coordination number for (a) the R-1234yf  $C_{1/2}-N_C$  interaction, and (b) the R-1234ze(E)  $C_{1/2}-N_C$  interaction.

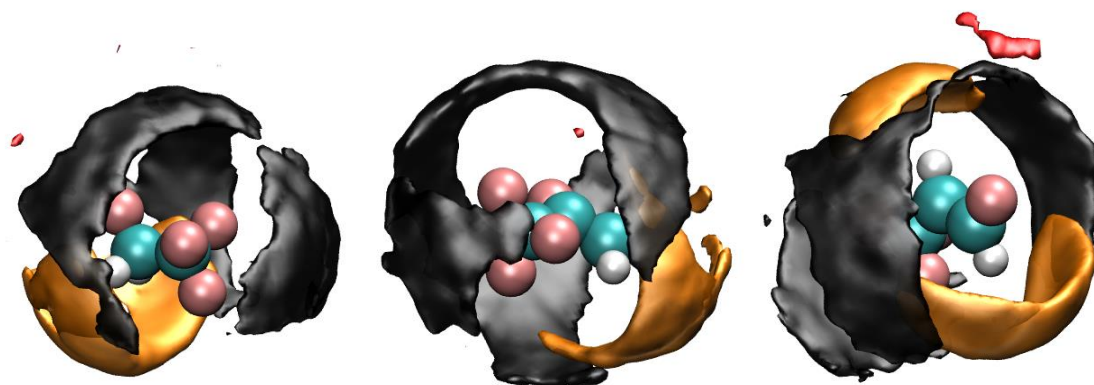


Figure S12. Spatial distribution function for selected atoms of  $[C_4C_{1im}][tcm]$  around R-134a (left), R-1234yf (middle), and R-1234ze(E) (right). The black surface corresponds to  $C_T$  atoms (isodensity contour at 3.3 (R-1234yf) and 3 (R-134a and R-1234ze(E)) times the average density), the orange surface corresponds to  $N_C$  atoms (isodensity contour at 2.6 times the average density), and the red surface corresponds to  $C_R$  atoms (isodensity contour at 1.6 (R-1234yf) and 1.8 (R-134a and R-1234ze(E)) times the average density).

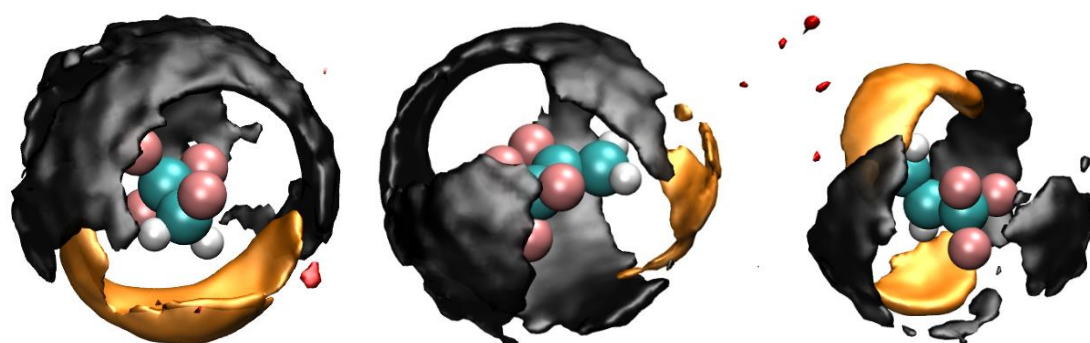


Figure S13. Spatial distribution function for selected atoms of  $[C_6C_{1im}][tcm]$  around R-134a (left), R-1234yf (middle), and R-1234ze(E) (right). The black surface corresponds to  $C_T$  atoms (isodensity contour at 3.3 (R-134a) and 3.9 (R-1234yf and R-1234ze(E)) times the average density), the orange surface corresponds to  $N_C$  atoms (isodensity contour at 2.6 times the average density), and the red surface corresponds to  $C_R$  atoms (isodensity contour at 1.6 times the average density).

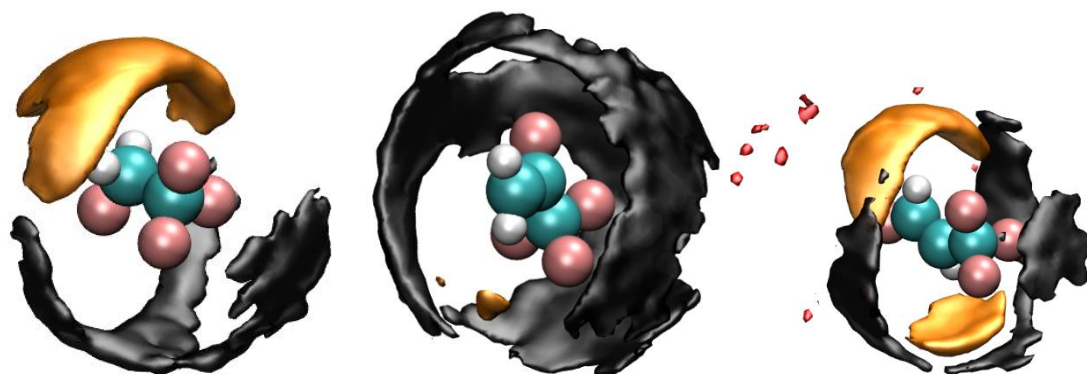


Figure S14. Spatial distribution function for selected atoms of  $[\text{C}_8\text{C}_1\text{im}][\text{tcm}]$  around R-134a (left), R-1234yf (middle), and R-1234ze(E) (right). The black surface corresponds to  $\text{C}_T$  atoms (isodensity contour at 3.9 times the average density), the orange surface corresponds to  $\text{N}_C$  atoms (isodensity contour at 2.6 times the average density), and the red surface corresponds to  $\text{C}_R$  atoms (isodensity contour at 1.6 times the average density).

## References

- (1) Sosa, J. E.; Ribeiro, R. P. P. L.; Castro, P. J.; Mota, J. P. B.; Araújo, J. M. M.; Pereiro, A. B. Absorption of Fluorinated Greenhouse Gases Using Fluorinated Ionic Liquids. *Ind. Eng. Chem. Res.* 2019, 58, 20769–20778. <https://doi.org/10.1021/acs.iecr.9b04648>.
- (2) Lepre, L. F.; Andre, D.; Denis-Quanquin, S.; Gautier, A.; Pádua, A. A. H.; Costa Gomes, M. F. Ionic Liquids Can Enable the Recycling of Fluorinated Greenhouse Gases. *ACS Sustain. Chem. Eng.* 2019, 7, 16900–16906. <https://doi.org/10.1021/acssuschemeng.9b04214>.
- (3) Wentworth, W. E. Rigorous Least Squares Adjustment: Application to Some Non-Linear Equations, *I. J. Chem. Educ.* 1965, 42 (2), 96–103. <https://doi.org/10.1021/ed042p96>.
- (4) Bell, I. H.; Wronski, J.; Quoilin, S.; Lemort, V. Pure and Pseudo-Pure Fluid Thermophysical Property Evaluation and the Open-Source Thermophysical Property Library CoolProp. *Ind. Eng. Chem. Res.* 2014, 53 (6), 2498–2508. <https://doi.org/10.1021/ie4033999>.
- (5) Tassios, D. P. *Applied Chemical Engineering Thermodynamics*; Springer-Verlag: Berlin, 1993; Vol. 67. <https://doi.org/10.1007/978-3-662-01645-9>.
- (6) Walas, S. M. *Phase Equilibria in Chemical Engineering*; Butterworth: Boston, 1985.

**Results**

---

**summary**

---

**Resumen de**

---

**resultados**

---



## 4. Results summary

The present thesis has been devoted to the development of an integrated framework for the design of processes based on the absorption of F-gases in ILs. This development has been based in three pillars. Firstly, an extensive and critical revision of the absorption and separation of F-gases using ILs was performed. Important trends and correlations were identified, as well as fields where there is still a lack of knowledge for the development of F-gas separation processes. Also, all the literature data were compiled and provided in the UC-RAIL database. The second pillar consists of the experimental determination of the solubility and diffusivity of HFCs and HFOs currently important in the RACHP sector in different ILs to use them in the design of separation processes and absorption refrigeration systems. The last objective of the thesis advanced in the mathematical modeling of F-gas/IL mixtures using both the classical thermodynamic regression approaches, as well as powerful computational methods that will help in different tasks towards the design of processes using ILs as selective F-gases entrainers for mixture separation, or as high-capacity absorbents in absorption refrigeration systems. This is, the work performed using the NRTL model will allow the process design based on the regressed parameters, the predictive tool shows that artificial intelligence can be of great help in the selection of solvents for different processes, and molecular dynamics provide very valuable insights at the microscale on the mechanisms leading the absorption of refrigerants in ILs.

### 4.1. Experimental results

The solubility and diffusivity of five refrigerant gases, three of them HFCs (R32, R134a, and R125) and two HFOs (R1234yf and R1234ze(E)), in ILs have been determined using the isochoric saturation and the semi-infinite volume methods. The experiments started studying the absorption in common ILs of low viscosity, namely  $[\text{C}_2\text{mim}][\text{BF}_4]$ ,  $[\text{C}_2\text{mim}][\text{OTf}]$ , and  $[\text{C}_2\text{mim}][\text{Tf}_2\text{N}]$ . The results show that the solubility of all the gases increases in ILs with higher molar volumes and more fluorine atoms in their structure, but that the solubility selectivity increases the other way around, using ILs with lower molar volumes and less fluorinated. For that reason, the IL  $[\text{C}_2\text{mim}][\text{SCN}]$  was tested owing to its small size and lack of fluorine atoms, achieving the highest selectivity values ever achieved for the separation of R32 from R125 and R1234yf, and R134a from R1234yf, three mixtures of interest due to their application as commercial refrigerant blends and the difficulty to separate them in pure components because of their close-boiling or azeotropic nature. Following studies with other cyanide based ILs showed that  $[\text{C}_2\text{mim}][\text{dca}]$  improves even further the selectivity for the separation of R134a



from R1234yf. Additionally, the solubility increases with higher molar volumes for the cyanide based ILs studied, which include  $[C_4\text{mim}][\text{dca}]$  and  $[C_n\text{mim}][\text{tcm}]$ , with  $n = 2, 4, 6,$  and  $8$ . However, no clear trends were found for the diffusion coefficients, as they were all very similar for every F-gas and IL. Taking together the experiments aimed at determining new VLE systems and the systems studied for validation of the experimental setup, a total of 875 solubility datapoints have been published. This thesis does not include the results of solubility of R32 and R125 in the  $[C_n\text{mim}][\text{tcm}]$  ILs, with  $n = 2, 4, 6,$  and  $8$ , because they have not yet been published and represent around 300 additional experimental datapoints. Table 7 summarizes the 42 systems studied during the thesis period plus the 2 systems studied for validation. This table does not include other systems that were also studied but have never been published, such as for example the absorption of  $\text{CO}_2$  in  $[C_4\text{mim}][\text{PF}_6]$  that was used for extra validation of the experimental setup. Finally, as the separation of R134a and R1234ze(E) remains a challenge, some experiments were done to study reactive absorption approaches could be applied to separate mixtures of both. To that end, the absorption of R1234ze(E) and R1234yf was studied in a solution formed by  $[C_2\text{mim}][\text{BF}_4]$  with silver salt with the same anion,  $\text{AgBF}_4$ , to verify if these two HFOs could form complexes with silver sharing their  $\pi$ -bond electrons with the metal. The results are not published nor presented here because no interaction was observed. Furthermore, the Gaussian determination of atomic charges presented in Table S14 of publication 8 shows that the fluorine atoms of the HFOs are so electronegative that the volume around the double bond of the molecules have local positive charge, meaning that the electrons of the  $\pi$ -bond have been attracted to the fluorine atoms of the molecule and removed from there, hindering their complexation capability.

Finally, a review article was published analyzing all the available information on the absorption of F-gases using ILs. The thermodynamic and transport properties were reviewed and regarded as a whole, compiled in the UC-RAIL database, and some trends for the solubility were identified using, for example, the Regular Solution Theory. The Regular Solution Theory gives interesting insights that give a good approximation of the system behavior, but it does not consider enthalpic interactions, so other models need to be used for the regression of the VLE. Additionally, the information available in separation process design was reviewed showing that they have the potential to be developed at an industrial scale for the recovery of F-gases from RAC equipment at its end of life.

Table 7. Summary of F-gas/IL systems studied during the thesis. (P): published system, (V): system used for validation of the experimental setup and published, and (F): system to be published in the future.

		F-gases				
		HFCs			HFOs	
		R32	R134a	R125	R1234yf	R1234ze(E)
Ionic liquids	[C <sub>2</sub> mim][BF <sub>4</sub> ]	P	P		V	
	[C <sub>2</sub> mim][dca]	P	P	P	P	P
	[C <sub>2</sub> mim][OTf]	V	P		P	P
	[C <sub>2</sub> mim][SCN]	P	P	P	P	P
	[C <sub>2</sub> mim][tcm]	F	P	F	P	P
	[C <sub>2</sub> mim][Tf <sub>2</sub> N]				P	P
	[C <sub>4</sub> mim][dca]	P	P	P	P	P
	[C <sub>4</sub> mim][tcm]	F	P	F	P	P
	[C <sub>6</sub> mim][tcm]	F	P	F	P	P
	[C <sub>8</sub> mim][tcm]	F	P	F	P	P

## 4.2. Computational results

Three types of models have been applied throughout the thesis with three different goals in the field of the VLE of F-gas/IL systems: data regression, data prediction, and molecular interaction analysis. The results achieved with each of them are discussed below.

### 4.2.1. Data regression

Two different models have been used for the regression of VLE data, one approach is based on the use of the NRTL activity coefficient model and the other one is based on the use of the soft-SAFT EoS. Both approaches led to good fitting of the experimental results.

For the NRTL method, the VLE were fitted mainly with two parameters, using four parameters when needed to decrease the relative error below 10%, which only happened in the systems with the lowest solubilities, such as the absorption of R125 in [C<sub>2</sub>mim][SCN]. The soft-SAFT EoS showed its accuracy after fitting the two binary parameters for association energy and volume correction, where the volume one was constant and transferable through compounds of the same family with the sole exception of the system formed by R125 and [C<sub>4</sub>mim][PF<sub>6</sub>] due to the convex behavior of the VLE isotherms at low temperatures. Once fitted the binary VLE, soft-SAFT was able to predict the VLLE behavior of the systems. NRTL was used to predict the VLLE

immiscibility regions too, but there were not VLE data available for the systems studied to check its accuracy. In any case, the determination of the VLE has not been an objective of this thesis because this region has little interest for process design for the separation of F-gas mixtures and absorption refrigeration processes.

The phase behavior of ternary mixtures was predicted using the binary interaction parameters with the NRTL method and the soft-SAFT EoS, and these ternary diagrams were used for the calculation of one-stage flash separators using the Rachford-Rice equation. The results show that [C<sub>2</sub>mim][SCN] would give the highest separation factor for the mixtures of R32 with R125 and R32 with R1234yf, and that [C<sub>2</sub>mim][dca] would be the best solvent to separate R134a from R1234yf.

The main current disadvantage of the soft-SAFT EoS is that it is not available in commercial software, which hinders its utilization despite its accuracy and transferability. More complex process design was therefore done with the NRTL method only and involved the design of an extractive distillation column and absorption refrigeration systems.

### 4.2.2. Data prediction

The experimental work necessary to find the optimal IL for each separation is expensive and time-consuming. For that reason, this thesis addressed the task of developing a tool able to generate reliable predictions of the VLE to be used in the screening stages of the process design. This becomes a matter of great interest when ILs are used as absorption solvents due to the enormous amount of anion and cation combinations that could be ideally used. To that end, the machine learning method of ANNs was used, resulting in an ANN able to predict the VLE of F-gases and ILs with a relative error of 10%, an outstandingly good result considering the great number of gases, ILs, and total datapoints involved (24, 52 and 4396, respectively). An especially remarkable result is its capability to predict the VLE of systems not existing in the original dataset, including the VLE of a new HFO, the R1243zf, whose solubility in ILs had not been studied before and was predicted with errors around 10%. The article related to its development includes as Supplementary Material an easy-to-use software tool so that the scientific community can take advantage and make use of it without the need to deeply know the methodology, only knowing the pure component properties for the solute and the solvent.

### 4.2.3. Interaction analysis

The analysis of solute-solvent interactions was done by means of molecular dynamics simulations using the CL&Pol force field for ILs and polarizing fixed-charge force fields available in the literature for the F-gases. Firstly, the theoretical approach was validated by means of free

energy perturbation calculations, which showed that the solubility expressed as Henry's law constants can be predicted using this methodology with a level of agreement that represents well the solute-solvent interactions. Afterwards, the solvation behavior was studied in terms of radial and spatial distribution functions. Despite the polarity of the F-gas molecules, they showed nonpolar domains in the  $-CF_3$  terminal groups. While the other regions of the molecule could form hydrogen bonds with the anion of the ILs, the main interaction in these mixtures is through nonpolar-nonpolar interactions between the F-gases  $-CF_3$  groups and the cation alkyl chains of the IL. This indicates that improving the selectivity to separate mixtures of R134a and R1234ze(E), a complex separation due to the high solubility of R1234ze(E) in comparison with its isomer R1234yf, should be achieved modifying the ILs' cation alkyl chains to make them interact differently with each of the molecules of interest. Also, the results showed that the difference between the solubility of the two HFO isomers may be due to the existence of two positive centers in the  $C_1$  and  $C_2$  of R1234ze(E) able to form hydrogen bonds with the ILs against only one center in the  $C_1$  of R1234yf.

### 4.3. Process design

The results of the process design showed that the absorption of F-gases using ILs can be used for the two types of processes evaluated in this thesis, but that different ILs should be used in each case: for flash separators and extractive distillation processes the use of selective solvent should be favored, while for the design of absorption refrigeration processes the main objective should be using an IL with a high absorption capacity, which normally is related to ILs with low selectivity values.

Publication 5 assessed the performance of 16 working pairs for absorption refrigeration systems. These pairs were formed from low-GWP HFCs and very-low-GWP HFOs combined with low viscosity ILs. The results show that the *COP* values for the single-effect absorption refrigeration systems are low, being the best working pair the one formed by R32/[C<sub>2</sub>mim][BF<sub>4</sub>] with a *COP* of 0.41 to be compared to the 0.75 value of the traditional H<sub>2</sub>O/LiBr working pair. Compression-assisted absorption refrigeration improves the *COP* and expands the range of working temperatures with respect to single-effect systems. In this case, the pair of R32/[C<sub>2</sub>mim][Tf<sub>2</sub>N] presents a *COP* of 0.74, competitive with the classic working pair. The definition of the pair R32/[C<sub>2</sub>mim][Tf<sub>2</sub>N] outperforms the F-gas/IL pairs reported previously using the same configuration. The key consideration in absorption refrigeration systems is the high refrigerant solubility in the IL to minimize the amount solvent used.

For the separation of HFCs and HFOs, the identification of selective ILs is key. The ILs identified in this thesis to perform the separations of interest were used in publication 6 to calculate flash separators of the mixtures, achieving separation factors with values around five at 303 K and 5 bar, a clear improvement with respect to the values around 1.6 for the separation factor of the ILs considered in publication 2, which were the ones for which there were data available in the literature. The ILs identified in this thesis triplicate the separation factors of the ones used previously, and extractive distillation process design is being done in the University of Cantabria pointing towards important reductions in the capital and operation expenditures just by selecting the appropriate IL for each separation.

### **4.4. Assembling the framework**

A classical approach to process design consists of testing different solvents until the suitable one is found, then the experimental data are regressed, and the model is used for the process design. However, this task is expensive and time-consuming, and it can even fail if the right solvent never gets to be tested. In the current context of the RACHP sector, where the refrigerant blends are evolving fast, new compounds are added to the mixtures and some mixtures will be short-lived because of the progressive change of the regulation limits, it is necessary to have a fast way to develop new processes and select the ILs for each of the applications. For that reason, the framework presented here helps decreasing the costs associated to basic research and accelerates the investigation to arrive faster at the industrial scale. The steps to follow in this framework are the following:

1. Objective definition. What is the aim of the absorption of F-gases with ILs? A process which requires high absorption of the refrigerant? Or is it a process in which high selectivity for the separation of a mixture of refrigerant gases is needed?
2. Review of the available information. This step could be time consuming, but thanks to the review article forming part of this thesis most of the work is already done with the significant trends already elucidated and the experimental data compiled in the UC-RAIL database. If needed, only the data from articles published after August 2021 should be included to check if even new trends arise thanks to a higher data availability.
3. Computational study of the solvation. Using molecular dynamics, the interactions of the F-gases and the ILs can be studied at an atomistic level gaining a deep understanding of the mixture behavior. If the aim is to develop an absorption refrigeration system, the study should aim to find the solvent characteristics that lead to a high solubility of the refrigerant. On the other hand, if the project is searching for an IL able to separate a

---

new refrigerant mixture, the study should focus on finding an IL that interacts strongly with one of the mixture components and not with the rest, or that interacts with all of them but one. That way, a series of candidates based on its molecular features can be preselected.

4. Data prediction using the machine learning tool. Thanks to the ANN developed in this thesis, the pure component properties can be used to predict the VLE of F-gases mixtures with ILs. The pure component properties are easily obtainable: molar mass of the anion and cation of the IL, molar volume and fluorine atoms of the IL, and molar mass, critical properties, acentric factor, vapor pressure, and fluorine atoms of the refrigerant gas. Then, all the candidates identified with the computational study can be screened fast, and the most promising be selected for continuing the study.
5. Experimental determination of the absorption of the F-gases in the selected IL. This allows the precise knowledge of the VLE, decreasing the uncertainty derived from the use of the ANN, which is lower than 10% in most cases, but can result in higher deviations when the values are far from those used to train the network.
6. Regression of the experimental data. The process design and simulation require the use of an accurate thermodynamic model. In this thesis, the NRTL activity coefficient model has been the most used for the design of flash separators, extractive distillation columns, and absorbers and desorbers in the absorption refrigeration systems. Nevertheless, as soon as soft-SAFT becomes widely available, it should be used because it can present a slightly improved accuracy with parameters transferable between different absorption pairs.
7. Process design itself. Once all the previous steps have been successfully completed, the pilot plant or industrial process design can be carried out following typical simulation and optimization procedures in the field of chemical engineering.

## 4. Resumen de resultados

La presente tesis se ha dedicado al desarrollo de un marco de trabajo integrado para el diseño de procesos basados en la absorción de gases fluorados en líquidos iónicos. Este desarrollo se ha basado en tres pilares. Primero, se ha realizado una revisión bibliográfica extensa y crítica sobre la absorción y separación de gases refrigerantes fluorados en líquidos iónicos (LIs). Al hacer la revisión se identificaron tendencias y correlaciones de interés para comprender el comportamiento de los sistemas estudiados, así como campos en los que hay que realizar todavía esfuerzos de investigación importantes para el desarrollo de procesos de separación de gases refrigerantes fluorados. Además, todos los datos existentes fueron recopilados en la base de datos UC-RAIL, suministrada como material suplementario. El segundo pilar consiste en la determinación experimental de la solubilidad y difusividad en diferentes LIs de los HFCs y HFOs importantes en la actualidad en el sector de la refrigeración, aire acondicionado y bombas de calor para usarlos en el diseño de procesos de separación y de sistemas de refrigeración por absorción. El último pilar avanza en el modelado matemático de mezclas de gases refrigerantes fluorados con LIs utilizando diferentes métodos que ayudarán en varias tareas encaminadas al diseño de procesos basados en el uso de LIs para absorber gases fluorados de forma selectiva en separaciones de mezclas o en gran cantidad en refrigeraciones basadas en absorción. Así, el trabajo realizado utilizando el modelo NRTL permite el diseño de procesos basado en los parámetros de regresión, mientras que la herramienta de predicción muestra que la inteligencia artificial puede ser de gran ayuda en la selección de disolventes para distintos procesos y la dinámica molecular da información muy valiosa al nivel de la microescala sobre los mecanismos que controlan la absorción de refrigerantes en LIs.

### 4.1. Resultados experimentales

La solubilidad y difusividad de cinco gases refrigerantes, tres de ellos HFCs (R32, R134a y R125) y dos HFOs (R1234yf y R1234ze(E)), en LIs se han determinado utilizando el método de saturación isocórica y el de volumen semi-infinito. Los experimentos comenzaron por el estudio de la absorción en LIs comunes de baja viscosidad:  $[\text{C}_2\text{mim}][\text{BF}_4]$ ,  $[\text{C}_2\text{mim}][\text{OTf}]$  y  $[\text{C}_2\text{mim}][\text{Tf}_2\text{N}]$ . Los resultados muestran que la solubilidad de todos los gases aumenta en LIs de mayor volumen molar y más átomos de flúor en su estructura, pero que la selectividad aumenta en sentido contrario, usando LIs de menor volumen molar y menos fluorados. Por ese motivo, el LI  $[\text{C}_2\text{mim}][\text{SCN}]$  se probó por su pequeño tamaño y ausencia de átomos de flúor, con lo que se consiguieron los valores de selectividad más altos hasta la fecha para la separación de R32 de R125 y R1234yf, y de R134a de R1234yf, tres mezclas de interés por su existencia en mezclas

refrigerantes comerciales y por la dificultad existente para separarlas en los componentes puros por su naturaleza azeotrópica o de proximidad de sus puntos de burbuja y rocío. Los experimentos siguientes con otros líquidos iónicos con aniones basados en el cianuro mostraron que la  $[C_2mim][dca]$  mejora más todavía la selectividad de la separación de R134a de R1234yf. Asimismo, la solubilidad aumenta con el aumento de volumen molar de los LIs basados en el cianuro, que incluyen los estudiados  $[C_4mim][dca]$  y  $[C_nmim][tcm]$  con  $n = 2, 4, 6$  y  $8$ . Sin embargo, no se encontraron tendencias claras para los coeficientes de difusión, ya que todos ellos son muy similares para todos los gases y LIs. Entre la determinación de nuevos sistemas y el estudio de sistemas para validar el equipo experimental, se han publicado un total de 875 puntos experimentales de solubilidad. Esta tesis no incluye los resultados de solubilidad de R32 y R125 en los LIs  $[C_nmim][tcm]$  con  $n = 2, 4, 6$  y  $8$  (alrededor de 300 puntos experimentales más) porque todavía no han sido publicados. La Tabla 8 resume los 42 sistemas estudiados durante el periodo de la tesis más los 2 sistemas estudiados como validación. Esta tabla no incluye otros sistemas que también se han estudiado pero que no se han publicado, como por ejemplo la absorción de  $CO_2$  en  $[C_4mim][PF_6]$  que se realizó como método de validación de la fiabilidad del montaje experimental. Por último, como la separación de R134a y R1234ze(E) sigue siendo un reto, se hicieron algunos experimentos para determinar si estos dos gases son separables por absorción reactiva. Para ello, se estudió la absorción de R124ze(E) y R1234yf en una disolución formada por  $[C_2mim][BF_4]$  con una sal de plata de anión común disuelta, el  $AgBF_4$ , para comprobar si estas dos HFOs podrían formar complejos con la plata compartiendo los electrones de su enlace  $\pi$  con el metal. Los resultados no están publicados ni presentados en este documento porque no se observó ninguna interacción. Además, la determinación de Gaussian de las cargas atómicas presentada en la Tabla S14 de la publicación 8 muestra que los átomos de flúor son tan electronegativos que el volumen alrededor del doble enlace de las HFOs tiene carga local positiva, lo que quiere decir que los electrones del enlace  $\pi$  se ven atraídos por los átomos de flúor de la molécula y desplazados del enlace doble, dificultando e impidiendo su capacidad para formar complejos organometálicos.

Finalmente, se publicó un artículo de revisión analizando todos los datos disponibles relacionados con la absorción de gases fluorados en LIs. Las propiedades termodinámicas y de transporte se revisaron y analizadas en conjunto, recopiladas en la base de datos UC-RAIL y se identificaron tendencias en la solubilidad usando, por ejemplo, la Teoría de Soluciones Regulares. Esta teoría da una aproximación que sirve para conocer mejor los sistemas, pero no tiene en cuenta interacciones entálpicas, por lo que hace falta usar otros modelos para la descripción del equilibrio líquido-vapor. Asimismo, se hizo una revisión de la información



disponible sobre el diseño de procesos de separación que muestra el potencial que tienen para ser desarrollados a escala industrial para la recuperación de gases fluorados provenientes de equipos de refrigeración en el fin de su vida útil.

Tabla 8. Resumen de sistemas de gases fluorados refrigerantes y líquidos iónicos estudiados durante la tesis. (P): sistema publicado, (V): sistema utilizado para validar el equipo experimental y publicado, y (F): sistema a publicar en el futuro.

		F-gases				
		HFCs			HFOs	
		R32	R134a	R125	R1234yf	R1234ze(E)
Líquidos iónicos	[C <sub>2</sub> mim][BF <sub>4</sub> ]	P	P		V	
	[C <sub>2</sub> mim][dca]	P	P	P	P	P
	[C <sub>2</sub> mim][OTf]	V	P		P	P
	[C <sub>2</sub> mim][SCN]	P	P	P	P	P
	[C <sub>2</sub> mim][tcm]	F	P	F	P	P
	[C <sub>2</sub> mim][Tf <sub>2</sub> N]				P	P
	[C <sub>4</sub> mim][dca]	P	P	P	P	P
	[C <sub>4</sub> mim][tcm]	F	P	F	P	P
	[C <sub>6</sub> mim][tcm]	F	P	F	P	P
	[C <sub>8</sub> mim][tcm]	F	P	F	P	P

## 4.2. Resultados computacionales

Se han aplicado tres tipos de modelos durante la tesis con tres metas diferentes en el campo del equilibrio líquido-vapor de sistemas de gases refrigerantes y LIs: regresión de datos experimentales, predicción de datos y análisis de interacciones moleculares. Los resultados conseguidos con cada uno de ellos se explican a continuación.

### 4.2.1. Regresión de datos

Se han utilizado dos modelos diferentes para la regresión de datos experimentales de equilibrio líquido-vapor, uno basado en el modelo de coeficientes de actividad NRTL y otro en el uso de la ecuación de estado soft-SAFT. Los dos enfoques dieron como resultado una buena descripción de los resultados experimentales.

Para el método NRTL, los equilibrios líquido-vapor se ajustaron principalmente con dos parámetros, o cuatro parámetros en el caso de necesitarlos para disminuir el error relativo por debajo del 10%, lo que ocurrió solo en los sistemas con solubilidades más bajas, como la

absorción de R125 en [C<sub>2</sub>mim][SCN]. La ecuación de estado soft-SAFT demostró su precisión ajustando los dos parámetros binarios de corrección de energía y volumen de asociación, de los que el parámetro de corrección de volumen era constante y transferible a compuestos de la misma familia con la única excepción del sistema formado por R125 con [C<sub>4</sub>mim][PF<sub>6</sub>] debido al comportamiento convexo de las isothermas del equilibrio líquido-vapor a bajas temperaturas. Tras ajustar el equilibrio líquido vapor binario, soft-SAFT fue capaz de predecir el equilibrio líquido-líquido-vapor de los sistemas. El modelo NRTL se usó también para predecir las regiones de inmiscibilidad líquido-líquido-vapor, pero no había datos disponibles para contrastar las predicciones de la región trifásica. En todo caso, no ha sido objeto de esta tesis doctoral la determinación del equilibrio líquido-líquido-vapor, ya que se trata de una región de escaso interés para el diseño de procesos de separación de mezclas de gases fluorados y de procesos de refrigeración basados en absorción en disolventes.

El equilibrio de fases de mezclas ternarias a partir de los parámetros binarios fue predicho con el método NRTL y la ecuación de estado soft-SAFT, y estos diagramas ternarios se usaron para el cálculo de separadores flash utilizando la ecuación de Rachford-Rice. Los resultados muestran que el [C<sub>2</sub>mim][SCN] daría el factor de separación más altos para las mezclas de R32 con R125 y R32 con R1234yf, y que [C<sub>2</sub>mim][dca] sería el mejor disolvente para separar R134a de R1234yf.

La principal desventaja en la actualidad de la ecuación de estado soft-SAFT es que no está disponible en software comercial, lo que dificulta su utilización a pesar de su precisión y transferibilidad. Por tanto, solo se usó NRTL para realizar diseños de proceso más complejos como una columna de destilación extractiva y sistemas de absorción por refrigeración.

#### 4.2.2. Predicción de datos

El trabajo experimental necesario para encontrar el LI óptimo para cada separación es caro y tedioso. Por ese motivo, esta tesis abordó la tarea de desarrollar una herramienta capaz de generar predicciones fiables del equilibrio líquido-vapor para utilizarla en etapas de exploración del diseño de procesos. Esta cuestión resulta de especial interés en el caso de utilizar como disolventes de absorción los LIs, dada la inmensa cantidad de combinaciones de aniones y cationes que se podrían idealmente utilizar. Para ello se utilizó el método de aprendizaje automático de las redes neuronales artificiales, con el que se obtuvo una red neuronal capaz de predecir el equilibrio líquido-vapor de gases fluorados y LIs con un error relativo del 10%, un resultado especialmente bueno si se considera el gran número de gases, LIs, y puntos totales utilizados (24, 52 y 4396, respectivamente). Un resultado especialmente remarcable es la capacidad de la red para predecir el equilibrio líquido-vapor de sistemas que no existían en la

base de datos original, incluyendo el de un nuevo gas de tipo HFO, el R1234zf, cuya solubilidad en LIs no se había estudiado con anterioridad y ha podido ser predicha con un error en torno al 10%. El artículo relacionado con el desarrollo de la red neuronal incluye como Material Suplementario una herramienta software de fácil utilización para permitir su uso por la comunidad científica sin necesidad de conocer la metodología en profundidad, a partir únicamente de las propiedades de compuesto puro del soluto y el disolvente.

#### 4.2.3. Análisis de interacciones

El análisis de interacciones soluto-disolvente se hizo por medio de simulaciones de dinámica molecular utilizando el campo de fuerza (force field) CL&Pol para los LIs y campos de fuerza de carga fija disponibles en la literatura para los gases fluorados. Primero, este enfoque teórico se validó por medio de cálculos de perturbación de energía libre, que mostraron que la solubilidad expresada en términos de valores de las constantes de Henry se puede predecir con esta metodología con un nivel de precisión adecuado para el estudio de las interacciones soluto-disolvente. A continuación, la solvatación se estudió en forma de funciones de distribución radiales y espaciales. A pesar de la polaridad de las moléculas de los gases fluorados, los grupos terminales  $-CF_3$  presentan dominios apolares. Mientras que otras regiones de la molécula podrían formar puentes de hidrógeno con los aniones de los LIs, la interacción principal en estas mezclas se realiza por medio de fuerzas de tipo apolar-apolar entre los grupos  $-CF_3$  de los gases fluorados y las cadenas alquílicas del catión del LI. Esto indica que mejorar la selectividad para separar mezclas de R134a y R1234ze(E), una separación compleja debido a la elevada solubilidad del R1234ze(E) en comparación con su isómero R1234yf, debería conseguirse a través de una modificación de la cadena alquílica del catión de los LIs para que esta interactuase de forma diferente con las moléculas de cada uno de los gases de interés. Además, los resultados mostraron que la diferencia de solubilidad entre los dos isómeros de HFO podría deberse a la existencia de dos centros positivos en los carbonos  $C_1$  y  $C_2$  del R1234ze(E) capaces de formar puentes de hidrógeno con los LIs, mientras que el R1234yf solo tiene uno en el  $C_1$ .

#### **4.3. Diseño de procesos**

Los resultados del diseño mostraron que la absorción de gases fluorados con LIs puede utilizarse para los dos tipos de procesos evaluados en esta tesis, pero que los LIs utilizados en cada caso deberían ser diferentes: para separadores flash y procesos de destilación extractiva, el uso de un disolvente selectivo se ve favorecido, mientras que para el diseño de procesos de refrigeración por absorción el objetivo principal debería ser utilizar LIs con alta capacidad de absorción, una característica normalmente relacionada con LIs de baja selectividad.

La publicación 5 evalúa el desempeño de 16 pares de trabajo para sistemas de refrigeración por absorción. Estos pares están formados por HFCs de bajo potencial de calentamiento atmosférico (PCA) y HFOs de muy bajo PCA combinados con LIs de baja viscosidad. Los resultados muestran que los valores de *COP* en los sistemas de refrigeración por absorción de efecto simple son bajos, donde el mejor par de trabajo es el formado por R32/[C<sub>2</sub>mim][BF<sub>4</sub>] con un *COP* de 0.41 a comparar con el valor de 0.75 del par de trabajo tradicional H<sub>2</sub>O/LiBr. La refrigeración por absorción con compresión asistida mejora el *COP* y expande el rango de temperaturas de trabajo respecto a los sistemas de efecto simple. En este caso, el par de R32/[C<sub>2</sub>mim][Tf<sub>2</sub>N] presenta un *COP* de 0.74, competitivo con el par de trabajo clásico, y con desempeños mejores que los de los pares de trabajo reportados previamente utilizando la misma configuración. La consideración clave en los sistemas de absorción por refrigeración es la alta solubilidad de refrigerante en el LI para minimizar la cantidad de disolvente utilizado.

Para la separación de HFCs y HFOs, identificar LIs selectivos es primordial. Los LIs identificados en este tesis para realizar las separaciones de interés se usaron en la publicación 6 para calcular separadores flash de la mezclas, alcanzando factores de separación con valores alrededor de cinco a 303 K y 5 bar, una mejora clara respecto a los valores alrededor de 1.6 para los factores de separación de los LIs considerados en la publicación 2, que eran para los que había datos disponibles en la literatura. Los LIs identificados en esta tesis triplican los de los utilizados previamente, y el diseño de procesos de destilación extractiva que se está realizando en la Universidad de Cantabria indica que se pueden alcanzar reducciones importantes in los costes de capital y operación simplemente al elegir el LI apropiado para cada separación.

#### **4.4. Creación del marco de trabajo**

Un enfoque clásico del diseño de procesos consiste en probar diferentes disolventes hasta encontrar uno adecuado, ajustar los datos experimentales con un modelo y usar este modelo para el diseño de procesos. Sin embargo, esta tarea consume mucho tiempo y puede fallar si el disolvente correcto no llega a probarse nunca. En el contexto actual del sector de la refrigeración, el aire acondicionado y las bombas de calor, en el que las mezclas refrigerantes evolucionan rápidamente y algunas de ellas van a poder utilizarse poco tiempo a causa del cambio progresivo de los límites de la regulación, es necesario tener una forma rápida de desarrollar nuevos procesos y seleccionar los LIs destinados a cada una de las aplicaciones. Por tanto, el marco de trabajo presentado aquí ayuda a disminuir los costes asociados a la investigación básica y acelera la investigación para llegar más rápido a la escala industrial. Los pasos a seguir en este marco son los siguientes:

1. Definición del objetivo. ¿Qué se quiere conseguir con la absorción de gases fluorados en LIs? ¿Un proceso con una alta capacidad de absorción de refrigerante? ¿O un proceso con una alta selectividad para la separación de una mezcla de gases refrigerantes?
2. Revisar la información disponible. Este paso podría consumir bastante tiempo, pero gracias al artículo de revisión que forma parte de esta tesis la mayoría de los datos están recopilados en la base de datos UC-RAIL. En caso de necesitarlo, solo habría que incluir los datos publicados después de agosto de 2021 para comprobar si se pueden elucidar nuevas tendencias gracias a la mayor disponibilidad de información.
3. Estudio computacional de la solvatación. Con la dinámica molecular, las interacciones de los gases fluorados y los LIs se pueden estudiar a un nivel atómico para comprender en profundidad el comportamiento de la mezcla. Si el objetivo es desarrollar un sistema de refrigeración por absorción, el estudio debería intentar encontrar unas características del disolvente que lleven a una alta solubilidad del refrigerante. Por otro lado, si el proyecto busca un LI capaz de separar una mezcla refrigerante nueva, el estudio debería enfocarse en encontrar un LI que interactúe fuertemente con uno de los componentes de la mezcla y no con el resto, o con todos excepto uno. De este modo se puede preseleccionar una serie de candidatos en base a sus características moleculares.
4. Predicción de datos usando la herramienta de aprendizaje automático. Gracias a la red neuronal artificial desarrollada en esta tesis, las propiedades de los compuestos puros se pueden utilizar para predecir el equilibrio líquido-vapor de mezclas de gases fluorados con LIs. Además, son propiedades de fácil acceso: masa molar del anión y catión del LI, volumen molar y átomos de flúor del LI, y la masa molar, propiedades críticas, factor acéntrico, presión de vapor y átomos de flúor del gas refrigerante. Así, todos los candidatos identificados con el estudio computacional se pueden evaluar rápidamente para seleccionar el más prometedor para continuar el estudio.
5. Determinación experimental de la absorción de los gases fluorados en el LI seleccionado. Esto permite el conocimiento preciso del equilibrio líquido-vapor, lo que disminuye la incertidumbre derivada del uso de la red neuronal, que es menor al 10% en la mayoría de los casos, pero puede dar errores mayores en casos específicos alejados de los valores usados para entrenar la red neuronal.
6. Regresión de los datos experimentales. El diseño y la simulación de procesos requieren el uso de un modelo termodinámico preciso. En esta tesis, el modelo de coeficientes de actividad NRTL se ha utilizado más para el diseño de separadores flash, columnas de destilación extractiva y absorbedores y desorbedores en los sistemas de refrigeración

por absorción. Sin embargo, la ecuación de estado soft-SAFT debería utilizarse tan pronto como esté disponible al público general porque puede presentar un ligero aumento en la precisión de la regresión con parámetros transferibles entre pares de absorción diferentes.

7. Diseño de procesos. Una vez que todos los pasos anteriores se han completado exitosamente, el diseño de la planta piloto o el proceso industrial puede llevarse a cabo siguiendo los procedimientos de simulación y optimización habituales en el campo de la ingeniería química.



**Conclusions and**  
**future perspectives**

**Conclusiones y**  
**perspectivas futuras**





---

## 5. Conclusions and future perspectives

The RACHP market is currently living a revolution to reduce the environmental impact associated with its direct and indirect emissions. At present, we are amid the evolution process, where there is a need to improve the use of resources and the energy efficiency to reduce waste and pollution.

On the one hand, residual streams from waste refrigeration equipment still contain CFCs that were banned in 1996 by the signing parties of the Montreal Protocol, but at the same time they start to contain the new fourth generation HFO refrigerants. Since the beginning of this thesis in October 2019, we have witnessed the entry into the market of yet newer HFO and HCFO molecules. Nowadays, in Europe the “waste” refrigerant gases should be collected for direct reuse or incinerated in special facilities, but there is still a portion that are released to the atmosphere due to leakages in RAC equipment or to illegal practices. This context presents a new paradigm of circular economy, expressed as the recovery of high-added-value refrigerant gases avoiding its destruction to reuse them in the new refrigerant blends that are being synthesized with low GWP HFCs and HFOs.

On the other hand, the importance of RAC sector as a global consumer of electricity in the grid mix makes clear that a reduction in the equipment consumption maintaining the same refrigeration capacity (i.e., an increase in the equipment efficiency) is of uttermost interest to build sustainable communities and promote green and sustainable development models.

In this thesis, both objectives have been addressed through the assessment of the absorption of F-gases in ILs, as these are considered green solvents, do not contaminate the gaseous streams, and their structure can be carefully selected to match the needs of each process. In the recovery of added-value refrigerants, ILs can act as entrainers in extractive distillation processes, separating the components for its reuse or incineration depending on their environmental impact. In the field of energy efficiency, ILs can be used as solvents in absorption refrigeration processes, which reduce the electricity consumption by using low-grade thermal energy that can come from renewable or waste sources. This thesis has approached the challenges of experimental and modeling studies. The conclusions derived from this thesis are:

1. There is not an IL that can be used for both separation and absorptive refrigeration purposes: an IL will be either very selective but low sorbing, or it will present a low selectivity, but a high absorption capacity. In that sense:

- a. Cyanide-based ILs are a good choice for the development of F-gas separation processes. Among the catalog of ILs that have been experimentally tested, [C<sub>2</sub>mim][SCN] proved to give the highest selectivity for the separation of R32 from R125 and R1234yf, and [C<sub>2</sub>mim][dca] performed the best separation of R134a from its mixtures with R1234yf.
  - b. For the design of absorption refrigeration systems, high molar volume and heavily fluorinated ILs such as [C<sub>2</sub>mim][Tf<sub>2</sub>N] will work the best because the solubility of fluorinated refrigerant gases is favored in these liquids. However, for scale-up purposes, the increase in molar volume and fluorination should be balanced with the possible increase in viscosity, as a stagnant fluid will not be suitable for the operation of the refrigeration system.
  - c. A general trend has been identified for the solubility of F-gases in ILs, where the absorption capacity of the IL will be lower for smaller (lower molar volume) ILs, but its selectivity will be higher.
2. The equilibrium and mass transport information on the absorption of F-gases in ILs have been reviewed, analyzed, and compiled in the UC-RAIL database. The conclusions resulting of this review should be used in the future to guide the IL selection in separation and absorption refrigeration processes, for example, ILs with low molar volume would be chosen for separation processes, and ILs with high molar volume would be used for absorption refrigeration. The resulting trends and correlations can be extended as new data are published. Additionally, trends that could only be identified for ILs that have been studied with a lot of gases could be extended to other ILs if the gaps on information for the many existing F-gases are filled. The UC-RAIL database gathers all the available information up to August 2021, and an easier access to the data will impulse their use in process design.
  3. The NRTL activity-coefficient method and the soft-SAFT EoS are successful thermodynamic models that have proved their prowess for the regression of the VLE of F-gases and ILs. Currently, NRTL is the most easily available in process simulation software and its use is widely extended. However, when soft-SAFT becomes widely available, its accuracy combined with the parameter transferability between compounds of the same family should make it a very interesting choice as thermodynamic model for advanced process design.

4. The machine learning method of ANNs have been used to develop a predictive tool to be used in the screening of suitable solvents for the application of interest. The easy-to-use tool is publicly available and capable of predicting the VLE of F-gases in ILs with average absolute relative deviation of 10%, even for new HFOs that were not included in the original training dataset. This tool works using as input common properties of the compounds forming the solute-solvent pair, namely, the critical properties, acentric factor and vapor pressure of the refrigerant gas, and the molar volume, molar mass and fluorine atoms of the refrigerant gas and the IL, all of them properties that are commonly studied and available in the open literature.
5. Molecular dynamics simulations are a powerful computational tool for the analysis of the interactions between F-gases and ILs. Using this tool will help in the selection of suitable ILs for each application based on its molecular features. For example, for the separation of R134a and R1234ze(E), the simulations have identified that modifying the cation alkyl chain of imidazolium ILs could improve the selectivity of the separation.

As a global conclusion, it can be said that this thesis has successfully developed and integrated a research framework based on experimental, thermodynamic modeling, machine learning, and computational chemistry that will allow the design of processes based on the absorption of F-gases in ILs. Furthermore, the proposed workflow can be repeated to generate the same tools allowing the study of the absorption of different compounds in different solvents.

Future steps of this work should take advantage of the developed framework for the design and optimization of processes. For example, the design and comparison of extractive distillation processes using [C<sub>2</sub>mim][SCN] and other ILs has already been done in the Department of Chemical Engineering of the University of Cantabria and will be published in the near future. Additionally, the interest on recovering the compounds with very high purities suggests that obtaining more information on the VLE of multicomponent mixtures in zones of high concentration of the components could be one of the important perspectives for future work to ensure the mixtures are separable and no pinch behaviors are observed.

Apart from the process design derived from this thesis, the framework could be further developed improving the predictive capabilities of the machine learning tool. Now, it is suitable for screening uses, and the VLE of the F-gases with the chosen solvent should be verified experimentally. A tool improvement should make the predictions good enough to completely

avoid the need of experimental testing. The work done using molecular dynamics showed that polarity has an important effect on the solvation of F-gases in ILs, which is a factor that is not considered in the current artificial neural network. To describe the polarity of the F-gases, dipole moments may be enough to train the ANN. However, describing the polarity of the IL is cumbersome due to the existence of polar, nonpolar and fluorinated nano-segregated domains in the bulk of the liquid. During the development of the thesis, the inclusion of Kamlet-Taft parameters as inputs of the ANN was considered, but there were not data available for all the ILs contained in the dataset. Then, the options pass through the extensive determination of the Kamlet-Taft parameters for many ILs or using some other polarity-related variable, maybe derived from quantum chemistry calculations. However, the options available during the thesis made these alternatives more difficult than actually making the VLE experiments, and if the more predictive tool is ever developed, it should be done with some property more easily accessible for the general public than determining experimentally the VLE itself.

Finally, another point where some future work should be carried out is the separation of mixtures of R134a and R1234ze(E). The molecular study using force fields showed that the main interaction of the  $[C_n\text{mim}][\text{tcm}]$  with these F-gases is through nonpolar-nonpolar interactions with the cation alkyl chain. Disturbing the nonpolar domain of the IL can improve the selectivity. This perturbation could be achieved through the introduction of moieties in the alkyl chains. For example, using ether alkyl chains ( $\text{CH}_3-(\text{CH}_2)_n-\text{O}-(\text{CH}_2)_m$ -imidazolium ring) will add some polarity to the chain and will promote hydrogen bonding between the F-gases positive centers (one in R134a and two in R1234ze(E)) and the oxygen degenerated electrons, so it may improve the selectivity of the absorption.

---

## 5. Conclusiones y perspectivas futuras

El mercado de la refrigeración, aire acondicionado y bombas de calor está viviendo una revolución para reducir el impacto medioambiental asociado a sus emisiones directas e indirectas. Actualmente, nos encontramos en medio del proceso de evolución, en el que hace falta mejorar la eficiencia energética y de uso de recursos para reducir los residuos y la contaminación derivados de la actividad del sector.

Por una parte, los residuos gaseosos procedentes de equipos de refrigeración fuera de uso contienen todavía CFCs prohibidos en 1996 por los firmantes del Protocolo de Montreal, pero al mismo tiempo empiezan a incluir las nuevas HFOs de la cuarta generación de refrigerantes. Desde que dio comienzo esta tesis en octubre de 2019, hemos sido testigos de la entrada al mercado de moléculas de HFOs y HCFOs aún más nuevas. Actualmente, en Europa, los gases refrigerantes “residuales” deberían recogerse para su reutilización directa o ser incinerados en instalaciones especializadas, pero todavía hay una porción que se emite a la atmósfera debido a fugas de equipos de refrigeración y aire acondicionado o a prácticas ilegales. Este contexto ofrece oportunidades en el nuevo paradigma de la economía circular, expresada como la recuperación de los gases refrigerantes de alto valor añadido evitando su destrucción para reusarlos en las nuevas mezclas refrigerantes que se están preparando con HFCs y HFOs con potenciales de calentamiento atmosférico bajos.

Por otro lado, la importancia del sector de la refrigeración y aire acondicionado como consumidor global en la red eléctrica deja claro que una reducción en el consumo de los equipos manteniendo la misma capacidad de refrigeración (esto es, un aumento en la eficiencia de los equipos) es del mayor interés para construir comunidades sostenibles y promover modelos de desarrollo sostenible.

En esta tesis, ambos objetivos se han abordado a través de la evaluación de la absorción de gases fluorados en líquidos iónicos (LIs), ya que estos se consideran disolventes verdes, no contaminan las corrientes gaseosas y su estructura puede ser elegida cuidadosamente para cumplir con las necesidades de cada proceso. En la recuperación de refrigerantes con valor añadido, los LIs pueden funcionar como absorbentes en procesos de destilación extractiva para separar los componentes de las mezclas refrigerantes para reutilizarlos o incinerarlos en función de su impacto medioambiental. En el campo de la eficiencia energética, los LIs se pueden usar como disolventes en procesos de refrigeración por absorción, que reducen el consumo eléctrico gracias al uso de energía térmica de baja energía de origen renovable o residual. Esta tesis se ha

aproximado a los retos de investigación a través de estudios experimentales y de modelado matemático. Las conclusiones derivadas de la tesis son:

1. No hay LIs universales que puedan usarse tanto para la separación de refrigerantes como para procesos de refrigeración por absorción: un LI puede ser o muy selectivo, pero con baja capacidad de absorción, o poco selectivo por la alta solubilidad de los gases. En ese sentido:
  - a. Los LIs que contengan grupos cianuro son una buena elección para el desarrollo de procesos de separación de gases fluorados. Dentro de la gama de LIs que se han estudiado experimentalmente, el  $[\text{C}_2\text{mim}][\text{SCN}]$  aporta la selectividad más alta para la separación de R32 de R125 y R1234yf, y la  $[\text{C}_2\text{mim}][\text{dca}]$  realiza la mejor separación de R134a de sus mezclas con R1234yf.
  - b. Para el diseño de sistemas de refrigeración por absorción, los LIs de volumen molar alto y que contenga mucho flúor como el  $[\text{C}_2\text{mim}][\text{Tf}_2\text{N}]$  funcionarán mejor porque la solubilidad de los gases refrigerantes fluorados se ve favorecida en estos LIs. Sin embargo, los incrementos en volumen molar y fluoración deberían equilibrarse con la posible subida de viscosidad del LI, pues un fluido viscoso aumentará el consumo de energía del sistema de refrigeración y no permite el buen funcionamiento del proceso.
  - c. Se ha identificado una tendencia en la solubilidad de los gases fluorados en LIs, según la cual la capacidad de absorción del LI será menor para LIs de menor volumen molar, pero su selectividad será mayor.
  
2. La información disponible sobre la absorción de gases fluorados en LIs se ha revisado, analizado y recopilado en la base de datos UC-RAIL. Esta incluye tanto propiedades de equilibrio como de transporte de materia, y las conclusiones resultantes de la revisión bibliográfica deberían utilizarse en el futuro como guía en la selección de LIs en procesos de separación o de refrigeración por absorción. Por ejemplo, LIs con bajo volumen molar servirían como agentes de separación en destilaciones extractivas mientras que LIs con elevado volumen molar se usarían como disolventes en procesos de separación por absorción. Las tendencias y correlaciones identificadas se pueden extender añadiendo los nuevos datos a medida que se publiquen. Además, las tendencias que solo se han podido identificar para LIs estudiados con muchos gases diferentes se podrían extender a otros LIs si se completa la información con los gases fluorados refrigerantes que faltan.

---

La base de datos UC-RAIL reúne toda la información disponible hasta agosto de 2021, y un acceso más fácil a estos datos impulsará su utilización en diseño de procesos.

3. Los modelos termodinámicos basados bien en coeficientes de actividad NRTL, o en la ecuación de estado soft-SAFT han demostrado su capacidad para la regresión del equilibrio líquido-vapor de gases fluorados en LIs. En la actualidad, el modelo NRTL es más fácil de utilizar por su disponibilidad en programas de simulación de procesos y su uso está muy extendido. Sin embargo, a medida que la ecuación soft-SAFT aparezca en los distintos programas de simulación de procesos, su precisión y la transferibilidad de parámetros entre compuestos de la misma familia deberían hacer de esta ecuación de estado una elección muy interesante como modelo termodinámico en el diseño avanzado de procesos.
4. El método de aprendizaje automático (machine learning) conocido como redes neuronales artificiales se ha usado para desarrollar una herramienta predictiva para la búsqueda de disolventes adecuados para la aplicación de interés. La herramienta está disponible al público y es capaz de predecir el equilibrio líquido-vapor con una desviación relativa absoluta media del 10%, incluso para HFOs que no estaban incluidos en la base de datos inicial. Esta herramienta funciona utilizando como input propiedades de los compuestos formando el par soluto-disolvente comunes, tales como las propiedades críticas, factor acéntrico y presión de vapor del gas refrigerante, y el volumen molar, masa molar y átomos de flúor del gas refrigerante y el líquido iónico, todas ellas propiedades comúnmente estudiadas y disponibles en la literatura abierta.
5. Las simulaciones de dinámica molecular son una herramienta computacional de gran utilidad para el análisis de las interacciones existentes entre gases fluorados y LIs. Usar esta herramienta ayudará en la selección de líquidos iónicos adecuados para cada aplicación basándose en su estructura molecular. Por ejemplo, para la separación de R134a y R1234ze(E), las simulaciones han identificado que modificar la cadena alquílica del catión de los LIs basados en imidazolio podría mejorar la selectividad de la separación.

La conclusión global de esta tesis es que ha desarrollado e integrado exitosamente un marco de investigación basado en la experimentación, el modelado termodinámico, el aprendizaje automático y la química computacional que permitirá el diseño de procesos basados en la



absorción de gases fluorados en LIs. Es más, el modo de trabajo aplicado se puede repetir para generar las mismas herramientas para el estudio de la absorción de compuestos diferentes en otros disolventes.

Como etapas futuras de continuación de esta tesis, se debería aprovechar el trabajo desarrollado para diseñar y optimizar procesos. Por ejemplo, el diseño y comparación de procesos de destilación extractiva utilizando  $[C_2mim][SCN]$  y otros LIs ya se ha llevado a cabo en el Departamento de Ingenierías Química y Biomolecular de la Universidad de Cantabria y se va a publicar próximamente. Asimismo, el interés en recuperar los compuestos con muy altas purezas sugiere que obtener más información sobre el equilibrio líquido-vapor de mezclas multicomponente en zonas de alta concentración podría ser una de las perspectivas importantes de trabajo futuro para asegurar que las mezclas son separables y no se observa un comportamiento de difícil separación por unión de las curvas de burbuja y de rocío.

Además del diseño de procesos derivado de esta tesis, el marco de trabajo se podría mejorar aún más a través de la mejora de las capacidades predictivas de la herramienta de aprendizaje automático. En este momento, la herramienta es adecuada para la búsqueda rápida de disolventes, y el equilibrio líquido-vapor de los gases fluorados con el LI elegido debería ser verificado experimentalmente. Una mejora de la herramienta debería hacer las predicciones lo suficientemente buenas para eliminar completamente la necesidad de realización de experimentos. El trabajo realizado con dinámica molecular mostró que la polaridad tiene un efecto importante en la solvatación de gases fluorados en LIs, un factor que no se considera en la red neuronal actual. Describir la polaridad de los gases fluorados es posible con el momento dipolar de las moléculas, que puede ser suficiente para el entrenamiento de la red. Sin embargo, describir la polaridad de los LIs es complicado debido a la existencia de dominios nano-segregados polares, apolares y fluorados en el seno del fluido. Durante el desarrollo de esta tesis, se consideró la inclusión de parámetros de Kamlet-Taft como entradas de la red neuronal, pero no existen suficientes datos en la literatura para cubrir todos los LIs considerados en la base de datos. De esta forma, las opciones pasan por una determinación extensiva de los parámetros de Kamlet-Taft para muchos LIs o utilizar otra variable relacionada con la polaridad, puede que proveniente de cálculos de química cuántica. Sin embargo, las opciones disponibles durante la tesis hacían estas alternativas más difíciles que determinar el propio equilibrio líquido-vapor experimentalmente. Si la más predictiva se desarrolla, debería hacerse con alguna propiedad de más fácil acceso para el público general que la determinación del equilibrio líquido-vapor.

---

Para finalizar, otro punto donde se debería continuar trabajando es la separación de mezclas de R134a y R1234ze(E). El estudio molecular usando campos de fuerza (force fields) demostró que la interacción principal de los  $[C_n\text{mim}][\text{tcm}]$  con los gases fluorados es a través de interacciones apolares con la cadena alquílica del catión. Perturbar el dominio apolar del LI puede mejorar la selectividad. Esta perturbación se podría conseguir con la introducción de grupos distintos en las cadenas alquílicas. Por ejemplo, usar cadenas alquílicas con éter ( $\text{CH}_3-(\text{CH}_2)_n-\text{O}-(\text{CH}_2)_m$ -anillo de imidazolio) puede añadir algo de polaridad a la cadena y promover puentes de hidrógeno en los centros positivos de los gases fluorados (uno en el R134a y dos en el R1234ze(E)) y los electrones degenerados del oxígeno, mejorando la selectividad de la absorción.

## ANEXO. DIFUSIÓN DE RESULTADOS


### 1. Artículos en revistas científicas

1. Salvador Asensio-Delgado, Fernando Pardo, Gabriel Zarca, Ane Urriaga. Absorption separation of fluorinated refrigerant gases with ionic liquids: Equilibrium, mass transport, and process design. *Separation and Purification Technology*, 276 (2021), 119363. Factor de impacto JCR: 9.136. Chemical engineering: primer cuartil, primer decil, 14/142. 
2. Salvador Asensio-Delgado, Daniel Jovell, Gabriel Zarca, Ane Urriaga, Fèlix Llovell. Thermodynamic and process modeling of the recovery of R410A compounds with ionic liquids. *International Journal of Refrigeration*, 118 (2020), 365-375. Factor de impacto JCR: 3.629. Mechanical engineering: segundo cuartil, 34/133. Thermodynamics: segundo cuartil, 17/60. 
3. Salvador Asensio-Delgado, Fernando Pardo, Gabriel Zarca, Ane Urriaga. Vapor-liquid equilibria and diffusion coefficients of difluoromethane, 1,1,1,2-tetrafluoroethane, and 2,3,3,3-tetrafluoropropene in low-viscosity ionic liquids. *Journal of Chemical & Engineering Data*, 65 (2020), 4242-4251. Factor de impacto JCR: 2.694. Thermodynamics: segundo cuartil, 27/63. Chemical engineering: tercer cuartil, 77/143. Multidisciplinary chemistry: tercer cuartil, 98/179. 
4. Salvador Asensio-Delgado, Fernando Pardo, Gabriel Zarca, Ane Urriaga. Enhanced absorption separation of hydrofluorocarbon/hydrofluoroolefin refrigerant blends using ionic liquids. *Separation and Purification Technology*, 249 (2020), 117136. Factor de impacto JCR: 7.312. Chemical engineering: primer cuartil, 16/143. 
5. José M. Asensio-Delgado, Salvador Asensio-Delgado, Gabriel Zarca, Ane Urriaga. Analysis of hybrid compression absorption refrigeration using low-GWP HFC or HFO/ionic liquid working pairs. *International Journal of Refrigeration*, 134 (2022), 232-241. Factor de impacto JCR (año 2021): 4.140. Mechanical engineering: primer cuartil, 34/137. Thermodynamics: segundo cuartil, 17/63. 




6. Salvador Asensio-Delgado, Miguel Viar, Fernando Pardo, Gabriel Zarca, Ane Urtiaga. Gas solubility and diffusivity of hydrofluorocarbons and hydrofluoroolefins in cyanide-based ionic liquids for the separation of refrigerant mixtures. *Fluid Phase Equilibria*, 549 (2021), 113210. Factor de impacto JCR: 2.745. Thermodynamics: segundo cuartil, 29/63. Chemical engineering: tercer cuartil, 81/142. Physical chemistry: tercer cuartil, 110/163.
- 
7. Salvador Asensio-Delgado, Fernando Pardo, Gabriel Zarca, Ane Urtiaga. Machine learning for predicting the solubility of high-GWP fluorinated refrigerants in ionic liquids. *Journal of Molecular Liquids*, 367 (2022), 120472. Factor de impacto JCR (año 2021): 6.633. Atomic, molecular & chemical physics: primer cuartil, 6/36. Physical chemistry: segundo cuartil, 48/163.
- 
8. Salvador Asensio-Delgado, Miguel Viar, Agílio A.H. Pádua, Gabriel Zarca, Ane Urtiaga. Understanding the molecular features controlling the solubility differences of R-134a, R-1234ze(E) and R-1234yf in 1-alkyl-3-methylimidazolium tricyanomethanide ionic liquids. *ACS Sustainable Chemistry & Engineering*, 10 (2022), 15124-15134. Factor de impacto JCR (año 2021): 9.224. Chemical engineering: primer cuartil, primer decil, 13/143. Multidisciplinary chemistry: primer cuartil, 29/179. Green & sustainable science & technology: primer cuartil, 10/47.
- 

## 2. Contribuciones a congresos

1. Salvador Asensio-Delgado, Fernando Pardo, Gabriel Zarca, Ane Urtiaga. Novel ionic liquid-based separation processes for the recycling of fluorinated refrigerant gases. Comunicación oral. 13<sup>th</sup> European Congress of Chemical Engineering and 6<sup>th</sup> European Congress of Applied Biotechnology. Celebrado de modo virtual. 20-23 de septiembre de 2021.
- 
2. Salvador Asensio-Delgado, Fernando Pardo, Gabriel Zarca, Ane Urtiaga. Ionic liquids as entrainers of fluorinated refrigerant gases: from vapor-liquid equilibrium to separation process design. Presentación flash y póster. 31<sup>st</sup> European Symposium on Applied Thermodynamics. Celebrado de modo virtual. 5-7 de julio de 2021.
- 

3. Salvador Asensio-Delgado, Fernando Pardo, Gabriel Zarca, Ane Urriaga. Using the Regular Solution Theory to select ionic liquids for the separation of fluorinated refrigerants. Comunicación oral. 6<sup>th</sup> Iberoamerican Meeting on Ionic Liquids. Celebrado de modo virtual.  24-26 de mayo 2021.
4. Salvador Asensio-Delgado, Fernando Pardo, Gabriel Zarca, Ane Urriaga. Solubility differences of refrigerant gases in ionic liquids. Comunicación oral. 14<sup>th</sup> Mediterranean Congress of Chemical Engineering. Celebrado de modo virtual. 16-20 de noviembre de 2020. ISBN: 978-84-09-25244-2.

### 3. Contribuciones a congresos como coautor

1. Gabriel Zarca, Salvador Asensio-Delgado, Fernando Pardo, Ane Urriaga. Separation of close-boiling refrigerant mixtures using ionic liquid-based absorption and membrane processes. Comunicación oral.  5<sup>th</sup> International Conference on Ionic Liquids in Separation and Purification Technology. Scottsdale, Arizona, EEUU, 5-8 de febrero de 2023.
2. Miguel Viar, Salvador Asensio-Delgado, Fernando Pardo, Gabriel Zarca, Ane Urriaga. Extractive distillation for refrigerant blends separation: solvent selection and process simulation. Comunicación oral.  20<sup>th</sup> International Symposium on Solubility Phenomena and Related Equilibrium Processes. Celebrado de modo virtual 4-9 de septiembre de 2022. ISBN: 978-972-75-308-5.
3. Miguel Viar, Salvador Asensio-Delgado, Fernando Pardo, Gabriel Zarca, Ane Urriaga. Extractive distillation process design for the recovery of fluorinated gases from refrigerant blends. Póster.  XXXVIII Reunión Bienal de la Real Sociedad Española de Química. Granada, 27-30 de junio de 2022. ISBN: 978-84-09-42159-6.

### 4. Contribuciones a congresos anteriores al doctorado

Como autor:

1. Salvador Asensio Delgado, Gabriel Zarca, Ane Urriaga, Fèlix Llovell. Evaluating the performance of ionic liquids to separate refrigerant gases using the soft-SAFT EoS.



- Comunicación oral. 3<sup>rd</sup> International Congress of Chemical Engineering ANQUE-ICCE 3. Santander, 19-21 de junio de 2019. ISBN: 978-84-09-12430-5.
- Salvador Asensio Delgado, Fernando Pardo, Ane Urriaga, Gabriel Zarca. Innovative separation processes for the recyclability of refrigerant gases. Póster. Student Conference ANQUE-ICCE 3. Santander, 17-18 de junio de 2019. ISBN: 978-84-09-12437-4.
  - Salvador Asensio Delgado, Gabriel Zarca, Ane Urriaga, Fèlix Llovell. Evaluación termodinámica mediante la ecuación de estado soft-SAFT del uso de líquidos iónicos para la separación selectiva de hidrofluorocarbonos. XXXV Jornadas Nacionales de Ingeniería Química. Salamanca, 4-5 de julio de 2018. ISBN: 978-84-09-02497-1.



Como coautor:

- Lourdes F. Vega, Carlos Albà, Salvador Asensio, Gabriel Zarca, Ane Urriaga, Fèlix Llovell. Assessing the use of ionic liquids as a novel solvent platform for the selective recovery of F-gases with the soft-SAFT EoS. International Conference on Properties and Phase Equilibria for Product and Process Design. Vancouver, 12-16 de mayo de 2019.



International Conference on Properties and Phase Equilibria  
for Product and Process Design  
Vancouver, Canada, May 12-16, 2019

## 5. Otras actividades

Participación en la VIII edición de la Noche Europea de los Investigadores organizada por la Unidad de Cultura Científica y Organización (UCC+i) de la Universidad de Cantabria. Organización del taller “¿Cómo afectan los equipos de refrigeración y aire acondicionado al cambio climático?”. 27 de noviembre de 2020.



Participación como voluntario en el comité de organización del tercer congreso ANQUE-ICCE y primer congreso CIBIQ 2019 celebrados entre el 19 y el 21 de junio de 2019.

Revisión de artículo científico para la revista Chemical Engineering & Technology.

Artículo en revisión en el Journal of Environmental Chemical Engineering. In the quest for ionic liquid entrainers for the recovery of R-32 and R-125 by extractive distillation under rate-based considerations. Viar, M., Asensio-Delgado, S., Pardo, F., Zarca, G., Urriaga, A.



Salvador Asensio Delgado was born on February 2<sup>nd</sup>, 1996, in Santander (Cantabria, Spain). In 2018, he completed the Degree of Chemical Engineering at the University of Cantabria, where he had been to Cornell University in Fall 2017, enrolled the European Project Semester in Winter 2018, and was awarded with Honors in Chemical Engineering, academic year 2017-2018 (Premio Extraordinario de Fin de Grado), and the IV Award AQUIQÁN to the Best Bachelor Thesis of the year.

In October 2019, he obtained an Interuniversity's Master's Degree in Chemical Engineering (UC and UPV/EHU) and obtained the awards to the Best Master Thesis in Chemical Engineering from the School of Industrial and Telecommunication Engineering and the first award to the Master Theses about Circular Economy from the MARE Chair of the University of Cantabria. During his academic period, he has received honors in 17 different subjects.

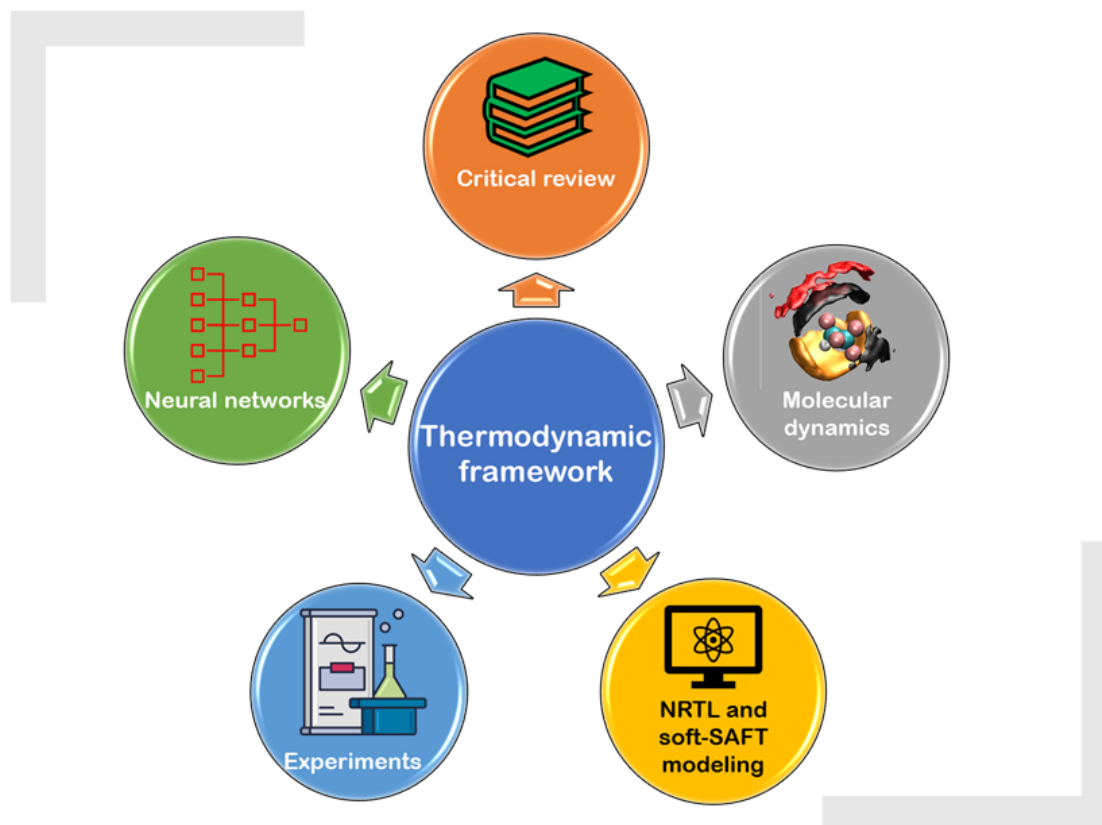
At the end of 2019, he started his doctoral studies funded by a FPU grant (FPU18/03939) from the Spanish Ministry of Science and Innovation. These studies were framed in the PhD program of Chemical Engineering, Energy and Processes at the University of Cantabria under the supervision of Prof. Dr. Ane Urtiaga and Dr. Gabriel Zarca Lago, in the research group of Environmental Technologies and Bioprocesses. He has been involved in the project KET4F-Gas, cofounded by the European Interreg Sudoe programme, aimed at reducing the environmental impact of fluorinated gases by means of key enabling technologies.

During his PhD, he has carried out a research stay at the Laboratoire de Chimie of the ENS de Lyon supervised by Prof. Dr. Agílio Pádua.

At the time of writing, he is the author of 8 scientific articles and 11 conference contributions.

In January 2022, he joined the Research and Innovation Center at Lyon of Rhodia Opérations of the Solvay's Group as a Research Process Engineer to work in the development of separation processes in the Laboratoire de Recherche de Procédés department.





El sector de la refrigeración y aire acondicionado tiene un elevado impacto ambiental ocasionado por las emisiones indirectas asociadas al consumo de energía de los equipos de refrigeración, así como a las emisiones directas de los gases refrigerantes de efecto invernadero. Esta tesis está consagrada al desarrollo de un marco de trabajo que combina estudios experimentales, modelado matemático y herramientas computacionales novedosas destinado a la selección de líquidos iónicos que proporcionen las características termodinámicas más adecuadas para su uso como disolventes de hidrofluorocarbonos e hidrofluoroolefinas en dos tipos de aplicaciones: i) sistemas de refrigeración por absorción con eficiencia energética mejorada, y ii) destilaciones extractivas para separar mezclas de refrigerantes obtenidas a partir de dispositivos al final de su vida útil, y recuperar los gases con bajo potencial de calentamiento atmosférico para su reutilización. La presente tesis doctoral contribuye a la evolución del sector de la refrigeración hacia la economía circular y propone las herramientas necesarias para el desarrollo de procesos que faciliten esta transición y la mitigación de los efectos del cambio climático.

The refrigeration and air conditioning sector has an elevated environmental impact resulting from the indirect emissions derived of its energy consumption, and from the direct emissions of GWP hydrofluorocarbons from equipment at its end of life. This thesis develops an integrated framework that combines experimental studies, mathematical modeling, and novel computational tools for the selection of ionic liquids with the adequate thermodynamic properties for their use as solvents of hydrofluorocarbons and hydrofluoroolefins in two applications: i) absorption refrigeration systems that increase the efficiency of the refrigeration devices, and ii) extractive distillations aimed to separate azeotropic and close-boiling-point mixtures of fluorinated gases, with the goal of recovering low-GWP refrigerants from end-of-life equipment. This doctoral thesis contributes to the evolution of the refrigeration sector towards the circular economy and proposes the necessary tools for the development of processes that facilitate this transition, as well as the mitigation of the effects of climate change.